UNIVERSITÀ DELLA
CALABRIA

UNIVERSITA' DELLA CALABRIA

Dipartimento di Ingegneria Meccanica Energetica e Gestionale (DIMEG)

Dottorato di Ricerca in

Ingegneria Civile e Industriale

CICLO

XXXIII°

TITOLO TESI

Towards the Clean Energy Building Community: multi-objective optimization of photovoltaic-wind-battery assisted heat pump systems in the presence of electric vehicle charging stations

Settore Scientifico Disciplinare ING-IND/11

Coordinatore: Ch.mo Prof. Enrico Conte

Firma ___ Firma oscurata in base alle linee guida del Garante della privacy

Supervisore: Ch.mo Prof. Giuseppe Oliveti

Firma ___ Firma oscurata in base alle linee guida del Garante della privacy

Co-supervisore: Ch.mo Ing. Ph.D. Domenico Mazzeo

Firma ___ Firma oscurata in base alle linee guida del Garante della privacy

Dottorando: Dott./ssa Nicoletta Matera

Firma ___ Firma oscurata in base alle linee guida del Garante della privacy

UNIVERSITÀ DELLA CALABRIA

UNIVERSITA' DELLA CALABRIA

Dipartimento di Ingegneria Meccanica Energetica e Gestionale (DIMEG)

Dottorato di Ricerca in

Ingegneria Civile e Industriale

CICLO

XXXIII°

TITOLO TESI

Towards the Clean Energy Building Community: multi-objective optimization of photovoltaic-wind-battery assisted heat pump systems in the presence of electric vehicle charging stations

Settore Scientifico Disciplinare ING-IND/11

Coordinatore: Ch.mo Prof. Enrico Conte

Firma _____

Supervisore: Ch.mo Prof. Giuseppe Oliveti

Firma_____

Co-supervisore: Ch.mo Ing. Ph.D. Domenico Mazzeo

Firma_____

Dottorando: Dott./ssa Nicoletta Matera

Firma _____

Towards the Clean Energy Building Community: multi-objective optimization of photovoltaic-wind-battery assisted heat pump systems in the presence of electric vehicle charging stations

Abstract

La tesi di dottorato si propone di analizzare l'abbinamento di sistemi ibridi rinnovabili con sistemi di accumulo al fine di mitigare l'incertezza e l'intermittenza di tali risorse e, quindi, di raggiungere una maggiore affidabilità nel soddisfare il carico richiesto e ridurre l'energia in eccesso.

La ricerca si è focalizzata sullo studio di una "Comunità a Energia Pulita" in cui sistemi ibridi tri-generativi composti da sistemi eolici, fotovoltaici, di accumulo e pompe di calore sono impiegati per la produzione di energia elettrica ed energia termica "calda" e "fredda" per la climatizzazione degli edifici, per fornire elettricità a distretti di edifici residenziali o di uffici e per alimentare stazioni di ricarica dei veicoli elettrici.

Viene fornite una panoramica e un database matriciale aggiornabile dei 550 articoli scientifici più rilevanti nella letteratura scientifica pubblicati nel periodo 1995-2020, propone diversi strumenti di dimensionamento e previsione delle performance della comunità a servizio dei progettisti e dei legislatori. Sonpo state considerate, tenendo conto degli aspetti energetici, economici e ambientali:

- diverse applicazioni;
- varie configurazioni di impianto stand-alone e grid-connected (con e senza batterie di accumulo, con e senza sistemi eolici, con e senza sistemi fotovoltaici, con e senza pompe di calore e con e senza stazioni di ricarica di veicoli elettrici);
- differenti condizioni di carico e località nel mondo.

Le procedure proposte si basano su analisi dinamiche e sul confronto sistematico e l'ottimizzazione di opportuni indicatori di performance, per individuare le migliori condizioni climatiche nel mondo e profili di carico e per determinare l'affidabilità energetica del sistema, oltre che la massima convenienza economica e il massimo abbattimento di emissioni inquinanti.

Infine, il consistente database creato è stato impiegato per creare un tool per il dimensionamento e per la previsione delle performance della comunità ad energia pulita impiegando tecniche di intelligenza artificiale basate sulle reti neurali artificiali. Il tool previsionale è applicabile ad una qualsiasi comunità ad energia pulita, con una qualsiasi potenza nominale installata, senza limitazioni geografiche, da implementare potenzialmente in qualsiasi località del mondo, e abbinabile a qualsiasi andamento di carico. Lo strumento, inoltre, con pochi dati annuali in input è in grado di determinare direttamente le prestazioni annuali della comunità senza eseguire alcuna simulazione dinamica ottenendo risultati molto accurati quanto quelli derivanti da simulazioni orarie.

Index

Introduction

The research activities carried out during the PhD related to the study of a "Clean Energy Community for multi-objective optimization of photovoltaic-wind-battery assisted heat pump systems in the presence of electric vehicle charging station".

The context of the research is within the current attention placed by governments, researchers and professionals on atmospheric concentrations of greenhouse gases, which have risen substantially in recent years due to increased anthropogenic emissions from population growth. It is widely recognized that this rapid increase is the primary cause of ongoing climate change.

The world population is a gigantic network of interconnected communities, more than 60% of whose population will live in urban areas by 2030. Furthermore, cities are responsible for more than 70% of global CO_2 emissions and consume more than two-thirds of global energy.

In particular, electricity demand could increase dramatically over the next 20 years, given expectations for the spread of electric vehicles and heat pumps for building air conditioning. This diffusion could change the peak demand for electricity and, more generally, the hourly profile of consumption, which is of particular interest from the perspective of power grid stability. As for electric vehicles, the International Energy Agency has predicted that they could experience exponential growth, leading to a stock of electric vehicles ranging from 9 million to 20 million by 2020 and 40 million to 70 million by 2025. It appears, therefore, of utmost importance to invest in the development of sustainable cities or communities for the reduction of greenhouse gas emissions and energy needs.

The 2016 UN Paris Agreement was a landmark agreement to combat climate change, putting a limit on global temperature rise. This development could be supported by new EU-wide regulations, such as the Clean Energy Package, the set of initiatives aimed at making the European Union more competitive in the energy transition and reshaping the profile of the European electricity market. There are three main objectives: achieving energy efficiency, becoming a leader in the renewable energy sector and conceiving the consumer as an active player in the electricity market. Finally, the Clean Mobility Package, which aims to reduce vehicle emissions by 30% by 2030 compared to 2021. From this context comes the concept of "Clean Energy Community" (CEC) that aims to initiate a transition from conventional centralized energy systems to distributed and decentralized systems that use renewable resources available locally. The "Clean Energy Community" (CEC) is an organizational and social structure that operates in a given target area, consisting of private and public users, with specific goals shared by the members, such as the production, storage, consumption, supply and distribution of cleaner energy. This transition configures consumers no longer as passive subjects, but rather as active figures in the achievement of the objectives established by international agreements. The realization of CEC requires the integration of technologies with high energy performance, called "Integrated community energy systems" (ICES) that is: the use of innovative and sustainable technologies that involve the use of multiple renewable technologies with the presence of storage systems. The architecture of ICES in a given CEC depends on available resources and the corresponding market, incentive and local regulatory framework.

In this context, the research activities focused on the study of a Clean Energy Community (CEC) in which renewable trigenerative hybrid systems (RHTS) consisting of photovoltaic, wind, and battery storage systems, used to assist heat pumps for building air conditioning, to supply electricity to residential or office buildings, and power electric vehicle charging stations.

The coupling of more renewable systems with storage systems allows mitigation of the high uncertainty and intermittence of the renewable resources and, therefore, the achievement of greater reliability in satisfying the load and reducing energy in excess.
The PhD thesis aims to provide an overview on this topic and different forecasting tools to assist designers and policy-makers in the sizing of PV-wind-battery hybrid system worldwide, for different load conditions, by taking into account energy, economic and environmental aspects. The methods proposed and results obtained have a general nature and can be applied in any climatic condition, system size and considering different intended uses. Finally, to condense results, artificial intelligence was used to provide a comprehensive artificial neural network tool for the analysis and sizing of these systems.

In Chapter 1, a literature review and statistical analysis were performed from data extracted from the 550 most relevant and recent articles regarding hybrid systems, published between 1995 and 2020. The review aim was to produce an upgradable matrix literature database that schematizes the content of all articles in terms of different categories, such as the geographical distribution, their component configurations, operating mode and the auxiliary components used to support it, their intended uses and study methodologies (simulation, experimental, economic, energy, environmental and social analysis etc.) and software used. In addition, all the optimization algorithm, energy, economic, environmental and social indicators available in the literature were extracted and elaborated to identify the most used. The 550 articles were analysed, compared, and classified into several categories to provide an overall framework of the state of the art. The objective is to clearly and appropriately show important trends and findings in the development of hybrid wind and solar PV experimental, simulation and optimisation projects. Data are elaborated to obtain a statistical analysis for each category or a combination of categories. The statistical analysis carried out in this work has led to the identification of the most interesting topics in the current research of hybrid systems, highlighting the more focused topics and, specularly, those on which further in-depth investigations are still required. The picture provided is nevertheless auspicious for the future, suggesting that the branch of research on hybrid systems is only at the beginning. The matrix database and literature review developed can be updated for future investigations aiming to detect the research trend in this field.

The research activities contained in this chapter led to the publication of the paper:
D. Mazzeo, N. Matera, P. De Luca, C. Baglivo, P. M. Congedo, G. Oliveti, A literature review and statistical analysis of PV-wind hybrid renewable system researches by considering the most relevant 550 articles: an upgradable matrix literature database, Journal of Cleaner Production, 2021, 126070, ISSN 0959-6526, https://doi.org/10.1016/j.jclepro.2021.126070.

From the literature emerged some important gaps, such as the development of general procedures for system sizing and optimization, that this PhD thesis tried to fill up in the next chapters.

In Chapter 2, a multi-objective optimization method for the dimensioning of hybrid photovoltaic-wind-battery systems HPWBS characterized by high-energy reliability is proposed. The energy reliability-constrained (ERC) method permits choosing the most proper indicators combination to be constrained or optimized as a function of the specific application. The ERC method is applicable to grid-connected and stand-alone hybrid systems with and without storage battery, for residential as

well as for other uses. The ERC method proposed, for the multi-objective optimization of PV-wind hybrid systems, employs several indicators to identify the most energy reliable system configurations. In addition, it can be applied in both the design phase and performance verification phase of a specific HPWBS.

Based on the literature, energy, economic and environmental indicators were rarely simultaneously employed in the optimization of a hybrid renewable system. In addition, there is no procedures or a set of indicators to be applied uniformly in all applications for the shared analysis.

In Chapter 3, a novel benchmark procedure was developed consisting of width energy, economic and environmental analysis based on a parametric analysis for the evaluation of a set of indicators and subsequently multi-objective analysis. The procedure compares the entire PV-wind-battery system configuration with the PV-wind, PV-battery and wind-battery system sub-configurations. A width parametric and multi-optimization analysis permit the identification of the most proper nominal powers of each system component. Finally, the effect of battery lifespan and incentives on the project feasibility was investigated.

The research activities contained in chapter 2-3 led to the publication of the paper:
D. Mazzeo, C. Baglivo, N. Matera, P. M. Congedo, G. Oliveti, A novel energy-economic-environmental multi-criteria decision-making in the optimization of a hybrid renewable system, Sustainable Cities and Society, Volume 52, 2020, 101780, ISSN 2210-6707, https://doi.org/10.1016/j.scs.2019.101780.

Increasing costs of petroleum derivatives, limitations on pollutant emissions and development of photovoltaic (PV) and electrical storage systems are seen as important factor to accelerate and support the growth of electric vehicle (EV) use. Despite the growing interest in this topic in recent decades, the literature survey has shown that nowadays further researches are requested to provide worldwide qualitative and quantitative results useful to optimize PV-battery system size for EV charging simultaneously taking into account the 3E objectives (energy, economic and environmental).
A higher number of researches regarded daytime EV charging when solar energy availability makes this combination quite promising. None of the papers analysed in-depth the effect of nocturnal EV charging by using PV and battery system in the presence and absence of a residential load.
Special attention must also be paid to the nocturnal EV charge, a scenario very likely in the residential sector, in those real estate units where users tend to move to the workplace during the daytime and then recharge the EV in the evening or at night. In these conditions, the coupling between EV-PV is feasible only in the presence of an appropriate storage system.

In Chapter 4, an in-depth analysis is developed regarding the energy reliability, economic rentability and emission abatement achievable by combining a PV-battery system with the nocturnal EV charging in a residential user. In particular, the self-consumed solar energy produced, the net present value of the investment and abatement of CO_2 emissions were evaluated for different daily distances travelled in various scenarios of EV charging: presence and absence of the PV-battery system, with or without electrical residential load; EV purchased as an alternative to a diesel or petrol

vehicle. Furthermore, a wide range of variation of the PV power and battery capacity was considered to evaluate the effects produced on the satisfied EV load, surplus energy sent to the grid, investment profitability and reduction of emissions. For this purpose, the system configurations that comply with these objectives were selected. The PV-battery and EV coupling performance was assessed by modelling and simulating the dynamic behaviour of each component and the entire system, by considering the temporal trend of the fuel, management and maintenance costs in the Italian territory.

The research activities contained in this chapter led to the publication of the papers:
D. Mazzeo, N. Matera, Oliveti G, Enhancement of self-consumption, energy utilization and profitability of a photovoltaic-battery powered electric vehicle in a residential user. In: 73st Conference of the Italian Thermal Machines Engineering Association (ATI),2018.

In addition to the electric transport area, another important sector interested in electrical energy is building air-conditioning. The increasingly electric energy demand is also owing to the widespread of use heat pumps, in addition to the use of electric vehicles in urban contexts. For this reason, in the next few years, strong employment of renewable energy systems and appropriate storage systems will be required.

In Chapter 5, a dynamic and energy reliability analysis of a renewable hybrid trigeneration system (RHTS) consisting of a photovoltaic generator, a wind micro-generator and an electric storage battery (electric renewable hybrid system ERHS) was developed. The load scenario considered foresees the employment of the ERHS to supply electric energy to an EV charging station, electric office devices, and heat pump used for building heating and cooling air conditioning. The RHTS and subsystem grid-connected ERHS considered are employed to satisfy the reference office building energy demand in a Mediterranean area. The dynamic simulation results are employed to study the dynamic interaction between the ERHS with the three electric loads in different characteristic weeks. Different indices are defined and evaluated, in the absence and presence of a battery storage system, to identify the most contemporary load compared with the availability of renewable sources and to determine the system energy reliability.

The research activities contained in this chapter led to the publication of the paper:
D. Mazzeo, N. Matera, G. Oliveti, Interaction Between a Wind-PV-Battery-Heat Pump Trigeneration System and Office Building Electric Energy Demand Including Vehicle Charging," 2018 IEEE International Conference on Environment and Electrical Engineering and 2018 IEEE Industrial and Commercial Power Systems Europe (EEEIC / I&CPS Europe), Palermo, 2018, pp. 1-5, doi: 10.1109/EEEIC.2018.8493710.

In Chapter 6, a novel weekly deterministic and yearly statistical analysis were developed to detect the average reliability and reliability uncertainty of a renewable hybrid system (ERHS), composed by photovoltaic (PV) and wind systems with battery storage, which is employed to power the heat pump, an EV charging station and building electric devices.
In particular, in the statistical analysis, each indicator was subdivided into the average and uncertainty contribution, defined with two different perspectives. The first set of indicators allows quantification of the ERHS capability: to satisfy the overall load by means of the overall PV-wind fraction; to utilize

the entire renewable energy produced by means of the utilization factor, to operate in nominal conditions by means of the dimensionless manufacturability; to cover the overall load over time by means of the overall time contemporaneity factor. The second set of indicators permits the comparison of the three different electric loads among them in terms of: renewable energy sent by the ERHS to each load by means of the energy contemporaneity factors; satisfaction of every single load by means of the PV-wind fractions; satisfaction of every single load in relation to the overall load by means of the weighted PV-wind fractions; satisfaction of every single load over time by means of the time contemporaneity factors.

For this issue, a dynamic simulation tool in the TRNSYS environment containing sophisticated models and proper algorithms and made up of three subroutines respectively for the building, HP and ERHS systems, was developed. In particular, a new algorithm to simulate the performance of a reversible multi-stage air-source HP was created. Different system configurations and system sizes were parametrically analyzed to identify, by means of the use of a novel set of dimensionless indicators, the ERHS with the most reliable and the least uncertain in reliability terms.

By considering an RHTS employed for supplying an office building energy demand located in the Mediterranean area, a weekly deterministic analysis has allowed evaluation of the reliability of the ERHS in the presence and absence of electric storage, while a yearly statistical analysis has allowed the identification of the system configurations with the highest average reliability and lowest reliability uncertainty by varying of the battery capacity, PV and wind power.

In this context, another important topic that was rarely carried out in the literature is the direct comparison between the techno-economic performance of stand-alone and grid-connected systems under the same operating conditions. Additionally, most of the researches are limited to specific weather conditions.

In Chapter 7, a worldwide techno-economic mapping and optimization of stand-alone (SA) and grid-connected (GC) photovoltaic (PV)-wind hybrid renewable energy systems (HRES) to supply the electrical demand of an office building district was carried out. For this purpose, energy and economic optimization problems were formulated to find the optimal SA and GC systems worldwide among 343 HRES system power configurations located in 48 different localities, uniformly divided in the sub-group of the Koppen classification. The energy reliability and economic profitability of optimal systems were geographically mapped worldwide.

The research activities contained in this chapter led to the publication of the papers:

1. *D. Mazzeo, N. Matera, P. De Luca, C. Baglivo, P. M. Congedo, G. Oliveti, Worldwide geographical mapping and optimization of stand-alone and grid-connected hybrid renewable system techno-economic performance across Köppen-Geiger climates, Applied Energy, Volume 276, 2020, 115507, ISSN 0306-2619, https://doi.org/10.1016/j.apenergy.2020.115507.*
2. *D. Mazzeo, C. Baglivo, N. Matera, P. De Luca, P. M. Congedo, G. Oliveti, Energy and economic dataset of the worldwide optimal photovoltaic-wind hybrid renewable energy systems, Data in Brief, Volume 33, 2020, 106476, ISSN 2352-3409, https://doi.org/10.1016/j.dib.2020.106476.*
3. *D. Mazzeo, C. Baglivo, N. Matera, P.M. Congedo, G. Oliveti, Impact of climatic conditions of different world zones on the energy performance of the photovoltaic-wind-battery hybrid system, IOP Conference Series: Earth and Environmental Science, Volume 410, Sustainability in the built*

environment for climate change mitigation: SBE19 Thessaloniki 23–25 October 2019, Thessaloniki, Greece, 10.1088/1755-1315/410/1/012044

Given the significant attention and promising usefulness demonstrated in different research area by artificial intelligence (AI), the last objective of this PhD thesis is to adopt artificial neural network algorithms in the topic addressed. In particular, this type of methodology is showing great potential also in the field of renewable systems, even though the present research is very recent and still in an embryonic state. For this reason, further investigations are needed to aim for artificial intelligence penetration in this sector.

In Chapter 8, an Artificial Neural Network (ANN) for the sizing and energy performance prediction of a CEC consisting of PV-wind-battery hybrid renewable energy system (HRES) used to supply electrical energy for office buildings equipped with electric vehicle charging stations was developed and validated.

The ANN was trained using an extremely large database composed of 49392 yearly simulations carried out on an hourly basis considering 48 locations around the world. These simulations were conducted according to the Koppen climate classification and, different system power configurations and loads, which were obtained by changing the number of buildings in the district. An ANN optimization was performed by determining the number of neurons needed to optimize the accuracy, quantified by using some accuracy metrics, such as the root mean square error RMSE and regression R. The ANN summarizes the hourly behaviour of the PV-wind HRES in relation to the existing climate and load conditions to directly provides the yearly energy performance and can directly determine the yearly energy performance of the PV-wind HRES deriving from the implementation of sophisticated dynamic models to predict the thermo-electrical performance of a PV system coupled to the electrical performance of a wind turbine in dynamic simulations that requires hourly climatic data. The ANN requires as inputs the component powers installed, yearly mean and standard deviations values of dynamic variables, such as external air temperature, horizontal solar radiation, wind speed and electrical load. In addition, the yearly energy performance evaluated by the ANN considers the hourly balance of the system that changes if the power generated is lower or greater than the power load.

The ANN was validated by considering different localities, system power configurations and power loads that differ from those used to create the database. This demonstrated the universal validity, namely, for any locality around the world, any system power configuration, and power load level.

Definitively, the ANN proposed allows designers and researchers to immediately obtain the yearly energy performance of a PV-wind HRES in any location and for any power installed and load. The result obtained from ANN is almost equivalent to what would be obtained by a sophisticated hourly simulation based on detailed component electrical models. The advantages are related to the reduction of input data required, only yearly average and standard deviations, and the lack of required expertise needed to use specific transient simulation tools that in many cases require an expensive license to be used.

The research activities contained in this chapter led to the publication of the papers:
D.Mazzeo, M. Sacit Herdem, N. Matera, M. Bonini, J. Z. Wen, J. Nathwani, G. Oliveti, Artificial intelligence application for the performance prediction of a clean energy community.
The paper is currently under review in Energy Journal.

Chapter 1

**A literature review and statistical analysis of
PV-wind hybrid renewable system researches by considering
the most relevant 550 articles: an upgradable matrix literature database**

Chapter 1

A literature review and statistical analysis of PV-wind hybrid renewable system researches by considering the most relevant 550 articles: an upgradable matrix literature database

Chapter 1

A literature review and statistical analysis of
PV-wind hybrid renewable system researches by considering
the most relevant 550 articles: an upgradable matrix literature database

Chapter 1

A literature review and statistical analysis of PV-wind hybrid renewable system researches by considering the most relevant 550 articles: an upgradable matrix literature database

Abstract

In recent years, research has shown a growing interest in the use of hybrid wind photovoltaic (PV) systems that provide better performance compared to the use of a single component due to complementarity in meeting electricity demand. Over the past twenty-five years, hundreds of articles have addressed the topic of hybrid systems considering different configurations and final uses and, over the past decades, many reviews have made a comprehensive summary of various results obtained. However, some reviews deal with the research in a too general and qualitative way, without providing quantitative data, and other reviews are too focused on a specific topic aspect.

To provide a qualitative-quantitative prospect of the research trend in the last twenty-five years, the present work is aimed at carrying out a literature review and statistical analysis starting from data extracted from the 550 most relevant and recent articles concerning hybrid systems, published between 1995 and 2020. The review aim was to produce an upgradable matrix literature database that schematizes the content of all articles in terms of different categories, such as the geographical distribution, their component configurations, operating mode and the auxiliary components used to support it, their intended uses and study methodologies (simulation, experimental, economic, energy, environmental and social analysis etc.) and software used. In addition, all the optimization algorithm, energy, economic, environmental and social indicators available in the literature were extracted and elaborated to identify the most used. The 550 articles were analysed, compared, and classified into several categories to provide an overall framework of the state of the art. The objective is to clearly and appropriately show important trends and findings in the development of hybrid wind and solar PV experimental, simulation and optimisation projects.

Data are elaborated to obtain a statistical analysis for each category or a combination of categories. In particular, the analysis highlighted that research is more focused on testing systems in warm or temperate localities, with the Köppen climate groups B and C prevalent over the others. From the geographical point of view, Asia is the continent most involved in world research (with China, India and Iran the first three countries for total publications produced). However, also in other parts of the world, a growing interest was noticed in this technology. The prevalent tested system configuration mode is the stand-alone hybrid systems, in a wide variety of climates and especially for residential uses. Simulations are mostly implemented in the analysed publications, mainly through HOMER and MATLAB software. Parametric analysis is widely used for optimal system design with a large variety of techniques. In particular, the system performance is examined mostly from an energy point of view. Economic analysis is also very common, alone or in combination with energy analysis. The most frequently used optimization algorithms are the particle swarm optimization (PSO) and genetic algorithm (GA), while the loss of power supply probability (LPSP) and renewable fraction (RE) for the energy analysis, the net present cost (NPC) and cost of energy (COE) for the economic analysis and the emissions (E) of CO_2 for the environmental analysis are most widespread indicators.

Finally, an analysis on the size of the system components is performed to study which renewable source is more preferred at low and high installed power, for stand-alone, grid-connected systems and

Chapter 1

A literature review and statistical analysis of
PV-wind hybrid renewable system researches by considering
the most relevant 550 articles: an upgradable matrix literature database

overall, considering different intended uses. The analysis highlights that PV systems are preferred at low installed powers, especially for residential use and stand-alone mode, while wind systems, in addition to being extensively used for low installed powers, demonstrates higher employment compared to PV systems as the power increases.

The paper findings and upgradable matrix literature database are proposed as a valuable tool for engineers, experts and national and international policymakers.

Keywords: Literature review; Renewable hybrid systems; Matrix database; Methodology; Indicators; Applications

- 550 relevant papers were reviewed and used to create an upgradable matrix literature database
- Asia is the continent most involved in world research with Iran, India, and China.
- The dry and temperate climate zones of Köppen climate group BWh are the most investigated.
- Stand-alone hybrid systems and residential use are the most explored applications.
- The use of a photovoltaic system is preferred for low installed powers, while wind systems also for high installed powers.

Chapter 1

A literature review and statistical analysis of PV-wind hybrid renewable system researches by considering the most relevant 550 articles: an upgradable matrix literature database

1. Introduction

The growing concern about environmental issues and the progressive depletion of fossil fuels has driven research towards renewable resources. Many renewable energy sources such as sun, wind and water are inexhaustible and will be the focus of the energy sector in the coming decades.

The possibility of integrating photovoltaic (PV) and wind systems allows a higher energy production than the individual system; PV and wind systems are technologies with low economic impact and compensate each other in terms of energy availability. Solar radiation is present during the day and summer season, while the wind compensates for the absence of solar production during the night and its decrease in winter. The unpredictability of these renewable sources leads to combining these systems with auxiliary energy systems such as diesel generators, fuel cells or storage systems such as batteries. The integration of PV and wind technologies into a hybrid system can partially solve the problem of high investment, maintenance and depreciation costs required. Most of the studies examined are aimed at assessing the economic and/or energy efficiency of the hybrid system compared to the non-hybrid system (PV or wind only) or at finding the optimal configuration in terms of an adequate number of PV panels and wind turbines.

In the case of stand-alone systems, a storage system can increase system reliability when both energy sources are insufficient. For grid-connected systems, the energy deficit can be compensated by drawing directly from the grid when the energy produced by the system is not enough to support the load. the system energy production increases and the excess energy can be channelled into the grid or stored in storage systems. Other storage systems, such as hydraulics, thermal, compressed air or hydrogen, electrolytic and fuel cell storages are also being coupled to hybrid systems.

Overall, defining P_g as the energy generated by the system and P_l as the energy required by the load, three cases can occur:

1) $P_g > P_l$: the power generated by the system is higher than that required by the load; the excess energy is stored in the battery and the remaining energy is sent to the grid or dissipated.

2) $P_g = P_l$: the power generated by the system is equal to that required; there is no excess or deficit.

3) $P_g < P_l$: the power generated by the system is insufficient to satisfy the load; the battery releases to the load the energy previously stored and, if the system is grid-connected, the further energy required is drawn from the grid.

Auxiliary energy production systems such as diesel generators can also be integrated into a stand-alone system in the event of failure of renewable sources, increasing the overall cost of the system. It is also possible to integrate other technologies such as hydropower, biomass systems, solar concentration systems and geothermal systems.

The analysis carried out in the present work aimed at giving a quantitative measurement of the various information concerning the hybrid systems examined in the publications, collected in a matrix database which will be illustrated below. In particular, the analysis aims to pursue the following objectives:

- Identification of the localities where simulations or experiments are carried out, reporting the most common localities and the research frequency in each world climatic group.
- Determination of the research frequency with simulation and experimental analysis or both.
- Investigation of the prevalence of stand-alone or grid-connected and the most frequent auxiliary components used.
- Identification of the most frequent intended uses, considering also the mixed uses for the same installation.

Chapter 1
A literature review and statistical analysis of
PV-wind hybrid renewable system researches by considering
the most relevant 550 articles: an upgradable matrix literature database

- Analysis of the study methodologies most frequently conducted and the most widely used software for this purpose.
- Development of statistical analysis to identify the ranges of installed component powers on which the research is most focused.

In addition, the data relating to the installations will be combined to obtain a more complete framework of the information collected, for example by linking the number of stand-alone installations in a given climate group or the intended uses with a grid-connected installation and so on).

The objective of this review is to create a schematic database and statistically analyse the overall trend of the most relevant articles in the topic PV-wind hybrid renewable systems by considering 550 recent papers [1-550].

Many reviews were developed in recent years. Table 1 shows a schematic view of the most relevant reviews developed on PV-wind hybrid renewable systems. The table reports general data and impact of reviews, the main focus and keywords, system configuration, indicators, methodology, algorithms and software used.

Table 1. Literature review of reviews on PV-wind hybrid renewable systems.

Ref.	Paper	Authors	University/Institute	Year of publication	Journal	Cit.*	Main focus and Keywords	System configuration	Indicators	Methodology/Algorithms/Software
[551]	Optimal sizing of renewable hybrids energy systems: A review of methodologies	R. Luna-Rubio, M. Trejo-Perea, D. Vargas-Vázquez, G.J. Ríos-Moreno	Universidad Autónoma de Querétaro, Santiago de Querétaro, Mexico	2012	Solar Energy	283	Sizing methodologies, indicators	Stand-alone/Grid connected	**Energy** (LPSP, SOC, LA, EENS), **Economic** (LCE, TAC, NPV, ACS)	Probabilistic, Analytical (HOMER), Iterative (PSO, GA, ARENA 12), Hybrid (Hybrid algorithms, ANN)
[552]	Real-time stochastic power management strategies in hybrid renewable energy systems: A review of key applications and perspectives	D.-A. Ciupageanua, L. Barelli, G. Lazaroiu	University of Perugia, Perugia, Italy / University Politehnica of Bucharest, Bucharest, Romania	2020	Electric Power Systems Research	0	Energy storage, Real-time power management, Renewable energy, Stochastic optimization, Gradient-based optimization	Undefined		Model predictive control (MPC), Stochastic game theory, Stochastic linear programming, Lyapunov optimization, Simultaneous perturbation stochastic approximation (SPSA)
[553]	Review of software tools for hybrid renewable energy systems	S. Sinha, S.S. Chandel	Centre for Energy and Environment, National Institute of Technology, Hamirpur, Himachal Pradesh, India	2014	Renewable and Sustainable Energy Reviews	340	Hybrid energy system, Simulation tools, Software	Undefined		HOMER, Hybrid2, RETScreen, iHOGA, INSEL, TRNSYS, iGRHYSO, HYBRIDS, RAPSIM, SOMES, SOLSTOR, HySim, HybSim, IPSYS, HySys, Dymola/Modelica, ARES, SOLSIM and HYBRIDDESIGNER.
[554]	Review of recent trends in optimization techniques for solar photovoltaic–wind-based hybrid energy systems	S. Sinha, S.S. Chandel	Centre for Energy and Environment, National Institute of Technology, Hamirpur, Himachal Pradesh, India	2015	Renewable and Sustainable Energy Reviews	195	Optimization techniques, Hybrid algorithms	Undefined	**Energy** (LPSP, LLP/LOLP, UL, SPL, LOLH, LOLR, LA), **Economic** (NPC, LCC, COE)	**Traditional approach** (Graphical construction, iterative, probabilistic, trade-off, linear programming), **New generation** (GA, PSO, SA, ACO, ABC, HS, BBO, GSA, ICA, TS), **Hybrid algorithms**
[555]	Review of solar photovoltaic and wind hybrid energy systems for sizing strategies optimization techniques and cost analysis methodologies	F.A. Khan, N. Pal, S.H. Saeed	Integral University, Lucknow, India / Indian Institute of Technology (Indian School of Mines), Dhanbad, India	2018	Renewable and Sustainable Energy Reviews	37	Sizing schemes, Optimization techniques and cost analysis	Undefined	**Energy** (LPSP, UL, LOLP/LLP, DPSP, LOLH, SPL, LOR, LOEE, LOLE), **Economic** (NPC, ACS, COE, LCC, LCUC, LCOE/LCE/LEC)	**Traditional techniques** (Iterative, probabilistic, linear programming, graphical construction, trade-off method), **Modern techniques** (GA, PSO, SA, ACA, BFO, ABC, hybrid algorithms), **Software**
[556]	A review on recent size optimization methodologies for standalone solar and wind hybrid renewable energy system	M.D.A. Al-falahi, S.D.G. Jayasinghe, H. Enshaei	Australian Maritime College, University of Tasmania, Tasmania, Australia	2017	Energy Conversion and Management	166	Off-grid, Optimization, Standalone, Algorithms, Software	Stand-alone	**Energy** (LPSP, LOLP/LLP, LOLR, LOLE, LOEE, UL, DPSP, EENS, ENS, EIR, ELF, D, TED, WRE, REP, FEE, LEP, KI, P(R), P(H)), **Economic** (NPC/TPC/NPV/TC, TIC, LCC, COE/LCE/LCOE, TAC/ASC, savings), **Environmental** (E, EE, LCA) and **Social** (HDI, JC, SCC, Socio-demographic factor)	**Classical methods** (Iterative, Linear Programming, Graphical, Analytical), **Modern methods** [Single algorithms (GA, NSGA-II, MBA, PSO, MPSO, MOPSO, MLUCA, ACO, ABC, PICEA, FOA, BBO, ABSO, ICA, CS, DHS, A-STRONG), Hybrid algorithms (HBB-BC, TLBO, Hybrid GA and exhaustive search technique, IPF, MESCA, MOEA-GA, ANN-GA-MCS, SA-TS, Markov based GA, DCHSSA, HSBCS, Hybrid iterative/GA, SAPSO, NSPSO, PSOMCS and FPA/SA)] and **Computer tools** (HOMER/HOMERpro and I-HOGA)
[557]	A review on recent sizing methodologies of hybrid renewable energy systems	J. Lian, Y. Zhang, C. Ma, Y. Yang, E. Chaima	Tianjin University, Tianjin, China	2019	Energy Conversion and Management	16	Classification, Evaluation indicator, Sizing methodology, Software tool	Stand-alone/Grid-connected	**Energy** (LPSP, LOLP; EENS, EIR, DPSP, DPS, LOLE, LOEE, LOE, LA, SOC, UL, MTBF, REP, LPP), **Economic** (TAC, ACS, COE, LCC, LCOE, NPV, NPC, TIC, TCC, PBP), **Environmental** (CE, EE, CFOE, LCA, LCE, FC, FE) and **Social** (HDI, JC, PR, Sa, SCC)	**Traditional methods** (graphic construction, probabilistic, iterative, numerical, analytical), **Artificial intelligence methods** (GA, PSO, SA, ACO, ABC, HS, CS, PICEA, MLUCA, GWO, BBO, EA), **Hybrid methods** (SA-TS, HBB-BC, GA-MILP, MOPSO-NSGA-II, ACO-CDIP), **Software tools** (HOMER, HOGA, HYBRID2, HYBRIDS)
[558]	A review on hybrid renewable energy systems	K.S. Krishna, K.S. Kumar	VIT University, Vellore, Tamilnadu, India	2015	Renewable and Sustainable Energy Reviews	111	Distributed generation, Energy management system, Maximum power point tracking technique	Stand-alone/Grid-connected	**Economic** (TC)	PSO, WSM, GA
[559]	A review of optimum sizing of hybrid PV–		Nizwa College of Technology, Oman	2016	Renewable and Sustainable	88	Sizing and optimization	Stand-alone		**Sizing techniques** (Annual monthly average sizing, Most unfavourable month,

Chapter 1

**A literature review and statistical analysis of
PV-wind hybrid renewable system researches by considering
the most relevant 550 articles: an upgradable matrix literature database**

Ref	Title	Authors	Affiliation	Year	Journal	No.	Topics	Configuration	Parameters	Methods
	Wind renewable energy systems in Oman	A.S. Al Busaidi, H.A. Kazem, A.H. Al-Badi, M.F. Khan	Sohar University, Oman; Sultan Qaboos University, Oman		Energy Reviews					LPSP technique), **Optimization techniques** (Graphic construction, probabilistic, iterative, artificial intelligence)
[560]	Solar–wind hybrid renewable energy system: A review	V. Khare, S. Nema, P. Baredar	MANIT, Bhopal, India	2016	Renewable and Sustainable Energy Reviews	232	Pre-feasibility analysis, optimum sizing, modelling, control aspects and reliability	Undefined		**Evolutionary techniques** (PSO, GA, FL, Neural Networks) and **Game theory**
[561]	A review on planning, configurations, modeling and optimization techniques of hybrid renewable energy systems for off grid applications	R. Siddaiah, R.P. Saini	Indian Institute of Technology, Roorkee, Uttarakhand, India	2016	Renewable and Sustainable Energy Reviews	131	HRES configurations, Planning, Economic modelling, Reliability modelling, Modeling and optimization techniques	Stand-alone		Classical methods, Artificial intelligence methods and hybrid methods
[562]	Energy management strategies in hybrid renewable energy systems: A review	L. Olatomiwa, S. Mekhilef, M.S. Ismail, M. Moghavvemi	University of Malaya, Kuala Lumpur, Malaysia; Palestine Technical University-Kadoorie, Tulkarm, Palestine; University of Science and Culture, Tehran, Iran; Federal University of Technology, Minna, Nigeria	2016	Renewable and Sustainable Energy Reviews	177	Energy management, Standalone hybrid systems, Grid-connected hybrid systems	Stand-alone/Grid-connected		Linear programming techniques, Intelligent techniques (FC, NN), Software techniques (HOMER, TRNSYS)
[563]	Performance evaluation of stand alone, grid connected and hybrid renewable energy systems for rural application: A comparative review	S. Goel, R. Sharma	Siksha 'O' Anusandhan University, Bhubaneswar, India	2017	Renewable and Sustainable Energy Reviews	70	Stand-alone, Grid-connected, Rural electrification, Plug-in-electric vehicle	Stand-alone/Grid-connected		
[564]	Review of hybrid renewable energy systems with comparative analysis of off-grid hybrid system	Y. Sawle, S.C. Gupta, A.K. Bohre	MANIT, Bhopal, India	2018	Renewable and Sustainable Energy Reviews	54	Modelling, Homer, PSO techniques	Stand-alone/Grid-connected	**Economic** (TNPC, COE)	PSO and HOMER
[565]	Sizing methods and optimization techniques for PV-wind based hybrid renewable energy system: A review	K. Anoune, M. Bouya, A. Astito, A.B. Abdellah	International University of Rabat (UIR), Sala Al Jadida, Morocco; Abdelmalek-Essaadi University (UAE), Ziaten, Tangier, Morocco	2018	Renewable and Sustainable Energy Reviews	60	Sizing and Optimization techniques	Undefined	**Energy** (LPS, SOC, LOLE, LOEE, LPSP, DPS, DPSP, LLP), **Economic** (LCC)	**Deterministic and stochastic methods** (Yearly average monthly method, worst month, Typical meteorological year), **Software** (HOMER, HYBRID2, HOGA, HYBRIDS, TRNSYS, HYDRO GEMS, RETScreen, GAMS, INSEL, ARES, SOLSIM, SOMES, H2RES), **Algorithm method** (GA, PSO, HSA, SA, ACA, BFO, ABC, CS), **Multi-objective design**, **Iterative method**, **Analytical method**, **Probabilistic method**, **Graphic construction**
[566]	Study of the different structures of hybrid systems in renewable energies: A review	J. Kartite, M. Cherkaoui	Mohammedia School of Engineers, Rabat, Morocco	2019	Energy Procedia	7	Hybrid Renewable Energy System (HRES), Photovoltaic, Wind energy, Storage capacity	Stand-alone/Grid-connected	**Energy** (LPSP), **Economic** (Cost of energy produced)	**Software** (HYBRID2, HOMER, RAPSIM), **Algorithms** (GA)
[567]	A current and future state of art development of hybrid energy system using wind and PV-solar: A review	P. Nema, R.K. Nema, S. Rangnekar	Maulana Azad National Institute of Technology, Bhopal, India	2009	Renewable and Sustainable Energy Reviews	409	Pre-feasibility, Modeling, Optimization, Controller	Stand-alone/Grid-connected		
[568]	Hybrid wind/photovoltaic energy system developments: Critical review and findings	A. Mahesh, K.S. Sandhu	National Institute of Technology, Kurukshetra, Haryana, India	2015	Renewable and Sustainable Energy Reviews	91	Size optimization	Stand-alone/Grid-connected	**Energy** (LPSP), **Economic** (LCE, LCC, ALCC, NPV)	Iterative techniques, graphical methods, stochastic approaches, artificial intelligent techniques, software (HOMER, RETScreen, HYBRID2, iHOGA, Hybrids)
[569]	State-of-art review of the optimization methods to design the configuration of hybrid renewable energy systems (HRESs)	M. Faccio, M. Gamberi, M. Bortolini, M. Nedaei	University of Padua, Vicenza Department, Italy; University of Bologna, Bologna, Italy	2018	Frontiers in energy	6	Design and optimization, Environmental pollutions	Stand-alone/Grid-connected	**Energy** (LLP, LPSP, LST, EIR, EENS, WRE, EEF, DPSP, DPS, VSI), **Environmental** (GWP, LCE, emission factors), **Economic** (BGED, EAC, NPV, LCC, LCOE), **Grid Parameters** (IGP, GGP)	**1** (Probabilistic, Analytical, Iterative, Hybrid models), **2** (Conventional techniques and artificial intelligence), **3** [heuristic based (GA, PSO, LP), simulation and sampling (HSS, SA, MCS), software and others (HOMER, Lingo, Matlab Simulink, MPC, B&B, GRG, iHOGA)]
[570]	Hybrid renewable energy systems for off-grid electric power: Review of substantial issues	Y.S. Mohammed, M.W. Mustafa, N. Bashir	Universiti Teknologi Malaysia, Johor Bahru, Malaysia	2014	Renewable and Sustainable Energy Reviews	47	Off-grid, Optimization, Simulation	Stand-alone		HOMER, iHOGA, HYBRID2 (Only mentioned, TRNSYS, HYDROGEMS, HYBRIDS, SOLSIM, INSEL, RAPSIM, SOMES)
[571]	A review on the utilization of hybrid renewable energy	S. Guo, Q. Liu, J. Sun, H. Jin	Chinese Academy of Sciences, Beijing, China; University of Science and Technology, Baotou, China; Xi'an Jiaotong University, Xi'an, China	2018	Renewable and Sustainable Energy Reviews	69	Hybrid renewable energy utilization, Solar energy, Biomass energy, Wind energy, Geothermal energy	Stand-alone/Grid-connected		
[572]	A review on configurations, control and sizing methodologies of hybrid energy systems	S. Upadhyay, M.P. Sharma	Indian Institute of Technology Roorkee, Uttarakhand, India	2014	Renewable and Sustainable Energy Reviews	146	Optimization techniques, Indicators, Sizing methodologies, Control and energy management	Stand-alone/Grid-connected	**Energy** (LPSP, ELF, LOLE, LOL, TEL, LA, SOC), **Economic** (LCE, TAC, Cn, Cav, NPV, ACS, FC), **Socio-political** (SA), **Environmental** (E)	Graphic construction, probabilistic, analytical, iterative, artificial intelligence, hybrid, software (HOMER, HYBRID2, HYBRIDS, RETScreen, IHOGA, TRNSYS)
[573]	A review of optimization approaches for hybrid distributed energy generation systems: Off-grid and grid-connected systems	S. Twaha, M.A.M. Ramli	University of Nottingham, United Kingdom; King Abdulaziz University, Saudi Arabia	2018	Sustainable Cities and Society	43	Optimization techniques, Off-grid systems, Grid-connected systems	Stand-alone/Grid-connected		**Mathematical** {Combinatorial, dynamic, numerical/analytical [stand-alone (MCS, MILP, DER-CAM, ARMA, GTI)], [grid connected (RHO, MILP, IMO and others)]}, **Computer programming** {Linear programming, dynamic programming, metaheuristic single methods [stand-alone (PSO, GA, DHS, WCA, BBO)], [grid connected (CS, BB-BC and others)] and hybrid methods [stand-alone (FPA-SA, TS-PSO-HS-SA, PSO-LP, HSBCS)],[grid connected (ACO-ABC, HBB-BC, MTLBO, SGHSA)]}
[574]	Modeling, planning, application and management of energy systems for	Y. Liu, S. Yu, Y. Zhu, D. Wang, J. Liu	Xi'an University of Architecture and Technology, Xi'an, PR China	2018	Renewable and Sustainable Energy Reviews	37	Isolated areas, Renewable energy, Modelling,	Stand-alone		Physical method, Statistical models, artificial intelligence

Chapter 1

**A literature review and statistical analysis of
PV-wind hybrid renewable system researches by considering
the most relevant 550 articles: an upgradable matrix literature database**

Ref	Title	Authors	Institution	Year	Journal	Citations	Topics	System	Indicators	Methods
[575]	isolated areas: A review / Multi-objective optimization of a stand-alone hybrid renewable energy system by using evolutionary algorithms: A review	M. Fadaee, M.A.M. Radzi	University Putra Malaysia, Serdang, Malaysia	2012	Renewable and Sustainable Energy Reviews	226	Planning, Energy systems / Multi-objective optimization, Stand-alone, Evolutionary algorithms, Pareto front	Stand-alone		MOEA, GA, PSO
[576]	Design and implementation of hybrid renewable energy systems on micro-communities: A review on case studies	D. Neves, C.A. Silva, S. Connors	Universidade de Lisboa, Portugal / Massachusetts Institute of Technology, USA	2014	Renewable and Sustainable Energy Reviews	115	Isolated micro-communities, Off-grid islands, Remote villages	Stand-alone/Grid-connected		
[577]	Effective utilization of excess energy in standalone hybrid renewable energy systems for improving comfort ability and reducing cost of energy: A review and analysis	M.S. Ismail, M. Moghavvemi, T.M.I. Mahlia, K.M. Muttaqi, S. Moghavvemi	Palestine Technical University—Kadoorie, Tulkarm, Palestine / University of Malaya, Kuala Lumpur, Malaysia / University of Science and Culture, Tehran, Iran / Universiti Tenaga Nasional, Kajang, Selangor, Malaysia / Syiah Kuala University, Banda Aceh, Indonesia / University of Wollongong, Wollongong, NSW, Australia	2015	Renewable and Sustainable Energy Reviews	40	Dump load, Excess energy	Stand-alone	**Energy** (EE), **Economic** (COE)	
[578]	Control strategies for a hybrid renewable energy system: A review	P.G. Arul, Vigna K. Ramachandaramurthy, R.K. Rajkumar	Universiti Tenaga Nasional, Putrajaya Campus, Kajang, Selangor, Malaysia	2015	Renewable and Sustainable Energy Reviews	94	Power converters, Control strategies	Stand-alone/Grid-connected		
[579]	Optimal planning of hybrid renewable energy systems using HOMER: A review	S. Bahramara, M. Parsa Moghaddam, M.R. Haghifam	Tarbiat Modares University, Tehran, Iran	2016	Renewable and Sustainable Energy Reviews	163	HOMER, Optimal sizing	Stand-alone/Grid-connected	**Economic** (COE)	HOMER
[580]	A review of energy management strategies for renewable hybrid energy systems with hydrogen backup	F.J. Vivas, A. De las Heras, F. Segura, J.M. Andújar	Universidad de Huelva, Spain	2018	Renewable and Sustainable Energy Reviews	66	State of art revision, Energy management strategy, Hydrogen backup	Stand-alone/Grid-connected		
[581]	A hybrid renewable energy system as a potential energy source for water desalination using reverse osmosis: A review	M.A.M. Khan, S. Rehman, F.A. Al-Sulaiman	King Fahd University of Petroleum & Minerals, Dhahran, Saudi Arabia	2018	Renewable and Sustainable Energy Reviews	25	RO Desalination	Stand-alone/Grid-connected		Algorithm method, Software method
[582]	Hybrid renewable mini-grids on non-interconnected small islands: Review of case studies	A.A. Eras-Almeida, M.A. Egido-Aguilera	Universidad Politécnica de Madrid, Madrid, Spain	2019	Renewable and Sustainable Energy Reviews	3	Hybrid renewable mini-grids, Non-interconnected, Small islands, Access to electricity, Business models	Stand-alone		

*The number of citations were extracted from the Scopus database on 13/07/2020

Luna-Rubio et al. [551] illustrated an overview of optimal sizing techniques for hybrid systems (both stand-alone and grid-connected), defining different economic (LCE, TAC, NPV, ACS) and energy (LPSP, SOC, LA, EENS) indicators and describing four categories in which the various methodologies (probabilistic, analytical, iterative, hybrid) can be included. In particular, the study concludes that iterative and hybrid techniques give better results in system sizing, considering the greater reliability they offer in multi-objective problems and their robustness even in the absence of meteorological data.

Ciupageanua et al. [552] carried out a study focused on methodologies for the optimization and optimal management of stochastic energy (in hybrid, non-hybrid and micro-grid systems), aimed at addressing the uncertainties characteristic of these processes (uncertainties in energy sources, modelling, analysis). In particular, the study focuses on Model Predictive Control (MPC) methodologies, stochastic game theory, linear stochastic programming, Lyapunov optimization and the Simultaneous Perturbation Stochastic Approximation (SPSA) algorithm. The study concludes that the last two methodologies (based on the gradient method) are the most performing.

Sinha and Chandel [553] provided a literature review of 19 software used for the optimal sizing of hybrid systems, devoting a large space to studies based on HOMER (which is the most widely used software) and a section on studies based on some of the other software. It has not been possible to illustrate the status of some of the lesser-used software. The study also compared HOMER and

Chapter 1   **A literature review and statistical analysis of**
PV-wind hybrid renewable system researches by considering
the most relevant 550 articles: an upgradable matrix literature database

RETScreen software for the optimization of a PV- battery system (case 1) and a PV-wind-battery system (case 2).

The same authors [554] developed a wider and more general study than the previous one on the optimization techniques of hybrid systems, that can be divided into traditional ones (graphic construction, iterative, probabilistic, trade-off and linear programming approaches) and the new generation ones (single algorithms and hybrid algorithms). They emphasized their advantages and disadvantages and pointed out that the optimization techniques of the new generation are becoming more employed. The study also defined energy and economic optimization criteria, illustrating the main indicators used for this purpose.

Khan et al. [555] also performed a similar study, dividing the optimization techniques into traditional, modern and software-based, and presented a sample of articles dealing with systems sized using these techniques according to economic and energy criteria. The study extracted the same conclusions, showing that modern techniques are becoming wider than traditional ones.

Similarly, Al-falahi et al. [556] carried out an in-depth study of the techniques for optimal sizing of stand-alone hybrid systems, dividing them into three categories: classical methods (iterative, linear programming, graphical and analytical), modern methods (single algorithms, hybrid algorithms) and software (HOMER, HOMERpro and iHOGA are analysed). The study presented a compendium of many studies using these methods and illustrated a certain tendency until 2017 to rely on modern techniques and software (especially hybrid algorithms, which return optimal solutions in very short computational time). The study also compared the performance of the various algorithms and highlighted the main factors that influence system sizing.

Lian et al. [557] proposed a study on the current state of research on hybrid installations (until 2019), classifying installations according to the type of component coupling (with particular attention to the presence or absence of hydroelectric sources or hydraulic storage systems) and providing an overview of the most used indicators and optimization techniques. In particular, the study divided the techniques into traditional methods (graphical, probabilistic, iterative, numerical, analytical), methods based on artificial intelligence (algorithms), hybrid methods (hybrid algorithms or hybridisation between algorithms and traditional techniques) and software (in particular, HOMER, HOGA, HYBRID2 and HYBRIDS) and listed their advantages and disadvantages. The study highlighted the trends in which the research is currently focused and suggests possible ways to improve the research quality.

Krishna and Kumar [558] considered many studies that analyse various aspects related to the systems management and configurations, dividing them according to the system mode analysed (stand-alone, grid-connected, both). They also dedicated a section to the description of the various methods for the optimal system sizing, describing techniques such as PSO and GA.

Al Busaidi et al. [559] illustrated sizing (monthly average, most unfavourable month and LPSP-based techniques) and optimization techniques (graphic construction, probabilistic, iterative and artificial intelligence) available in the literature and presented some case studies of hybrid systems carried out in Oman.

Khare et al. [560] presented the phases required for the correct sizing and management of a hybrid system, starting from pre-feasibility studies, through optimal sizing, modelling, system management and energy reliability analysis, reviewing many studies for each of these categories. The analysis focused particularly on the use of evolutionary algorithmic techniques (GA, PSO, FL, Neural Networks) and on the application of game theory in the field of hybrid systems.

Chapter 1   **A literature review and statistical analysis of**
PV-wind hybrid renewable system researches by considering
the most relevant 550 articles: an upgradable matrix literature database

Siddaiah and Saini [561] proposed a review on hybrid systems, dividing them according to the type of DC/AC or AC/DC static conversion used and the intended use (small such as villages or large such as districts and communities). In addition, the analysis classified the modelling and optimization techniques into classical, artificial intelligence and hybrid, and proposed a further division into economic and energy-based techniques.

Olatomiwa et al. [562] reviewed the system management strategies of various studies, dividing the techniques into three main types: linear programming, intelligent and software. Each of the techniques was analysed separately for stand-alone and grid-connected systems giving particular attention to the use of the Fuzzy Logic technique. The analysis exposed a dense collection of studies, describing in detail the configurations studied and the conclusions reached by each survey.

Goel and Sharma [563] presented a sample of studies on hybrid systems divided into four categories: stand-alone systems, grid-connected systems, systems used for rural electrification and charging of electric vehicles using renewable energy. The study highlighted the research results on hybrid systems (until 2017) and dedicated a short space for software optimization.

Sawle et al. [564] provided a detailed description of hybrid system components, modelling techniques, system control and optimisation and carried out a case study aimed at the system economic optimisation using HOMER and PSO.

Analogously, Anoune et al. [565] illustrated an extensive examination of sizing and optimization techniques for hybrid systems. The study classified the systems according to the type of DC/AC connection, illustrated the mathematical models of the system components and listed the main energy and economic indicators used for optimization. A description of different system sizing approaches was provided with the following categories: deterministic and stochastic techniques, software, algorithmic methods, approaches for multi-objective optimization, iterative, analytical, probabilistic and graphical construction approaches. In particular, similarly to several previous studies, the analysis highlighted the importance acquired by artificial intelligence techniques, which increasingly overshadow the traditional ones. However, they concluded that an optimal technique for all areas cannot be established, since the deficiencies of one technique are often compensated by the strengths of another.

Kartite and Cherkaoui [566] proposed a rather general review on hybrid systems, reporting their classification according to operating mode, components and system size, main optimization criteria and software used for this purpose. The analysis mentioned several studies related to system optimization through different methodologies (genetic algorithm, economic evaluation through HOMER, optimization through LPSP, etc.).

Nema et al. [567] presented the sizing process phase by phase, illustrating the pre-feasibility studies, the modelling of components, the system sizing and optimization and the tools for control and management of energy flows in the system, reviewing many studies dealing with these topics. The analysis carried out in 2009 concluded by predicting the system cost reduction considering the increase in the cost of conventional energy, and the diffusion of artificial intelligence techniques to optimize energy management operations.

Mahesh and Sandhu [568] carry out a very detailed review on various aspects of hybrid systems: optimal sizing, component modelling, energy and economic analysis and optimization techniques (iterative techniques, graphic methods, stochastic approaches, artificial intelligence and software). The study also covered new review topics, such as the electrical components of the system, the performance evaluation of existing systems, the locations where the applications were carried out.

Chapter 1

**A literature review and statistical analysis of
PV-wind hybrid renewable system researches by considering
the most relevant 550 articles: an upgradable matrix literature database**

Faccio et al. [569] reviewed 100 articles concerning renewable hybrid systems, showing that the most frequent configurations are composed of PV and wind systems integrated. The study continues illustrating the main journals involved in the research, the energy, economic and environmental indicators most commonly used for sizing and optimization techniques, reported in various categories.

Instead, many other literature reviews treated renewable energy and hybrid systems in a general perspective and then focused on PV and wind hybrid systems.

Mohammed et al. [570] produced an explanatory study on hybrid systems in general, describing their advantages and illustrating the main energy, economic, environmental and socio-political factors that influence their development. The analysis indicated the main renewable energy sources most suitable to be part of a hybrid system (PV, wind, biomass, hydroelectric) and provided a brief overview of studies related to the sizing or optimization of various configurations of hybrid systems and the software used for this purpose.

Guo et al. [571] analysed the possibilities of integration of various renewable sources (biomass, PV, solar thermal, wind, geothermal), listing their main characteristics, advantages and disadvantages. A particular focus was done on the processes of hydrogen production, drying and energy multi-generation (heat and electricity) obtained through the simultaneous production of different renewable energy sources (solar-geothermal and others).

Upadhyay and Sharma [572] proposed a study on renewable hybrid systems, with a special focus on PV-wind systems. They illustrated the main energy, economic, socio-political and environmental indicators used for sizing, optimization techniques (graphic construction, iterative, analytical, probabilistic, artificial intelligence, hybrid) and the problems that this technology may entail.

Twaha and Ramli [573] proposed an in-depth review of optimization techniques for hybrid power generation systems, citing many studies dealing with PV-wind hybrid systems. In particular, optimization techniques are divided into two categories: mathematical methods (combiners, dynamic and numerical/analytical) and computer methods (linear programming, dynamic programming and metaheuristic methods with single and hybrid algorithms). The analysis further subdivides these techniques, treating them separately when used for stand-alone or grid-connected systems.

Liu et al. [574] carried out an analysis of forecasting models for the use of renewable energy installations (hybrid and non-hybrid) for isolated locations, analysing physical methods, statistical models, artificial intelligence techniques and software.

Many other studies focused on much more specific aspects. Fadaee and Radzi [575] reviewed the evolutionary algorithms for the multi-objective optimization (through the search for the Pareto Optimum) of stand-alone hybrid systems, reporting many studies using PSO and GA.

Neves et al. [576] proposed a comparative study of various analyses carried out on hybrid systems serving small communities on islands or in remote locations. The study provided both the starting data of the various articles (population, consumption, costs) and those resulting from the overall analysis (percentage of stand-alone/grid-connected systems, percentage of energy from renewable sources by location, etc.), being very exhaustive from a quantitative point of view.

Ismail et al. [577] presented an analysis of studies focusing on the dissipation or possible use of excess energy from hybrid systems and proposed a case study to demonstrate that the use of such energy can lead to a decrease in the cost of energy (COE).

Chapter 1   **A literature review and statistical analysis of**
PV-wind hybrid renewable system researches by considering
the most relevant 550 articles: an upgradable matrix literature database

Arul et al. [578] described the hybrid system configurations proposed in various studies, examining the wide range of wiring diagrams and components for energy conversion and system stabilisation under various use conditions.

Bahramara et al. [579] presented a sample of studies using HOMER software for the optimization of hybrid systems, with particular attention given to the energy cost resulting from the simulation for each study. The analysis described in detail the software architecture and the use possibilities and provided conclusions on the geographical distribution of software use, the simulated installed power ranges and the most common system modes.

Vivas et al. [580] performed a state of the art analysis of publications concerning the integration of hydrogen systems (electrolytic cells and fuel cells) with hybrid systems and other storage systems such as batteries. In particular, hybrid systems were classified according to the mode (stand-alone or grid-connected), the methods of integration of electrical components (DC/AC, AC/DC, hybrid connections) and the elements that compose the system considering the generation from a single energy source and single or hybrid storage system, generation from multiple energy sources and single or hybrid storage system). The analysis illustrated a large sample of studies that explore techno-economic criteria, optimization techniques and system management strategies, offering a remarkable point of reference for researchers who want to deepen the development of hydrogen technology, which is in a strong ascent phase.

Khan et al. [581] analysed the possibilities of using renewable energy systems to supply water desalination systems. In particular, configurations with PV systems only, wind systems only and PV-wind hybrid systems were explored. The analysis condensed many studies on this subject and briefly focused on optimization techniques using algorithm and software. Finally, the authors evaluated the solar and wind resources in Saudi Arabia for possible uses aimed at feeding desalination systems.

Eras-Almeida and Egido-Aguilera [582] developed a literature review of mini-grids integrated from renewable sources in the service of islands with no connection to the mainland and with a population between 10000 and 100000 inhabitants. By considering ten case studies, they analysed the potential of islands to host technologies for the exploitation of renewable energy, focused on their economic aspect, policies and business models to identify the key factors that favour or disadvantage the development of renewable energy.

Most of the reviews described the deal with sizing techniques and optimization of hybrid systems or a specific aspect of this topic.

All the reviews processed in this paper were published after 2008, in correspondence with the growing interest that this technology has aroused in the last decade.

This work aims to join many of the aspects found in the reviews illustrated, by analysing a sample of the most relevant 550 articles available in the literature, to provide a broad overview covering the most varied aspects on the subject of hybrid systems. The geographical and climatic distribution of the studies, the system configuration, operating mode and size, the intended uses, and the study methodologies (sizing techniques, analysis typology, software used) are examined and categorized to provide a qualitative-quantitative picture of the current state of research on hybrid systems.

The paper is organized in the following way. In Section 2, the matrix literature database built to summerize articles, indicators and algorithms used in the studies are illustrated. In Section 3, geographical mapping of the research is developed to establish the distribution of the localities where the installations are most tested. In Section 4, the system configurations and the types of auxiliary components used are analysed. In Section 5, a mapping of the most widespread intended uses is

Chapter 1   **A literature review and statistical analysis of**
PV-wind hybrid renewable system researches by considering
the most relevant 550 articles: an upgradable matrix literature database

carried out. In Section 6, the types and methods of investigation are analysed. In Section 7, a combined analysis of the previous aspects is illustrated. In Section 8, the system component sizes considered in the research selected are elaborated to perform a statistical distribution analysis. Finally, the conclusions of the analysis are described in Section 9.

2. Creation of the article database

This review provides an analysis of 550 relevant articles [1-550] published from 1995 to 2020, selected from ScienceDirect [583] and Scopus [584] platforms. Articles were reviewed to verify the pertinency with the researched topic, excluding those not relevant. Data were extrapolated and reported in a matrix built-in Microsoft Excel, available as supplementary data file "Literature matrix database.xls". The construction of the matrix database has required one year in the period January - December 2019 and citations reported are related to this period. Figure 1 illustrates the ensembles of columns filled for each article to build the upgradable matrix database developed for the literature review and statistical analysis.
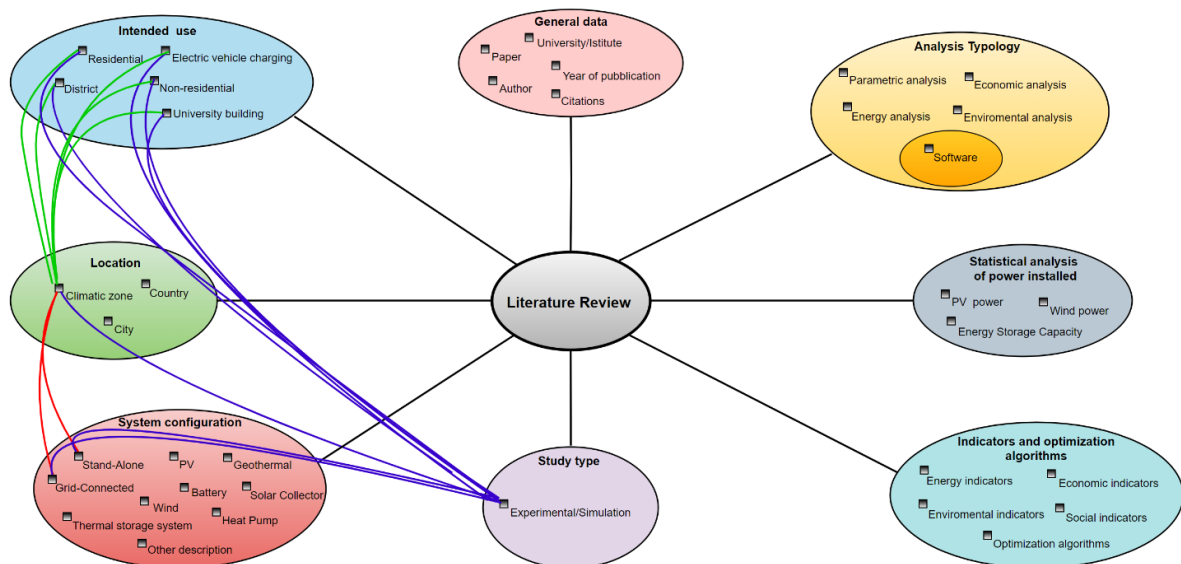
Figure 1. Schematic view of the upgradable matrix database developed for the literature review and statistical analysis.

The 550 articles were read, analysed, compared, and contracted to obtain and discuss findings on the topic. Then, they were classified into different categories for a better understanding of readers. The objective is to clearly and appropriately show important trends and findings in the development of hybrid wind and solar PV experimental, simulation and optimisation projects. Overall, the matrix database is constituted of the following ensembles each composed of different items/columns: general data, location, study type, system configuration, intended use, analysis typology, indicators and optimization algorithm and statistical analysis of the power installed. Each column of these ensembles was filled by taking data when declared from articles. The matrix was employed to statistically analyse singularly each item/column and to perform a combined analysis interweaving different ensembles.

Chapter 1

A literature review and statistical analysis of
PV-wind hybrid renewable system researches by considering
the most relevant 550 articles: an upgradable matrix literature database

2.1 General data

This item contains general information regarding:
- **Paper**: title of the article;
- **Author**: author/authors of the article;
- **University/Institute**: university and/or institution involved in the study;
- **Year of publication:** year in which the article was accepted and appeared in the ScienceDirect or Scopus platforms;
- **Journal**: scientific international journal on which the article is published;
- **Citations**: number of citations received by other articles after the article publication.

2.2 Location

This item regards the location in which the hybrid system was investigated:
- **Country:** country where the system was installed or simulated;
- **City:** city where the system was installed or simulated;
- **Climate Zone (Köppen classification):** climate zone of the city considered in the paper according to the Köppen-Geiger classification [585, 586].

2.3 Study Type

Each article was classified according to the study type, experimental (analysis of existing systems) investigation or simulation investigation with the help of software or algorithms. A study may contain both study types. For the item *"Experimental/Simulation"* four possible combinations are associated:
- **Yes/Yes:** articles with experimental and simulation analysis of the hybrid system;
- **Yes/No:** articles with only experimental analysis;
- **No/Yes:** articles with only simulation analysis;
- **No/No:** articles in which neither experimental nor simulation analysis was performed.

2.4 System Configuration

This item collects information about all the auxiliary components integrated with the PV-wind hybrid system:
- **PV**;
- **Wind**;
- **Battery**;
- **Thermal Storage systems**;
- **Heat Pump**;
- **Geothermal**;
- **Solar Collector**;
- **Other/Description** additional components not covered by the above items (diesel generator, hydroelectric turbines, hydrogen storage systems, etc.).

In addition, this item aims to specify if a connection with the grid is considered:
- **Stand-Alone:** systems that are autonomous from the electricity grid;
- **Grid-Connected:** systems connected to the electricity grid.

Chapter 1   **A literature review and statistical analysis of**
PV-wind hybrid renewable system researches by considering
the most relevant 550 articles: an upgradable matrix literature database

2.5 Intended Use

These items group the most common uses that are covered by the hybrid system:

- **Residential:** isolated houses, condominiums, etc.;
- **District:** villages or urban agglomerations with the presence of non-residential building such as hospitals, schools, shopping centres;
- **University building:** it includes a great variety of uses, such as residential (student housing), non-residential (offices, university classrooms, laboratories), district (entire university campuses) or experimental prototypes. Many articles analysed both residential and non-residential buildings within campuses;
- **Non- Residential:** offices, hospitals, shopping centres, industries;
- **Electric Vehicle Charging:** charging systems for electric vehicles.

In the same article, it is also possible to find different uses for the same system configuration or different system configurations intended for different uses.

2.6 Analysis typology

This item specifies which analysis typology was performed, such as:

- **Parametric Analysis** includes all articles in which the system sizing was carried out through parametric analyses, in economic, energy, environmental, social and/or environmental terms.
- **Energy Analysis** indicates the articles in which the analysis was developed using indicators that represent the system energy reliability and efficiency.
- **Economic Analysis** pointed out the article in which the analysis of the hybrid system is based on cost, revenue and profitability indicators.
- **Environmental Analysis** groups all the articles in which the emission savings and environmental impacts due to the use of the hybrid system are analysed.

In addition, the software used was memorized in the matrix database when a simulation analysis is foreseen.

2.7 Indicators and optimization algorithms

For each article, the optimization algorithm and the indicator used for the energy, economic, environmental or social analysis were extracted. For each optimization algorithms and energy, economic, environmental and social indicators, identified among the 550 articles considered, the upgradable matrix database presents a list of articles that have used it. The definition and description of algorithms and indicators selected are made available with this review in the file *"Supplementary material.docx"*.

2.7.1. Energy indicators

The system energy reliability represents the ability to ensure an adequate supply of electricity to loads. Therefore, the reliability analysis of the energy produced represents an essential step in the dimensioning of hybrid systems. Energy reliability indicators express numerically various factors such as energy production and capacity of system components, load characteristics and relative uncertainty, and operating conditions. They are used to assess system performance in relation to minimum reliability requirements. Among the most important are LPSP (Loss of Power Supply

Chapter 1

A literature review and statistical analysis of PV-wind hybrid renewable system researches by considering the most relevant 550 articles: an upgradable matrix literature database

Probability), indicating the probability that the hybrid system will not be able to meet the energy demand, and RF (Renewable Fraction), representing the fraction of energy supplied to the load from renewable sources.

2.7.2. Economic indicators

The economic sustainability is analysed considering the corresponding investment feasibility. The main costs affecting the system are the initial investment, operation and maintenance costs, as well as the cost of electricity production and the cost of replacing the various components of the system once their useful life is over. The economic analysis takes also into account the incentive and financing mechanisms and the discount rate. Among the most frequent economic indicators used to analyse the economic performance of a hybrid system found in the analysed article sample, there are the Net Present Cost (NPC) and the Cost Of Energy (COE).

2.7.3. Environmental indicators

The environmental analysis considers the possible system impacts of the hybrid system on the environment, intending to define measures for the reduction of emissions. The use of these indicators can be considered as less frequent than energy and economic analysis. However, many indicators are available with the amount of CO_2 emissions (E) the most important.

2.7.4. Social indicators

The social indicators quantify the negative and positive impacts due to the presence of renewable systems on human health related to the emission of substances harmful and human social well-being related to the creation of availability of new jobs. This type of analysis is infrequent with few indicators found in the literature.

2.7.5. Optimization algorithms

The articles analysed proposed different algorithms of optimization, sizing and control to improve the performance of hybrid systems, the algorithms most commonly found are PSO (Particle Swarm Optimization) and GA (Genetic Algorithm).

2.7.6. Probability density distribution of photovoltaic and wind power and battery capacity

In papers with parametric analysis, the maximum and minimum values of the nominal installed PV and wind power in kW and the storage battery capacity in kWh were extracted. When a parametric analysis is not performed, both minimum and maximum values of wind and PV powers and battery capacities were set equal to those of the sole analysed hybrid system. When the PV power is not directly available and the PV system area is available, a peak power factor of 0.15 kW/m2 was considered. Similarly, when the storage capacity is declared in terms of voltage in Volt and electric charge in Ampere-hour, the storage capacity in kWh is calculated by their multiplication (i.e. considering a 24 V & 150 Ah battery, the capacity calculated is 3.6 kWh). The objective of this extrapolation is the determination of the probability density distribution of PV and wind power installed and battery capacity in the parametric analysis. In addition, the analysis foresees the subdivision of the overall distribution in those related to the stand-alone and grid-connected systems and the residential and non-residential uses.

Chapter 1   **A literature review and statistical analysis of**
PV-wind hybrid renewable system researches by considering
the most relevant 550 articles: an upgradable matrix literature database

3. Geographical distribution of articles

3.1 Countries and locations

The hybrid system performance and diffusion strongly depend on climatic conditions worldwide [587]. In many articles, the location where the hybrid system was placed is declared, which does not necessarily coincide with the location where the study was developed. In some articles, data with which the simulation or experimentation were carried out derive from experimental measurements taken from stations located in the national borders. In particular, the data from the 550 article samples showed that:

-    452 articles (82.2% of the sample) declare the country where the hybrid system was located.
-    Among these, 16 articles (2.9%) stated that the hybrid system was located in more than one country.
-    Among the 436 articles reporting only one country, 43 (7.8%) considered different cities.
-    Among the 16 articles that considered more than one country, 3 articles selected more than one location in at least one of the reported countries.
-    98 articles do not declare the country where the hybrid system was investigated.

In the figure, only the countries and localities with the most occurrences are reported in histogram form. As can be seen, Asian countries (in particular Iran, India and China) are more productive than the others, confirming that in these countries there is a tendency to research within their national borders. Also, in global terms, looking at the occurrences of the continents in the publications, Asia is the place where the most studies are carried out, almost balancing the number of publications made in all the other continents. Research in Africa and Europe is widely frequent, while in Oceania this research sector is still at an early stage. The research highlighted the presence of 462 locations where the analyses were carried out; some locations are more present than others given their particular climatic importance or because they host important research sites.

Iran cities are present four times in the ranking, for a total of 31 publications produced. Spain and Italy are the leading European countries, confirming Europe's fair incisiveness in this sector. Algeria is the only African country detected in the top rank, with a total of 14 occurrences.

Chapter 1   **A literature review and statistical analysis of**
PV-wind hybrid renewable system researches by considering
the most relevant 550 articles: an upgradable matrix literature database
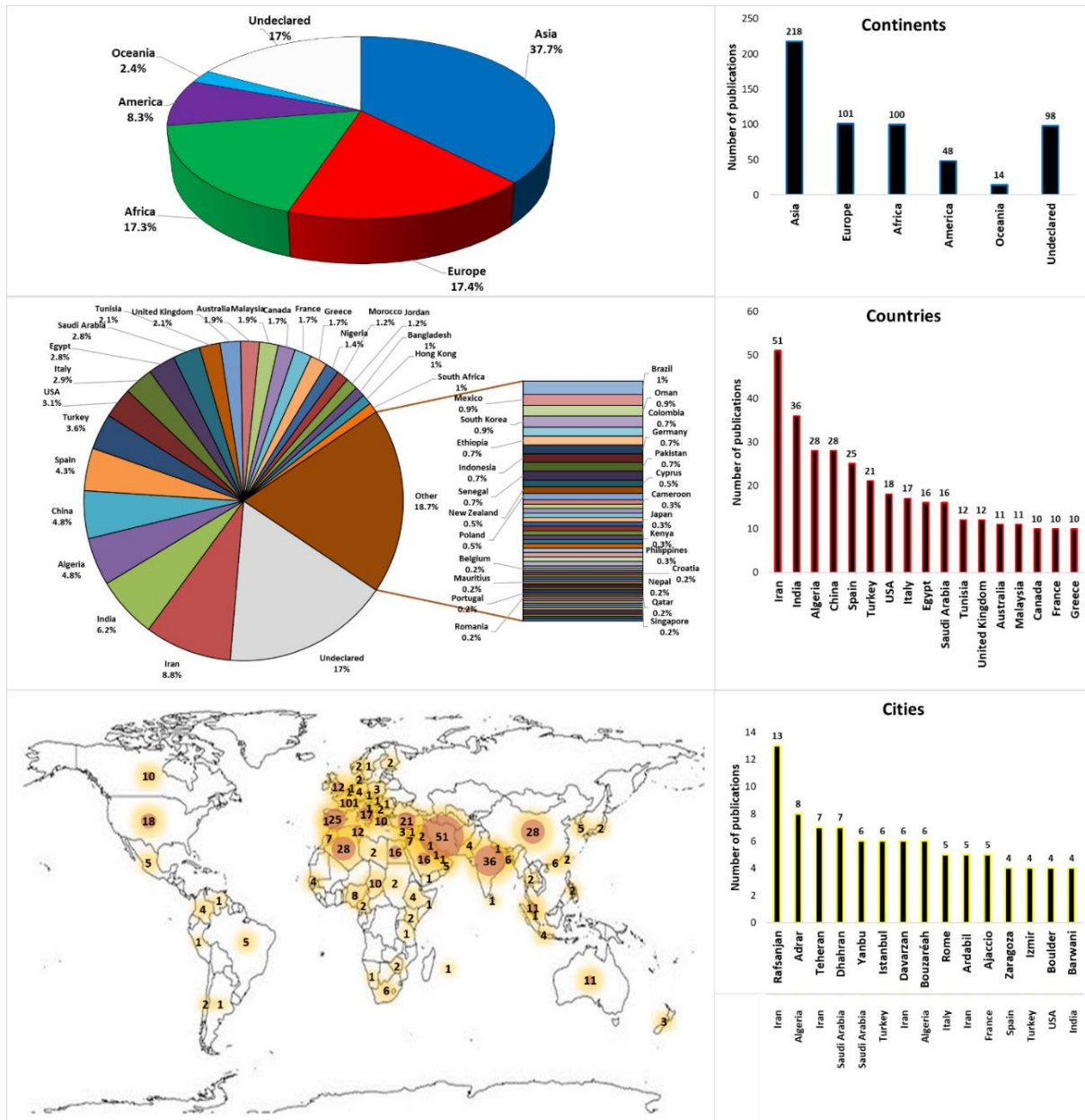
Figure 2. Geographical distribution map and number of articles by continent, country and location.

3.2 Koppen climate groups

Each location considered in the article sample was grouped using the Köppen classification [586]. The locations considered fall within the first four main groups of the overall five groups (A, B, C, D and E) and 20 different climate subgroups of the overall 30 sub-groups. The 20 climate subgroups found are:

- Group A: Af (tropical rainforest climate), Am (tropical monsoon climate) and Aw (tropical wet savanna climate);
- Group B: BSh (hot semi-arid (steppe) climate), BSk (cold semi-arid (steppe) climate), BWh (hot desert climate), BWk (cold desert climate);
- Group C: Cfa (humid subtropical climate), Cfb (temperate oceanic climate), Cfc (sub-polar oceanic climate), Csa (hot-summer Mediterranean climate), Csb (Warm-summer climate), Cwa

Chapter 1

**A literature review and statistical analysis of
PV-wind hybrid renewable system researches by considering
the most relevant 550 articles: an upgradable matrix literature database**

(monsoon-influenced humid subtropical climate) and Cwb (subtropical highland climate or temperature oceanic climate with dry winters);

- Group D: Dfa (hot-summer humid continental climates), Dfb (warm-summer humid continental climate), Dfc (subarctic climate), Dsa (hot, dry-summer continental climate), Dsb (warm, dry-summer continental climate), Dwa (monsoon-influenced hot-summer humid continental climate) and Dwb (Monsoon-influenced warm-summer humid continental climate).

The words "undeclared" indicates that the climate classification for a given location could not be traced, because it is too remote to be mapped or it is located on a boundary zone between several climate zones or concerns publications that declare only the country. Figure 3 shows the distribution of the sample locations in the climate zones and the number of occurrences of each climatic zone.
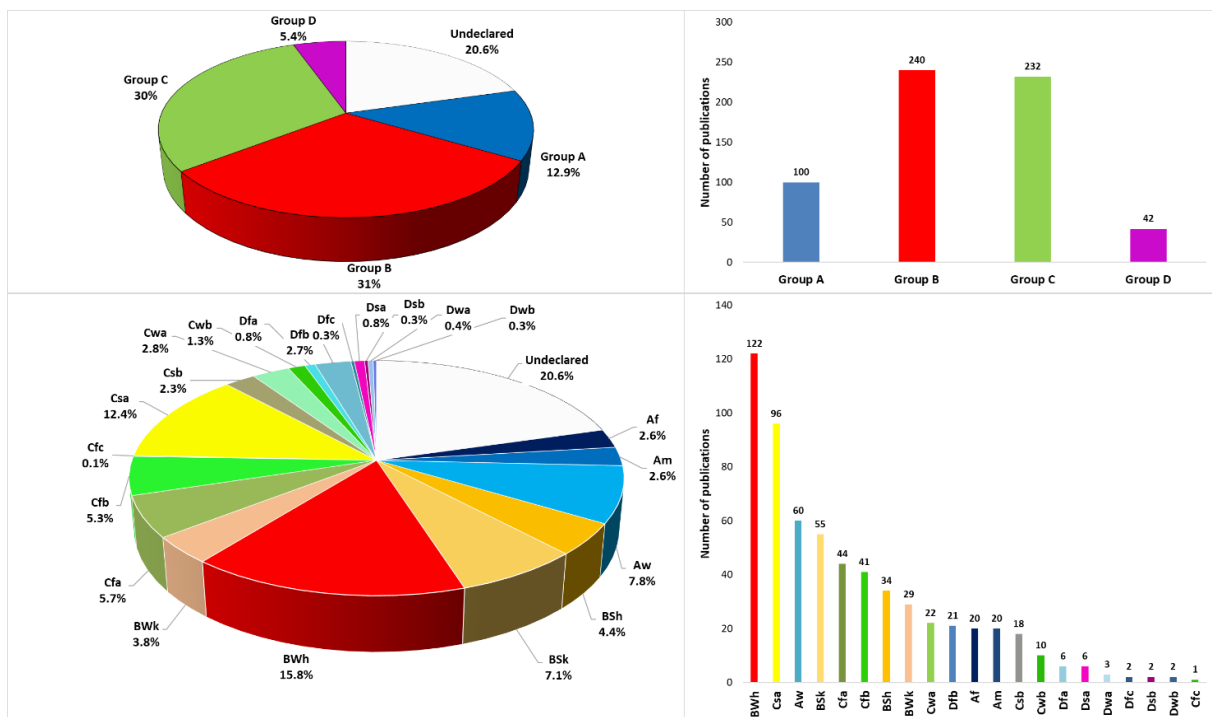
Figure 3. Number of publications in each climate subgroup according to the Koppen climate classification.

As can be seen from the graphs, the hot desert climate (BWh) is the most frequent within the papers analysed. This is certainly due to the strong presence of the countries of Saharan Africa (Algeria, Tunisia, Egypt, Libya, Morocco), the Arabian Peninsula (Saudi Arabia, United Arab Emirates, Oman, Yemen) and Middle East Asia, whose countries fall in many climatic zones (Iran, Iraq). The trend of research of these countries is to focus on the PV component, to exploit the solar resource that is naturally present on the national territories in large quantities. Each main climate group has a subgroup that stands out for the number of presences (BWh, Aw, Csa). For group B, other subgroups are strongly present compared to the other groups since they cover a large part of the territories where the investigations were carried out (Africa, Middle East, part of Asia overlooking the Indian Ocean on the Middle Eastside and a good part of the Chinese national territory).

As regards group A, it is evident that the typical climate of the savanna (Aw) is prevalent. It is present in most of the Brazilian national territory (the remaining part of which falls in the other climates of group A), in the Central African belt (Nigeria, Cameroon, part of Chad and part of Ethiopia) and the territories of the Indian Ocean, namely the Indochinese side, i.e. part of India and Malaysia, which is

Chapter 1   **A literature review and statistical analysis of
PV-wind hybrid renewable system researches by considering
the most relevant 550 articles: an upgradable matrix literature database**

the most recurrent country in the area of the Indonesian archipelago. These territories are strongly windy, so they are ideal locations for the installation and study of hybrid systems, with particular attention to the wind component.

Within Group C, the hot-summer Mediterranean climate (Csa) is the prevalent subgroup climate. It is less frequent compared to the other subgroups of other main groups; however, it represents the important Mediterranean area of Italian islands and peninsular, French coast, Spain, Portugal, most of the Greek territory, northern Algeria and Morocco, the coast of Turkey, Cyprus and the Arab territories overlooking the Mediterranean. The Csa climate zone is less widespread than Bwh but more distributed in the sample territories.

The other subgroups are less frequent in percentage but widely spread, such as the rest of Europe, the Australian coast, the Atlantic part of the United States, a good part of the Chinese territory and numerous areas of Africa and Central-Southern South America.

Group D and Group C highlight the majority of climatic subgroups (7 in total), but with a substantial difference in percentage. The D climatic subgroups are generally cold or humid territories − northern Canada, the United States in the Rocky Mountains area, Siberian Russia, parts of Iran and a relevant part of Turkish territory − not suitable for the exploitation of the solar source.

Table 2 shows the most recurrent country for each climate subgroup.

Table 2. Countries with the most occurrences per climate zone.

Climatic group	Country	Occurrences
Af	Malaysia	11
Am	Nigeria	7
Aw	India	23
BSh	India/Chad	6
BSk	Iran	33
BWh	Saudi Arabia	29
BWk	Iran	26
Cfa	China	20
Cfb	United Kingdom	9
Cfc	Australia	1
Csa	Italy/Turkey	16
Csb	France	7
Cwa	India	11
Cwb	India	5
Dfa	South Korea	3
Dfb	Sweden	10
Dfc	Canada	2
Dsa	Iran	6
Dsb	Iran	2
Dwa	China	2
Dwb	China	2

The wide coverage of group B is confirmed, considering that with four subgroups it outnumbers the articles in group C, despite this latter is present with seven subgroups. The analysis points out that research on hybrid systems is more concentrated in locations with arid or temperate climates since they offer better exploitation of a renewable source like the solar one. India, China and Iran appear four times in the table, confirming that in these countries hybrid systems are studied under different climatic conditions.

Chapter 1   **A literature review and statistical analysis of**
PV-wind hybrid renewable system researches by considering
the most relevant 550 articles: an upgradable matrix literature database

4. System configurations, auxiliary components and system modes

4.1 System configurations and auxiliary components

Numerous articles investigated the energy efficiency and/or economic profitability of the hybrid system compared to non-hybrid configurations. 55 articles developed a comparative or sizing analysis of hybrid systems considering also non-hybrid configurations, i.e. only PV and/or only wind systems (with or without auxiliary components). For the 100% of articles selected, hybrid systems with at least both wind and PV components were considered.

The auxiliary components were divided into the following two macro-categories:

- ✓ Auxiliary energy generation systems: components that generate the missing electrical energy to be sent to the load in case of failure of renewable sources or other generation systems coupled to the electrical one to create cogeneration, trigeneration or multigeneration system (electricity, heat, cold, hydrogen and so on).
- ✓ Energy storage systems: to store excess energy from renewable sources via electrical, thermal, hydrogen or other storage systems.

The survey showed that:

- The battery is the most widely used storage system. A total of 401 articles (73%) describe a system equipped with a battery and 16 of these carried out a comparative study between a hybrid system equipped with a battery and the same hybrid system equipped with other auxiliary components. In 228 articles, the battery is coupled with another auxiliary component and in 4 of these cases with a different storage system;
- In 321 articles (58.6%), the hybrid system is equipped with another auxiliary component and in 103 articles more than one auxiliary component is used;
- The diesel generator is the most widely used auxiliary generation system with 147 articles. For 139 times, it is coupled with a battery and 31 times with other components;
- Fuel cells, alone or in combination, are the most widely used auxiliary generation system after the diesel generator with 103 articles, of which 67 in combination with a battery;
- Hydrogen systems, which combine electrolyser cells, fuel cells and hydrogen tanks, are widely used with 79 articles and act both as excess energy storage systems to produce the hydrogen to be stored and auxiliary generation systems burning the hydrogen produced in the event of failure of renewable sources. In 45 articles, these systems are combined with batteries, 13 articles with diesel generators and 12 articles with other components.

Figure 4 shows the percentage occurrences of the main auxiliary components in the article sample. To give a more complete idea, the same analysis was carried out, individually, for auxiliary generation systems and storage systems.

Chapter 1   **A literature review and statistical analysis of**
PV-wind hybrid renewable system researches by considering
the most relevant 550 articles: an upgradable matrix literature database
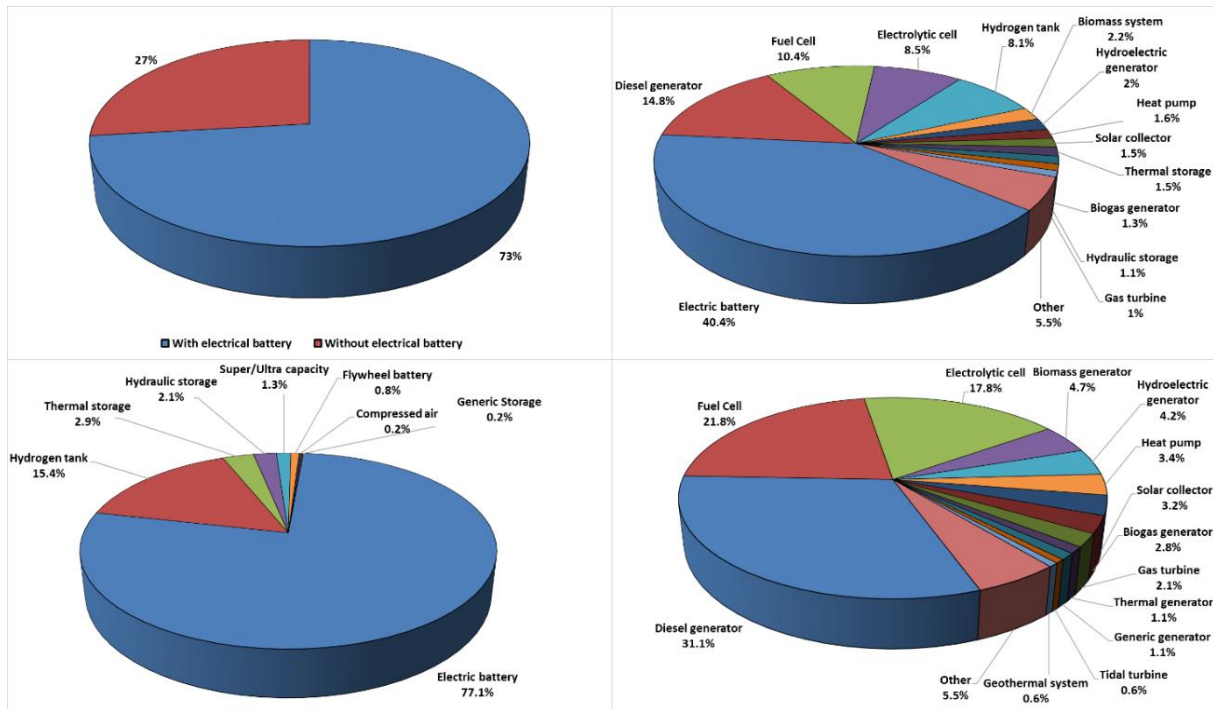
Figure 4. Percentage of occurrence of electric battery presence, auxiliary components, auxiliary generation systems, and storage systems.

As regards the generation systems, it is evident a massive use of the diesel generator, which can guarantee great reliability despite it is characterized by high values of emissions and consumption., Fuel cells occupy the second position, used alone or in combination with electrolytic cells to compose the hydrogen systems. The use of such systems is constantly increasing, as shown by the growing number of couplings made with hybrid systems over the years (see Figure 5).

The battery is the most widely used storage system. Of great importance are also the hydrogen tanks, used in combination with electrolytic cells and fuel cells to form the hydrogen systems. With lower frequency, but no less important are alternative storage systems such as thermal and hydraulic storage.
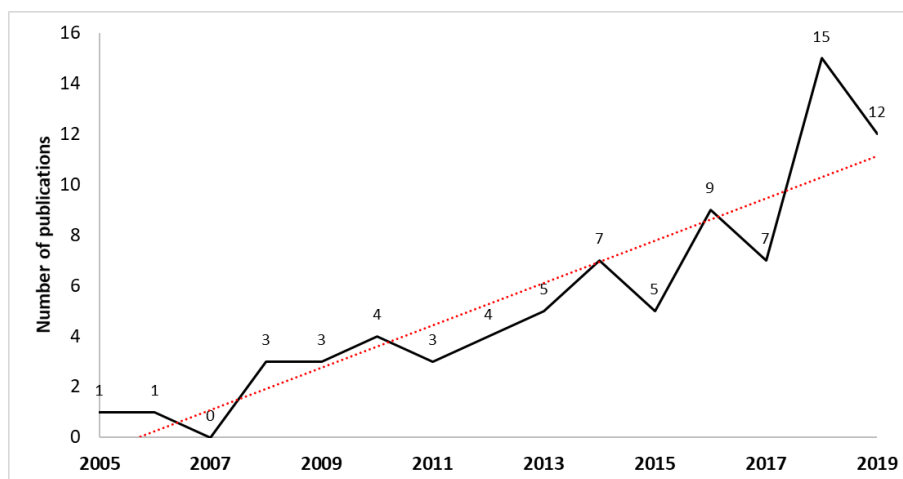
Figure 5. Time trend of publications related to hybrid systems coupled to hydrogen systems.

Chapter 1   **A literature review and statistical analysis of**
PV-wind hybrid renewable system researches by considering
the most relevant 550 articles: an upgradable matrix literature database

4.2 System installation mode

The installation mode is an important system feature, as it characterizes the final uses. The investigation has shown that:

- 319 articles focus on stand-alone systems;
- 168 articles focus on grid-connected systems;
- 18 articles focus on both stand-alone and grid-connected systems to perform a comparison or equip the system with various auxiliary components;
- 47 articles do not state the system mode;
- 2 articles describe different hybrid systems that are located in several localities with or without a connection to the grid.

Figure 6 highlights the distribution of articles in relation to the system installation mode.
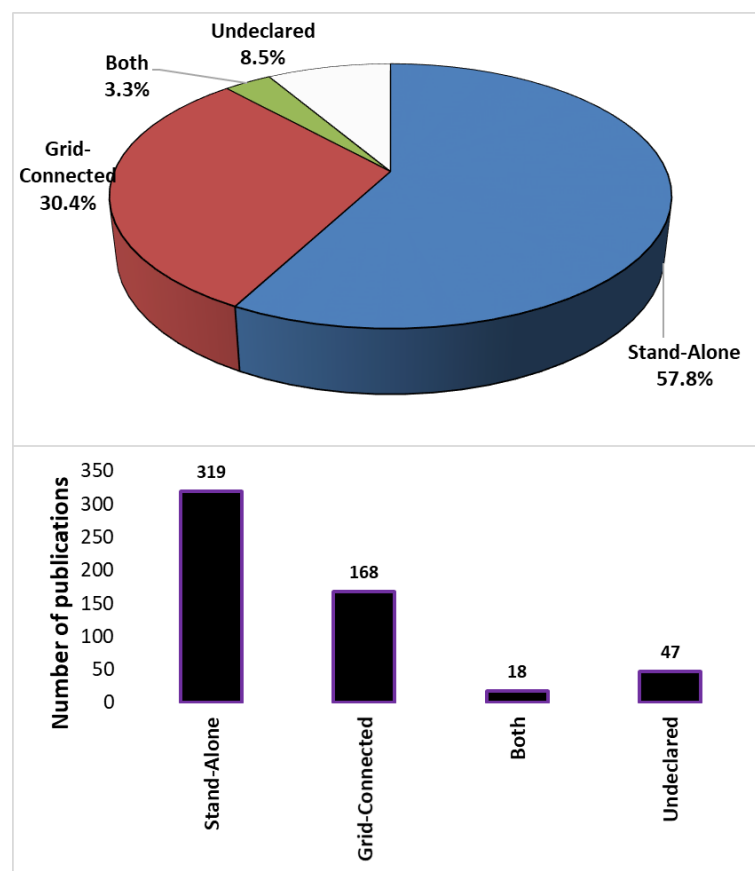
Figure 6. *Percentage of occurrence and occurrences of the installation modes.*

Research tends to be focused especially on stand-alone systems, satisfying isolated users and ensuring greater autonomy from the national electricity grid. Grid-connected system investigations account for about half of the stand-alone system applications. It is clear that the hybrid system sector is still growing and that it is not yet possible to avoid the support of an auxiliary source such as the national grid or an additional component.

Chapter 1   **A literature review and statistical analysis of**
PV-wind hybrid renewable system researches by considering
the most relevant 550 articles: an upgradable matrix literature database

5. Intended uses

The intended use represents the load type to be fed by the hybrid system. In the analysed articles, the use is prevalently declared, especially for research focused on sizing and optimization problems. The survey showed that:

- 405 articles (73.9%) declare a specific or generic use;
- 29 of these articles declare a generic load or unspecified intended use;
- 31 articles declare a mixed-use, i.e. for several intended uses at the same time, e.g. residential and non-residential;
- 6 articles compare the same hybrid system for different intended uses not simultaneously analysed.

Figure 7 shows the occurrences of the different intended uses and mixed users.
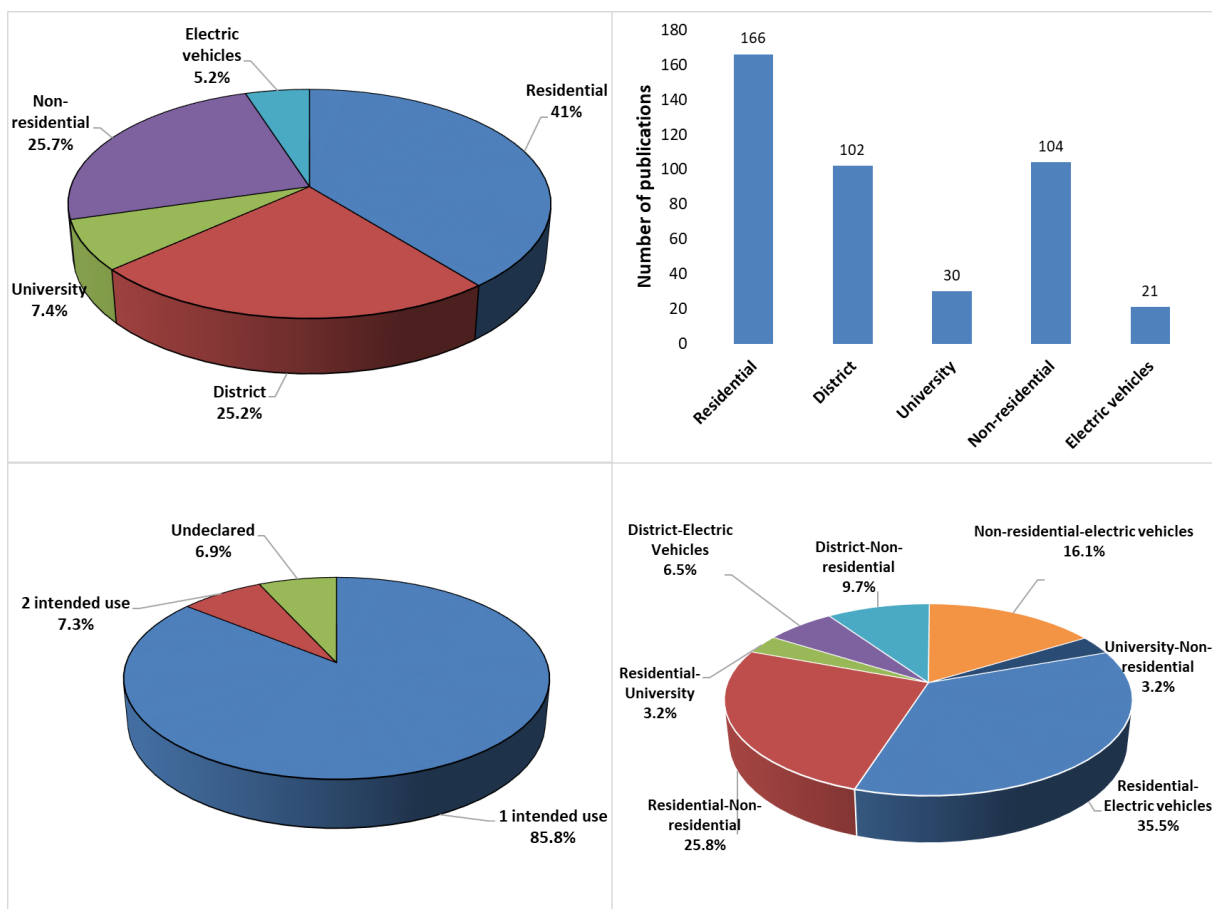
Figure 7. *Percentage of intended use types, intended use type occurrences, percentage of the number of uses and percentage of mixed users.*

The most frequent use is the residential one, followed by the non-residential and district uses. The use of hybrid systems is mainly aimed at satisfying people's electrical energy demand. The non-residential uses represent mainly agricultural and industrial, and university uses.

The latter represent hybrid systems tested in university facilities or used to feed specific loads or those more strictly related to the university energy demand. In this way, the hybrid system is investigated and, at the same time, is used for the power supply of the university loads. In addition, the power supply of electric vehicles is becoming increasingly important. The tendency to use the same system

Chapter 1　　　　　　　　　　　**A literature review and statistical analysis of**
PV-wind hybrid renewable system researches by considering
the most relevant 550 articles: an upgradable matrix literature database

for several intended uses is still not very widespread. However, an embryonic increasing trend can also be noted in this type of "mixed" users.

In mixed users, residential use remains predominant compared to the others, while non-residential use is much higher than district use, in contrast with the not mixed-use, where non-residential and district uses had almost the same percentage. Of particular interest is the percentage of mixed uses with electric vehicle charging stations, especially in combination with residential use. This is probably due to the increasing diffusion of the so-called "smart home" market.

Overall, the research trend demonstrated a wide hybrid system employment to serve residential or neighbourhood loads to satisfy people well-being.

6. Study methodologies

6.1 Study types

Different study types were applied in the articles analysed, such as numerical simulations, experimentation carried out on real systems or both methods, comparing the data obtained by simulation with those obtained by experimentation or vice versa. All publications were classified as "Experimental/Simulation".

As shown in Figure 8, the statistical survey revealed the following results:

- 472 articles (85.7%) present a study in which only simulations were performed (No/Yes);
- 32 articles (5.8%) illustrate a purely experimental study (Yes/No);
- 46 articles (8.3%) present simulation calculations compared with experimental results (Yes/Yes);
- One publication presents a study without both simulation and experimental investigation (No/No);
- One publication presents several hybrid systems studied differently from a simulation and experimental point of view.

The results show that the general trend of the research is to develop numerical simulations for the study of hybrid systems. This is due to the lower execution time and tools required by the numerical simulation compared to experimental analyses, which involve problems in terms of costs and technical issues arising from the system installation and operation. The experimental investigations are much smaller than simulation ones, as demonstrated by the trend of the number of publications over the years (see Figure 9).

Chapter 1

A literature review and statistical analysis of
PV-wind hybrid renewable system researches by considering
the most relevant 550 articles: an upgradable matrix literature database
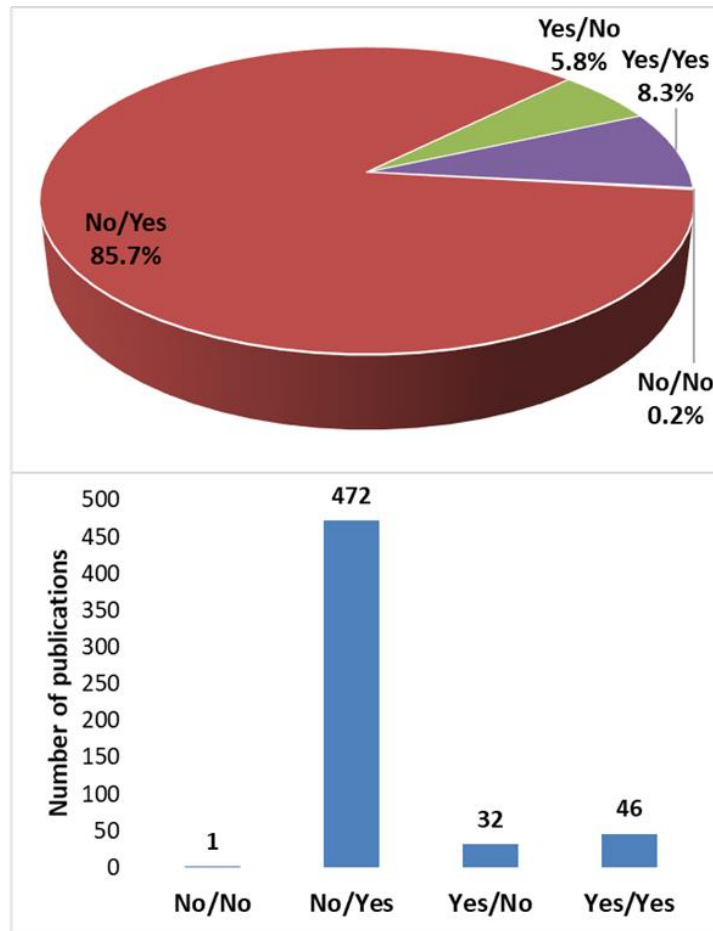
Figure 8. Occurrences and percentage of study categories.

The trend of experimental/simulated studies has been on the rise since 2005, with growth in the last decade and a peak in 2018 (the data for 2020 is partial). By considering articles with only experimental investigations a curious trend can be noted. In addition to the peak of 2018, the trend shows an irregular behaviour preserved until today by the number of articles.
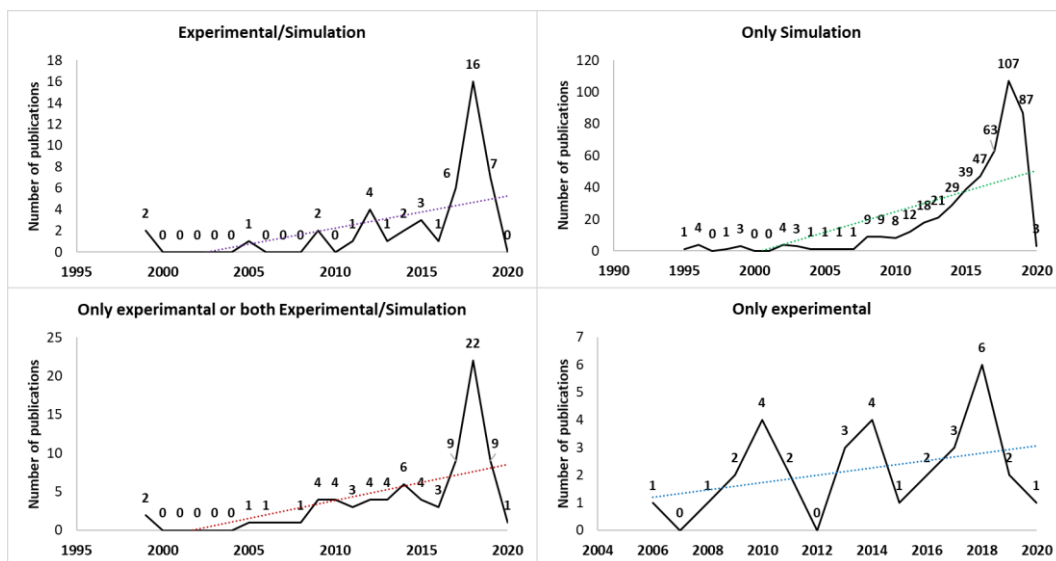
Figure 9. Trend in the years of publications in the presence and absence of experimental and simulation studies.

Chapter 1   **A literature review and statistical analysis of**
PV-wind hybrid renewable system researches by considering
the most relevant 550 articles: an upgradable matrix literature database

Despite the increasing availability of funds for researchers over the last decades, even today they prefer numerical simulations given the higher reliability of the prediction models available in this topic that provide results very close to the acquired experimental data.

The graph also shows that the combination of simulations and experimental investigations is becoming more popular than the only experimental investigation. For all categories, the trend line is increasing.

6.2 Analysis typology

All articles were classified according to the analysis typology in the following categories:
- Parametric analysis, aimed at optimizing parameters using algorithms for the sizing of hybrid systems.
- Non-parametric analysis, aimed at analysing the performance of a specific system, in economic, energy or environmental terms.

Both of these analysis typologies may be related to one or a combination of energy, economic, environmental analysis. The analysis highlighted the following results:
- 378 articles (68.7%) proposed a parametric analysis;
- 163 articles (29.6%) developed a non-parametric analysis;
- 9 articles (1.6%) produced other study types that cannot be placed in one of the previous categories;
- 404 articles declared the software used to carry out the study;
- 74 of these articles used more than one software.

Figure 10 shows the percentage distribution among the study types divided into parametric and non-parametric analyses, in turn, classified in the other categories.
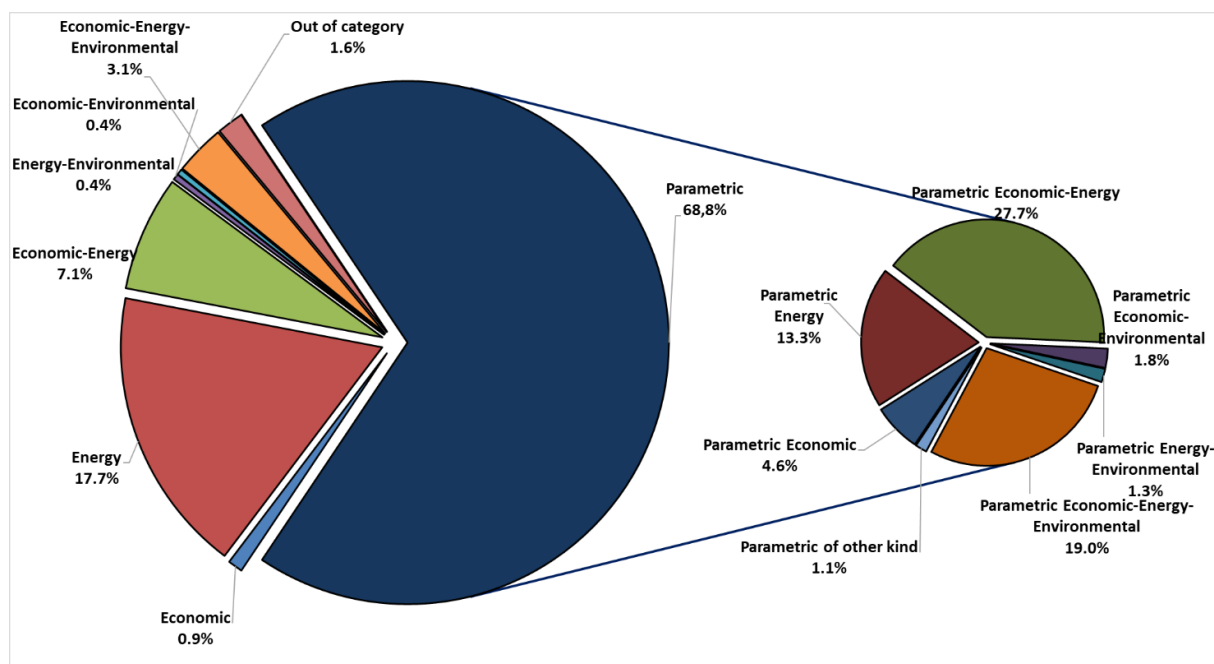
Figure 10. *Percentage distribution of analysis typologies.*

Most publications developed parametric analysis, focusing on optimal sizing, which is a very delicate phase and depends on a multitude of factors such as installation site, investment capital and availability of renewable resources. By isolating the parametric and non-parametric analyses of Figure 10, the percentage distributions of Figure 11 are obtained.
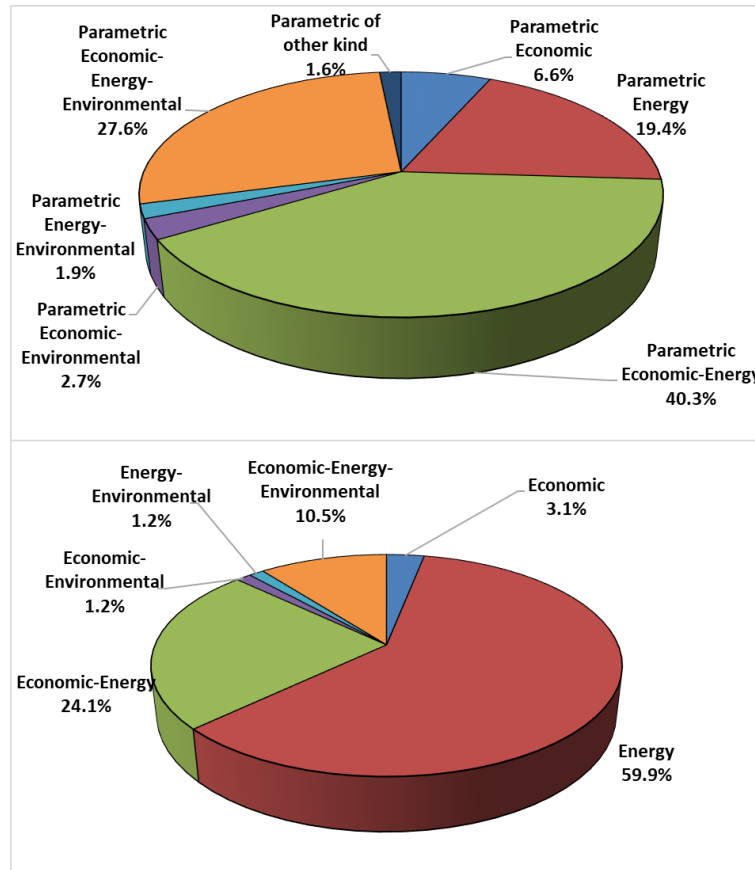
Figure 11. *Distribution of parametric and non-parametric studies.*

In parametric studies, the energy analyses are predominant, followed by the economic one. This means that the main type of optimization involves energy and economic objective functions, which have the greatest weight in the system installation and management. Purely environmental parametric analyses are absent. The environmental aspect is examined in a much smaller percentage and only in combination with one or more of the other analysis types.

By isolating the non-parametric analyses, similar evaluations can be made. The energy analyses are the most performed, especially not combined with other analysis types. This means that once the problem of sizing and investment capital has been overcome, it is necessary to monitor and analyse the systems to ensure acceptable energy reliability throughout their useful life. The economic analyses are in the second position in terms of occurrences; in this case, a greater detachment is observed since articles analysing the economic return of a specific system is rarer. The absence of purely environmental analyses is confirmed. The environmental analysis is usually coupled with the others and in a considerably smaller percentage than the others. The number of articles investigating harmful emission savings and relative environmental impact associated with hybrid systems is strangely limited compared to the other analysis types. This makes the hybrid system environmental analysis a research topic of less interest at least until now.

Chapter 1   **A literature review and statistical analysis of**
PV-wind hybrid renewable system researches by considering
the most relevant 550 articles: an upgradable matrix literature database

6.3 Software

The analysis revealed the use of different 58 software in the article sample. The same software with different versions was included in the same count. Figure 12 shows the distribution of software used overall, for parametric analyses and non-parametric analyses.
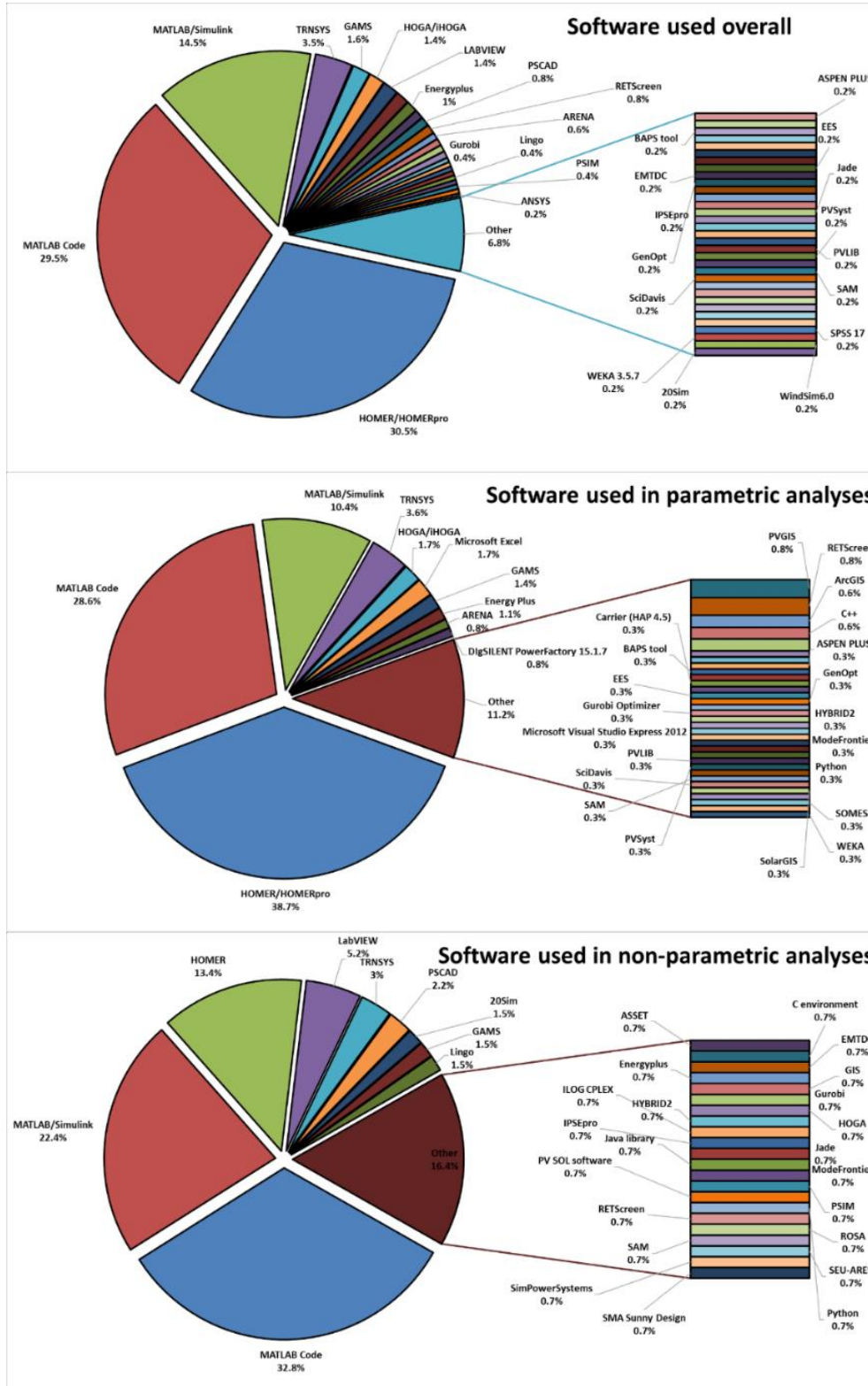
Figure 12. *Distribution of software used overall, for parametric analyses and non-parametric analyses.*

Chapter 1　　　　　　　　　　　　　　　**A literature review and statistical analysis of**
PV-wind hybrid renewable system researches by considering
the most relevant 550 articles: an upgradable matrix literature database

HOMER, MATLAB codes and Simulink toolbox software were used in almost 75% of the article sample. This result is not surprising, considering that HOMER is the software par excellence for the optimization of hybrid systems, while MATLAB has a considerable use versatility. In the top rank, TRNSYS (in different versions), HOGA (other software used for optimization) and GAMS occupy the successive positions.

Among the software for parametric analyses, the predominant presence of HOMER is highlighted, while MATLAB codes and Simulink toolbox retain their importance. This three software cover more than 75% of the occurrences. The following positions are still occupied by TRNSYS, HOGA and GAMS, confirming the trend already seen in the overall distribution. This means that parametric analyses have a greater influence on the general trend of the distribution. For non-parametric analyses, the software rank changes significantly.

The HOMER is less applied, while MATLAB codes and Simulink toolbox confirm its predominant position, assured by its great versatility. The other software appears in rather low percentages.

6.4 Indicators and optimization algorithms

For each publication, all the indicators used were collected, consisting of 80 energy indicators, 63 economic indicators, 18 environmental indicators and 4 social indicators. The full list and definition of all indicators can be found in the Supplementary file "Supplementary material.docx".

Furthermore, all the optimization algorithms used in the sample publications were reported (for a total of 164 algorithms). Figure 13 shows the occurrences and distribution of the indicators used in the article sample in the following order: energy indicators, economic indicators, environmental indicators, social indicators.

As regards the energy indicators, reliability is the most frequent system measure of the ability to meet the load using the LPSP, LPS, and LLP indicators. This confirms that the achievement of a reliable system is the priority objective of energy analysis. Other widespread indicators are the renewable fraction (RF), which determines the amount of energy produced from renewable sources, and the excess energy (EE), that can be stored or dissipated. The unserved load (UL) can be included among the indicators that provide a measure of energy reliability.

The two main relevant parameters in the economic analyses are the COE and NPC which represent, respectively, the cost of the energy and the cost of the system. In some articles, they are defined in other forms or under other names, such as LCOE and LCE for the cost of energy and TAC, LCC, NPV for the cost of the system. On the other hand, the indicators representing the economic return of the system are much less frequent. In the histogram in the figure, in descending order, the first of these parameters is Payback Time (PBT), which is the time needed to recover the project initial investment. Consequently, the main economic concern is that of the costs to be faced, which can represent an inhibiting element for research in the sector.

Although there are fewer environmental analyses, it is clear that existing studies are targeted towards emission analysis. In this context, the E parameter is the main and most used and most other parameters are related to the quantification of emissions, both carbon and other gases often expressed in terms of carbon equivalent.

It is difficult to make assumptions about social indicators, as the study on the impact that a hybrid system can have on people's well-being (in terms of health, employment, etc.) is very specific and

Chapter 1

**A literature review and statistical analysis of
PV-wind hybrid renewable system researches by considering
the most relevant 550 articles: an upgradable matrix literature database**

requires a considerable amount of information. Being only five articles of the sample analysed involved in this analysis type, nothing statistically significant emerges.
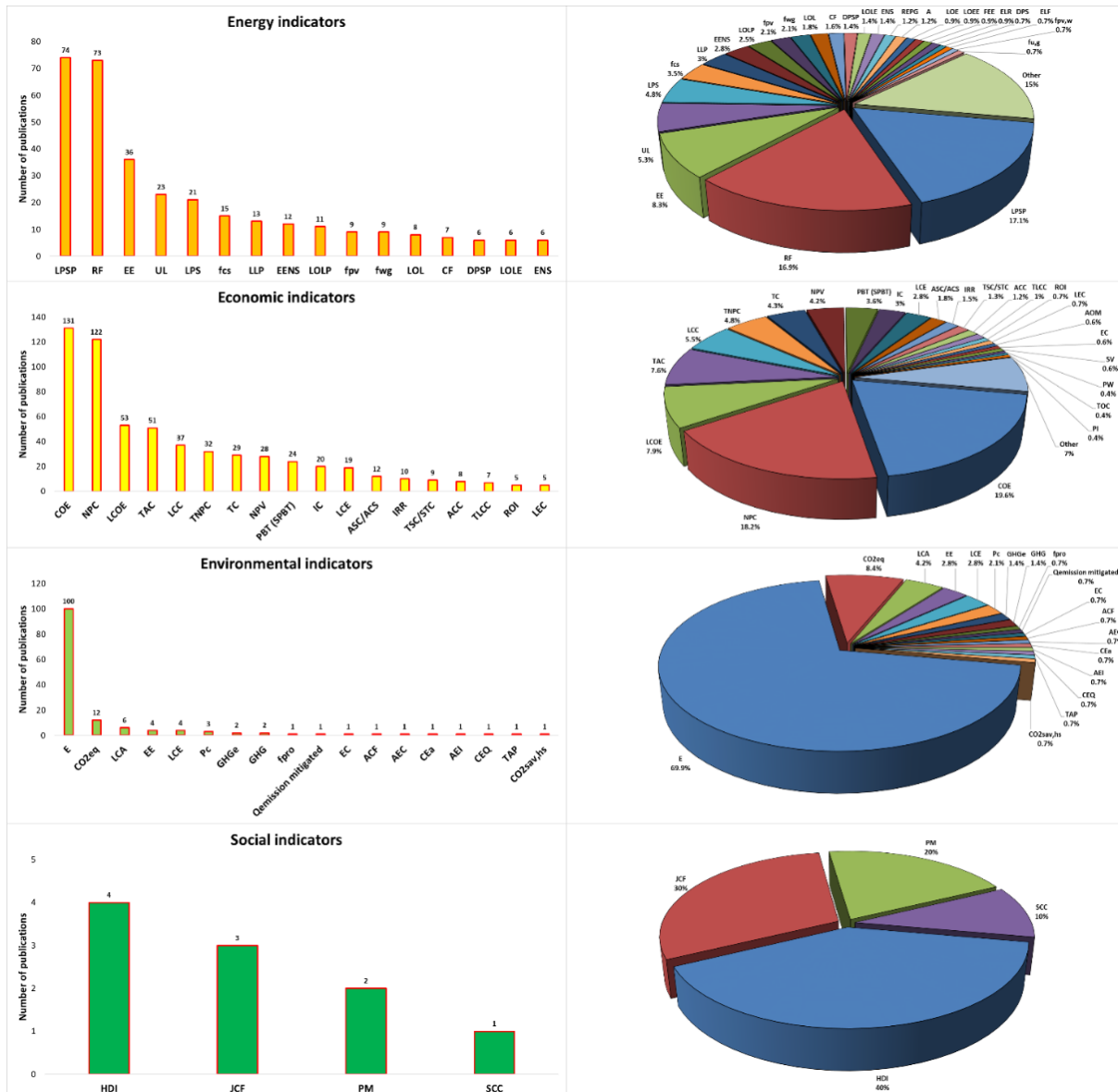
Figure 13. *Occurrences and distribution of energy, economic, environmental and social indicators.*

As shown in Figure 14, the number of algorithms used is very wide. Techniques that have at most four occurrences in the sample constitute more than 40% of the article sample. The survey showed that 53 articles seek optimality following the Pareto procedure. The most used algorithms are the Particle Swarm Optimization (PSO) and Genetic Algorithm (GA) in their basic version, while their improved or compounded versions with other algorithms are less frequent but considerably numerous. This highlights the great use versatility of these algorithms, which are predominant in research on hybrid systems. Also, the Fuzzy Logic (FL) technique and the SA (Simulated Annealing), HS (Harmony Search) and CS (Chaotic Search) algorithms were quite employed. These algorithms are often used for comparative studies to determine which is the best hybrid system configuration in term of installed component power.

Chapter 1

**A literature review and statistical analysis of
PV-wind hybrid renewable system researches by considering
the most relevant 550 articles: an upgradable matrix literature database**
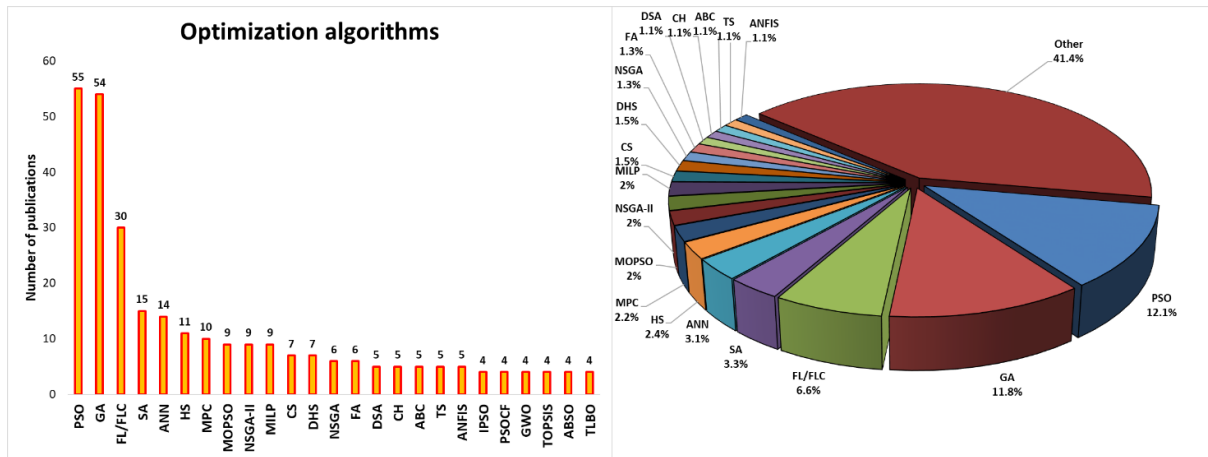
Figure 14. Occurrences and distribution of optimization algorithms.

7. Combined analysis

The items concerning each article were combined, refining the information in relation to climate zones, study types, system modes and intended uses. In particular, the data of different columns of the matrix database which appear to have a certain correlation in common were combined to obtain more detailed results.

7.1 Climate zones and study types

To obtain a deeper knowledge of the geographical distribution of the studies, data from various columns of the matrix were combined with the climate groups. To begin with, the distribution of the study types (experimental/simulation, only simulation and only experimental) in the various climate subgroups and the percentage of their presence in each subgroup were examined.
Figure 15 shows the distribution of the study types in climate zones.
The analysis showed that Iran holds the record as a country where more studies with simulation are carried out. Spain and India are the countries where, respectively, more investigations with experimentation and more with experimental/simulation analyses were carried out. However, this is a primacy statistically irrelevant given the low number of experimental investigations compared to the simulation ones. The only study with neither simulation nor experimentation comes from Singapore. As can be seen, the geographical distribution of research with the only simulation follows very closely the general distribution of studies (see Figure 3, left bottom). It is evident that a large number of simulation research strongly influences the general trend of geographical distribution. Specifically, a great variety of subgroups with a quite uniform distribution of occurrences can be observed. Group C is the most numerically tested climate zone, followed almost identically by Group B and A, and with very low articles, by Group D. Group BWh is the climate zone with the highest number of simulated hybrid systems.
As regards the distribution of only experimental investigations, there is a lower frequency in climate group B in favour of groups C and A, which is prevalent given to the European contributions. Only experimental investigations were not addressed in Group D, and in some subgroup zones of group B, where numerical simulations are preferred. The low frequency of the experimental study methodology makes the results less statistically significant.

**A literature review and statistical analysis of
PV-wind hybrid renewable system researches by considering
the most relevant 550 articles: an upgradable matrix literature database**
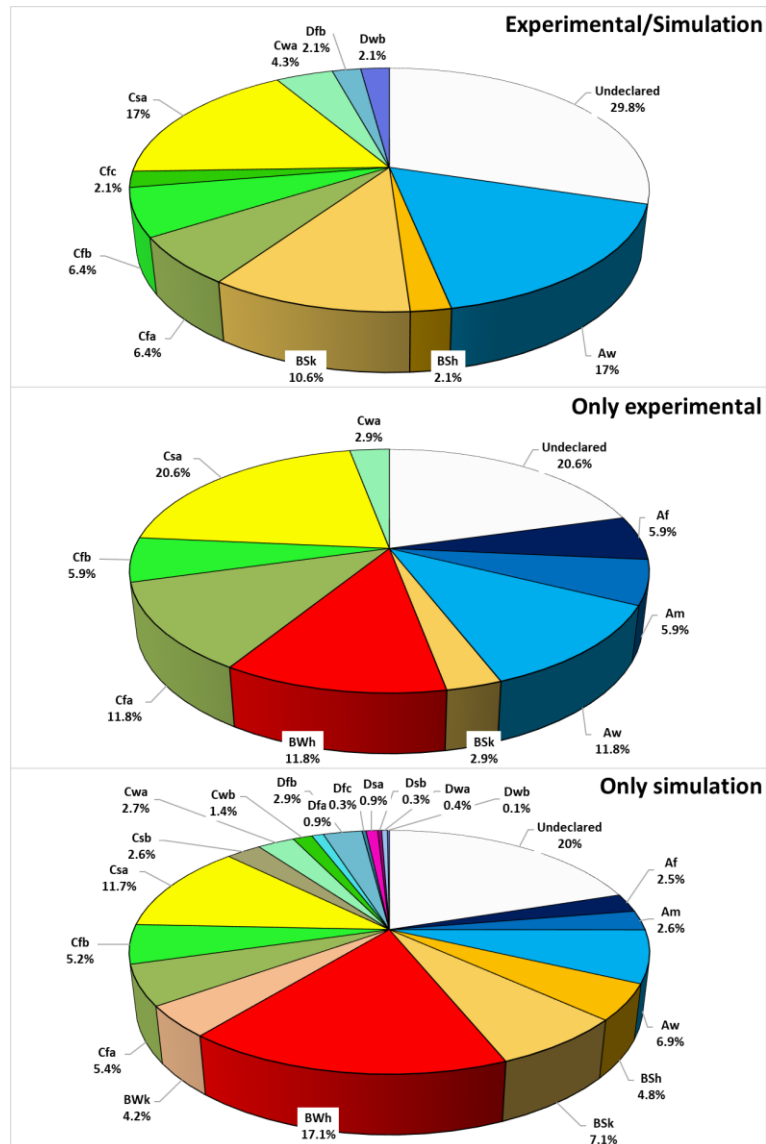
Figure 15. Distribution of the study types in climate zones.

Finally, similar considerations can be highlighted also for articles with experimental/simulation analyses: Group C prevails also in this case; Group B undergoes a further decrease compared to only experimental analyses, with the BWh subgroup, generally the most present, absent in the occurrences; group D shows some investigation of this type, even if with a low frequency; in the group A, only group Aw is present, which undergoes a considerable increase, becoming the most frequent subgroup. The distribution of the study types in each climate zone was investigated further.

In Group A, the tendency to use simulation is prevalent; Group Aw has the highest frequency in the sample and the highest number of countries. In Group B, simulations are even more used than in Group A, with group BWk characterized by 100% of the investigations carried out by simulation only. In Group C, the trend is more or less the same for all subgroups: the simulation analyses are over 80% in all the subgroups present; for the Csb and Cwb subgroups, 100% of the studies are simulations only; the only analysis belonging to the Cfc subgroup is experimental/simulation. The trend in simulation analysis is also confirmed in Group D wherein Dfa, Dfc, Dsa, Dsb Dwa, and Dwb subgroups 100% of the articles used simulation only.

Chapter 1   **A literature review and statistical analysis of**
PV-wind hybrid renewable system researches by considering
the most relevant 550 articles: an upgradable matrix literature database

In general, it can be concluded that for all climate zones, articles employing simulation are the most widespread, which indicates that worldwide research on hybrid systems prefer to analyse predicted results before concentrating more frequently on practical applications

7.2 Climate zones and planting modes

The geographical distribution in the climate zones and the frequency percentage for each climate zone of system installation modes were examined exactly as done for the study types. On one hand, the analysis has shown that Iran is the country where most studies on stand-alone installations were carried out and where the combination of stand-alone and grid-connected systems for the same installation is compared. India and Algeria follow Iran in rank with a great detachment. On the other hand, China is the country where the grid-connected systems are most studied, followed by Spain, India and Italy. Figure 16 illustrates the distribution of articles with stand-alone, grid-connected and both system modes in the different climatic zones.
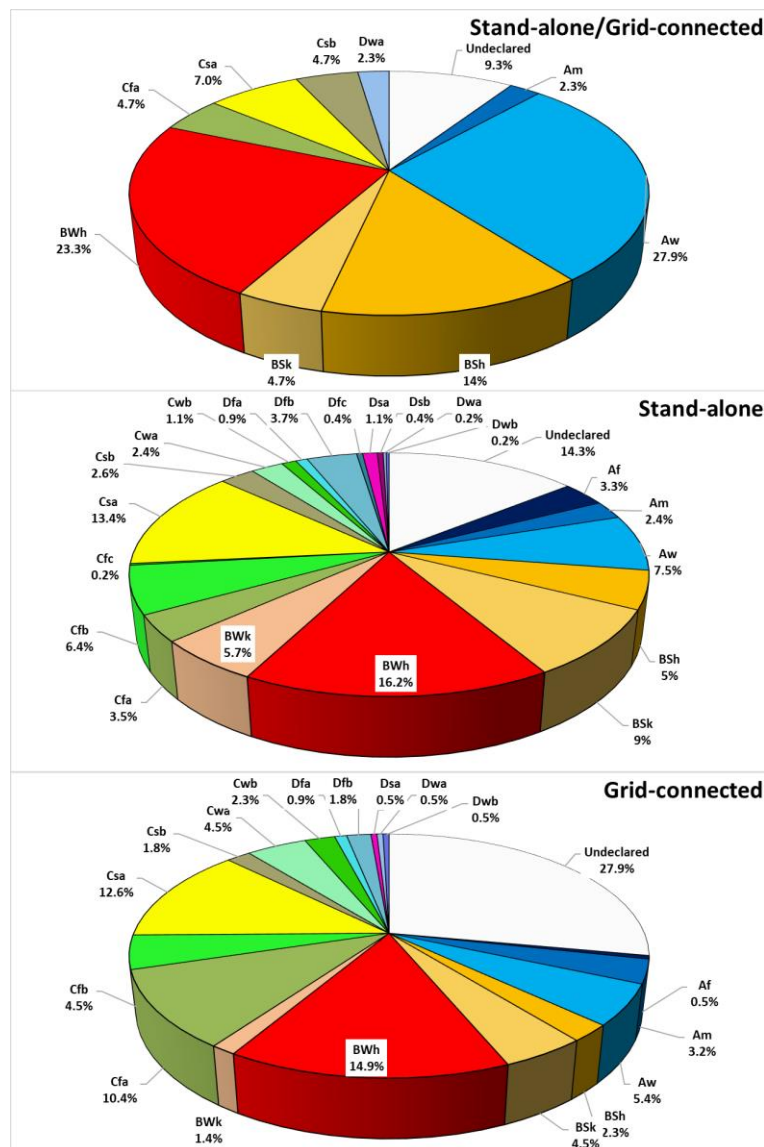
Figure 16. *Distribution of system installation modes in the climate zones.*

The distribution of the stand-alone installation modes is the one that most closely follows the distribution of research in the climate zones (see Figure 3). This is certainly due to the overwhelming presence of stand-alone installations in the applications in the article sample. As far as grid-connected system installations are concerned, there is a more or less important decrease in percentage in almost all climate zones compared to the stand-alone distribution. The only noticeable increase is found in Group C, while in Group D this increase is by a few tenths of a percentage. In particular, the noticeable percentage increase revealed in the Cfa subgroup is certainly due to China research, while the slight increase in the Cwa subgroup is caused by the presence of India contributions. On the contrary, the percentage of areas whose climate zone was not declared doubled. This is a determining factor in the percentage decrease of the other climate zones and implies that the climatic zone is certainly considered more important for articles concerning stand-alone systems. To deepen the level of detail, a comparison of occurrences of countries where the hybrid system was located for both system installation modes was made in Figure 17.
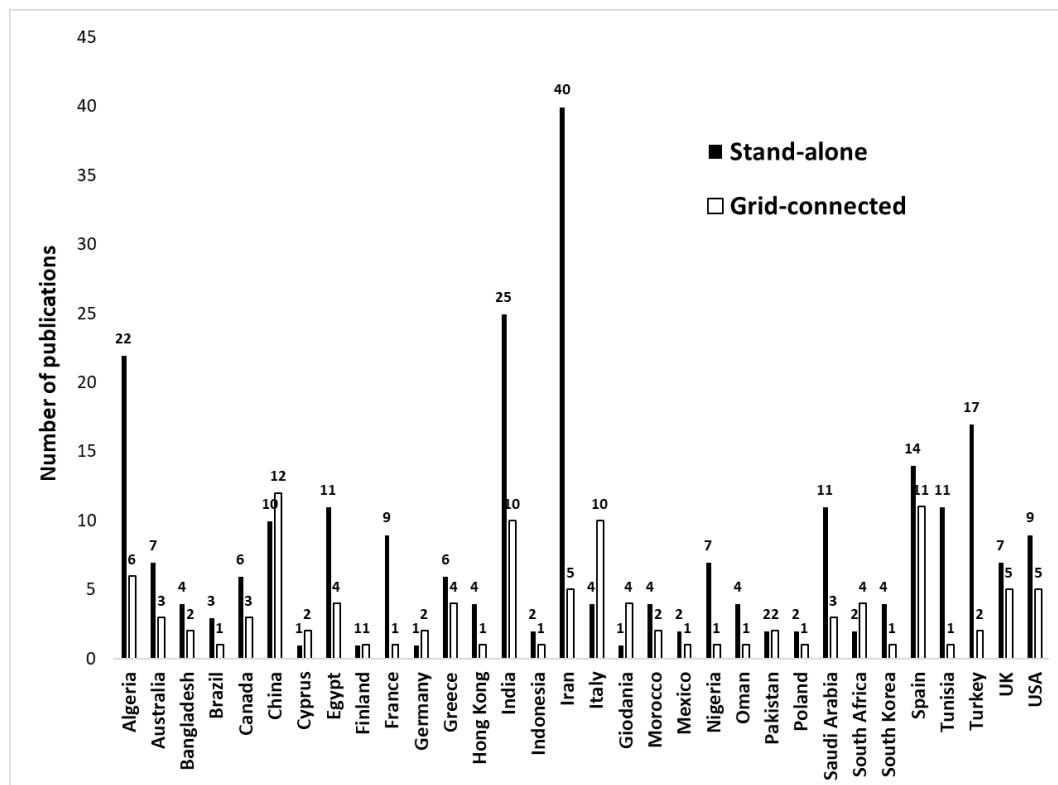
Figure 17. Occurrences of countries withstand-alone and grid-connected system installation modes.

It is evident the prevalence of stand-alone systems compared to grid-connected systems. It is quite rare for the latter to exceed the number of stand-alone system research in a country. Only for China, Germany, Jordan, and South Africa grid-connection system modes slightly overcome the stand-alone ones for few occurrences. Only in the case of grid-connection system modes in Italy, the occurrence difference is relevant with 10 against 4. By considering the countries with a considerable number of articles, China and Spain are the most balanced countries.

In addition, the same comparison was developed considering the main climatic groups. In climate group A, a remarkable presence of articles related to stand-alone systems compared to grid-connected systems is evident, especially in the Af subgroup. The gap is much smaller in the Am range. The Aw subgroup, including a higher number of countries, is more in line with the general trend (see Figure

Chapter 1　　　　　　　　　　　　**A literature review and statistical analysis of**
PV-wind hybrid renewable system researches by considering
the most relevant 550 articles: an upgradable matrix literature database

6, top) and is statistically more significant. The preponderant presence of stand-alone modes is confirmed even more in Group B. The climate zones in this group are divided over many more countries than in group A, making it the most statistically significant group. Consequently, the most frequent BSk and BWh subgroups correspond very closely to the general trend (see Figure 6, top). In the BSh subgroup, articles with grid-connected systems are even surpassed by those that compare stand-alone mode with grid connection, which is not the case in any other subgroup.

In Group C, there is a reversal of the trend. The most frequent systems in the Cfa subgroup are those with a grid connection, although the stand-alone systems follow them numerically very closely. This is due to China contributions in this climate zone, which is characterized by many investigations on grid-connected systems. The Cwa and Cwb climate zones also show a similar trend with a much smaller number of occurrences. The Cfc climate has just one stand-alone system.

Group D does not present any particular novelty, except for the Dwa subgroup, equally divided with one study for each category. This group has the lowest number of occurrences and can be considered statistically irrelevant. The only exception is the Dfb subgroup which is the only one with more than twenty occurrences. In the Dfc and Dsb subgroups, 100% of the studies carried out regarding stand-alone systems

7.3 Climate zones and intended uses

The geographical distribution of intended uses in climate zones and the frequency percentage for each climate zone were also examined.

The analysis has shown that Iran is the location where systems are tested for residential and non-residential use with the highest numerical incidence, while in China the systems are mainly investigated for district uses. This is not a case since China also holds the primacy for grid-connected systems. University uses are more frequent in Turkey, while uses for electric vehicles are mainly widespread in Italy, Canada and the United States. Electric vehicle use is less frequent compared to the other ones and has less statistical relevance.

Figure 18 shows the distribution of intended uses in climate zones.

Chapter 1

**A literature review and statistical analysis of
PV-wind hybrid renewable system researches by considering
the most relevant 550 articles: an upgradable matrix literature database**
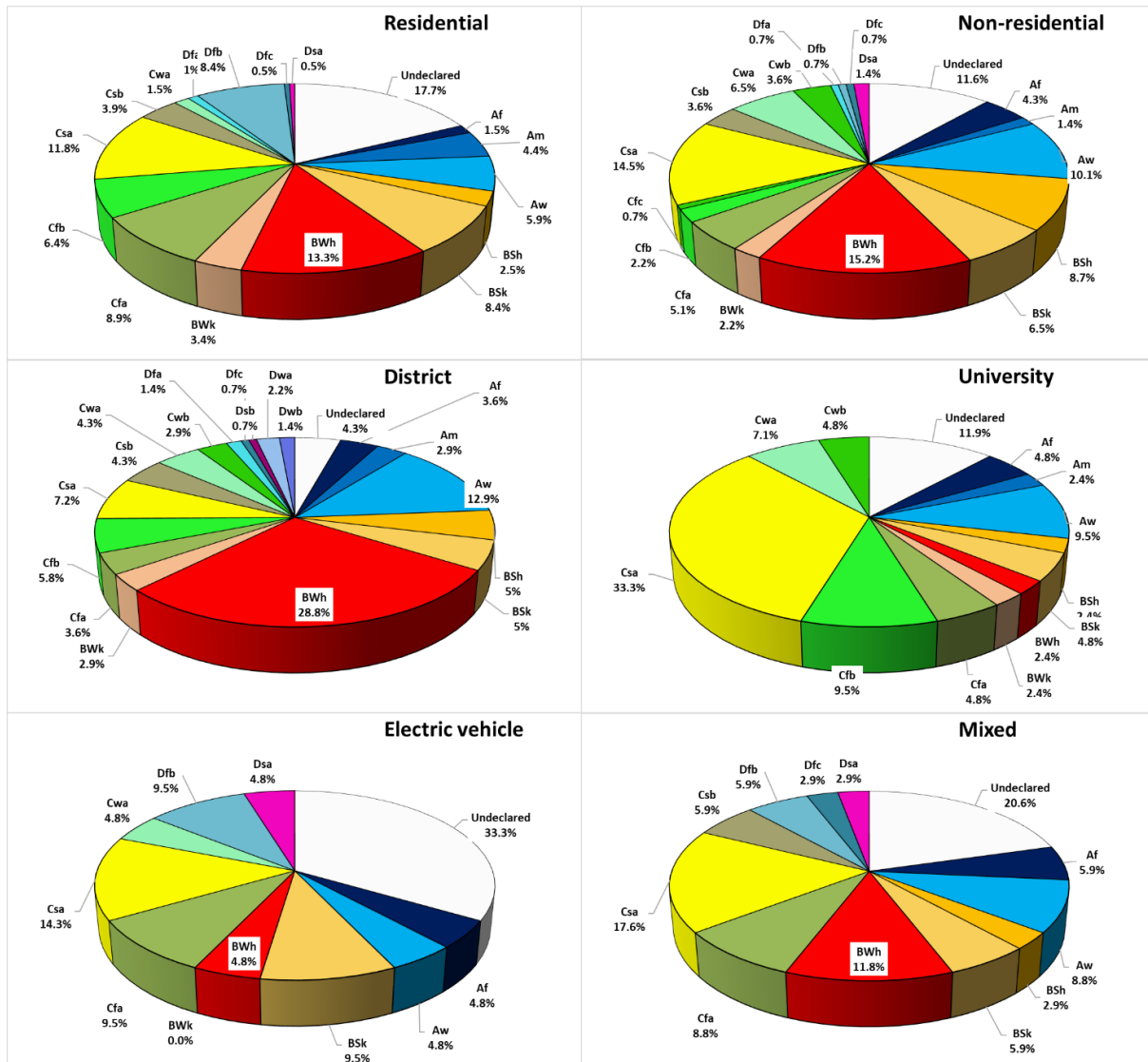
Figure 18. Distribution of intended uses in climate zones.

The residential and non-residential uses are the most homogeneously distributed in the different subgroups, with particular relevance covered by climatic groups B and C. Group A keeps the same percentages in all uses found in the article sample, which indicates that researchers in this climate group are almost equally concentrated on several fronts. Group D shows particular relevance only in residential uses, especially the Dfb subgroup which is the most frequent, while university uses were never investigated. In Group B a remarkable frequency, more than 40% of district uses can be observed and, in particular, the BWh subgroup with almost 30%. This implies that in hot desert climates, the sector is particularly focused on identifying alternative sustainable generation systems to meet the energy needs of entire districts using renewable energy sources. Group C has the highest percentage of analyses carried out for university uses, with the Csa subgroup, in which European countries, characterized by over 33%. This implies that the European countries, especially those with a Mediterranean climate, are more focused on university type uses and practical applications on campus. Articles with applications in Group B are rarely interested in these user types.

The insignificant presence of the intended use for the electric vehicle charging stations in the sample makes the left bottom graph in Figure 18 statistically irrelevant. The frequency of the main subgroups is confirmed and particular relevance is assumed also by group D.

Chapter 1

**A literature review and statistical analysis of
PV-wind hybrid renewable system researches by considering
the most relevant 550 articles: an upgradable matrix literature database**

Further analysis to identify the frequency of each intended use within each climate group was developed.

Group A shows irregular behaviour among their subgroups. In the subgroups Af and Aw, respectively, the non-residential and the district uses prevail. In the Am subgroup, residential use is predominant. The generic or undeclared uses are kept around 20% in all subgroups. In Group B, generic or undeclared loads are particularly important. This shows that in studies from this climate group, declaring the intended load is of minor importance, especially in the BWk subgroup, where the intended use is not declared in almost 50% of articles. Residential use varies between 14% and 30% in the different B subgroups, while district and non-residential uses have wider ranges of variation and are more or less relevant in each subgroup, but always with significant presence. This confirms that university uses are of low relevance in all B subgroups, while electric vehicle use is even absent in some of them. In Group C, the university use is of considerable importance. The intended use is declared for the majority of articles and the frequency of residential, district and non-residential uses change for each C subgroup. In the Cwb subgroup, the residential use was never considered, while in the Cfc subgroup, the only article related to this climate subgroup is a system for non-residential use.

As already highlighted, climatic group D have relative statistical relevance given the low number of publications. However, the emerging trend moves towards the use of hybrid systems for the charge of electric vehicles. The residential and non-residential uses are present in all subgroups in a more or less significant percentage, while the university use was never considered. District use is present in some subgroups and absent in others. In this regard, for the Dsb, Dwa and Dwb subgroups in 100% of the articles regard a district use.

7.4 Study types and system installation modes

Cross-referencing the data concerning the study type (simulation - experimental) with the system modes (stand-alone – grid-connected), it was found that the articles that carried out simulations occupy percentages higher than 85% for all the system modes (see Figure 19). This confirms what was already observed in the analysis of the system modes (see Figure 8). The other study methodologies have percentages lower than 10%, which makes the simulation the most widely used methodology both for all climate zones and system modes.

To further refine the level of detail, the same analysis was carried out in reverse by crossing the system modes for the different study types. For all the study methodologies, the percentage distributions follow the general trend of the system modes (see Figure 6), with the stand-alone ones prevailing over the others. There are no particular variations to be reported.

Chapter 1   **A literature review and statistical analysis of**
PV-wind hybrid renewable system researches by considering
the most relevant 550 articles: an upgradable matrix literature database
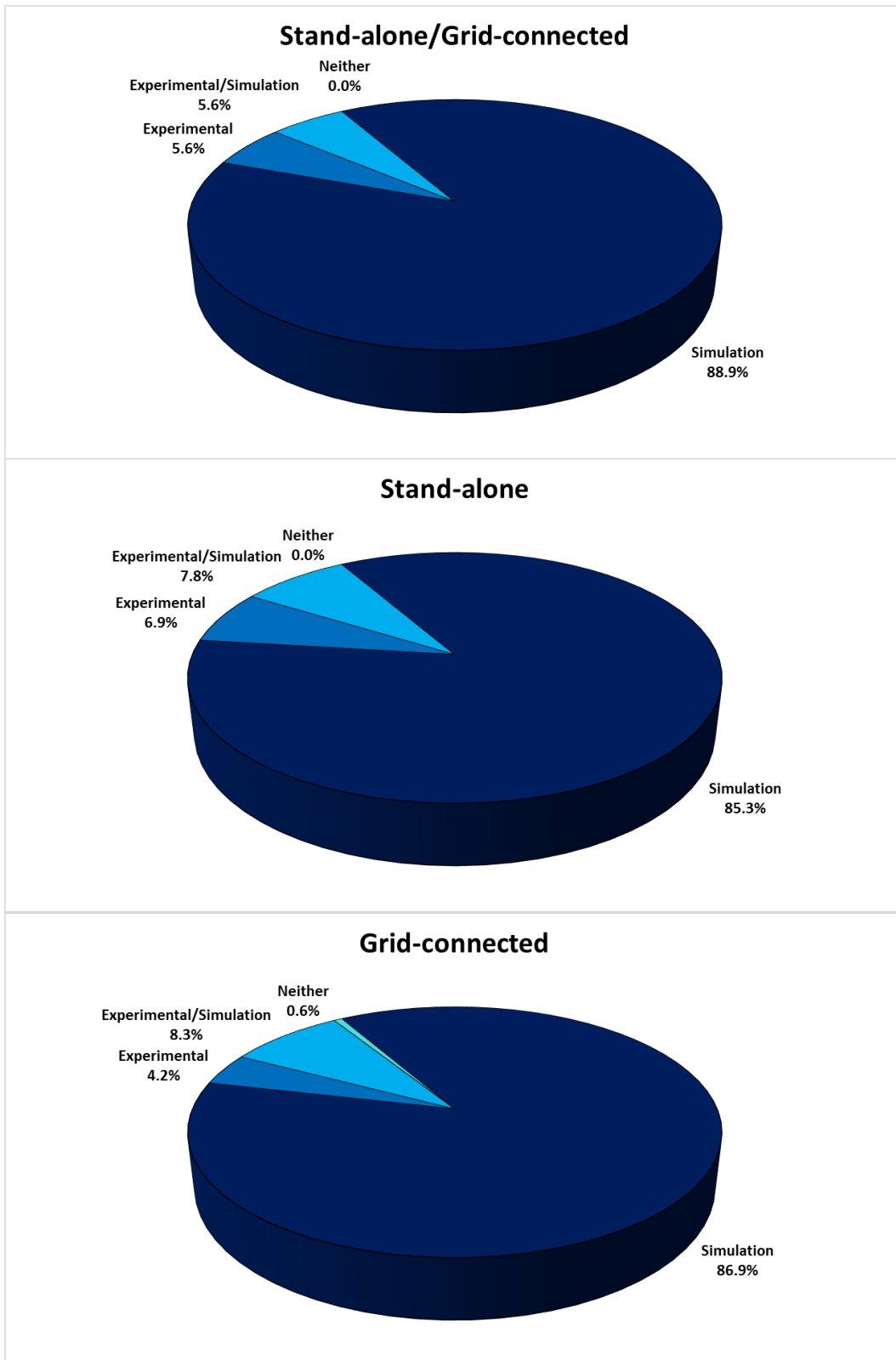
Figure 19. *Distribution of the study methodologies in the installation modes.*

Chapter 1   **A literature review and statistical analysis of**
PV-wind hybrid renewable system researches by considering
the most relevant 550 articles: an upgradable matrix literature database

7.5 Study types and intended uses

To further verify the distribution of the study methodologies, data on the intended uses were also cross-checked. Figure 20 illustrates the percentage distribution of study types for each intended use. The results confirm a prevalence of articles with simulation in all intended uses.
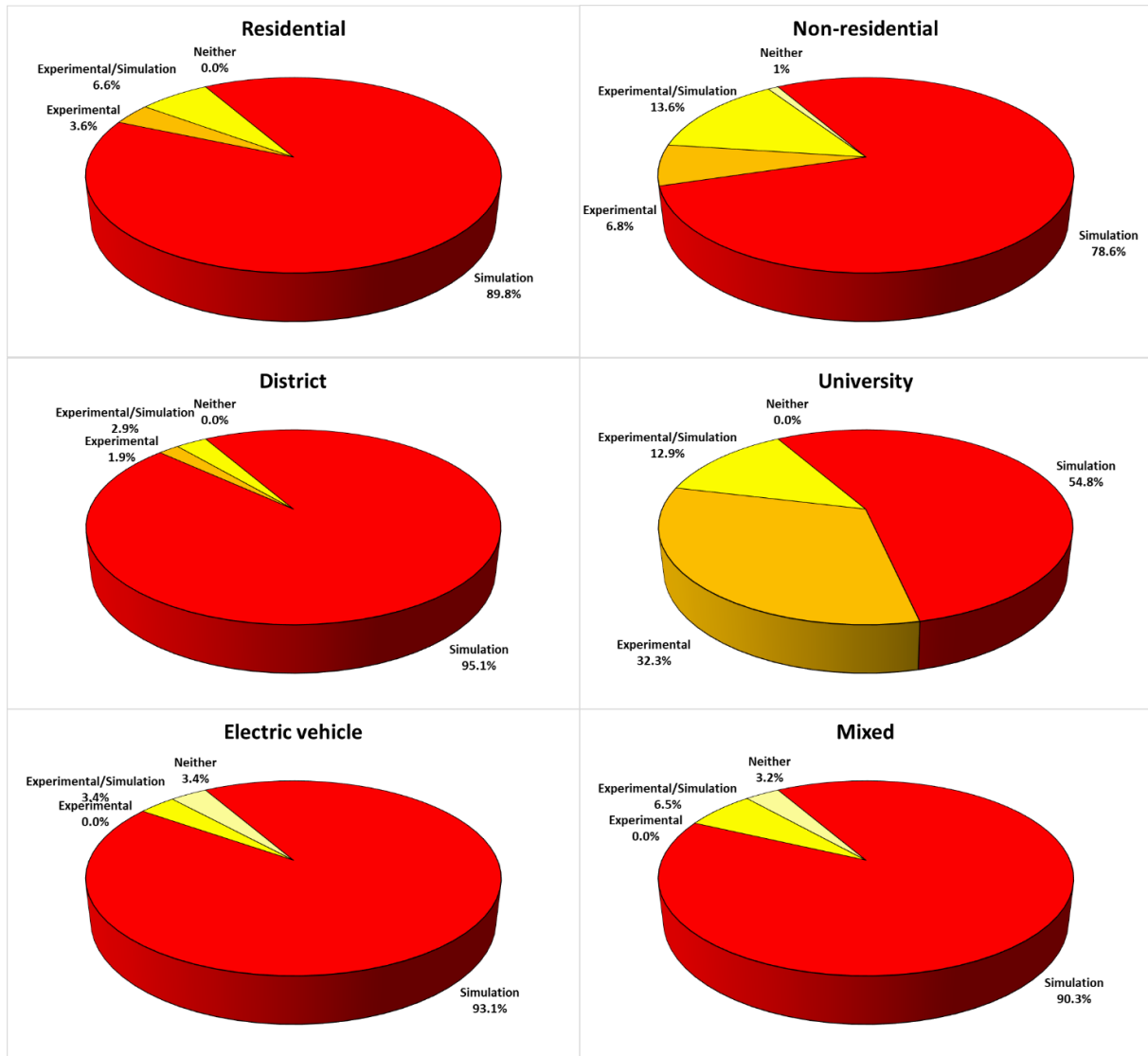
Figure 20. Distribution of study methodologies in intended uses.

The only exception is the university use that plays a relevant role for experimental analysis since a large number of existing systems are located on university campuses and are tested for experimental purposes and/or used to supply energy to university environments. Similarly to the other combined analysis, also a reverse analysis was developed by analysing the distribution of intended uses in the various study methodologies.

A rather variegated trend can be observed by identifying the most widely intended use for each study methodology. As expected, university use has a higher percentage in experimental investigations, residential use in simulation investigations, non-residential use in experimental/simulation comparisons. Only one article used neither simulations nor experiments.

Chapter 1
A literature review and statistical analysis of
PV-wind hybrid renewable system researches by considering
the most relevant 550 articles: an upgradable matrix literature database

7.6 System configurations and system installation modes

The distribution of the system configurations with different auxiliary components in stand-alone and grid-connected systems was separately investigated. For the articles with different system configurations analysed, each configuration was treated as a separate system. The analysis showed that:

- More than 70% of the auxiliary components belong to stand-alone systems;
- In both system installation modes, more than half of the auxiliary components consist of energy storage systems (54% for stand-alone systems and 51% for grid-connected systems).
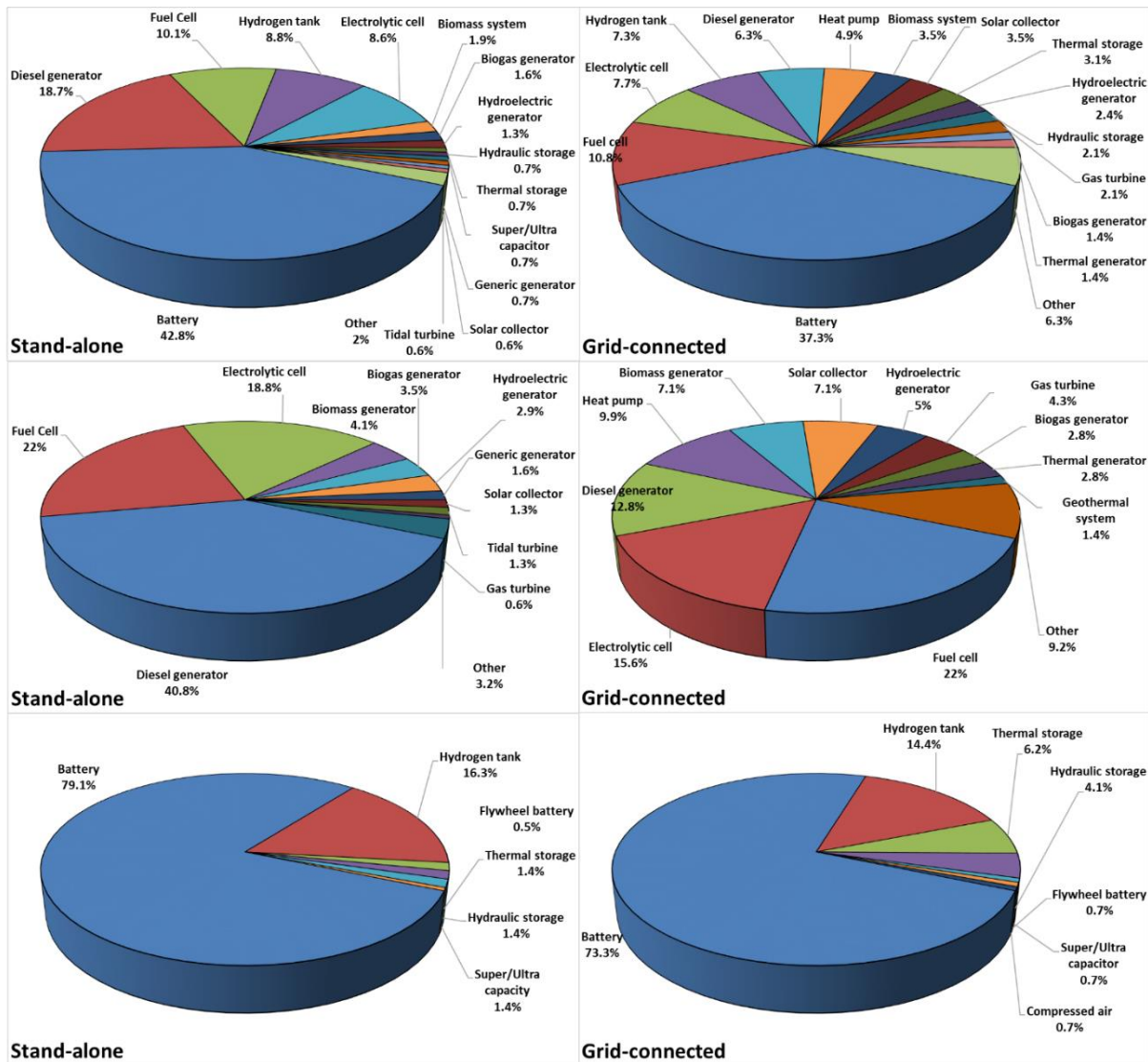
Figure 21. *Percentage of occurrence of auxiliary components, auxiliary generation systems and storage systems for stand-alone and grid-connected installation modes.*

The distribution of auxiliary components for stand-alone installations is extremely close to the general one (see Figure 4, top right). This implies that stand-alone installations have a very strong influence on the general distribution. Similar considerations can be made for auxiliary generation systems and storage systems. The only important difference for auxiliary generation systems is related to the diesel generators, with a clear percentage increase from 31.1% for the general distribution (see Figure 4, bottom right) to 40.8% in only stand-alone systems.

For the stand-alone systems, the battery is confirmed to be the most used storage system, followed by hydrogen tanks, exactly as in Figure 21 bottom left. The results obtained are not surprising, considering that stand-alone systems need an integration system; in more than 120 articles, battery and diesel generator are used in combination.

For grid-connected systems, the battery is always the most used component but with a smaller percentage, as well as the components for hydrogen systems. As expected, the diesel generator is less frequent in grid-connected systems being more reliable than stand-alone systems and less dependent on auxiliary systems. It emerges that the diesel generators are usually coupled with a large number of energy generation systems of various types, such as biomass, hydroelectric, thermal, meaning that the optimal configuration for a grid-connected system is still in the testing phase. Considerations for auxiliary generation systems (see Figure 21, central right) are similar to those of auxiliary systems since the fuel cells are the most employed and the diesel generators are relegated to third place. For storage systems, there are no particular variations compared with the general trend (see Figure 4, bottom left) and stand-alone distributions. The battery is always the most widely used component although in a slightly lower percentage, while the frequency of other storage systems is quite low.

7.7 System installation modes and intended uses

To conclude the cross statistical analysis, the data on the system installation modes and the intended uses were combined. The analysis results shown in Figure 22 show that stand-alone installations are the most widely used in the majority of intended uses, especially for residential and district use with very similar distributions. The tendency is different for university and non-residential uses. In particular, the stand-alone installations in the university uses are only slightly higher than grid-connected ones. This implies that university research focuses on both system modes. Instead, a complete reversal distribution is highlighted for electric vehicle charging stations, powered by grid-connected systems in more than 60% of articles. The employment of stand-alone systems for charging electric vehicles is still too early stage, while grid-connected charging stations are more widespread. Similarly, when mixed uses are used simultaneously, grid-connected systems were more employed than stand-alone ones since higher reliability is required when many different load types are considered.

Chapter 1

**A literature review and statistical analysis of
PV-wind hybrid renewable system researches by considering
the most relevant 550 articles: an upgradable matrix literature database**
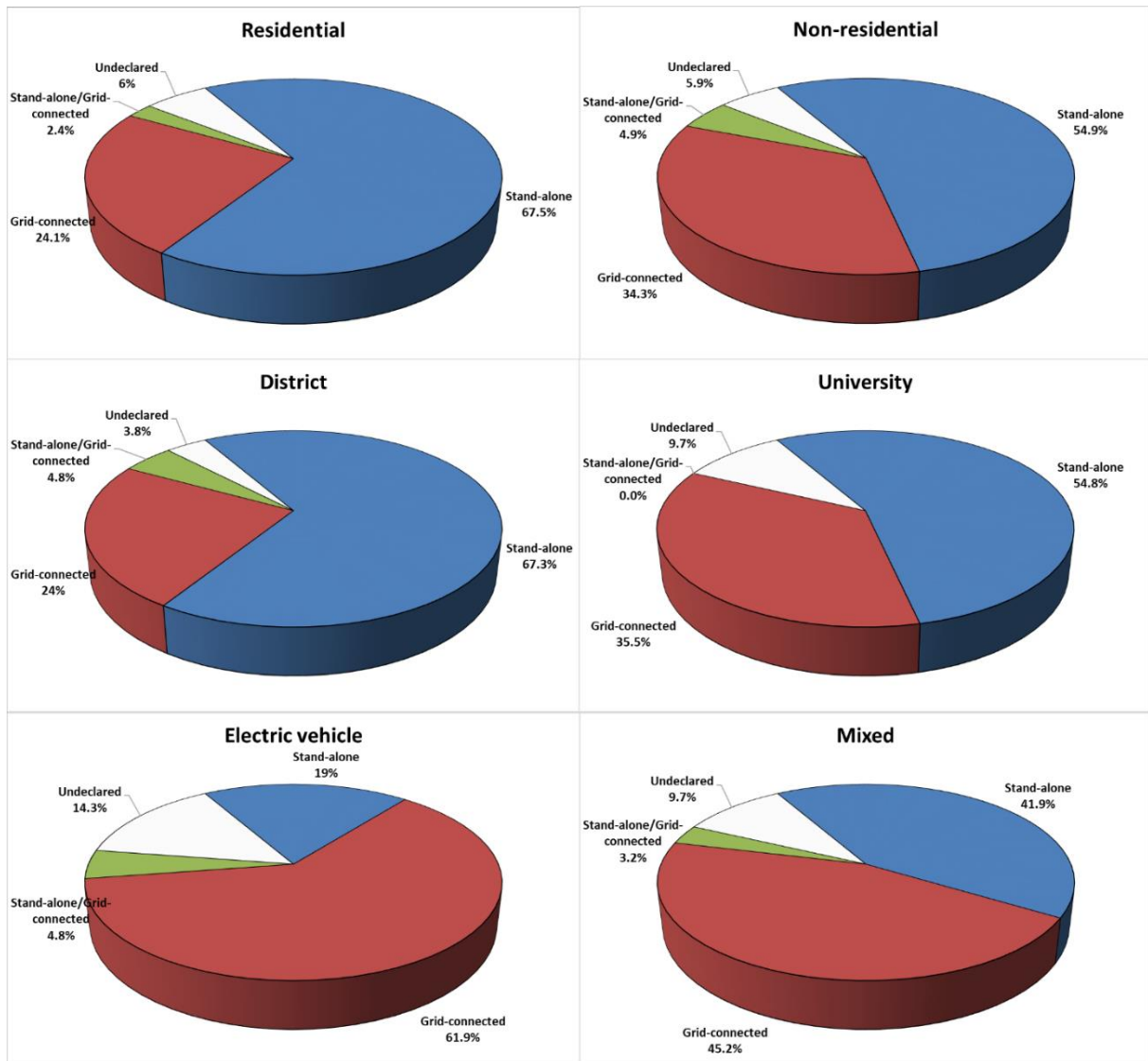
Figure 22. Distribution of intended uses in system modes.

The reversal analysis obtained by analysing the distribution of different intended uses for each system installation mode, stand-alone has a rather homogeneous percentage for each intended use, while articles with grid-connected electric vehicle charging stations are higher than the grid-connected university hybrid systems. In more than 1/3 of articles with grid-connected systems, the intended use is considered of minor importance since it is generic or undeclared.

8. Statistical analysis of power installed in the parametric analyses of hybrid systems

8.1 Analysis procedure

To identify the most frequent PV and wind powers and battery capacities installed in hybrid systems, the variation ranges related to PV and wind nominal powers and battery capacity were collected for each article. The minimum and maximum values of this range were reported in the matrix database. Articles that were not developed parametric analyses or did not deal with system sizing declare only one value of PV and wind power, as well as of battery capacity, which are reported as both minimum and maximum.

Chapter 1   **A literature review and statistical analysis of**
PV-wind hybrid renewable system researches by considering
the most relevant 550 articles: an upgradable matrix literature database

The analysis showed that:

- In the article sample, 475 articles declare data concerning the PV power installed; among these, 213 do not declare a variation range.
- 470 articles provide data concerning wind power installed; among these, 241 articles do not declare a variation range.
- 305 articles describe battery capacity data. among these, 139 articles do not declare a variation range.

The absolute minimum and the absolute maximum of powers and capacity related to all articles were identified. Subsequently, the variation ranges were divided into classes to identify the frequency in each class. For each article, a unitary value is set in all classes in which fall the values considered in the parametric analysis. Consequently, a frequency matrix was obtained composed of 550 rows and columns equal to the number of classes considered. This process was developed for the PV power installed, wind power installed and battery capacity. producing a frequency matrix for different classes. By adding the values contained in each column, a vector containing the frequency of each class was determined to trace probability distributions. For each system component (PV, wind and battery), different probability density distributions were obtained: for all article sample, for stand-alone and grid-connected systems, and residential and non-residential uses. Finally, the probability associated with each class was calculated by considering both constant and incremental ranges.

8.2 Photovoltaic system

Figure 23 shows the probability density distribution of PV power installed by considering all articles, articles with stand-alone and grid-connected systems. Table 3 lists the overall, stand-alone and grid-connected PV system power probability by using an incremental and constant range.
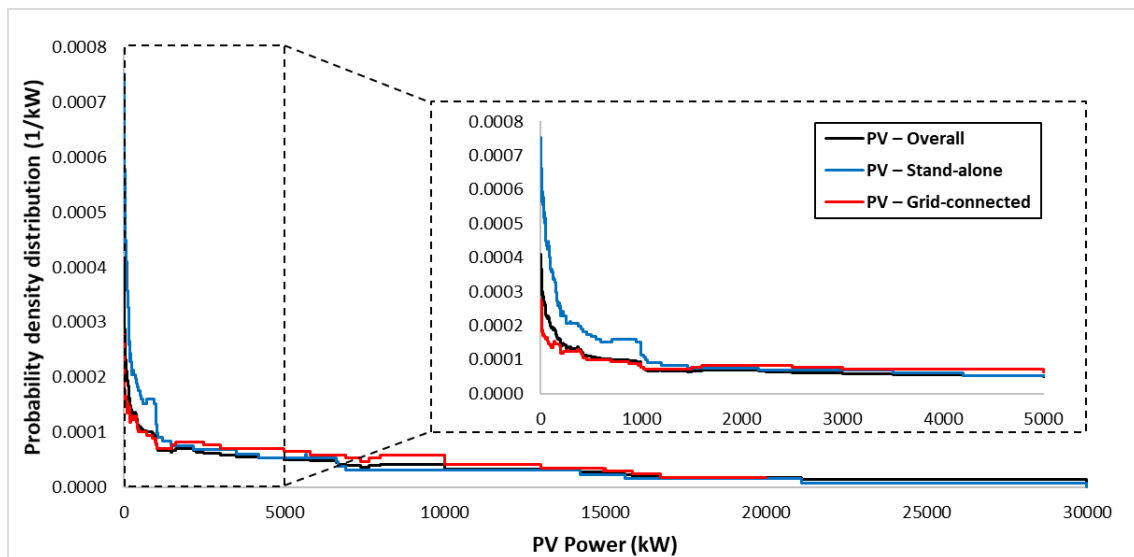
Figure 23. Overall, stand-alone and grid-connected photovoltaic system power probability density distributions.

Chapter 1　　　　　　　　　　　　　　　　**A literature review and statistical analysis of**
PV-wind hybrid renewable system researches by considering
the most relevant 550 articles: an upgradable matrix literature database

Table 3. *Overall, stand-alone and grid-connected photovoltaic system power probability distributions by using an incremental and constant range.*

PV – Overall				PV – Stand-alone				PV – Grid-connected			
Incremental range		Constant range		Incremental range		Constant range		Incremental range		Constant range	
Power (kW)	Prob. (%)	Power (kW)	Prob. (%)	Power (kW)	Prob. (%)	Power (kW)	Prob. (%)	Power (kW)	Prob. (%)	Power (kW)	Prob. (%)
0-5	0.2	0-2500	23.4	0-5	0.3	0-2500	33.7	0-5	0.1	0-2000	19.1
5-10	0.2	2500-5000	14.1	5-10	0.3	2500-5000	15.4	5-10	0.1	2000-4000	15.0
10-20	0.3	5000-7500	11.4	10-20	0.6	5000-7500	11.6	10-20	0.2	4000-6000	13.4
20-40	0.6	7500-10000	10.3	20-40	1.1	7500-10000	7.6	20-40	0.3	6000-8000	11.0
40-80	0.9	10000-12500	8.4	40-80	1.8	10000-12500	7.6	40-80	0.6	8000-10000	11.8
80-160	1.5	12500-15000	7.6	80-160	2.8	12500-15000	7.0	80-160	1.2	10000-12000	8.2
160-320	2.3	15000-17500	5.1	160-320	3.7	15000-17500	4.3	160-320	2.1	12000-14000	7.7
320-640	3.7	17500-20000	4.2	320-640	5.7	17500-20000	3.8	320-640	3.5	14000-16000	6.3
640-1280	5.5	20000-22500	3.8	640-1280	8.2	20000-22500	2.7	640-1280	5.3	16000-18000	4.0
1280-2560	8.6	22500-25000	3.5	1280-2560	9.6	22500-25000	1.9	1280-2560	10.2	>18000	3.5
2560-5120	14.4	25000-27500	3.5	2560-5120	15.6	25000-27500	1.9	2560-5120	18.3		
5120-10240	21.9	27500-30000	3.5	5120-10240	19.3	27500-30000	1.9	5120-10240	29.3		
10240-20480	25.2	>30000	1.4	10240-20480	22.7	>30000	0.7	>10240	28.7		
>20480	14.8			>20480	8.4						

PV systems are characterized prevalently on low-medium installed power values and above 2500 kW the frequency decreases very quickly leading to low frequencies of PV high-power installed in articles. This implies that research tends to investigate small and medium PV system sizes in hybrid systems.

Stand-alone PV systems show the same trend but much more marked, presenting higher probability in the first intervals which decrease much faster in the following ones. Instead, the grid-connected system distribution is more uniform and decreases much more slowly, being used even for high powers installed. This implies, that the behaviour of the stand-alone PV system power probability density distribution is very incisive on the overall distribution.

8.3 Wind system

Figure 24 shows the probability density distribution of wind power installed by considering all articles, articles with stand-alone and grid-connected systems. Table 4 lists the overall, stand-alone and grid-connected wind system power probability by using an incremental and constant range.
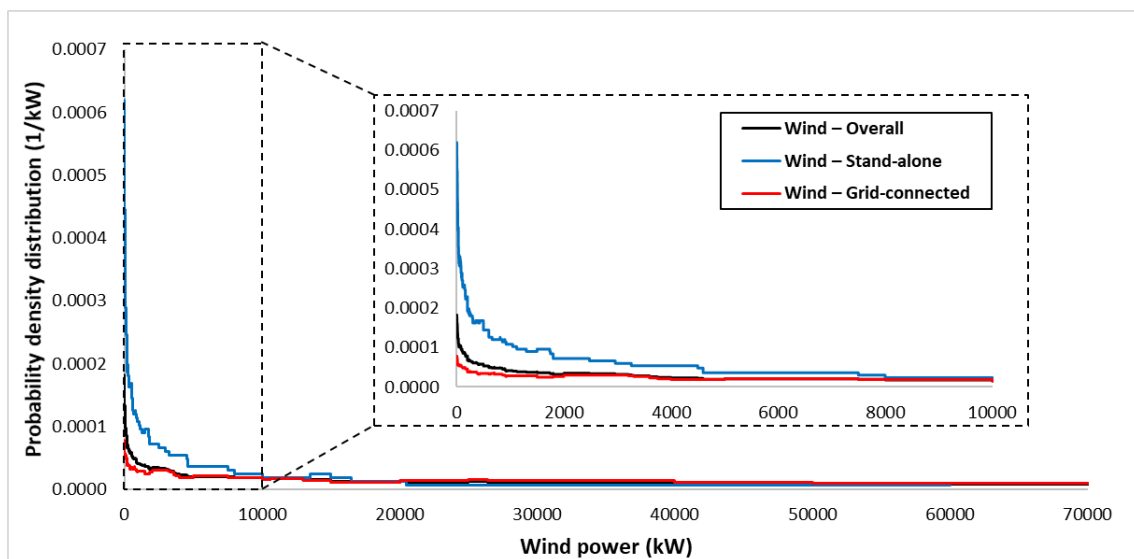
Figure 24. *Overall, stand-alone and grid-connected wind system power probability density distributions.*

Chapter 1

**A literature review and statistical analysis of
PV-wind hybrid renewable system researches by considering
the most relevant 550 articles: an upgradable matrix literature database**

Table 4. *Overall, stand-alone and grid-connected wind system power probability by using an incremental and constant range.*

Wind – Overall				Wind – Stand-alone				Wind – Grid-connected			
Incremental range		Constant range		Incremental range		Constant range		Incremental range		Constant range	
Power (kW)	Prob. (%)	Power (kW)	Prob. (%)	Power (kW)	Prob. (%)	Power (kW)	Prob. (%)	Power (kW)	Prob. (%)	Power (kW)	Prob. (%)
0-5	0.1	0-10000	28.1	0-5	0.3	0-5000	43.5	0-5	0.04	0-10000	24.0
5-10	0.1	10000-20000	14	5-10	0.3	5000-10000	15.3	5-10	0.04	10000-20000	13.5
10-20	0.1	20000-30000	11.9	10-20	0.5	10000-15000	9.9	10-20	0.1	20000-30000	13.7
20-40	0.2	30000-40000	11.7	20-40	0.7	15000-20000	6.9	20-40	0.1	30000-40000	13.4
40-80	0.4	40000-50000	10.4	40-80	1.3	20000-25000	3.3	40-80	0.2	40000-50000	11.0
80-160	0.7	50000-60000	9.1	80-160	2.1	25000-30000	3	80-160	0.4	50000-60000	9.6
160-320	1.1	60000-70000	7.8	160-320	3.1	30000-35000	3	160-320	0.6	60000-70000	9.6
320-640	1.8	>70000	7.1	320-640	4.9	35000-40000	3	320-640	1.1	>70000	4.8
640-1280	2.8			640-1280	7.0	40000-45000	3	640-1280	1.9		
1280-2560	4.5			1280-2560	10.3	45000-50000	3	1280-2560	3.6		
2560-5120	6.7			2560-5120	13.5	50000-55000	3	2560-5120	6.1		
5120-10240	9.9			5120-10240	15.3	>55000	3	5120-10240	10.2		
10240-20480	14.3			10240-20480	17.0			10240-20480	13.7		
20480-40960	23.9			20480-40960	12.3			20480-40960	27.5		
>40960	33.3			>40960	11.4			>40960	34.3		

The trend of the wind power probability density distribution is similar to the PV trends (see Figure 23) but with fewer oscillations; the stand-alone system prevails for low systems, while the grid connection remains mostly constant throughout the range. In particular, the wind power probability density distribution at high powers installed is greater than the PV one. Above 10000 kW, the probability density distribution of the installed wind power stabilizes and decreases slightly, implying that the wind system is an essential component for large systems. Stand-alone systems have a much more pronounced concavity curve in the range of 0-5000 kW. The 43.5% of occurrences fall within this range, meaning that stand-alone wind systems have a high concentration for low power values. The rest of the interval is more or less equally distributed from the medium to large power ranges. The grid-connected systems show a reversal of the trend since the typical decrease that is revealed with the increase in power is immediate. For wind powers higher than 500 kW, the probability density distribution remains more or less constant throughout the range until it reaches very high-power values. This shows that, in addition to having a significant impact on the overall trend, the grid-connected mode is mainly used for large installations since 76 % of occurrences are concentrated in the range above 20000 kW.

8.4 Comparison between photovoltaic and wind systems

In Figure 25, the PV and wind distributions were also compared, using the overall distribution and the stand-alone and grid-connected modes individually. The results show that PV is much more frequent and used for lower power values, while wind power is more uniformly distributed over a much wider range. This shows that wind power is a more important component as power increases. The stand-alone distributions are almost overlapping with a very slight prevalence of PV. The differences in the overall distribution are strongly influenced by the grid-connected mode. For medium-low power values less than 20000 kW, grid-connected systems are prevalently composed of PV power installed, while the two distributions become very close as power increases.

Chapter 1   **A literature review and statistical analysis of**
PV-wind hybrid renewable system researches by considering
the most relevant 550 articles: an upgradable matrix literature database
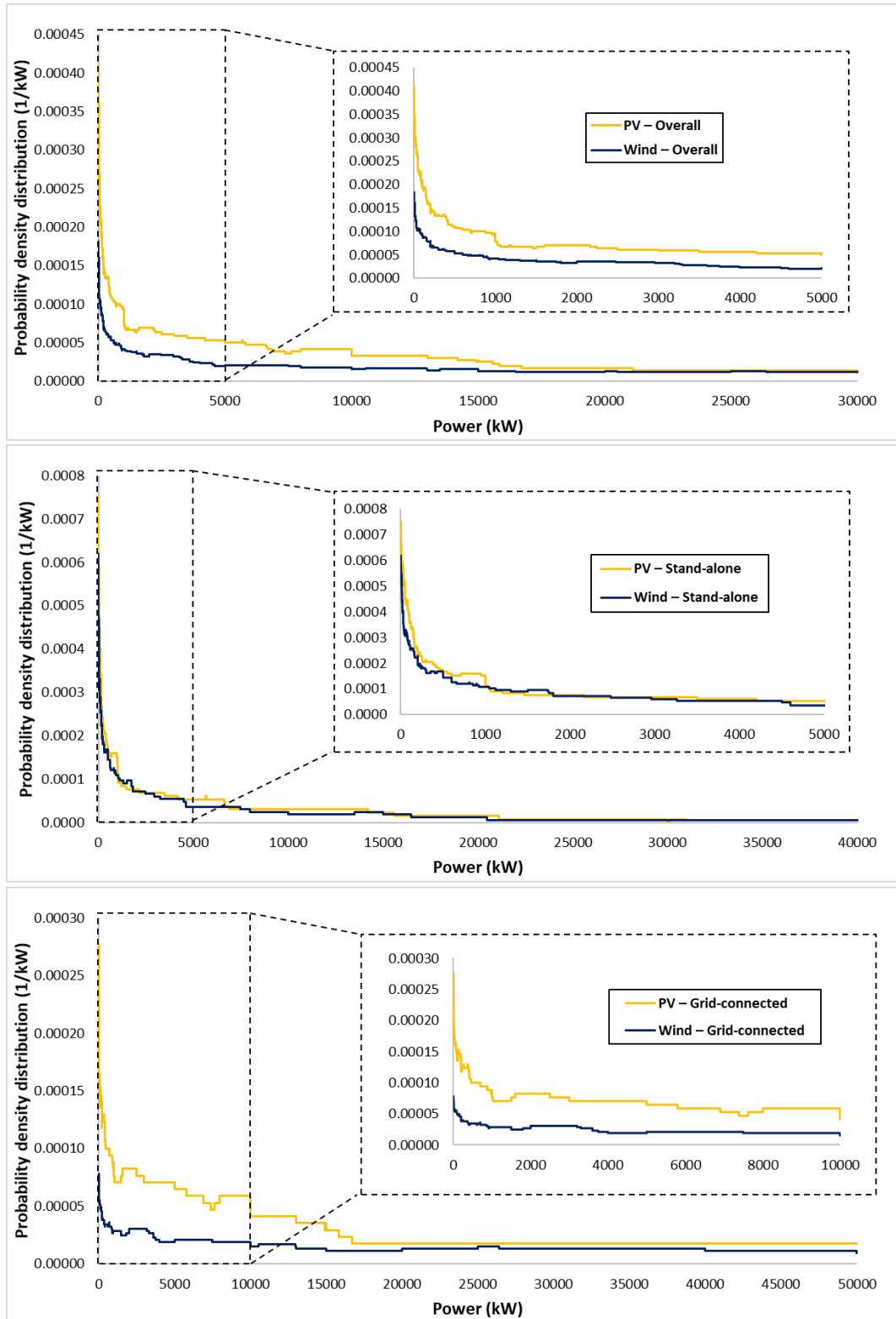
Figure 25. *Overall, stand-alone and grid-connected photovoltaic and wind system power probability density distributions.*

Chapter 1   **A literature review and statistical analysis of**
PV-wind hybrid renewable system researches by considering
the most relevant 550 articles: an upgradable matrix literature database

8.5 Battery storage system

The same type of analysis was carried out with the storage battery capacity. Figure 26 shows the probability density distribution of battery capacity installed by considering all articles, articles with stand-alone and grid-connected systems. Table 5 lists the overall, stand-alone and grid-connected battery capacity probability by using an incremental and constant range.
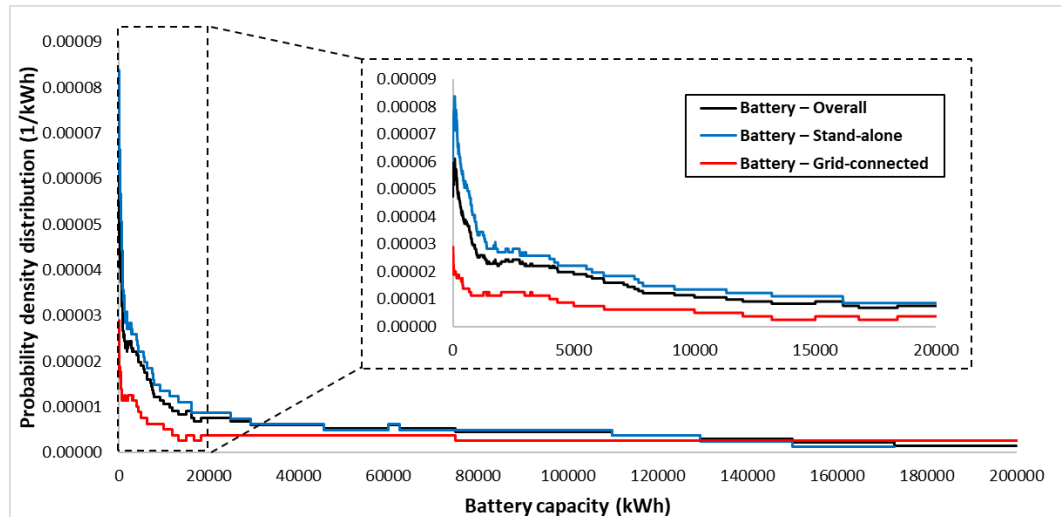
Figure 26. *Overall, stand-alone and grid-connected storage system capacity probability density distributions.*

The overall storage capacity found in articles is extremely large, even until 200000 kWh.
The distribution shows that the storage capacities used are more concentrated until 20 000 kWh, namely in almost 1/3 of the total interval. Above this value, the distribution decreases quicker since the presence of a battery is less necessary for large hybrid systems.
The storage capacity for batteries used in stand-alone systems shows a similar trend but with higher frequencies for low-medium capacities.
For grid-connected systems, the distribution trend slightly changes since a more uniform distribution of frequencies with a higher value for low-capacity values is observed, mainly due to the relatively low number of articles that couple the battery to this system installation mode, namely about forty compared to a total of 550. In these cases, the presence of the grid makes it less necessary to rely on an energy storage system.
The trend of the three curves is similar to those of PV systems in Figure 23 and wind power in Figure 24, with the stand-alone prevailing for low values and the grid-connected more evenly distributed throughout the range.

Chapter 1   **A literature review and statistical analysis of**
PV-wind hybrid renewable system researches by considering
the most relevant 550 articles: an upgradable matrix literature database

Table 5. Overall, stand-alone and grid-connected storage system capacity probability by using an incremental and constant range.

Battery – Overall				Battery – Stand-alone				Battery – Grid-connected			
Incremental range		Constant range		Incremental range		Constant range		Incremental range		Constant range	
Capacity (kWh)	Prob. (%)	Capacity (kWh)	Prob. (%)	Capacity (kWh)	Prob. (%)	Capacity (kWh)	Prob. (%)	Capacity (kWh)	Prob. (%)	Capacity (kWh)	Prob. (%)
0-20	0.1	0-20000	28.9	0-20	0.1	0-20000	35.4	0-50	0.1	0-30000	16.7
20-40	0.1	20000-40000	13.3	20-40	0.1	20000-40000	14.1	50-100	0.1	30000-60000	11.3
40-80	0.2	40000-60000	11.1	40-80	0.3	40000-60000	10.5	100-200	0.2	60000-90000	9.5
80-160	0.4	60000-80000	10.5	80-160	0.6	60000-80000	10.2	200-400	0.4	90000-120000	7.6
160-320	0.8	80000-100000	9.2	160-320	1.0	80000-100000	9.9	400-800	0.5	120000-150000	7.6
320-640	1.3	100000-120000	8.4	320-640	1.7	100000-120000	8.6	800-1600	0.9	150000-180000	7.6
640-1280	1.8	120000-140000	6.8	640-1280	2.5	120000-140000	6.1	1600-3200	1.9	180000-210000	7.6
1280-2560	3.0	140000-160000	5.3	1280-2560	3.6	140000-160000	3.7	3200-6400	2.9	210000-240000	7.6
2560-5120	5.5	160000-180000	4.0	2560-5120	6.3	>160000	1.6	6400-12800	3.6	240000-270000	7.6
5120-10240	7.3	>180000	2.4	5120-10240	8.6			12800-25600	4.4	270000-300000	7.6
10240-20480	8.7			10240-20480	10.8			25600-51200	9.7	300000-330000	4.8
20480-40960	13.5			20480-40960	14.3			51200-102400	15.9	330000-360000	3.8
40960-81920	21.9			40960-81920	21.1			102400-204800	25.8	>360000	1
81920-163840	29.7			81920-163840	27.8			>204800	33.6		
>163840	5.5			>163840	1.1						

8.6 Residential and non-residential uses

The previous probability density distributions were further elaborated by considering the main system intended uses, residential and non-residential ones. The non-residential uses include district, university and non-residential uses of the categories listed in Section 2.5. The analysis examines PV and wind powers installed and battery capacities installed separately, considering grid-connected and stand-alone systems.

8.6.1. Residential and non-residential photovoltaic systems

Figure 27 illustrates the comparison of overall, stand-alone and grid-connected residential PV power probability density distributions.

Chapter 1
A literature review and statistical analysis of
PV-wind hybrid renewable system researches by considering
the most relevant 550 articles: an upgradable matrix literature database
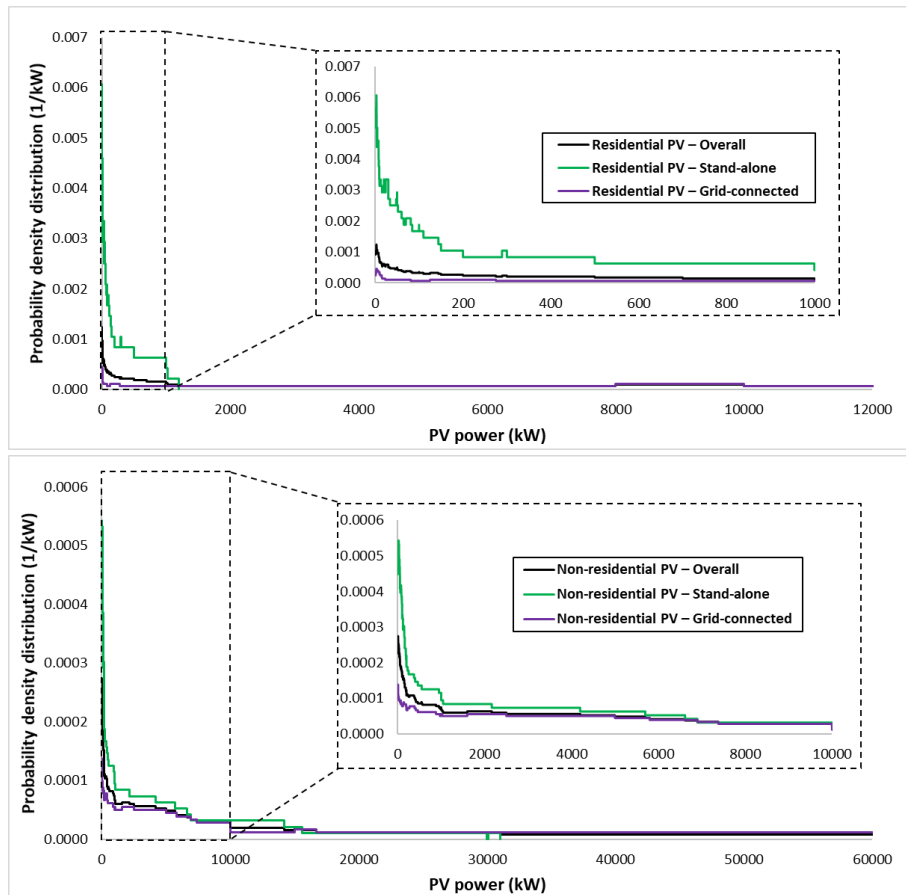
Figure 27. Overall, stand-alone and grid-connected residential and non-residential photovoltaic power probability density distributions.

PV powers installed in residential uses are contracted in a limited range in low- medium powers no higher than 13000 kW for all system installation modes. There is a large number of articles dealing with systems intended for the supply of electrical energy to individual houses and above 1000 kW this number decreases considerably. This is even more evident when stand-alone systems are considered. The stand-alone PV residential distribution reaches up to a maximum value of 1200 kW, with the highest frequencies lower than 200 kW. On the other hand, the grid-connected PV residential distribution has a rather uniform trend in a higher power interval. Stand-alone systems are preferred for residential use.

The stand-alone non-residential PV distribution show trends similar to those of residential one but distributed throughout a much wider range. This distribution strongly influences the overall trend for low PV powers, while the grid-connected prevails for high powers.

As shown in Figure 27, residential PV is focused on low PV powers and its probability density distribution always exceeds the non-residential one since this latter is extended over a much wider range. This also occurs in stand-alone and grid-connected systems. For grid-connected, the uniform trend is justified considering the relatively low presence of articles found.

8.6.2. Residential and non-residential wind systems

Figure 28 illustrates the comparison of overall, stand-alone and grid-connected residential wind power probability density distributions.

Chapter 1　　　　　　　　　　　　　　　　　　　**A literature review and statistical analysis of**
PV-wind hybrid renewable system researches by considering
the most relevant 550 articles: an upgradable matrix literature database

The overall residential wind distribution is rather evenly distributed throughout the range, except for the typical higher frequency at low power values. The stand-alone residential wind distribution shows the most pronounced frequencies at low powers, while the grid-connected distribution exhibits the most uniform trend in the power range.

Non-residential wind power distribution has a much more jagged trend, considering a large number of articles found and large-scale uses falling in this use. The power range is much larger than the residential one.

The overall distribution is certainly influenced to a greater extent by the grid-connected distribution, which remains relatively stable throughout the range, while the stand-alone distribution has a constant trend above 10000 kW.

Overall, by comparing the residential and non-residential distributions, it emerges that wind powers installed for residential use are distributed with greater concentration at low power, while non-residential wind power is much more uniform over a much wider range. The two stand-alone distributions have similar curves below 10000 kW, making the difference in the overall distribution given by the different grid-connected distributions in the two uses.
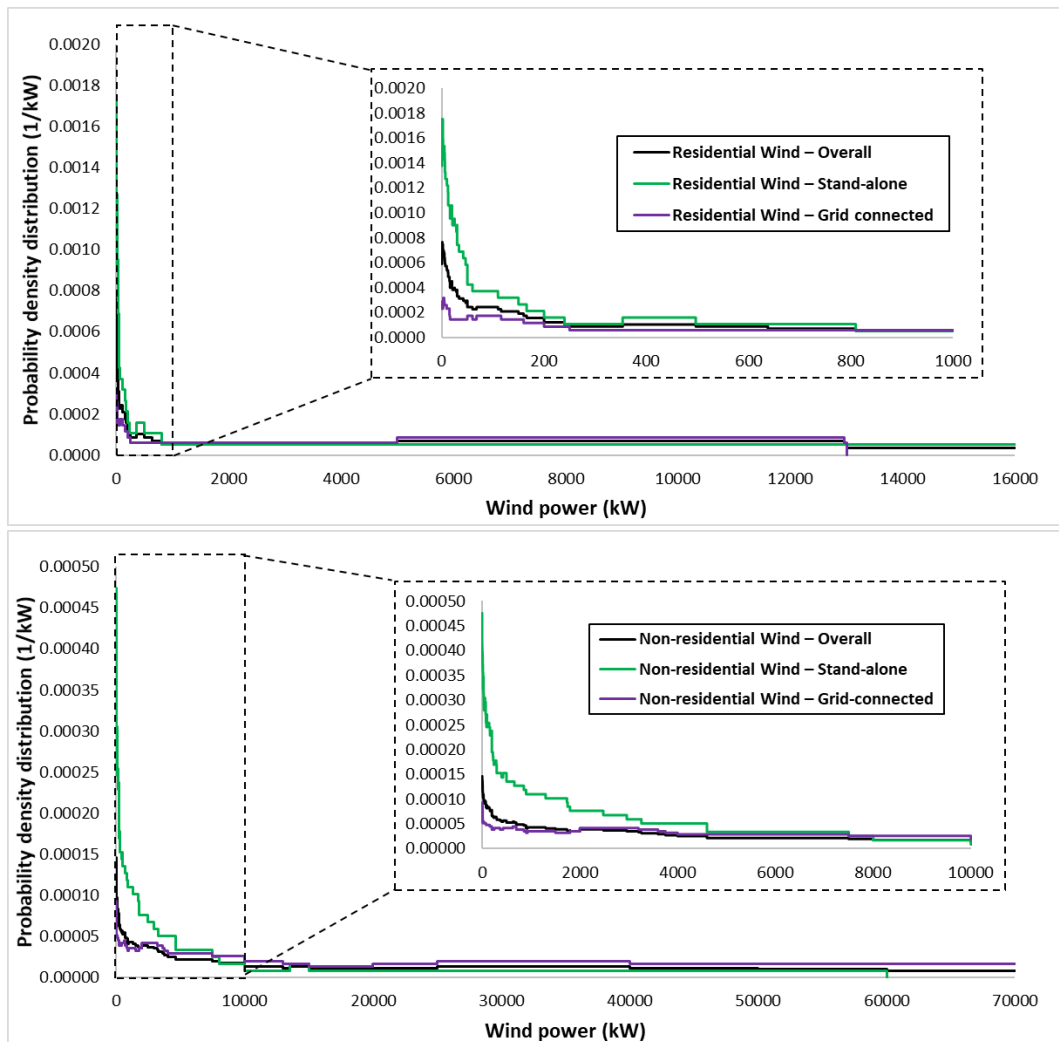
Figure 28. *Overall, stand-alone and grid-connected residential and non-residential wind power probability density distributions.*

Chapter 1   **A literature review and statistical analysis of**
PV-wind hybrid renewable system researches by considering
the most relevant 550 articles: an upgradable matrix literature database

8.6.3. Residential and non-residential battery storage systems

Figure 29 illustrates the comparison of overall, stand-alone and grid-connected battery capacity probability density distributions.

The range of battery storage capacities used in the residential sector is very wide with higher frequencies for low capacity values. This is more evident for stand-alone and this high frequency represents all articles dealing with the energy satisfaction of buildings located in remote locations, where an auxiliary storage system is indispensable in case of failure of renewable sources. The grid-connected has an almost uniform distribution.

The overall non-residential battery storage capacity probability distributions show a higher concentration than residential batteries at low capacities. More than 50% of probability is concentrated below 20000 kWh. The battery employment in variegated non-residential uses leads to a more indented trend than the residential one.

The overall distribution is certainly more influenced by the stand-alone distribution, which exhibits an overlapped behaviour. The more uniform trend of grid-connected distribution is justified by the scarcity of articles on the use of batteries in grid-connected systems for non-residential use, about twenty of a total of 550 articles. It is clear that in these applications, the auxiliary energy support to the user is provided mainly by the grid, while the use of batteries is rarely applied. In grid-connection systems, the variation range of battery capacities employed is very lower than that of the stand-alone one

By comparing the residential and non-residential distributions, the use of the battery for non-residential uses prevails for low-medium storage capacity values. On the other hand, batteries for residential use have a more homogeneous distribution compared to the non-residential one.

Chapter 1   **A literature review and statistical analysis of**
PV-wind hybrid renewable system researches by considering
the most relevant 550 articles: an upgradable matrix literature database
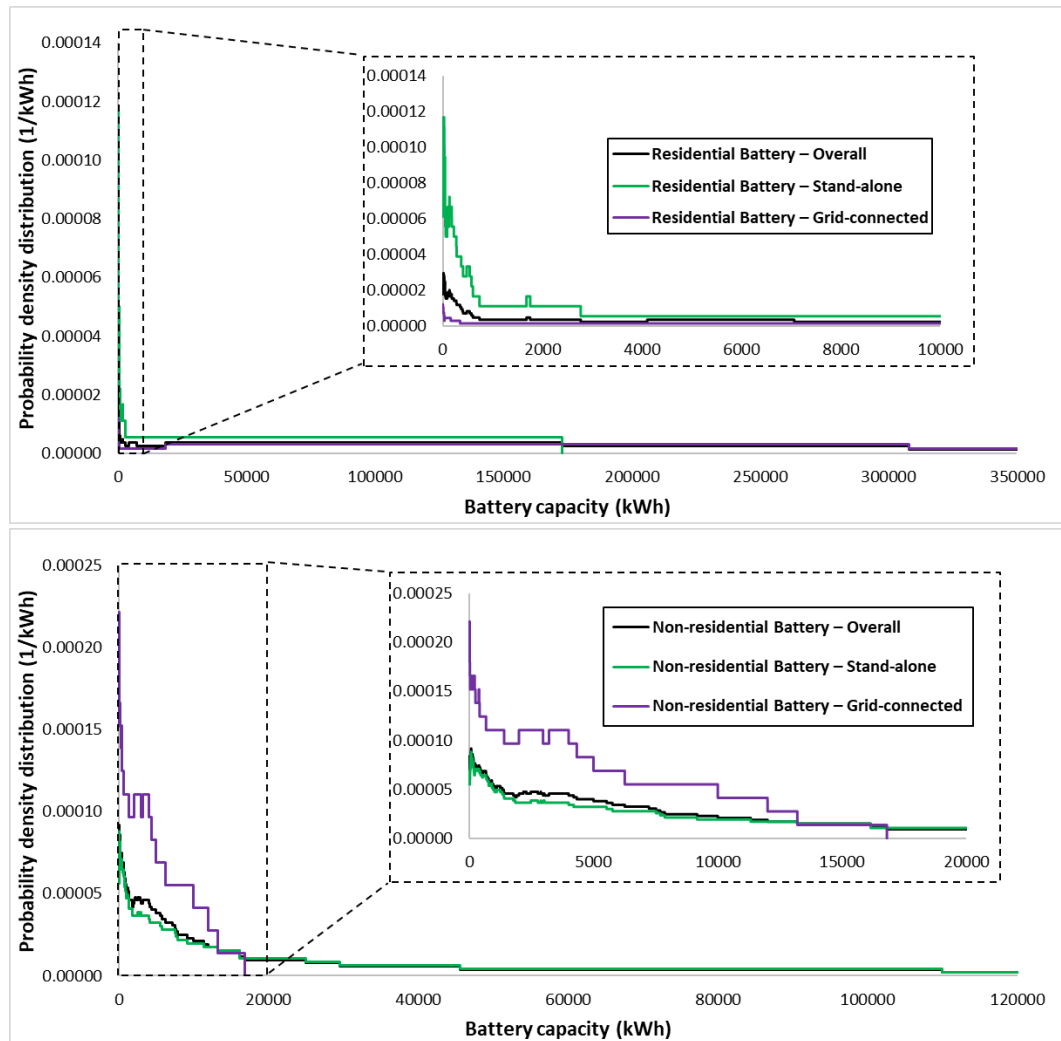
Figure 29. Overall, stand-alone and grid-connected residential and non-residential battery capacity probability density distributions.

9. Conclusions

The matrix database collecting the main data of the most relevant 550 articles published over the last 25 years has permitted performing a statistical analysis to provide a quantitative measure of trends on which PV-wind hybrid-system research has focused. In particular, it emerged that:

- Iran, India and China are the countries with the highest number of applications in the world.
- The dry and temperate climate zones are those where most research was made; in particular, the climatic group BWh is the most recurring. This trend is also confirmed by grouping the articles by analysis methodology, system installation mode and intended use.
- The most prevalent study methodology is the simulation, even grouping articles by climatic zone, system installation mode and intended use.
- The battery is the most widely used auxiliary component, both for stand-alone and grid-connected systems. Diesel generator for stand-alone systems and fuel cells for grid-connected systems are the second most utilized auxiliary components.
- Stand-alone systems are more investigated than grid-connected systems or both simultaneously, even grouping articles by study methodology, climatic zone and intended use.

- Residential use is the most intended use, even grouping articles by climatic zone, study methodology and system installation mode.
- Parametric analysis is the most developed analysis type, focusing on the optimal sizing of hybrid systems and HOMER is the most widely used software.
- The most used indicators are the LPSP and RF for the energy analysis, the NPC and COE for the economic analysis and the emissions of CO_2 (E) for the environmental analysis.
- The most used optimization techniques are the PSO and GA, used individually or in combination with other algorithms or alternatives versions, i.e. multi-objective versions.
- As regards the system installed power, the use of PV systems is preferred for low power, while wind systems take on greater importance for large-scale systems. However, wind systems are more uniformly distributed systems in the power variation range identified than PV systems, which are particularly used in low-medium power systems.
- The residential use is mainly couple to medium-low powers installed, while the non-residential use distribution as a function of the power installed is more variable and can reach also several tens of MW.

The statistical analysis carried out in this work has led to the identification of the most interesting topics in the current research of hybrid systems, highlighting the more focused topics and, specularly, those on which further in-depth investigations are still required. The picture provided is nevertheless auspicious for the future, suggesting that the branch of research on hybrid systems is only at the beginning.

The matrix database and literature review developed can be updated for future investigations aiming to detect the research trend in this field.

References

[1] Sichilalu, S., Tazvinga, H., & Xia, X. (2016). Optimal control of a fuel cell/wind/PV/grid hybrid system with thermal heat pump load. Solar Energy, 135, 59–69. https://doi.org/10.1016/j.solener.2016.05.028

[2] Sichilalu, S., Mathaba, T., & Xia, X. (2017). Optimal control of a wind–PV-hybrid powered heat pump water heater. Applied Energy, 185, 1173–1184. https://doi.org/10.1016/j.apenergy.2015.10.072

[3] Arcos-Aviles, D., Pascual, J., Marroyo, L., Sanchis, P., Guinjoan, F., & Marietta, M. P. (2015). Optimal Fuzzy Logic EMS design for residential grid-connected microgrid with hybrid renewable generation and storage. IEEE International Symposium on Industrial Electronics, 2015-September, 742–747. https://doi.org/10.1109/ISIE.2015.7281561

[4] Bonanno, F., Capizzi, G., Gagliano, A., & Napoli, C. (2012). Optimal management of various renewable energy sources by a new forecasting method. SPEEDAM 2012 - 21st International Symposium on Power Electronics, Electrical Drives, Automation and Motion, 934–940. https://doi.org/10.1109/SPEEDAM.2012.6264603

[5] Madboly, D. A., Aleem, S. H. E. A., & Ibrahim, A. M. (2017). Optimal sizing of different configurations of renewable distributed generation systems for a green building in Egypt. 2016 18th International Middle-East Power Systems Conference, MEPCON 2016 - Proceedings, 107–116. https://doi.org/10.1109/MEPCON.2016.7836879

[6] Pal, P., Mukherjee, V., & Maleki, A. (2018). Economic and performance investigation of hybrid PV/wind/battery energy system for isolated Andaman and Nicobar islands, India. International Journal of Ambient Energy, 0(0), 1–19. https://doi.org/10.1080/01430750.2018.1525579

[7] Papadopoulos, V., Desmet, J., Knockaert, J., & Develder, C. (2018). Improving the utilization factor of a PEM electrolyzer powered by a 15 MW PV park by combining wind power and battery storage –

Chapter 1
                                              A literature review and statistical analysis of
                                              PV-wind hybrid renewable system researches by considering
                                              the most relevant 550 articles: an upgradable matrix literature database

Feasibility study. International Journal of Hydrogen Energy, 43(34), 16468–16478. https://doi.org/10.1016/j.ijhydene.2018.07.069

[8] Parida, A., & Chatterjee, D. (2018). Stand-alone AC-DC microgrid-based wind-solar hybrid generation scheme with autonomous energy exchange topologies suitable for remote rural area power supply. International Transactions on Electrical Energy Systems, 28(4), 1–13. https://doi.org/10.1002/etep.2520

[9] Pavan Kumar, Y. V., & Bhimasingu, R. (2015). Renewable energy based microgrid system sizing and energy management for green buildings. Journal of Modern Power Systems and Clean Energy, 3(1), 1–13. https://doi.org/10.1007/s40565-015-0101-7

[10] Praveen Kumar, T., Subrahmanyam, N., & Sydulu, M. (2019). CMBSNN for Power Flow Management of the Hybrid Renewable Energy–Storage System-Based Distribution Generation. IETE Technical Review (Institution of Electronics and Telecommunication Engineers, India), 36(3), 303–314. https://doi.org/10.1080/02564602.2018.1465860

[11] Sun, F., Hou, W., Yin, B., & Xi, H. (2009). Preliminary studies on the linking of building hybrid energy system and distributed power generation system. 1st International Conference on Sustainable Power Generation and Supply, SUPERGEN '09, 1–6. https://doi.org/10.1109/SUPERGEN.2009.5348238

[12] Priyadarshi, N., Ramachandaramurthy, V. K., Padmanaban, S., & Azam, F. (2019). An ant colony optimized mppt for standalone hybrid pv-wind power system with single cuk converter. Energies, 12(1). https://doi.org/10.3390/en12010167

[13] Priyadarshi, N., Padmanaban, S., Ionel, D. M., Mihet-Popa, L., & Azam, F. (2018). Hybrid PV-Wind, micro-grid development using quasi-Z-source inverter modeling and control-experimental investigation. Energies, 11(9). https://doi.org/10.3390/en11092277

[14] Ramasamy, P., & Krishnasamy, V. (2018). Common Mode Voltage Reduction Using 3D-SVPWM for 3-level CI-NPC Inverter with Hybrid Energy System. Electric Power Components and Systems, 46(4), 391–405. https://doi.org/10.1080/15325008.2018.1446198

[15] Ramli, M. A. M., Bouchekara, H. R. E. H., & Alghamdi, A. S. (2018). Optimal sizing of PV/wind/diesel hybrid microgrid system using multi-objective self-adaptive differential evolution algorithm. Renewable Energy, 121, 400–411. https://doi.org/10.1016/j.renene.2018.01.058

[16] Ramli, M. S., Wahid, S. S. A., & Hassan, K. K. (2017). A comparison of renewable energy technologies using two simulation softwares: HOMER and RETScreen. AIP Conference Proceedings, 1875(August). https://doi.org/10.1063/1.4998384

[17] Rathaiah, M., Ram Kishore Kumar Reddy, P., & Sujatha, P. (2018). Adaptive fuzzy controller design for solar and wind based hybrid system. International Journal of Engineering and Technology(UAE), 7(2), 283–290. https://doi.org/10.14419/ijet.v7i2.24.12065

[18] Razmjoo, A., & Davarpanah, A. (2019). Developing various hybrid energy systems for residential application as an appropriate and reliable way to achieve Energy sustainability. Energy Sources, Part A: Recovery, Utilization and Environmental Effects, 41(10), 1180–1193. https://doi.org/10.1080/15567036.2018.1544996

[19] Reddy, S. S. (2018). Emergency reserve activation considering demand-side resources and battery storage in a hybrid power system. Electrical Engineering, 100(3), 1589–1599. https://doi.org/10.1007/s00202-017-0637-9

[20] Reddy, S. S. (2017). Optimal power flow with renewable energy resources including storage. Electrical Engineering, 99(2), 685–695. https://doi.org/10.1007/s00202-016-0402-5

[21] Reddy, S. S. (2017). Optimal scheduling of thermal-wind-solar power system with storage. Renewable Energy, 101, 1357–1368. https://doi.org/10.1016/j.renene.2016.10.022

[22] Lamedica, R., Santini, E., Ruvio, A., Palagi, L., & Rossetta, I. (2018). A MILP methodology to optimize sizing of PV - Wind renewable energy systems. Energy, 165, 385–398. https://doi.org/10.1016/j.energy.2018.09.087

Chapter 1
A literature review and statistical analysis of
PV-wind hybrid renewable system researches by considering
the most relevant 550 articles: an upgradable matrix literature database

[23]   Leskarac, D., Moghimi, M., Liu, J., Water, W., Lu, J., & Stegen, S. (2018). Hybrid AC/DC Microgrid testing facility for energy management in commercial buildings. Energy and Buildings, 174, 563–578. https://doi.org/10.1016/j.enbuild.2018.06.061

[24]   Radhakrishnan, A., & Selvan, M. P. (2015). Load scheduling for smart energy management in residential buildings with renewable sources. 2014 18th National Power Systems Conference, NPSC 2014. https://doi.org/10.1109/NPSC.2014.7103825

[25]   Lotfy, M. E., Senjyu, T., Farahat, M. A. F., Abdel-Gawad, A. F., & Matayoshi, H. (2017). A polar fuzzy control scheme for hybrid power system using vehicle-to-grid technique. Energies, 10(8), 1–25. https://doi.org/10.3390/en10081083

[26]   López-González, A., Domenech, B., & Ferrer-Martí, L. (2018). Sustainability and design assessment of rural hybrid microgrids in Venezuela. Energy, 159, 229–242. https://doi.org/10.1016/j.energy.2018.06.165

[27]   Lu, J., Wang, W., Zhang, Y., & Cheng, S. (2017). Multi-objective optimal design of stand-alone hybrid energy system using entropy weight method based on HOMER. Energies, 10(10). https://doi.org/10.3390/en10101664

[28]   Mabrouk, S. Ben, Oueslati, H., Mabrouk, A. Ben, Zizzo, G., La Cascia, D., Dusonchet, L., … Massaro, F. (2017). Simulation of photovoltaic installation connected to the grid with storage system. Energy Procedia, 139, 609–616. https://doi.org/10.1016/j.egypro.2017.11.261

[29]   Mahesh, A., & Sandhu, K. S. (2020). A genetic algorithm based improved optimal sizing strategy for solar-wind-battery hybrid system using energy filter algorithm. Frontiers in Energy, 14(1), 139–151. https://doi.org/10.1007/s11708-017-0484-4

[30]   Maleki, A. (2018). Modeling and optimum design of an off-grid PV/WT/FC/diesel hybrid system considering different fuel prices. International Journal of Low-Carbon Technologies, 13(2), 140–147. https://doi.org/10.1093/ijlct/cty006

[31]   Saadatmandi, M., Hakimi, S. M., & Hajizadeh, A. (2018). Management of plug-in hybrid electrical vehicle to increase renewable energy penetration in smart grid. 2018 International Conference on Smart Energy Systems and Technologies, SEST 2018 - Proceedings, 1–6. https://doi.org/10.1109/SEST.2018.8495734

[32]   Mandal, S., Das, B. K., & Hoque, N. (2018). Optimum sizing of a stand-alone hybrid energy system for rural electrification in Bangladesh. Journal of Cleaner Production, 200, 12–27. https://doi.org/10.1016/j.jclepro.2018.07.257

[33]   Mandelli, S., Brivio, C., Leonardi, M., Colombo, E., Molinas, M., Park, E., & Merlo, M. (2016). The role of electrical energy storage in sub-Saharan Africa. Journal of Energy Storage, 8, 287–299. https://doi.org/10.1016/j.est.2015.11.006

[34]   Marzband, M., Ghazimirsaeid, S. S., Uppal, H., & Fernando, T. (2017). A real-time evaluation of energy management systems for smart hybrid home Microgrids. Electric Power Systems Research, 143, 624–633. https://doi.org/10.1016/j.epsr.2016.10.054

[35]   Ma, T., & Javed, M. S. (2019). Integrated sizing of hybrid PV-wind-battery system for remote island considering the saturation of each renewable energy resource. Energy Conversion and Management, 182(December 2018), 178–190. https://doi.org/10.1016/j.enconman.2018.12.059

[36]   Spertino, F., Ahmad, J., Chicco, G., Ciocia, A., & Di Leo, P. (2015). Matching between electric generation and load: Hybrid PV-wind system and tertiary-sector users. Proceedings of the Universities Power Engineering Conference, 2015-November, 6–11. https://doi.org/10.1109/UPEC.2015.7339787

[37]   Ma, W., Xue, X., Liu, G., & Zhou, R. (2018). Techno-economic evaluation of a community-based hybrid renewable energy system considering site-specific nature. Energy Conversion and Management, 171, 1737–1748. https://doi.org/10.1016/j.enconman.2018.06.109

Chapter 1   **A literature review and statistical analysis of**
PV-wind hybrid renewable system researches by considering
the most relevant 550 articles: an upgradable matrix literature database

[38]   Tabanjat, A., Becherif, M., Hissel, D., & Ramadan, H. S. (2018). Energy management hypothesis for hybrid power system of H2/WT/PV/GMT via AI techniques. International Journal of Hydrogen Energy, 43(6), 3527–3541. https://doi.org/10.1016/j.ijhydene.2017.06.085

[39]   Taghipour Broujeni, S., Fathi, S. H., & Milimonfared, J. (2017). Multivariable controller for a novel topology of double-input converter applied in distributed hybrid photovoltaic/wind power system. International Transactions on Electrical Energy Systems, 27(2), 1–17. https://doi.org/10.1002/etep.2261

[40]   Tahani, M., Babayan, N., & Pouyaei, A. (2015). Optimization of PV/Wind/Battery stand-alone system, using hybrid FPA/SA algorithm and CFD simulation, case study: Tehran. Energy Conversion and Management, 106, 644–659. https://doi.org/10.1016/j.enconman.2015.10.011

[41]   Tawfik, T. M., Badr, M. A., El-Kady, E. Y., & Abdellatif, O. E. (2018). Optimization and energy management of hybrid standalone energy system: a case study. Renewable Energy Focus, 25(June), 48–56. https://doi.org/10.1016/j.ref.2018.03.004

[42]   Fazelpour, F., Farahi, S., & Soltani, N. (2016). Techno-economic analysis of hybrid power systems for a residential building in Zabol, Iran. EEEIC 2016 - International Conference on Environment and Electrical Engineering. https://doi.org/10.1109/EEEIC.2016.7555649

[43]   Timmerberg, S., & Kaltschmitt, M. (2019). Hydrogen from renewables: Supply from North Africa to Central Europe as blend in existing pipelines – Potentials and costs. Applied Energy, 237(November 2018), 795–809. https://doi.org/10.1016/j.apenergy.2019.01.030

[44]   Tudu, B., Mandal, K. K., & Chakraborty, N. (2019). Optimal design and development of PV-wind-battery based nano-grid system: A field-on-laboratory demonstration. Frontiers in Energy, 13(2), 269–283. https://doi.org/10.1007/s11708-018-0573-z

[45]   Tutkun, N. (2014). Minimization of operational cost for an off-grid renewable hybrid system to generate electricity in residential buildings through the SVM and the BCGA methods. Energy and Buildings, 76, 470–475. https://doi.org/10.1016/j.enbuild.2014.03.003

[46]   Wang, R., Li, G., Ming, M., Wu, G., & Wang, L. (2017). An efficient multi-objective model and algorithm for sizing a stand-alone hybrid renewable energy system. Energy, 141, 2288–2299. https://doi.org/10.1016/j.energy.2017.11.085

[47]   Wang, Z., Wang, L., Dounis, A. I., & Yang, R. (2012). Integration of plug-in hybrid electric vehicles into energy and comfort management for smart building. Energy and Buildings, 47, 260–266. https://doi.org/10.1016/j.enbuild.2011.11.048

[48]   Wanjiru, E. M., Sichilalu, S. M., & Xia, X. (2017). Optimal control of heat pump water heater-instantaneous shower using integrated renewable-grid energy systems. Applied Energy, 201, 332–342. https://doi.org/10.1016/j.apenergy.2016.10.041

[49]   Wei, Y., Hou, X., Zhang, X., Xiong, S., & Peng, F. (2018). Performance optimization of a hybrid micro-grid based on double-loop MPPT and SVC-MERS. IOP Conference Series: Earth and Environmental Science, 121(4). https://doi.org/10.1088/1755-1315/121/4/042036

[50]   Restrepo-Garcés, A. R., Manotas-Duque, D. F., & Lozano, C. A. (2017). Multicriteria Hybrid Method - ROA, for the choice of generation of renewable sources: case study in shopping centers. Ingeniare. Revista Chilena de Ingeniería, 25(3), 399–414. https://doi.org/10.4067/s0718-33052017000300399

[51]   Rezvani, A., Esmaeily, A., Etaati, H., & Mohammadinodoushan, M. (2019). Intelligent hybrid power generation system using new hybrid fuzzy-neural for photovoltaic system and RBFNSM for wind turbine in the grid connected mode. Frontiers in Energy, 13(1), 131–148. https://doi.org/10.1007/s11708-017-0446-x

[52]   Roy, K., Krishna Mandal, K., Chandra Mandal, A., & Narayan Patra, S. (2018). Analysis of energy management in micro grid – A hybrid BFOA and ANN approach. Renewable and Sustainable Energy Reviews, 82(August 2017), 4296–4308. https://doi.org/10.1016/j.rser.2017.07.037

[53]   Sadati, S. M. S., Jahani, E., Taylan, O., & Baker, D. K. (2018). Sizing of Photovoltaic-Wind-Battery Hybrid System for a Mediterranean Island Community Based on Estimated and Measured Meteorological

Chapter 1
                                   A literature review and statistical analysis of
PV-wind hybrid renewable system researches by considering
the most relevant 550 articles: an upgradable matrix literature database

Data. Journal of Solar Energy Engineering, Transactions of the ASME, 140(1), 1–12. https://doi.org/10.1115/1.4038466

[54] Salkuti, S. R. (2019). Day-ahead thermal and renewable power generation scheduling considering uncertainty. Renewable Energy, 131, 956–965. https://doi.org/10.1016/j.renene.2018.07.106

[55] Sandhu, K. S., & Mahesh, A. (2018). Optimal sizing of PV/wind/battery hybrid renewable energy system considering demand side management. International Journal on Electrical Engineering and Informatics, 10(1), 79–93. https://doi.org/10.15676/ijeei.2018.10.1.6

[56] Santra, S. B., Kumar, K., Biswal, P., & Panigrahi, C. K. (2018). Lyapunov Based Fast Terminal Sliding Mode Q-V Control of Grid Connected Hybrid Solar PV and Wind System. IEEE Access, 6, 39139–39153. https://doi.org/10.1109/ACCESS.2018.2850453

[57] Sawle, Y., Gupta, S. C., & Bohre, A. K. (2018). A novel methodology for scrutiny of autonomous hybrid renewable energy system. International Journal of Energy Research, 42(2), 570–586. https://doi.org/10.1002/er.3841

[58] Sawle, Y., Gupta, S. C., & Bohre, A. K. (2018). Review of hybrid renewable energy systems with comparative analysis of off-grid hybrid system. Renewable and Sustainable Energy Reviews, 81(May 2017), 2217–2235. https://doi.org/10.1016/j.rser.2017.06.033

[59] Sawle, Y., Gupta, S. C., & Bohre, A. K. (2018). Socio-techno-economic design of hybrid renewable energy system using optimization techniques. Renewable Energy, 119, 459–472. https://doi.org/10.1016/j.renene.2017.11.058

[60] Shaik, A. G., & Mahela, O. P. (2018). Power quality assessment and event detection in hybrid power system. Electric Power Systems Research, 161, 26–44. https://doi.org/10.1016/j.epsr.2018.03.026

[61] Shaikh, P. H., Leghari, Z. H., Mirjat, N. H., Shaikh, F., Solangi, A. R., Jan, T., & Uqaili, M. A. (2018). Wind-PV-based hybrid DC microgrid (DCMG) development: An experimental investigation and comparative economic analysis. Energies, 11(5). https://doi.org/10.3390/en11051295

[62] Shaahid, S. M. (2011). Review of research on autonomous wind farms and solar parks and their feasibility for commercial loads in hot regions. Renewable and Sustainable Energy Reviews, 15(8), 3877–3887. https://doi.org/10.1016/j.rser.2011.07.017

[63] Stroe, D. I., Zaharof, A., & Iov, F. (2018). Power and energy management with battery storage for a hybrid residential PV-wind system - A case study for Denmark. Energy Procedia, 155, 464–477. https://doi.org/10.1016/j.egypro.2018.11.033

[64] Spiru, P., & Lizica-Simona, P. (2018). Technical and economical analysis of a PV/wind/diesel hybrid power system for a remote area. Energy Procedia, 147, 343–350. https://doi.org/10.1016/j.egypro.2018.07.102

[65] Giriantari, I. A. D., & Irawati, R. (2017). Smart microgrid system with hybrid system supply: Udayana university pilot project design. 2016 International Conference on Smart Green Technology in Electrical and Information Systems: Advancing Smart and Green Technology to Build Smart Society, ICSGTEIS 2016 - Proceedings, (October), 178–181. https://doi.org/10.1109/ICSGTEIS.2016.7885785

[66] Liu, W., Li, N., Jiang, Z., Chen, Z., Wang, S., Han, J., … Liu, C. (2018). Smart Micro-grid System with Wind/PV/Battery. Energy Procedia, 152, 1212–1217. https://doi.org/10.1016/j.egypro.2018.09.171

[67] Sharafi, M., & ElMekkawy, T. Y. (2015). Stochastic optimization of hybrid renewable energy systems using sampling average method. Renewable and Sustainable Energy Reviews, 52, 1668–1679. https://doi.org/10.1016/j.rser.2015.08.010

[68] Xiao, J., Zhao, T., Hai, K. L., & Wang, P. (2017). Smart energy hub - Modularized hybrid AC/DC microgrid: System design and deployment. 2017 IEEE Conference on Energy Internet and Energy System Integration, EI2 2017 - Proceedings, 2018-January, 1–6. https://doi.org/10.1109/EI2.2017.8245453

[69] Singh, R., Bansal, R. C., Singh, A. R., & Naidoo, R. (2018). Multi-Objective Optimization of Hybrid Renewable Energy System Using Reformed Electric System Cascade Analysis for Islanding and Grid

Chapter 1   **A literature review and statistical analysis of**
PV-wind hybrid renewable system researches by considering
the most relevant 550 articles: an upgradable matrix literature database

Connected   Modes   of   Operation.   IEEE   Access,   6,   47332–47354.
https://doi.org/10.1109/ACCESS.2018.2867276

[70]   Khan, A., Alghamdi, T. A., Khan, Z. A., Fatima, A., Abid, S., Khalid, A., & Javaid, N. (2019).
Enhanced Evolutionary Sizing Algorithms for Optimal Sizing of a Stand-Alone PV-WT-Battery Hybrid
System. Applied Sciences, 9(23), 5197. https://doi.org/10.3390/app9235197

[71]   Andalib-Bin-Karim, C., Liang, X., & Chowdhury, H. U. A. (2017). Generation reliability assessment
of stand-alone hybrid power system - A case study. Proceedings of the IEEE International Conference on
Industrial Technology, 434–439. https://doi.org/10.1109/ICIT.2017.7913270

[72]   Ghorbani, N., Kasaeian, A., Toopshekan, A., Bahrami, L., & Maghami, A. (2018). Optimizing a hybrid
wind-PV-battery system using GA-PSO and MOPSO for reducing cost and increasing reliability. Energy,
154, 581–591. https://doi.org/10.1016/j.energy.2017.12.057

[73]   Giallanza, A., Porretto, M., Puma, G. L., & Marannano, G. (2018). A sizing approach for stand-alone
hybrid photovoltaic-wind-battery systems: A Sicilian case study. Journal of Cleaner Production, 199, 817–
830. https://doi.org/10.1016/j.jclepro.2018.07.223

[74]   Gökçek, M., & Kale, C. (2018). Techno-economical evaluation of a hydrogen refuelling station
powered by Wind-PV hybrid power system: A case study for İzmir-çeşme. International Journal of
Hydrogen Energy, 43(23), 10615–10625. https://doi.org/10.1016/j.ijhydene.2018.01.082

[75]   Gonzalez, A., Riba, J. R., Esteban, B., & Rius, A. (2018). Environmental and cost optimal design of a
biomass–Wind–PV   electricity   generation   system.   Renewable   Energy,   126,   420–430.
https://doi.org/10.1016/j.renene.2018.03.062

[76]   Akinyele, D. O., Rayudu, R. K., Nair, N. K. C., 2015. Grid-independent renewable energy solutions
for residential use: The case of an off-grid house in wellington, New Zealand. In: 2015 IEEE PES Asia-
Pacific Power and Energy Engineering Conference (APPEEC), Brisbane, QLD, Australia, pp. 1-5, doi:
10.1109/APPEEC.2015.7380969.

[77]   Guangqian, D., Bekhrad, K., Azarikhah, P., & Maleki, A. (2018). A hybrid algorithm based
optimization on modeling of grid independent biodiesel-based hybrid solar/wind systems. Renewable
Energy, 122, 551–560. https://doi.org/10.1016/j.renene.2018.02.021

[78]   Ifaei, P., Farid, A., & Yoo, C. K. (2018). An optimal renewable energy management strategy with and
without hydropower using a factor weighted multi-criteria decision making analysis and nation-wide big
data - Case study in Iran. Energy, 158, 357–372. https://doi.org/10.1016/j.energy.2018.06.043

[79]   Wang, Z., Wang, L., Dounis, A. I., & Yang, R. (2011). Integration of plug-in hybrid electric vehicles
into building energy management system. IEEE Power and Energy Society General Meeting, 1–8.
https://doi.org/10.1109/PES.2011.6039275

[80]   Mazzeo, D., Matera, N., & Oliveti, G. (2018). Interaction between a Wind-PV-Battery-Heat Pump
Trigeneration System and Office Building Electric Energy Demand Including Vehicle Charging.
Proceedings - 2018 IEEE International Conference on Environment and Electrical Engineering and 2018
IEEE Industrial and Commercial Power Systems Europe, EEEIC/I and CPS Europe 2018.
https://doi.org/10.1109/EEEIC.2018.8493710

[81]   Jayalakshmi, N. S., & Gaonkar, D. N. (2017). An integrated control and management approach of
stand-alone hybrid wind/PV/battery power generation system with maximum power extraction capability.
Distributed   Generation   and   Alternative   Energy   Journal,   32(2),   7–26.
https://doi.org/10.1080/21563306.2017.11869107

[82]   Jeong, Y., Lee, M., & Kim, J. (2017). Scenario-Based Design and Assessment of renewable energy
supply   systems   for   green   building   applications.   Energy   Procedia,   136,   27–33.
https://doi.org/10.1016/j.egypro.2017.10.259

[83]   Galvan, E., Mandal, P., Haque, A. U., & Tseng, T. L. (Bill). (2017). Optimal Placement of Intermittent
Renewable Energy Resources and Energy Storage System in Smart Power Distribution Networks. Electric
Power Components and Systems, 45(14), 1543–1553. https://doi.org/10.1080/15325008.2017.1362605

Chapter 1

**A literature review and statistical analysis of
PV-wind hybrid renewable system researches by considering
the most relevant 550 articles: an upgradable matrix literature database**

[84]   Jurasz, J., Mikulik, J., Krzywda, M., Ciapała, B., & Janowski, M. (2018). Integrating a wind- and solar-powered hybrid to the power system by coupling it with a hydroelectric power station with pumping installation. Energy, 144, 549–563. https://doi.org/10.1016/j.energy.2017.12.011

[85]   Jurasz, J., Dąbek, P. B., Kaźmierczak, B., Kies, A., & Wdowikowski, M. (2018). Large scale complementary solar and wind energy sources coupled with pumped-storage hydroelectricity for Lower Silesia (Poland). Energy, 161, 183–192. https://doi.org/10.1016/j.energy.2018.07.085

[86]   Kartite, J., & Cherkaoui, M. (2018). What solution for Morocco: photovoltaic alone, wind alone or both? case study of Dakhla city. In SCA '18: Proceedings of the 3rd International Conference on Smart City Applications. ACM Proceedings, pp. 1–5,59, https://doi.org/10.1145/3286606.3286836.

[87]   Kaygusuz, A., Keles, C., Alagoz, B. B., & Karabiber, A. (2013). Renewable energy integration for smart sites. Energy and Buildings, 64, 456–462. https://doi.org/10.1016/j.enbuild.2013.05.031

[88]   Kazem, H. A., Al-Badi, H. A. S., Al Busaidi, A. S., & Chaichan, M. T. (2017). Optimum design and evaluation of hybrid solar/wind/diesel power system for Masirah Island. Environment, Development and Sustainability, 19(5), 1761–1778. https://doi.org/10.1007/s10668-016-9828-1

[89]   Khan, M. A., Zeb, K., Sathishkumar, P., Himanshu, L., Srinivasa Rao, S., Gopi, C. V. V. M., & Kim, H. J. (2018). A novel off-grid optimal hybrid energy system for rural electrification of Tanzania using a closed loop cooled solar system. Energies, 11(4), 1–22. https://doi.org/10.3390/en11040905

[90]   Khan, M. J., & Mathew, L. (2019). Fuzzy logic controller-based MPPT for hybrid photo-voltaic/wind/fuel cell power system. Neural Computing and Applications, 31(10), 6331–6344. https://doi.org/10.1007/s00521-018-3456-7

[91]   Cerone, A. (2015). Sefm 2015. International Conference on Software Engineering and Formal Methods, 9509, 139–144. https://doi.org/10.1007/978-3-662-49224-6

[92]   Iqbal, Z., Javaid, N., Iqbal, S., Aslam, S., Khan, Z. A., Abdul, W., … Alamri, A. (2018). A domestic microgrid with optimized home energy management system. Energies, 11(4), 1–39. https://doi.org/10.3390/en11041002

[93]   Marmouh, S., Boutoubat, M., & Mokrani, L. (2018). Performance and power quality improvement based on DC-bus voltage regulation of a stand-alone hybrid energy system. Electric Power Systems Research, 163, 73–84. https://doi.org/10.1016/j.epsr.2018.06.004

[94]   Duman, A. C., & Güler, Ö. (2018). Techno-economic analysis of off-grid PV/wind/fuel cell hybrid system combinations with a comparison of regularly and seasonally occupied households. Sustainable Cities and Society, 42(May), 107–126. https://doi.org/10.1016/j.scs.2018.06.029

[95]   He, L., Zhang, S., Chen, Y., Ren, L., & Li, J. (2018). Techno-economic potential of a renewable energy-based microgrid system for a sustainable large-scale residential community in Beijing, China. Renewable and Sustainable Energy Reviews, 93,631–641. https://doi.org/10.1016/j.rser.2018.05.053

[96]   Ogunjuyigbe, A. S. O., Ayodele, T. R., & Akinola, O. A. (2016). Optimal allocation and sizing of PV/Wind/Split-diesel/Battery hybrid energy system for minimizing life cycle cost, carbon emission and dump energy of remote residential building. Applied Energy, 171, 153–171. https://doi.org/10.1016/j.apenergy.2016.03.051

[97]   Olatomiwa, L., Blanchard, R., Mekhilef, S., & Akinyele, D. (2018). Hybrid renewable energy supply for rural healthcare facilities: An approach to quality healthcare delivery. Sustainable Energy Technologies and Assessments, 30(February), 121–138. https://doi.org/10.1016/j.seta.2018.09.007

[98]   Nakomčić-Smaragdakis, B. B., & Dragutinović, N. G. (2016). Hybrid renewable energy system application for electricity and heat supply of a residential building. Thermal Science, 20(2), 695–706. https://doi.org/10.2298/TSCI150505144N

[99]   Nayak, C. K., Kasturi, K., & Nayak, M. R. (2019). Economical management of microgrid for optimal participation in electricity market. Journal of Energy Storage, 21(December 2018), 657–664. https://doi.org/10.1016/j.est.2018.12.027

Chapter 1

**A literature review and statistical analysis of
PV-wind hybrid renewable system researches by considering
the most relevant 550 articles: an upgradable matrix literature database**

[100] Mazzeo, D., Baglivo, C., Matera, N., Congedo, P. M., & Oliveti, G. (2020). A novel energy-economic-environmental multi-criteria decision-making in the optimization of a hybrid renewable system. Sustainable Cities and Society, 52(July 2019), 101780. https://doi.org/10.1016/j.scs.2019.101780

[101] Nyeche, E. N., & Diemuodeke, E. O. (2020). Modelling and optimisation of a hybrid PV-wind turbine-pumped hydro storage energy system for mini-grid application in coastline communities. Journal of Cleaner Production, 250(xxxx), 119578. https://doi.org/10.1016/j.jclepro.2019.119578

[102] Nassourou, M., Puig, V., & Blesa, J. (2017). Robust Optimization based Energy Dispatch in Smart Grids Considering Simultaneously Multiple Uncertainties: Load Demands and Energy Prices. IFAC-PapersOnLine, 50(1), 6755–6760. https://doi.org/10.1016/j.ifacol.2017.08.1175

[103] Mohammed, O. H., Amirat, Y., & Benbouzid, M. (2018). Economical evaluation and optimal energy management of a stand-alone hybrid energy system handling in genetic algorithm strategies, 7(10). https://doi.org/10.3390/electronics7100233

[104] Bae, H., Choi, K., Park, T., Lee, S., & Lee, S. (2012). A battery management scheme for versatile power transfer in smart microgrids. 2012 IEEE Global High Tech Congress on Electronics, GHTCE 2012, 101–105. https://doi.org/10.1109/GHTCE.2012.6490133

[105] Prodanović, M., Gafurov, T., & Téllez, M. B. (2012). A demand based approach to optimisation of energy supply mix for smart buildings. 2012 IEEE PES Innovative Smart Grid Technologies, ISGT 2012, 1–8. https://doi.org/10.1109/ISGT.2012.6175731

[106] Buonomano, A., Calise, F., d'Accadia, M. D., & Vicidomini, M. (2018). A hybrid renewable system based on wind and solar energy coupled with an electrical storage: Dynamic simulation and economic assessment. Energy, 155, 174–189. https://doi.org/10.1016/j.energy.2018.05.006

[107] Baygi, S. M. H., Elahi, A., & Karsaz, A. (2018). A novel framework for optimal sizing of hybrid stand-alone renewable energy system: A gray Wolf optimizer. 3rd Conference on Swarm Intelligence and Evolutionary Computation, CSIEC 2018, 1–7. https://doi.org/10.1109/CSIEC.2018.8405415

[108] Soysal, O. A., & Soysal, H. S. (2008). A residential example of hybrid wind-solar Energy system: WISE. IEEE Power and Energy Society 2008 General Meeting: Conversion and Delivery of Electrical Energy in the 21st Century, PES, 1–5. https://doi.org/10.1109/PES.2008.4596536

[109] Aagreh, Y., & Al-Ghzawi, A. (2013). Feasibility of utilizing renewable energy systems for a small hotel in Ajloun city, Jordan. Applied Energy, 103, 25–31. https://doi.org/10.1016/j.apenergy.2012.10.008

[110] Abarkan, M., Errahimi, F., M'Sirdi, N. K., & Naamane, A. (2013). Analysis of energy consumption for a building using wind and solar energy sources. Energy Procedia, 42, 567–576. https://doi.org/10.1016/j.egypro.2013.11.058

[111] Abdallah, I., Gehin, A. L., & Ould Bouamama, B. (2018). Event driven Hybrid Bond Graph for Hybrid Renewable Energy Systems part I: Modelling and operating mode management. International Journal of Hydrogen Energy, 43(49), 22088–22107. https://doi.org/10.1016/j.ijhydene.2017.10.144

[112] Abdelkader, A., Rabeh, A., Mohamed Ali, D., & Mohamed, J. (2018). Multi-objective genetic algorithm based sizing optimization of a stand-alone wind/PV power supply system with enhanced battery/supercapacitor hybrid energy storage. Energy, 163, 351–363. https://doi.org/10.1016/j.energy.2018.08.135

[113] Abdullah, M. A., Muttaqi, K. M., & Agalgaonkar, A. P. (2015). Sustainable energy system design with distributed renewable resources considering economic, environmental and uncertainty aspects. Renewable Energy, 78, 165–172. https://doi.org/10.1016/j.renene.2014.12.044

[114] Boudoudouh, S., & Maaroufi, M. (2018). Agent-based self-adaptive DC-DC converter for hybrid energetic system control. Proceedings - 2018 6th International Istanbul Smart Grids and Cities Congress and Fair, ICSG 2018, 44–48. https://doi.org/10.1109/SGCF.2018.8408939

[115] Ahn, J., Kim, J. G., Seo, I. Y., Roh, J. H., Song, S. H., Song, J., … Kwak, H. Y. (2017). Thermoeconomic installation limit of PV/WT hybrid energy systems for Off-grid islands. International Journal of Green Energy, 14(11), 961–969. https://doi.org/10.1080/15435075.2017.1340296

Chapter 1   **A literature review and statistical analysis of**
PV-wind hybrid renewable system researches by considering
the most relevant 550 articles: an upgradable matrix literature database

[116]   Akinyele, D. (2017). Techno-economic design and performance analysis of nanogrid systems for households in energy-poor villages. Sustainable Cities and Society, 34, 335–357. https://doi.org/10.1016/j.scs.2017.07.004

[117]   Akram, U., Khalid, M., & Shafiq, S. (2017). An innovative hybrid wind-solar and battery-supercapacitor microgrid system—development and optimization. IEEE Access, 5, 25897–25912. https://doi.org/10.1109/ACCESS.2017.2767618

[118]   Alam, M., & Bhattacharyya, S. (2016). Decentralized renewable hybrid mini-grids for sustainable electrification of the off-grid coastal areas of Bangladesh. Energies, 9(4). https://doi.org/10.3390/en9040268

[119]   Al-Ghussain, L., Taylan, O., & Baker, D. K. (2019). An investigation of optimum PV and wind energy system capacities for alternate short and long-term energy storage sizing methodologies. International Journal of Energy Research, 43(1), 204–218. https://doi.org/10.1002/er.4251

[120]   Al-Ghussain, L., Ahmed, H., & Haneef, F. (2018). Optimization of hybrid PV-wind system: Case study Al-Tafilah cement factory, Jordan. Sustainable Energy Technologies and Assessments, 30, 24–36. https://doi.org/10.1016/j.seta.2018.08.008

[121]   Al-Ghussain, L., & Taylan, O. (2019). Sizing methodology of a PV/wind hybrid system: Case study in cyprus. Environmental Progress and Sustainable Energy, 38(3), 1–7. https://doi.org/10.1002/ep.13052

[122]   Al-Ghussain, L., Taylan, O., & Fahrioglu, M. (2018). Sizing of a Photovoltaic-Wind-Oil Shale Hybrid System: Case Analysis in Jordan. Journal of Solar Energy Engineering, Transactions of the ASME, 140(1), 1–12. https://doi.org/10.1115/1.4038048

[123]   Al-Hamdani, A. H., Dawood, A. F., Abdullah, K. N., Hasan, H. M., Sarhan, M., Shareef, H., & Tarik, R. (2018). Potential of Renewable Energy in Al-Fourat Al-Awsat: Al Najaf City Case Study. Journal of Physics: Conference Series, 1032(1). https://doi.org/10.1088/1742-6596/1032/1/012014

[124]   Alharthi, Y. Z., Siddiki, M. K., & Chaudhry, G. M. (2018). Resource assessment and techno-economic analysis of a grid-connected solar PV-wind hybrid system for different locations in Saudi Arabia. Sustainability (Switzerland), 10(10). https://doi.org/10.3390/su10103690

[125]   Alkhalidi, A., Qoaider, L., Khashman, A., Al-Alami, A. R., & Jiryes, S. (2018). Energy and water as indicators for sustainable city site selection and design in Jordan using smart grid. Sustainable Cities and Society, 37(November 2017), 125–132. https://doi.org/10.1016/j.scs.2017.10.037

[126]   Al-Masri, H. M. K., AbuElrub, A., Almehizia, A. A., & Ehsani, M. (2019). Multi-figure of merit optimization for global scale sustainable power systems. Renewable Energy, 134, 538–549. https://doi.org/10.1016/j.renene.2018.11.053

[127]   Al-Saadi, S., & Krarti, M. (2015). Evaluation of optimal hybrid distributed generation systems for an isolated rural settlement in masirah island, Oman. Distributed Generation and Alternative Energy Journal, 30(2), 23–42. https://doi.org/10.1080/21563306.2015.11431662

[128]   Ameer, B., & Krarti, M. (2017). Design of Carbon-Neutral Residential Communities in Kuwait. Journal of Solar Energy Engineering, Transactions of the ASME, 139(3), 1–12. https://doi.org/10.1115/1.4036054

[129]   Tutkun, N., & Celebi, N. (2017). An improved approach to minimise energy cost in a small wind-photovoltaic hybrid system. Proceedings of 2016 International Renewable and Sustainable Energy Conference, IRSEC 2016, 858–862. https://doi.org/10.1109/IRSEC.2016.7983981

[130]   Gafurov, T., Téllez, M. B., & Prodanović, M. (2011). An integrated approach to optimization of energy supply mix in smart buildings. IEEE PES Innovative Smart Grid Technologies Conference Europe, 1–8. https://doi.org/10.1109/ISGTEurope.2011.6162693

[131]   Ayoub, N., Musharavati, F., Pokharel, S., & Gabbar, H. A. (2018). ANN Model for Energy Demand and Supply Forecasting in a Hybrid Energy Supply System. 2018 6th IEEE International Conference on Smart Energy Grid Engineering, SEGE 2018, 25–30. https://doi.org/10.1109/SEGE.2018.8499514

Chapter 1   **A literature review and statistical analysis of**
PV-wind hybrid renewable system researches by considering
the most relevant 550 articles: an upgradable matrix literature database

[132]   Anoune, K., Laknizi, A., Bouya, M., Astito, A., & Ben Abdellah, A. (2018). Sizing a PV-Wind based hybrid system using deterministic approach. Energy Conversion and Management, 169(May), 137–148. https://doi.org/10.1016/j.enconman.2018.05.034

[133]   Arabzadeh Saheli, M., Fazelpour, F., Soltani, N., & Rosen, M. A. (2019). Performance analysis of a photovoltaic/wind/diesel hybrid power generation system for domestic utilization in winnipeg, manitoba, canada. Environmental Progress and Sustainable Energy, 38(2), 548–562. https://doi.org/10.1002/ep.12939

[134]   Ariyo, B. O., Akorede, M. F., Omeiza, I. O. A., Amuda, S. A. Y., & Oladeji, S. A. (2018). Optimisation analysis of a stand-alone hybrid energy system for the senate building, university of Ilorin, Nigeria. Journal of Building Engineering, 19(August 2017), 285–294. https://doi.org/10.1016/j.jobe.2018.05.015

[135]   Arnaoutakis, N., Kanellos, F., & Papaefthimiou, S. (2018). Combined operation, modeling and life cycle assessment of a generic hybrid power system installed in Crete. Energy Systems, 9(2), 343–359. https://doi.org/10.1007/s12667-017-0241-0

[136]   Arul, P. G., & Ramachandaramurthy, V. K. (2017). Mitigating techniques for the operational challenges of a standalone hybrid system integrating renewable energy sources. Sustainable Energy Technologies and Assessments, 22, 18–24. https://doi.org/10.1016/j.seta.2017.05.004

[137]   Bhandari, R., Gerstner, J., Belhassan, H., Gtz, D., & Hausmann, H. (2018). Autonomous Electricity Supply with Hybrid Renewable Configuration in Ghana. 2018 7th International Energy and Sustainability Conference, IESC 2018. https://doi.org/10.1109/IESC.2018.8439991

[138]   Awan, A. B., Zubair, M., Sidhu, G. A. S., Bhatti, A. R., & Abo-Khalil, A. G. (2019). Performance analysis of various hybrid renewable energy systems using battery, hydrogen, and pumped hydro-based storage units. International Journal of Energy Research, 43(12), 6296–6321. https://doi.org/10.1002/er.4343

[139]   Bagheri, M., Shirzadi, N., Bazdar, E., & Kennedy, C. A. (2018). Optimal planning of hybrid renewable energy infrastructure for urban sustainability: Green Vancouver. Renewable and Sustainable Energy Reviews, 95(November 2017), 254–264. https://doi.org/10.1016/j.rser.2018.07.037

[140]   Bartolucci, L., Cordiner, S., Mulone, V., Rocco, V., & Rossi, J. L. (2018). Renewable source penetration and microgrids: Effects of MILP – Based control strategies. Energy, 152, 416–426. https://doi.org/10.1016/j.energy.2018.03.145

[141]   Behravesh, V., Keypour, R., & Foroud, A. A. (2018). Stochastic analysis of solar and wind hybrid rooftop generation systems and their impact on voltage behavior in low voltage distribution systems. Solar Energy, 166(June 2017), 317–333. https://doi.org/10.1016/j.solener.2018.03.063

[142]   Behzadi Forough, A., & Roshandel, R. (2017). Multi objective receding horizon optimization for optimal scheduling of hybrid renewable energy system. Energy and Buildings, 150, 583–597. https://doi.org/10.1016/j.enbuild.2017.06.031

[143]   Beke, T., 2015. A simple model for the energy supply of a stand-alone house using a hybrid wind–solar power system. European Journal of Physics 37 (1), 143–148. doi:10.1088/0143-0807/37/1/015804.

[144]   Belouda, M., Hajjaji, M., Sliti, H., & Mami, A. (2018). Bi-objective optimization of a standalone hybrid PV–Wind–battery system generation in a remote area in Tunisia. Sustainable Energy, Grids and Networks, 16, 315–326. https://doi.org/10.1016/j.segan.2018.09.005

[145]   Benali, A., Khiat, M., Allaoui, T., & Denaï, M. (2018). Power Quality Improvement and Low Voltage Ride Through Capability in Hybrid Wind-PV Farms Grid-Connected Using Dynamic Voltage Restorer. IEEE Access, 6, 68634–68648. https://doi.org/10.1109/ACCESS.2018.2878493

[146]   Beshr, E. H., Abdelghany, H., & Eteiba, M. (2018). Novel optimization technique of isolated microgrid with hydrogen energy storage. PLoS ONE, 13(2), 1–17. https://doi.org/10.1371/journal.pone.0193224

[147]   Bhattacharjee, S., & Acharya, S. (2015). PV-wind hybrid power option for a low wind topography. Energy Conversion and Management, 89, 942–954. https://doi.org/10.1016/j.enconman.2014.10.065

Chapter 1
A literature review and statistical analysis of
PV-wind hybrid renewable system researches by considering
the most relevant 550 articles: an upgradable matrix literature database

[148] Bouchebbat, R., & Gherbi, S. (2017). A Novel Optimal Control and Management Strategy of Stand-Alone Hybrid PV/Wind/Diesel Power System. Journal of Control, Automation and Electrical Systems, 28(2), 284–296. https://doi.org/10.1007/s40313-016-0290-y

[149] Boussetta, M., El Bachtiri, R., Khanfara, M., & El Hammoumi, K. (2017). Assessing the potential of hybrid PV–Wind systems to cover public facilities loads under different Moroccan climate conditions. Sustainable Energy Technologies and Assessments, 22, 74–82. https://doi.org/10.1016/j.seta.2017.07.005

[150] Brinda, M. D., Suresh, A., & Rashmi, M. R. (2019). Optimal sizing and distribution system reconfiguration of hybrid FC/WT/PV system using cluster computing based on harmony search algorithm. Cluster Computing, 22, 6849–6854. https://doi.org/10.1007/s10586-017-1605-x

[151] Dagdougui, H., Minciardi, R., Ouammi, A., Robba, M., & Sacile, R. (2012). Modeling and optimization of a hybrid system for the energy supply of a "green" building. Energy Conversion and Management, 64, 351–363. https://doi.org/10.1016/j.enconman.2012.05.017

[152] Dekkiche, M., Tahri, T., Bettahar, A., & Belmadani, B. (2017). Weather data analysis and optimal design of hybrid pv-wind-diesel power system for a village in Chlef, Algeria. Desalination and Water Treatment, 79, 125–134. https://doi.org/10.5004/dwt.2017.20714

[153] Fernando, W., Gupta, N., Linn, H. H., & Ozveren, C. S. (2018). Design of optimum configuration of a hybrid power system for Abertay University campus. Proceedings of the 2018 IEEE Conference of Russian Young Researchers in Electrical and Electronic Engineering, ElConRus 2018, 1795–1800. https://doi.org/10.1109/EIConRus.2018.8317454

[154] Diemuodeke, E. O., Addo, A., Oko, C. O. C., Mulugetta, Y., & Ojapah, M. M. (2019). Optimal mapping of hybrid renewable energy systems for locations using multi-criteria decision-making algorithm. Renewable Energy, 134, 461–477. https://doi.org/10.1016/j.renene.2018.11.055

[155] Elhadidy, M. A. (2002). Performance evaluation of hybrid (wind/solar/diesel) power systems. Renewable Energy, 26(3), 401–413. https://doi.org/10.1016/S0960-1481(01)00139-2

[156] Elhadidy, M. A., & Shaahid, S. M. (2004). Promoting applications of hybrid (wind+photovoltaic+diesel+battery) power systems in hot regions. Renewable Energy, 29(4), 517–528. https://doi.org/10.1016/j.renene.2003.08.001

[157] Elma, O., & Selamogullari, U. S. (2012). A comparative sizing analysis of a renewable energy supplied stand-alone house considering both demand side and source side dynamics. Applied Energy, 96, 400–408. https://doi.org/10.1016/j.apenergy.2012.02.080

[158] Eltamaly, A. M., Mohamed, M. A., Al-Saud, M. S., & Alolah, A. I. (2017). Load management as a smart grid concept for sizing and designing of hybrid renewable energy systems. Engineering Optimization, 49(10), 1813–1828. https://doi.org/10.1080/0305215X.2016.1261246

[159] Erdinc, O., Elma, O., Uzunoglu, M., Selamogullari, U. S., Vural, B., Ugur, E., … Dusmez, S. (2012). Experimental performance assessment of an online energy management strategy for varying renewable power production suppression. International Journal of Hydrogen Energy, 37(6), 4737–4748. https://doi.org/10.1016/j.ijhydene.2011.12.042

[160] Escalante Soberanis, M. A., Mithrush, T., Bassam, A., & Mérida, W. (2018). A sensitivity analysis to determine technical and economic feasibility of energy storage systems implementation: A flow battery case study. Renewable Energy, 115, 547–557. https://doi.org/10.1016/j.renene.2017.08.082

[161] Hailu Kebede, M., & Bekele Beyene, G. (2018). Feasibility Study of PV-Wind-Fuel Cell Hybrid Power System for Electrification of a Rural Village in Ethiopia. Journal of Electrical and Computer Engineering, 2018. https://doi.org/10.1155/2018/4015354

[162] Hamilton, J., Negnevitsky, M., Wang, X., & Lyden, S. (2019). High penetration renewable generation within Australian isolated and remote power systems. Energy, 168, 684–692. https://doi.org/10.1016/j.energy.2018.11.118

Chapter 1   **A literature review and statistical analysis of**
PV-wind hybrid renewable system researches by considering
the most relevant 550 articles: an upgradable matrix literature database

[163]   Haratian, M., Tabibi, P., Sadeghi, M., Vaseghi, B., & Poustdouz, A. (2018). A renewable energy solution for stand-alone power generation: A case study of KhshU Site-Iran. Renewable Energy, 125, 926–935. https://doi.org/10.1016/j.renene.2018.02.078

[164]   Hatata, A. Y., Osman, G., & Aladl, M. M. (2018). An optimization method for sizing a solar/wind/battery hybrid power system based on the artificial immune system. Sustainable Energy Technologies and Assessments, 27(December 2017), 83–93. https://doi.org/10.1016/j.seta.2018.03.002

[165]   Hemanand, T., Subramaniam, N. P., & Venkateshkumar, M. (2018). Comparative analysis of intelligent controller based microgrid integration of hybrid PV/wind power system. Journal of Ambient Intelligence and Humanized Computing,https://doi.org/10.1007/s12652-018-0961-6

[166]   Hu, J., Shan, Y., Xu, Y., & Guerrero, J. M. (2019). A coordinated control of hybrid ac/dc microgrids with PV-wind-battery under variable generation and load conditions. International Journal of Electrical Power and Energy Systems, 104(April 2018), 583–592. https://doi.org/10.1016/j.ijepes.2018.07.037

[167]   Rathore, A. K. (2012). Hybrid micro-grid (μG) Based residential utility interfaced smart energy system: Applications for green data centers and commercial buildings. Proceedings of the 2012 7th IEEE Conference on Industrial Electronics and Applications, ICIEA 2012, 2063–2068. https://doi.org/10.1109/ICIEA.2012.6361070

[168]   Gioutsos, D. M., Blok, K., van Velzen, L., & Moorman, S. (2018). Cost-optimal electricity systems with increasing renewable energy penetration for islands across the globe. Applied Energy, 226, 437–449. https://doi.org/10.1016/j.apenergy.2018.05.108

[169]   Broy, A., & Sourkounis, C. (2014). Guidelines for renewable energy based supply system for various types of buildings. ENERGYCON 2014 - IEEE International Energy Conference, 968–974. https://doi.org/10.1109/ENERGYCON.2014.6850543

[170]   Aki, H. (2010). Independent hybrid renewable energy systems: Example applications around the world. IEEE PES General Meeting, PES 2010, 1–4. https://doi.org/10.1109/PES.2010.5589565

[171]   Arun, S. L., & Selvan, M. P. (2018). for Dynamic Demand Response in Smart Buildings. IEEE Systems Journal, 12(2), 1329–1340. https://doi.org/10.1109/JSYST.2017.2647759

[172]   Kabalcı, E. (2018). An islanded hybrid microgrid design with decentralized DC and AC subgrid controllers. Energy, 153, 185–199. https://doi.org/10.1016/j.energy.2018.04.060

[173]   Mazur, M., Partyka, J., & Rakhimov, K. (2014). Analiza możliwości wykorzystania hybrydowego autonomicznego systemu zasilania w budynku mieszkalnym. Przeglad Elektrotechniczny, 90(3), 207–210. https://doi.org/10.12915/pe.2014.03.47

[174]   Mekhamer, S., Abdelaziz, A., & Algabalawy, M. (2018). Design of hybrid power generation systems connected to utility grid and natural gas distribution network: A new contribution. Engineering Review, 38(2), 204–214. https://doi.org/10.30765/er.38.2.8

[175]   Mendoza-Vizcaino, J., Sumper, A., & Galceran-Arellano, S. (2017). PV, wind and storage integration on small islands for the fulfilment of the 50-50 renewable electricity generation target. Sustainability (Switzerland), 9(6). https://doi.org/10.3390/su9060905

[176]   Kemper, P., & Witkowski, U. (2017). Model Based Design of a Renewable Energy Supply with Hybrid Energy Storage System. Proceedings - UKSim-AMSS 2016: 10th European Modelling Symposium on Computer Modelling and Simulation, 117–123. https://doi.org/10.1109/EMS.2016.030

[177]   Mohamed, M. A., Eltamaly, A. M., Alolah, A. I., & Hatata, A. Y. (2019). A novel framework-based cuckoo search algorithm for sizing and optimization of grid-independent hybrid renewable energy systems. International Journal of Green Energy, 16(1), 86–100. https://doi.org/10.1080/15435075.2018.1533837

[178]   Mohammadi, M., Ghasempour, R., Razi Astaraei, F., Ahmadi, E., Aligholian, A., & Toopshekan, A. (2018). Optimal planning of renewable energy resource for a residential house considering economic and reliability criteria. International Journal of Electrical Power and Energy Systems, 96, 261–273. https://doi.org/10.1016/j.ijepes.2017.10.017

Chapter 1

A literature review and statistical analysis of PV-wind hybrid renewable system researches by considering the most relevant 550 articles: an upgradable matrix literature database

[179] Muh, E., & Tabet, F. (2019). Comparative analysis of hybrid renewable energy systems for off-grid applications in Southern Cameroons. Renewable Energy, 135, 41–54. https://doi.org/10.1016/j.renene.2018.11.105

[180] Mumtaz, S., & Khan, L. (2017). Adaptive control paradigm for photovoltaic and solid oxide fuel cell in a grid-integrated hybrid renewable energy system. PLoS ONE (Vol. 12). https://doi.org/10.1371/journal.pone.0173966

[181] Mazzeo, D. (2019). Solar and wind assisted heat pump to meet the building air conditioning and electric energy demand in the presence of an electric vehicle charging station and battery storage. Journal of Cleaner Production, 213, 1228–1250. https://doi.org/10.1016/j.jclepro.2018.12.212

[182] Mazzeo, D., Oliveti, G., Baglivo, C., & Congedo, P. M. (2018). Energy reliability-constrained method for the multi-objective optimization of a photovoltaic-wind hybrid system with battery storage. Energy, 156, 688–708. https://doi.org/10.1016/j.energy.2018.04.062

[183] Xiao, Z. xia, Guerrero, J. M., Shuang, J., Sera, D., Schaltz, E., & Vásquez, J. C. (2018). Flat tie-line power scheduling control of grid-connected hybrid microgrids. Applied Energy, 210, 786–799. https://doi.org/10.1016/j.apenergy.2017.07.066

[184] Yang, Y., Bremner, S., Menictas, C., Meng, K., Dong, Z. Y., & Kay, M. (2018). An economic optimization for BESS sizing in a hybrid PV and wind power plant. 2017 IEEE Innovative Smart Grid Technologies - Asia: Smart Grid for Smart Community, ISGT-Asia 2017, 1–6. https://doi.org/10.1109/ISGT-Asia.2017.8378353

[185] Yanine, F. F., Caballero, F. I., Sauma, E. E., & Córdova, F. M. (2014). Homeostatic control, smart metering and efficient energy supply and consumption criteria: A means to building more sustainable hybrid micro-generation systems. Renewable and Sustainable Energy Reviews, 38, 235–258. https://doi.org/10.1016/j.rser.2014.05.078

[186] Yimen, N., Hamandjoda, O., Meva'a, L., Ndzana, B., & Nganhou, J. (2018). Analyzing of a photovoltaic/wind/biogas/pumped-hydro off-grid hybrid system for rural electrification in Sub-Saharan Africa - Case study of Djoundé in Northern Cameroon. Energies, 11(10). https://doi.org/10.3390/en11102644

[187] Yousef, H., Al-Badi, A. H., & Polycarpou, A. (2018). Power management for hybrid distributed generation systems. International Journal of Sustainable Engineering, 11(1), 65–74. https://doi.org/10.1080/19397038.2017.1387825

[188] Zafar, S., & Dincer, I. (2014). Energy, exergy and exergoeconomic analyses of a combined renewable energy system for residential applications. Energy and Buildings, 71, 68–79. https://doi.org/10.1016/j.enbuild.2013.12.006

[189] Zaibi, M., Champenois, G., Roboam, X., Belhadj, J., & Sareni, B. (2018). Smart power management of a hybrid photovoltaic/wind stand-alone system coupling battery storage and hydraulic network. Mathematics and Computers in Simulation, 146, 210–228. https://doi.org/10.1016/j.matcom.2016.08.009

[190] Zailan, R., Zaini, S. N., Mohd Rashid, M. I., & Abdul Razak, A. (2017). Feasibility Study of Standalone PV-Wind-Diesel Energy Systems for Coastal Residential Application in Pekan, Pahang. MATEC Web of Conferences, 131, 0–5. https://doi.org/10.1051/matecconf/201713102001

[191] Zebraoui, O., & Bouzi, M. (2018). Robust sliding mode control based MPPT for a PV/Wind hybrid energy system. International Journal of Intelligent Engineering and Systems, 11(5), 290–300. https://doi.org/10.22266/IJIES2018.1031.27

[192] Zhang, Y., Yan, Z., Li, L., & Yao, J. (2018). A hybrid building power distribution system in consideration of supply and demand-side: A short overview and a case study. Energies, 11(1). https://doi.org/10.3390/en11113082

[193] Zhu, Z., Liu, D., Liao, Q., Tang, F., Zhang, J. J., & Jiang, H. (2018). Optimal power scheduling for a medium voltage AC/DC hybrid distribution network. Sustainability (Switzerland), 10(2), 1–22. https://doi.org/10.3390/su10020318

Chapter 1

A literature review and statistical analysis of PV-wind hybrid renewable system researches by considering the most relevant 550 articles: an upgradable matrix literature database

[194]   Zubair, M., Bilal Awan, A., Al-Ahmadi, A., & Ahmed, G. A. K. (2018). NPC based design optimization for a net zero office building in hot climates with pv panels as shading device. Energies, 11(6). https://doi.org/10.3390/en11061391

[195]   Sharafi, M., ElMekkawy, T. Y., & Bibeau, E. L. (2015). Optimal design of hybrid renewable energy systems in buildings with low to high renewable energy ratio. Renewable Energy, 83, 1026–1042. https://doi.org/10.1016/j.renene.2015.05.022

[196]   Sharma, H., Pal, N., Kumar, P., & Yadav, A. (2017). A control strategy of hybrid solar-wind energy generation system. Archives of Electrical Engineering, 66(2), 241–251. https://doi.org/10.1515/aee-2017-0018

[197]   Shi, Z. S., Wang, R., Zhang, X. Y., Zhang, Y., & Zhang, T. (2017). Optimal design of grid-connected hybrid renewable energy systems using multi-objective evolutionary algorithm. Scientia Iranica, 24(6), 3148–3156. https://doi.org/10.24200/sci.2017.4578

[198]   Sigarchian, S. G., Malmquist, A., & Fransson, T. (2014). Modeling and control strategy of a hybrid PV/Wind/Engine/Battery system to provide electricity and drinkable water for remote applications. Energy Procedia, 57, 1401–1410. https://doi.org/10.1016/j.egypro.2014.10.087

[199]   Shin, Y., Koo, W. Y., Kim, T. H., Jung, S., & Kim, H. (2015). Capacity design and operation planning of a hybrid PV-wind-battery-diesel power generation system in the case of Deokjeok Island. Applied Thermal Engineering, 89, 514–525. https://doi.org/10.1016/j.applthermaleng.2015.06.043

[200]   Jarrou, A., & Sauter, D. (2017). Simulation, analysis and identification of a Renewable energy system. Proceedings - 2017 IEEE 15th International New Circuits and Systems Conference, NEWCAS 2017, 401–404. https://doi.org/10.1109/NEWCAS.2017.8010190

[201]   Singh, A., & Letha, S. S. (2019). Emerging energy sources for electric vehicle charging station. Environment, Development and Sustainability, 21(5), 2043–2082. https://doi.org/10.1007/s10668-018-0151-x

[202]   Singh, G., Baredar, P., Singh, A., & Kurup, D. (2017). Optimal sizing and location of PV, wind and battery storage for electrification to an island: A case study of Kavaratti, Lakshadweep. Journal of Energy Storage, 12, 78–86. https://doi.org/10.1016/j.est.2017.04.003

[203]   Swartz, J., Ghofrani, A., & Jafari, M. (2017). Sizing methodology for combined renewable energy systems. 2017 IEEE Power and Energy Society Innovative Smart Grid Technologies Conference, ISGT 2017. https://doi.org/10.1109/ISGT.2017.8085958

[204]   Sreeraj, E. S., Chatterjee, K., & Bandyopadhyay, S. (2010). Design of isolated renewable hybrid power systems. Solar Energy, 84(7), 1124–1136. https://doi.org/10.1016/j.solener.2010.03.017

[205]   McGowan, J. G., & Manwell, J. F. (1999). Hybrid wind/pv/diesel system experiences. Renewable Energy, 16(1-4–4 pt 2), 928–933. https://doi.org/10.1016/S0960-1481(98)00319-X

[206]   Campana, P. E., Wästhage, L., Nookuea, W., Tan, Y., & Yan, J. (2019). Optimization and assessment of floating and floating-tracking PV systems integrated in on- and off-grid hybrid energy systems. Solar Energy, 177, 782–795. https://doi.org/10.1016/j.solener.2018.11.045

[207]   Cao, S., & Alanne, K. (2015). Technical feasibility of a hybrid on-site H2 and renewable energy system for a zero-energy building with a H2 vehicle. Applied Energy, 158, 568–583. https://doi.org/10.1016/j.apenergy.2015.08.009

[208]   Chen, P. J., & Wang, F. C. (2018). Design optimization for the hybrid power system of a green building. International Journal of Hydrogen Energy, 43(4), 2381–2393. https://doi.org/10.1016/j.ijhydene.2017.12.020

[209]   Coma, E., & Jones, P. (2015). "Buildings as Power Stations": an energy simulation tool for housing. Procedia Engineering, 118, 58–71. https://doi.org/10.1016/j.proeng.2015.08.404

[210]   Cao, S., & Alanne, K. (2018). The techno-economic analysis of a hybrid zero-emission building system integrated with a commercial-scale zero-emission hydrogen vehicle. Applied Energy, 211, 639–661. https://doi.org/10.1016/j.apenergy.2017.11.079

Chapter 1

A literature review and statistical analysis of PV-wind hybrid renewable system researches by considering the most relevant 550 articles: an upgradable matrix literature database

[211] Faquir, S., Yahyaouy, A., Tairi, H., & Sabor, J. (2018). Energy Management of An Extended Hybrid Renewable Energy System for Isolated Sites Using A Fuzzy Logic Controller. IOP Conference Series: Materials Science and Engineering, 353(1). https://doi.org/10.1088/1757-899X/353/1/012025

[212] Farahi, S., & Fazelpour, F. (2019). Techno-economic assessment of employing hybrid power system for residential, public, and commercial buildings in different climatic conditions of Iran. Environmental Progress and Sustainable Energy, 38(2), 614–623. https://doi.org/10.1002/ep.12961

[213] Fathabadi, H. (2018). Novel high-efficient large-scale stand-alone solar/wind hybrid power source equipped with battery bank used as storage device. Journal of Energy Storage, 17(November 2017), 485–495. https://doi.org/10.1016/j.est.2018.04.008

[214] Fathima, A. H., Palanisamy, K., Padmanaban, S., & Subramaniam, U. (2018). Intelligence-based battery management and economic analysis of an optimized dual-Vanadium Redox Battery (VRB) for a wind-PV hybrid system. Energies, 11(10). https://doi.org/10.3390/en11102785

[215] Hasan, K., Fatima, K., & Sohel Mahmood, M. (2011). Feasibility of hybrid power generation over wind and solar standalone system. 2011 5th International Power Engineering and Optimization Conference, PEOCO 2011 - Program and Abstracts, (June), 139–143. https://doi.org/10.1109/PEOCO.2011.5970430

[216] Feng, H., Tian, X., Cao, S., Zhao, J., & Deng, S. (2016). Match performance analysis for a solar-driven energy system in net zero energy building. Energy Procedia, 88, 394–400. https://doi.org/10.1016/j.egypro.2016.06.010

[217] Forough, A. B., & Roshandel, R. (2018). Lifetime optimization framework for a hybrid renewable energy system based on receding horizon optimization. Energy, 150, 617–630. https://doi.org/10.1016/j.energy.2018.02.158

[218] Fulzele, J. B., & Daigavane, M. B. (2018). Design and Optimization of Hybrid PV-Wind Renewable Energy System. Materials Today: Proceedings, 5(1), 810–818. https://doi.org/10.1016/j.matpr.2017.11.151

[219] Javed, M. S., Song, A., & Ma, T. (2019). Techno-economic assessment of a stand-alone hybrid solar-wind-battery system for a remote island using genetic algorithm. Energy, 176, 704–717. https://doi.org/10.1016/j.energy.2019.03.131

[220] Padrón, I., Avila, D., Marichal, G. N., & Rodríguez, J. A. (2019). Assessment of Hybrid Renewable Energy Systems to supplied energy to Autonomous Desalination Systems in two islands of the Canary Archipelago. Renewable and Sustainable Energy Reviews, 101(October 2018), 221–230. https://doi.org/10.1016/j.rser.2018.11.009

[221] Samy, M. M., Barakat, S., & Ramadan, H. S. (2020). Techno-economic analysis for rustic electrification in Egypt using multi-source renewable energy based on PV/ wind/ FC. International Journal of Hydrogen Energy, 45(20), 11471–11483. https://doi.org/10.1016/j.ijhydene.2019.04.038

[222] Krishan, O., & Suhag, S. (2019). Techno-economic analysis of a hybrid renewable energy system for an energy poor rural community. Journal of Energy Storage, 23, 305–319. https://doi.org/10.1016/j.est.2019.04.002

[223] Diaf, S., Notton, G., Belhamel, M., Haddadi, M., & Louche, A. (2008). Design and techno-economical optimization for hybrid PV/wind system under various meteorological conditions. Applied Energy, 85(10), 968–987. https://doi.org/10.1016/j.apenergy.2008.02.012

[224] Sharafi, M., & ELMekkawy, T. Y. (2014). Multi-objective optimal design of hybrid renewable energy systems using PSO-simulation based approach. Renewable Energy, 68, 67–79. https://doi.org/10.1016/j.renene.2014.01.011

[225] Sawle, Y., Gupta, S. C., & Bohre, A. K. (2017). Optimal sizing of standalone PV/Wind/Biomass hybrid energy system using GA and PSO optimization technique. Energy Procedia, 117, 690–698. https://doi.org/10.1016/j.egypro.2017.05.183

Chapter 1   **A literature review and statistical analysis of**
PV-wind hybrid renewable system researches by considering
the most relevant 550 articles: an upgradable matrix literature database

[226]   Bakić, V., Pezo, M., Stevanović, Ž., Živković, M., & Grubor, B. (2012). Dynamical simulation of PV/Wind hybrid energy conversion system. Energy, 45(1), 324–328. https://doi.org/10.1016/j.energy.2011.11.063

[227]   Mohammed, O. H., Amirat, Y., & Benbouzid, M. (2019). Particle swarm optimization of a hybrid wind/tidal/PV/battery energy system. Application to a remota area in Bretagne, France. Energy Procedia, 162, 87–96. https://doi.org/10.1016/j.egypro.2019.04.010

[228]   Razmjoo, A., Shirmohammadi, R., Davarpanah, A., Pourfayaz, F., & Aslani, A. (2019). Stand-alone hybrid energy systems for remote area power generation. Energy Reports, 5, 231–241. https://doi.org/10.1016/j.egyr.2019.01.010

[229]   Akhtari, M. R., & Baneshi, M. (2019). Techno-economic assessment and optimization of a hybrid renewable co-supply of electricity, heat and hydrogen system to enhance performance by recovering excess electricity for a large energy consumer. Energy Conversion and Management, 188, 131–141. https://doi.org/10.1016/j.enconman.2019.03.067

[230]   Gebrehiwot, K., Mondal, M. A. H., Ringler, C., & Gebremeskel, A. G. (2019). Optimization and cost-benefit assessment of hybrid power systems for off-grid rural electrification in Ethiopia. Energy, 177, 234–246. https://doi.org/10.1016/j.energy.2019.04.095

[231]   Dihrab, S. S., & Sopian, K. (2010). Electricity generation of hybrid PV/wind systems in Iraq. Renewable Energy, 35(6), 1303–1307. https://doi.org/10.1016/j.renene.2009.12.010

[232]   Maleki, A., Ameri, M., & Keynia, F. (2015). Scrutiny of multifarious particle swarm optimization for finding the optimal size of a PV/wind/battery hybrid system. Renewable Energy, 80, 552–563. https://doi.org/10.1016/j.renene.2015.02.045

[233]   Rehman, S., Mahbub Alam, M., Meyer, J. P., & Al-Hadhrami, L. M. (2012). Feasibility study of a wind-pv-diesel hybrid power system for a village. Renewable Energy, 38(1), 258–268. https://doi.org/10.1016/j.renene.2011.06.028

[234]   Nandi, S. K., & Ghosh, H. R. (2010). Prospect of wind-PV-battery hybrid power system as an alternative to grid extension in Bangladesh. Energy, 35(7), 3040–3047. https://doi.org/10.1016/j.energy.2010.03.044

[235]   Li, C., Ge, X., Zheng, Y., Xu, C., Ren, Y., Song, C., & Yang, C. (2013). Techno-economic feasibility study of autonomous hybrid wind/PV/battery power system for a household in Urumqi, China. Energy, 55, 263–272. https://doi.org/10.1016/j.energy.2013.03.084

[236]   Ngan, M. S., & Tan, C. W. (2012). Assessment of economic viability for PV/wind/diesel hybrid energy system in southern Peninsular Malaysia. Renewable and Sustainable Energy Reviews, 16(1), 634–647. https://doi.org/10.1016/j.rser.2011.08.028

[237]   Ould Bilal, B., Sambou, V., Ndiaye, P. A., Kébé, C. M. F., & Ndongo, M. (2013). Study of the influence of load profile variation on the optimal sizing of a standalone hybrid PV/Wind/Battery/Diesel system. Energy Procedia, 36, 1265–1275. https://doi.org/10.1016/j.egypro.2013.07.143

[238]   Maleki, A., & Askarzadeh, A. (2014). Optimal sizing of a PV/wind/diesel system with battery storage for electrification to an off-grid remote region: A case study of Rafsanjan, Iran. Sustainable Energy Technologies and Assessments, 7, 147–153. https://doi.org/10.1016/j.seta.2014.04.005

[239]   Sultan, H. M., Zaki Diab, A. A., Kuznetsov Oleg, N., & Zubkova Irina, S. (2018). Design and evaluation of PV-wind hybrid system with hydroelectric pumped storage on the National Power System of Egypt. Global Energy Interconnection, 1(3), 301–311. https://doi.org/10.14171/j.2096-5117.gei.2018.03.001

[240]   Hemeida, A. M., El-Ahmar, M. H., El-Sayed, A. M., Hasanien, H. M., Alkhalaf, S., Esmail, M. F. C., & Senjyu, T. (2020). Optimum design of hybrid wind/PV energy system for remote area. Ain Shams Engineering Journal, 11(1), 11–23. https://doi.org/10.1016/j.asej.2019.08.005

Chapter 1   **A literature review and statistical analysis of**
PV-wind hybrid renewable system researches by considering
the most relevant 550 articles: an upgradable matrix literature database

[241] Bianchini, A., Magnelli, N., Ferrara, G., Carnevale, E. A., & Ferrari, L. (2015). Optimization of a PV-wind-diesel hybrid system for a remote stand-alone application. Energy Procedia, 81, 133–145. https://doi.org/10.1016/j.egypro.2015.12.068

[242] Seraphim, O. J., Siqueira, J. A. C., Putti, F. F., Filho, L. R. A. G., Cremasco, C. P., & Daltin, R. S. (2014). Energetic exploitation from a hybrid pvwind power micro-generation rural electrification. Energy Procedia, 57, 1475–1484. https://doi.org/10.1016/j.egypro.2014.10.092

[243] Abu-Hijleh, B. (2016). Use of Hybrid PV and Wind Turbine - Grid Connected System in a Local Emirati Home in Dubai-UAE. Energy Procedia, 100, 463–468. https://doi.org/10.1016/j.egypro.2016.10.203

[244] Maouedj, R., Mammeri, A., Draou, M. D., & Benyoucef, B. (2014). Performance evaluation of hybrid photovoltaic-wind power systems. Energy Procedia, 50, 797–807. https://doi.org/10.1016/j.egypro.2014.06.098

[245] Petras Baršauskas, Tadas Šarapovas, Aurelijus Cvilikas, (2008) "The evaluation of e-commerce impact on business efficiency", Baltic Journal of Management, Vol. 3 Issue: 1, pp.71-91, doi:10.1108/17465260810844275.

[246] Vick, B. D., & Neal, B. A. (2012). Analysis of off-grid hybrid wind turbine/solar PV water pumping systems. Solar Energy, 86(5), 1197–1207. https://doi.org/10.1016/j.solener.2012.01.012

[247] Maleki, A., & Pourfayaz, F. (2015). Optimal sizing of autonomous hybrid photovoltaic/wind/battery power system with LPSP technology by using evolutionary algorithms. Solar Energy, 115, 471–483. https://doi.org/10.1016/j.solener.2015.03.004

[248] Ahmadi, S., & Abdi, S. (2016). Application of the Hybrid Big Bang-Big Crunch algorithm for optimal sizing of a stand-alone hybrid PV/wind/battery system. Solar Energy, 134, 366–374. https://doi.org/10.1016/j.solener.2016.05.019

[249] Belfkira, R., Zhang, L., & Barakat, G. (2011). Optimal sizing study of hybrid wind/PV/diesel power generation unit. Solar Energy, 85(1), 100–110. https://doi.org/10.1016/j.solener.2010.10.018

[250] Askarzadeh, A. (2013). A discrete chaotic harmony search-based simulated annealing algorithm for optimum design of PV/wind hybrid system. Solar Energy, 97, 93–101. https://doi.org/10.1016/j.solener.2013.08.014

[251] Merei, G., Berger, C., & Sauer, D. U. (2013). Optimization of an off-grid hybrid PV-Wind-Diesel system with different battery technologies using genetic algorithm. Solar Energy, 97, 460–473. https://doi.org/10.1016/j.solener.2013.08.016

[252] Kaabeche, A., & Ibtiouen, R. (2014). Techno-economic optimization of hybrid photovoltaic/wind/diesel/battery generation in a stand-alone power system. Solar Energy, 103, 171–182. https://doi.org/10.1016/j.solener.2014.02.017

[253] Syed, I. M. (2017). Near-optimal standalone hybrid PV/WE system sizing method. Solar Energy, 157, 727–734. https://doi.org/10.1016/j.solener.2017.08.085

[254] Beyer, H. G., & Langer, C. (2013). A method for the identification of configurations of PV/wind hybrid systems for the reliable supply of small loads. Solar Energy, 57(5), 381-391. https://doi.org/10.1016/S0038-092X(96)00118-1

[255] Rajkumar, R. K., Ramachandaramurthy, V. K., Yong, B. L., & Chia, D. B. (2011). Techno-economical optimization of hybrid pv/wind/battery system using Neuro-Fuzzy. Energy, 36(8), 5148–5153. https://doi.org/10.1016/j.energy.2011.06.017

[256] Arribas, L., Cano, L., Cruz, I., Mata, M., & Llobet, E. (2010). PV-wind hybrid system performance: A new approach and a case study. Renewable Energy, 35(1), 128–137. https://doi.org/10.1016/j.renene.2009.07.002

[257] Maheri, A. (2014). Multi-objective design optimisation of standalone hybrid wind-PV-diesel systems under uncertainties. Renewable Energy, 66, 650–661. https://doi.org/10.1016/j.renene.2014.01.009

Chapter 1   **A literature review and statistical analysis of**
PV-wind hybrid renewable system researches by considering
the most relevant 550 articles: an upgradable matrix literature database

[258]   Shilaja, C., & Arunprasath, T. (2019). Internet of medical things-load optimization of power flow based on hybrid enhanced grey wolf optimization and dragonfly algorithm. Future Generation Computer Systems, 98, 319–330. https://doi.org/10.1016/j.future.2018.12.070

[259]   Madhlopa, A., Sparks, D., Keen, S., Moorlach, M., Krog, P., & Dlamini, T. (2015). Optimization of a PV-wind hybrid system under limited water resources. Renewable and Sustainable Energy Reviews, 47, 324–331. https://doi.org/10.1016/j.rser.2015.03.051

[260]   Dursun, E., & Kilic, O. (2012). Comparative evaluation of different power management strategies of a stand-alone PV/Wind/PEMFC hybrid power system. International Journal of Electrical Power and Energy Systems, 34(1), 81–89. https://doi.org/10.1016/j.ijepes.2011.08.025

[261]   Eid, A. (2014). Utility integration of PV-wind-fuel cell hybrid distributed generation systems under variable load demands. International Journal of Electrical Power and Energy Systems, 62, 689–699. https://doi.org/10.1016/j.ijepes.2014.05.020

[262]   Maleki, A., Khajeh, M. G., & Ameri, M. (2016). Optimal sizing of a grid independent hybrid renewable energy system incorporating resource uncertainty, and load uncertainty. International Journal of Electrical Power and Energy Systems, 83, 514–524. https://doi.org/10.1016/j.ijepes.2016.04.008

[263]   Elkazaz, M., Sumner, M., & Thomas, D. (2020). Energy management system for hybrid PV-wind-battery microgrid using convex programming, model predictive and rolling horizon predictive control with experimental validation. International Journal of Electrical Power and Energy Systems, 115, 105483. https://doi.org/10.1016/j.ijepes.2019.105483

[264]   Celik, A. N. (2003). Techno-economic analysis of autonomous PV-wind hybrid energy systems using different sizing methods. Energy Conversion and Management, 44(12), 1951–1968. https://doi.org/10.1016/S0196-8904(02)00223-6

[265]   El-Shatter, T. F., Eskander, M. N., & El-Hagry, M. T. (2006). Energy flow and management of a hybrid wind/PV/fuel cell generation system. Energy Conversion and Management, 47(9–10), 1264–1280. https://doi.org/10.1016/j.enconman.2005.06.022

[266]   Essalaimeh, S., Al-Salaymeh, A., & Abdullat, Y. (2013). Electrical production for domestic and industrial applications using hybrid PV-wind system. Energy Conversion and Management, 65, 736–743. https://doi.org/10.1016/j.enconman.2012.01.044

[267]   Behravesh, V., Keypour, R., & Akbari Foroud, A. (2019). Control strategy for improving voltage quality in residential power distribution network consisting of roof-top photovoltaic-wind hybrid systems, battery storage and electric vehicles. Solar Energy, 182(June 2018), 80–95. https://doi.org/10.1016/j.solener.2019.02.037

[268]   Behravesh, V., Akbari Foroud, A., & Keypour, R. (2018). Optimal sizing methodology for photovoltaic and wind hybrid rooftop generation systems in residential low voltage distribution networks. Solar Energy, 173(April), 17–33. https://doi.org/10.1016/j.solener.2018.07.054

[269]   Khalilnejad, A., & Riahy, G. H. (2014). A hybrid wind-PV system performance investigation for the purpose of maximum hydrogen production and storage using advanced alkaline electrolyzer. Energy Conversion and Management, 80, 398–406. https://doi.org/10.1016/j.enconman.2014.01.040

[270]   Sinha, S., & Chandel, S. S. (2015). Prospects of solar photovoltaic-micro-wind based hybrid power systems in western Himalayan state of Himachal Pradesh in India. Energy Conversion and Management, 105, 1340–1351. https://doi.org/10.1016/j.enconman.2015.08.078

[271]   Baneshi, M., & Hadianfard, F. (2016). Techno-economic feasibility of hybrid diesel/PV/wind/battery electricity generation systems for non-residential large electricity consumers under southern Iran climate conditions. Energy Conversion and Management, 127, 233–244. https://doi.org/10.1016/j.enconman.2016.09.008

[272]   Sarkar, T., Bhattacharjee, A., Samanta, H., Bhattacharya, K., & Saha, H. (2019). Optimal design and implementation of solar PV-wind-biogas-VRFB storage integrated smart hybrid microgrid for ensuring

Chapter 1

A literature review and statistical analysis of PV-wind hybrid renewable system researches by considering the most relevant 550 articles: an upgradable matrix literature database

zero loss of power supply probability. Energy Conversion and Management, 191(January), 102–118. https://doi.org/10.1016/j.enconman.2019.04.025

[273]   Diaf, S., Diaf, D., Belhamel, M., Haddadi, M., & Louche, A. (2007). A methodology for optimal sizing of autonomous hybrid PV/wind system. Energy Policy, 35(11), 5708–5718. https://doi.org/10.1016/j.enpol.2007.06.020

[274]   Dufo-López, R., Bernal-Agustín, J. L., & Mendoza, F. (2009). Design and economical analysis of hybrid PV-wind systems connected to the grid for the intermittent production of hydrogen. Energy Policy, 37(8), 3082–3095. https://doi.org/10.1016/j.enpol.2009.03.059

[275]   Nandi, S. K., & Ghosh, H. R. (2009). A wind-PV-battery hybrid power system at Sitakunda in Bangladesh. Energy Policy, 37(9), 3659–3664. https://doi.org/10.1016/j.enpol.2009.04.039

[276]   Ekren, O., Ekren, B. Y., & Ozerdem, B. (2009). Break-even analysis and size optimization of a PV/wind hybrid energy conversion system with battery storage - A case study. Applied Energy, 86(7–8), 1043–1054. https://doi.org/10.1016/j.apenergy.2008.09.024

[277]   Ekren, B. Y., & Ekren, O. (2009). Simulation based size optimization of a PV/wind hybrid energy conversion system with battery storage under various load and auxiliary energy conditions. Applied Energy, 86(9), 1387–1394. https://doi.org/10.1016/j.apenergy.2008.12.015

[278]   Ekren, O., & Ekren, B. Y. (2010). Size optimization of a PV/wind hybrid energy conversion system with battery storage using simulated annealing. Applied Energy, 87(2), 592–598. https://doi.org/10.1016/j.apenergy.2009.05.022

[279]   Bekele, G., & Tadesse, G. (2012). Feasibility study of small Hydro/PV/Wind hybrid system for off-grid rural electrification in Ethiopia. Applied Energy, 97, 5–15. https://doi.org/10.1016/j.apenergy.2011.11.059

[280]   Morshed, M. J., Hmida, J. Ben, & Fekih, A. (2018). A probabilistic multi-objective approach for power flow optimization in hybrid wind-PV-PEV systems. Applied Energy, 211(December 2017), 1136–1149. https://doi.org/10.1016/j.apenergy.2017.11.101

[281]   Panahandeh, B., Bard, J., Outzourhit, A., & Zejli, D. (2011). Simulation of PV-wind-hybrid systems combined with hydrogen storage for rural electrification. International Journal of Hydrogen Energy, 36(6), 4185–4197. https://doi.org/10.1016/j.ijhydene.2010.07.151

[282]   Eroglu, M., Dursun, E., Sevencan, S., Song, J., Yazici, S., & Kilic, O. (2011). A mobile renewable house using PV/wind/fuel cell hybrid power system. International Journal of Hydrogen Energy, 36(13), 7985–7992. https://doi.org/10.1016/j.ijhydene.2011.01.046

[283]   Akyuz, E., Oktay, Z., & Dincer, I. (2012). Performance investigation of hydrogen production from a hybrid wind-PV system. International Journal of Hydrogen Energy, 37(21), 16623–16630. https://doi.org/10.1016/j.ijhydene.2012.02.149

[284]   Maleki, A., & Askarzadeh, A. (2014). Comparative study of artificial intelligence techniques for sizing of a hydrogen-based stand-alone photovoltaic/wind hybrid system. International Journal of Hydrogen Energy, 39(19), 9973–9984. https://doi.org/10.1016/j.ijhydene.2014.04.147

[285]   Kaabeche, A., Belhamel, M., & Ibtiouen, R. (2011). Sizing optimization of grid-independent hybrid photovoltaic/wind power generation system. Energy, 36(2), 1214–1222. https://doi.org/10.1016/j.energy.2010.11.024

[286]   Hiendro, A., Kurnianto, R., Rajagukguk, M., Simanjuntak, Y. M., & Junaidi. (2013). Techno-economic analysis of photovoltaic/wind hybrid system for onshore/remote area in Indonesia. Energy, 59, 652–657. https://doi.org/10.1016/j.energy.2013.06.005

[287]   Caballero, F., Sauma, E., & Yanine, F. (2013). Business optimal design of a grid-connected hybrid PV (photovoltaic)-wind energy system without energy storage for an Easter Island's block. Energy, 61, 248–261. https://doi.org/10.1016/j.energy.2013.08.030

Chapter 1
A literature review and statistical analysis of
PV-wind hybrid renewable system researches by considering
the most relevant 550 articles: an upgradable matrix literature database

[288] Sigarchian, S. G., Paleta, R., Malmquist, A., & Pina, A. (2015). Feasibility study of using a biogas engine as backup in a decentralized hybrid (PV/wind/battery) power generation system - Case study Kenya. Energy, 90, 1830–1841. https://doi.org/10.1016/j.energy.2015.07.008

[289] Shayeghi, H., & Hashemi, Y. (2015). Application of fuzzy decision-making based on INSGA-II to designing PV-wind hybrid system. Engineering Applications of Artificial Intelligence, 45, 1–17. https://doi.org/10.1016/j.engappai.2015.04.013

[290] Shezan, S. A., Julai, S., Kibria, M. A., Ullah, K. R., Saidur, R., Chong, W. T., & Akikur, R. K. (2016). Performance analysis of an off-grid wind-PV (photovoltaic)-diesel-battery hybrid energy system feasible for remote areas. Journal of Cleaner Production, 125, 121–132. https://doi.org/10.1016/j.jclepro.2016.03.014

[291] Ai, B., Yang, H., Shen, H., & Liao, X. (2003). Computer-aided design of PV/wind hybrid system. Renewable Energy, 28(10), 1491–1512. https://doi.org/10.1016/S0960-1481(03)00011-9

[292] Nelson, D. B., Nehrir, M. H., & Wang, C. (2006). Unit sizing and cost analysis of stand-alone hybrid wind/PV/fuel cell power generation systems. Renewable Energy, 31(10), 1641–1656. https://doi.org/10.1016/j.renene.2005.08.031

[293] Sopian, K., Ibrahim, M. Z., Wan Daud, W. R., Othman, M. Y., Yatim, B., & Amin, N. (2009). Performance of a PV-wind hybrid system for hydrogen production. Renewable Energy, 34(8), 1973–1978. https://doi.org/10.1016/j.renene.2008.12.010

[294] Fathy, A. (2016). A reliable methodology based on mine blast optimization algorithm for optimal sizing of hybrid PV-wind-FC system for remote area in Egypt. Renewable Energy, 95, 367–380. https://doi.org/10.1016/j.renene.2016.04.030

[295] Abbassi, A., Dami, M. A., & Jemli, M. (2017). A statistical approach for hybrid energy storage system sizing based on capacity distributions in an autonomous PV/Wind power generation system. Renewable Energy, 103, 81–93. https://doi.org/10.1016/j.renene.2016.11.024

[296] Zamani, M. H., & Riahy, G. H. (2008). Introducing a new method for optimal sizing of a hybrid (wind/PV/battery) system considering instantaneous wind speed variations. Energy for Sustainable Development, 12(2), 27–33. https://doi.org/10.1016/S0973-0826(08)60426-3

[297] Mondal, A. H., & Denich, M. (2010). Hybrid systems for decentralized power generation in Bangladesh. Energy for Sustainable Development, 14(1), 48–55. https://doi.org/10.1016/j.esd.2010.01.001

[298] Aien, M., Rashidinejad, M., & Firuz-Abad, M. F. (2015). Probabilistic optimal power flow in correlated hybrid wind-PV power systems: A review and a new approach. Renewable and Sustainable Energy Reviews, 41, 1437–1446. https://doi.org/10.1016/j.rser.2014.09.012

[299] Al Busaidi, A. S., Kazem, H. A., Al-Badi, A. H., & Farooq Khan, M. (2016). A review of optimum sizing of hybrid PV-Wind renewable energy systems in oman. Renewable and Sustainable Energy Reviews, 53, 185–193. https://doi.org/10.1016/j.rser.2015.08.039

[300] Maatallah, T., Ghodhbane, N., & Ben Nasrallah, S. (2016). Assessment viability for hybrid energy system (PV/wind/diesel) with storage in the northernmost city in Africa, Bizerte, Tunisia. Renewable and Sustainable Energy Reviews, 59, 1639–1652. https://doi.org/10.1016/j.rser.2016.01.076

[301] Nadjemi, O., Nacer, T., Hamidat, A., & Salhi, H. (2017). Optimal hybrid PV/wind energy system sizing: Application of cuckoo search algorithm for Algerian dairy farms. Renewable and Sustainable Energy Reviews, 70(December 2016), 1352–1365. https://doi.org/10.1016/j.rser.2016.12.038

[302] Shi, B., Wu, W., & Yan, L. (2017). Size optimization of stand-alone PV/wind/diesel hybrid power generation systems. Journal of the Taiwan Institute of Chemical Engineers, 73, 93–101. https://doi.org/10.1016/j.jtice.2016.07.047

[303] Chaib, A., Achour, D., & Kesraoui, M. (2016). Control of a Solar PV/wind Hybrid Energy System. Energy Procedia, 95, 89–97. https://doi.org/10.1016/j.egypro.2016.09.028

[304]　Adefarati, T., & Bansal, R. C. (2017). The Impacts of PV-Wind-Diesel-Electric Storage Hybrid System on the Reliability of a Power System. Energy Procedia, 105, 616–621. https://doi.org/10.1016/j.egypro.2017.03.364

[305]　Hossain, M., Mekhilef, S., & Olatomiwa, L. (2017). Performance evaluation of a stand-alone PV-wind-diesel-battery hybrid system feasible for a large resort center in South China Sea, Malaysia. Sustainable Cities and Society, 28, 358–366. https://doi.org/10.1016/j.scs.2016.10.008

[306]　Rajesh K., Kulkarni, A. D., & Ananthapadmanabha, T. (2015). Modeling and Simulation of Solar PV and DFIG Based Wind Hybrid System. Procedia Technology, 21, 667–675. https://doi.org/10.1016/j.protcy.2015.10.080

[307]　Sinha, S., & Chandel, S. S. (2017). Improving the reliability of photovoltaic-based hybrid power system with battery storage in low wind locations. Sustainable Energy Technologies and Assessments, 19, 146–159. https://doi.org/10.1016/j.seta.2017.01.008

[308]　Kumar, R., Gupta, R. A., & Bansal, A. K. (2013). Economic analysis and power management of a stand-alone wind/photovoltaic hybrid energy system using biogeography based optimization algorithm. Swarm and Evolutionary Computation, 8, 33–43. https://doi.org/10.1016/j.swevo.2012.08.002

[309]　Maleki, A., & Pourfayaz, F. (2015). Sizing of stand-alone photovoltaic/wind/diesel system with battery and fuel cell storage devices by harmony search algorithm. Journal of Energy Storage, 2, 30–42. https://doi.org/10.1016/j.est.2015.05.006

[310]　Bendary, A. F., & Ismail, M. M. (2019). Battery charge management for hybrid PV/wind/fuel cell with storage battery. Energy Procedia, 162, 107–116. https://doi.org/10.1016/j.egypro.2019.04.012

[311]　Bagul, A.D., Salameh, Z.M., Borowy, B., 1996. Sizing of a stand-alone hybrid wind-photovoltaic system using a three-event probability density approximation. Solar Energy 56 (4), 323–335. 10.1016/0038-092X(95)00116-9.

[312]　Gomaa, S., Aboul Seoud, A.K., Kheiralla, H.N., 1995. Design and analysis of photovoltaic and wind energy hybrid systems in Alexandria, Egypt. Renewable Energy 6 (5–6), 643–647. doi:10.1016/0960-1481(95)00044-K.

[313]　Askarzadeh, A. (2013). Developing a discrete harmony search algorithm for size optimization of wind-photovoltaic hybrid energy system. Solar Energy, 98(PC), 190–195. https://doi.org/10.1016/j.solener.2013.10.008

[314]　Maleki, A., & Askarzadeh, A. (2014). Artificial bee swarm optimization for optimum sizing of a stand-alone PV/WT/FC hybrid system considering LPSP concept. Solar Energy, 107, 227–235. https://doi.org/10.1016/j.solener.2014.05.016

[315]　Smaoui, M., Abdelkafi, A., & Krichen, L. (2015). Optimal sizing of stand-alone photovoltaic/wind/hydrogen hybrid system supplying a desalination unit. Solar Energy, 120, 263–276. https://doi.org/10.1016/j.solener.2015.07.032

[316]　Hocaoğlu, F. O., Gerek, Ö. N., & Kurban, M. (2009). A novel hybrid (wind-photovoltaic) system sizing procedure. Solar Energy, 83(11), 2019–2028. https://doi.org/10.1016/j.solener.2009.07.010

[317]　Nasiraghdam, H., & Jadid, S. (2012). Optimal hybrid PV/WT/FC sizing and distribution system reconfiguration using multi-objective artificial bee colony (MOABC) algorithm. Solar Energy, 86(10), 3057–3071. https://doi.org/10.1016/j.solener.2012.07.014

[318]　Bayod-Rújula, Á. A., Haro-Larrodé, M. E., & Martínez-Gracia, A. (2013). Sizing criteria of hybrid photovoltaic-wind systems with battery storage and self-consumption considering interaction with the grid. Solar Energy, 98(PC), 582–591. https://doi.org/10.1016/j.solener.2013.10.023

[319]　Tazvinga, H., Zhu, B., & Xia, X. (2014). Energy dispatch strategy for a photovoltaic-wind-diesel-battery hybrid power system. Solar Energy, 108, 412–420. https://doi.org/10.1016/j.solener.2014.07.025

[320]　Shi, Z., Wang, R., & Zhang, T. (2015). Multi-objective optimal design of hybrid renewable energy systems using preference-inspired coevolutionary approach. Solar Energy, 118, 96–106. https://doi.org/10.1016/j.solener.2015.03.052

Chapter 1

A literature review and statistical analysis of PV-wind hybrid renewable system researches by considering the most relevant 550 articles: an upgradable matrix literature database

[321] Tito, S. R., Lie, T. T., & Anderson, T. N. (2016). Optimal sizing of a wind-photovoltaic-battery hybrid renewable energy system considering socio-demographic factors. Solar Energy, 136, 525–532. https://doi.org/10.1016/j.solener.2016.07.036

[322] Maleki, A., Pourfayaz, F., & Ahmadi, M. H. (2016). Design of a cost-effective wind/photovoltaic/hydrogen energy system for supplying a desalination unit by a heuristic approach. Solar Energy, 139, 666–675. https://doi.org/10.1016/j.solener.2016.09.028

[323] Chaurasia, G. S., Singh, A. K., Agrawal, S., & Sharma, N. K. (2017). A meta-heuristic firefly algorithm based smart control strategy and analysis of a grid connected hybrid photovoltaic/wind distributed generation system. Solar Energy, 150, 265–274. https://doi.org/10.1016/j.solener.2017.03.079

[324] Bukar, A. L., Tan, C. W., & Lau, K. Y. (2019). Optimal sizing of an autonomous photovoltaic/wind/battery/diesel generator microgrid using grasshopper optimization algorithm. Solar Energy, 188, 685–696. https://doi.org/10.1016/j.solener.2019.06.050

[325] Carvalho, D. B., Guardia, E. C., & Marangon Lima, J. W. (2019). Technical-economic analysis of the insertion of PV power into a wind-solar hybrid system. Solar Energy, 191, 530–539. https://doi.org/10.1016/j.solener.2019.06.070

[326] Zhang, G., Wu, B., Maleki, A., & Zhang, W. (2018). Simulated annealing-chaotic search algorithm based optimization of reverse osmosis hybrid desalination system driven by wind and solar energies. Solar Energy, 173, 964–975. https://doi.org/10.1016/j.solener.2018.07.094

[327] Kershman, S. A., Rheinländer, J., & Gabler, H. (2003). Seawater reverse osmosis powered from renewable energy sources - Hybrid wind/photovoltaic/grid power supply for small-scale desalination in Libya. Desalination, 153(1–3), 17–23. https://doi.org/10.1016/S0011-9164(02)01089-5

[328] Mahmoudi, H., Abdul-Wahab, S. A., Goosen, M. F. A., Sablani, S. S., Perret, J., Ouagued, A., & Spahis, N. (2008). Weather data and analysis of hybrid photovoltaic-wind power generation systems adapted to a seawater greenhouse desalination unit designed for arid coastal countries. Desalination, 222(1–3), 119–127. https://doi.org/10.1016/j.desal.2007.01.135

[329] Maleki, A. (2018). Design and optimization of autonomous solar-wind-reverse osmosis desalination systems coupling battery and hydrogen energy storage by an improved bee algorithm. Desalination, 435(August 2017), 221–234. https://doi.org/10.1016/j.desal.2017.05.034

[330] Gökçek, M. (2018). Integration of hybrid power (wind-photovoltaic-diesel-battery) and seawater reverse osmosis systems for small-scale desalination applications. Desalination, 435(July 2017), 210–220. https://doi.org/10.1016/j.desal.2017.07.006

[331] Zare Oskouei, M., & Sadeghi Yazdankhah, A. (2015). Scenario-based stochastic optimal operation of wind, photovoltaic, pump-storage hybrid system in frequency- based pricing. Energy Conversion and Management, 105, 1105–1114. https://doi.org/10.1016/j.enconman.2015.08.062

[332] Khanjarpanah, H., Jabbarzadeh, A., & Seyedhosseini, S. M. (2018). A novel multi-period double frontier network DEA to sustainable location optimization of hybrid wind-photovoltaic power plant with real application. Energy Conversion and Management, 159(December 2017), 175–188. https://doi.org/10.1016/j.enconman.2018.01.013

[333] Saheb-Koussa, D., Haddadi, M., & Belhamel, M. (2009). Economic and technical study of a hybrid system (wind-photovoltaic-diesel) for rural electrification in Algeria. Applied Energy, 86(7–8), 1024–1030. https://doi.org/10.1016/j.apenergy.2008.10.015

[334] Suha Yazici, M., Yavasoglu, H. A., & Eroglu, M. (2013). A mobile off-grid platform powered with photovoltaic/wind/battery/fuel cell hybrid power systems. International Journal of Hydrogen Energy, 38(26), 11639–11645. https://doi.org/10.1016/j.ijhydene.2013.04.025

[335] Mezzai, N., Rekioua, D., Rekioua, T., Mohammedi, A., Idjdarane, K., & Bacha, S. (2014). Modeling of hybrid photovoltaic/wind/fuel cells power system. International Journal of Hydrogen Energy, 39(27), 15158–15168. https://doi.org/10.1016/j.ijhydene.2014.06.015

Chapter 1   **A literature review and statistical analysis of**
PV-wind hybrid renewable system researches by considering
the most relevant 550 articles: an upgradable matrix literature database

[336]   Zhang, D., Liu, J., Jiao, S., Tian, H., Lou, C., Zhou, Z., … Zuo, J. (2019). Research on the configuration and operation effect of the hybrid solar-wind-battery power generation system based on NSGA-II. Energy, 189, 116121. https://doi.org/10.1016/j.energy.2019.116121

[337]   Abbes, D., Martinez, A., & Champenois, G. (2014). Life cycle cost, embodied energy and loss of power supply probability for the optimal design of hybrid power systems. Mathematics and Computers in Simulation, 98, 46–62. https://doi.org/10.1016/j.matcom.2013.05.004

[338]   Ferrari, L., Bianchini, A., Galli, G., Ferrara, G., & Carnevale, E. A. (2018). Influence of actual component characteristics on the optimal energy mix of a photovoltaic-wind-diesel hybrid system for a remote off-grid application. Journal of Cleaner Production, 178, 206–219. https://doi.org/10.1016/j.jclepro.2018.01.032

[339]   Geem, Z. W. (2012). Size optimization for a hybrid photovoltaic-wind energy system. International Journal of Electrical Power and Energy Systems, 42(1), 448–451. https://doi.org/10.1016/j.ijepes.2012.04.051

[340]   Hong, C. M., & Chen, C. H. (2014). Intelligent control of a grid-connected wind-photovoltaic hybrid power systems. International Journal of Electrical Power and Energy Systems, 55, 554–561. https://doi.org/10.1016/j.ijepes.2013.10.024

[341]   Kamjoo, A., Maheri, A., Dizqah, A. M., & Putrus, G. A. (2016). Multi-objective design under uncertainties of hybrid renewable energy system using NSGA-II and chance constrained programming. International Journal of Electrical Power and Energy Systems, 74, 187–194. https://doi.org/10.1016/j.ijepes.2015.07.007

[342]   Kaldellis, J. K., & Zafirakis, D. (2012). Optimum sizing of stand-alone wind-photovoltaic hybrid systems for representative wind and solar potential cases of the Greek territory. Journal of Wind Engineering and Industrial Aerodynamics, 107–108, 169–178. https://doi.org/10.1016/j.jweia.2012.04.013

[343]   Bekelea, G., & Boneya, G. (2012). Design of a photovoltaic-wind hybrid power generation system for Ethiopian remote area. Energy Procedia, 14(0), 1760–1765. https://doi.org/10.1016/j.egypro.2011.12.1164

[344]   Yin, X. L., Cheng, L., Wang, X., Lu, J., & Qin, H. (2019). Optimization for hydro-photovoltaic-wind power generation system based on modified version of multi-objective whale optimization algorithm. Energy Procedia, 158, 6208–6216. https://doi.org/10.1016/j.egypro.2019.01.480

[345]   Celik, A. N. (2002). Optimisation and techno-economic analysis of autonomous photovoltaic-wind hybrid energy systems in comparison to single photovoltaic and wind systems. Energy Conversion and Management, 43(18), 2453–2468. https://doi.org/10.1016/S0196-8904(01)00198-4

[346]   Ahmed, N. A., Miyatake, M., & Al-Othman, A. K. (2008). Power fluctuations suppression of stand-alone hybrid generation combining solar photovoltaic/wind turbine and fuel cell systems. Energy Conversion and Management, 49(10), 2711–2719. https://doi.org/10.1016/j.enconman.2008.04.005

[347]   Aissou, S., Rekioua, D., Mezzai, N., Rekioua, T., & Bacha, S. (2015). Modeling and control of hybrid photovoltaic wind power system with battery storage. Energy Conversion and Management, 89, 615–625. https://doi.org/10.1016/j.enconman.2014.10.034

[348]   Gan, L. K., Shek, J. K. H., & Mueller, M. A. (2015). Hybrid wind-photovoltaic-diesel-battery system sizing tool development using empirical approach, life-cycle cost and performance analysis: A case study in Scotland. Energy Conversion and Management, 106, 479–494. https://doi.org/10.1016/j.enconman.2015.09.029

[349]   Sinha, S., & Chandel, S. S. (2016). Analysis of fixed tilt and sun tracking photovoltaic-micro wind based hybrid power systems. Energy Conversion and Management, 115, 265–275. https://doi.org/10.1016/j.enconman.2016.02.056

Chapter 1   **A literature review and statistical analysis of**
PV-wind hybrid renewable system researches by considering
the most relevant 550 articles: an upgradable matrix literature database

[350]   Devrim, Y., & Bilir, L. (2016). Performance investigation of a wind turbine–solar photovoltaic panels–fuel cell hybrid system installed at İncek region – Ankara, Turkey. Energy Conversion and Management, 126, 759–766. https://doi.org/10.1016/j.enconman.2016.08.062

[351]   Acuña, L. G., Lake, M., Padilla, R. V., Lim, Y. Y., Ponzón, E. G., & Soo Too, Y. C. (2018). Modelling autonomous hybrid photovoltaic-wind energy systems under a new reliability approach. Energy Conversion and Management, 172(January), 357–369. https://doi.org/10.1016/j.enconman.2018.07.025

[352]   Zhang, W., Maleki, A., Rosen, M. A., & Liu, J. (2019). Sizing a stand-alone solar-wind-hydrogen energy system using weather forecasting and a hybrid search optimization algorithm. Energy Conversion and Management, 180, 609–621. https://doi.org/10.1016/j.enconman.2018.08.102

[353]   Han, X., Pan, X., Yang, H., Xu, C., Ju, X., & Du, X. (2019). Dynamic output characteristics of a photovoltaic-wind-concentrating solar power hybrid system integrating an electric heating device. Energy Conversion and Management, 193(January), 86–98. https://doi.org/10.1016/j.enconman.2019.04.063

[354]   Kaabeche, A., & Bakelli, Y. (2019). Renewable hybrid system size optimization considering various electrochemical energy storage technologies. Energy Conversion and Management, 193, 162–175. https://doi.org/10.1016/j.enconman.2019.04.064

[355]   Liu, W., Zhu, F., Chen, J., Wang, H., Xu, B., Song, P., … Yang, M. (2019). Multi-objective optimization scheduling of wind–photovoltaic–hydropower systems considering riverine ecosystem. Energy Conversion and Management, 196, 32–43. https://doi.org/10.1016/j.enconman.2019.05.104

[356]   Elkadeem, M. R., Wang, S., Sharshir, S. W., & Atia, E. G. (2019). Feasibility analysis and techno-economic design of grid-isolated hybrid renewable energy system for electrification of agriculture and irrigation area: A case study in Dongola, Sudan. Energy Conversion and Management, 196, 1453–1478. https://doi.org/10.1016/j.enconman.2019.06.085

[357]   Diaf, S., Belhamel, M., Haddadi, M., & Louche, A. (2008). Technical and economic assessment of hybrid photovoltaic/wind system with battery storage in Corsica island. Energy Policy, 36(2), 743–754. https://doi.org/10.1016/j.enpol.2007.10.028

[358]   Marano, V., Rizzo, G., & Tiano, F. A. (2012). Application of dynamic programming to the optimal management of a hybrid power plant with wind turbines, photovoltaic panels and compressed air energy storage. Applied Energy, 97, 849–859. https://doi.org/10.1016/j.apenergy.2011.12.086

[359]   Ma, T., Yang, H., & Lu, L. (2014). A feasibility study of a stand-alone hybrid solar-wind-battery system for a remote island. Applied Energy, 121, 149–158. https://doi.org/10.1016/j.apenergy.2014.01.090

[360]   Bhandari, B., Lee, K. T., Lee, C. S., Song, C. K., Maskey, R. K., & Ahn, S. H. (2014). A novel off-grid hybrid power system comprised of solar photovoltaic, wind, and hydro energy sources. Applied Energy, 133, 236–242. https://doi.org/10.1016/j.apenergy.2014.07.033

[361]   Bantikatla, H., Nulu, L. D. S. M. P., Bhogoju, R., Narlanka, P., Siddi, V. R., Royal, K. K., & Hymavathi, A. (2019). Design and fabrication of hybrid solar silicon PV system. Materials Today: Proceedings, 19(xxxx), 761–766. https://doi.org/10.1016/j.matpr.2019.08.126

[362]   González, A., Riba, J. R., Rius, A., & Puig, R. (2015). Optimal sizing of a hybrid grid-connected photovoltaic and wind power system. Applied Energy, 154, 752–762. https://doi.org/10.1016/j.apenergy.2015.04.105

[363]   Amrollahi, M. H., & Bathaee, S. M. T. (2017). Techno-economic optimization of hybrid photovoltaic/wind generation together with energy storage system in a stand-alone micro-grid subjected to demand response. Applied Energy, 202, 66–77. https://doi.org/10.1016/j.apenergy.2017.05.116

[364]   Sun, K., Li, K. J., Pan, J., Liu, Y., & Liu, Y. (2019). An optimal combined operation scheme for pumped storage and hybrid wind-photovoltaic complementary power generation system. Applied Energy, 242(March), 1155–1163. https://doi.org/10.1016/j.apenergy.2019.03.171

Chapter 1   **A literature review and statistical analysis of**
PV-wind hybrid renewable system researches by considering
the most relevant 550 articles: an upgradable matrix literature database

[365]   Xu, B., Chen, D., Venkateshkumar, M., Xiao, Y., Yue, Y., Xing, Y., & Li, P. (2019). Modeling a pumped storage hydropower integrated to a hybrid power system with solar-wind power and its stability analysis. Applied Energy, 248(March), 446–462. https://doi.org/10.1016/j.apenergy.2019.04.125

[366]   Tan, Q., Ding, Y., Ye, Q., Mei, S., Zhang, Y., & Wei, Y. (2019). Optimization and evaluation of a dispatch model for an integrated wind-photovoltaic-thermal power system based on dynamic carbon emissions trading. Applied Energy, 253(July). https://doi.org/10.1016/j.apenergy.2019.113598

[367]   Shakya, B. D., Aye, L., & Musgrave, P. (2005). Technical feasibility and financial analysis of hybrid wind-photovoltaic system with hydrogen storage for Cooma. International Journal of Hydrogen Energy, 30(1), 9–20. https://doi.org/10.1016/j.ijhydene.2004.03.013

[368]   Calderón, M., Calderón, A. J., Ramiro, A., & González, J. F. (2010). Weather data and energy balance of a hybrid photovoltaic-wind system with hydrogen storage. International Journal of Hydrogen Energy, 35(15), 7706–7715. https://doi.org/10.1016/j.ijhydene.2010.05.067

[369]   Calderón, M., Calderón, A. J., Ramiro, A., González, J. F., & González, I. (2011). Evaluation of a hybrid photovoltaic-wind system with hydrogen storage performance using exergy analysis. International Journal of Hydrogen Energy, 36(10), 5751–5762. https://doi.org/10.1016/j.ijhydene.2011.02.055

[370]   Chávez-Ramírez, A. U., Cruz, J. C., Espinosa-Lumbreras, R., Ledesma-García, J., Durón-Torres, S. M., & Arriaga, L. G. (2013). Design and set up of a hybrid power system (PV-WT-URFC) for a stand-alone application in Mexico. International Journal of Hydrogen Energy, 38(28), 12623–12633. https://doi.org/10.1016/j.ijhydene.2012.11.019

[371]   García, P., Torreglosa, J. P., Fernández, L. M., & Jurado, F. (2013). Optimal energy management system for stand-alone wind turbine/photovoltaic/ hydrogen/battery hybrid system with supervisory control based on fuzzy logic. International Journal of Hydrogen Energy, 38(33), 14146–14158. https://doi.org/10.1016/j.ijhydene.2013.08.106

[372]   García-Triviño, P., Llorens-Iborra, F., García-Vázquez, C. A., Gil-Mena, A. J., Fernández-Ramírez, L. M., & Jurado, F. (2014). Long-term optimization based on PSO of a grid-connected renewable energy/battery/hydrogen hybrid system. International Journal of Hydrogen Energy, 39(21), 10805–10816. https://doi.org/10.1016/j.ijhydene.2014.05.064

[373]   Sanchez, V. M., Chavez-Ramirez, A. U., Duron-Torres, S. M., Hernandez, J., Arriaga, L. G., & Ramirez, J. M. (2014). Techno-economical optimization based on swarm intelligence algorithm for a stand-alone wind-photovoltaic-hydrogen power system at south-east region of Mexico. International Journal of Hydrogen Energy, 39(29), 16646–16655. https://doi.org/10.1016/j.ijhydene.2014.06.034

[374]   Tamalouzt, S., Benyahia, N., Rekioua, T., Rekioua, D., & Abdessemed, R. (2016). Performances analysis of WT-DFIG with PV and fuel cell hybrid power sources system associated with hydrogen storage hybrid energy system. International Journal of Hydrogen Energy, 41(45), 21006–21021. https://doi.org/10.1016/j.ijhydene.2016.06.163

[375]   Roumila, Z., Rekioua, D., & Rekioua, T. (2017). Energy management based fuzzy logic controller of hybrid system wind/photovoltaic/diesel with storage battery. International Journal of Hydrogen Energy, 42(30), 19525–19535. https://doi.org/10.1016/j.ijhydene.2017.06.006

[376]   Cherif, H., & Belhadj, J. (2011). Large-scale time evaluation for energy estimation of stand-alone hybrid photovoltaic-wind system feeding a reverse osmosis desalination unit. Energy, 36(10), 6058–6067. https://doi.org/10.1016/j.energy.2011.08.010

[377]   Lujano-Rojas, J. M., Dufo-López, R., & Bernal-Agustín, J. L. (2013). Probabilistic modelling and analysis of stand-alone hybrid power systems. Energy, 63, 19–27. https://doi.org/10.1016/j.energy.2013.10.003

[378]   Boukettaya, G., & Krichen, L. (2014). A dynamic power management strategy of a grid connected hybrid generation system using wind, photovoltaic and Flywheel Energy Storage System in residential applications. Energy, 71, 148–159. https://doi.org/10.1016/j.energy.2014.04.039

Chapter 1　　　　　　　　　　　　　　　　**A literature review and statistical analysis of**
PV-wind hybrid renewable system researches by considering
the most relevant 550 articles: an upgradable matrix literature database

[379]　Fazelpour, F., Soltani, N., & Rosen, M. A. (2014). Feasibility of satisfying electrical energy needs with hybrid systems for a medium-size hotel on Kish Island, Iran. Energy, 73, 856–865. https://doi.org/10.1016/j.energy.2014.06.097

[380]　Fathabadi, H. (2016). Novel highly accurate universal maximum power point tracker for maximum power extraction from hybrid fuel cell/photovoltaic/wind power generation systems. Energy, 116, 402–416. https://doi.org/10.1016/j.energy.2016.09.095

[381]　Sanajaoba Singh, S., & Fernandez, E. (2018). Modeling, size optimization and sensitivity analysis of a remote hybrid renewable energy system. Energy, 143, 719–731. https://doi.org/10.1016/j.energy.2017.11.053

[382]　Ahmad, J., Imran, M., Khalid, A., Iqbal, W., Ashraf, S. R., Adnan, M., … Khokhar, K. S. (2018). Techno economic analysis of a wind-photovoltaic-biomass hybrid renewable energy system for rural electrification: A case study of Kallar Kahar. Energy, 148, 208–234. https://doi.org/10.1016/j.energy.2018.01.133

[383]　Khiareddine, A., Ben Salah, C., Rekioua, D., & Mimouni, M. F. (2018). Sizing methodology for hybrid photovoltaic /wind/ hydrogen/battery integrated to energy management strategy for pumping system. Energy, 153, 743–762. https://doi.org/10.1016/j.energy.2018.04.073

[384]　Ben Ali, I., Turki, M., Belhadj, J., & Roboam, X. (2018). Optimized fuzzy rule-based energy management for a battery-less PV/wind-BWRO desalination system. Energy, 159, 216–228. https://doi.org/10.1016/j.energy.2018.06.110

[385]　Zhang, W., Maleki, A., Rosen, M. A., & Liu, J. (2018). Optimization with a simulated annealing algorithm of a hybrid system for renewable energy including battery and hydrogen storage. Energy, 163, 191–207. https://doi.org/10.1016/j.energy.2018.08.112

[386]　Ceran, B. (2019). The concept of use of PV/WT/FC hybrid power generation system for smoothing the energy profile of the consumer. Energy, 167, 853–865. https://doi.org/10.1016/j.energy.2018.11.028

[387]　Lee, J. Y., Aviso, K. B., & Tan, R. R. (2019). Multi-objective optimisation of hybrid power systems under uncertainties. Energy, 175, 1271–1282. https://doi.org/10.1016/j.energy.2019.03.141

[388]　Dhunny, A. Z., Doorga, J. R. S., Allam, Z., Lollchund, M. R., & Boojhawon, R. (2019). Identification of optimal wind, solar and hybrid wind-solar farming sites using fuzzy logic modelling. Energy, 188, 116056. https://doi.org/10.1016/j.energy.2019.116056

[389]　Habib, M. A., Said, S. A. M., El-Hadidy, M. A., & Al-Zaharna, I. (1999). Optimization procedure of a hybrid photovoltaic wind energy system. Energy, 24(11), 919–929. https://doi.org/10.1016/S0360-5442(99)00042-0

[390]　Ferrer-Martí, L., Domenech, B., García-Villoria, A., & Pastor, R. (2013). A MILP model to design hybrid wind-photovoltaic isolated rural electrification projects in developing countries. European Journal of Operational Research, 226(2), 293–300. https://doi.org/10.1016/j.ejor.2012.11.018

[391]　Charrouf, O., Betka, A., Abdeddaim, S., & Ghamri, A. (2020). Artificial Neural Network power manager for hybrid PV-wind desalination system. Mathematics and Computers in Simulation, 167(xxxx), 443–460. https://doi.org/10.1016/j.matcom.2019.09.005

[392]　Onar, O. C., Uzunoglu, M., & Alam, M. S. (2008). Modeling, control and simulation of an autonomous wind turbine/photovoltaic/fuel cell/ultra-capacitor hybrid power system. Journal of Power Sources, 185(2), 1273–1283. https://doi.org/10.1016/j.jpowsour.2008.08.083

[393]　Lai, C. M. (2006). Prototype development of the rooftop turbine ventilator powered by hybrid wind and photovoltaic energy. Energy and Buildings, 38(3), 174–180. https://doi.org/10.1016/j.enbuild.2005.06.004

[394]　Cetin, E., Yilanci, A., Ozturk, H. K., Colak, M., Kasikci, I., & Iplikci, S. (2010). A micro-DC power distribution system for a residential application energized by photovoltaic-wind/fuel cell hybrid energy systems. Energy and Buildings, 42(8), 1344–1352. https://doi.org/10.1016/j.enbuild.2010.03.003

Chapter 1   **A literature review and statistical analysis of**
PV-wind hybrid renewable system researches by considering
the most relevant 550 articles: an upgradable matrix literature database

[395] Skretas, S. B., & Papadopoulos, D. P. (2009). Efficient design and simulation of an expandable hybrid (wind-photovoltaic) power system with MPPT and inverter input voltage regulation features in compliance with electric grid requirements. Electric Power Systems Research, 79(9), 1271–1285. https://doi.org/10.1016/j.epsr.2009.03.010

[396] Alvarez-Mendoza, F., Angeles-Camacho, C., Bacher, P., & Madsen, H. (2018). Semi-dispatchable generation with wind-photovoltaic-fuel cell hybrid system to mitigate frequency disturbance. Electric Power Systems Research, 165(October 2017), 60–67. https://doi.org/10.1016/j.epsr.2018.08.021

[397] Mohammed, Z., Hizam, H., & Gomes, C. (2019). Lightning-induced transient effects in a hybrid PV– wind system and mitigation strategies. Electric Power Systems Research, 174(May), 105882. https://doi.org/10.1016/j.epsr.2019.105882

[398] Ravinder, K., & Bansal, H. O. (2019). Investigations on shunt active power filter in a PV-wind-FC based hybrid renewable energy system to improve power quality using hardware-in-the-loop testing platform. Electric Power Systems Research, 177(July). https://doi.org/10.1016/j.epsr.2019.105957

[399] Kellogg, W., Nehrir, M. H., Venkataramanan, G., & Gerez, V. (1996). Optimal unit sizing for a hybrid wind/photovoltaic generating system. Electric Power Systems Research, 39(1), 35–38. https://doi.org/10.1016/S0378-7796(96)01096-6

[400] Diab, F., Lan, H., Zhang, L., & Ali, S. (2016). An environmentally friendly factory in Egypt based on hybrid photovoltaic/wind/diesel/battery system. Journal of Cleaner Production, 112, 3884–3894. https://doi.org/10.1016/j.jclepro.2015.07.008

[401] Khaloie, H., Abdollahi, A., Shafie-Khah, M., Siano, P., Nojavan, S., Anvari-Moghaddam, A., & Catalão, J. P. S. (2020). Co-optimized bidding strategy of an integrated wind-thermal-photovoltaic system in deregulated electricity market under uncertainties. Journal of Cleaner Production, 242. https://doi.org/10.1016/j.jclepro.2019.118434

[402] Celik, A. N. (2002). The system performance of autonomous photovoltaic-wind hybrid energy systems using synthetically generated weather data. Renewable Energy, 27(1), 107–121. https://doi.org/10.1016/S0960-1481(01)00168-9

[403] Yang, H. X., Lu, L., & Burnett, J. (2003). Weather data and probability analysis of hybrid photovoltaic-wind power generation systems in Hong Kong. Renewable Energy, 28(11), 1813–1824. https://doi.org/10.1016/S0960-1481(03)00015-6

[404] Dufo-López, R., & Bernal-Agustín, J. L. (2008). Multi-objective design of PV-wind-diesel-hydrogen-battery systems. Renewable Energy, 33(12), 2559–2572. https://doi.org/10.1016/j.renene.2008.02.027

[405] Martínez, J., & Medina, A. (2010). A state space model for the dynamic operation representation of small-scale wind-photovoltaic hybrid systems. Renewable Energy, 35(6), 1159–1168. https://doi.org/10.1016/j.renene.2009.11.039

[406] Ould Bilal, B., Sambou, V., Ndiaye, P. A., Kébé, C. M. F., & Ndongo, M. (2010). Optimal design of a hybrid solar-wind-battery system using the minimization of the annualized cost system and the minimization of the loss of power supply probability (LPSP). Renewable Energy, 35(10), 2388–2390. https://doi.org/10.1016/j.renene.2010.03.004

[407] Türkay, B. E., & Telli, A. Y. (2011). Economic analysis of standalone and grid connected hybrid energy systems. Renewable Energy, 36(7), 1931–1943. https://doi.org/10.1016/j.renene.2010.12.007

[408] Sen, R., & Bhattacharyya, S. C. (2014). Off-grid electricity generation with renewable energy technologies inIndia: An application of HOMER. Renewable Energy, 62, 388–398. https://doi.org/10.1016/j.renene.2013.07.028

[409] Paliwal, P., Patidar, N. P., & Nema, R. K. (2014). Determination of reliability constrained optimal resource mix for an autonomous hybrid power system using Particle Swarm Optimization. Renewable Energy, 63, 194–204. https://doi.org/10.1016/j.renene.2013.09.003

Chapter 1

A literature review and statistical analysis of
PV-wind hybrid renewable system researches by considering
the most relevant 550 articles: an upgradable matrix literature database

[410] Ma, T., Yang, H., Lu, L., & Peng, J. (2014). Technical feasibility study on a standalone hybrid solar-wind system with pumped hydro storage for a remote island in Hong Kong. Renewable Energy, 69, 7–15. https://doi.org/10.1016/j.renene.2014.03.028

[411] Torreglosa, J. P., García, P., Fernández, L. M., & Jurado, F. (2015). Energy dispatching based on predictive controller of an off-grid wind turbine/photovoltaic/hydrogen/battery hybrid system. Renewable Energy, 74, 326–336. https://doi.org/10.1016/j.renene.2014.08.010

[412] Malheiro, A., Castro, P. M., Lima, R. M., & Estanqueiro, A. (2015). Integrated sizing and scheduling of wind/PV/diesel/battery isolated systems. Renewable Energy, 83, 646–657. https://doi.org/10.1016/j.renene.2015.04.066

[413] Haghighat Mamaghani, A., Avella Escandon, S. A., Najafi, B., Shirazi, A., & Rinaldi, F. (2016). Techno-economic feasibility of photovoltaic, wind, diesel and hybrid electrification systems for off-grid rural electrification in Colombia. Renewable Energy, 97, 293–305. https://doi.org/10.1016/j.renene.2016.05.086

[414] Acuña, L. G., Padilla, R. V., & Mercado, A. S. (2017). Measuring reliability of hybrid photovoltaic-wind energy systems: A new indicator. Renewable Energy, 106, 68–77. https://doi.org/10.1016/j.renene.2016.12.089

[415] Al-Hamidi, H., & Al Asfar, J. (2017). Hybrid renewable energy system with minimum noise wind turbine. Renewable Energy, 114, 581–587. https://doi.org/10.1016/j.renene.2017.07.015

[416] Tu, T., Rajarathnam, G. P., & Vassallo, A. M. (2019). Optimization of a stand-alone photovoltaic–wind–diesel–battery system with multi-layered demand scheduling. Renewable Energy, 131, 333–347. https://doi.org/10.1016/j.renene.2018.07.029

[417] Hadidian Moghaddam, M. J., Kalam, A., Nowdeh, S. A., Ahmadi, A., Babanezhad, M., & Saha, S. (2019). Optimal sizing and energy management of stand-alone hybrid photovoltaic/wind system based on hydrogen storage considering LOEE and LOLE reliability indices using flower pollination algorithm. Renewable Energy, 135, 1412–1434. https://doi.org/10.1016/j.renene.2018.09.078

[418] Rullo, P., Braccia, L., Luppi, P., Zumoffen, D., & Feroldi, D. (2019). Integration of sizing and energy management based on economic predictive control for standalone hybrid renewable energy systems. Renewable Energy, 140, 436–451. https://doi.org/10.1016/j.renene.2019.03.074

[419] Xu, X., Hu, W., Cao, D., Huang, Q., Chen, C., & Chen, Z. (2020). Optimized sizing of a standalone PV-wind-hydropower station with pumped-storage installation hybrid energy system. Renewable Energy, 147, 1418–1431. https://doi.org/10.1016/j.renene.2019.09.099

[420] Tobergte, D. R., & Curtis, S. (1998). Hybrid Photovoltaxjwind Grid-Connected Power Plants in Croatian Renewable Energy Program. Renewable Energy, 15(9), 594–597. https://doi.org/10.1017/CBO9781107415324.004

[421] Khiari, W., Turki, M., & Belhadj, J. (2019). Power control strategy for PV/Wind reverse osmosis desalination without battery. Control Engineering Practice, 89, 169–179. https://doi.org/10.1016/j.conengprac.2019.05.020

[422] Bentouba, S., & Bourouis, M. (2016). Feasibility study of a wind-photovoltaic hybrid power generation system for a remote area in the extreme south of Algeria. Applied Thermal Engineering, 99, 713–719. https://doi.org/10.1016/j.applthermaleng.2015.12.014

[423] Asrari, A., Ghasemi, A., & Javidi, M. H. (2012). Economic evaluation of hybrid renewable energy systems for rural electrification in Iran - A case study. Renewable and Sustainable Energy Reviews, 16(5), 3123–3130. https://doi.org/10.1016/j.rser.2012.02.052

[424] Fadaeenejad, M., Radzi, M. A. M., Abkadir, M. Z. A., & Hizam, H. (2014). Assessment of hybrid renewable power sources for rural electrification in Malaysia. Renewable and Sustainable Energy Reviews, 30, 299–305. https://doi.org/10.1016/j.rser.2013.10.003

Chapter 1   **A literature review and statistical analysis of**
PV-wind hybrid renewable system researches by considering
the most relevant 550 articles: an upgradable matrix literature database

[425]   Belmili, H., Haddadi, M., Bacha, S., Almi, M. F., & Bendib, B. (2014). Sizing stand-alone photovoltaic-wind hybrid system: Techno-economic analysis and optimization. Renewable and Sustainable Energy Reviews, 30, 821–832. https://doi.org/10.1016/j.rser.2013.11.011

[426]   Koussa, D. S., & Koussa, M. (2015). A feasibility and cost benefit prospection of grid connected hybrid power system (wind-photovoltaic) - Case study: An Algerian coastal site. Renewable and Sustainable Energy Reviews, 50, 628–642. https://doi.org/10.1016/j.rser.2015.04.189

[427]   Hosseinalizadeh, R., Shakouri G, H., Amalnick, M. S., & Taghipour, P. (2016). Economic sizing of a hybrid (PV-WT-FC) renewable energy system (HRES) for stand-alone usages by an optimization-simulation model: Case study of Iran. Renewable and Sustainable Energy Reviews, 54, 139–150. https://doi.org/10.1016/j.rser.2015.09.046

[428]   Amutha, W. M., & Rajini, V. (2016). Cost benefit and technical analysis of rural electrification alternatives in southern India using HOMER. Renewable and Sustainable Energy Reviews, 62, 236–246. https://doi.org/10.1016/j.rser.2016.04.042

[429]   Fan, X. chao, Wang, W. qing, Shi, R. jing, & Cheng, Z. jiang. (2017). Hybrid pluripotent coupling system with wind and photovoltaic-hydrogen energy storage and the coal chemical industry in Hami, Xinjiang. Renewable and Sustainable Energy Reviews, 72(1230), 950–960. https://doi.org/10.1016/j.rser.2017.01.085

[430]   Khan, M. J., Yadav, A. K., & Mathew, L. (2017). Techno economic feasibility analysis of different combinations of PV-Wind-Diesel-Battery hybrid system for telecommunication applications in different cities of Punjab, India. Renewable and Sustainable Energy Reviews, 76, 577–607. https://doi.org/10.1016/j.rser.2017.03.076

[431]   Qolipour, M., Mostafaeipour, A., & Tousi, O. M. (2017). Techno-economic feasibility of a photovoltaic-wind power plant construction for electric and hydrogen production: A case study. Renewable and Sustainable Energy Reviews, 78(May), 113–123. https://doi.org/10.1016/j.rser.2017.04.088

[432]   Fetanat, A., & Khorasaninejad, E. (2015). Size optimization for hybrid photovoltaic-wind energy system using ant colony optimization for continuous domains based integer programming. Applied Soft Computing Journal, 31, 196–209. https://doi.org/10.1016/j.asoc.2015.02.047

[433]   Cano, A., Jurado, F., Sánchez, H., Fernández, L. M., & Castañeda, M. (2014). Optimal sizing of stand-alone hybrid systems based on PV/WT/FC by using several methodologies. Journal of the Energy Institute, 87(4), 330–340. https://doi.org/10.1016/j.joei.2014.03.028

[434]   Sarker, K., Chatterjee, D., & Goswami, S. K. (2017). Grid integration of photovoltaic and wind based hybrid distributed generation system with low harmonic injection and power quality improvement using biogeography-based optimization. Renewable Energy Focus, 22–23(December), 38–56. https://doi.org/10.1016/j.ref.2017.10.004

[435]   Saheb-Koussa, D., Koussa, M., Belhamel, M., & Haddadi, M. (2011). Economic and environmental analysis for grid-connected hybrid photovoltaic-wind power system in the arid region. Energy Procedia, 6, 361–370. https://doi.org/10.1016/j.egypro.2011.05.042

[436]   Notton, G., Diaf, S., & Stoyanov, L. (2011). Hybrid photovoltaic/wind energy systems for remote locations. Energy Procedia, 6, 666–677. https://doi.org/10.1016/j.egypro.2011.05.076

[437]   Irwan, Y. M., Daut, I., Safwati, I., Irwanto, M., Gomesh, N., & Fitra, M. (2013). A new technique of photovoltaic/wind hybrid system in Perlis. Energy Procedia, 36, 492–501. https://doi.org/10.1016/j.egypro.2013.07.056

[438]   Belmili, H., Almi, M. F., Bendib, B., & Bolouma, S. (2013). A computer program development for sizing stand-alone Photovoltaic-Wind hybrid systems. Energy Procedia, 36, 546–557. https://doi.org/10.1016/j.egypro.2013.07.063

Chapter 1
A literature review and statistical analysis of
PV-wind hybrid renewable system researches by considering
the most relevant 550 articles: an upgradable matrix literature database

[439]   Rafa, S., Khenfri, F., & Diaf, S. (2013). Development and realization of an intelligent power strip for energy consumption management in hybrid wind/photovoltaic systems. Energy Procedia, 42, 530–538. https://doi.org/10.1016/j.egypro.2013.11.054

[440]   Tégani, I., Aboubou, A., Ayad, M. Y., Becherif, M., Saadi, R., & Kraa, O. (2014). Optimal sizing design and energy management of stand-alone photovoltaic/wind generator systems. Energy Procedia, 50, 163–170. https://doi.org/10.1016/j.egypro.2014.06.020

[441]   Maouedj, R., Mammeri, A., Draou, M. D., & Benyoucef, B. (2015). Techno-economic Analysis of a Standalone Hybrid Photovoltaic-wind System. Application in Electrification of a House in Adrar Region. Energy Procedia, 74, 1192–1204. https://doi.org/10.1016/j.egypro.2015.07.762

[442]   Bocklisch, T., & Lindner, J. (2016). Technical and Economic Investigation and Comparison of Photovoltaic - Wind Energy - Hybrid Systems with Battery and Heat-storage Path. Energy Procedia, 99, 350–359. https://doi.org/10.1016/j.egypro.2016.10.125

[443]   Chadel, A., Chadel, M., Aillerie, M., & Benyoucef, B. (2017). Technical and economic analysis of hybrid solar/wind energy source for the site of Tlemcen-Algeria. Energy Procedia, 119, 29–37. https://doi.org/10.1016/j.egypro.2017.07.043

[444]   Goddard, R., Zhang, L., & Xia, X. (2019). Optimal Sizing and Power Sharing of Distributed Hybrid Renewable Energy Systems Considering Socio-Demographic Factors. Energy Procedia, 159, 340–345. https://doi.org/10.1016/j.egypro.2019.01.005

[445]   Camargo, L. R., Gruber, K., Nitsch, F., & Dorner, W. (2019). Hybrid renewable energy systems to supply electricity self-sufficient residential buildings in Central Europe. Energy Procedia, 158, 321–326. https://doi.org/10.1016/j.egypro.2019.01.096

[446]   Javed, M. S., & Ma, T. (2019). Techno-economic assessment of a hybrid solar-wind-battery system with genetic algorithm. Energy Procedia, 158, 6384–6392. https://doi.org/10.1016/j.egypro.2019.01.211

[447]   Xu, B., Chen, D., Venkateshkumar, M., Xiao, Y., & Xing, Y. (2019). Modeling a pumped storage power integration to a hybrid power system with solar-wind power and its stability analysis. Energy Procedia, 158, 6225–6230. https://doi.org/10.1016/j.egypro.2019.01.475

[448]   Kolhe, M. L., Ranaweera, K. M. I. U., & Gunawardana, A. G. B. S. (2015). Techno-economic sizing of off-grid hybrid renewable energy system for rural electrification in Sri Lanka. Sustainable Energy Technologies and Assessments, 11(2015), 53–64. https://doi.org/10.1016/j.seta.2015.03.008

[449]   Prashanth, B. N., Pramod, R., & Kumar, G. B. V. (2018). Design and Development of Hybrid Wind and Solar Energy System for Power Generation. Materials Today: Proceedings, 5(5), 11415–11422. https://doi.org/10.1016/j.matpr.2018.02.109

[450]   Jansen, G., Dehouche, Z., Bonser, R., & Corrigan, H. (2019). Validation of autonomous renewable energy hybrid wind/photovoltaic/RHFC prototype for the cell tower industry using MATLAB/Simulink. Materials Today: Proceedings, 10, 408–418. https://doi.org/10.1016/j.matpr.2019.03.004

[451]   Bakir, H., & Kulaksiz, A. A. (2020). Modelling and voltage control of the solar-wind hybrid micro-grid with optimized STATCOM using GA and BFA. Engineering Science and Technology, 23(3), 576–584. https://doi.org/10.1016/j.jestch.2019.07.009

[452]   Nyemba, W. R., Chinguwa, S., Mushanguri, I., & Mbohwa, C. (2019). Optimization of the design and manufacture of a solar-wind hybrid street light. Procedia Manufacturing, 35, 285–290. https://doi.org/10.1016/j.promfg.2019.05.041

[453]   Yang, H., Zhou, W., Lu, L., & Fang, Z. (2008). Optimal sizing method for stand-alone hybrid solar-wind system with LPSP technology by using genetic algorithm. Solar Energy, 82(4), 354–367. https://doi.org/10.1016/j.solener.2007.08.005

[454]   Boonbumroong, U., Pratinthong, N., Thepa, S., Jivacate, C., & Pridasawas, W. (2011). Particle swarm optimization for AC-coupling stand alone hybrid power systems. Solar Energy, 85(3), 560–569. https://doi.org/10.1016/j.solener.2010.12.027

Chapter 1
A literature review and statistical analysis of
PV-wind hybrid renewable system researches by considering
the most relevant 550 articles: an upgradable matrix literature database

[455]   Eltamaly, A. M., Mohamed, M. A., & Alolah, A. I. (2016). A novel smart grid theory for optimal sizing of hybrid renewable energy systems. Solar Energy, 124, 26–38. https://doi.org/10.1016/j.solener.2015.11.016

[456]   Mohammadi, M., Hosseinian, S. H., & Gharehpetian, G. B. (2012). Optimization of hybrid solar energy sources/wind turbine systems integrated to utility grids as microgrid (MG) under pool/bilateral/hybrid electricity market using PSO. Solar Energy, 86(1), 112–125. https://doi.org/10.1016/j.solener.2011.09.011

[457]   Sagani, A., Vrettakos, G., & Dedoussis, V. (2017). Viability assessment of a combined hybrid electricity and heat system for remote household applications. Solar Energy, 151, 33–47. https://doi.org/10.1016/j.solener.2017.05.011

[458]   Sanajaoba, S. (2019). Optimal sizing of off-grid hybrid energy system based on minimum cost of energy and reliability criteria using firefly algorithm. Solar Energy, 188(February), 655–666. https://doi.org/10.1016/j.solener.2019.06.049

[459]   Murugaperumal, K., & Ajay D Vimal Raj, P. (2019). Feasibility design and techno-economic analysis of hybrid renewable energy system for rural electrification. Solar Energy, 188(July), 1068–1083. https://doi.org/10.1016/j.solener.2019.07.008

[460]   Manwell, J. F., McGowan, J. G., & Breger, D. (2018). A design and analysis tool for utility scale power systems incorporating large scale wind, solar photovoltaics and energy storage. Journal of Energy Storage, 19, 103–112. https://doi.org/10.1016/j.est.2018.07.010

[461]   Peng, W., Maleki, A., Rosen, M. A., & Azarikhah, P. (2018). Optimization of a hybrid system for solar-wind-based water desalination by reverse osmosis: Comparison of approaches. Desalination, 442(November 2017), 16–31. https://doi.org/10.1016/j.desal.2018.03.021

[462]   Zahboune, H., Zouggar, S., Krajacic, G., Varbanov, P. S., Elhafyani, M., & Ziani, E. (2016). Optimal hybrid renewable energy design in autonomous system using Modified Electric System Cascade Analysis and Homer software. Energy Conversion and Management, 126, 909–922. https://doi.org/10.1016/j.enconman.2016.08.061

[463]   Ifaei, P., Karbassi, A., Jacome, G., & Yoo, C. K. (2017). A systematic approach of bottom-up assessment methodology for an optimal design of hybrid solar/wind energy resources – Case study at middle east region. Energy Conversion and Management, 145(2017), 138–157. https://doi.org/10.1016/j.enconman.2017.04.097

[464]   Luta, D. N., & Raji, A. K. (2018). Decision-making between a grid extension and a rural renewable off-grid system with hydrogen generation. International Journal of Hydrogen Energy, 43(20), 9535–9548. https://doi.org/10.1016/j.ijhydene.2018.04.032

[465]   Jahangiri, M., Soulouknga, M. H., Bardei, F. K., Shamsabadi, A. A., Akinlabi, E. T., Sichilalu, S. M., & Mostafaeipour, A. (2019). Techno-econo-environmental optimal operation of grid-wind-solar electricity generation with hydrogen storage system for domestic scale, case study in Chad. International Journal of Hydrogen Energy, 44(54), 28613–28628. https://doi.org/10.1016/j.ijhydene.2019.09.130

[466]   Zahboune, H., Zouggar, S., Yong, J. Y., Varbanov, P. S., Elhafyani, M., Ziani, E., & Zarhloule, Y. (2016). Modified Electric System Cascade Analysis for optimal sizing of an autonomous Hybrid Energy System. Energy, 116, 1374–1384. https://doi.org/10.1016/j.energy.2016.07.101

[467]   Dufo-López, R., Cristóbal-Monreal, I. R., & Yusta, J. M. (2016). Optimisation of PV-wind-diesel-battery stand-alone systems to minimise cost and maximise human development index and job creation. Renewable Energy, 94, 280–293. https://doi.org/10.1016/j.renene.2016.03.065

[468]   Sikder, P. S., & Pal, N. (2019). Modeling of an intelligent battery controller for standalone solar-wind hybrid distributed generation system. Journal of King Saud University - Engineering Sciences, (xxxx). https://doi.org/10.1016/j.jksues.2019.02.002

[469]   Al-Sharafi, A., Sahin, A. Z., Ayar, T., & Yilbas, B. S. (2017). Techno-economic analysis and optimization of solar and wind energy systems for power generation and hydrogen production in Saudi

Chapter 1   **A literature review and statistical analysis of**
PV-wind hybrid renewable system researches by considering
the most relevant 550 articles: an upgradable matrix literature database

Arabia.   Renewable   and   Sustainable   Energy   Reviews,   69,   33–49.
https://doi.org/10.1016/j.rser.2016.11.157

[470]   Kaabeche, A., Diaf, S., & Ibtiouen, R. (2017). Firefly-inspired algorithm for optimal sizing of
renewable hybrid system considering reliability criteria. Solar Energy, 155, 727–738.
https://doi.org/10.1016/j.solener.2017.06.070

[471]   Das, D. C., Roy, A. K., & Sinha, N. (2012). GA based frequency controller for solar thermal-diesel-
wind hybrid energy generation/energy storage system. International Journal of Electrical Power and
Energy Systems, 43(1), 262–279. https://doi.org/10.1016/j.ijepes.2012.05.025

[472]   Said, B., Messaoud, H., Aek, S., Roca I Cabarrocas, P., Bourouis, M., Alberto, C., … Med Seghir, B.
(2013). Hybrid system and environmental evaluation case house in south of Algeria. Energy Procedia, 36,
1328–1338. https://doi.org/10.1016/j.egypro.2013.07.151

[473]   Loganathan, B., Chowdhury, H., Mustary, I., Sony, S. M., Rana, M. M., & Alam, F. (2019). Design
of hybrid houseshold power generation system for a rural area: A case study for oodnadatta, Australia.
Energy Procedia, 160, 827–833. https://doi.org/10.1016/j.egypro.2019.02.151

[474]   Bizon, N., Oproescu, M., & Raceanu, M. (2015). Efficient energy control strategies for a standalone
Renewable/Fuel Cell Hybrid Power Source. Energy Conversion and Management, 90, 93–110.
https://doi.org/10.1016/j.enconman.2014.11.002

[475]   Bizon, N. (2014). Load-following mode control of a standalone renewable/fuel cell hybrid power
source.   Energy   Conversion   and   Management,   77,   763–772.
https://doi.org/10.1016/j.enconman.2013.10.035

[476]   Baghdadi, F., Mohammedi, K., Diaf, S., & Behar, O. (2015). Feasibility study and energy conversion
analysis of stand-alone hybrid renewable energy system. Energy Conversion and Management, 105, 471–
479. https://doi.org/10.1016/j.enconman.2015.07.051

[477]   Derrouazin, A., Aillerie, M., Mekkakia-Maaza, N., & Charles, J. P. (2017). Multi input-output fuzzy
logic smart controller for a residential hybrid solar-wind-storage energy system. Energy Conversion and
Management, 148, 238–250. https://doi.org/10.1016/j.enconman.2017.05.046

[478]   Gökçek, M., & Kale, C. (2018). Optimal design of a Hydrogen Refuelling Station (HRFS) powered
by Hybrid Power System. Energy Conversion and Management, 161, 215–224.
https://doi.org/10.1016/j.enconman.2018.02.007

[479]   Abdelshafy, A. M., Hassan, H., & Jurasz, J. (2018). Optimal design of a grid-connected desalination
plant powered by renewable energy resources using a hybrid PSO–GWO approach. Energy Conversion
and Management, 173, 331–347. https://doi.org/10.1016/j.enconman.2018.07.083

[480]   Acevedo-Arenas, C. Y., Correcher, A., Sánchez-Díaz, C., Ariza, E., Alfonso-Solar, D., Vargas-
Salgado, C., & Petit-Suárez, J. F. (2019). MPC for optimal dispatch of an AC-linked hybrid
PV/wind/biomass/H2 system incorporating demand response. Energy Conversion and Management, 186,
241–257. https://doi.org/10.1016/j.enconman.2019.02.044

[481]   Sezer, N., & Koç, M. (2019). Development and performance assessment of a new integrated solar,
wind, and osmotic power system for multigeneration, based on thermodynamic principles. Energy
Conversion and Management, 188(March), 94–111. https://doi.org/10.1016/j.enconman.2019.03.051

[482]   Abdin, Z., & Mérida, W. (2019). Hybrid energy systems for off-grid power supply and hydrogen
production based on renewable energy: A techno-economic analysis. Energy Conversion and
Management, 196(January), 1068–1079. https://doi.org/10.1016/j.enconman.2019.06.068

[483]   Yang, H., Wei, Z., & Chengzhi, L. (2009). Optimal design and techno-economic analysis of a hybrid
solar-wind   power   generation   system.   Applied   Energy,   86(2),   163–169.
https://doi.org/10.1016/j.apenergy.2008.03.008

[484]   Ma, T., Yang, H., Lu, L., & Peng, J. (2015). Optimal design of an autonomous solar-wind-pumped
storage   power   supply   system.   Applied   Energy,   160,   728–736.
https://doi.org/10.1016/j.apenergy.2014.11.026

Chapter 1

A literature review and statistical analysis of PV-wind hybrid renewable system researches by considering the most relevant 550 articles: an upgradable matrix literature database

[485]   Bagheri, M., Delbari, S. H., Pakzadmanesh, M., & Kennedy, C. A. (2019). City-integrated renewable energy design for low-carbon and climate-resilient communities. Applied Energy, 239(June 2018), 1212–1225. https://doi.org/10.1016/j.apenergy.2019.02.031

[486]   Zhang, H., Lu, Z., Hu, W., Wang, Y., Dong, L., & Zhang, J. (2019). Coordinated optimal operation of hydro–wind–solar integrated systems. Applied Energy, 242, 883–896. https://doi.org/10.1016/j.apenergy.2019.03.064

[487]   Li, L., Yao, Z., You, S., Wang, C. H., Chong, C., & Wang, X. (2019). Optimal design of negative emission hybrid renewable energy systems with biochar production. Applied Energy, 243, 233–249. https://doi.org/10.1016/j.apenergy.2019.03.183

[488]   Wei, H., Hongxuan, Z., Yu, D., Yiting, W., Ling, D., & Ming, X. (2019). Short-term optimal operation of hydro-wind-solar hybrid system with improved generative adversarial networks. Applied Energy, 250(March), 389–403. https://doi.org/10.1016/j.apenergy.2019.04.090

[489]   Cao, S. (2019). The impact of electric vehicles and mobile boundary expansions on the realization of zero-emission office buildings. Applied Energy, 251(May), 113347. https://doi.org/10.1016/j.apenergy.2019.113347

[490]   Giannakoudis, G., Papadopoulos, A. I., Seferlis, P., & Voutetakis, S. (2010). Optimum design and operation under uncertainty of power systems using renewable energy sources and hydrogen storage. International Journal of Hydrogen Energy, 35(3), 872–891. https://doi.org/10.1016/j.ijhydene.2009.11.044

[491]   Calderón, M., Calderón, A. J., Ramiro, A., & González, J. F. (2010). Automatic management of energy flows of a stand-alone renewable energy supply with hydrogen support. International Journal of Hydrogen Energy, 35(6), 2226–2235. https://doi.org/10.1016/j.ijhydene.2009.12.028

[492]   García-Triviño, P., Fernández-Ramírez, L. M., Gil-Mena, A. J., Llorens-Iborra, F., García-Vázquez, C. A., & Jurado, F. (2016). Optimized operation combining costs, efficiency and lifetime of a hybrid renewable energy system with energy storage by battery and hydrogen in grid-connected applications. International Journal of Hydrogen Energy, 41(48), 23132–23144. https://doi.org/10.1016/j.ijhydene.2016.09.140

[493]   Chen, H., Yang, C., Deng, K., Zhou, N., & Wu, H. (2017). Multi-objective optimization of the hybrid wind/solar/fuel cell distributed generation system using Hammersley Sequence Sampling. International Journal of Hydrogen Energy, 42(12), 7836–7846. https://doi.org/10.1016/j.ijhydene.2017.01.202

[494]   Keskin Arabul, F., Arabul, A. Y., Kumru, C. F., & Boynuegri, A. R. (2017). Providing energy management of a fuel cell–battery–wind turbine–solar panel hybrid off grid smart home system. International Journal of Hydrogen Energy, 42(43), 26906–26913. https://doi.org/10.1016/j.ijhydene.2017.02.204

[495]   Saheb Koussa, D., & Koussa, M. (2016). GHGs (greenhouse gases) emission and economic analysis of a GCRES (grid-connected renewable energy system) in the arid region, Algeria. Energy, 102, 216–230. https://doi.org/10.1016/j.energy.2016.02.103

[496]   Rajanna, S., & Saini, R. P. (2016). Development of optimal integrated renewable energy model with battery storage for a remote Indian area. Energy, 111, 803–817. https://doi.org/10.1016/j.energy.2016.06.005

[497]   Baghaee, H. R., Mirsalim, M., Gharehpetian, G. B., & Talebi, H. A. (2016). Reliability/cost-based multi-objective Pareto optimal design of stand-alone wind/PV/FC generation microgrid system. Energy, 115, 1022–1041. https://doi.org/10.1016/j.energy.2016.09.007

[498]   Jurasz, J., Beluco, A., & Canales, F. A. (2018). The impact of complementarity on power supply reliability of small scale hybrid energy systems. Energy, 161, 737–743. https://doi.org/10.1016/j.energy.2018.07.182

[499]   Talaat, M., Farahat, M. A., & Elkholy, M. H. (2019). Renewable power integration: Experimental and simulation study to investigate the ability of integrating wave, solar and wind energies. Energy, 170, 668–682. https://doi.org/10.1016/j.energy.2018.12.171

Chapter 1   **A literature review and statistical analysis of**
PV-wind hybrid renewable system researches by considering
the most relevant 550 articles: an upgradable matrix literature database

[500]   Li, C., Wang, W., & Chen, D. (2019). Multi-objective complementary scheduling of hydro-thermal-RE power system via a multi-objective hybrid grey wolf optimizer. Energy, 171, 241–255. https://doi.org/10.1016/j.energy.2018.12.213

[501]   Nematollahi, O., Alamdari, P., Jahangiri, M., Sedaghat, A., & Alemrajabi, A. A. (2019). A techno-economical assessment of solar/wind resources and hydrogen production: A case study with GIS maps. Energy, 175, 914–930. https://doi.org/10.1016/j.energy.2019.03.125

[502]   Li, Q., Loy-Benitez, J., Nam, K. J., Hwangbo, S., Rashidi, J., & Yoo, C. K. (2019). Sustainable and reliable design of reverse osmosis desalination with hybrid renewable energy systems through supply chain forecasting using recurrent neural networks. Energy, 178, 277–292. https://doi.org/10.1016/j.energy.2019.04.114

[503]   Chong, W. T., Wang, X. H., Wong, K. H., Mojumder, J. C., Poh, S. C., Saw, L. H., & Lai, S. H. (2016). Performance assessment of a hybrid solar-wind-rain eco-roof system for buildings. Energy and Buildings, 127, 1028–1042. https://doi.org/10.1016/j.enbuild.2016.06.065

[504]   Baseer, M. A., Alqahtani, A., & Rehman, S. (2019). Techno-economic design and evaluation of hybrid energy systems for residential communities: Case study of Jubail industrial city. Journal of Cleaner Production, 237, 117806. https://doi.org/10.1016/j.jclepro.2019.117806

[505]   Zhang, W., Maleki, A., & Rosen, M. A. (2019). A heuristic-based approach for optimizing a small independent solar and wind hybrid power scheme incorporating load forecasting. Journal of Cleaner Production, 241, 117920. https://doi.org/10.1016/j.jclepro.2019.117920

[506]   Kashefi Kaviani, A., Riahy, G. H., & Kouhsari, S. M. (2009). Optimal design of a reliable hydrogen-based stand-alone wind/PV generating system, considering component outages. Renewable Energy, 34(11), 2380–2390. https://doi.org/10.1016/j.renene.2009.03.020

[507]   Sarker, S. (2016). Feasibility analysis of a renewable hybrid energy system with producer gas generator fulfilling remote household electricity demand in Southern Norway. Renewable Energy, 87, 772–781. https://doi.org/10.1016/j.renene.2015.11.013

[508]   Ramli, M. A. M., Hiendro, A., & Al-Turki, Y. A. (2016). Techno-economic energy analysis of wind/solar hybrid system: Case study for western coastal area of Saudi Arabia. Renewable Energy, 91, 374–385. https://doi.org/10.1016/j.renene.2016.01.071

[509]   Shafiullah, G. M. (2016). Hybrid renewable energy integration (HREI) system for subtropical climate in Central Queensland, Australia. Renewable Energy, 96, 1034–1053. https://doi.org/10.1016/j.renene.2016.04.101

[510]   Ali, L., & Shahnia, F. (2017). Determination of an economically-suitable and sustainable standalone power system for an off-grid town in Western Australia. Renewable Energy, 106, 243–254. https://doi.org/10.1016/j.renene.2016.12.088

[511]   Nag, A. K., & Sarkar, S. (2018). Modeling of hybrid energy system for futuristic energy demand of an Indian rural area and their optimal and sensitivity analysis. Renewable Energy, 118, 477–488. https://doi.org/10.1016/j.renene.2017.11.047

[512]   Salisu, S., Mustafa, M. W., Olatomiwa, L., & Mohammed, O. O. (2019). Assessment of technical and economic feasibility for a hybrid PV-wind-diesel-battery energy system in a remote community of north central Nigeria. Alexandria Engineering Journal, 58(4), 1103–1118. https://doi.org/10.1016/j.aej.2019.09.013

[513]   Abo-Elyousr, F. K., & Elnozahy, A. (2018). Bi-objective economic feasibility of hybrid micro-grid systems with multiple fuel options for islanded areas in Egypt. Renewable Energy, 128, 37–56. https://doi.org/10.1016/j.renene.2018.05.066

[514]   Duchaud, J. L., Notton, G., Darras, C., & Voyant, C. (2019). Multi-Objective Particle Swarm optimal sizing of a renewable hybrid power plant with storage. Renewable Energy, 131, 1156–1167. https://doi.org/10.1016/j.renene.2018.08.058

Chapter 1   **A literature review and statistical analysis of**
PV-wind hybrid renewable system researches by considering
the most relevant 550 articles: an upgradable matrix literature database

[515]   El Alimi, S., Maatallah, T., & Ben Nasrallah, S. (2014). Break-even analysis and optimization of a stand-alone hybrid system with battery storage for residential load consumption - A case study. Renewable and Sustainable Energy Reviews, 37, 408–423. https://doi.org/10.1016/j.rser.2014.04.059

[516]   Abdilahi, A. M., Mohd Yatim, A. H., Mustafa, M. W., Khalaf, O. T., Shumran, A. F., & Mohamed Nor, F. (2014). Feasibility study of renewable energy-based microgrid system in Somaliland's urban centers. Renewable and Sustainable Energy Reviews, 40, 1048–1059. https://doi.org/10.1016/j.rser.2014.07.150

[517]   Gupta, R. A., Kumar, R., & Bansal, A. K. (2015). BBO-based small autonomous hybrid power system optimization incorporating wind speed and solar radiation forecasting. Renewable and Sustainable Energy Reviews, 41, 1366–1375. https://doi.org/10.1016/j.rser.2014.09.017

[518]   Ajlan, A., Tan, C. W., & Abdilahi, A. M. (2017). Assessment of environmental and economic perspectives for renewable-based hybrid power system in Yemen. Renewable and Sustainable Energy Reviews, 75(October 2016), 559–570. https://doi.org/10.1016/j.rser.2016.11.024

[519]   Khare, R., & Kumar, Y. (2016). A novel hybrid MOL-TLBO optimized techno-economic-socio analysis of renewable energy mix in island mode. Applied Soft Computing Journal, 43, 187–198. https://doi.org/10.1016/j.asoc.2016.02.044

[520]   Heidary, B., Hashjin, T. T., Ghobadian, B., & Roshandel, R. (2018). Optimal integration of small scale hybrid solar wind RO-MSF desalination system. Renewable Energy Focus, 27(December), 120–134. https://doi.org/10.1016/j.ref.2018.05.003

[521]   Amer, M., Namaane, A., & M'Sirdi, N. K. (2013). Optimization of hybrid renewable energy systems (HRES) using PSO for cost reduction. Energy Procedia, 42, 318–327. https://doi.org/10.1016/j.egypro.2013.11.032

[522]   Jayachandran, M., & Ravi, G. (2017). Design and Optimization of Hybrid Micro-Grid System. Energy Procedia, 117, 95–103. https://doi.org/10.1016/j.egypro.2017.05.111

[523]   Duchaud, J. L., Notton, G., Fouilloy, A., & Voyant, C. (2019). Wind, solar and battery micro-grid optimal sizing in Tilos Island. Energy Procedia, 159, 22–27. https://doi.org/10.1016/j.egypro.2018.12.012

[524]   Zhang, H., Hu, W., Yu, R., & Tang, M. (2019). Coordinated optimal short-term operation of hydro-wind-solar integrated systems. Energy Procedia, 158, 6260–6265. https://doi.org/10.1016/j.egypro.2019.01.460

[525]   Li, J., Lu, J., Yao, L., Cheng, L., & Qin, H. (2019). Wind-Solar-Hydro power optimal scheduling model based on multiobjective dragonfly algorithm. Energy Procedia, 158, 6217–6224. https://doi.org/10.1016/j.egypro.2019.01.476

[526]   Saad, N. H., El-Sattar, A. A., & Mansour, A. E. A. M. (2018). A novel control strategy for grid connected hybrid renewable energy systems using improved particle swarm optimization. Ain Shams Engineering Journal, 9(4), 2195–2214. https://doi.org/10.1016/j.asej.2017.03.009

[527]   Yahyaoui, I., Yahyaoui, A., Chaabene, M., & Tadeo, F. (2016). Energy management for a stand-alone photovoltaic-wind system suitable for rural electrification. Sustainable Cities and Society, 25, 90–101. https://doi.org/10.1016/j.scs.2015.12.002

[528]   Mosaad, M. I., Abed El-Raouf, M. O., Al-Ahmar, M. A., & Bendary, F. M. (2019). Optimal PI controller of DVR to enhance the performance of hybrid power system feeding a remote area in Egypt. Sustainable Cities and Society, 47, 101469. https://doi.org/10.1016/j.scs.2019.101469

[529]   Algabalawy, M. A., Abdelaziz, A. Y., Mekhamer, S. F., & Abdel Aleem, S. H. E. (2018). Considerations on optimal design of hybrid power generation systems using whale and sine cosine optimization algorithms. Journal of Electrical Systems and Information Technology, 5(3), 312–325. https://doi.org/10.1016/j.jesit.2018.03.004

[530]   Fathabadi, H. (2017). Novel standalone hybrid solar/wind/fuel cell power generation system for remote areas. Solar Energy, 146, 30–43. https://doi.org/10.1016/j.solener.2017.01.071

Chapter 1

**A literature review and statistical analysis of
PV-wind hybrid renewable system researches by considering
the most relevant 550 articles: an upgradable matrix literature database**

[531] Shivaie, M., Mokhayeri, M., Kiani-Moghaddam, M., & Ashouri-Zadeh, A. (2019). A reliability-constrained cost-effective model for optimal sizing of an autonomous hybrid solar/wind/diesel/battery energy system by a modified discrete bat search algorithm. Solar Energy, 189, 344–356. https://doi.org/10.1016/j.solener.2019.07.075

[532] Ziogou, C., Ipsakis, D., Elmasides, C., Stergiopoulos, F., Papadopoulou, S., Seferlis, P., & Voutetakis, S. (2011). Automation infrastructure and operation control strategy in a stand-alone power system based on renewable energy sources. Journal of Power Sources, 196(22), 9488–9499. https://doi.org/10.1016/j.jpowsour.2011.07.029

[533] Rathore, A., & Patidar, N. P. (2019). Reliability assessment using probabilistic modelling of pumped storage hydro plant with PV-Wind based standalone microgrid. International Journal of Electrical Power and Energy Systems, 106(October 2018), 17–32. https://doi.org/10.1016/j.ijepes.2018.09.030

[534] Li, L., You, S., & Wang, X. (2019). Optimal design of standalone hybrid renewable energy systems with biochar production in remote rural areas: A case study. Energy Procedia, 158, 688–693. https://doi.org/10.1016/j.egypro.2019.01.185

[535] Xu, J., Wang, F., Lv, C., Huang, Q., & Xie, H. (2018). Economic-environmental equilibrium based optimal scheduling strategy towards wind-solar-thermal power generation system under limited resources. Applied Energy, 231, 355–371. https://doi.org/10.1016/j.apenergy.2018.09.113

[536] Chen, S., Kumar, A., Wong, W. C., Chiu, M. Sen, & Wang, X. (2019). Hydrogen value chain and fuel cells within hybrid renewable energy systems: Advanced operation and control strategies. Applied Energy, 233–234(October 2018), 321–337. https://doi.org/10.1016/j.apenergy.2018.10.003

[537] Patel, A. M., & Singal, S. K. (2019). Optimal component selection of integrated renewable energy system for power generation in stand-alone applications. Energy, 175, 481–504. https://doi.org/10.1016/j.energy.2019.03.055

[538] Rad, M. A. V., Ghasempour, R., Rahdan, P., Mousavi, S., & Arastounia, M. (2020). Techno-economic analysis of a hybrid power system based on the cost-effective hydrogen production method for rural electrification, a case study in Iran. Energy, 190. https://doi.org/10.1016/j.energy.2019.116421

[539] Sharma, B., Dahiya, R., & Nakka, J. (2019). Effective grid connected power injection scheme using multilevel inverter based hybrid wind solar energy conversion system. Electric Power Systems Research, 171(December 2018), 1–14. https://doi.org/10.1016/j.epsr.2019.01.044

[540] Neto, P. B. L., Saavedra, O. R., & Oliveira, D. Q. (2020). The effect of complementarity between solar, wind and tidal energy in isolated hybrid microgrids. Renewable Energy, 147, 339–355. https://doi.org/10.1016/j.renene.2019.08.134

[541] Kaabeche, A., Belhamel, M., & Ibtiouen, R. (2011). Techno-economic valuation and optimization of integrated photovoltaic/wind energy conversion system. Solar Energy, 85(10), 2407–2420. https://doi.org/10.1016/j.solener.2011.06.032

[542] García-Triviño, P., Gil-Mena, A. J., Llorens-Iborra, F., García-Vázquez, C. A., Fernández-Ramírez, L. M., & Jurado, F. (2015). Power control based on particle swarm optimization of grid-connected inverter for hybrid renewable energy system. Energy Conversion and Management, 91, 83–92. https://doi.org/10.1016/j.enconman.2014.11.051

[543] Azaza, M., & Wallin, F. (2017). Multi objective particle swarm optimization of hybrid micro-grid system: A case study in Sweden. Energy, 123, 108–118. https://doi.org/10.1016/j.energy.2017.01.149

[544] Vaccari, M., Mancuso, G. M., Riccardi, J., Cantù, M., & Pannocchia, G. (2019). A Sequential Linear Programming algorithm for economic optimization of Hybrid Renewable Energy Systems. Journal of Process Control, 74, 189–201. https://doi.org/10.1016/j.jprocont.2017.08.015

[545] Iverson, Z., Achuthan, A., Marzocca, P., & Aidun, D. (2013). Optimal design of hybrid renewable energy systems (HRES) using hydrogen storage technology for data center applications. Renewable Energy, 52, 79–87. https://doi.org/10.1016/j.renene.2012.10.038

Chapter 1

**A literature review and statistical analysis of
PV-wind hybrid renewable system researches by considering
the most relevant 550 articles: an upgradable matrix literature database**

[546] Maleki, A., Hafeznia, H., Rosen, M. A., & Pourfayaz, F. (2017). Optimization of a grid-connected hybrid solar-wind-hydrogen CHP system for residential applications by efficient metaheuristic approaches. Applied Thermal Engineering, 123, 1263–1277. https://doi.org/10.1016/j.applthermaleng.2017.05.100

[547] Ray, P. K., & Mohanty, A. (2019). A robust firefly–swarm hybrid optimization for frequency control in wind/PV/FC based microgrid. Applied Soft Computing Journal, (xxxx), 105823. https://doi.org/10.1016/j.asoc.2019.105823

[548] Lee, K., & Kum, D. (2019). Complete design space exploration of isolated hybrid renewable energy system via dynamic programming. Energy Conversion and Management, 196, 920–934. https://doi.org/10.1016/j.enconman.2019.05.078

[549] Gholami, K., & Dehnavi, E. (2019). A modified particle swarm optimization algorithm for scheduling renewable generation in a micro-grid under load uncertainty. Applied Soft Computing Journal, 78, 496–514. https://doi.org/10.1016/j.asoc.2019.02.042

[550] Kennedy, N., Miao, C., Wu, Q., Wang, Y., Ji, J., & Roskilly, T. (2017). Optimal Hybrid Power System Using Renewables and Hydrogen for an Isolated Island in the UK. Energy Procedia, 105, 1388–1393. https://doi.org/10.1016/j.egypro.2017.03.517

[551] Luna-Rubio, R., Trejo-Perea, M., Vargas-Vázquez, D., & Ríos-Moreno, G. J. (2012). Optimal sizing of renewable hybrids energy systems: A review of methodologies. Solar Energy, 86, 1077-1088. https://doi.org/10.1016/j.solener.2011.10.016

[552] Ciupageanu, D. A., Barelli, L., & Lazaroiu, G. (2020). Real-time stochastic power management strategies in hybrid renewable energy systems: A review of key applications and perspectives. Electric Power Systems Research, 187, 106497. https://doi.org/10.1016/j.epsr.2020.106497.

[553] Sinha, S., & Chandel, S. S. (2014). Review of software tools for hybrid renewable energy systems. Renewable and Sustainable Energy Reviews, 32, 192-205. https://doi.org/10.1016/j.rser.2014.01.035

[554] Sinha, S., & Chandel, S. S. (2015). Review of recent trends in optimization techniques for solar photovoltaic-wind based hybrid energy systems. Renewable and Sustainable Energy Reviews, 50, 755-769, https://doi.org/10.1016/j.rser.2015.05.040

[555] Khan, F. A., Pal, N., & Saeed, S. H. (2018). Review of solar photovoltaic and wind hybrid energy systems for sizing strategies optimization techniques and cost analysis methodologies. Renewable and Sustainable Energy Reviews, 92, 937-947, https://doi.org/10.1016/j.rser.2018.04.107

[556] Al-falahi, M. D. A., Jayasinghe, S. D. G., & Enshaei, H. (2017). A review on recent size optimization methodologies for standalone solar and wind hybrid renewable energy system. In Energy Conversion and Management, 143, 252-274. https://doi.org/10.1016/j.enconman.2017.04.019

[557] Lian, J., Zhang, Y., Ma, C., Yang, Y., & Chaima, E. (2019). A review on recent sizing methodologies of hybrid renewable energy systems. Energy Conversion and Management, 199, 112027. https://doi.org/10.1016/j.enconman.2019.112027

[558] Shivarama Krishna, K., & Sathish Kumar, K. (2015). A review on hybrid renewable energy systems. In Renewable and Sustainable Energy Reviews, 52, 907-916. https://doi.org/10.1016/j.rser.2015.07.187

[559] Al Busaidi, A. S., Kazem, H. A., Al-Badi, A. H., & Farooq Khan, M. (2016). A review of optimum sizing of hybrid PV-Wind renewable energy systems in oman. Renewable and Sustainable Energy Reviews, Volume 53, 185-193. https://doi.org/10.1016/j.rser.2015.08.039

[560] Khare, V., Nema, S., & Baredar, P. (2016). Solar-wind hybrid renewable energy system: A review. In Renewable and Sustainable Energy Reviews, 58, 23-33. https://doi.org/10.1016/j.rser.2015.12.223

[561] Siddaiah, R., & Saini, R. P. (2016). A review on planning, configurations, modeling and optimization techniques of hybrid renewable energy systems for off grid applications. Renewable and Sustainable Energy Reviews, 58, 376-396. https://doi.org/10.1016/j.rser.2015.12.281

Chapter 1

A literature review and statistical analysis of PV-wind hybrid renewable system researches by considering the most relevant 550 articles: an upgradable matrix literature database

[562]   Olatomiwa, L., Mekhilef, S., Ismail, M. S., & Moghavvemi, M. (2016). Energy management strategies in hybrid renewable energy systems: A review. Renewable and Sustainable Energy Reviews. 62, 821-835. https://doi.org/10.1016/j.rser.2016.05.040.

[563]   Goel, S., & Sharma, R. (2017). Performance evaluation of stand alone, grid connected and hybrid renewable energy systems for rural application: A comparative review. Renewable and Sustainable Energy Reviews, 78, 1378-1389. https://doi.org/10.1016/j.rser.2017.05.200

[564]   Sawle, Y., Gupta, S. C., & Bohre, A. K. (2018). Review of hybrid renewable energy systems with comparative analysis of off-grid hybrid system. Renewable and Sustainable Energy Reviews, 81, 2217-2235. https://doi.org/10.1016/j.rser.2017.06.033

[565]   Anoune, K., Bouya, M., Astito, A., & Abdellah, A. Ben. (2018). Sizing methods and optimization techniques for PV-wind based hybrid renewable energy system: A review. Renewable and Sustainable Energy Reviews, 93, 652-673. https://doi.org/10.1016/j.rser.2018.05.032

[566]   Kartite, J., & Cherkaoui, M. (2019). Study of the different structures of hybrid systems in renewable energies: A review. Energy Procedia, 157, 323-330https://doi.org/10.1016/j.egypro.2018.11.197

[567]   Nema, P., Nema, R. K., & Rangnekar, S. (2009). A current and future state of art development of hybrid energy system using wind and PV-solar: A review. Renewable and Sustainable Energy Reviews, 13, 2096-210. https://doi.org/10.1016/j.rser.2008.10.006

[568]   Mahesh, A., & Sandhu, K. S. (2015). Hybrid wind/photovoltaic energy system developments: Critical review and findings. Renewable and Sustainable Energy Reviews, 52, 1135-1147. https://doi.org/10.1016/j.rser.2015.08.008.

[569]   Faccio, M., Gamberi, M., Bortolini, M., & Nedaei, M. (2018). State-of-art review of the optimization methods to design the configuration of hybrid renewable energy systems (HRESs). Frontiers in Energy. 12, 591–622. https://doi.org/10.1007/s11708-018-0567-x

[570]   Mohammed, Y. S., Mustafa, M. W., & Bashir, N. (2014). Hybrid renewable energy systems for off-grid electric power: Review of substantial issues. Renewable and Sustainable Energy Reviews, 35,527-539. https://doi.org/10.1016/j.rser.2014.04.022

[571]   Guo, S., Liu, Q., Sun, J., & Jin, H. (2018). A review on the utilization of hybrid renewable energy. Renewable and Sustainable Energy Reviews, 91, 1121-1147. https://doi.org/10.1016/j.rser.2018.04.105

[572]   Upadhyay, S., & Sharma, M. P. (2014). A review on configurations, control and sizing methodologies of hybrid energy systems. In Renewable and Sustainable Energy Reviews, 38, 47-63https://doi.org/10.1016/j.rser.2014.05.057

[573]   Twaha, S., & Ramli, M. A. M. (2018). A review of optimization approaches for hybrid distributed energy generation systems: Off-grid and grid-connected systems. Sustainable Cities and Society, 41, 320-331. https://doi.org/10.1016/j.scs.2018.05.027

[574]   Liu, Y., Yu, S., Zhu, Y., Wang, D., & Liu, J. (2018). Modeling, planning, application and management of energy systems for isolated areas: A review. Renewable and Sustainable Energy Reviews, 82, 460-470. https://doi.org/10.1016/j.rser.2017.09.063

[575]   Fadaee, M., & Radzi, M. A. M. (2012). Multi-objective optimization of a stand-alone hybrid renewable energy system by using evolutionary algorithms: A review. Renewable and Sustainable Energy Reviews, 16, 3364-3369. https://doi.org/10.1016/j.rser.2012.02.071

[576]   Neves, D., Silva, C. A., & Connors, S. (2014). Design and implementation of hybrid renewable energy systems on micro-communities: A review on case studies. Renewable and Sustainable Energy Reviews, 31, 935-946. https://doi.org/10.1016/j.rser.2013.12.047

[577]   Ismail, M. S., Moghavvemi, M., Mahlia, T. M. I., Muttaqi, K. M., & Moghavvemi, S. (2015). Effective utilization of excess energy in standalone hybrid renewable energy systems for improving comfort ability and reducing cost of energy: A review and analysis. Renewable and Sustainable Energy Reviews,42, 726-734. https://doi.org/10.1016/j.rser.2014.10.051

Chapter 1   **A literature review and statistical analysis of**
PV-wind hybrid renewable system researches by considering
the most relevant 550 articles: an upgradable matrix literature database

[578]   Arul, P. G., Ramachandaramurthy, V. K., & Rajkumar, R. K. (2015). Control strategies for a hybrid renewable energy system: A review. In Renewable and Sustainable Energy Reviews, 42, 597-608. https://doi.org/10.1016/j.rser.2014.10.062

[579]   Bahramara, S., Moghaddam, M. P., & Haghifam, M. R. (2016). Optimal planning of hybrid renewable energy systems using HOMER: A review. Renewable and Sustainable Energy Reviews, 62, 609-620. https://doi.org/10.1016/j.rser.2016.05.039

[580]   Vivas, F. J., De las Heras, A., Segura, F., & Andújar, J. M. (2018). A review of energy management strategies for renewable hybrid energy systems with hydrogen backup. In Renewable and Sustainable Energy Reviews, 82,126-155. https://doi.org/10.1016/j.rser.2017.09.014

[581]   Khan, M. A. M., Rehman, S., & Al-Sulaiman, F. A. (2018). A hybrid renewable energy system as a potential energy source for water desalination using reverse osmosis: A review. Renewable and Sustainable Energy Reviews, 97, 456-477. https://doi.org/10.1016/j.rser.2018.08.049

[582]   Eras-Almeida, A. A., & Egido-Aguilera, M. A. (2019). Hybrid renewable mini-grids on non-interconnected small islands: Review of case studies. Renewable and Sustainable Energy Reviews, 116, 109417. https://doi.org/10.1016/j.rser.2019.109417

[583]   ScienceDirect, www.sciencedirect.com

[584]   Scopus, www.scopus.com

[585]   Rubel, F., & Kottek, M. (2010). Observed and projected climate shifts 1901–2100 depicted by world maps of the Köppen-Geiger climate classification, Meteorol Z, 19, 135-141, http://koeppen-geiger.vu-wien.ac.at/shifts.htm

[586]   The Koppen Climate Classification. Available online: https://www.mindat.org/climate.php. [accessed: 17/12/2020].

[587]   Mazzeo, D., Matera, N., De Luca, P., Baglivo, C., Congedo, P. M. & Oliveti, G. (2020). Worldwide geographical mapping and optimization of stand-alone and grid-connected hybrid renewable system techno-economic performance across Köppen-Geiger climates. Applied Energy, 276, 115507. https://doi.org/10.1016/j.apenergy.2020.115507.

Chapter 2

Energy reliability-constrained method
for the multi-objective optimization
of a photovoltaic-wind hybrid system with battery storage

Chapter 2

Energy reliability-constrained method for the multi-objective optimization of a photovoltaic-wind hybrid system with battery storage

Chapter 2   **Energy reliability-constrained method
for the multi-objective optimization
of a photovoltaic-wind hybrid system with battery storage**
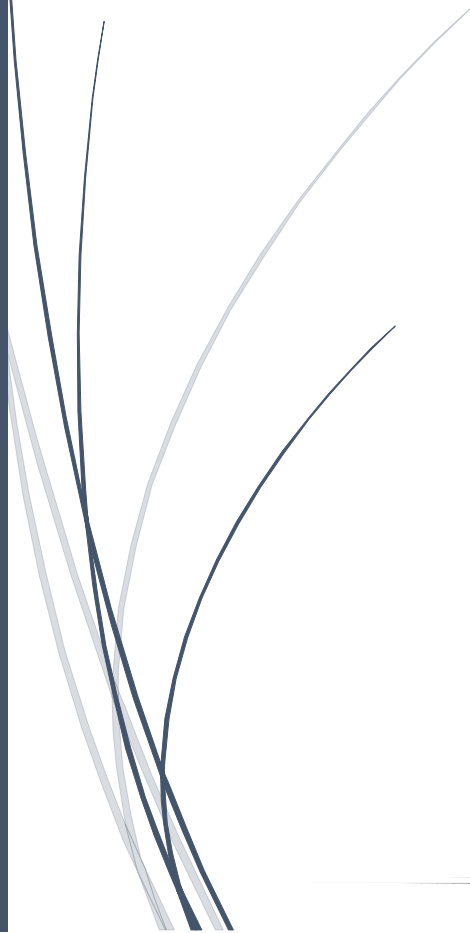
Chapter 2

Energy reliability-constrained method for the multi-objective optimization of a photovoltaic-wind hybrid system with battery storage

Abstract

A multi-objective optimization method for the dimensioning of hybrid photovoltaic-wind-battery systems HPWBS characterized by high-energy reliability is proposed. The energy reliability-constrained (ERC) method permits choosing the most proper indicators combination to be constrained or optimized as a function of the specific application. The ERC method is applicable to grid-connected and stand-alone hybrid systems with and without storage battery, for residential as well as for other uses. The reliability indicators defined are: the photovoltaic-wind fraction; energy fraction required by the load satisfied by the HPWBS; the utilization factor; energy fraction produced sent to the load; the manufacturability that characterized the system in relation to the available renewable sources and load. The ERC method was employed for the multi-objective optimization of a grid-connected hybrid system with and without storage battery for the electric energy supply to an urban residential building in a Mediterranean climate. A parametric analysis, for different loads, by varying the photovoltaic and wind power and the battery storage capacity, was developed to evaluate the annual energy reliability in a dimensionless form of 450 system configurations. The results allowed obtaining empiric correlations to be used in the system design. Finally, the ERC method application allowed achieving optimal system configurations with greater reliability compared with those provided by the Pareto-front method.

Keywords: Renewable Energy; Photovoltaic, Wind, Storage; TRNSYS; Simulation; Optimization; Hybrid system

- Energy reliability-constrained ERC method for the multi-objective optimization of an HPWBS.
- ERC method applied to a grid-connected HPWBS to supply a variable load in a Mediterranean climate.
- HPWBS was simulated under dynamic conditions by means of TRNSYS software.
- Analytic correlations for the system dimensioning are proposed.
- ERC method was compared with the Pareto-front method in the identification of the optimal system configurations.

Chapter 2   **Energy reliability-constrained method
for the multi-objective optimization
of a photovoltaic-wind hybrid system with battery storage**

1. Introduction

Recent European directives have promoted the improvement of energy performances in the construction sector. The direct effect of these policies is the increase in studies addressed to the development of innovative technological solutions aimed at reducing overall energy consumption, dependence on fossil fuels and greenhouse emissions into the atmosphere. The hybrid systems result in the best solutions to satisfy the provisions of the new directives. This term indicates the use of multiple technologies like, for example, wind, photovoltaic and geothermal plants integrated into the same system. In the electricity sector, wind and photovoltaic systems have been developing considerably in recent years, thanks to the wider availability in terms of installation costs. However, the significant intermittence and uncertainty of energy sources, also due to climate changes, may make the single use of those systems unreliable in terms of meeting the load. A combination of these two technologies (hybrid photovoltaic-wind system HPWS) allows the uncertainty issue to partially overcome, while the integration of an energy storage system (hybrid photovoltaic-wind-battery system HPWBS) mitigates the intermittence issue. The greater energy reliability of hybrid systems allows their installation even in remote areas, without access to the electricity grid (stand-alone systems), or in areas with access to the electricity grid (grid-connected). When the energy production results more or less than the required load, the difference can be exchanged with the public grid by a net metering service. Moreover, hybrid systems can be used in locations without access to reliable power, thus being an emergency system for significantly long periods in alternative to the traditional uninterruptible power supply (UPS).

In the last decade, in several research, the reliability criterion has turned out to be the most important in the sizing phase of hybrid systems. A correct sizing requires the use of proper reliability indicators and optimization analysis. The survey of the literature has highlighted that most of the reliability analysis methods on hybrid systems are related to stand-alone systems [1-13] rather than grid-connected ones [14-16]. As regards the stand-alone systems, different reliability indicators were defined by considering only the unsatisfied load [17-21] in terms of time fraction, energy fraction or probabilistic, such as the loss of power supply probability (LPSP), loss of load probability (LOLP), unmet load (UL), system performance level (SPL), loss of load hours (LOLH), loss of load risk (LOLR), level of autonomy (LA), deficiency in power supply probability (DPSP), expected energy not supplied (EENS), and maxENS. In general, from an energy point of view, further reliability indicators should be employed to make a proper coupling between the renewable energy sources of a locality, system components and load. In addition, for the size design of a reliable grid-connected system, other important factors should be considered in order to reduce the energy produced in excess.

Generally, a hybrid system optimization criterion requires the maximization or the minimization of one or more indicators, and the Pareto-front is one of the most applied methods [5, 21-23]. It is the authors' belief, in accordance with recent researches [22], in addition to optimizing some indicators, it is necessary to constrain other ones to assign a weight to each indicator and guarantee appropriate reliability. Moreover, the indicators to be constrained and those to be optimized should be chosen in relation to the importance associated with each of the objectives to be achieved and to the specific application.
The present research proposes the use of the energy reliability-constrained (ERC) method. The method allows differently constraining the reliability indicators and can be applied in the design or in the performance verification phase of a specific HPWS or HPWBS, whether grid-connected or stand-alone, for residential users as well as for other users. In the design phase, when the location is defined,

Chapter 2   Energy reliability-constrained method
for the multi-objective optimization
of a photovoltaic-wind hybrid system with battery storage

the ERC method allows the identification of the proper technical characteristic and the overall nominal power of the system components, or the identification of a suitable location for specific system components. Such flexibility makes the ERC method of a general nature from a methodological point of view.

Other critical aspects, emerged from the previous studies, regard: a scarcity of applications for grid-connected hybrid systems; the infrequency of a direct comparison between HPWS and HPWBS; specific cases studies, relating to certain power sizes of the system or fixed load levels; the prevalent use of estimated weather data rather than experimentally measured instantaneous actual data sets. In addition, as mentioned previously and highlighted in Ref. [18], several size optimization applications have been conducted worldwide and mostly the locations are characterized by high winds, such as remotely located hilly areas, where the transmission extension may not be feasible, or coastal areas [6-14, 22-26]. The studies in the urban context with low wind regime are very limited [4, 15, 25-27]. Instead, a great number of researches were conducted in the Mediterranean area [1-3, 9-13, 15, 26-28], where the elevated availability of solar radiation makes the use of these systems very promising.

For all these reasons, the ERC method was applied to a grid-connected hybrid system with and without electric battery storage for urban residential use. A width range of variation of the component sizes, for different hourly average daily load values, was considered. The climatic data used in this study were measured at the Solar Engineering Laboratory located on the roof of a building of the University of Calabria Campus, in Southern Italy. This study is the first in this area of Italy, and the results obtained are useful for similar climate regions of the Mediterranean area.

2. Methodology

The procedure consists in the energy reliability evaluation of the hybrid system in accordance with the following phases: (i) mathematical modelling to describe the non-linear characteristics of the system components; (ii) hourly dynamic simulation to obtain the powers in input and in output from each component; (ii) evaluation of the annual energies associated with these powers; (iii) dimensionless representation of the results by means of the fractions referring to the energy required by the load and referring to energy generated; (iv) definition and calculation of proper indicators that identify the system energy reliability; (v) parametric analysis to evaluate the effects of the components size variation on the system energy reliability; (vi) multi-objective optimization analysis development by means of ERC method used to identify, for a certain load, the optimal system configurations that simultaneously ensure maximization of some indicators and, for the other ones, higher values than predetermined constraints.

2.1 Mathematical modeling

Figure 1 shows the scheme of the grid-connected HPWBS for residential use.

Chapter 2   **Energy reliability-constrained method
for the multi-objective optimization
of a photovoltaic-wind hybrid system with battery storage**
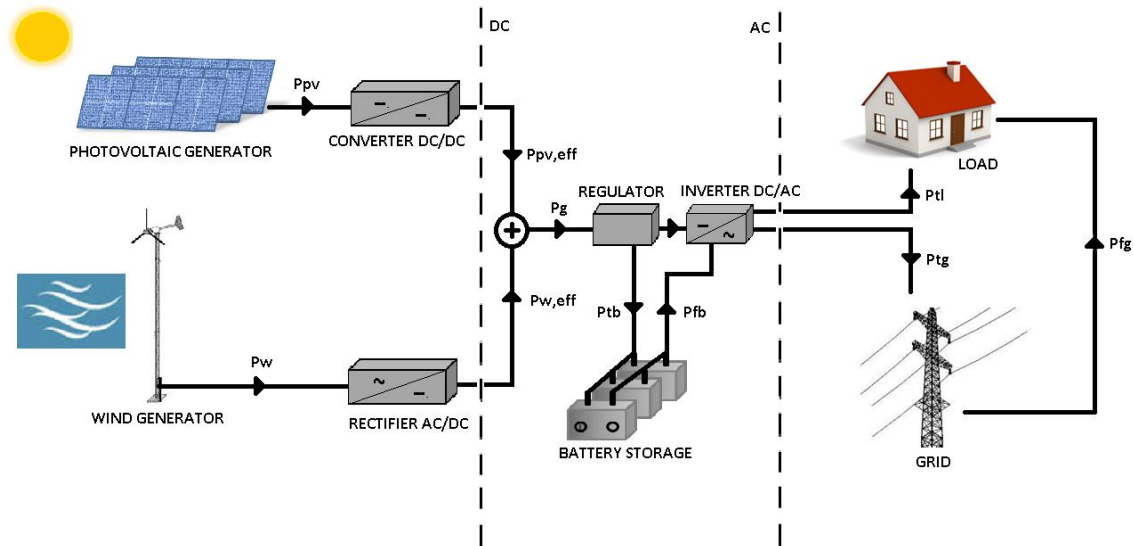
Figure 1. Scheme of the grid-connected HPWBS for residential use.

The plant consists of a wind micro-generator and an AC/DC rectifier, a photovoltaic (PV) generator
and an AC/AC converter, an electric battery storage system, a regulator and a DC/AC inverter.

2.1.1. Photovoltaic generator

The hourly solar radiation G incident on the inclined plane of the PV generator is the sum of direct,
diffuse and reflected radiation [29]:

$$G = G_{b,h}R_b + G_{d,h}R_d + \left(G_{b,h} + G_{d,h}\right)R_r \tag{1}$$

where $G_{b,h}$ and $G_{d,h}$ are the hourly direct and diffuse solar radiations on the horizontal surface, R_b is
the hourly average geometry factor of the direct radiation, R_d and R_r are the geometry factors of
diffuse and reflected radiation.

The PV generator performances are determined by solving the equivalent electric circuit consisting
of a direct/ideal-current generator, a diode and two resistances [30].

The current-voltage characteristic of the circuit is represented by the following equation:

$$I = I_L - I_0 \left[e^{\frac{V+IR_s}{a}} - 1\right] - \frac{V + IR_s}{R_{sh}} \tag{2}$$

with

$$a = \frac{N_s n_I k T_c}{q} \tag{3}$$

Chapter 2

**Energy reliability-constrained method
for the multi-objective optimization
of a photovoltaic-wind hybrid system with battery storage**

where,

q is the electron charge, k is Boltzmann's constant, n_I is the usual ideality factor (dimensionless diode curve-fitting factor, with a minimum possible), N_s is the number of cells in series and Tc is the cell temperature.

The model parameters that characterize the electric circuit, as a function of absorbed solar radiation and cell temperature, are: the light current I_L, the diode reverse saturation current I_0, the series resistance R_s, the shunt resistance R_{sh} and the modified ideality factor a.

In the reference conditions, $I_{L,ref}$, $I_{0,ref}$, $R_{s,ref}$, $R_{sh,ref}$ and a_{ref} are obtained using the simplified hypothesis introduced by Fry [31], which determines the shunt resistance directly from the slope in the short-circuit point of the I-V curve. In this way, the unknown quantities are reduced to four parameters and are obtained by imposing the conditions at the open-circuit point, short-circuit point and maximum power point into Eq. (2), and using the analytic expression of the voltage derivative compared to the temperature in open-circuit conditions, namely temperature coefficient of open-circuit voltage. The system, consisting of the four equations, is solved by an iterative search routine, which provides the values of $I_{L,ref}$, $I_{0,ref}$, $R_{s,ref}$ and a_{ref}. The parameter values under operating conditions are obtained by updating the I_L and I_0 values, as a function of solar radiation absorbed and the cell temperature respectively. The latter is calculated using the nominal operating cell temperature (NOCT). In this way, the characteristic curve is updated at each time instant as a function of the cell temperature and the solar radiation absorbed [32]. In addition, absorbed solar power is evaluated considering the incidence angle modifier IAM [33]. The electric PV power produced is calculated at the maximum power point of the characteristic curve by Eq. (4):

$$P_{pv}(t) = I_{mp}(t)V_{mp}(t) \tag{4}$$

2.1.2. Wind generator

The wind electric power as a function of the wind speed is evaluated through the reference experimental power curve. This curve is determined to a specific value of the air density using the wind speed values measured at the turbine hub height. Under operating conditions, the power delivered is determined using a calculation algorithm, which employs at each instant the following steps [34]:

(i)   calculation of the air density at the actual operating height z_h of the wind turbine, as a function of air temperature and pressure;

(ii) calculation of the wind speed $v_h(t)$ at the actual operating height z_h of the wind turbine, starting from the wind speed $v_{an}(t)$ at the anemometric height z_{an}, by Eq. (5), known the shear exponent $\alpha(t)$;

(iii) evaluation of the turbine power $P_0(t)$ at the actual operating height through the use of the experimental power curve traced for a reference air density ρ_0;

(iv) determination of the correct power $P_\rho(t)$ and the correct nominal speed $v_{nom,\rho}$, respectively by means of Eq. (6) and Eq. (7), in order to consider the updated air density value, in relation to the method of power control mode;

Chapter 2   Energy reliability-constrained method
for the multi-objective optimization
of a photovoltaic-wind hybrid system with battery storage

(v)   calculation of net power $P_{\rho,net}$ considering the miscellaneous losses ℓ (Eq. 8).

$$\frac{v_h(t)}{v_{an}(t)} = \left(\frac{z_h}{z_{an}}\right)^{\alpha(t)} \tag{5}$$

$$\frac{P_\rho(t)}{P_0(t)} = \frac{\rho(t)}{\rho_0} \tag{6}$$

$$\frac{v_{nom,\rho}(t)}{v_{nom,\rho_0}} = \left(\frac{\rho_0}{\rho(t)}\right)^{1/3} \tag{7}$$

$$P_w(t) = P_{\rho,net}(t) = P_\rho(t)\left(1 - \frac{\ell}{100}\right) \tag{8}$$

2.1.3. Electric storage battery

Battery performances are evaluated through a model, which uses the instantaneous balance equation of the state of charge (SOC). In the charging phase, the charge rate is obtained from:

$$\frac{dSOC}{dt} = P(t)\,\eta_{bat} = P_{tb}(t) \tag{9}$$

In the discharge phase, the discharge rate is obtained from:

$$\frac{dSOC}{dt} = P(t) = -P_{fb}(t) \tag{10}$$

where, η_{bat} is the battery efficiency, $P(t)$ is the power sent to the battery or the power drawn from the battery.

SOC at the successive time instant $t+1$ is determined discretizing Eq. (9) and Eq. (10):

$$\begin{cases} SOC(t+1) = SOC(t) + P_{tb}(t)\eta_{bat}\Delta t & P(t) > 0 \\ SOC(t+1) = SOC(t) - P_{fb}(t)\,\Delta t & P(t) < 0 \end{cases} \tag{11}$$

Chapter 2   **Energy reliability-constrained method
for the multi-objective optimization
of a photovoltaic-wind hybrid system with battery storage**

At any time, the SOC is subjected to the constraints $SOC_{min}(t) < SOC(t) < SOC_{max}$, with SOC_{max} and $SOC_{min}(t)$ the maximum and minimum allowable SOC. Once the SOC is known, the charge fraction f_{SOC} is calculated as a function of the battery capacity C_{bat} by Eq. (12):

$$f_{SOC}(t+1) = \frac{SOC(t+1)}{C_{bat}} \tag{12}$$

2.1.4. Static converters

The output electric power from each of the static converters shown in Figure 1 is calculated, starting from the input values, through an electric conversion efficiency:

- DC/DC converter

$$P_{pv,eff}(t) = P_{pv}(t)\, \eta_{DC/DC} \tag{13}$$

where, $P_{pv,eff}(t)$ is the output power and $P_{pv}(t)$ input power coming from the PV generator.
- AC/DC rectifier

$$P_{w,eff}(t) = P_w(t)\, \eta_{AC/DC} \tag{14}$$

where, $P_{w,eff}(t)$ is the output power and $P_w(t)$ input power coming from the wind generator.
- DC/AC inverter

$$P_{inv,out} = P_{inv,in}\, \eta_{inv} \tag{15}$$

where, $P_{inv,out}$ is the output power and $P_{inv,inp}$ input power coming from the two generators and battery.

In the Eqs. (13)-(15), $\eta_{AC/AC}$, $\eta_{AC/DC}$ and η_{inv} are the efficiencies of the correspondent static converters.

2.1.5. Regulator

The regulator, characterized by an efficiency η_{reg}, at each instant compares the power generated $P_g(t)$, sum of the power produced by the PV system $P_{pv,eff}(t)$ and wind system $P_{w,eff}(t)$, with the instantaneous load $P_L(t)$. The result of the comparison between $P_g(t)$ and $P_L(t)$ at any time instant determines the system operating and the power provided by HPWBS to the load $P_{tl}(t)$.

Chapter 2

**Energy reliability-constrained method
for the multi-objective optimization
of a photovoltaic-wind hybrid system with battery storage**

2.2. Dynamic simulation and instantaneous balance

The system was simulated on an hourly basis for a whole year using a computational model built-in TRNSYS 17 (Transient System Simulation) environment [35], see Figure 2.
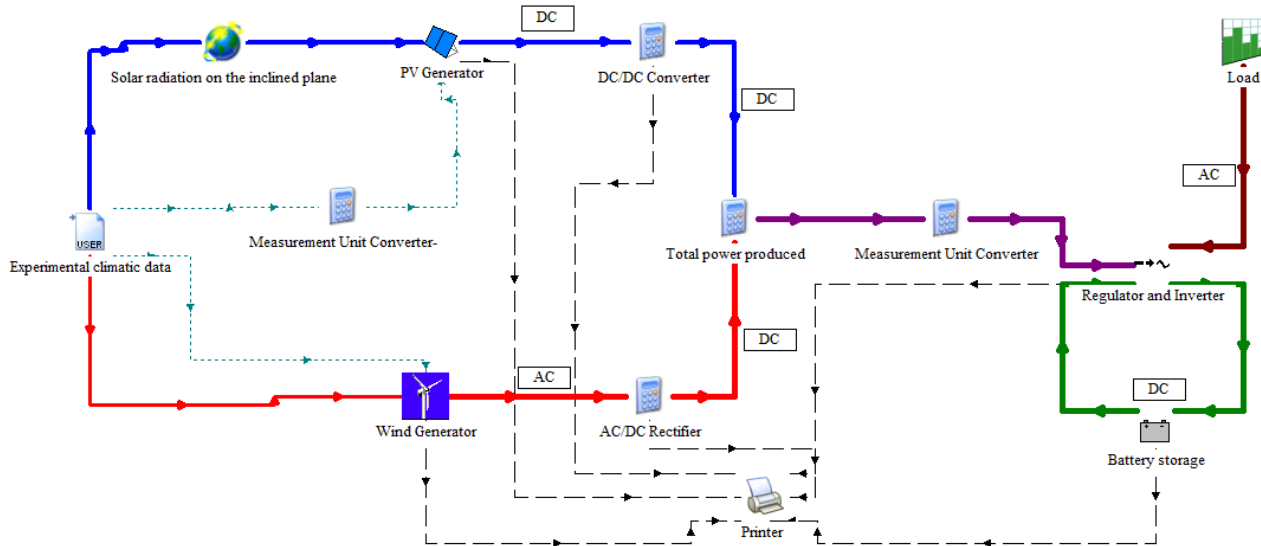
Figure 2. Assembled model of the HPWBS in TRNSYS environment.

   The system components are simulated under dynamic conditions, using mathematical models, described in the previous Section 2.1, implemented in specific Types. In particular: Type 94 simulates the PV generator, Type 90 the wind generator, Type 48 the storage battery, Type 47 the regulator and inverter, equation blocks the static converters and Type 14 the load trend; Type 9 allows to import the experimental climate data; Type 16 reports on the inclined surface the incident solar radiation on the horizontal surface; Type 25 allows results to be printed. Through the parameters setting of each Type, it is possible to determine, at any time instant, the power produced by the PV $P_{pv}(t)$ and wind generator $P_w(t)$, output power from the AC/DC rectifier $P_{w,eff}(t)$, from the DC/DC static converter $P_{pv,eff}(t)$ and from the DC/AC inverter $P_{inv,out}$, input $P_{tb}(t)$ or output $P_{fb}(t)$ power from the battery, power delivered to the load $P_{tl}(t)$, excess power $P_{tg}(t)$ and power drawn from the grid $P_{fg}(t)$.
Three different system operating modes can be identified:

Mode 1): $\eta_{reg}\eta_{inv}P_g(t) > P_L(t)$

When the overall net power generated $\eta_{reg}\eta_{inv}P_g(t)$ is greater than the power required by the load $P_L(t)$, the excess power is used to charge the battery $P_{tb}(t)$ and, in the totally charged conditions, is sent to the grid $P_{tg}(t)$. In this operation mode, the power drawn from the battery $P_{fb}(t)$ and from the grid $P_{fg}(t)$ are null.

Referring to Figure 1, the balance equation of the generated power is:

$$P_g(t) = \left[P_{pv,eff}(t) + P_{w,eff}(t)\right] = \frac{P_{tl}(t)}{\eta_{reg}\eta_{inv}} + \frac{P_{tb}(t)}{\eta_{reg}} + \frac{P_{tg}(t)}{\eta_{reg}\eta_{inv}} \qquad (16)$$

Chapter 2   **Energy reliability-constrained method**
for the multi-objective optimization
of a photovoltaic-wind hybrid system with battery storage

Mode 2): $\eta_{inv}\eta_{reg}P_g(t) < P_L(t)$

When the overall net power generated $\eta_{reg}\eta_{inv}P_g(t)$ is less than that required by the load $P_L(t)$, the missing power is drawn from the battery $P_{fb}(t)$ and, if necessary, from the grid $P_{fg}(t)$. Under such conditions, the power sent to the battery $P_{tb}(t)$ and the excess power $P_{tg}(t)$ are null.

Referring to Figure 1, the balance equation of the power sent to the load is:

$$P_{tl}(t) = P_g(t)\eta_{reg}\eta_{inv} + P_{fb}(t)\eta_{inv} = \left[P_{pv,eff}(t) + P_{w,eff}(t)\right]\eta_{reg}\eta_{inv} + P_{fb}(t)\eta_{inv} \qquad (17)$$

Mode 3): $\eta_{inv}\eta_{reg}P_g(t) = P_L(t)$

When the net overall power generated $\eta_{reg}\eta_{inv}P_g(t)$ is equal to the load $P_L(t)$, the power sent to and drawn from the battery, $P_{tb}(t)$ and $P_{fb}(t)$, and that sent to and drawn from the grid, $P_{tg}(t)$ and $P_{fg}(t)$, are null.

Referring to Figure 1, the balance equation of the generated power is:

$$P_g(t) = \left[P_{pv,eff}(t) + P_{w,eff}(t)\right] = \frac{P_{tl}(t)}{\eta_{reg}\eta_{inv}} \qquad (18)$$

Referring to the instantaneous load:

- Both in Mode 1) and Mode 3), the power required by the load is supplied entirely from the system:

$$P_L(t) = P_{tl}(t) \qquad (19)$$

- In Mode 2), the power required by the load is partly provided by HPWBS and partially withdrawn from the grid:

$$P_L(t) = P_{tl}(t) + P_{fg}(t) \qquad (20)$$

2.3. Annual energy balance

The overall annual energy required by the load E_L is partly provided by the HPWBS E_{tl} and partly by the grid E_{fg}:

$$E_L = E_{tl} + E_{fg} \qquad (21)$$

Chapter 2

**Energy reliability-constrained method
for the multi-objective optimization
of a photovoltaic-wind hybrid system with battery storage**

The overall annual energy produced by the PV and wind generator is:

$$E_g = E_{pv}\, \eta_{DC/DC} + E_w\, \eta_{AC/DC} \tag{22}$$

E_g is partly sent directly to the load, E_{dtl}, partly stored in the battery, E_{tb}, and partly sent to the grid, E_{tg}:

$$E_g = \frac{E_{dtl}}{\eta_{reg}\eta_{inv}} + \frac{E_{tb}}{\eta_{reg}} + \frac{E_{tg}}{\eta_{reg}\eta_{inv}} \tag{23}$$

Where, the energy sent directly to the load E_{dtl} can be obtained from the Eq. (24).

$$E_{tl} = E_{dtl} + E_{fb}\eta_{inv} \tag{24}$$

In Eq. (24) the overall energy produced by the HPWBS sent to the load E_{tl} is the sum of the energy sent directly to the load E_{dtl} and that received from the battery $E_{fb}\eta_{inv}$.

The balance Eq. (23) can be made dimensionless by dividing each term to the energy required by the load E_L. In addition, multiplying both members of Eq. (23) for the regulator and inverter efficiencies $\eta_{reg}\eta_{inv}$, Eq. (25) is obtained.

$$\frac{E_g}{E_L}\eta_{reg}\eta_{inv} = \frac{E_{dtl}}{E_L} + \frac{E_{tb}}{E_L}\eta_{inv} + \frac{E_{tg}}{E_L} \tag{25}$$

Eq. (25) can be written in the corresponding form:

$$e_g = e_{dtl} + e_{tb} + e_{tg} \tag{26}$$

Considering Eq. (27) of the annual energy balance of the battery:

$$E_{fb} = \eta_{bat}E_{tb} \tag{27}$$

Chapter 2

**Energy reliability-constrained method
for the multi-objective optimization
of a photovoltaic-wind hybrid system with battery storage**

and extracting E_{tl} from Eqs. (23) and (24) and replacing it into Eq. (21), the balance equation of the energy required by the load is obtained:

$$E_L = E_g \eta_{reg} \eta_{inv} - \left[E_{tb}(1 - \eta_{bat}) \eta_{inv} \right] - E_{tg} + E_{fg} \tag{28}$$

The annual energy required by the load is the sum of two contributions: (i) the overall net energy produced by the generators, $E_g \eta_{reg} \eta_{inv}$, reduced by the energy lost in the battery and then in the inverter $E_{tb}(1 - \eta_{bat}) \eta_{inv}$, and by the excess energy sent to the grid E_{tg}; (ii) the energy drawn from the grid E_{fg}. The balance Eq. (28) can be made dimensionless by dividing each term to the energy required by the load E_L:

$$1 = \frac{E_g}{E_L} \eta_{reg} \eta_{inv} - \left[\frac{E_{tb}}{E_L}(1 - \eta_{bat}) \eta_{inv} \right] - \frac{E_{tg}}{E_L} + \frac{E_{fg}}{E_L} \tag{29}$$

Eq. (29) can be written in the corresponding form:

$$1 = e_g - e_{lb} - e_{tg} + e_{fg} \tag{30}$$

Replacing Eq. (26) into Eq. (30), and taking into account that $e_{tb} - e_{lb} = e_{fb}$, a new relation of the energy balance equation of the energy required by the load (load balance LB) is obtained:

$$1 = e_{dtl} + e_{fb} + e_{fg} \tag{31}$$

The addends of the second member in Eq. (31) are the fractions, referred to the energy required by the load, of the energy sent directly to the load (e_{dtl}), energy extracted from the battery (e_{fb}) and from the grid $\left(e_{fg} \right)$.

The balance equation of the energy generated (generated energy balance GEB), per unit of energy required by the load, e_g, expressed by Eq. (26), can be written as follows:

$$1 = \frac{e_{dtl}}{e_g} + \frac{e_{tb}}{e_g} + \frac{e_{tg}}{e_g} \tag{32}$$

Chapter 2   **Energy reliability-constrained method**
for the multi-objective optimization
of a photovoltaic-wind hybrid system with battery storage

The addends of the second member in Eq. (32) are the fractions, referred to the energy generated, of energy sent directly to the load e_{dtl}/e_g energy sent directly to the battery e_{tb}/e_g , and excess energy sent to the network e_{tg}/e_g.

Eqs. (31)-(32) are used in Sections 4.1.1 and 4.1.2 to evaluate the energy reliability of the system as a function of the following dimensionless parameters:

$$p_w = \frac{P_W}{P_W + P_{PV}} \tag{33}$$

$$p_b = \frac{P_B}{P_n} = \frac{P_B}{P_W + P_{PV} + P_B} \tag{34}$$

$$p_l = \frac{P_L}{P_W + P_{PV}} \tag{35}$$

$$p_{hbl} = \frac{P_L}{P_n} = \frac{P_L}{P_W + P_{PV} + P_B} \tag{36}$$

where,

- p_w represents the *wind fraction*, the ratio of the wind nominal power P_W to the overall nominal PV-wind power. The p_w parameter runs between zero and one: when $p_w = 0$ the system is without the wind generator, for $p_w = 1$ the system is devoid of the PV generator.
- p_b is the *storage fraction*, the ratio of the nominal battery power P_B (maximum stored energy in one hour) to the overall nominal power P_n of the HPWBS, the sum of the nominal PV, wind and battery power. The p_b parameter ranges between 0 and 1: when $p_b = 0$ the system is without battery, for $p_b = 1$ the system is constituted only by the storage battery, since $P_W + P_{PV} = 0$.
- p_l is the *load fraction*, the ratio of the hourly average daily load P_L to the nominal PV-wind power. Parameter p_l can be less or greater than 1; when it is greater, the hourly average daily power required by the load is higher than the sum of the PV and wind nominal power.
- p_{hbl} is the *load overall fraction*, the ratio of the hourly average daily load P_L to the overall nominal power P_n of the HPWBS.

2.4. Energy reliability indicators

This section defines the dimensionless indicators to be used in the energy reliability analysis to identify the optimal system configurations. The indicators are:

Chapter 2   **Energy reliability-constrained method**
for the multi-objective optimization
of a photovoltaic-wind hybrid system with battery storage

- the **photovoltaic-wind fraction $f_{pv,w}$** (-) defined as the ratio of the energy supplied by the HPWBS to the load E_{tl} to the energy required by the load E_L. Considering Eq. (31), this indicator can be expressed as the sum of the energy fractions e_{dtl} and e_{fb}:

$$f_{pv,w} = \frac{E_{tl}}{E_L} = e_{dtl} + e_{fb} \qquad (37)$$

  $f_{pv,w}$ measures the fraction of energy required by the load satisfied by the system (the complement to one is the energy fraction missing to meet the load), and it varies between 0 and 1; for $f_{pv,w} = 1$, all the energy required by the load is provided by the system and the energy supplied by the grid is zero.

- the **utilization factor** of the generated energy **f_u** (-) defined as the ratio of the energy supplied by the HPWBS to the load E_{tl} to the generated energy E_g. Considering Eq. (32), this indicator is expressed as the sum of the energy fractions e_{dtl}/e_g and e_{tb}/e_g:

$$f_u = \frac{E_{tl}}{E_g} = \frac{e_{dtl}}{e_g} + \frac{e_{tb}}{e_g} \qquad (38)$$

  f_u quantifies the fraction of produced energy employed to satisfy the load (the complement to one is the excess energy fraction), and it varies between 0 and 1; for $f_u = 1$, all the energy generated is supplied to the load, and the excess energy is zero.

- the **system manufacturability h_{hl}** (kWh/kWh) defined as the ratio of the energy supplied by the HPWBS to the load E_{tl} to the overall nominal power of the HPWBS P_n. Considering Eqs. (36)-(37), this indicator is expressed as the product of the load overall fraction p_{hbl} and the PV-wind fraction:

$$h_{hl} = \frac{E_{tl}}{P_n} = 8760 \, p_{hbl} \, f_{pv,w} \qquad (39)$$

  Where, 8760 are the hours of one year.
  This indicator provides the energy sent to the load per each kW installed, namely the number of operating equivalent hours of the system in a year in which all the system components operate simultaneously in the nominal conditions.

2.5. Multi-objective optimization

This section presents the multi-objective optimization methods used, such as the Pareto-front method and the energy reliability-constrained (ERC) method proposed by the authors.

Chapter 2   **Energy reliability-constrained method**
for the multi-objective optimization
of a photovoltaic-wind hybrid system with battery storage

In general, in multi-objective optimization, there is no one unique solution satisfying all objectives simultaneously, and then it is necessary to find a trade-off between a set of *n* conflicting objective functions O_i:

$$\{O_1(r), O_2(r), ..., O_n(r)\} \tag{40}$$

each of which depends on the *r* parameters $r = (r_1, r_2, ..., r_r)$.

In the application at hand, these objective functions are the maximization of the energy reliability indicators described in Section 2.4, namely the PV-wind fraction $f_{pv,w}$, utilization factor of the generated energy f_u, system manufacturability h_{hl} or a combination of these latter. A multi-objective optimization based on the Pareto-front method [36], described in subsection 2.5.1, is requested since the three indicators have different trends by varying the sizes of the system components. For example, an increase of the overall nominal power of the system determines higher energy produced sent to the load with a greater $f_{pv,w}$, and simultaneously, higher energy in excess with a lower f_u. Instead, the variation of h_{hl} is not determinable beforehand. Alternatively to the Pareto-front, the ERC method, described in subsection 2.5.2, can be applied to guarantee that some reliability indicators were higher than predetermined constraints.

2.5.1. Pareto-front method

In a multi-objective maximization, the Pareto optimal solutions are based on the following definition of dominance, where a feasible solution r* is said to Pareto dominate another solution $r^{'}$ if:

$$O_i(r^*) \geq O_i(r^{'}) \ \forall i \in \{1,2, ... n\} \quad \text{and} \quad O_j(r^*) > O_j(r^{'}) \ \text{for at least one j} \in \{1,2, ... n\} \tag{41}$$

that is, r* is as good as $r^{'}$ in all objectives and is strictly better than $r^{'}$ in at least one. An r* not dominated by any other is called Pareto optimal solution. The set of all Pareto optimal solutions constitutes the Pareto-front.

The application of this method to an HPWBS allows the identification of the trade-off system configurations. These configurations might not assure high energy reliability since among these are also included those configurations with a high value of an objective and a low value of the other. Hybrid systems with high reliability are those that ensure values of indicators exceeding prefixed constraints. For this reason, the objective functions must be constrained.

2.5.2. Energy reliability-constrained (ERC) method

In the method proposed some solutions are excluded subjecting *m* objective functions to prefixed constraints:

$$\{O_1(r) < \bar{O}_1, O_2(r) < \bar{O}_2, ..., O_m(r) < \bar{O}_m\} \tag{42}$$

Chapter 2   **Energy reliability-constrained method**
for the multi-objective optimization
of a photovoltaic-wind hybrid system with battery storage

In this way, some Pareto optimal solutions are excluded and others not belonging to the Pareto-front are considered. Among the solutions not excluded, the optimal solutions are those that optimize the other *n-m* objective functions:

$$max \; or \; min \; \{O_{n-m}(r), O_{n-m+1}(r), \dots, O_n(r)\} \tag{43}$$

Therefore, the ERC method is a general procedure that in the case of the absence of objective functions to be constrained (m=0) becomes the Pareto-front method.

In the case of an HPWBS, some indicators are subjected to the prefixed constraints: $f_{pv,w} > \bar{f}_{pv,w}$, or $f_u > \bar{f}_u$, or $h_{hl} > \bar{h}_{hl}$, or a combination of these latter, with $\bar{f}_{pv,w}$, $\bar{f}_u$, and $\bar{h}_{hl}$ constraint values. Then, the optimal system configurations are identified by maximizing the remaining indicators.

The choice of the indicators to be constrained or to be maximized depends on the presence or absence of a grid connection:

- in an energy reliable grid-connected HPWBS, the energy drawn from the grid and the energy produced in excess must be limited ($f_{pv,w} > \bar{f}_{pv,w}$ and $f_u > \bar{f}_u$);
- in an energy reliable stand-alone HPWBS, only the missing energy to meet the load must be limited ($f_{pv,w} > \bar{f}_{pv,w}$), while and the energy produced in excess must be minimized (max f_u).

In both cases, the indicator h_{hl} must be maximized. Consequently, in the grid-connected HPWBS m=2 and n=1, while in the stand-alone HPWBS m=1 and n=2.

3. Case study

In this section are presented: the experimental climatic data of the location (Section 3.1); the technical data relative to all the system components (Section 3.2); the hourly trend of the daily electric load (Section 3.3); the different configurations of the HPWBS considered in the parametric analysis (Section 3.4).

3.1. Climatic data

The experimental meteorological data regards the values collected during the entire 2015 year in an urban context, namely in the Solar Engineering laboratory located at the Department of Mechanical, Energetics and Management Engineering (DIMEG) at the University of Calabria, Cosenza (Italy). The Mediterranean climate of Cosenza, identified as Csa in the Köppen climate classification [37], has moderate temperatures with changeable and rainy weather in winter, while summers are hot and dry.
In Figure 3 the hourly values, on the left, and the monthly average daily, on the right, of the solar radiation on the horizontal surface G_h, external air temperature T_{ea}, and wind speed v are shown. The measurements were carried out on the roof of a university building at a height of 10 meters from the ground. As regards solar radiation, the values on the PV generator inclined surface, exposed to the South and inclined at a $\beta = 33 \,°$ angle, were obtained with Type 16a which employs Eq. (1). Instead,

Chapter 2

**Energy reliability-constrained method
for the multi-objective optimization
of a photovoltaic-wind hybrid system with battery storage**

Type 90 reports the wind speed data from the anemometric measure height to the hub height of the wind turbine by Eq. (5).
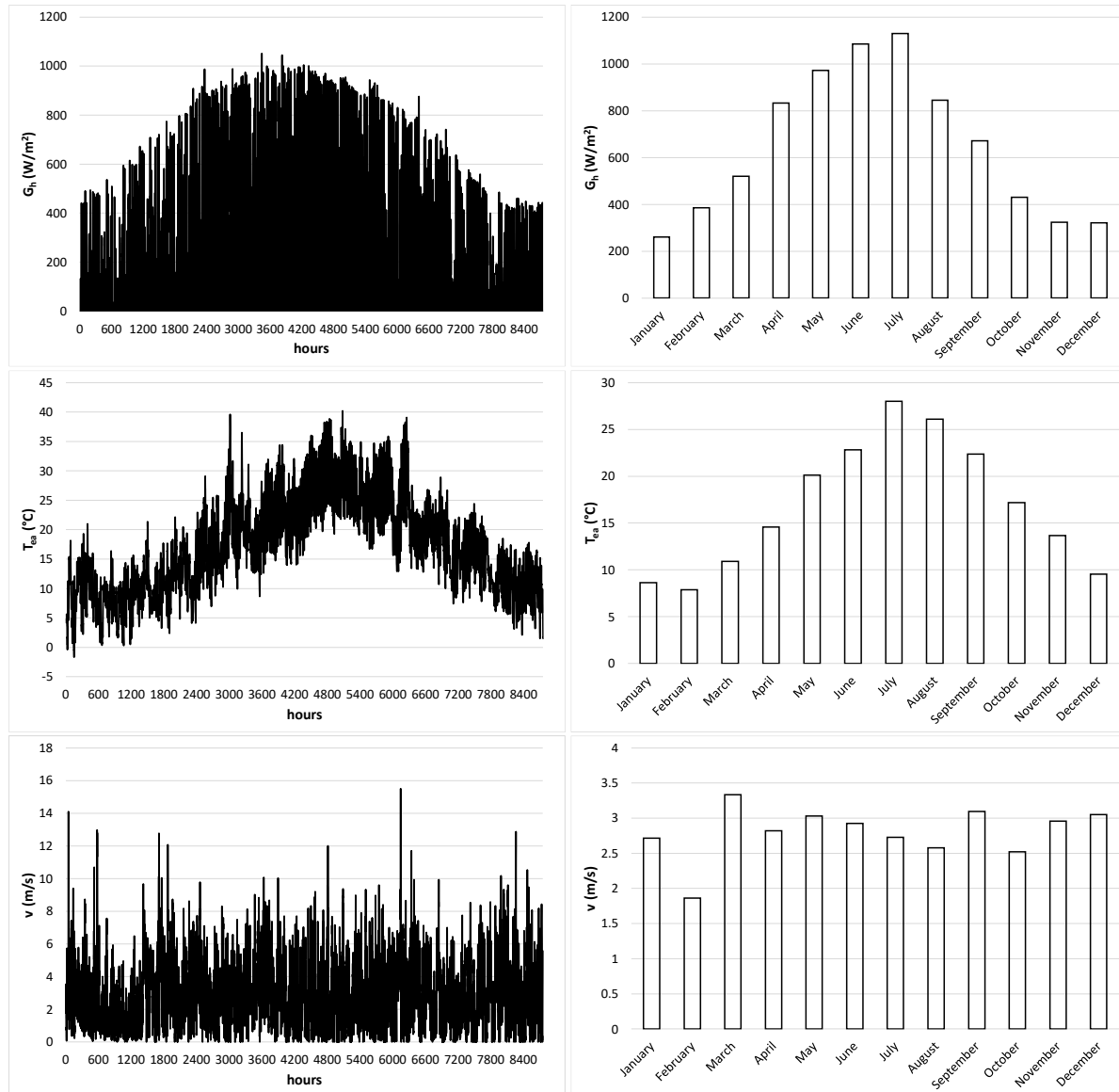
Figure 3. Hourly and monthly average daily solar radiation on the horizontal plane, external air temperature and wind speed in Cosenza (Italy).

3.2. System components

The PV generator consists of Sharp modules [38] with polycrystalline silicon cells, each of which has a dimension of (15.65 cm $\times$ 15.65 cm). The wind micro-generator employed is the Proven Energy of Angel Wind Energy [39]. The wind micro-generator was placed 5 meters higher from the roof, i.e. 15 meters in height from the ground. The electric storage is a set of Type BAT-2.0-A-SE-10 batteries, at lithium ions of LG Chem [40]. The main electric and thermal characteristics of the system components taken from the manufacturer's datasheet and the parameters used in the TRNSYS software are shown in Table 1. In addition, Table 1 shows the type and efficiency of the DC/DC converter [41], AC/DC rectifier [42], DC/AC inverter [43] and regulator [44].

Table 1. Characteristics at reference conditions of the components and parameters set in TRNSYS.

Chapter 2

**Energy reliability-constrained method
for the multi-objective optimization
of a photovoltaic-wind hybrid system with battery storage**

Photovoltaic module		Wind generator		DC/AC Inverter	
Sharp - ND-Serie A5		**Angel Wind Energy - ProvenEnergy**		**ABB Group- PVI-6000-TL-OUTD**	
Power at maximum power point P_{mp} (W)	250	Rated power of the turbine P_W (kW)	2.5	Efficiency η_{inv} (-)	0.97
Open-circuit voltage V_{sc} (V)	37.6	Rated wind speed $v_{nom,\rho o}$ (m/s)	12	**Regulator**	
Short-circuit current I_{sc} (A)	8.68	Hub height z_h (m)	14.5	Steca - Steca Solarix MPPT	
Voltage at maximum power point V_{mp} (V)	30.9	Turbine power loss ℓ (%)	6	Regulator efficiency η_{reg} (-)	0.98
Current at maximum power point I_{mp} (A)	8.10	Rotor Diameter D (m)	3.5	High limit on f_{SOC} (-)	0.97
Module conversion efficiency η_{pv} (%)	15.2	Air density ρ_0 (kg/m^3)	1.225	Low limit on f_{SOC} (-)	0.10
NOCT (°C)	47.5	Data collection height z_{an} (m)	10	**Battery storage**	
Cell area A_c (cm^2)	156.5	Site shear exponent α (-)	0.14	Lg chem - BAT-2.0-A-SE-10	
Module area A_m (m^2)	1.65	Barometric pressure p (kPa)	101.3	Energy capacity C_B (kWh)	2
Number of cells wired in series n_c (-)	60	Site elevation alt (m)	220	Charging efficiency η_{bat} (-)	0.98
Temperature coefficient of I_{sc} μ_{Isc} (-)	0.038	**AC/DC Rectifier**			
Temperature coefficient of V_{oc} μ_{Voc} (-)	-0.329	3D Company -EOREG700V54			
Array slope β (degrees)	33	Efficiency $\eta_{DC/DC}$ (-)	0.90		
DC/DC Converter					
EpSolar - 20A Serie A					
Efficiency $\eta_{DC/DC}$ (-)	0.94				

3.3. Electric loads

The electric load considered is typical of residential use with a daily trend variable hourly. Figure 4 shows the values of electric loads obtained by varying the hourly average daily value and keeping the trend unchanged. Globally, five hourly average daily loads P_L ranges between 0.5 kW and 10 kW were considered. The corresponding annual energy required by the load E_L varies between 4.38 MWh and 87.6 MWh.

Chapter 2   **Energy reliability-constrained method**
for the multi-objective optimization
of a photovoltaic-wind hybrid system with battery storage
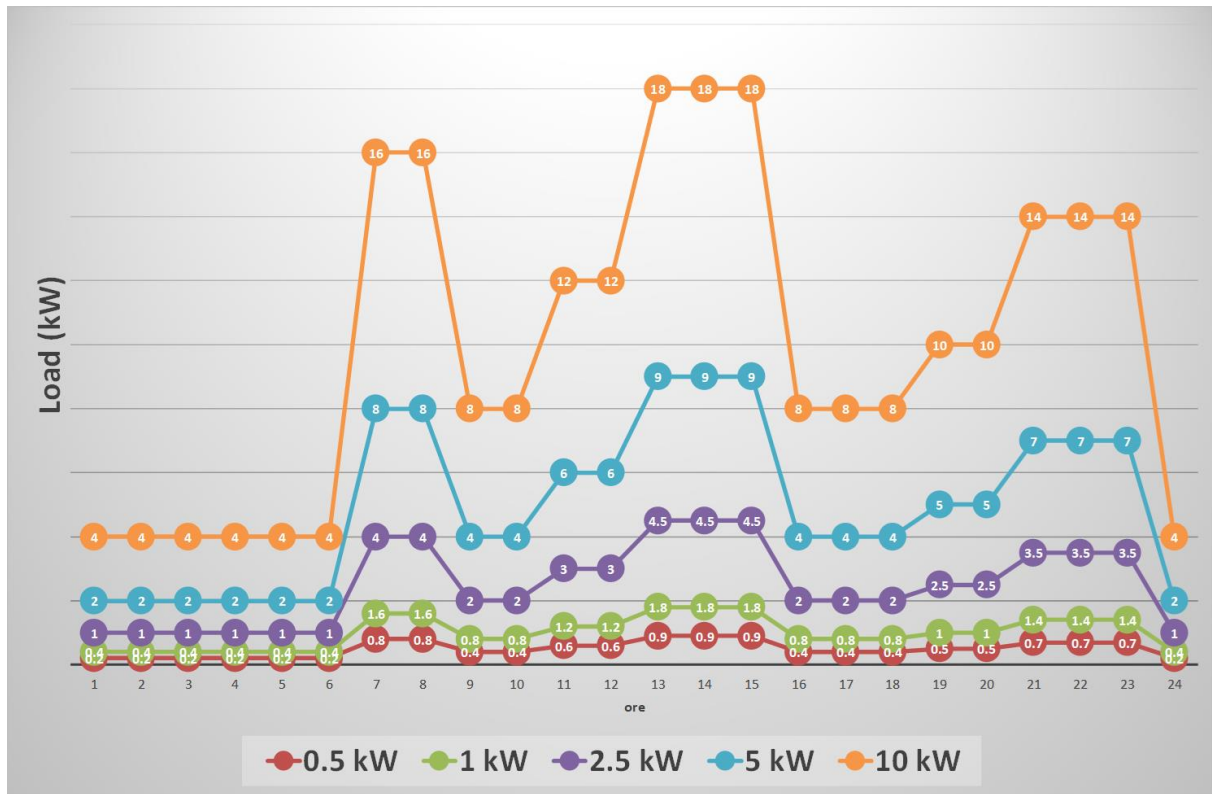
Figure 4. Hourly trends of the daily load for different hourly average daily values.

3.4. Parametric analysis

Referring to Table 2, the calculation scheme developed in TRNSYS was used to perform an annual energy parametric analysis of different hybrid system configurations in the presence and absence of a storage battery, for each considered load.

Table 2. Parametric analysis: nominal powers of the PV and wind micro-generator, and storage capacity of the electric battery.

P_{PV} (kW)	P_W (kW)	C_B (kWh)
2.5	2.5	0
5	5	2
10	7.5	4
	10	6
	15	8
		10

Overall, 450 system configurations were considered in the parametric analysis, obtained by varying: (i) the nominal power of the PV generator by changing the number of PV modules; (ii) the nominal power of the wind generator by modifying the number of wind micro-generators; (iii) the storage capacity by varying the number of storage batteries. For each case, the calculation scheme of TRNSYS was used to calculate the hourly values of the output powers from each component defined in Sections 2.1 and 2.2. These powers were used for the calculation of the relative hourly and annual

Chapter 2

**Energy reliability-constrained method
for the multi-objective optimization
of a photovoltaic-wind hybrid system with battery storage**

energy defined in Section 2.3, used to evaluate the dimensionless fractions, Eqs. (31)-(32) and Eqs. (37)-(39), defined in Section 2.4.

4. Results and discussion

In Section 4.1, the system energy reliability was studied by varying the wind fraction p_w, storage fraction p_b and t load fraction p_l, evaluating the influence on the energy fractions of the LB, Eq. (31), and comparing them with the energy fractions of GEB, Eq. (32). These energy fractions and the reliability indicators, Eqs. (37)-(39), were also studied as a function of the load overall fraction p_{hbl}, by providing some analytic correlations. In Section 4.2, an energy reliability multi-objective optimization was developed to identify the optimal system configurations based on the ERC method. These optimal configurations were compared with those obtained by using the Pareto-front method.

4.1. Parametric analysis

4.1.1. Balance of the energy required by the load LB

Figures 5-7 show, as a function of the wind fraction p_w, the trends of the energy fraction sent directly to the load e_{dtl}, energy fraction taken from the battery e_{fb}, and energy fraction extracted from the grid e_{fg}. The figures regard three different load values P_L, 0.5 kW, 2.5 kW and 10 kW. In each figure, four images obtained by assigning to the storage capacity C_B the values 0 kWh, 2 kWh, 6 kWh and 10 kWh are reported. Each image shows the trend of e_{dtl}, e_{fb} and e_{fg} as a function of p_w for three different values of the nominal power of the PV generator P_{PV}, 2.5 kW, 5 kW and 10 kW, considering P_L and C_B constants.
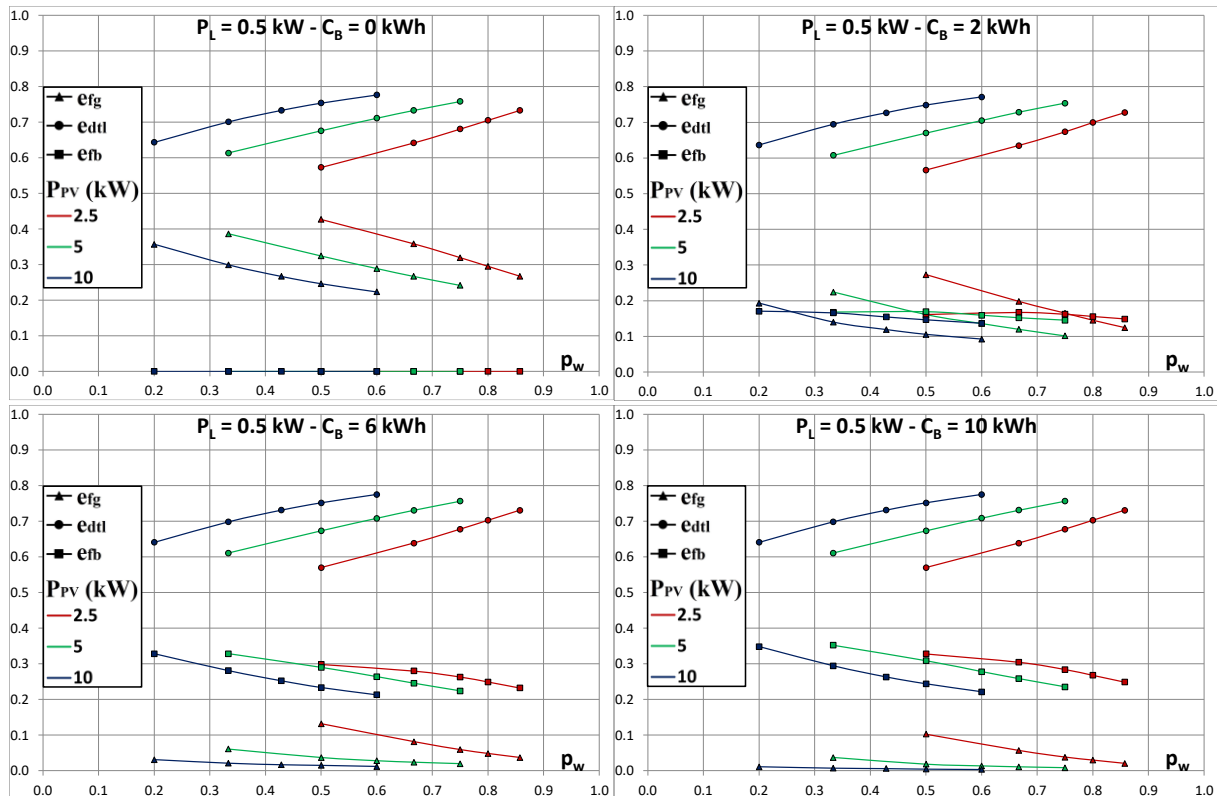
Figure 5. *Energy fraction sent directly to the load, energy fraction drawn from the battery and energy fraction drawn from the grid as a function of the wind fraction.* $P_L = 0.5$ kW.

Chapter 2

**Energy reliability-constrained method
for the multi-objective optimization
of a photovoltaic-wind hybrid system with battery storage**
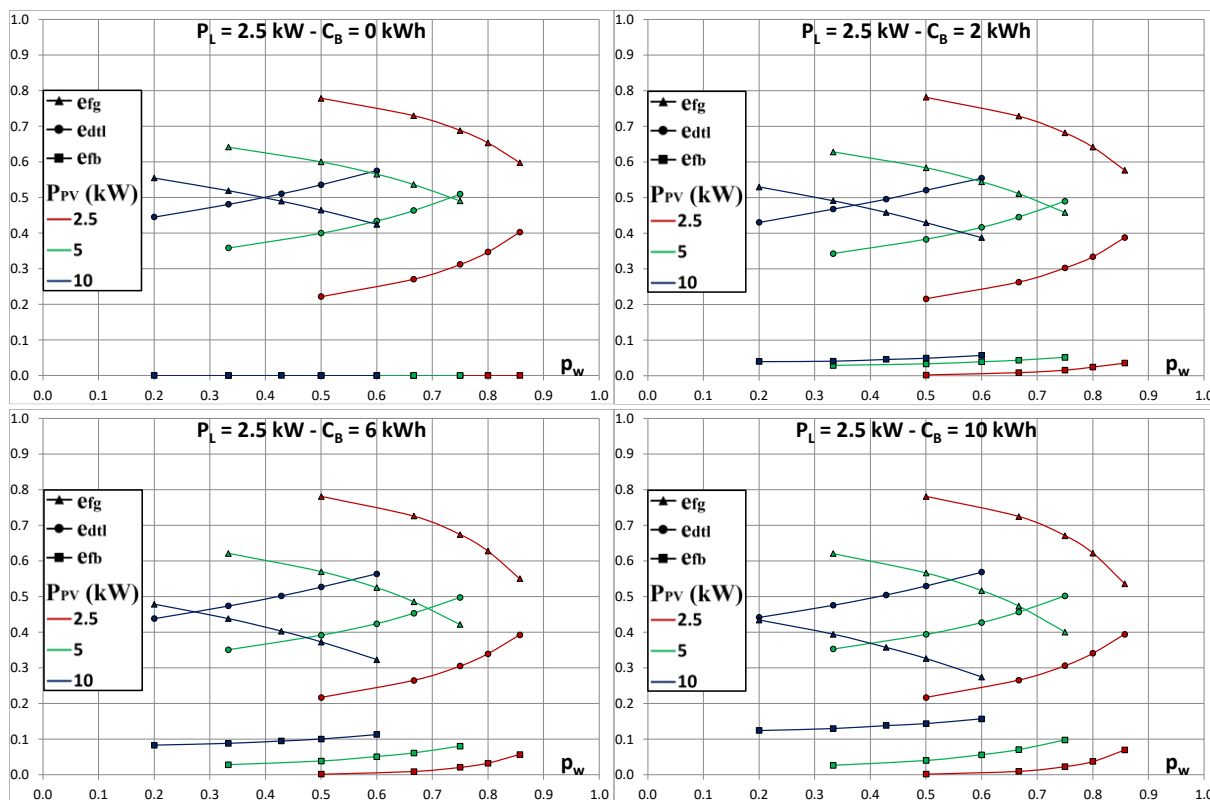
Figure 6. *Energy fraction sent directly to the load, energy fraction drawn from the battery and energy fraction drawn from the grid as a function of the wind fraction.* $P_L = 2.5$ kW.
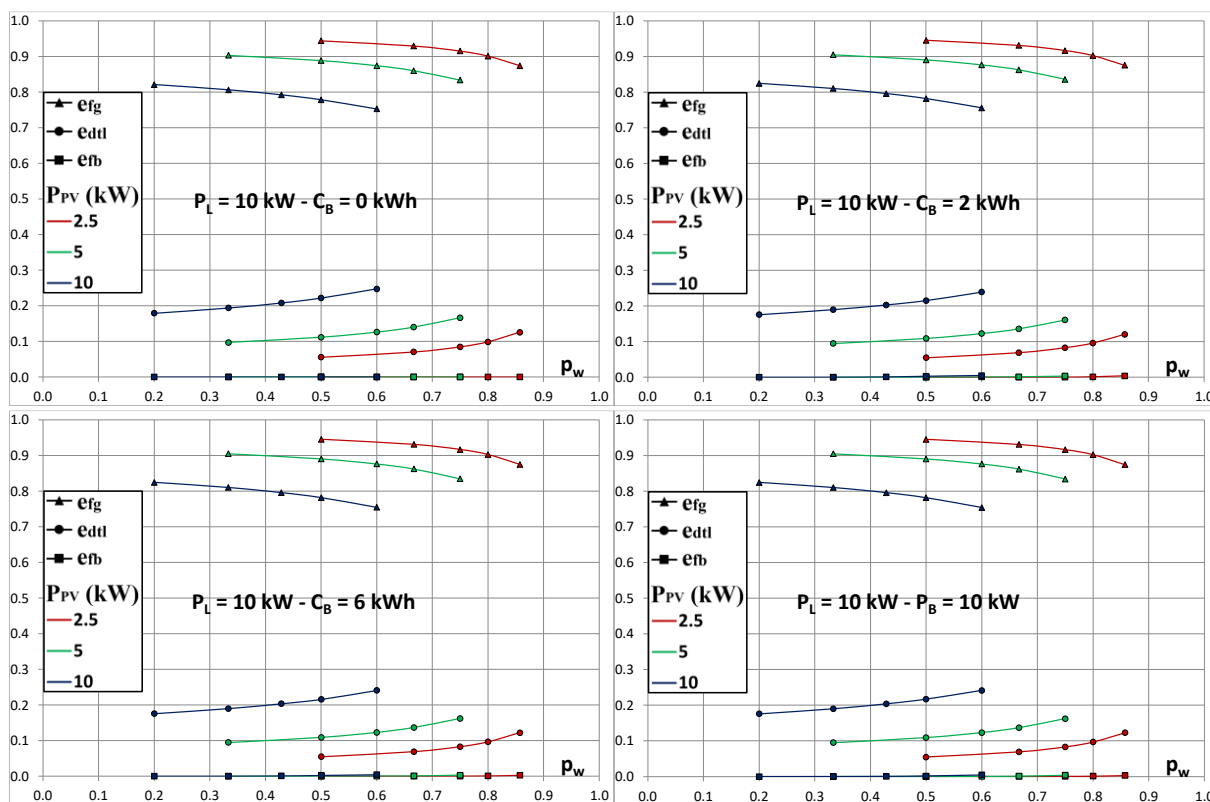
Figure 7. *Energy fraction sent directly to the load, energy fraction drawn from the battery and energy fraction drawn from the grid as a function of the wind fraction.* $P_L = 10$ kW.

Chapter 2

**Energy reliability-constrained method
for the multi-objective optimization
of a photovoltaic-wind hybrid system with battery storage**

In Figures 8-10 are reported, as a function of the storage fraction p_b, the trends of the energy fraction sent directly to the load e_{dtl}, energy fraction drawn from the battery e_{fb}, and energy fraction extracted from the grid e_{fg}. The figures are obtained by considering three different load values P_L, 0.5 kW, 2.5 kW and 10 kW. In each figure, three images obtained by assigning to the nominal power of the PV generator P_{PV} the values 2.5 kW, 5 kW and 10 kW are reported. Each image shows the trend of e_{dtl}, e_{fb} and e_{fg} by varying p_b for five different values of the nominal power of the wind generator P_W, 2.5 kW, 5 kW, 7.5 kW, 10 kW and 15 kW, with P_L and C_B constants.

Chapter 2

Energy reliability-constrained method
for the multi-objective optimization
of a photovoltaic-wind hybrid system with battery storage
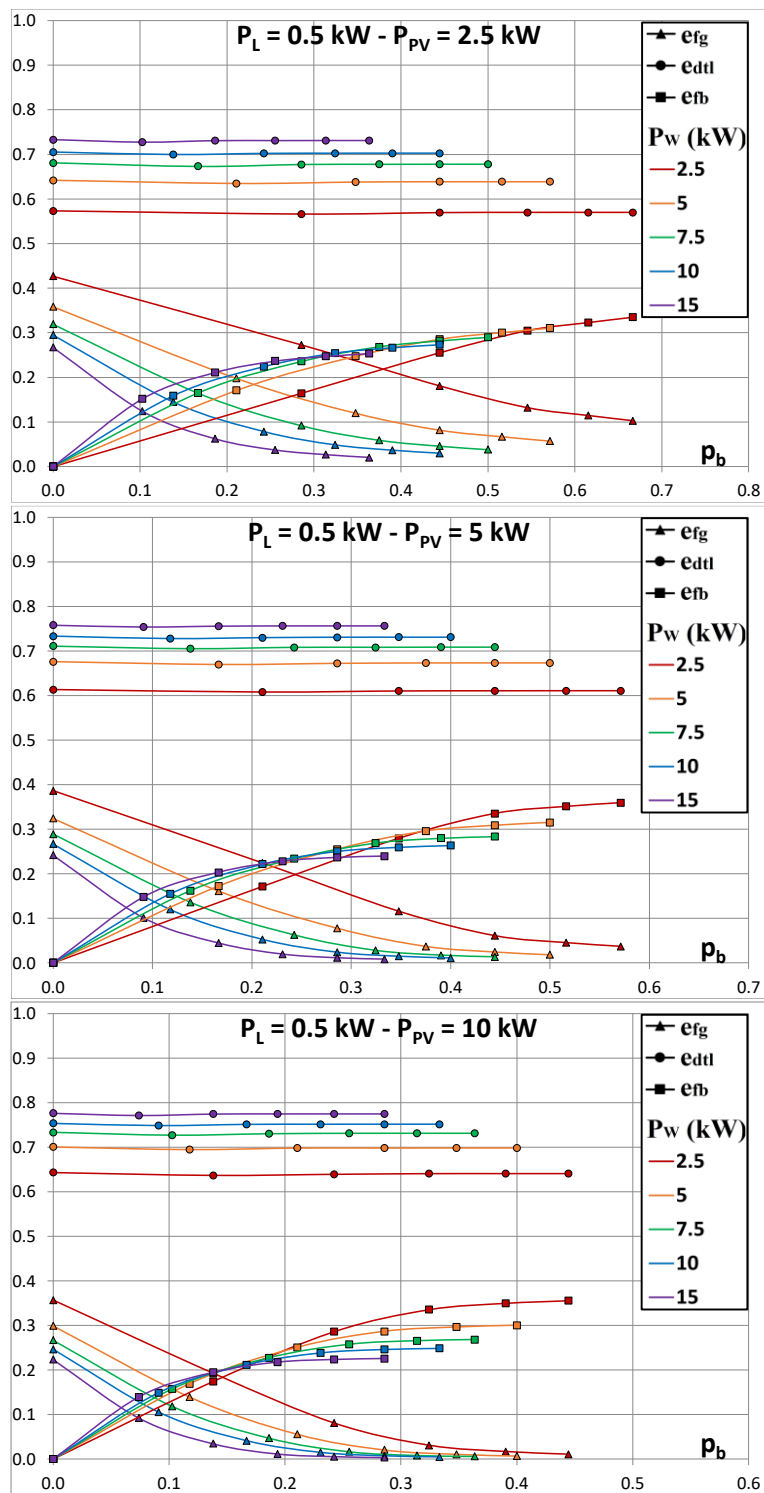
Figure 8. Energy fraction sent directly to the load, energy fraction drawn from the battery and energy fraction taken from the grid as a function of the storage fraction. $P_L = 0.5$ kW.
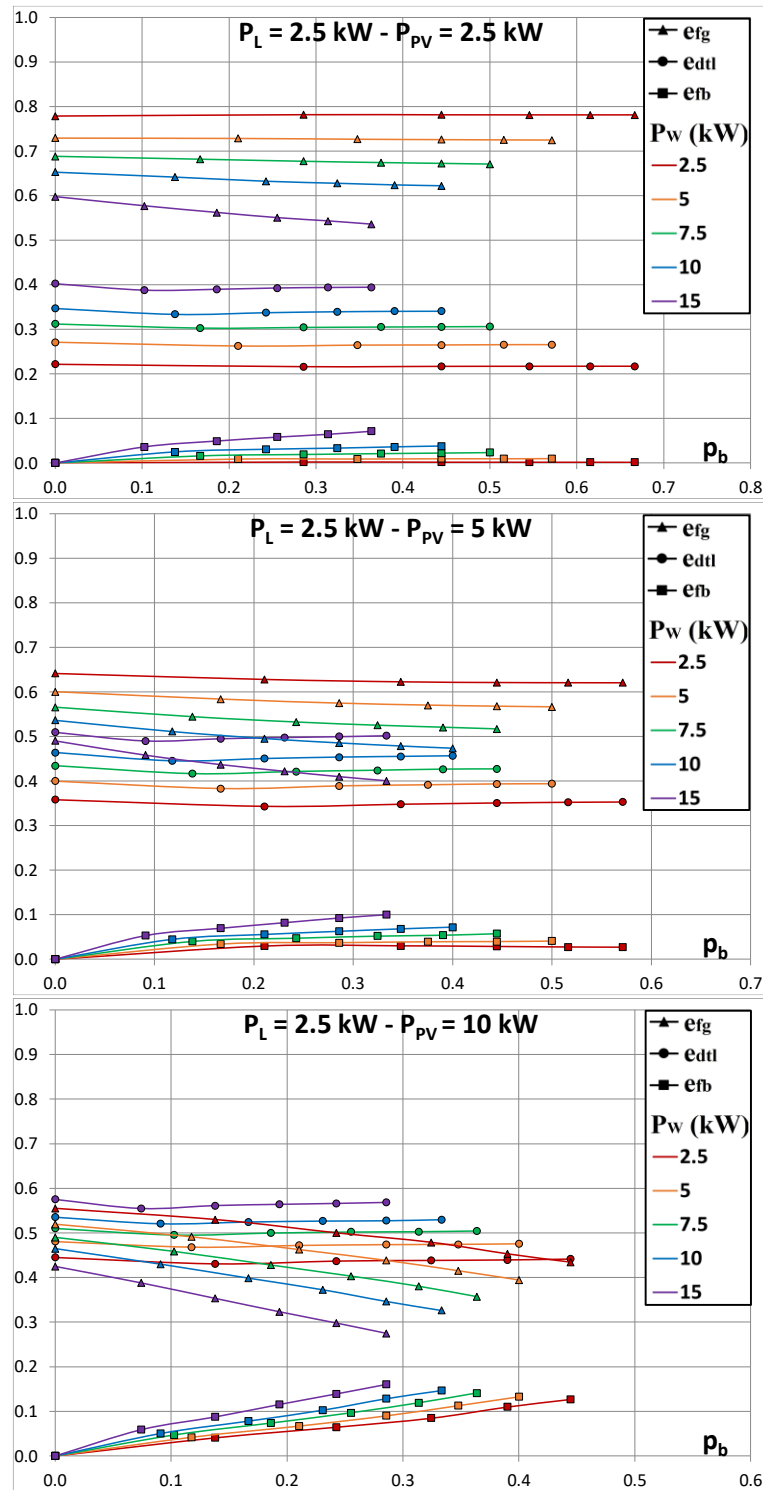
Figure 9. Energy fraction sent directly to the load, energy fraction drawn from the battery and energy fraction taken from the grid as a function of the storage fraction. $P_L = 2.5$ kW.

Chapter 2   **Energy reliability-constrained method**
for the multi-objective optimization
of a photovoltaic-wind hybrid system with battery storage
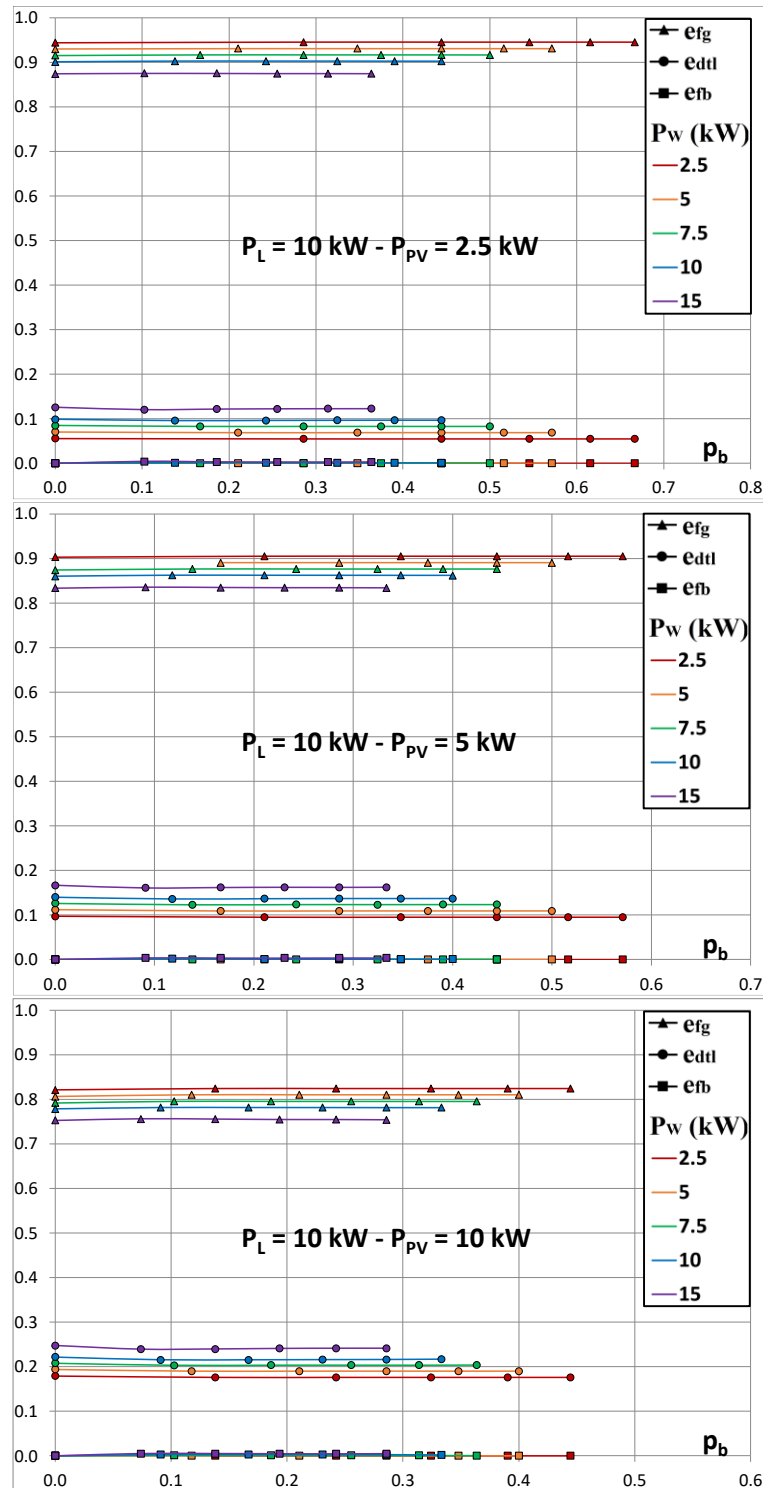
Figure 10. *Energy fraction sent directly to the load, energy fraction drawn from the battery and energy fraction taken from the grid as a function of the storage fraction.* $P_L = 10$ kW.

Figures 11-13 report, by varying the load fraction p_l, the trends of the energy fraction sent directly to the load e_{dtl}, energy fraction drawn from the battery e_{fb} and energy fraction extracted from the grid e_{fg}. The figures are obtained considering three different values of the nominal power of the PV generator P_{PV}, 2.5 kW, 5 kW and 10 kW. In each figure, three images obtained by assigning to the nominal power of the wind generator P_W the values 2.5 kW, 7.5 kW and 15 kW are reported. Each

Chapter 2

**Energy reliability-constrained method
for the multi-objective optimization
of a photovoltaic-wind hybrid system with battery storage**

image shows the trend of e_{dtl}, e_{fb} and e_{fg} by varying the load fraction p_l, for six different values of storage capacity C_B, 0 kWh, 2 kWh, 4 kWh, 6 kWh, 8 kWh, and 10 kWh, with P_{PV} and P_W constants.
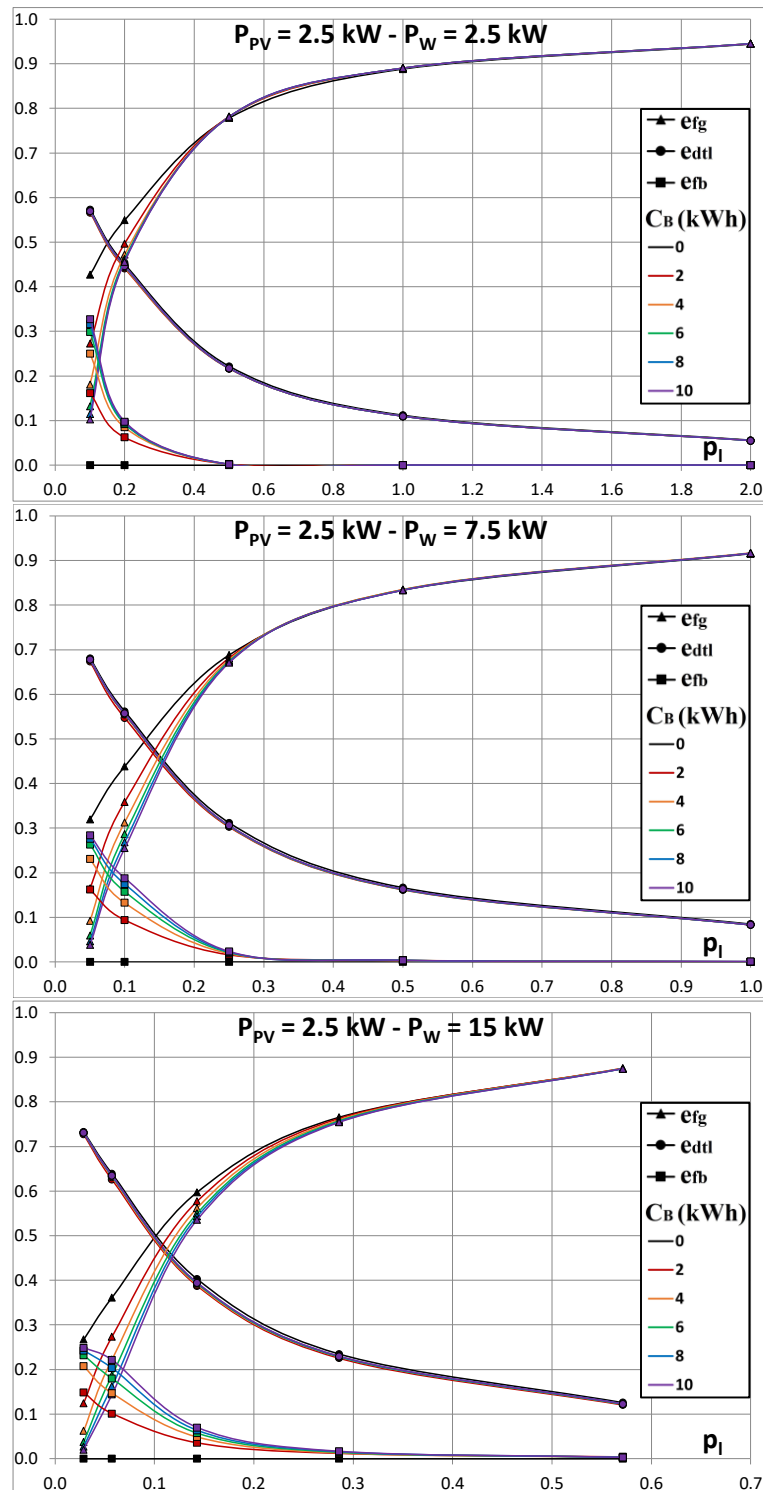
Figure 11. *Energy fraction sent directly to the load, energy fraction drawn from the battery and energy fraction taken from the grid as a function of the storage fraction.* $P_{PV} = 2.5$ kW.

Chapter 2

**Energy reliability-constrained method
for the multi-objective optimization
of a photovoltaic-wind hybrid system with battery storage**
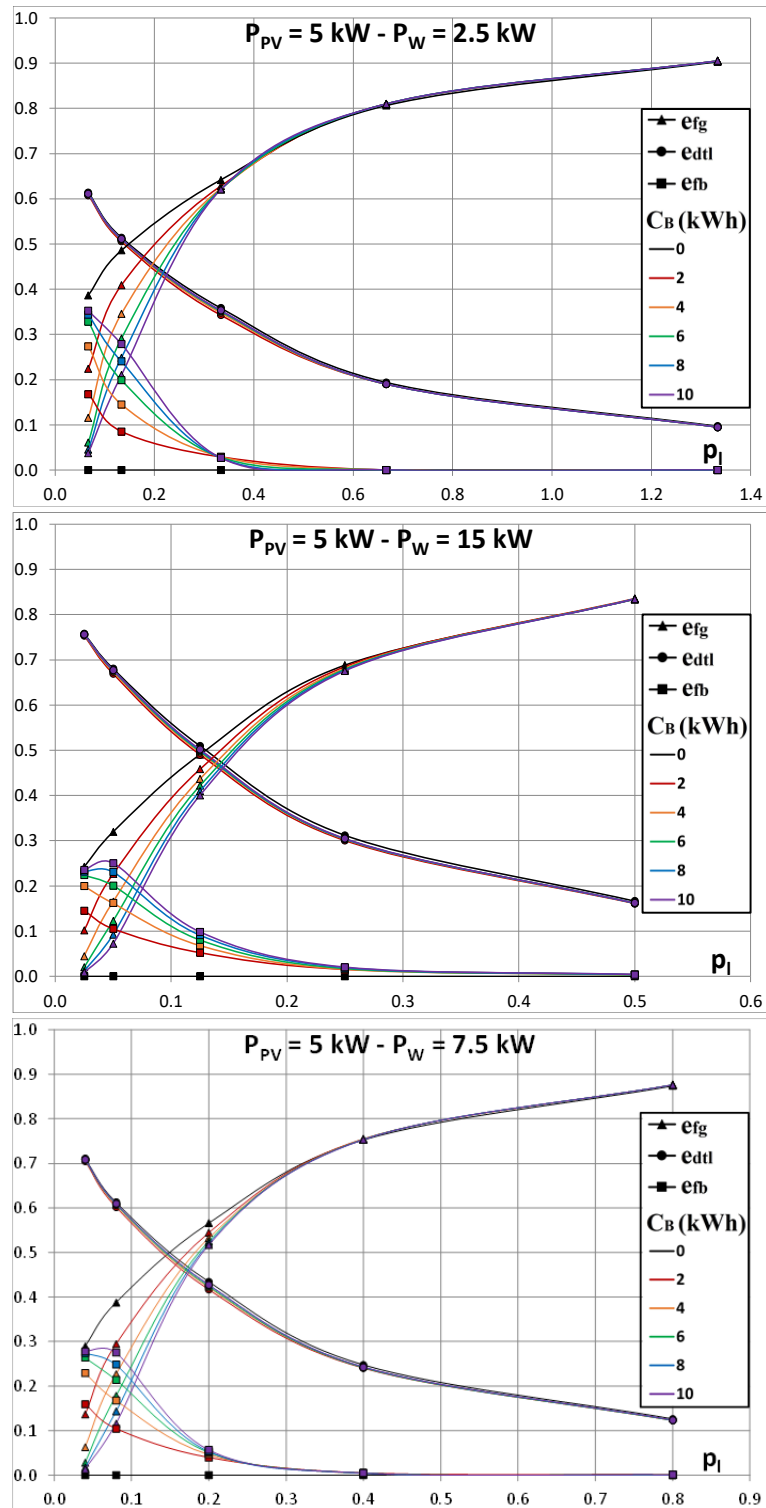
Figure 12. *Energy fraction sent directly to the load, energy fraction drawn from the battery and energy fraction taken from the grid as a function of the storage fraction.* $P_{PV} = 5$ kW.

Chapter 2

**Energy reliability-constrained method
for the multi-objective optimization
of a photovoltaic-wind hybrid system with battery storage**
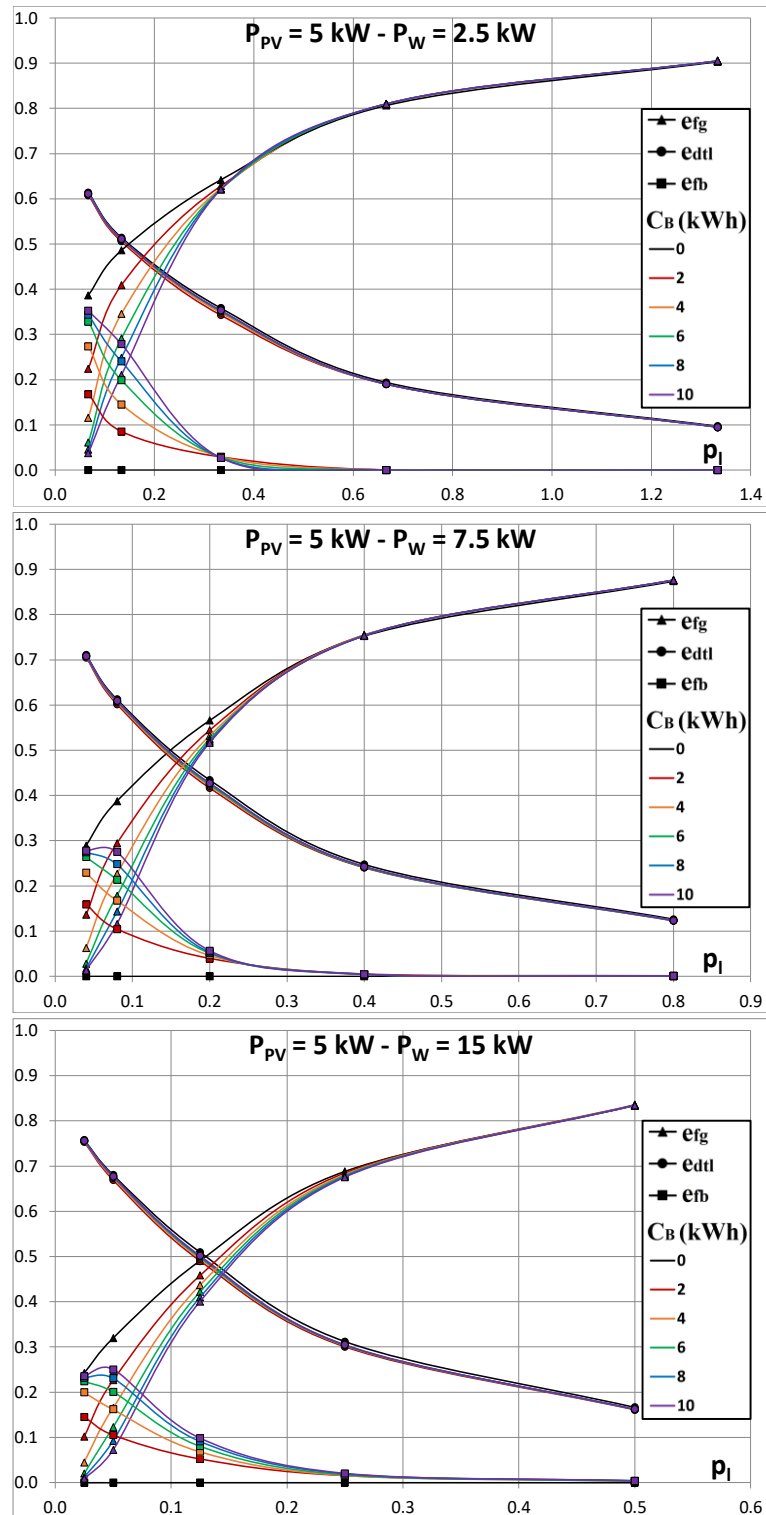
Figure 13. *Energy fraction sent directly to the load, energy fraction drawn from the battery and energy fraction taken from the grid as a function of the storage fraction.* $P_{PV} = 10$ kW.

4.1.2. Comparison of the LB and GEB

Figures 14-16 show a comparison, through unitary histograms obtained as the sum of different color bars, of the LB (on the right), and the GEB (on the left). The histograms were obtained for different

Chapter 2

**Energy reliability-constrained method
for the multi-objective optimization
of a photovoltaic-wind hybrid system with battery storage**

values of load P_L, storage capacity C_B, and nominal power of the PV generator P_{PV} and wind generator P_W. For a combination of these values:

- the GEB is expressed by the sum of the energy fraction sent directly to the load e_{dtl}/e_g (green), energy fraction sent to the battery e_{tb}/e_g (blue), and energy fraction in excess sent to the grid e_{tg}/e_g (yellow);
- the LB is expressed by the sum of the energy fraction sent directly to the load e_{dtl} (light blue), energy fraction taken from the battery e_{fb} (cyan) and energy fraction taken from the grid e_{fg} (red).
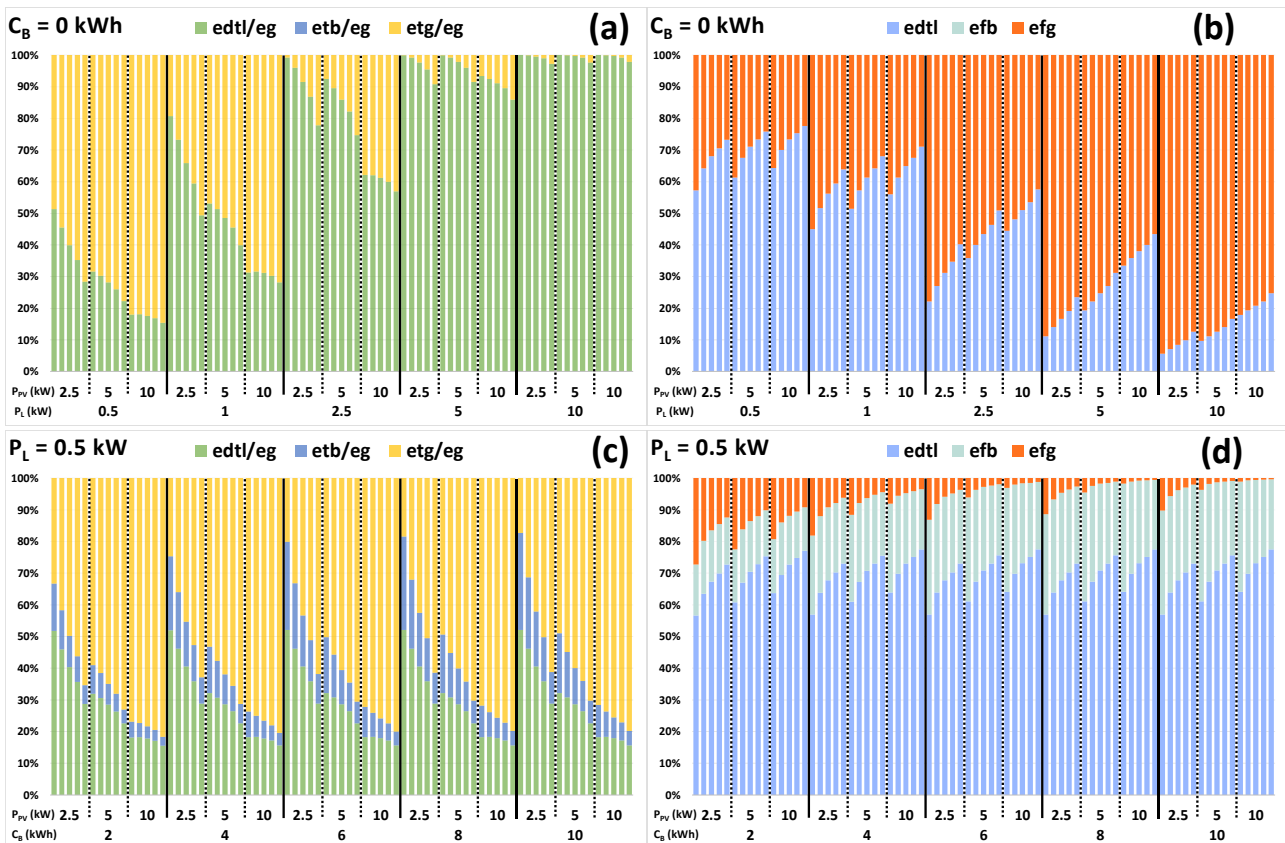
Figure 14. *(a) and (b) GEB and LB for different load values without the storage battery; (c) and (d) GEB and LB in the presence of a battery storage for* $P_L = 0.5$ *kW.*

Chapter 2

**Energy reliability-constrained method
for the multi-objective optimization
of a photovoltaic-wind hybrid system with battery storage**
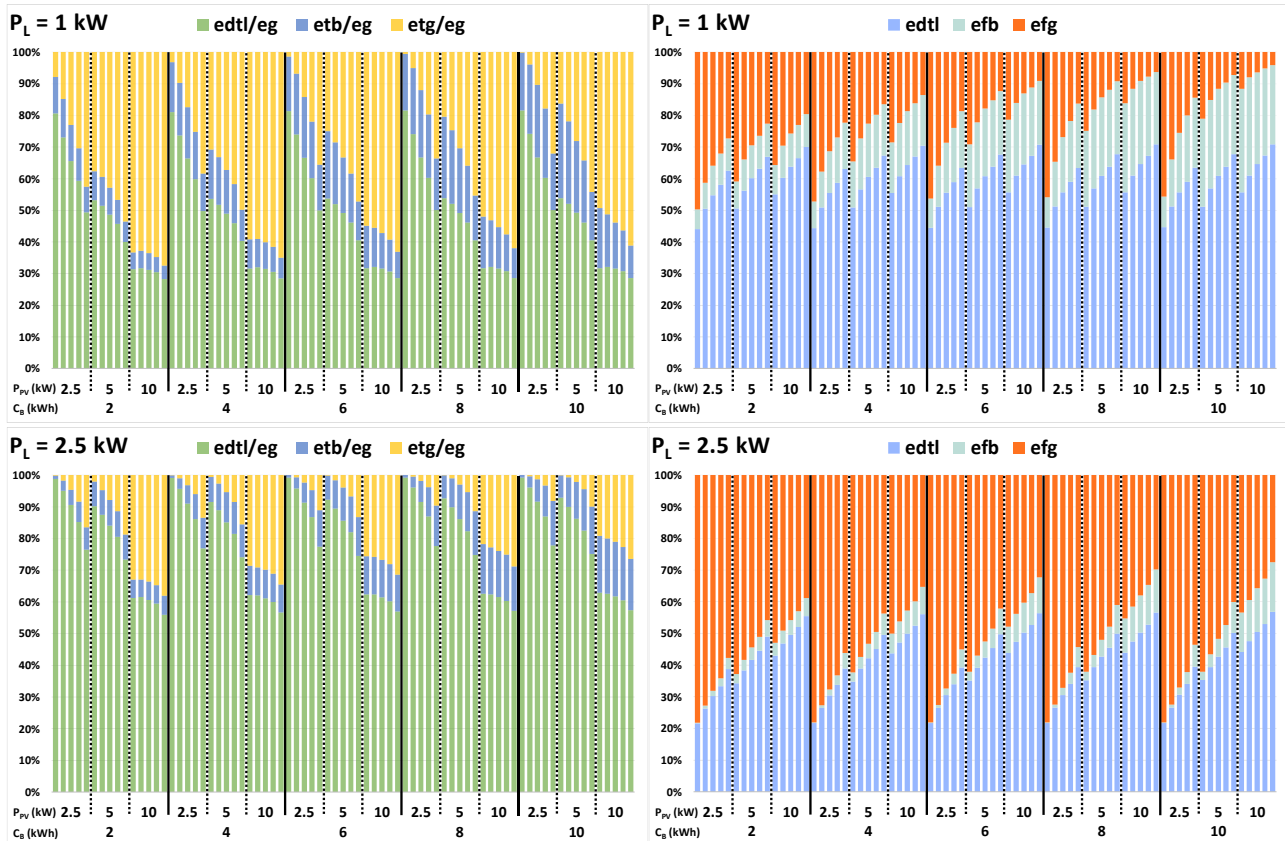
Figure 15. *GEB and LB in the presence of a battery storage.* $P_L = 1$ kW; $P_L = 2.5$ kW.
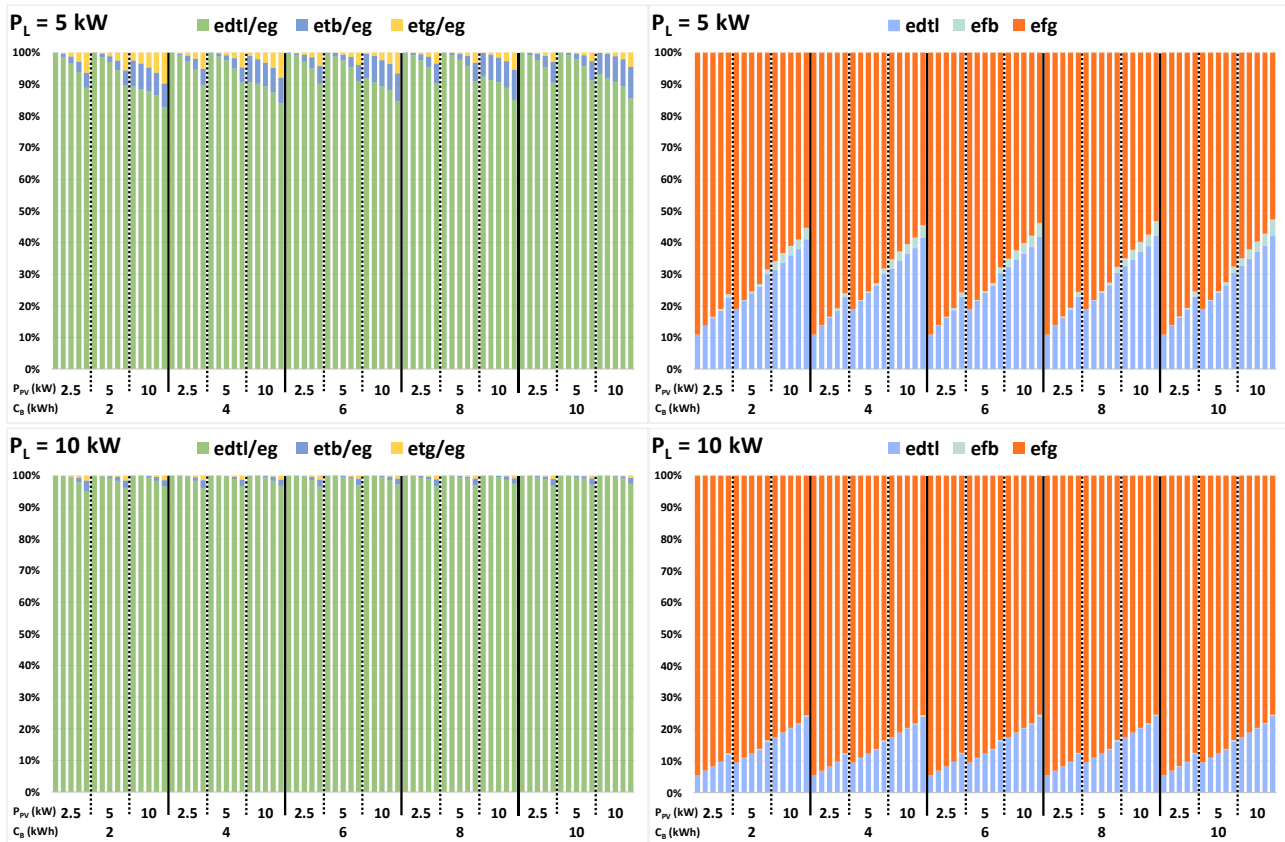
Figure 16. *GEB and LB in the presence of a battery storage.* $P_L = 5$ kW; $P_L = 10$ kW.

Chapter 2

Energy reliability-constrained method
for the multi-objective optimization
of a photovoltaic-wind hybrid system with battery storage

Images 14a and 14b concern the system configurations in the absence of battery storage, $C_B = 0$, and the histograms are related to different values of P_L and P_{PV}. Fixed P_L and P_{PV}, the five bars, from the left toward right, represent the increasing values of P_W. Images 14c and 14d and each image of Figures 15 and 16, relative to a given value of P_L, are obtained by varying C_B and P_{PV}. Fixed C_B and P_{PV}, the five bars, from the left toward right, represent increasing values of P_W. The comparison of the HPWBS with HPWS shows that the presence of a battery, highlighted by the ratios e_{tb}/e_g and e_{fb}: in GEB, does not modify e_{dtl}/e_g and leads to a reduction of di e_{tg}/e_g; in the LB, determines a reduction of e_{fg} with e_{dtl} constant. In addition, Figures 14-16 permit indirect determination of the utilization factor f_u and the PV-wind fraction $f_{pv,w}$. The f_u value is obtained from the histograms of the GEB by summing e_{dtl}/e_g and e_{tb}/e_g (green and blue bars), while the $f_{pv,w}$ value is obtained from the histograms of the LB adding up e_{dtl} and e_{fb} (light blue and cyan bars). Consequently, to identify the PV-wind fraction and utilization factor, it is necessary to read the corresponding value in the ordinate axes to the cumulative histogram of the first 2 bars.

4.1.3. General considerations on the LB and GEB

From the previous parametric analysis, both in the absence and presence of a storage battery, the following considerations may be deduced:

- an increase in nominal power of the wind and PV generators results in a reduction of the energy fraction extracted from the grid, with an increase of the energy fraction produced in excess; by increasing the wind fraction, the variation of the fractions of the LB and GEB is determined by the load value and storage capacity. This is due to the time shift between the availability of wind power and solar power and the load.
- A rise in load determines an increase of the energy drawn fraction from the grid and a reduction of the energy fraction in excess.
- The energy fraction sent directly to the load, which appears in the LB, increases as the nominal powers of the wind and PV generator grow, and it decreases as the load value increases. In addition, it is not determined by the storage capacity; this is owing to the operation mode of the system, which gives priority in the distribution of the energy produced to the satisfaction of the load and, in the case of excess energy, to the charge of the battery.
- The energy fraction sent directly to the load, that appears in the GEB, regardless of the storage capacity, with the increase of the wind and PV nominal powers, for low loads is reduced while for high loads increases; this is owing to the variation of the energy fraction in excess when the nominal powers increase. The energy fraction in excess for low loads increases significantly whereas for high loads the increase is less remarkable.

The presence of a storage battery causes a reduction in the energy fraction drawn from the grid and energy fraction produced in excess; these reductions are more evident by raising the storage capacity since the energy fraction in excess recovered is higher. As regards, the energy fraction drawn from the battery:

- for small nominal powers of the generators and storage capacity, it is reduced when the load increases, since the energy produced is mainly sent to the load;
- for high values of the nominal power of the generators and storage capacity, there is a load value where the stored energy fraction is maximum and, independently of the nominal power

Chapter 2   **Energy reliability-constrained method**
for the multi-objective optimization
of a photovoltaic-wind hybrid system with battery storage

of the generators, a subsequent load value above which the energy fraction drawn from the battery is null, since there is no recoverable energy fraction in excess;

- an increase of the nominal power of the generators determines a reduction in the produced energy fraction stored by the battery for reduced load values, and an increase for higher load values; this is due to the sharp increase in the energy fraction sent directly to the load for reduced loads, while for high loads this increase is limited.

In addition, the results obtained can be employed valuably also to evaluate the energy reliability of the same HPWBS without a grid connection, namely a stand-alone system, in the locality considered. In this case, as previously highlighted in Section 2.5.2, the main indicator is the PV-wind fraction, which identifies the energy missing to meet the load. Instead, the utilization factor, which is complementary to that of the energy produced in excess, becomes energy to be dissipated.

4.1.4. Analytic correlations

Figure 17 shows, as a function of the load overall fraction p_{hbl}, the values of the energy fractions which appear in the LB and GEB, and the values of the reliability indicators f_u and $f_{pv,w}$. In particular, image 17a reports the energy fractions e_{dtl}/e_g and e_{tb}/e_g, image 17b e_{tg}/e_g and f_u, image 17c e_{dtl} and e_{fb}, image 17d e_{fg} and $f_{pv,w}$.
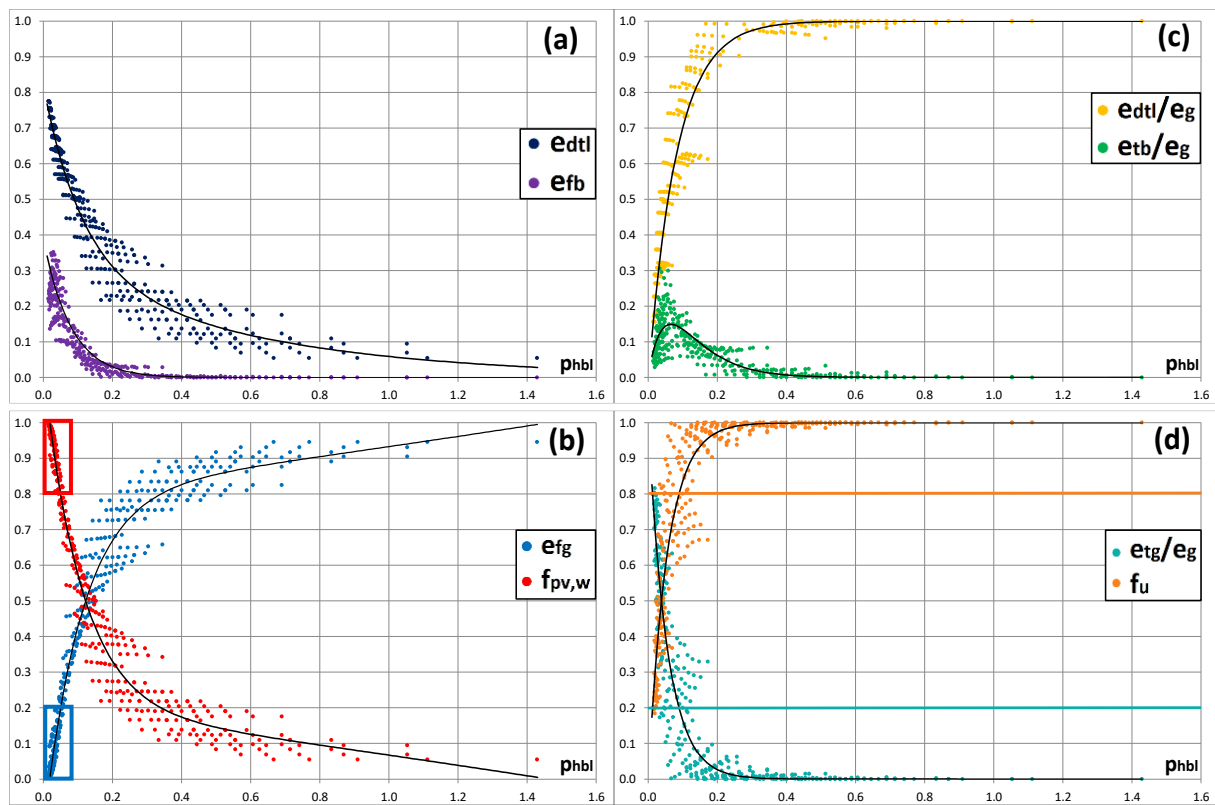
Figure 17. *a) and b) Energy fractions of the LB and PV-wind fraction; c) and d) energy fractions of the GEB and utilization factor.*

The figures show that all the energy fractions of the LB and GEB are dependent on p_{hbl}; this parameter influences the two energy balances to a more remarkable extent than the p_w, p_b and p_l parameters. In particular, the fractions e_{dtl} and e_{fg} have a high correlation with a low dispersion for $p_{hbl} \leq 0.15$ and

Chapter 2

**Energy reliability-constrained method
for the multi-objective optimization
of a photovoltaic-wind hybrid system with battery storage**

a growing dispersion for higher values of p_{hbl}. Instead, the e_{fb} fraction presents a reduced dispersion throughout the variation range of p_{hbl}.

Even fractions e_{tg}/e_g and e_{dtl}/e_g are dependent on p_{hbl} with a higher dispersion than the fractions of the LB, while for e_{tb}/e_g the dispersions are more pronounced.

Empiric equations obtained by the nonlinear regression technique, for the energy fractions of the LB, are:

$$e_{dtl} = 0.4958 \exp(-8.492\, p_{hbl}) + 0.3202 \exp(-1.693\, p_{hbl}) \qquad R^2 = 0.9563 \qquad (44)$$

$$e_{fb} = -0.2659 \exp(-10\, p_{hbl}) + 0.6071 \exp(-11.4\, p_{hbl}) \qquad R^2 = 0.8743 \qquad (45)$$

$$e_{fg} = 0.8028 \exp(0.1502\, p_{hbl}) - 0.9477 \exp(-8.959\, p_{hbl}) \qquad R^2 = 0.9711 \qquad (46)$$

For the energy fractions of the GEB, the empiric equations are:

$$e_{tg}/e_g = \exp(-18.31\, p_{hbl}) \qquad R^2 = 0.8599 \qquad (47)$$

$$e_{dtl}/e_g = 1 - \exp(-12.12\, p_{hbl}) \qquad R^2 = 0.9308 \qquad (48)$$

The e_{tb}/e_g empiric equation can be obtained by replacing Eqs. (47) and (48) into Eq. (32).

As regards the empiric equations of the indicators f_u and $f_{pv,w}$, as they have complementary trends to e_{tg}/e_g and e_{fg}, they can be obtained by Eqs. (37)-(38). These correlations can be used to evaluate the p_{hbl} value, which permits obtaining predefined values of energy fractions that appear in the LB and the GEB, utilization factor and PV-wind fraction. After determining the value of p_{hbl} and, once known the hourly average daily power required by the load P_L, it is possible to determine the overall nominal power of the system P_n required.

Images 17c and 17d permit identification of the variation range of p_{hbl} within which f_u and $f_{pv,w}$ show the highest values. In addition, they show that with an p_{hbl} increase is associated a reduction of f_u and a rise of $f_{pv,w}$. For this reason, for the identification of the most energy reliable system configurations, a trade-off multi-objective optimization is required.

4.2. Multi-objective optimization

The results of the parametric analysis were employed to develop energy reliability multi-objective optimization based on the Pareto-front method and the ERC method described, respectively, in

Chapter 2   **Energy reliability-constrained method
for the multi-objective optimization
of a photovoltaic-wind hybrid system with battery storage**

Sections 2.5.1 and 2.5.2. The multi-objective optimization consists in the identification of the system configurations that simultaneously ensure high values of the utilization factor of the generated energy f_u, PV-wind fraction $f_{pv,w}$ used to meet the load, and manufacturability h_{hl}.

In Figures 18-22, for each value of the considered load P_L, there is a comparison of the values of f_u and $f_{pv,w}$ at the variation of the storage capacity C_B, and for the different values of the nominal power of the PV generator P_{PV} and wind generator P_W. For the determination of the points that identify the optimal configurations, each image reports a graphical representation of the Pareto-front and constraint and objective function values employed in the ERC method.
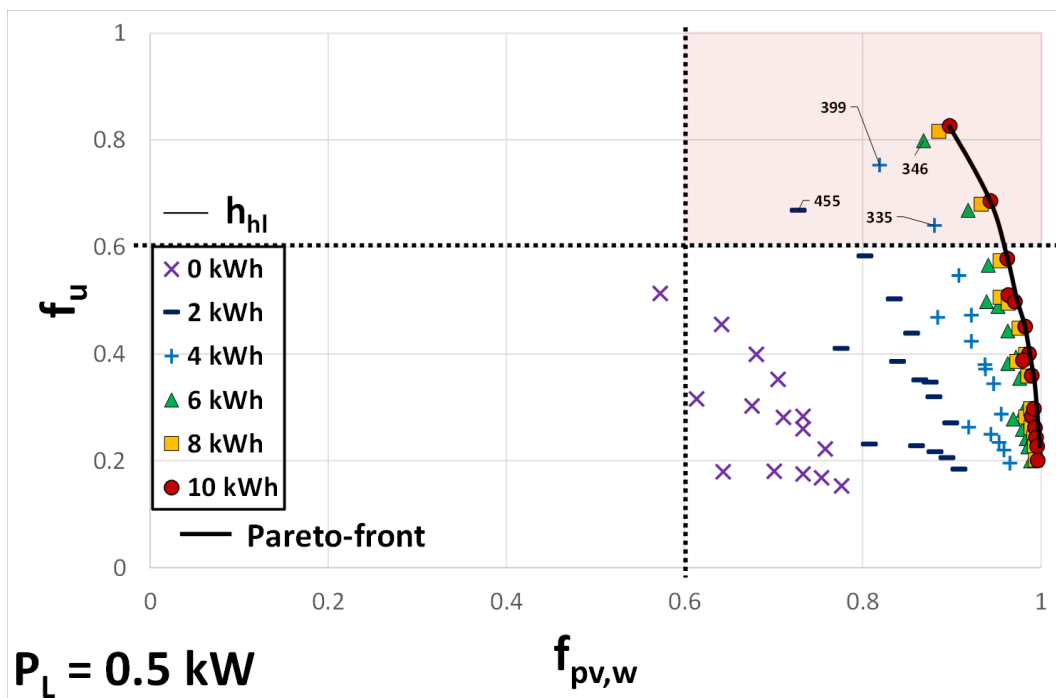
Figure 18. *Results of the multi-objective optimization analysis.* P_L = 0.5 kW.

Chapter 2

**Energy reliability-constrained method
for the multi-objective optimization
of a photovoltaic-wind hybrid system with battery storage**
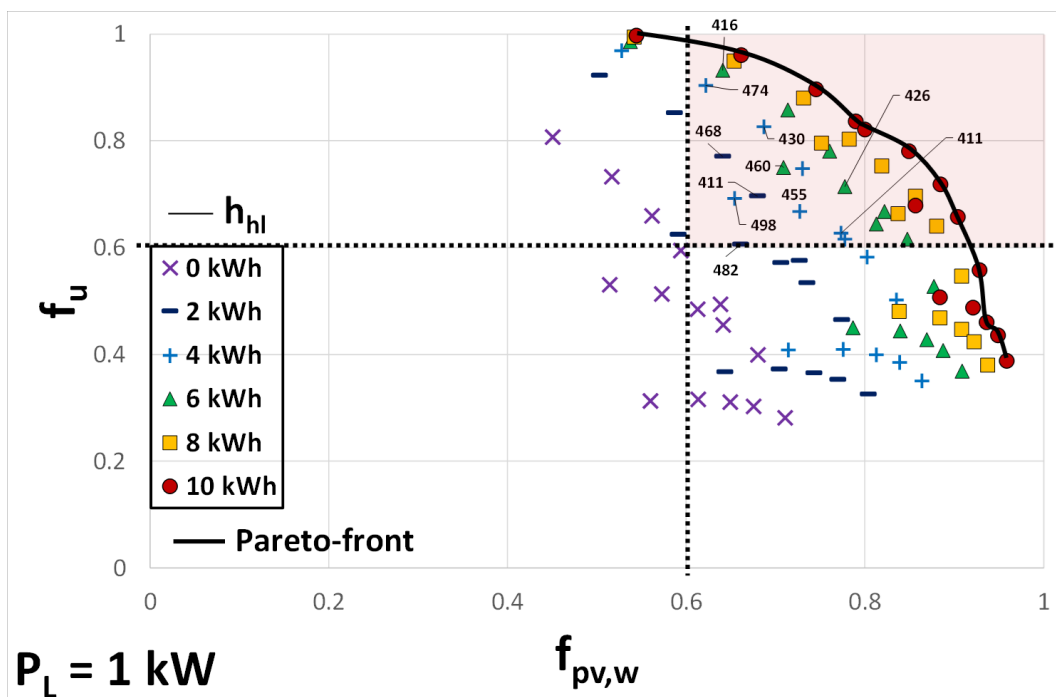
Figure 19. Results of the multi-objective optimization analysis. $P_L = 1$ kW.
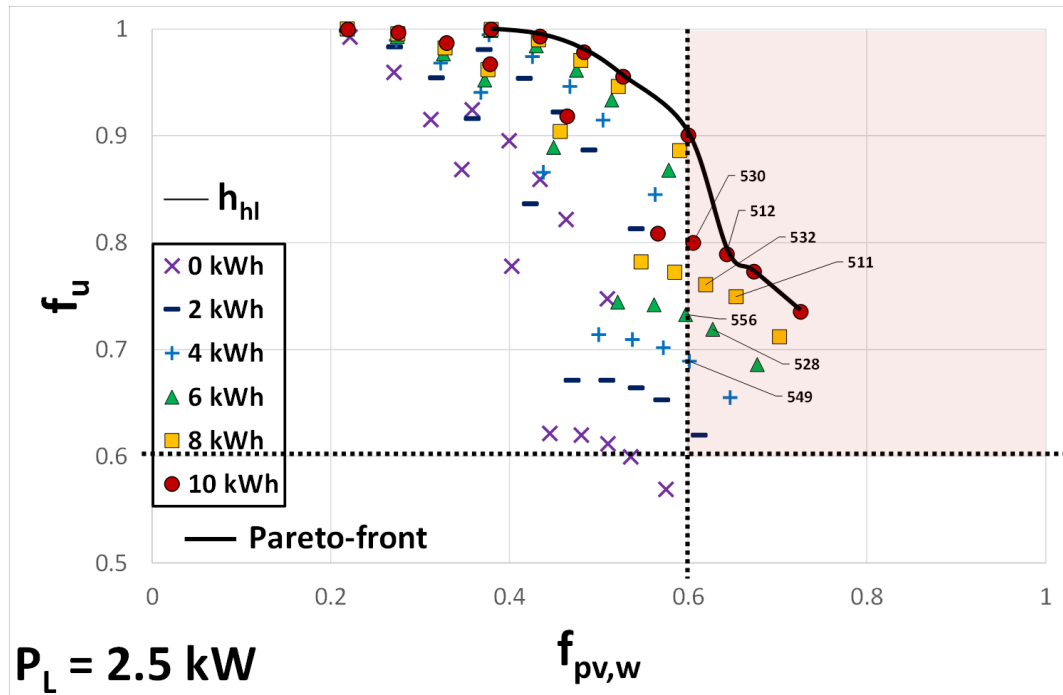
$P_L = 2.5$ kW

Figure 20. Results of the multi-objective optimization analysis. $P_L = 2.5$ kW.
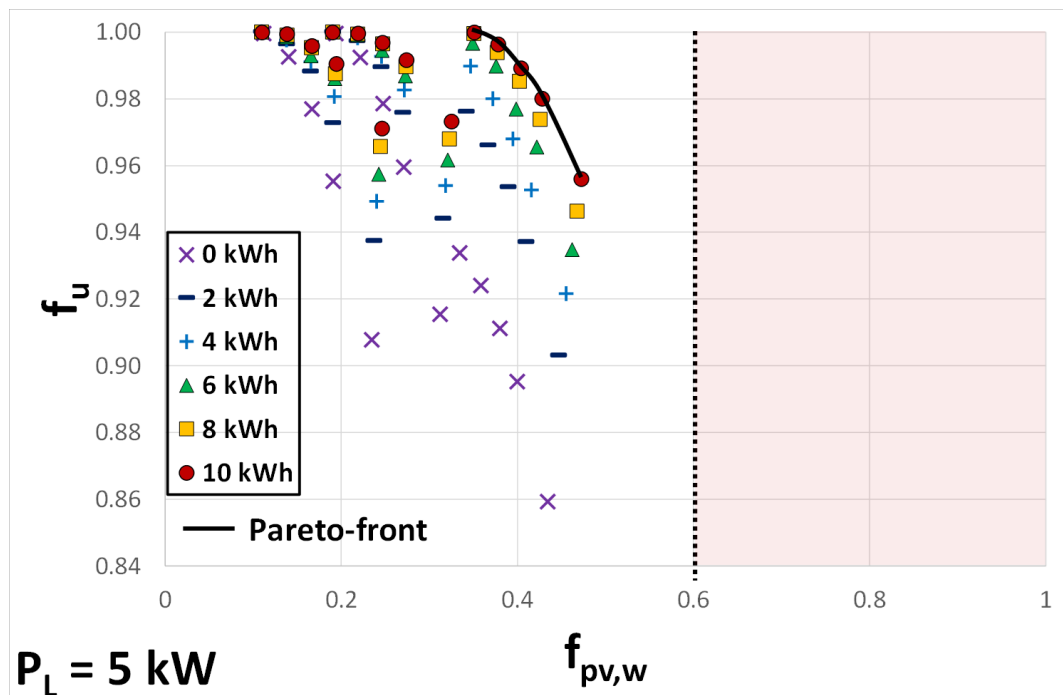
$P_L = 5$ kW

Figure 21. Results of the multi-objective optimization analysis. $P_L = 5$ kW.

Chapter 2

**Energy reliability-constrained method
for the multi-objective optimization
of a photovoltaic-wind hybrid system with battery storage**
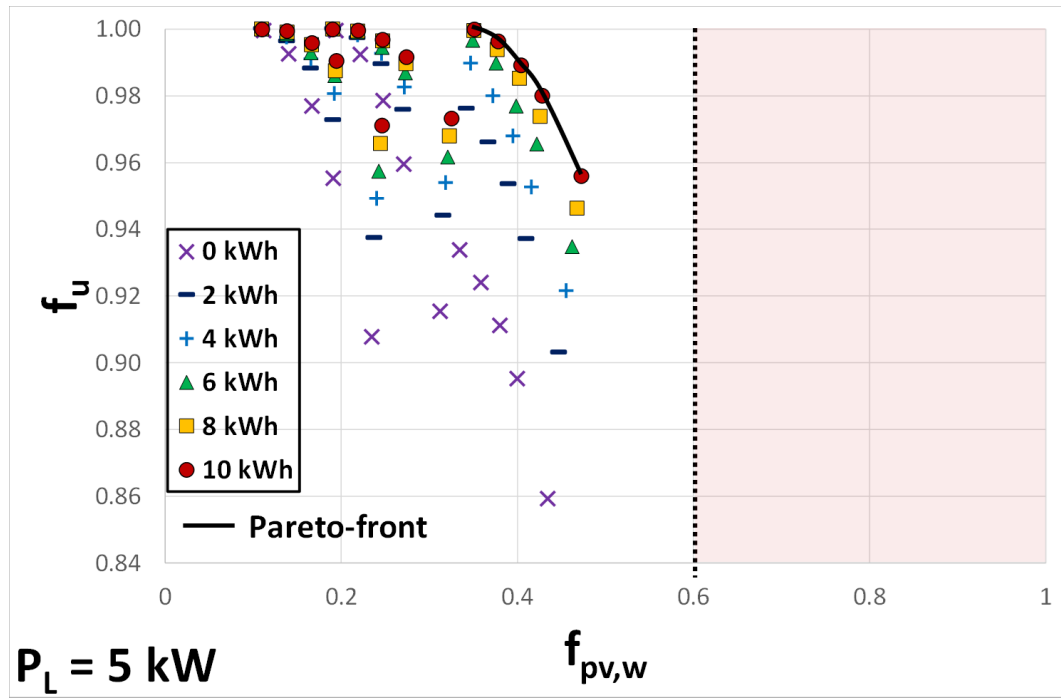
Figure 22. *Results of the multi-objective optimization analysis*. $P_L = 10$ kW.

4.2.1. Pareto-front method

Figures 18-22 show that, for all load values, almost all system configurations on the Pareto-front have a storage capacity of the battery equal to the maximum (10 kWh). For fixed values of the PV and wind power, as battery capacity decreases, the points move away from the Pareto-front determining a reduction of both of f_u and $f_{pv,w}$. Furthermore, as the load increases, the Pareto-front moves towards higher values of utilization factors and lower values of the PV-wind fraction.

Table 3 reports the PV, wind and battery nominal powers, and the corresponding values of the indicators associated with the Pareto-front points for each load value.

Table 3. *Pareto-front optimal HPWBS configurations.*

P_L (kW)		P_B (kW)	P_{PV} (kW)	P_W (kW)	P_n (kW)	$f_{pv,w}$ (-)	f_u (-)
	1	10	2.5	2.5	15	0.90	0.83
	2	10	2.5	5	17.5	0.94	0.69
	3	10	2.5	7.5	20	0.96	0.58
0.5 kW	4	10	2.5	10	22.5	0.97	0.50
	5	10	5	5	20	0.98	0.45
	6	8	5	5	18	0.98	0.45
	7	10	5	7.5	22.5	0.99	0.40
	8	10	10	10	30	1.00	0.23
	1	10	2.5	2.5	15	0.54	1.00
	2	10	2.5	5	17.5	0.66	0.96
	3	10	2.5	7.5	20	0.75	0.90
	4	10	5	2.5	17.5	0.79	0.84
1 kW	5	10	2.5	10	22.5	0.80	0.82
	6	10	5	5	20	0.85	0.78
	7	10	5	7.5	22.5	0.88	0.72
	8	10	5	10	25	0.90	0.66
	9	10	5	15	30	0.93	0.56
	10	10	10	7.5	27.5	0.94	0.46

Chapter 2

Energy reliability-constrained method
for the multi-objective optimization
of a photovoltaic-wind hybrid system with battery storage

	11	10	10	10	30	0.95	0.44
	12	10	10	15	35	0.96	0.39
2.5 kW	1	10	5	2.5	17.5	0.38	1.00
	2	8	5	2.5	15.5	0.38	1.00
	3	6	5	2.5	13.5	0.38	1.00
	4	10	5	5	20	0.43	0.99
	5	8	5	5	18	0.43	0.99
	6	10	5	7.5	22.5	0.48	0.98
	7	10	5	10	25	0.53	0.96
	8	10	5	15	30	0.60	0.90
	9	10	10	5	25	0.61	0.80
	10	10	10	7.5	27.5	0.64	0.79
	11	10	10	10	30	0.67	0.77
	12	10	10	15	35	0.73	0.74
5 kW	1	10	2.5	2.5	18.50	0.35	1.00
	2	10	10	5	25	0.38	1.00
	3	10	10	7.5	27.5	0.40	0.99
	4	10	10	10	30	0.43	0.98
	5	10	10	15	35	0.47	0.96
10 kW	1	8	10	10	28	0.22	1.00
	2	6	10	10	26	0.22	1.00
	3	4	10	10	24	0.22	1.00
	4	2	10	10	22	0.22	1.00
	5	10	10	15	35	0.25	0.99
	6	8	10	15	33	0.25	0.99
	7	6	10	15	31	0.25	0.99

The table highlights the trade-off behavior of the optimization problem, showing for each load value that to an increase of an indicator is associated a reduction of the other one. In particular, an increase in the nominal power of the PV or wind generator results in a rise of $f_{pv,w}$ and a reduction of f_u. Since high values of f_u and $f_{pv,w}$ are simultaneously requested to energy reliability grid-connected HPWBS, then some Pareto-front optimal system configurations have a low energy reliability. In addition, the table shows that different values of the overall nominal power installed P_n correspond to these optimal configurations.

4.2.2. Energy reliability-constrained (ERC) method

The identification of the most energy reliable system configurations requires the application of the ERC method. In the application of the method the power P_n was considered by means of the use of the manufacturability indicator h_{hl}, which normalizes the energy delivered to the load compared to the nominal power installed. Since, for a grid-connected hybrid system, the number of indicators to be constrained and to be optimized are equal to, respectively, m=2 and n=1, then this goal has been achieved: (i) tracing the quadrant (light red in Figures 18-22) which identifies the system configurations that satisfy the constraints described in Section 2.5.2, in this case $\bar{f}_{pv,w} = 0.60$ and $\bar{f}_u = 0.60$; (ii) identifying the system configurations within this quadrant resulting in the higher values of manufacturability h_{hl}.

For a load of 5 kW and 10 kW, no system configuration falls within the selected quadrant since higher component powers are requested. For loads of 0.5 kW, 1 kW and 2.5 kW, in the selected quadrant, only the optimal system configurations with the maximum values of h_{hl} in hours/year are shown. For these system configurations, Table 4 reports, for load values P_L of 0.5 kW, 1 kW and 2.5 kW, the

Chapter 2

**Energy reliability-constrained method
for the multi-objective optimization
of a photovoltaic-wind hybrid system with battery storage**

nominal powers of the PV generator P_{PV} and wind generator P_W, maximum storable energy in 1 h by the battery P_B, overall power of the system P_n, wind fraction p_w, storage fraction p_b, load fraction p_l, and load overall fraction p_{hbl}. Furthermore, the energy fractions that appear in the GEB and LB, Eqs. (26), (30)-(32), utilization factor f_u, PV-wind fraction $f_{pv,w}$ and manufacturability h_{hl} are reported.

The table shows that the optimal HPWBS configurations obtained with the ERC method are not necessarily those with the maximum battery capacity, unlike what proved with the Pareto-front optimal configurations. The optimal configurations are characterized by a load overall fraction p_{hbl} between 0.05 and 0.11, storage fraction p_b from 0.17 to 0.55, and wind fraction p_w between 0.33 and 0.75. These system configurations ensure e_{dtl} values between 0.48 and 0.64, e_{fb} values between 0.08 and 0.30, e_{fg} values between 0.12 and 0.40, e_{dtl}/e_g values between 0.46 and 0.74, e_{tb}/e_g values between 0.09 and 0.28, and e_{tg}/e_g values between 0.07 and 0.39. In these conditions, the reliability indicators are included in the following ranges: f_u between 0.61 and 0.93, $f_{pv,w}$ between 0.60 and 0.88, and h_{hl} between 335 h/year and 556 h/year.

Table 4. ERC optimal HPWBS configurations.

P_L (kW)	P_B (kW)	P_{PV} (kW)	P_W (kW)	P_n (kW)	p_w (-)	p_b (-)	p_l (-)	p_{hbl} (-)	e_{dtl} (-)	e_{fb} (-)	e_{fg} (-)	e_g (-)	e_{lb} (-)	e_{tb} (-)	e_{tg} (-)	e_{dtl}/e_g (-)	e_{tb}/e_g (-)	e_{tg}/e_g (-)	$f_{pv,w}$ (-)	f_u (-)	h_{hl} (h)
0.5	6	2.5	2.5	11	0.50	0.55	0.10	0.05	0.57	0.30	0.13	1.09	0.01	0.30	0.22	0.52	0.28	0.20	0.87	0.80	345.6
0.5	4	2.5	2.5	9	0.50	0.44	0.10	0.06	0.57	0.25	0.18	1.09	0.01	0.26	0.27	0.52	0.23	0.25	0.82	0.75	398.6
0.5	2	2.5	2.5	7	0.50	0.29	0.10	0.07	0.57	0.16	0.27	1.09	0.00	0.16	0.36	0.52	0.15	0.33	0.73	0.67	455.0
0.5	4	2.5	5	11.5	0.67	0.35	0.07	0.04	0.64	0.24	0.12	1.38	0.01	0.25	0.50	0.46	0.18	0.36	0.88	0.64	335.3
1	6	2.5	5	13.5	0.67	0.44	0.13	0.07	0.51	0.13	0.36	0.69	0.00	0.13	0.05	0.74	0.19	0.07	0.64	0.93	416.0
1	4	2.5	5	11.5	0.67	0.35	0.13	0.09	0.51	0.11	0.38	0.69	0.00	0.12	0.07	0.74	0.17	0.10	0.62	0.90	473.8
1	4	2.5	7.5	14	0.75	0.29	0.10	0.07	0.55	0.13	0.31	0.84	0.00	0.14	0.15	0.66	0.16	0.17	0.69	0.83	429.9
1	8	5	2.5	15.5	0.33	0.52	0.13	0.06	0.51	0.24	0.25	0.95	0.01	0.25	0.19	0.54	0.26	0.20	0.75	0.80	424.7
1	2	2.5	7.5	12	0.75	0.17	0.10	0.08	0.55	0.09	0.36	0.84	0.00	0.10	0.19	0.66	0.11	0.23	0.64	0.77	468.0
1	6	5	2.5	13.5	0.33	0.44	0.13	0.07	0.51	0.20	0.29	0.95	0.00	0.20	0.24	0.54	0.21	0.25	0.71	0.75	460.0
1	6	5	5	16	0.50	0.38	0.10	0.06	0.57	0.21	0.22	1.09	0.00	0.21	0.31	0.52	0.19	0.29	0.78	0.71	425.8
1	4	5	2.5	11.5	0.33	0.35	0.13	0.09	0.51	0.15	0.35	0.95	0.00	0.15	0.29	0.54	0.16	0.31	0.65	0.69	498.2
1	4	5	5	14	0.50	0.29	0.10	0.07	0.57	0.16	0.27	1.09	0.00	0.16	0.36	0.52	0.15	0.33	0.73	0.67	455.0
1	4	5	7.5	16.5	0.60	0.24	0.08	0.06	0.61	0.17	0.23	1.24	0.00	0.17	0.46	0.49	0.14	0.37	0.77	0.63	410.6
1	2	5	5	12	0.50	0.17	0.10	0.08	0.56	0.10	0.34	1.09	0.00	0.10	0.43	0.51	0.09	0.39	0.66	0.61	482.3
2.5	10	10	5	25	0.33	0.40	0.17	0.10	0.48	0.13	0.39	0.76	0.00	0.13	0.15	0.63	0.17	0.20	0.61	0.80	530.4
2.5	10	10	7.5	27.5	0.43	0.36	0.14	0.09	0.50	0.14	0.36	0.82	0.00	0.14	0.17	0.62	0.17	0.21	0.64	0.79	511.9
2.5	8	10	7.5	25.5	0.43	0.31	0.14	0.10	0.50	0.12	0.38	0.82	0.00	0.12	0.20	0.62	0.15	0.24	0.62	0.76	532.2
2.5	8	10	10	28	0.50	0.29	0.13	0.09	0.53	0.13	0.35	0.88	0.00	0.13	0.22	0.60	0.15	0.25	0.65	0.75	511.0
2.5	6	10	7.5	23.5	0.43	0.26	0.14	0.11	0.50	0.09	0.40	0.82	0.00	0.10	0.22	0.61	0.12	0.27	0.60	0.73	556.4
2.5	6	10	10	26	0.50	0.23	0.13	0.10	0.53	0.10	0.37	0.88	0.00	0.10	0.25	0.60	0.12	0.28	0.63	0.72	528.4
2.5	4	10	10	24	0.50	0.17	0.13	0.10	0.52	0.08	0.40	0.88	0.00	0.08	0.27	0.60	0.09	0.31	0.60	0.69	548.7

5. Conclusions

The ERC method proposed, for the multi-objective optimization of PV-wind hybrid systems, employs several indicators to identify the most energy reliable system configurations. It can be

Chapter 2

**Energy reliability-constrained method
for the multi-objective optimization
of a photovoltaic-wind hybrid system with battery storage**

applied easily to a grid-connected and stand-alone PV-wind hybrid system with and without storage battery, in any climate context and load conditions, and allows optimizing the system in accordance with the specific application and the objectives. In addition, it can be applied in both the design phase and performance verification phase of a specific HPWBS.

The ERC method was applied to a grid-connected HPWBS and HPWS used to supply a variable load on an hourly basis in an urban residential context with a Mediterranean climate, and it was compared with the classic multi-objective optimization Pareto-front method.
The results of the energy reliability parametric analysis, obtained considering 450 different system configurations, have shown that:

- the energy reliability is determined by the wind fraction, storage fraction and load fraction;
- the energy fractions that appear in the LB and GEB, turned out to be correlated strongly to the load overall fraction, which takes into account the size of all system components. The obtained empiric correlations are to be used for the system sizing;
- the presence of a storage battery gives rise to an increase in the utilization factor and the PV-wind fraction, which present complementary trends, respectively to that of the energy fraction in excess and to that of the energy fraction drawn from the grid.
- high values of the PV-wind fraction, variable between 1 and 0.80, can be obtained with a load overall fraction ranging from 0 to 0.05, while high values of the utilization factor can be obtained throughout the variation range of load overall fraction.

In addition, the results of the parametric analysis can also be employed in the locality considered to evaluate the energy reliability of the same hybrid system without grid connection, namely a stand-alone system, with the PV-wind fraction that assumes the meaning of energy missing to meet the load.

The comparison between the ERC and Pareto-front multi-objective optimization methods has highlighted that:

- the Pareto-front optimal configurations are those with the highest values of the battery storage capacity, and among these configurations, just some assure high energy reliability;
- the ERC method identifies the most energy reliable system configurations, which ensure simultaneously high values of the PV-wind fraction and utilization factor. These optimal configurations are not necessarily those with the maximum battery capacity; in addition, among these system configurations, the ERC method allows the selection of those with the greatest values of energy sent to the load per kW installed, by means of the use of the further indicator manufacturability.

The optimal HPWBS, found by means of the ERC method, needs an overall nominal power of 10-20 times the hourly average daily load, a storage capacity of the battery between 17 % and 55 % of the overall nominal power, and a wind fraction between 33% and 75%. These system configurations ensure utilization factor values between 0.61 and 0.93, PV-wind fractions between 0.60 and 0.88, and manufacturability between 335 h/ year and 556 h/year.

References

[1] A. Abbassi, M. A. Dami, M. Jemli, A statistical approach for hybrid energy storage system sizing based on capacity distributions in an autonomous PV/Wind power generation system. Renew Energy, Volume 103, 2017, Pages 81-93, ISSN 0960-1481, https://doi.org/10.1016/j.renene.2016.11.024.

Chapter 2

**Energy reliability-constrained method
for the multi-objective optimization
of a photovoltaic-wind hybrid system with battery storage**

[2] A. Kaabeche, M. Belhamel, R. Ibtiouen, Sizing optimization of grid-independent hybrid photovoltaic/wind power generation system, Energy, Volume 36, Issue 2, 2011,Pages 1214-1222, ISSN 0360-5442, https://doi.org/10.1016/j.energy.2010.11.024.

[3] R. Maouedj, A. Mammeri, M.D. Draou, B. Benyoucef, Techno-economic Analysis of a Standalone Hybrid Photovoltaic-wind System. Application in Electrification of a House in Adrar Region, Energy Procedia, Volume 74, 2015, Pages 1192-1204, ISSN 1876-6102, https://doi.org/10.1016/j.egypro.2015.07.762.

[4] B. Getachew, P. Björn, Feasibility study for a standalone solar–wind-based hybrid energy system for application in Ethiopia, Applied Energy Volume 87, Issue 2, 2010, Pages 487-495, ISSN 0306-2619, https://doi.org/10.1016/j.apenergy.2009.06.006.

[5] N. Ghorbani, A. Kasaeian, A. Toopshekan, L. Bahrami, A. Maghami, Optimizing a Hybrid Wind-PV-Battery System Using GA-PSO and MOPSO for Reducing Cost and Increasing Reliability, Energy, 2017, ISSN 0360-5442, https://doi.org/10.1016/j.energy.2017.12.057

[6] H.C. Chen, Optimum capacity determination of stand-alone hybrid generation system considering cost and reliability, Applied Energy, Volume 103, 2013, Pages 155-164, ISSN 0306-2619,

[7] https://doi.org/10.1016/j.apenergy.2012.09.022.

[8] T. Ma, H. Yang, L. Lu, A feasibility study of a stand-alone hybrid solar–wind– battery system for a remote island, Applied Energy, Volume 121, 2014, Pages 149-158, ISSN 0306-2619, https://doi.org/10.1016/j.apenergy.2014.01.090.

[9] B. Ould Bilal, V. Sambou, P.A. Ndiaye, C.M.F. Kébé, M. Ndongo, Optimal design of a hybrid solar–wind-battery system using the minimization of the annualized cost system and the minimization of the loss of power supply probability (LPSP), Renewable Energy, Volume 35, Issue 10, 2010, Pages 2388-2390, ISSN 0960-1481, https://doi.org/10.1016/j.renene.2010.03.004.

[10]   P.S. Georgilakis, Y.A. Katsigiannis, Reliability and economic evaluation of small autonomous power systems containing only renewable energy sources, Renewable Energy, Volume 34, Issue 1, 2009, Pages 65-70, ISSN 0960-1481, https://doi.org/10.1016/j.renene.2008.03.004.

[11]   A. Kaabeche, S. Diaf, R. Ibtiouen, Firefly-inspired algorithm for optimal sizing of renewable hybrid system considering reliability criteria, Solar Energy, Volume 155, 2017, Pages 727-738, ISSN 0038-092X, https://doi.org/10.1016/j.solener.2017.06.070.

[12]   S. Diaf, D. Diaf, M. Belhamel, M. Haddadi, A. Louche, A methodology for optimal sizing of autonomous hybrid PV/wind system, Energy Policy, Volume 35, Issue 11,2007, Pages 5708-5718, ISSN 0301-4215, https://doi.org/10.1016/j.enpol.2007.06.020.

[13]   S. Diaf, M. Belhamel, M. Haddadi, A. Louche, A. Technical and economic assessment of hybrid photovoltaic/wind system with battery storage in Corsica Island, Energy Policy, Volume 36, Issue 2, 2008, Pages 743-754, ISSN 0301-4215, https://doi.org/10.1016/j.enpol.2007.10.028.

[14]   S. Diaf, G. Notton, M. Belhamel, M. Haddadi, A. Louche, Design and techno-economical optimization for hybrid PV/wind system under various meteorological conditions, Applied Energy, Volume 85, Issue 10, 2008, Pages 968-987, ISSN 0306-2619, https://doi.org/10.1016/j.apenergy.2008.02.012.

[15]   F. Caballero, E. Sauma, F. Yanine, Business optimal design of a grid-connected hybrid PV (photovoltaic)-wind energy system without energy storage for an Easter Island's block, Energy, Volume 61, 2013, Pages 248-261, ISSN 0360-5442, https://doi.org/10.1016/j.energy.2013.08.030.

[16]   A. González, J.R. Riba, A. Rius, R. Puig, Optimal sizing of a hybrid grid-connected photovoltaic and wind power system, Applied Energy, Volume 154, 2015, Pages 752-762, ISSN 0306-2619, https://doi.org/10.1016/j.apenergy.2015.04.105.

[17]   M.Z. Daud, A. Mohamed, M.A. Hannan, An improved control method of battery energy storage system for hourly dispatch of photovoltaic power sources, Energy Conversion and Management, Volume 73, 2013, Pages 256-270, ISSN 0196-8904, https://doi.org/10.1016/j.enconman.2013.04.013.

[18]   S. Sinha, S.S. Chandel, Review of recent trends in optimization techniques for solar photovoltaic–wind-based hybrid energy systems, Renewable and Sustainable Energy Reviews, Volume 50,

Chapter 2

**Energy reliability-constrained method
for the multi-objective optimization
of a photovoltaic-wind hybrid system with battery storage**

[19]   2015, Pages 755-769, ISSN 1364-0321, https://doi.org/10.1016/j.rser.2015.05.040.

[20]   A. Mahesh, K.S. Sandhu, Hybrid wind/photovoltaic energy system developments: Critical review and findings, Renewable and Sustainable Energy Reviews, Volume 52, 2015, Pages 1135-1147,

[21]   ISSN 1364-0321, https://doi.org/10.1016/j.rser.2015.08.008.

[22]   V. Khare, S. Nema, P. Baredar, Solar – wind hybrid renewable energy system: A review, Renewable and Sustainable Energy Reviews, Volume 58, 2016, Pages 23-33, ISSN 1364-0321, https://doi.org/10.1016/j.rser.2015.12.223.

[23]   R. Luna-Rubio, M. Trejo-Perea, D. Vargas-Vázquez, G.J. Ríos-Moreno, Optimal sizing of renewable hybrids energy systems: A review of methodologies, Solar Energy, Volume 86, Issue 4, 2012, Pages 1077-1088, ISSN 0038-092X, https://doi.org/10.1016/j.solener.2011.10.016.

[24]   H.R. Baghaee, M. Mirsalim, G.B. Gharehpetian, H.A. Talebi, Reliability/cost-based multi-objective Pareto optimal design of stand-alone wind/PV/FC generation microgrid system, Energy, Volume 115, Part 1, 2016, Pages 1022-1041, ISSN 0360-5442, https://doi.org/10.1016/j.energy.2016.09.007.

[25]   L.G. Acuña, R.V. Padilla, A.S. Mercado, Measuring reliability of hybrid photovoltaic-wind energy systems: A new indicator, Renewable Energy, Volume 106, 2017, Pages 68-77, ISSN 0960-1481, https://doi.org/10.1016/j.renene.2016.12.089.

[26]   M.A.M. Ramli, H.R.E.H. Bouchekara, A.S. Alghamdi, Optimal Sizing of PV/wind/diesel hybrid microgrid system using multi-objective self-adaptive differential evolution algorithm, Renewable Energy 2018, ISSN 0960-1481, https://doi.org/10.1016/j.renene.2018.01.058.

[27]   M.A. Ramli, A. Hiendro, Y.A. Al-Turki, Techno-economic energy analysis of wind/solar hybrid system: Case study for western coastal area of Saudi Arabia, Renewable Energy, Volume 91, 2016, Pages 374-385, ISSN 0960-1481, https://doi.org/10.1016/j.renene.2016.01.071.

[28]   S. Sinha, S.S. Chandel, Improving the reliability of photovoltaic-based hybrid power system with battery storage in low wind locations, Sustainable Energy Technologies and Assessments, Volume 19, 2017, Pages 146-159, ISSN 2213-1388, https://doi.org/10.1016/j.seta.2017.01.008.

[29]   S. Aissou, D. Rekioua, N. Mezzai, T. Rekioua, S. Bacha, Modeling and control of hybrid photovoltaic wind power system with battery storage, Energy Conversion and Management, Volume 89, 2015, Pages 615-625, ISSN 0196-8904, https://doi.org/10.1016/j.enconman.2014.10.034.

[30]   M. Boussetta, R. El Bachtiri, M. Khanfara, K. El Hammoumi Assessing the potential of hybrid PV–Wind systems to cover public facilities loads under different Moroccan climate conditions, Sustainable Energy Technologies and Assessments, Volume 22, 2017, Pages 74-82, ISSN 2213-1388, https://doi.org/10.1016/j.seta.2017.07.005.

[31]   O. Ekren, B.Y. Ekren, Size optimization of a PV/wind hybrid energy conversion system with battery storage using simulated annealing, Applied Energy, Volume 87, Issue 2, 2010, Pages 592-598, ISSN 0306-2619, https://doi.org/10.1016/j.apenergy.2009.05.022.

[32]   D.G. Erbs, S.A. Klein, J.A. Duffie, Estimation of the diffuse radiation fraction for hourly, daily and monthly-average global radiation, Solar Energy, Volume 28, Issue 4, 1982, Pages 293-302, ISSN 0038-092X, http://dx.doi.org/10.1016/0038-092X(82)90302-4.

[33]   J.A. Duffie, W.A. Beckman, Solar Engineering of Thermal Processes 4th Edition, Solar Energy Laboratory University of Wisconsin-Madison, John Wiley & Sons, 2013.

[34]   Fry, A. Bryan, Simulation of Grid-Tied Building Integrated Photovoltaic Systems. M. S. Thesis –Solar Energy Laboratory, University of Wisconsin, Madison: 1999.

[35]   R. Chenni, M. Makhlouf, T. Kerbache, A. Bouzid, A detailed modeling method for photovoltaic cells, Energy, Volume 32, Issue 9, 2007, Pages 1724-1730, ISSN 0360-5442, https://doi.org/10.1016/j.energy.2006.12.006.

[36]   D. L. King, J.A. Kratochvil, W.E. Boyson, Measuring the Solar Spectral and Angle-of-Incidence Effects on Photovoltaic Modules and Irradiance Sensors, Proceedings of the 1994 IEEE Photovoltaics Specialists Conference. Sept 30-Oct 3, 1997. pp. 1113-1116.

Chapter 2   **Energy reliability-constrained method**
for the multi-objective optimization
of a photovoltaic-wind hybrid system with battery storage

[37]   P. J. A. Quinlan, Time series modeling of hybrid wind photovoltaic diesel power systems. M. S. Thesis –Solar Energy Laboratory, University of Wisconsin, Madison: 1996.

[38]   TRNSYS; Version 17. (2012) Solar Energy Laboratory University of Wisconsin-Madison: Madison, WI, USA.

[39]   A.M. Kanakkithodi, G. Pilania, R. Ramprasad, T. Lookman, J.E. Gubernatis, Multi-objective optimization techniques to design the Pareto front of organic dielectric polymers, Computational Materials Science, Volume 125, 2016, Pages 92-99, ISSN 0927-0256, https://doi.org/10.1016/j.commatsci.2016.08.018.

[40]   M. Kottek, J. Grieser, C. Beck, B. Rudolf, F. Rubel, World Map of the Köppen-Geiger climate classification updated, Meteorologische Zeitschrift 15.3 (2006): 259-263. DOI: 10.1127/0941-2948/2006/0130.

[41]   Sharp Energy Solutions, Hamburg (Germany). Website: www.sharp.eu/cps/rde/xchg/eu/, last access: 23/02/2018.

[42]   Angel Wind Energy Inc., Onarga, IL (United States). Website: www.angelwindenergy.com/, last access: 23/02/2018.

[43]   LG Chem Michigan Inc., Seoul (Korea). Website: www.lgchem.com/, last access: 23/02/2018.

[44]   EPsolar Technology CO., Ltd., Beijing (China). Website: www.epsolarpv.com, last access: 23/02/2018.

[45]   Ditta 3T s.r.l., Perugia (Italy). Website: www.ditta3t.com, last access: 23/02/2018.

[46]   ABB Ltd., Zürich(Switzerland). Website: www.abb.com/, last access: 23/02/2018.

[47]   Steca Elektronik GmbH, Memmingen (Germany). Website: www.steca.com, last access: 23/02/2018.

Nomenclature

Abbreviations

ERC	energy reliability-constrained
GEB	generated energy balance (-)
HPWBS	hybrid photovoltaic-wind-battery system
HPWS	hybrid photovoltaic-wind system
IAM	incidence angle modifier (-)
LB	load balance (-)
NOCT	nominal operating cell temperature (K)
PV	photovoltaic
UPS	uninterruptible power supply

Symbols

a	modified ideality factor (eV)
C_{bat}	battery capacity (kWh)
e_{dtl}	energy fraction sent directly to the load (-)
e_{fb}	energy fraction drawn from the battery (-)
e_{fg}	energy fraction drawn from the grid (-)
e_g	energy fraction produced by the generators (-)
e_{lb}	energy fraction lost in the battery (-)
e_{tb}	energy fraction sent to the battery (-)
e_{tg}	energy fraction in excess sent to the grid (-)
E_{dtl}	annual energy sent directly to the load (Wh)
E_{fb}	annual energy drawn from the battery (Wh)
E_{fg}	annual energy drawn from the power grid (Wh)

Chapter 2

**Energy reliability-constrained method
for the multi-objective optimization
of a photovoltaic-wind hybrid system with battery storage**

E_g	annual energy produced by the generators (Wh)
E_{lb}	annual energy lost in the battery (Wh)
E_L	annual energy required by the load (Wh)
E_{pv}	annual energy produced by the photovoltaic generator (Wh)
$E_{pv,eff}$	annual effective energy produced by the photovoltaic generator (Wh)
E_{tb}	annual energy sent to the battery (Wh)
E_{tl}	annual energy produced sent to the load (Wh)
E_{tg}	annual energy in excess sent to the grid (Wh)
E_w	annual energy produced by the wind generator (Wh)
$E_{w,eff}$	annual effective energy produced by the wind generator (Wh)
$f_{pv,w}$	photovoltaic-wind fraction (-)
$\bar{f}_{pv,w}$	constraint on the photovoltaic-wind fraction (-)
f_{SOC}	charge fraction (-)
f_u	utilization factor (-)
$\bar{f}_u$	constraint on the utilization factor (-)
G	hourly solar radiation on the inclined surface (W/m^2)
$G_{b,h}$	beam solar radiation on the horizontal surface (W/m^2)
$G_{d,h}$	diffuse solar radiation on the horizontal surface (W/m^2)
h_{hl}	manufacturability (Wh/W)
$\bar{h}_{hl}$	constraint on the manufacturability (Wh/W)
k	Boltzmann's constant (1.38066E–23 J/K)
I	current (A)
I_o	diode reverse saturation current (A)
I_L	light current (A)
$I_{mp}(t)$	current at maximum power point (A)
ℓ	miscellaneous losses (%)
n_I	usual ideality factor (-)
N_s	number of cells in series (-)
O	objective function
$\bar{O}$	constraint on the objective function
p_b	storage fraction (-)
p_{hbl}	load overall fraction (-)
p_l	load fraction (-)
p_w	wind fraction (-)
$P(t)$	power (W)
$P_o(t)$	wind turbine power at the actual operating height for a reference air density (W)
P_B	maximum stored energy in one hour by the battery (W)
$P_g(t)$	overall power generated (W)
$P_{fb}(t)$	power drawn from the battery (W)
$P_{fg}(t)$	power drawn from the grid (W)
$P_{inv,out}(t)$	inverter output power(W)
$P_{inv,inp}(t)$	inverter input power(W)
$P_L(t)$	power required by the load (W)
P_n	overall nominal power of the HPWBS (W)
$P_{pv}(t)$	power produced by the photovoltaic generator (W)
$P_{pv,eff}(t)$	effective power produced by the photovoltaic generator (W)
P_{PV}	nominal power of the photovoltaic generator (W)
$P_{tb}(t)$	power sent to the battery (W)

Chapter 2
                                      Energy reliability-constrained method
for the multi-objective optimization
of a photovoltaic-wind hybrid system with battery storage

$P_{tg}(t)$	power in excess sent to the grid (W)
$P_{tl}(t)$	power produced sent to the load (W)
$P_w(t)$	power produced by the wind generator (W)
$P_{w,eff}(t)$	effective power produced by the wind generator (W)
P_W	nominal power of the photovoltaic generator (W)
$P_\rho(t)$	wind turbine power as a function of air density (W)
$P_{\rho,net}(t)$	power produced by the wind generator (W)
q	electron charge (1.60218E–19 C)
r	parameters of the objective functions
R_b	hourly average geometry factor of the beam radiation (-)
R_d	geometry factor of the diffuse radiation (-)
R_r	geometry factor of the reflected radiation (-)
R_s	series resistance (Ω)
R_{sh}	shunt resistance (Ω)
$SOC(t)$	state of charge of the battery (Wh)
$SOC_{max}(t)$	maximum allowable SOC (Wh)
$SOC_{min}(t)$	minimum allowable SOC (Wh)
t	time (s)
T_c	cell temperature (°C)
$T_{ea}(t)$	external air temperature (K)
$v(t)$	wind speed (m/s)
$V_{mp}(t)$	voltage at maximum power point (V)
v_{an}	wind speed at the anemometric height (m/s)
$v_h(t)$	wind speed at the actual operating height of the wind turbine (m/s)
$v_{nom,\rho}$	nominal wind speed as a function of air density (m/s)
$v_{nom,\rho o}$	nominal wind speed at the reference air density (m/s)
V	voltage (V)
z_{an}	anemometric height (m)
z_h	actual operating height of the wind turbine (m)

Greek letters

$\alpha(t)$	wind shear exponent (-)
β	inclination angle of the photovoltaic surface (°)
Δt	time interval (s)
$\eta_{AC/AC}$	DC/DC converter efficiency (-)
$\eta_{AC/DC}$	AC/DC rectifier efficiency (-)
η_{bat}	battery efficiency (-)
η_{inv}	inverter efficiency (-)
η_{reg}	regulator efficiency (-)
$\rho(t)$	air density (kg/ m^3)
ρ_0	power curve air density (kg/m^3)

Subscripts

i	i-th objective function
j	j-th objective function
m	number of constrained objective functions
n	number of objective functions
r	number of parameters of the objective functions
ref	at the reference conditions

Chapter 3

A novel energy economic-environmental
multi-criteria decision-making
in the optimization of a hybrid renewable system

Chapter 3

A novel energy economic-environmental multi-criteria decision-making in the optimization of a hybrid renewable system

Chapter 3   **A novel energy economic-environmental**
multi-criteria decision-making
in the optimization of a hybrid renewable system
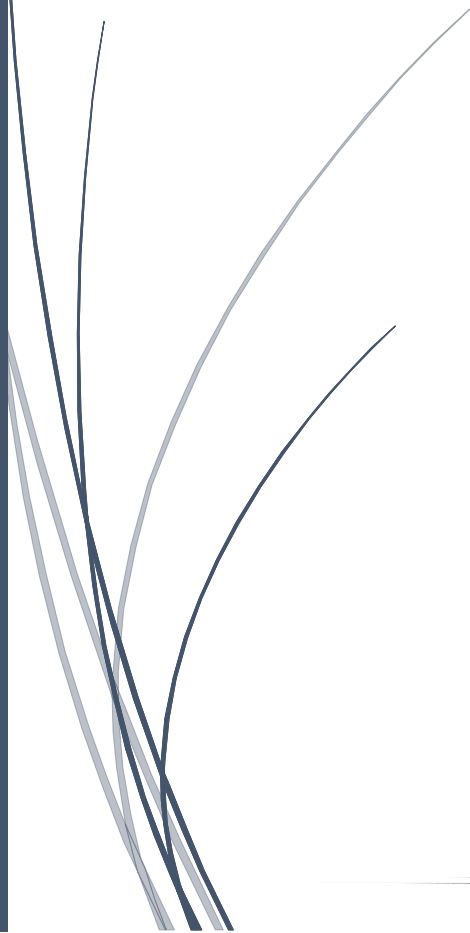
Chapter 3

A novel energy economic-environmental multi-criteria decision-making in the optimization of a hybrid renewable system

Abstract

The development of hybrid renewable systems is an economically competitive solution to reach energy decarbonization and reduction of greenhouse gasses.

Based on the literature, energy, economic and environmental indicators were rarely simultaneously employed in the optimization of a hybrid renewable system. In addition, there is no procedures or a set of indicators to be applied uniformly in all applications for the shared analysis.

The paper presents a novel energy-economic-environmental multi-criteria decision-making in the optimization of a hybrid renewable system, based on a new set of dimensionless indicators, proposed as a standard for future applications. The procedure compares the entire PV-wind-battery system configuration with the PV-wind, PV-battery and wind-battery system sub-configurations. A width parametric and multi-optimization analysis permit the identification of the most proper nominal powers of each system component.

The procedure proposed was applied in a Mediterranean residential building, demonstrating that some system configurations allow complying simultaneously with at least two of the three energy objectives proposed, the cost-optimal level and the maximum reduction of emissions, for specific values of the load. The solar source was the most suitable both from an energy, environmental and economic point of view, while the use of the wind source leads to a greater system operating time in the nominal power conditions. The study pointed out and quantified that for specific loads, PV, wind and battery powers, the development of incentives for wind systems and of battery systems with a higher lifespan, can help to make the hybrid systems more economically competitive.

Keywords: Renewable Energy; PV-wind hybrid system; Battery storage; Energy, economic and environmental analysis; Sizing and optimization; Incentives

- A novel decision-making procedure for the hybrid system analysis is proposed.
- A new set of dimensionless energy, economic and environmental indicators are defined.
- A width parametric analysis for different system configurations and loads is made.
- Multi-objective optimization with the selection of the best system configurations.
- Impact of battery lifespan increase and incentives is evaluated

Chapter 3

**A novel energy economic-environmental
multi-criteria decision-making
in the optimization of a hybrid renewable system**

1. Introduction

Worldwide, there is growing attention of the governments in promoting actions targeting energy decarbonisation and greenhouse gas reduction toward the achievement of more sustainable cities and societies. As mentioned by Alkhalidi et al. [1], the idea of sustainable cities was introduced to meet and overcome the challenges facing urban development. A clean urban development requires the use of renewable systems able to produce energy in the most reliable way, namely continuously and in a sufficient manner. Among the different types of energy, the electrical energy demand is undergoing drastic growth owing to the electrification of transport and air-conditioning sectors.

The electrical hybrid system exploits different renewable energy sources to balance better the advantages and disadvantages of each technology involved, using the strengths of one to compensate for the shortcomings of the other. As a consequence of the increasing complexity of the system, the investigation for optimal sizing has become more complicated due to the variability over time of renewable sources and loads, large number of parameters that must be considered, non-linearity of the components and interdependence of the optimal configuration and strategy control. It is possible to obtain different best solutions for different specific applications, climate and energy demands. Appropriate control techniques and optimization procedures are also necessary for the management of components and loads in order to make the system economically sustainable, minimizing the production costs and harmful emissions. Recent technological developments, especially in the field of electronic components, allow the coupling of renewable technologies that were previously difficult to be compatible.

As well known, the integration of solar and wind energy systems is a common solution to produce electrical energy more continuously. A focus is necessary for the use of storage batteries, which allow the reduction of excess energy when the request is absent or reduced.

The integration of these technologies allows the conception of several cleaner and sustainable promising applications, such as in the transport sector for the electric vehicle charge [2-5], in the air conditioning systems and domestic hot water production to supply heat pumps [6-8] and also, in general, to satisfy the electrical energy demand of non-residential and residential buildings [9, 10].

The potential of this integration is evident when the uncertainty of each resource is considered. The abundance of solar source permits the use of photovoltaic (PV) system almost anywhere, but it requires a large energy storage system to avoid interruption of service during the night hours (or during periods characterized by poor irradiation). Production via wind turbine is also intermittent and depends on the wind characteristics of the selected site. By exploiting the complementarity of the various resources (on a daily or seasonal basis), the efficiency and reliability of the system can be increased, avoiding an oversizing of renewable systems.

The current market underlines that the hybrid system is strongly affected by the costs of the battery and wind turbine. For this reason, it is very important to focus on the correct selection of storage capacity, which is often oversized. Furthermore, the development of new micro-turbines suitable for low wind locations is crucial to overcome the obstacle of high cut-in and rated speed of the wind turbines. However, the hybrid system is characterized by high initial investment, while the operating and maintenance costs are low thanks to the absence of fuel.

In the last years, several investigations have addressed this topic that has undergone exponential growth; hereafter, the main objectives and results obtained by some works developed are summarized. Cao et al. [11] have presented a parametric analysis to evaluate the system performance obtained from the combination of ground source heat pump, PV and wind systems in Finnish and German

Chapter 3

A novel energy economic-environmental multi-criteria decision-making in the optimization of a hybrid renewable system

climates. The results highlight the reduction in the electricity consumption of the heating system that can be achieved by using a geothermal heat pump. In similar research, the potential of active control on the heat pump in a residential building coupled with a PV and wind system, to limit the building maximum power requirements and maximize the self-consumption of locally produced electricity, was highlighted [12]. Also Stanek et al. [13] investigated the behaviour of a heat pump coupled with PV panels or wind turbines by using some thermo-ecological cost indices. The case study regards a residential building in the Katowice region. In a small hybrid system composed of geothermal heat pump, solar PV panels, and wind turbines for residential building power supply in Serbia, it was demonstrated that the investments for geothermal heat pump and PV panels are profitable, on the contrary, it is less convenient for a small wind turbine [14]. Finally, Park et al. [15] have investigated the performance of wind turbines, PV panels, converters, and batteries for power generation on an island in South Korea.

Another important aspect treated regards the hybrid system optimization by using a techno-economic analysis. For example, in the study [16] an optimization analysis of stand-alone hybrid systems composed of PV, wind, diesel generator, converter and battery for a tourist centre was developed. Instead, in another work, the minimization of the costs has permitted to identify the optimal size of a stand-alone PV-wind-diesel-battery system by using a two-stage mixed-integer linear programming model [17]. Grande et al. [18] have focused on the techno and economic feasibility of off-grid PV and battery systems for electric vehicle charging stations. The aim was the minimization of the electricity taken from the grid, monitoring the economic impact. A techno-economic analysis was also conducted in [19] for several hybrid system combinations considering regular and seasonal building occupancy. The study [20] have shown a techno-economic design and analysis, applicable for future electrification of several rural communities in the world, of a nano-grid system for energy-poor villages in Nigeria. In the techno-economic analysis, a significant factor that influences the investment feasibility is represented by the national incentives. Recently, it was demonstrated that the wind system is unable to obtain a desirable financial result from the investment by employing the Colombian Law 1715 for wind and solar systems [21].

A thorough analysis of studies in the last ten years on hybrid systems was conducted and a selected list [22-39], characteristic of the most substantial works published in prestigious journals, is presented in Table 1. Table 1 points out, for each paper, the weather data source, uses and hybrid system configurations.

Table 1. *Literature overview: weather data, uses and hybrid system configurations.*

REFERENCES	LOCALITY	WEATHER DATA*					USE	SYSTEM CONFIGURATIONS			
		Köppen Climate classification**	Solar irrad.	Wind speed	Ext. Temp.	Frequency, Time period		PV	WIND	ENERGY STORAGE	SA/ GC***
[22]	Saudi Arabia	BWh	√	LM	√	Hourly, one year	District	√	√	√	SA
[23]	Belgrade, Serbia	Cfa	TMY	TMY	-	Hourly, one year	Residential building	√	√	-	GC
[24]	Qazvin, Iran	Csa	MO	MO	-	Hourly, one year	District	√	√	√	SA
[25]	Ghardaia, Algeria	BWh	NASA	MO	-	Hourly, one year	Residential building, agricultural farm	√	√	√	GC
[26]	Naples, Italy	Csa	TMY	TMY	-	Hourly, one year	Supermaket, tourist centre, hotel, offices	√	√	√	SA/GC
[27]	Kerman, Iran	BSk	√	√	-	Hourly, one year	District	√	√	√	SA
[28]	Yavatmal, India	Aw	MO	NASA	-	Monthly, one year	District	√	√	√	SA

Chapter 3

A novel energy economic-environmental
multi-criteria decision-making
in the optimization of a hybrid renewable system

[29]	Shenyang, China	Dwa	LM	LM	-	Hourly, one year	Office	√	√	√	SA
	Shangai, China	Cfa	LM	LM	-	Hourly, one year	Office	√	√	√	SA
	Guangzhou, China	Cfa	LM	LM	-	Hourly, one year	Office	√	√	√	SA
[30]	Hamirpur, India	Cwa	LM	LM	LM	Hourly, one year	Office	√	√	√	GC
	Bilaspur, India	Cwa	NASA	NASA	NASA	Hourly, one year	Office	√	√	√	GC
	Chamba, India	Cwa	NASA	NASA	NASA	Hourly, one year	Office	√	√	√	GC
	Kangra, India	Cwa	NASA	NASA	NASA	Hourly, one year	Office	√	√	√	GC
	Kinnaur, India	Dsb	NASA	NASA	NASA	Hourly, one year	Office	√	√	√	GC
	Kullu, India	Cfb	NASA	NASA	NASA	Hourly, one year	Office	√	√	√	GC
	Lahaul & Spiti, India	Dsb	NASA	NASA	NASA	Hourly, one year	Office	√	√	√	GC
	Mandi, India	Cwb	NASA	NASA	NASA	Hourly, one year	Office	√	√	√	GC
	Shimla, India	Cwb	NASA	NASA	NASA	Hourly, one year	Office	√	√	√	GC
	Sirmour, India	Cwb	NASA	NASA	NASA	Hourly, one year	Office	√	√	√	GC
	Solan, India	Cwb	NASA	NASA	NASA	Hourly, one year	Office	√	√	√	GC
	Una, India	Cwa	NASA	NASA	NASA	Hourly, one year	Office	√	√	√	GC
[31]	Urumqi, China	Bsk	NASA	NASA	NASA	Hourly, one year	Residential building	√	√	√	SA
[32]	Bouzaréah, Algeria	Csa	LM	LM	LM	Hourly, one year	Residential building	√	√	√	SA
[33]	Ghardaıa, Algeria	BWh	MO	MO	MO	Hourly, one year	Residential building	√	√	√	SA
[34]	Rabat, Morocco	Csa	TMY	TMY	TMY	Hourly, one year	University campus	√	√	√	GC
[35]	Tehran, Iran	BSk	MO	MO	-	Hourly, one year	Residential building	√	√	√	SA
[36]	Boulder, Colorado, USA	BSk	MO	MO	MO	5-min, one year	Residential building	√	√	-	SA
[37]	Izmir-Cesme, Turkey	Csa	NASA	NASA	-	Monthly, one year	Hydrogen refuelling station	√	√	√	SA
[38]	Rafsanjan regions, Iran	Bsk	√	√	-	Hourly, one year	Residential building	√	√	√	SA
[39]	Izmir, Turkey	Csa	TMY	TMY	TMY	Hourly, one year	Residential building	√	√	-	GC
	Madrid, Spain	Csa	TMY	TMY	TMY	Hourly, one year	Residential building	√	√	-	GC
	Budapest, Hungary	Dfb	TMY	TMY	TMY	Hourly, one year	Residential building	√	√	-	GC
	Paris, France	Cfb	TMY	TMY	TMY	Hourly, one year	Residential building	√	√	-	GC
	Helsinki, Finland	Dfb	TMY	TMY	TMY	Hourly, one year	Residential building	√	√	-	GC

The source of the weather is indicated with LM for locally measured data, MO for data from a meteorological organization, NASA for data from the national aeronautics and space administration and TMY for the typical meteorological year. The weather data are highlighted using the Köppen Climate classification [40]. The following considerations were carried out in Table 1:

- the climate most frequently exploited is Csa (Temperate/Dry_summer/Hot_Summer), tested for an equal number in stand-alone SA and grid-connected GC systems;
- in BSk (Arid/Steppe/Cold) climates only SA applications are considered;
- Cwa (Temperate/Dry_Winter/Hot_Summer) and Cwb (Temperate/Dry_Winter/Warm_Summer) are tested for GC systems;
- in tropical/megathermal climates A and dry (desert and semi-arid) climates B, SA systems are prevalently studied;
- in temperate/mesothermal climates C, both GC and SA systems are investigated
- in continental/microthermal climates D, the GC systems are more frequent than the SA one.

Chapter 3

**A novel energy economic-environmental
multi-criteria decision-making
in the optimization of a hybrid renewable system**

The main uses considered for hybrid systems are districts, residential buildings, or no residential buildings, such as offices, supermarkets, and so on.

With reference to the research of Table 1, a first investigation has allowed the identification of papers that employ energy, economic or environmental analysis and indicators to optimize a hybrid renewable system, as shown in Table 2.

Table 2. Literature overview: optimization, energy, economic and environmental analysis and indicators.

REFERENCES	Energy analysis	Energy Indicators	Economic analysis	Economic Indicators	Environmental analysis	Environmental Indicators
[22]	√	-	√	COE, NPC	-	-
[23]	√	-	-	-	√	E
[24]	√	ENS	√	TPC	-	-
[25]	√	GPAP	√	-	√	E
[26]	√	-	√	PI	-	-
[27]	√	-	√	LCC	-	-
[28]	√	-	√	NPC	-	-
[29]	√	-	-	-	-	-
[30]	√	-	√	COE, NPC	-	-
[31]	√	-	√	COE, NPC	-	-
[32]	√	DPSP	√	LUEC	-	-
[33]	√	TED	√	TNPC, EC	√	E
[34]	√	-	√	-	√	CO₂ mitigation
[35]	√	LPS, LPSP	√	NPC, LCE	-	-
[36]	√	-	-	-	-	-
[37]	√	-	√	LCOE, NPC	-	-
[38]	√	-	√	TAC	-	-
[39]	√	-	√	EPBT, SPBT	-	-

ENERGY	LPSP LPS	Loss of Power Supply Probability Loss of Power Supply	The probability of unmet load over the total energy produced.	
	DPSP	Deficiency in Power Supply Probability	The amount of power shortage at each hour.	
	ENS	Energy not supplied	The amount of load energy not supplied during a period.	
	TED	Total Energy Deficit	The ratio of energy not supplied to the consumer when was requested on the total energy required.	
	GPAP	Grid Power Absorption Probability	The probability that the system needs to purchase electricity from the utility grid when renewable energy is unable to feed the load.	
ECONOMIC	TNPC NPC TPC	Total Net Present Cost Net Present Cost Total Percent Cost	The total investment, maintenance, operation and replacement costs throughout the life time of the system.	
	LCC	Life Cycle Cost	The costs of system operation throughout the lifetime. Does not include manufacturing and disposal costs.	
	PI	Profit index	Assessment of the economic profitability of the plant under investigation,	
	COE LCE LCOE	Levelised cost of energy	The ratio of the costs and total energy consumed by the load throughout the lifetime of the system.	
	LUEC	Levelised Unit Electricity Cost	The total cost of the whole hybrid system divided by the energy supplied from the hybrid system.	
	EC	Energy Cost	The total cost of the whole hybrid system at the annual electrical energy produced by the system.	
	TAC	Total Annual Cost	The summation of capital costs, replacement costs, operation costs and annual maintenance costs.	
	EPBT	Energy Payback Time	Evaluation of the sustainability of the analysed renewable systems, i.e. the time necessary for a given plant to produce an amount of energy equal to that used for its realization.	
	SPBT	Simple Payback Time	The ratio of the initial investment and the annual saving.	
ENVIRONMENTAL	E	Total CO₂ Emissions or fuel emissions	The total amount of kg of CO₂ emissions produced by the system throughout a period.	
	CO₂ mitigation	CO₂ mitigation	The quantity of gas emission mitigated by using the hybrid system	

Table 2 highlights that the energy analysis is always addressed in all the researches often by coupling it to the economic analysis. Instead, the environmental analysis was developed in few papers. In the energy analysis, the past papers aimed to analyze and optimize indicators related to the unmet electrical load in deterministic or statistical terms. Instead, the economic indicators regard the profitability and total cost of the whole hybrid system, while the environmental ones mainly quantify the CO_2 emissions.

As shown in Table 3, by considering papers [22-39], the second investigation was conducted for the identification of the ranges of nominal powers of hybrid system components and of the optimal solutions.

Chapter 3

A novel energy economic-environmental
multi-criteria decision-making
in the optimization of a hybrid renewable system

Table 3. *Literature overview: combo of hybrid solar/wind/battery systems.*

INTERNAL REFERENCES	Combo	Use	Photovoltaic power [kW]	Wind power [kW]	Energy storage [kWh]
[8]	1_Optimal	District	200	200	4560-9120-287270
	2_ Optimal	District	400	200	4560
	3_ Optimal	District	200	400	4560
	4_ Optimal	District	400	400	4560
[9]	1_ Optimal	Residential building	3	1	-
	2_ Optimal	Residential building	3	3	-
	3_ Optimal	Residential building	3	5	-
[10]	Range	District	[0-400]	[0-400]	[0-900]
	1_ Optimal	District	330	-	555
	2_ Optimal	District	237	-	515
	3_ Optimal	District	185	-	440
	4_ Optimal	District	-	363	843
	5_ Optimal	District	-	277	529
	6_ Optimal	District	-	210	343
	7_ Optimal	District	186	57	434
	8_ Optimal	District	141	56	338
	9_ Optimal	District	106	57	222
[11]	Range	All	[0-15] (0-100 m^2) *	[0-20]	[0-100]
	1_ Optimal	Residential building	7,7 (51 m^2) *	1	12.5
	2_ Optimal	Residential building	3,8 (25 m^2) *	1.5	23.5
	3_ Optimal	Residential building	4,7 (31 m^2) *	1	11
	4_ Optimal	Residential building	4,0 (26,5 m^2) *	2	10
	5_ Optimal	Residential building	2,9 (19 m^2) *	2	8.5
	6_ Optimal	Residential building	2,8 (18,5 m^2) *	2	8.5
	7_ Optimal	Farm	10,1 (67 m^2) *	3.5	47
	8_ Optimal	Farm	10,1 (67 m^2) *	3.5	47
	9_ Optimal	Farm	10,1 (67 m^2) *	1.5	37.5
	10_ Optimal	Farm	10,1 (67 m^2) *	1.5	37
	11_ Optimal	Farm	6,5 (43 m^2) *	3.5	30
	12_ Optimal	Farm	6,5 (43 m^2) *	3.5	30
[12]	1_ Optimal	Supermarket	190	10	-
	2_ Optimal	Supermarket	190	10	400
	3_ Optimal	Touristic centre	190	10	-
	4_ Optimal	Touristic centre	190	10	400
	5_ Optimal	Hotel	60	10	-
	6_ Optimal	Hotel	60	10	140
	7_ Optimal	Offices	60	10	-
	8_ Optimal	Offices	60	10	140
[13]	Range	District	≥ 0	≥ 0	≥ 0
	1_ Optimal	District	4.935	4	226.8 (63)**
	2_ Optimal	District	7.520	-	669.6 (186)**
	3_ Optimal	District	-	10	1224 (340) **
[14]	Range	District	≥ 0.19	[50-500]	≥ 1.27
	1_ Optimal	District	251.94	217.43	1462.8
[15]	1_ Optimal	Office	0.280	0.4	4.8 (4)***
	2_ Optimal	Office	0.280	0.4	4.8 (4)***
[16]	Range	Office	[1-8]	[1-13]	18 (10) ****
	1_ Optimal	Office	1	5	18 (10) ****
	2_ Optimal	Office	8	1	18 (10) ****
	3_ Optimal	Office	8	1	18 (10) ****
	4_ Optimal	Office	8	2	18 (10) ****
	5_ Optimal	Office	8	2	18 (10) ****
	6_ Optimal	Office	8	3	18 (10) ****
	7_ Optimal	Office	8	3	18 (10) ****
	8_ Optimal	Office	7	5	18 (10) ****
	9_ Optimal	Office	6	2	18 (10) ****
	10_ Optimal	Office	6	1	18 (10) ****
	11_ Optimal	Office	4	6	18 (10) ****
	12_ Optimal	Office	6	2	18 (10) ****
	13_ Optimal	Office	6	3	18 (10) ****
	14_ Optimal	Office	6	3	18 (10) ****
	15_ Optimal	Office	5	5	18 (10) ****
[17]	Range	Residential building	[0-30]	[12.5]	[0-222.08]
	1_ Optimal	Residential building	5	2.5	55.52
	2_ Optimal	Residential building	5	-	83. 28
	3_ Optimal	Residential building	-	7.5	111. 04
[18]	Range	Residential building	[0.774-2.58]	[0.4-4]	Variable
[19]	Range	Residential building	[5.28-24]	[1-10]	86,4
	1_ Optimal	Residential building	8.5	1	86,4
	2_ Optimal	Residential building	15.7	1	86,4
[20]	1_ Optimal	Campus university	9	1	-
	2_ Optimal	Campus university	12	1	30
[21]	Range	Residential building	[0-165]	[0-166]	[98-370]
	1_ Optimal	Residential building	82	25	190
	2_ Optimal	Residential building	61	22	434
	3_ Optimal	Residential building	35	30	360
	4_ Optimal	Residential building	165	54	350
	5_ Optimal	Residential building	62	25	148
	6_ Optimal	Residential building	47	25	98
	7_ Optimal	Residential building	0	166	370
	8_ Optimal	Residential building	0	120	230

Chapter 3

**A novel energy economic-environmental
multi-criteria decision-making
in the optimization of a hybrid renewable system**

	9_ Optimal	Residential building	0	92	150
	10_ Optimal	Residential building	144	0	241
	11_ Optimal	Residential building	104	0	224
	12_ Optimal	Residential building	81	0	192
[22]	1_ Optimal	Residential building	0	8	-
	2_ Optimal	Residential building	0.8	7.2	-
	3_ Optimal	Residential building	1.6	6.4	-
	4_ Optimal	Residential building	2.4	5.6	-
	5_ Optimal	Residential building	3.2	4.8	-
	6_ Optimal	Residential building	4	4	-
	7_ Optimal	Residential building	4.8	3.2	-
	8_ Optimal	Residential building	5.6	2.4	-
	9_ Optimal	Residential building	6.4	1.6	-
	10_ Optimal	Residential building	7.2	0.8	-
	11_ Optimal	Residential building	8	0	-
[23]	1_ Optimal	Hydrogen refuelling station	271	2	71
	2_ Optimal	Hydrogen refuelling station	279	2	86
	3_ Optimal	Hydrogen refuelling station	320	2	89
	4_ Optimal	Hydrogen refuelling station	224	2	93
	5_ Optimal	Hydrogen refuelling station	228	2	100
	6_ Optimal	Hydrogen refuelling station	413	2	115
[24]	Range	Residential building	[0 - 1040]	[0-4000]	[0-8200]
	1_ Optimal	Residential building	0	31-55	44.1-170.1
	2_ Optimal	Residential building	5.2-68.38	-	1803.9-2809.8
	3_ Optimal	Residential building	-	29-5	48.3-178.5
[25]	1_ Optimal	Residential building	2.5	2.5	-

* The photovoltaic power has been calculated from the PV system surface by the peak power factor of 0,15 kW/m².
** The storage power has been calculated considering 24 V & 150 Ah batteries of 3.6 kWh each one.
*** The storage power has been calculated considering 12 V & 100 Ah batteries of 1.2 kWh each one.
**** The storage power has been calculated considering 12 V & 150 Ah batteries of 1.8 kWh each one.

The energy, economic and environmental optimization criteria were rarely considered simultaneously. The optimal solutions found in the previous studies cannot be compared since they employ different indicators and are related to the optimization of one, two or three indicators in a non-uniform way. For this reason, it is needed to create a shared procedure that permits to establish when a hybrid system must be realized in substitution of a non-hybrid system and to size the system by considering all the three aspects.

2. Materials and methods

This section provides a detailed presentation of the benchmark procedure and case study proposed. The different configurations of the hybrid system, procedure and indicators employed for the energy, economic and environmental analysis and optimization are extensively described.

2.1 The PV-wind hybrid system configurations

As shown in Figure 1, four different system configurations were considered: (I) PV-Wind-Battery hybrid system; (II) PV-Wind hybrid system; (III) PV-Battery system; (IV) Wind-Battery system.
The system configuration (I) involves the production of electricity through a PV generator, a wind generator and a storage system to feed the load. The system has in support the following devices: DC/DC converter contains the device of maximum power point tracking of the PV generator; AC/DC rectifier transforms the alternating current produced by the wind generator into the direct current; a regulator limits the charge and discharge status of the battery; the inverter transforms the direct current coming from the wind system, the PV system and the battery in alternating current.
Starting from configuration (I), configuration (II) is obtained by eliminating the electrical storage system and the charge regulator (B), the configuration (III) by eliminating the wind system (C), and the configuration (IV) by removing the PV system (D).
In Figure 1, P_{pv} e P_w are, respectively, the outgoing power from the PV generator and the wind generator, $P_{pv,eff}$ e $P_{w,eff}$ the power outgoing from the PV and wind static converters, P_g is the total power produced, P_{tb} e P_{fb} are respectively the ingoing and outgoing powers from the storage system,

Chapter 3

A novel energy economic-environmental multi-criteria decision-making in the optimization of a hybrid renewable system

P_{tl} is the power coming from the hybrid system entering the load, P_{tg} is the power sent to the grid by the hybrid system, P_{fg} is the power drawn from the grid.
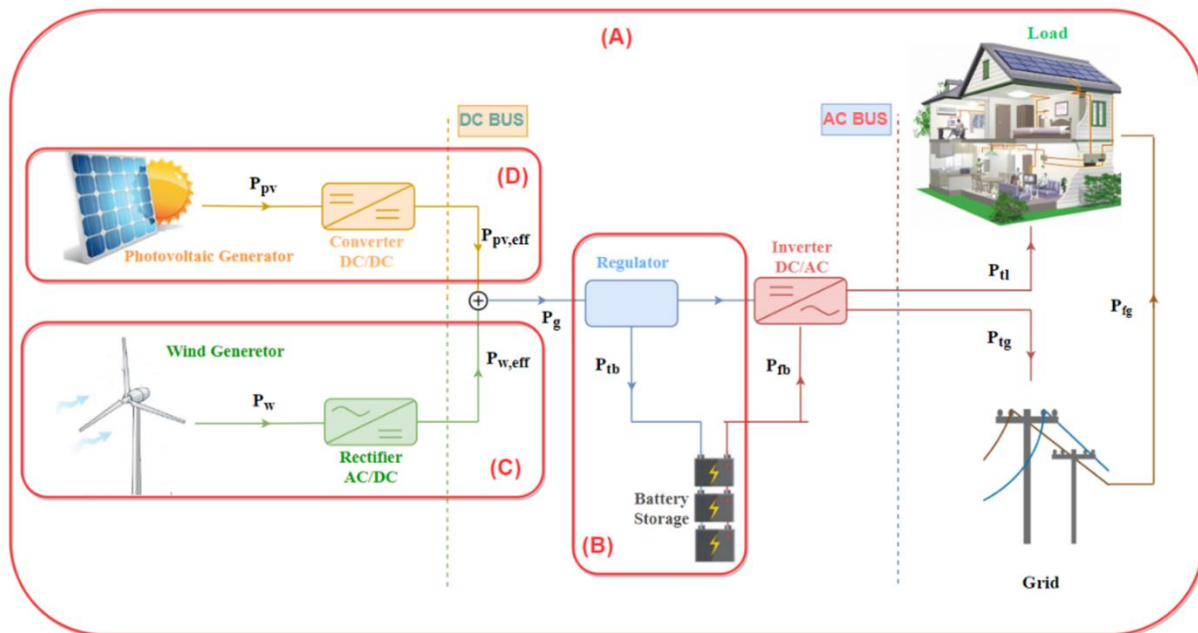
Figure 1. *Layout of the (I), (II), (III) and (IV) system configurations.*

2.2 Technical data of the system components

The PV generator, produced by Sharp, consists of modules of nominal power equal to 250 W, with polycrystalline silicon cells of area equal to (15.65 cm x 15.65 cm), efficiency under reference conditions of 15.2%, and nominal operating cell temperature NOCT of 47°C. The main data of the I-V curve: open-circuit voltage 37.5 V, short-circuit current 8.76 A, voltage at the point of maximum power 30.3 V, current at the point of maximum power 8.24 A, and temperature coefficients on open-circuit voltage and short-circuit current of, respectively, -0.31 %/°C and 0.05 %/°C.

The horizontal-axis wind micro-generator, produced by Angel Wind Energy, was placed 5 meters above the roof, i.e. 15 meters above the ground. The main technical characteristics are: nominal power of 2.5 kW, nominal wind speed 12 m/s, cut-in wind speed 2.5 m/s, cut on wind speed 20 m/s, and rotor diameter 3.5 m.

The storage system consists of lithium-ion batteries with a storage capacity (maximum state of charge SOC_{max}) of 2 kWh, an efficiency of 0.98, and a high limit and low limit on the fractional state of charge of 0.97 and 0.1, respectively. The efficiency of the static converter DC/DC, AC/DC rectifier, DC/AC inverter and regulator are respectively 0.94, 0.90, 0.97 and 0.98.

2.3 Description of the weather monitoring station

The methodology of this work can be applied to developed power simulations of a hybrid system located in any climate condition.

In the specific case study, the weather monitoring station for the detection of solar radiation on the horizontal plane, external air temperature and wind speed is located on the roof of a building of the University of Calabria, latitude 29° 22', longitude 16 ° 13.5', altitude 240 m a.s.l., see Figure 2.

Chapter 3

**A novel energy economic-environmental
multi-criteria decision-making
in the optimization of a hybrid renewable system**

Figure 2. Weather monitoring station for solar radiation on the horizontal plane, external air temperature and wind speed measurement.

In accordance with the Koppen classification [40], the location presents a Csa climate with a Hot-summer Mediterranean climate characterized by the coldest month averaging above 0 °C, at least one month's average temperature above 22 °C, and at least four months averaging above 10 °C.

In Figure 3, the daily average hourly values of the external air temperature and wind speed, and the daily value of the global solar energy incident on the horizontal plane are reported.
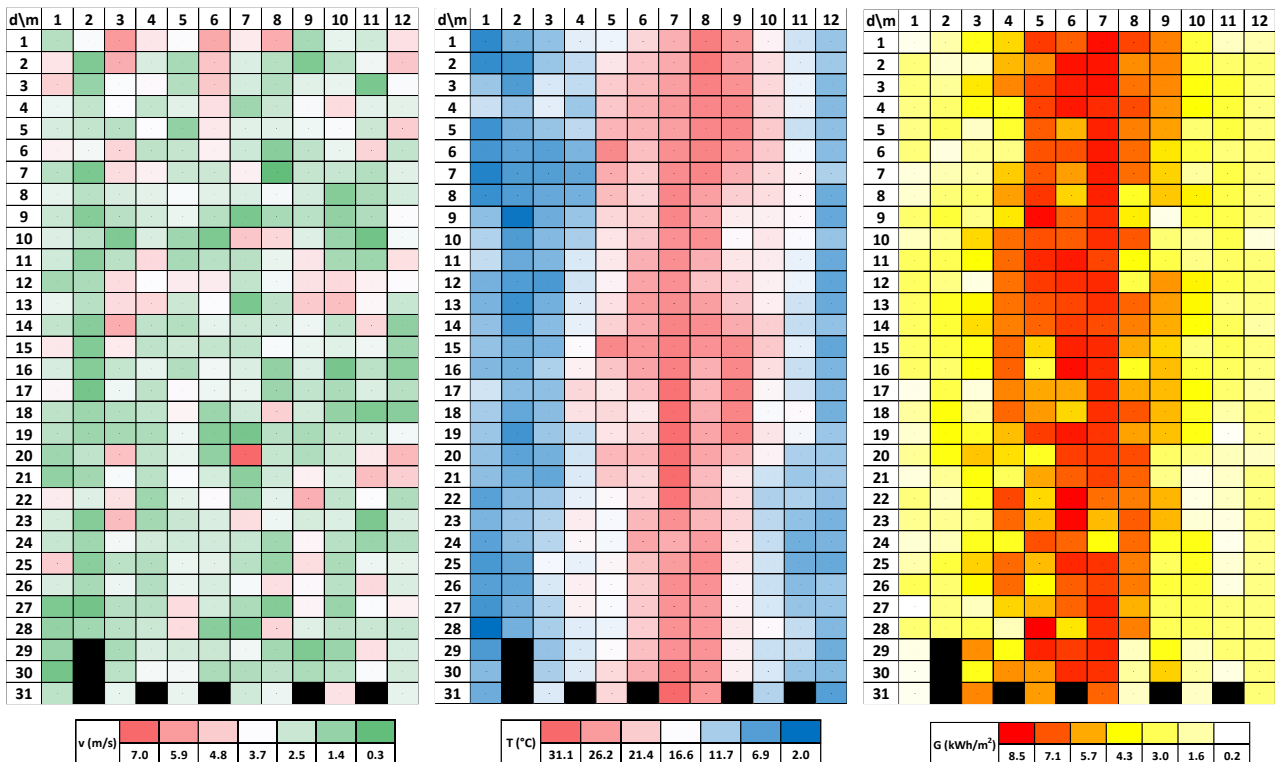
Figure 3. Daily average hourly wind speed and external air temperature, and daily solar energy on the horizontal plane measured at the University of Calabria. (d) days and (m) months through the year.

2.4 Description of electrical load

The methodology of this work can be applied to developed power simulations of a hybrid system used to supply any type of load, namely any type of end-use, with different time resolutions.

Chapter 3

**A novel energy economic-environmental
multi-criteria decision-making
in the optimization of a hybrid renewable system**

In the specific case study, for system configurations (I), (II), (III), and (IV), five different electrical loads were considered, characterized by the same time trend and different daily average hourly values, as shown in Figure 4. The daily trends considered are related to residential buildings with one or more apartments with average absorbed power ranging from 0.5 kW to 10 kW. In particular, yearly real bill data of an apartment with a floor area of 120 m^2 inhabited by four people were used to extract the daily trend related to the case of load with an hourly average of 0.5 kW. Consequently, the electrical load with hourly average power values of 1 kW, 2.5 kW, 5 kW and 10 kW are comparable respectively to 2, 5, 10, and 20 apartments, each of which has a floor area of 120 m^2 and is inhabited on average by four people.
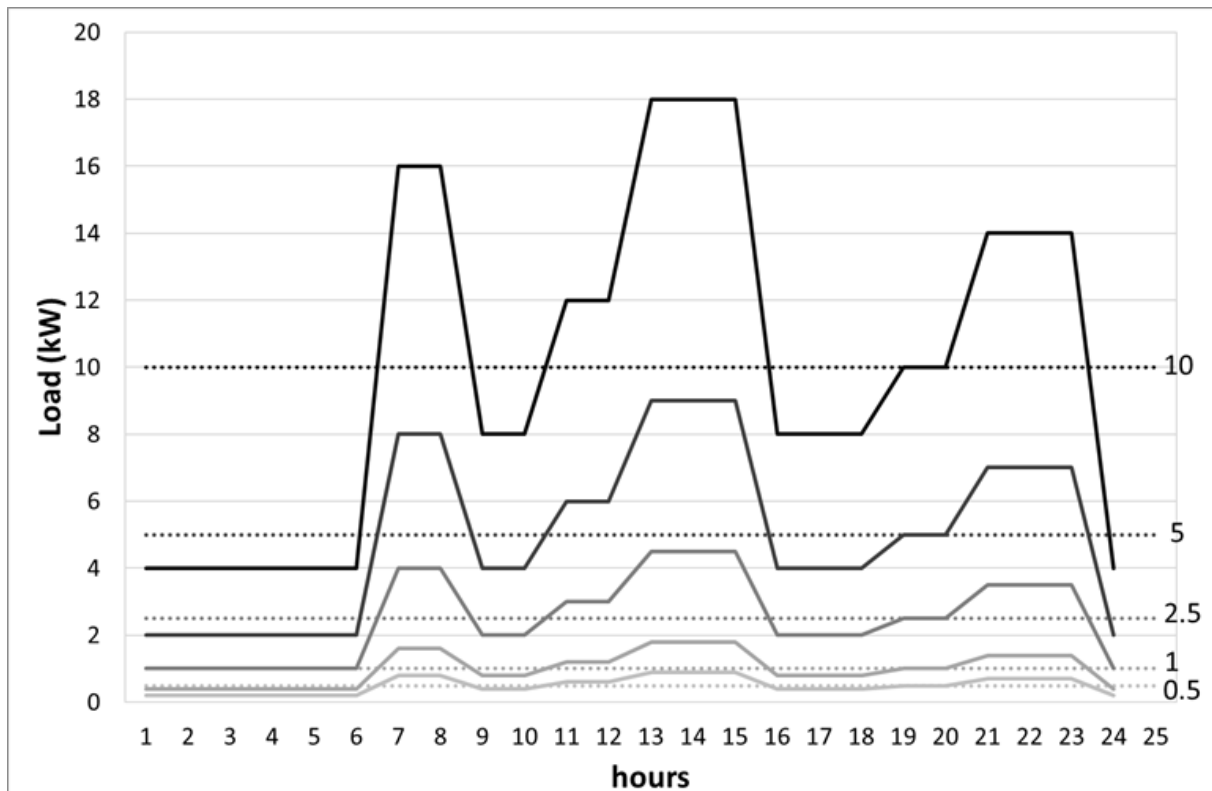
Figure 4. Daily trends of the electrical loads.

2.5 Energy, economic and environmental analysis

2.5.1 Parametric analysis

For each system configuration, a parametric analysis was developed by varying:
- the nominal power of the PV generator by varying the number of PV modules;
- the nominal power of the wind generator by varying the number of wind generators;
- the storage capacity by varying the number of electrical batteries.

As shown in Figure 5, there are 700 system scenarios considered in the parametric analysis: 375 scenarios are considered for the configuration (I), 75 scenarios for configuration (II), and 125 scenarios for configurations (III) and (IV). To make the results comparable, the variation range of the total nominal power is between 5 kW and 25 kW for all system configurations.

Chapter 3

A novel energy economic-environmental multi-criteria decision-making in the optimization of a hybrid renewable system
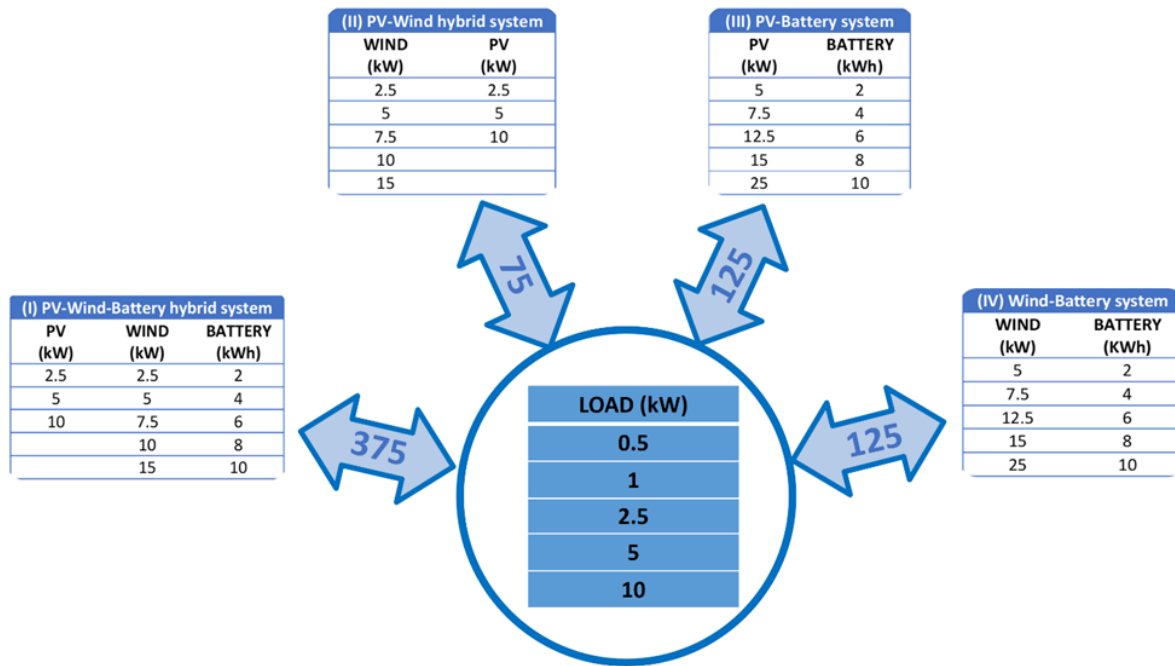
Figure 5. *Scheme of the parametric simulation.*

The methodology of this work can be applied to developed power simulations of a hybrid system with any time resolution. The simulations could be carried out considering 15-minute intervals or less, as reported also by the recent studies [41, 42], which investigate the influence of the time step in the simulation analysis. Ayala-Gilardón et al. [42] found that the self-sufficiency and self-consumption parameters are overestimated by around 9% when the time resolution is changed from 10 s to 1 hour.

Ref. [43] state that to identify a unique methodology capable of defining an acceptable time step before simulating hybrid systems can be very difficult.

The choice of the calculation time-step is strongly dependent on the time-step for the acquisition of the input data, namely the weather data and the electrical load, in addition to the available computational complexity and computational cost required. For example, when the climatic and electrical load data are available on an hourly basis, has no sense to simulate with a lower time-step. In the present case study, being hourly the climatic and load data employed, an hourly time-step was used. This permits to have short calculation time, useful when a high number of scenarios are to be simulated.

For each scenario, a dynamic simulation in the TRNSYS environment was used to calculate the hourly values of the output powers from each component. These make the procedure to calculate energy and economic output uniform, having the prices of the energy drawn from the grid and the energy sold to the grid, used in the economic analysis, usually an hourly trend. These powers were used for the calculation of the relative hourly and yearly energy, to evaluate the dimensionless fractions defined in Section 2.5.2.

The energy and economic analysis described in the following sections were summarized as annual values. Starting from the annual energies, an environmental analysis was developed. Subsequently, an analysis was carried out to identify the system scenarios for the different load values, which lead to a maximization of energy performance, economic convenience and abatement of CO_2 emissions.

Chapter 3

A novel energy economic-environmental
multi-criteria decision-making
in the optimization of a hybrid renewable system

Figure 6 shows the different steps of the calculation procedure for the energy, economic and environmental analysis.
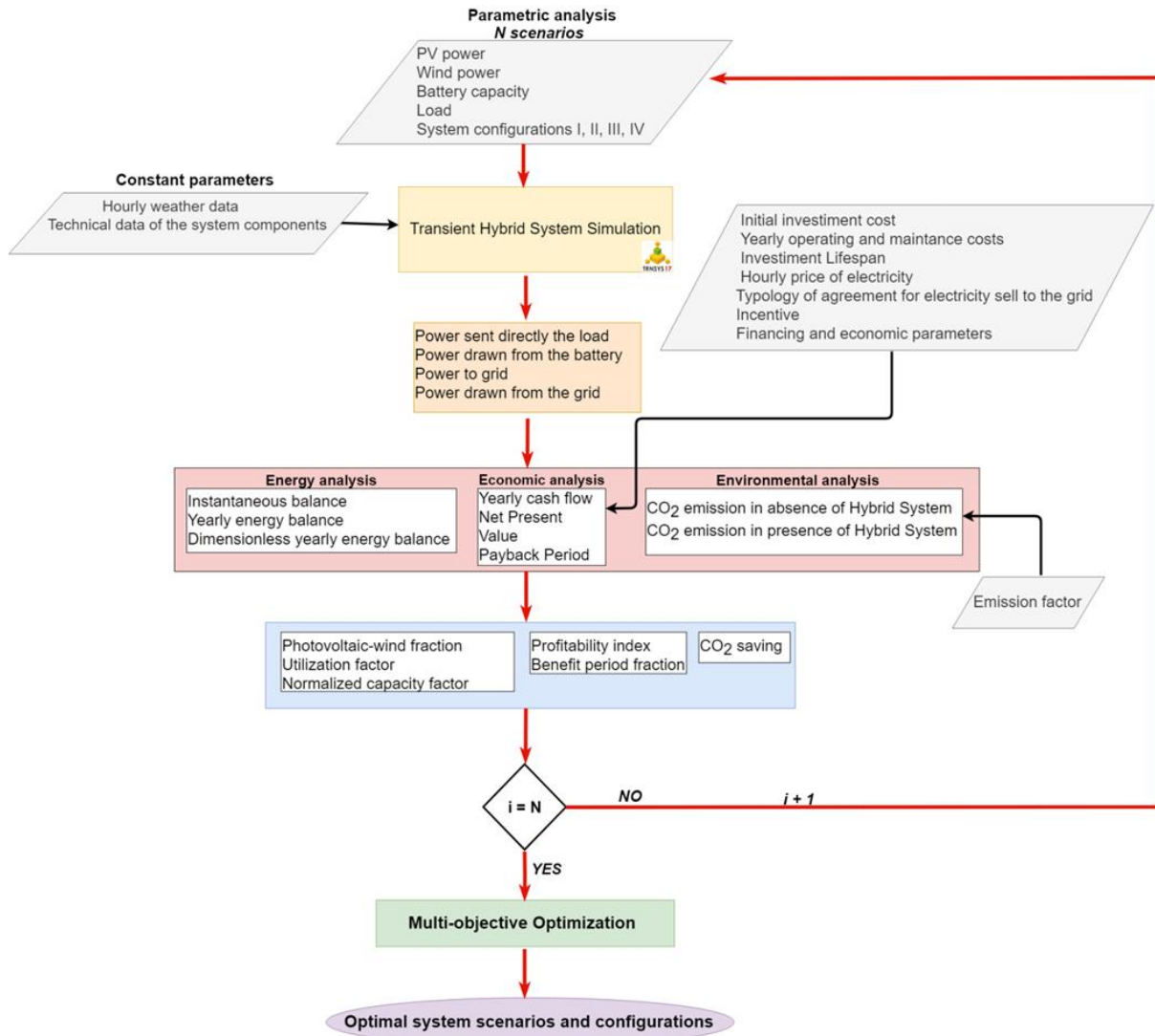
Figure 6. *Steps for the multi-objective energy, economic and environmental optimization.*

2.5.2. Energy analysis

The energy performance of the system components was evaluated on an hourly basis using the dynamic models shown in Table 4, implemented in the TRNSYS 17 environment [44, 45].

Chapter 3   **A novel energy economic-environmental
                                                   multi-criteria decision-making
                                   in the optimization of a hybrid renewable system**

Table 4. Mathematical models used for the simulation of system components.

System component	Mathematical model	Description of the model
Photovoltaic generator	Fry 5-parameter model [46, 47]	It resolves the equivalent electrical circuit described by a 5-parameter balance equation, which is updated at all times in function of the cell temperature and the absorbed solar irradiation.
Wind generator	Quinlan model [46, 48]	It reproduces the power experimental curve of the wind generator, updated at any time, as a function of air density at the generator hub.
Storage battery	State of charge SOC model [46]	It applies an energy balance equation to calculate the SOC at the successive instant as a function of the SOC at the previous time instant and power exchanged with generators and load.
DC/DC converter		It uses the average value of electrical efficiency for the evaluation of the electrical power outgoing from the component.
Rectifier AC/DC	Efficiency model	
Inverter DC/AC		
Regulator		

In this simulation environment, users can build more or less complex simulation models of hybrid systems by the most sophisticated dynamic models of the system components and implementing different battery control strategies. The main characteristic of TRNSYS is the high flexibility to modify models, control strategies and system configurations. This is confirmed by the overview conducted by Sinha et al. [49] on principal tools used for the simulation of hybrid systems, which underlies the extreme modelling flexibility of TRNSYS. A detail to be emphasized, highlighted by Sharma et al. [50], is related to the lower minimum time step employable (0.01 s) than that of other widespread software, such as HOMER, i-Hoga and so on.

For the PV cell, the Fry model [46, 47] permits to update the characteristic electrical parameters of the current-voltage I-V curve, such as voltage and current at the maximum power point, as a function of the cell temperature and absorbed solar radiation. To take into account the loss of PV efficiency over time, the power at the maximum power point $P_{mp} = V_{mp} \cdot I_{mp}$ must be reduced. In general, a linear trend of this loss is provided by PV companies:

$$P_{mp}(n) = V_{mp}(n)I_{mp}(n) = V_{mp}(0)I_{mp}(0)(1 - c_{PV}n) \tag{1}$$

Where, *n* is the time in years and c_{PV} is the PV degradation factor with values around 0.5-1.0 %/year.

The wind generator is simulated by using the Quinlan model [46, 48] that allows using directly the experimental power curve as a function of the wind speed to be updated at each time instant as a function of the air density.

For the storage system, an instantaneous power balance permits to update the state of charge SOC in relation to the power coming from the generator or drawn by the load [46]. Similarly to the PV cell, the real storage capacity of the battery decreases over time. This storage capacity loss can be considered by reducing each year the value of SOC_{max} through an equation similar to Eq. (1):

$$SOC_{max}(n) = SOC_{max}(0)(1 - c_{bat}n) \tag{2}$$

Where, c_{bat} is the battery degradation factor with values around 0.5-1.0 %/year.

Chapter 3   **A novel energy economic-environmental**
multi-criteria decision-making
in the optimization of a hybrid renewable system

To take into account the yearly variation of the efficiency and battery storage capacity, for each scenario of the considered 375 ones and each year of the investment lifespan N, one energy simulation of the hybrid system should be performed. Therefore, the computational cost exponentially increases from 375 energy simulations to 375 x N (with N = 25-30 years). Additionally, the economic and environmental analysis must be conducted year-by-year being variable the hourly energies in output from each component, and consequently the yearly energy contributions. In this work, to drastically reduce the computational cost of the analysis by maintaining, at the same time, the accuracy high, the average of the PV efficiencies (or powers at the maximum power point) and storage battery capacities during the entire investment lifespan was considered. By considering the PV and battery linear degradation considered in Eqs. (1) and (2), the average values are respectively:

$$\overline{P}_{mp} = \frac{P_{mp}(0) + P_{mp}(N_{PV})}{2} \quad (3a) \qquad\qquad \overline{SOC}_{max} = \frac{SOC_{max}(0) + SOC_{max}(N_{bat})}{2} \quad (3b)$$

Tables 5-8 show the power balance equation for the three system operating modes (overall power generated minor, equal or major of the power required by the load) and yearly dimensionless energy balances for each system configuration. These dimensionless energy balances were obtained by dividing the various energy contributions, respectively, for the annual energy generated by the system E_g and that required by the load E_L.

Table 5. Power balance equations for the three system operating modes and yearly dimensionless energy balances of the system configuration (I).

System operating mode	Balance equation of the generated energy by the hybrid system and the power required by the load $P_L(t)$	Dimensionless balance equation of the yearly energy produced by the hybrid system and the energy required by the load
$\eta_{inv}\eta_{reg}P_g(t) > P_L(t)$	$P_g(t) = \dfrac{P_{tl}(t)}{\eta_{inv}\eta_{reg}} + \dfrac{P_{tb}(t)}{\eta_{reg}} + \dfrac{P_{tg}(t)}{\eta_{inv}\eta_{reg}}$ (4)	$\dfrac{e_{dtl,w}}{e_g} + \dfrac{e_{dtl,pv}}{e_g} + \dfrac{e_{tb,w}}{e_g} + \dfrac{e_{tb,pv}}{e_g} + \dfrac{e_{tg,w}}{e_g} + \dfrac{e_{tg,pv}}{e_g} = 1$ (10)
	$P_L(t) = P_{tl}(t)$ (5)	
$\eta_{inv}\eta_{reg}P_g(t) < P_L(t)$	$P_g(t)\eta_{inv}\eta_{reg} + P_{fb}(t)\eta_{inv} = P_{tl}(t)$ (6)	
	$P_L(t) = P_{tl}(t) + P_{fg}(t)$ (7)	
$\eta_{inv}\eta_{reg}P_g(t) = P_L(t)$	$P_g(t) = \dfrac{P_{tl}(t)}{\eta_{inv}\eta_{reg}}$ (8)	$e_{dtl,w} + e_{dtl,pv} + e_{fb,w} + e_{fb,pv} + e_{fg} = 1$ (11)
	$P_L(t) = P_{tl}(t)$ (9)	

Table 6. Power balance equations for the three system operating modes and yearly dimensionless energy balances of the system configuration (II).

Chapter 3   **A novel energy economic-environmental**
multi-criteria decision-making
in the optimization of a hybrid renewable system

System operating mode	Balance equation of the generated energy by the hybrid system and the power required by the load $P_L(t)$		Dimensionless balance equation of the yearly energy produced by the hybrid system and the energy required by the load
$\eta_{inv}P_g(t) > P_L(t)$	$P_g(t) = \dfrac{P_{tl}(t)}{\eta_{inv}} + \dfrac{P_{tg}(t)}{\eta_{inv}}$	(12)	$\dfrac{e_{dtl,w}}{e_g} + \dfrac{e_{dtl,pv}}{e_g} + \dfrac{e_{tg,w}}{e_g} + \dfrac{e_{tg,pv}}{e_g} = 1 \quad (18)$
	$P_L(t) = P_{tl}(t)$	(13)	
$\eta_{inv}P_g(t) < P_L(t)$	$P_g(t)\eta_{inv} = P_{tl}(t)$	(14)	
	$P_L(t) = P_{tl}(t) + P_{fg}(t)$	(15)	
$\eta_{inv}P_g(t) = P_L(t)$	$P_g(t) = \dfrac{P_{tl}(t)}{\eta_{inv}}$	(16)	$e_{dtl,w} + e_{dtl,pv} + e_{fg} = 1 \quad (19)$
	$P_L(t) = P_{tl}(t)$	(17)	

Table 7. *Power balance equations for the three system operating modes and yearly dimensionless energy balances of the system configuration (III).*

System operating mode	Balance equation of the generated energy by the hybrid system and the power required by the load $P_L(t)$		Dimensionless balance equation of the yearly energy produced by the hybrid system and the energy required by the load
$\eta_{inv}\eta_{reg}P_{pv,eff}(t) > P_L(t)$	$P_{pv,eff}(t) = \dfrac{P_{tl}(t)}{\eta_{inv}\eta_{reg}} + \dfrac{P_{tb}(t)}{\eta_{reg}} + \dfrac{P_{tg}(t)}{\eta_{inv}\eta_{reg}}$	(20)	$\dfrac{e_{dtl,pv}}{e_g} + \dfrac{e_{tb,pv}}{e_g} + \dfrac{e_{tg,pv}}{e_g} = 1 \quad (26)$
	$P_L(t) = P_{tl}(t)$	(21)	
$\eta_{inv}\eta_{reg}P_{pv,eff}(t) < P_L(t)$	$P_{pv,eff}(t)\eta_{inv}\eta_{reg} + P_{fb}(t)\eta_{inv} = P_{tl}(t)$	(22)	
	$P_L(t) = P_{tl}(t) + P_{fg}(t)$	(23)	
$\eta_{inv}\eta_{reg}P_{pv,eff}(t) = P_L(t)$	$P_{pv,eff}(t) = \dfrac{P_{tl}(t)}{\eta_{inv}\eta_{reg}}$	(24)	$e_{dtl,pv} + e_{fb,pv} + e_{fg} = 1 \quad (27)$
	$P_L(t) = P_{tl}(t)$	(25)	

Chapter 3   **A novel energy economic-environmental**
multi-criteria decision-making
in the optimization of a hybrid renewable system

Table 8. *Power balance equations for the three system operating modes and yearly dimensionless energy balances of the system configuration (IV).*

System operating mode	Balance equation of the generated energy by the hybrid system and the power required by the load $P_L(t)$	Dimensionless balance equation of the annual energy produced by the hybrid system and the energy required by the load
$\eta_{inv}\eta_{reg}P_{w,eff}(t) > P_L(t)$	$P_{w,eff}(t) = \dfrac{P_{tl}(t)}{\eta_{inv}\eta_{reg}} + \dfrac{P_{tb}(t)}{\eta_{reg}} + \dfrac{P_{tg}(t)}{\eta_{inv}\eta_{reg}}$ (28) $P_L(t) = P_{tl}(t)$ (29)	$\dfrac{e_{dtl,w}}{e_g} + \dfrac{e_{tb,w}}{e_g} + \dfrac{e_{tg,w}}{e_g} = 1$ (34)
$\eta_{inv}\eta_{reg}P_{w,eff}(t) < P_L(t)$	$P_{w,eff}(t)\eta_{inv}\eta_{reg} + P_{fb}(t)\eta_{inv} = P_{tl}(t)$ (30) $P_L(t) = P_{tl}(t) + P_{fg}(t)$ (31)	
$\eta_{inv}\eta_{reg}P_{w,eff}(t) = P_L(t)$	$P_{w,eff}(t) = \dfrac{P_{tl}(t)}{\eta_{inv}\eta_{reg}}$ (32) $P_L(t) = P_{tl}(t)$ (33)	$e_{dtl,w} + e_{fb,w} + e_{fg} = 1$ (35)

For each system configuration, the system operating mode and the battery control strategy are determined by comparing the available power coming from the PV and wind generator and the power required by the load $P_L(t)$. In the analysis, the priority is to meet the electrical demand and subsequently to charge the battery.

- For the system configuration (I), the available power is given by the following equation:

$$\eta_{inv}\eta_{reg}P_g(t) = \eta_{inv}\eta_{reg}\left[P_{pv,eff}(t) + P_{w,eff}(t)\right] \qquad (36)$$

As reported in Table 5, when $\eta_{inv}\eta_{reg}P_g(t) > P_L(t)$, their difference is sent primarily to the battery, $P_{tb}(t)$, and once the maximum charge has been reached, the remaining part $P_{tg}(t)$ is sent to the grid. If $\eta_{inv}\eta_{reg}P_g(t) < P_L(t)$, their difference is drawn from the battery, $P_{fb}(t)$, and if this is not enough, the remaining part $P_{fg}(t)$ is taken from the grid. When $\eta_{inv}\eta_{reg}P_g(t) = P_L(t)$ the load is supplied entirely by the generators without the intervention of the storage system and grid.

- For the system configuration (II), the available power is given by the following equation:

$$\eta_{inv}P_g(t) = \eta_{inv}\left[P_{pv,eff}(t) + P_{w,eff}(t)\right] \qquad (37)$$

The removal of the storage battery and regulator determines, in the balance equations corresponding to the three modes of operation, the annulment of powers $P_{tb}(t)$ and $P_{fb}(t)$ and absence of losses in the battery ($\eta_{bat} = 1$) and regulator ($\eta_{reg} = 1$), see Table 6.

Chapter 3　　　　　　　　　　　　　　　　　　**A novel energy economic-environmental**
multi-criteria decision-making
in the optimization of a hybrid renewable system

- For the system configuration (III), the available power is given by the equation:

$$\eta_{inv}\eta_{reg}P_g(t) = \eta_{inv}\eta_{reg}P_{pv,eff}(t) \tag{38}$$

The removal of the wind system determines, in the balance equations corresponding to the three modes of operation, the annulment of powers $P_{w,eff}$ and the absence of losses in the rectifier ($\eta_{AC/DC} = 1$), see Table 7.

- For the system configuration (IV), the available power is given by the equation:

$$\eta_{inv}\eta_{reg}P_g(t) = \eta_{inv}P_{w,eff}(t) \tag{39}$$

The absence of the PV system leads, in the balance equations corresponding to the three modes of operation, the annulment of powers $P_{pv,eff}$ and the absence of losses in the static converter ($\eta_{DC/DC} = 1$), see Table 8.

The analysis of the annual energy balances in the dimensionless form are reported below:

- For configuration (I), the energy generated is distributed and flows into the fraction sent directly to the load e_{dtl} (sum of the component coming from the PV generator $e_{dtl,pv}$ and from the wind generator $e_{dtl,w}$), in the fraction of energy sent to the battery e_{tb} (sum of the component coming from the PV generator $e_{tb,pv}$ and from the wind generator $e_{tb,w}$) and in the fraction of energy sent to the grid e_{tg} (sum of the component coming from the PV generator $e_{tg,pv}$ and from the wind generator $e_{tg,w}$). The energy required by the load is supplied in part by the PV generator $e_{dtl,pv}$ and by the wind generator $e_{dtl,w}$, in part, it is taken from the storage system $e_{fb} = e_{fb,pv} + e_{fb,w}$, and in part, it is drawn from the grid e_{fg}.

- In configuration (II), the fractions of ingoing energy $e_{tb,pv}$, $e_{tb,w}$, and the fractions of outgoing energy $e_{fb,pv}$ and $e_{fb,w}$ from the battery are null.

- In configuration (III), the fractions of energy $e_{dtl,w}$, $e_{tb,w}$, $e_{tg,w}$, coming from the wind system are null.

- In configuration (IV), the fractions of energy $e_{dtl,pv}$, $e_{tb,pv}$, $e_{tg,pv}$ coming from the PV system are null.

2.5.3. Economic analysis

The use of complementary sources, such as solar and wind energy, permit to reach high system reliability. In addition, the time shift between energy generation and demand can be reduced by using battery storage systems. The contemporaneous use of such a system is more expensive than conventional ones. For this reason, an economic analysis is required that depends on main factors: PV, wind, and battery prices, PV, wind, and battery lifetimes, electricity prices and tariff structure, financial data and incentives.

2.5.3.1 NPV method
Once defined the energy performances of the different system configurations, the economic and financial planning processes were carried out using the Net Present Value (NPV) method, to verify

Chapter 3
A novel energy economic-environmental
multi-criteria decision-making
in the optimization of a hybrid renewable system

the effects of the investment project and the feasibility of the hybrid system. The NPV method was widely employed for the economic analysis of a hybrid system [51-53].

The investment operation can be represented by a succession of monetary inputs and outputs called cash flows. The method employed to calculate the cash flows of the investment project is the financial evaluation (considering the prices paid by the consumer, benefits and cost savings, including applicable taxes and subsidies).

The investment analysis must consider the following aspects:

- cost of installation, which essentially is determined by the type of structure and the installation complexity;
- operating, maintenance and replacement costs;
- benefits associated with the energy savings, not withdrawn from the grid;
- benefits related to the energy produced remuneration according to the type of sales contract;
- benefits associated with the local or national incentives for this type of investment.

The NPV is obtained by adding up all the financial flows and applying the discount rate to calculate the value at the initial year:

$$NPV = \sum_{\tau=0}^{N} \sum_{i} C_i(\tau) \cdot R_d(\tau) \tag{40}$$

Where:

N is the investment lifespan;

$C_i(\tau)$ represents the i-th cash flow, positive or negative, in the year τ, which for $\tau = 0$ is equal to the initial investment -I.

Some components, such as the battery and the inverter, usually have a lifespan lower than the lifespan of PV and wind generators; then a replacement cost for these components must be foreseen. The battery lifespan strongly depends on the energy generated and required by the load since they greatly influence the charge/discharge process of the battery and consequently the number of cycles made. In general, for each system configuration and scenario considered, the battery lifespan N_{bat} could be calculated by counting during the simulation the number of cycles made in one year C_n. To evaluate N_{bat}, the following equation is proposed:

$$N_{bat} = \frac{C_{max}}{C_n} \tag{41}$$

Where C_{max} is the total number of cycles that the battery can make.

$R_d(\tau)$ is the discount factor for year n, calculated on the basis of the discount rate r by the expression:

$$R_d(\tau) = \left(\frac{1}{1 + r/100}\right)^{\tau} \tag{42}$$

The last step is to define all the parameters associated with a possible bank financing of the initial expense. The discount rate r can be calculated as:

$$r = \frac{i_r}{i_r + 1} \tag{43}$$

Chapter 3

A novel energy economic-environmental
multi-criteria decision-making
in the optimization of a hybrid renewable system

where i_r is the real interest rate.

To define the benefits related to saving or sell electricity, it is necessary to consider the development rate of the price of electricity in addition to the discount rate.

The bank loan parameter is a key factor to determine the percentage of the initial expense to sustain as own capital invested. It is related to the duration of debt, the interest rate proposed by the creditor company and the debt ratio.

As regards the type of electricity tariffs and incentive plans for renewable systems, they change in a significant manner worldwide. Many European countries employ an electricity tariff system based on a price that varies differently according to the time when it is used. Mulder et al. [54] developed a survey on the tariff systems that are mostly subscribed by households in western European countries. They highlighted that many countries have a bi-tariff electricity meter with a day/night tariff or a similar peak/off-peak tariff, of which price difference varies substantially among the Countries. At a certain instant, the hybrid system can produce energy that is not used directly by the user or accumulated by the battery but sent to the public grid. There are several ways to sell electricity produced in excess, not compatible with each other: net metering service, simplified purchase and resale arrangements.

Net metering is a specific type of electrical energy valorization, enabling the producer to attain a form of self-consumption by entering the electricity produced in the grid, and then pick it up at a time different from that at which the production occurs. The contribution of net metering is a fictitious reimbursement that rewards the user for the energy that he puts into the network. The remuneration is not energy sales alone, but it is the sale of energy and the repayment of part of the network services: distribution, dispatching, measuring and some general system charges. However, taxes are not reimbursed.

Instead, the feed-in tariff system is a subsidy that pays system owners for all the PV electricity they generate over 20 years and an export tariff for electricity output to the national grid [55]. As a consequence of this tariff, with incentives that are considerably higher than the electricity price, in some countries, the installation of renewable systems is put in parallel with the domestic electricity grid to sell all the generated electricity [54]. In other countries, in addition to the self-consumption fee, a selling price for the electricity is provided.

As regards the incentive policies of renewable systems in other worldwide countries, useful researches were developed in the USA by Zhang et al. [56], in Australia by Yuan et al. [57], and in China by Simpson et al.[58].

2.5.3.2 The case study of Italy

To evaluate the economic convenience of the hybrid systems and sub-systems considered in this work, the NPV method was applied in an Italian context.

2.5.3.2.1 Price of electricity

The following data are reported in accordance with the definition of the Italian operator [59], considering three bands, F1 peak hours, F2 intermediate hours, F3 off-peak and festive hours, as shown in Table 9.

Table 9. Hourly detection of electricity consumption.

Chapter 3

A novel energy economic-environmental
multi-criteria decision-making
in the optimization of a hybrid renewable system

Detection of consumption		
Peak hours	*F1*	Mon-Fri from 8:00 to 19:00, excluding national holidays
Intermediate hours	*F2*	Mon-Fri from 7:00 to 8:00 and from 19:00 to 23:00 Saturday from 7:00 to 23:00, excluding national holidays
Off-peak and festive hours	*F3*	Mon-Sat from 23:00 to 7:00, Sundays and national holidays all day

The consumption may be billed according to two other options:
• F1-F23 (bi-hourly tariff) applies to domestic utilities, considering two different bands F1 and F23. The F23 band comprises all the hours included in the F2 and F3 bands;
• F0 (mono-hourly tariff) is applied when the meter cannot read the consumption band or from the customer's request. In this case, because there is no distinction for bands, the price of energy remains the same for all hours of the day and every day of the week.
Table 10 shows the price of electricity in different bands.

Table 10. Price of electricity in different bands.

Electricity tariffs			
Bi-hourly tariff	*F1*	€/kWh	0.194900
	F23	€/kWh	0.188663
Mono-hourly tariff	*F0*	€/kWh	0.164483

The tariff to be applied can be linked to several factors and is strongly determined by the performance of the electrical load. Looking at table 10, it is possible to choose the type of contract and to make a direct comparison of both the two cases described.
The minimum price guaranteed by the Manager of Energy Services (Gestore dei Servizi Energetici, GSE) for the sale of the energy produced by the PV generator and wind generator is, respectively, 0.0495 €/kWh and 0.0394 €/kWh [60].

2.5.3.2.2 Cost analysis

For the analysis of system costs, it is necessary to distinguish three categories: initial costs of installation; annual costs of maintenance, management and replacement. For each component of the system, accurate market analysis has been performed to define the reference prices of the elements.
Generally, a PV generator has a life of 25-30 years with a warranty that covers the entire project life; the average price of installation of a PV system is about 1045 €/kW, while the annual costs of maintenance and operation are 2% of the initial cost. About the disposal costs, according to the Legislative Decree No.49/2014 [61] for waste from plants with power less than 10 kW_p, the disposal responsibility is borne by producers, free for owners.
A wind micro-generator has a life of 25-30 years with a warranty that covers the entire period. The average price of installation is 3448.5 €/kW while operating and maintenance costs are 3% of the initial cost. For the disposal costs, a null value has been assumed, because possible recycling or reuse of the main elements (metallic support structure, steel hub, blades in plastic material reinforced with glass or aluminium fibres) has been considered.
Typically, an ion-lithium storage battery performs about 5000-6000 charge/discharge cycles. In this specific case study, to reduce the computational cost of simulations a permanent battery lifespan of

Chapter 3   **A novel energy economic-environmental**
multi-criteria decision-making
in the optimization of a hybrid renewable system

15 years with a replacement in the middle of the design life of the hybrid system was considered. This can be justified by considering that the solar source has a daily periodicity that leads approximately to 1 cycle per day having a charging process during the diurnal hours and a discharge process during the nocturnal hours. The average price of installation is 927 €/kWh. Further analysis has been carried out, for the different system configurations with battery storage, by varying the useful life of the battery N_{bat} from 15 years to 25-30 years, considering the new researches applied to ion-lithium batteries [62].

About the converters and the inverter, unit prices related to the installation power of the respective generators are considered. The average price of installation of the converters is about 75 €/kW, while for the inverter a cost of 327 €/kW was used, in reference to the entire system power. Analogously to the battery system, also the inverter was replaced in the 15th year.

Finally, a reduction of the unitary cost of the system as the system size increases was considered. The unitary costs previously listed are relative to the minimum powers of each component, namely 2.5 kW for the PV and wind generators, 2 kWh for the battery storage and 5 kW for the inverter. A unitary cost reduction of 3 % of those values was considered for each kW additionally installed.

2.5.3.2.3 Incentives and subsidies

As the 2017 Italian Stability Law indicates, those who install a PV system can take advantage of IRPEF tax deductions to recover 50% of costs incurred for the construction of the plant: those deductions are finalized to support the restructuring and the domestic PV and they are not to be confused with tax deductions of 65% for energy saving. These are only valid for solar thermal systems for domestic hot water and for interventions to improve the energy efficiency of buildings (insulation, windows, fixtures, boilers, heat pumps).

The key points of the law are: deductions regarding domestic PV systems up to 20 kW power; relief also applies to PV systems in condominiums; facilitated VAT benefit to 10%, instead of 22%, is added to that one of tax deductions IRPEF for buildings for residential use.

As stated by the Italian Revenue Agency [63] in Resolution N.22/E of April 2, 2013, the tariffs are not applied if IRPEF tax deductions have been recognized; on the contrary, the net metering service, like the simplified purchase, can be combined with tax relief.

Thus, the government does not provide incentives for producing energy, but it gives the possibility of halving the cost by returning half of the expenses incurred, up to a maximum of 96000 euro, including other possible renovations. This restitution is not enjoyed immediately, but it is provided in the form of tax relief divided into units of equal amount in the 10 years following the installation of the system.

The tax deduction for the installed PV is only valid in domestic-residential installations, while for companies, societies or businesses, there is the opportunity to take advantage of the super amortization of 140% if the plant is classified as a chattel.

The installation of a storage system may not be considered an intervention aimed at the achievement of energy savings. The use of a storage battery can be reduced to that category of interventions when the element purchase is contextual or following to the PV system, configured as an element functionally connected to the PV and able to improve the potential. Thus, the initial costs of DC/DC converter, inverter and battery were considered for tax deductions. Analogously, a wind micro-

Chapter 3   A novel energy economic-environmental
multi-criteria decision-making
in the optimization of a hybrid renewable system

generator installed on a building roof or in a building courtyard can also be an intervention aimed at the achievement of energy savings.

At the end of the analysis, the optimization of the incentives of the PV and wind systems has been done for the different system configurations, changing the tax deductions from 50% to 100% with a step of 10% considering the 10-year duration of deductions for all cases.

2.5.3.2.4 Financing

The rate values provided by the Italian National Institute of Statistics (Istituto Nazionale di Statistica) ISTAT [64] and the European Central Bank [65] were considered. To define the development rate of the electricity price, the table provided by the Authority for Electrical Energy, Gas and water System (AEEGSI), from January 2018 under the name of Italian Regulatory Authority for Energy, Networks and Environment (ARERA) [66], was used. It shows the parameters on the trend of electricity prices for domestic consumers. The used parameters are reported in Table 11.

Table 11. Economic and financial parameters of investment.

Economic parameters	
Inflation rate (%)	0.7
Market interest rate (%)	0.9
Rate of development of the price for electricity (%)	1.1
Investment lifespan (years)	30
Financial parameters	
Debt interest rate (%)	5.2
Debt term (years)	10

2.5.4. Environmental analysis

The yearly CO_2 emissions, in the absence of renewable systems, are expressed by Eq. (44).

$$CO_{2,\text{ahs}} = f_E \, E_L \tag{44}$$

Where, f_E is the overall electrical emission factor.

In the presence of the PV, wind and battery system only a part of the energy required by the load is drawn from the grid, while the surplus energy contributes to reducing the overall emissions since it is sent to the grid. In these conditions, the yearly CO_2 emissions are:

$$CO_{2,\text{phs}} = f_E\big(e_{\text{fg}} - e_{\text{tg}}\big)E_L \tag{45}$$

The CO_2 production was calculated by considering an emission factor of the electrical energy related to the average Italian emissions of the thermo-electric plants [67] of 0.531 kg_{CO2}/kWh.

2.5.5. Energy, economic and environmental performance indicators

Chapter 3

A novel energy economic-environmental multi-criteria decision-making in the optimization of a hybrid renewable system

The energy and economic analysis were obtained using dimensionless indicators which quantify the energy performance and the economic convenience of the investment.

For the energy analysis, the indicators defined are:

- the **PV-wind fraction $f_{pv,w}$** (-) defined as the ratio between the energy supplied from the HPWBS to the load E_{tl} and the energy required by the load E_L. This indicator is expressed as the sum of the energy fractions e_{dtl} and e_{fb}:

$$f_{pv,w} = \frac{E_{tl}}{E_L} = e_{dtl} + e_{fb} \qquad (46)$$

$f_{pv,w}$ varies between 0 and 1, for $f_{pv,w} = 1$ all the energy required by the load is provided by the system and the energy supplied from the grid is nil.

- the **utilization factor of the generated energy $f_{u,g}$** (-) defined as the ratio of the energy supplied by the system to load E_{tl} to the generated energy E_g. This indicator is expressed as the sum of the energy fractions e_{dtl}/e_g and e_{tb}/e_g:

$$f_{u,g} = \frac{E_{tl}}{E_g} = \frac{e_{dtl}}{e_g} + \frac{e_{tb}}{e_g} \qquad (47)$$

$f_{u,g}$ varies between 0 e 1, for $f_{u,g} = 1$ all the energy generated is supplied to the load, and the excess energy is nil.

- the **capacity factor of the hybrid system CF** (Wh/Wh) is defined as the ratio between the energy provided by the hybrid system to the load E_{tl} and the maximum energy that the system can supply with each component that works simultaneously in nominal conditions P_n. P_n is the overall system nominal power, sum of the PV power $P_{pv,n}$, wind power $P_{w,n}$ and battery power $P_{b,n}$, namely the constant power to be sent to the battery to charge it in one hour.

  Under such conditions, this indicator provides the fraction of operating equivalent hours of the system in a year needed to deliver the energy sent to the load. This indicator is expressed as the product of the PV-wind fraction $f_{pv,w}$ and the ratio of the daily average load to the nominal power P_n.

$$CF = \frac{E_{tl}}{P_n T} = \frac{P_L}{P_n} f_{pv,w} \qquad (48)$$

where, T is the number of hours in one year. CF varies between 0 and 1, for $CF = 1$ all the components of the hybrid system work always in the nominal conditions.

Since the PV generator can operate to the nominal power only for t=T/2, the wind generator can work to the nominal power only in a specific wind speed range, and battery storage cannot always work in the nominal conditions due to the charge and discharge phases, then $f_{u,hp}$ assumes very low values. To make it coherent with the previous indicators, the capacity factor was normalized with respect to the maximum value obtained in the parametric analysis for each scenario, obtaining the **normalized capacity factor $f_{u,hs}$** (-):

Chapter 3

A novel energy economic-environmental
multi-criteria decision-making
in the optimization of a hybrid renewable system

$$f_{u,hs} = CF/ (CF)_{max} \tag{49}$$

For the economic analysis, the indicators defined are:

- the **Profitability Index PI** (-) defined as the ratio of the net present value NPV and the initial investment cost I:

$$PI = \frac{NPV}{I} \tag{50}$$

PI can be negative and positive, for $PI = 0$ the initial investment cost is recovered without achieving any economic benefit.

- the **Benefit Period Fraction BPF** (-) defined as the fraction time length between the Payback Period PP and the lifespan of the investment N, namely the fraction of time in which the economic benefits are reached.

$$BPF = \frac{N - PP}{N} \tag{51}$$

Where, the PP is the time length required for NPV to become zero. Values close to one indicate that the time length of the economic benefits is close to the time length of the investment, while for values of zero there is not a period of economic benefits.

For the environmental analysis, the indicator defined is:

- the **yearly CO₂ savings** (kg) owing to the hybrid system are:

$$(CO_2)_{sav,hs} = CO_{2,ahs} - CO_{2,phs} = f_E(1 - e_{fg} + e_{tg})E_L \tag{52}$$

By considering Eq. (11) and by replacing e_{fg} into Eq. (52), a new expression for $(CO_2)_{sav,hp}$ is obtained:

$$(CO_2)_{sav,hs} = f_E(e_{dtl} + e_{fb} + e_{tg})E_L \tag{53}$$

3. Results and discussion

3.1. Results of the parametric analysis

Figures 7, 8 and 9 show the results of PV-wind hybrid systems (I) and (II) with and without battery storage, by varying the daily average load and battery capacity. The energy and economic results of the parametric analysis are related to different values of the nominal powers of the wind and PV generator $P_{w,n}$ and $P_{pv,n}$. Figure 7 is related to a daily average load of 0.5 kW, Figure 8 to a daily average load of 2.5 kW, and Figure 9 to a daily average load of 10 kW. The four images in each figure are related to four different values of the battery capacity (2, 6, 10, 0) kWh.

Chapter 3
A novel energy economic-environmental
multi-criteria decision-making
in the optimization of a hybrid renewable system

For each image, with equal load and storage capacity, 15 histograms are reported on the left axis, relating to the three PV powers considered $P_{pv,n}$ (2.5, 5, 10) kW, and for each of these powers, to the five wind powers installed $P_{w,n}$ (2.5, 5, 7.5, 10, 15) kW.
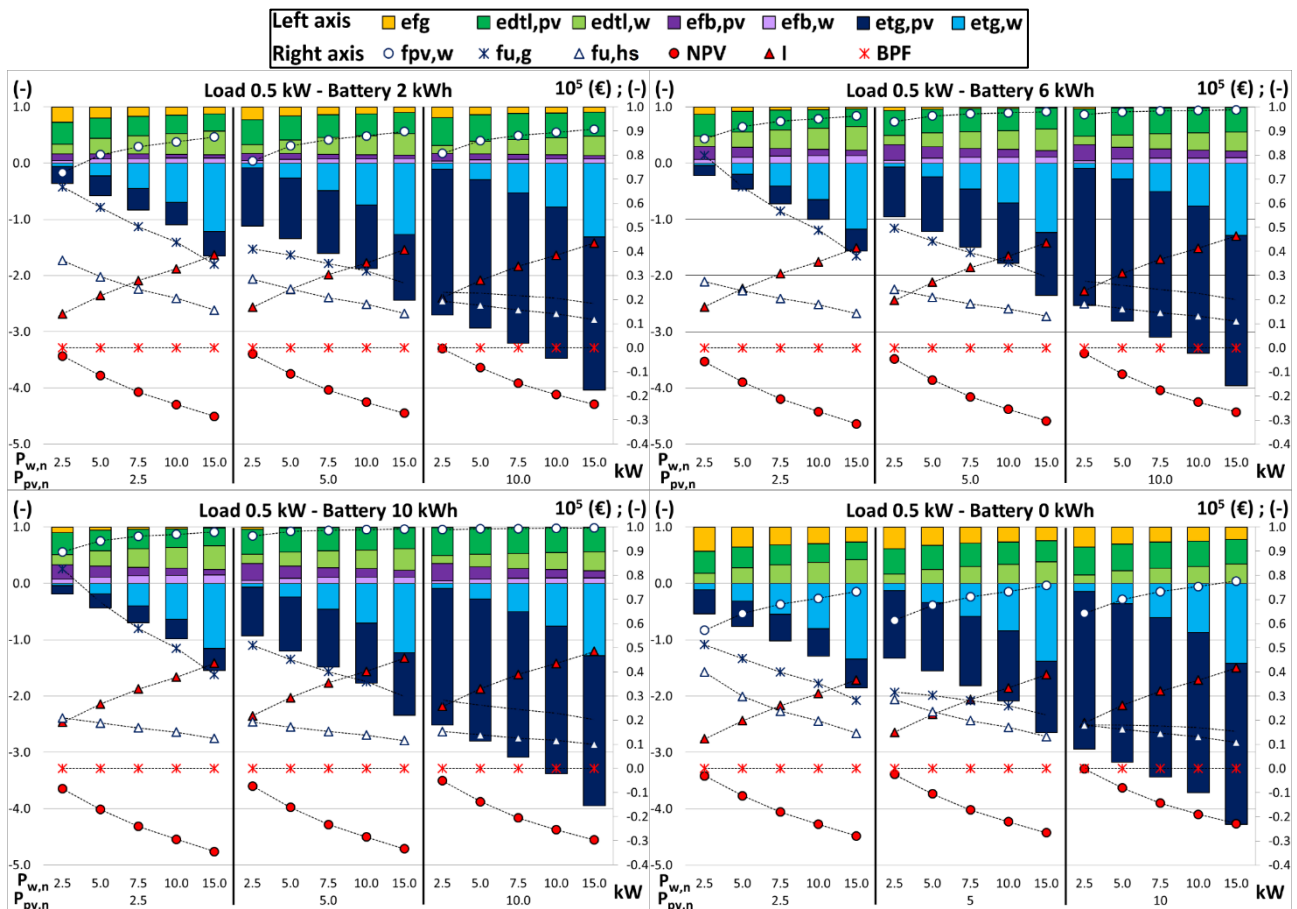
Figure 7. *Energy and economic results for system configuration (I) and (II) for a load of 0.5 kW.*

Each image was divided into three sub-images for each value of $P_{pv,n}$ containing five histograms for the five different values of $P_{w,n}$. Each histogram represents the cumulative contributions of the dimensionless energy balance expressed by Eq. (11), whose terms are e_{fg}, $e_{dtl,pv}$, $e_{dtl,w}$, $e_{fb,pv}$, and $e_{fb,w}$. The dimensionless energy in excess, which does not contribute to supply the load, is represented in all the images by a negative term, divided into the contribute due to the wind generator $e_{tg,w}$ and to the PV generator $e_{tg,pv}$. A different colour represents the previous dimensionless terms on the histogram. Finally, each image on the right axis shows the values of the energy indicators $f_{pw,w}$, $f_{u,g}$, $f_{u,hs}$ and economic indicators PI, represented by means of the NPV and I, and BPF.

In the case of a PV system with battery storage, namely system configuration (III), Figure 10 shows the energy and economic results of the parametric analysis for different values of the daily average load, obtained for different values of the nominal powers of the battery storage and PV generator $P_{b,n}$ and $P_{pv,n}$. The three images in the figure are related to the different values of the load (0.5, 2.5, 10) kW.

In each image, at equal load, 15 histograms are reported on the left axis, relating to three battery powers considered $P_{b,n}$ (2, 6, 10) kW and, for each of these powers, to the five PV powers installed

Chapter 3

**A novel energy economic-environmental
multi-criteria decision-making
in the optimization of a hybrid renewable system**

$P_{pv,n}$ (5, 7.5, 12.5, 15, 25) kW. Each image was divided into three sub-images for each value of $P_{b,n}$ containing five bars for the five different values of $P_{pv,n}$.

Analogously, in the case of a wind system with battery storage, namely system configuration (IV), Figure 11 shows the energy and economic results of the parametric analysis for different values of the daily average load, obtained for different values of the nominal powers of the battery storage and wind generator $P_{b,n}$ and $P_{w,n}$. The three images in the figure are related to the different values of the load (0.5, 2.5, 10) kWh.

In each image, at equal load, 15 histograms are reported on the left axis, relating to the three storage battery powers considered $P_{b,n}$ (2, 6, 10) kW and, for each of these powers, to the five wind powers installed $P_{w,n}$ (5, 7.5, 12.5, 15, 25) kW. Each image was divided into three sub-images for each valued of $P_{b,n}$ containing five bars for the five different values of $P_{w,n}$.
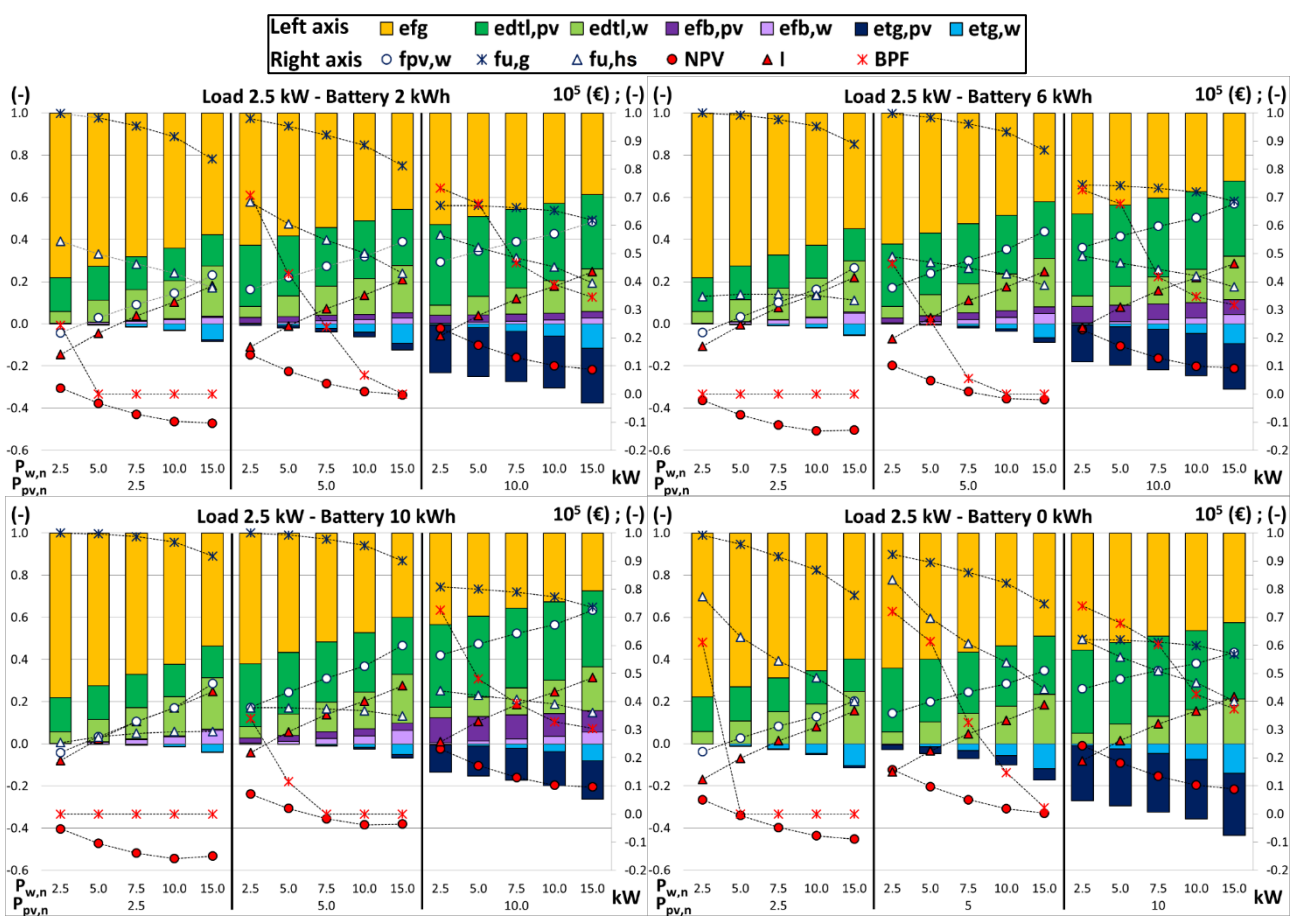
Figure 8. *Energy and economic results for system configuration (I) and (II) for a load of 2.5 kW.*

Chapter 3

**A novel energy economic-environmental
multi-criteria decision-making
in the optimization of a hybrid renewable system**
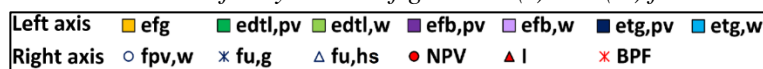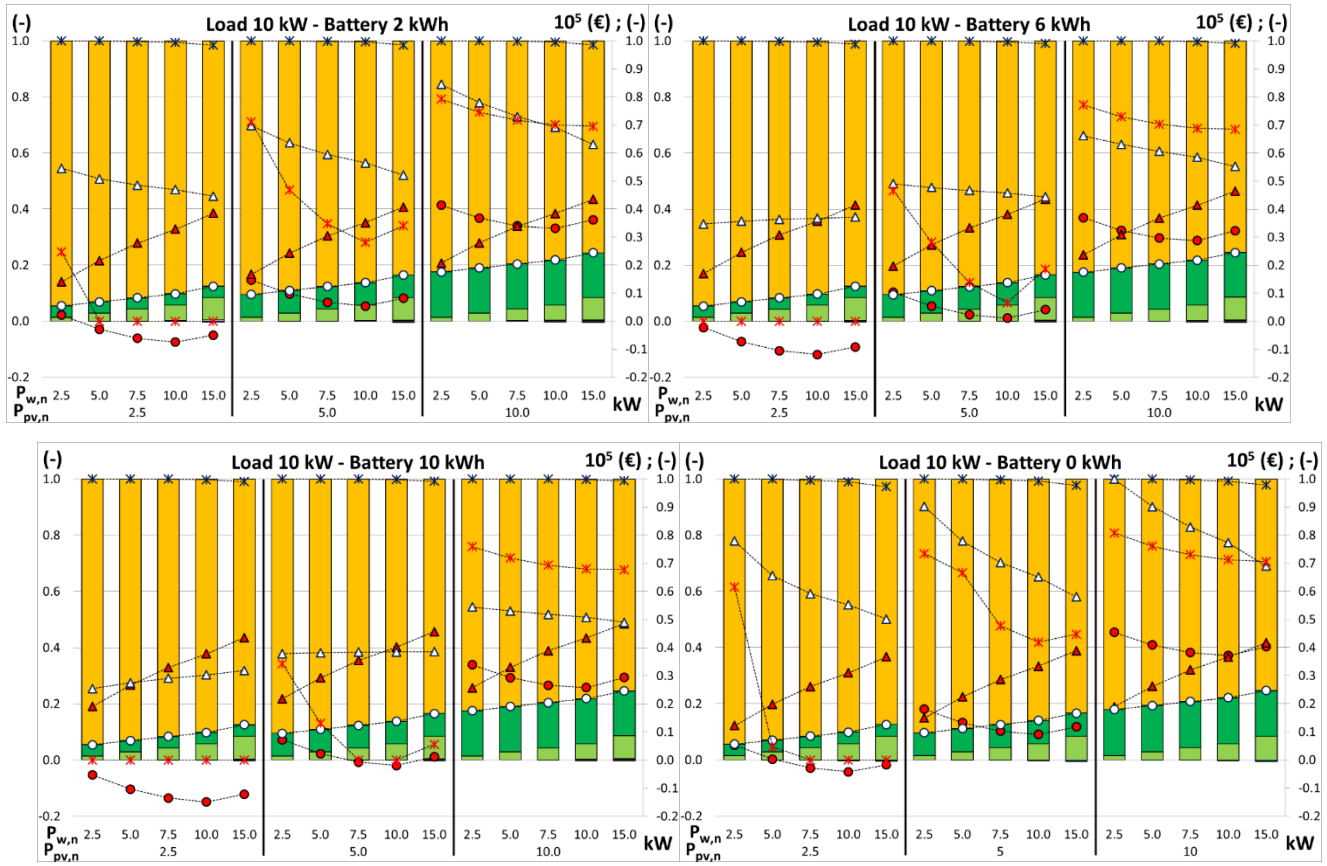
Figure 9. *Energy and economic results for system configuration (I) and (II) for a load of 10 kW.*

Chapter 3

**A novel energy economic-environmental
multi-criteria decision-making
in the optimization of a hybrid renewable system**
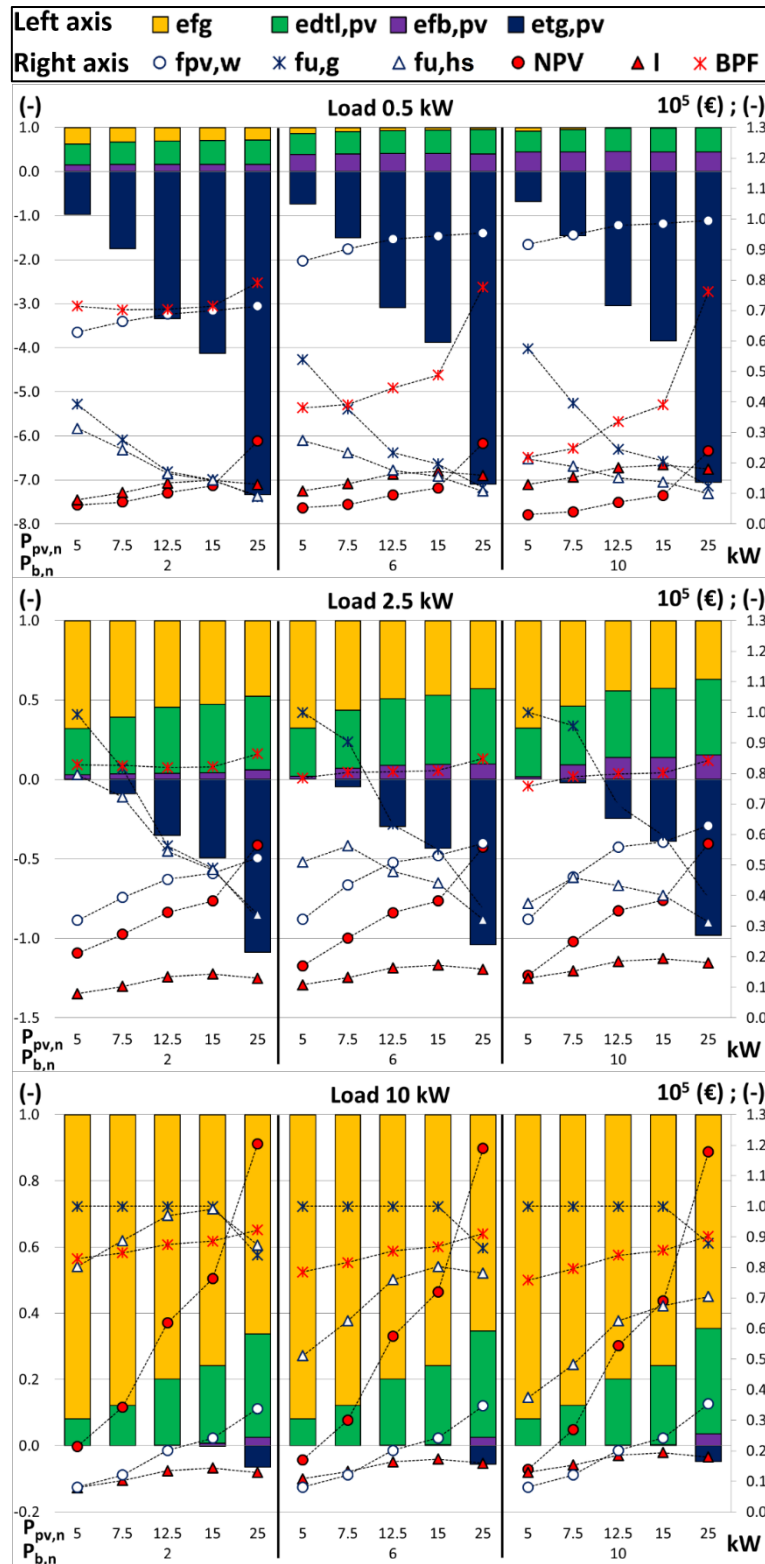
Figure 10. *Energy and economic results for system configuration (III)*

Chapter 3   **A novel energy economic-environmental**
multi-criteria decision-making
in the optimization of a hybrid renewable system
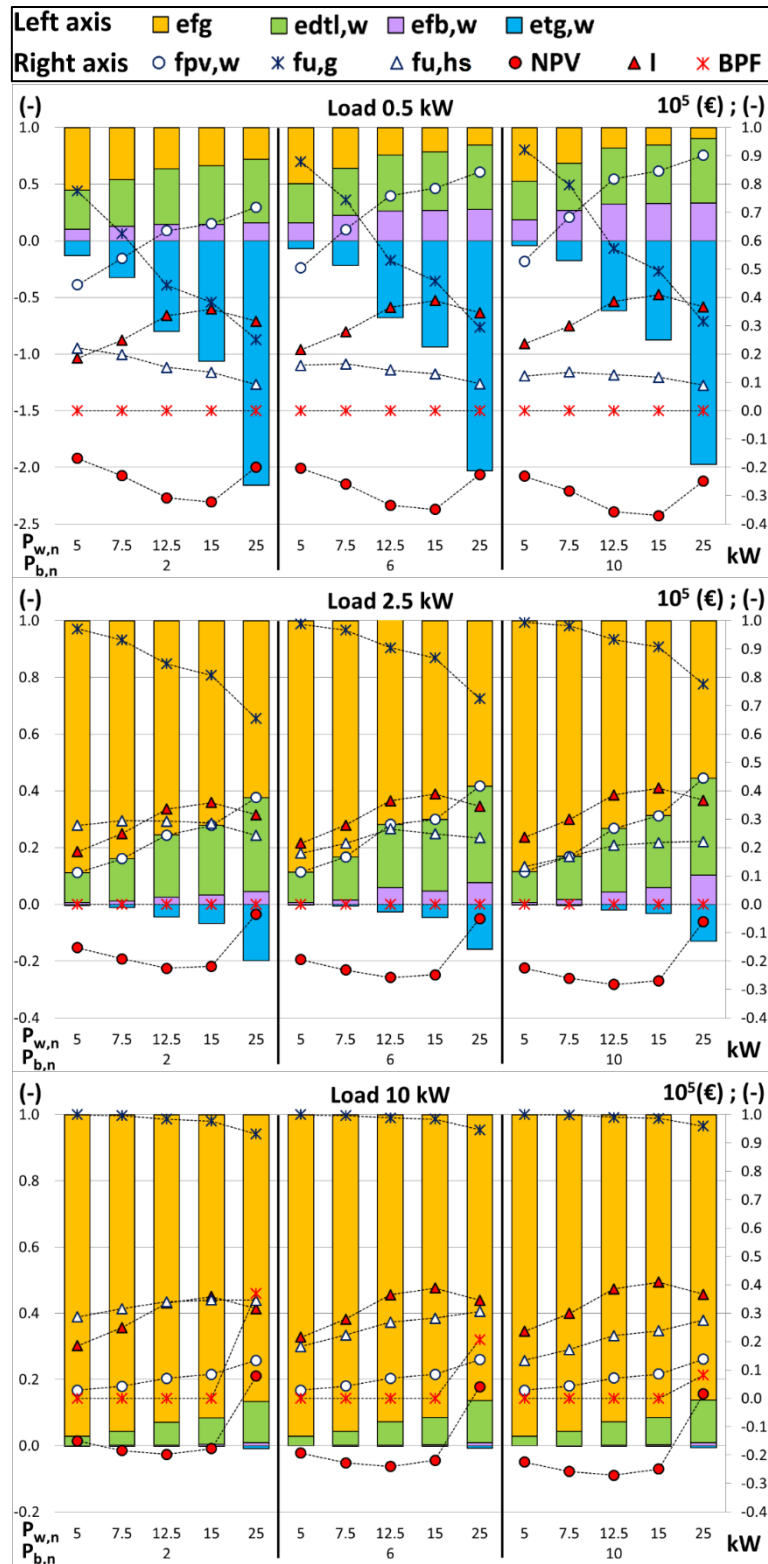
Figure 11. *Energy and economic results for system configuration (IV)*

3.1.1. Energy balance of the energy required by the load

The load is the factor that most significantly influences the distribution of energy contributions in the balance equations, Eqs. (8), (16), (24), (32). In particular, the growth of the load increases the fraction e_{fg} (yellow), and reduces the fractions e_{dtl} (dark and light green), e_{fb} (dark and light violet) and e_{tg} (dark and light blue). The increase of the storage capacity leads to a growth of the fractions $e_{fb,pv}$

Chapter 3   **A novel energy economic-environmental**
multi-criteria decision-making
in the optimization of a hybrid renewable system

(dark violet bar) and $e_{fb,w}$ (light violet), with consequent reduction of fractions e_{tg} (dark and light blue) and e_{fg} (yellow). In the absence of electrical storage, the null values of $e_{fb,pv}$ (dark violet) and $e_{fb,w}$ (light violet) determine an increase in the fractions e_{tg} (dark and light blue) and e_{fg} (yellow).

In the system configurations with the wind system, at fixed values of other powers (for each sub-image), a greater wind power increases the fractions $e_{dtl,w}$ (light green bar), $e_{fb,w}$ (light violet), and $e_{tg,w}$ (light blue). Instead, the fraction e_{fg} (yellow bar) is reduced. The magnitude of these variations is mainly determined by the daily average value of the load.

In the system configurations with the PV system, at fixed values of other powers (for each image for system configurations (I) and (II) and for each sub-image for system configuration (III)), similar considerations can be made on the effect of the growth in the PV power on the fractions $e_{dtl,pv}$ (dark green), $e_{tg,pv}$ (dark blue) and e_{fg} (yellow).

For any value of the load and storage capacity, and with the same wind and PV power installed, the fraction of PV energy produced and stored, one sent directly to the load, and one in excess are higher than wind ones. This is evident by comparing configuration (III) with (IV), Figures 10 and 11, for the same wind and PV power installed.

3.1.2. Energy indicators

The energy indicators $f_{pv,w}$, $f_{u,g}$, and $f_{u,hs}$ are mainly influenced by the load. In particular, the increase in the load determines a reduction of $f_{pv,w}$, and an increment of $f_{u,g}$ and $f_{u,hs}$.

The growth of the storage capacity leads to a significant increase in the fractions $f_{pv,w}$ and $f_{u,g}$ for low loads and to a slight increase for high loads. These changes are more noticeable for small battery capacity. In addition, the increase in storage capacity produces a substantial decrease in $f_{u,hs}$ for any load.

In the configurations with the wind system, at fixed values of other powers (namely for each sub-images), higher installed wind power leads to an increase in $f_{pv,w}$ and a reduction in $f_{u,g}$, especially for low loads. Similar considerations can be deducted in the configurations with the PV system by increasing nominal PV power, at fixed values of other powers (for each image for system configurations (I) and (II) and each sub-image for system configuration (III)).

The capacity factor of the hybrid system $f_{u,hs}$ presents, instead, a complex trend, as it depends on P_L/P_n and $f_{pv,w}$. As aforementioned, an increase of P_L leads to a reduction in $f_{pv,w}$, while the growth of P_n increases $f_{pv,w}$. As a result, an increase in P_L/P_n reduces $f_{pv,w}$. The value $\left(P_L/P_n \cdot f_{pv,w}\right)$ can increase or decrease when the wind power, PV power and battery capacity increase. For all system configurations, the increase in the load and storage capacity, for any combination of powers ($P_{pv,n}$, $P_{w,n}$) determine a reduction in $f_{u,hs}$.

In the case of system configuration (I), for a load of $P_L = 0.5$ kW, $f_{u,hs}$ undergoes a reduction for an increase in the wind power and PV power; for a load of 2.5 kW or 10 kW, the $f_{u,hs}$ trend, by varying the wind power, is determined by the PV power.

Also for system configuration (II), $f_{u,hs}$ is reduced at the increase in the $P_{w,n}$. The effect of $P_{pv,n}$ is determined by the powers (P_L, $P_{w,n}$).

For system configuration (III), the $f_{u,hs}$ trends as a function of the PV power are decreasing for small loads and become increasing for high loads. Analogous behaviour emerges for system configuration

Chapter 3

A novel energy economic-environmental
multi-criteria decision-making
in the optimization of a hybrid renewable system

(IV) by considering the $f_{u,hs}$ trends as a function of the wind power by passing from reduced loads to high ones.

By comparing system configuration (I) with system configuration (II), namely by removing the battery storage, with unchanged $P_{pv,n}$ and $P_{w,n}$, the indicators $f_{pv,w}$ and $f_{u,g}$ are reduced and this effect is less significant as the load increases; instead, $f_{u,hs}$ increases and this effect is more significant as the load increases.

By comparing system configuration (I) with system configuration (III), namely by removing the wind system, the indicator $f_{pv,w}$ is reduced while $f_{u,g}$ is increased, with unchanged $P_{pv,n}$ and $P_{b,n}$. Analogous behaviour of $f_{pv,w}$ and $f_{u,g}$ is obtained, by comparing system configuration (I) with system configuration (IV), namely by removing the PV system, with unchanged $P_{w,n}$ and $P_{b,n}$. All these effects are less significant as the load increases.

For both configurations, the $f_{u,hp}$ variations are determined by the load and battery capacity value.

Finally, at fixed load and battery capacity values, system configuration (III) presents higher values of $f_{pv,w}$ and $f_{u,hs}$, and lower values of $f_{u,g}$, than those related to the system configuration (IV), demonstrating that the PV generator satisfies the load more than the wind one, operates longer at the nominal conditions than the wind one, and the fraction of PV energy generated employed to satisfy the load is less than the corresponding fraction of wind one.

3.1.3. Economic indicators

The initial investment cost I is according to the overall installed power:
- For system configuration (I), it varies between 14.0 k€ (for $P_{b,n}$ = 2 kW, $P_{w,n}$ = 2.5 kW and $P_{pv,n}$ = 2.5 kW) and 49.0 k€ (for $P_{b,n}$ = 10 kW, $P_{w,n}$ = 15 kW and $P_{pv,n}$ = 10 kW).
- For system configuration (II), it varies between 12.3 k€ ($P_{w,n}$ = 2.5 kW and $P_{pv,n}$ = 2.5 kW) and 41.7 k€ ($P_{w,n}$ = 15 kW and $P_{pv,n}$ = 10 kW).
- For system configuration (III), it varies between 8.0 k€ (for $P_{b,n}$ = 2 kW and $P_{pv,n}$ = 5 kW) and 19.0 k€ (for $P_{b,n}$ = 10 kW and $P_{pv,n}$ = 15 kW).
- For system configuration (IV), it varies between 18.6 k€ (for $P_{b,n}$ = 2 kW and $P_{w,n}$ = 5 kW) and 40.9 k€ (for $P_{b,n}$ = 10 kW and $P_{w,n}$ = 15 kW).

The NPV trend grows as the load increases for all the system configurations. In particular, for system configuration (I) and (II):
- For a load of 0.5 kW, the NPV is always negative and slightly increases with increasing $P_{pv,n}$ and decreases markedly with increasing $P_{w,n}$.
- For a load of 2.5 kW, the NPV grows as $P_{pv,n}$ increases from negative to positive values; NPV rises as $P_{w,n}$ and $P_{b,n}$ decrease. Overall, the minimum value of NPV is -15.8 k€, obtained for $P_{pv,n}$ = 2.5 kW, $P_{w,n}$ = 10 kW and $P_{b,n}$ = 10 kW, while the maximum value is 24 k€, obtained for $P_{pv,n}$ = 10 kW, $P_{w,n}$ = 2.5 kW and $P_{b,n}$ = 0 kW.
- For a load of 10 kW, the NPV moderately increases when $P_{pv,n}$ grows and when $P_{b,n}$ decreases. Instead, as $P_{w,n}$ increases, the trend presents a minimum value. The minimum value of NPV is -14.9 k€, while the maximum value is 45 k€, obtained for the same combinations of ($P_{b,n}$, $P_{pv,n}$, $P_{w,n}$) relative to a load of 2.5 kW.

Chapter 3
                                           **A novel energy economic-environmental
multi-criteria decision-making
in the optimization of a hybrid renewable system**

By removing the wind system, namely by comparing system configuration (I) and (III), the NPV undergoes a strong rise reaching, for $P_{pv,n} = 25$ kW and $P_{b,n} = 2$ kW, a maximum values of 27 k€ for a load of 0.5 kW, of 57 k€ for a load of 2.5 kW and 120 k€ for a load of 10 kW.

The removal of the PV system, namely by comparing system configuration (I) and (III), determines a significant reduction in the NPV, which is always negative except for a load of 10 kW and the maximum wind power of 25 kW for the different values of the battery power. In this case, the NPV becomes positive but with a very reduced value.

The BPF trend is analogous to that of the NPV, with the difference that when the NPV is negative the BPF is nil. As a consequence, for system configurations (I) and (II) the BPF highest value is 0.81, obtained for $P_{pv,n} = 10$ kW, $P_{w,n} = 2.5$ kW and $P_{b,n} = 0$ kW, when the load is 10 kW. BPF is 0.74 and 0 for lower loads of, respectively, 2.5 kW and 0.5 kW. For system configuration (III), a BPF maximum value is 0.92, obtained for $P_{pv,n} = 25$ kW and $P_{b,n} = 2$ kW, when the load is 10 kW. BPF is 0.86 and 0.79 for lower loads of, respectively, 2.5 kW and 0.5 kW.

For system configuration (IV), the BPF maximum value is 0.37, obtained for $P_{w,n} = 25$ kW and $P_{b,n} = 2$ kW, when the load is 10 kW, and it is nil for a load of 2.5 kW and 0.5 kW.

The BPF trend discontinuities are owing to the substitution cost of the battery that leads in some configurations to two different PP during the investment lifespan, of which only the higher was considered.

3.1.4. Energy and economic comparison of the four configuration systems

The results of the energy and economic analysis, for the four system configurations and 700 scenarios, were summarized in Figure 12. In particular, the images report the economic indicator NPV/I on the vertical axes, while on the horizontal axes the images on the top, centre and bottom show, respectively, the energy indicators PV-wind fraction $f_{pv,w}$, utilization factor $f_{u,g}$ and normalized capacity factor $f_{u,hs}$. These three optimization criteria were labelled respectively as *a)*, *b)* and *c)*. The images permit a direct comparison of the economic convenience with energy performance, and identification of the system configurations and scenarios that assure the highest values of each indicator. The BPF was not considered since, as highlighted in Section 3.1.3, it presents an analogous trend of the NPV indicator. Therefore, the highest NPV value assures the maximum BPF.

Chapter 3

A novel energy economic-environmental multi-criteria decision-making in the optimization of a hybrid renewable system
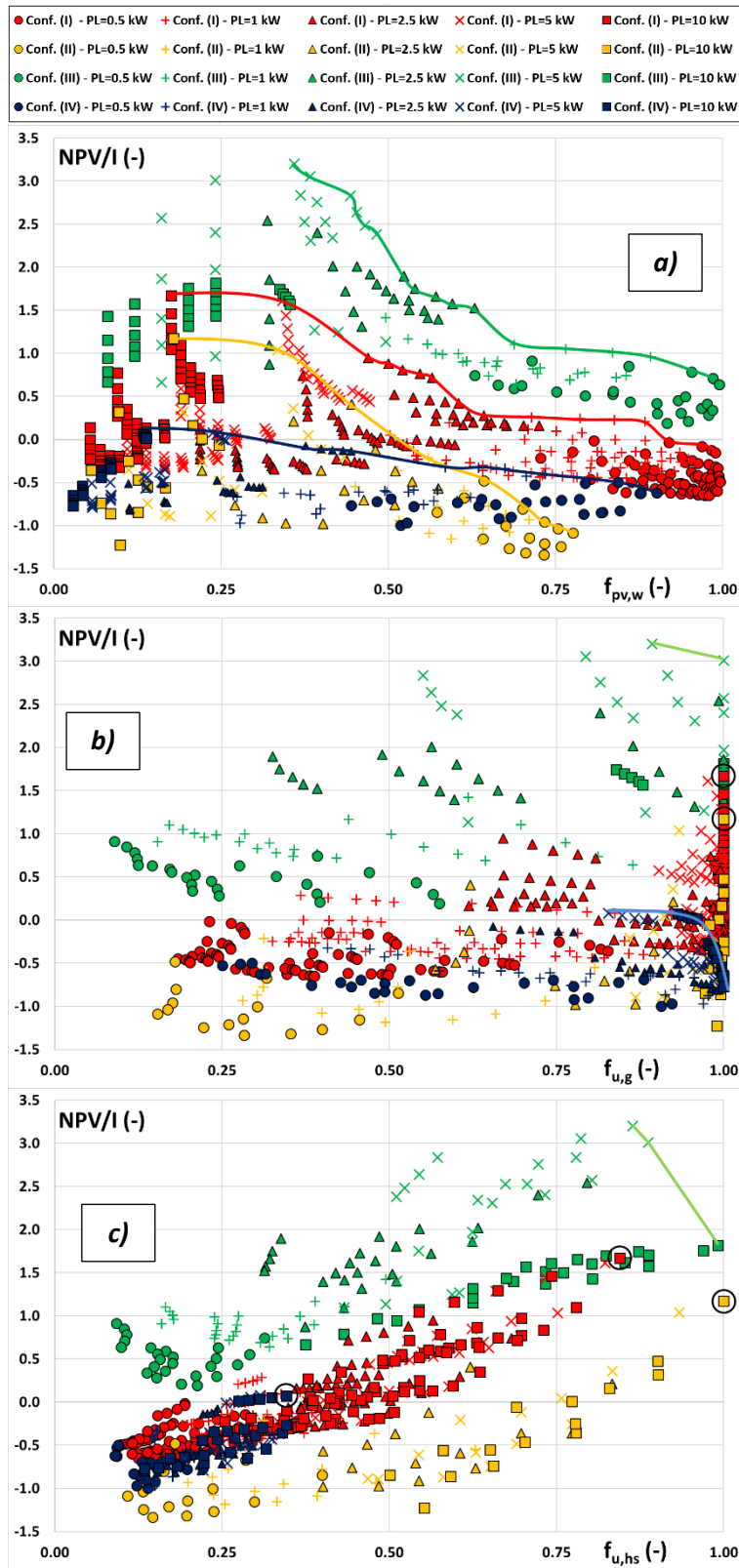
Figure 12. *Energy and economic results of the parametric analysis for the four system configurations*

Chapter 3   **A novel energy economic-environmental
multi-criteria decision-making
in the optimization of a hybrid renewable system**

3.1.4.1.   *Economic viability versus load satisfaction*

As regards the image at the top of Figure 12, there is no unique scenario that assures simultaneously, for all system configurations, the highest value of NPV/I and the maximum $f_{pv,w}$. For each configuration, the best scenarios are represented by the points within the Pareto-front [68, 69], identified by a continuous line. In general, the PV-battery system, PV-wind-battery system and PV-wind system present an analogous Pareto-front trend, while the Pareto-front trend of the wind-battery system is characterized by a reduction of NPV/I by increasing $f_{pv,w}$ more slowly than the other configurations.

The comparison of Pareto-fronts highlights that the PV-battery system is the best both in energy and economic terms, followed by the hybrid PV-wind-battery system. Instead, the worst system is determined by the (NPV/I, $f_{pv,w}$) combination. In particular, below of a specific value of NPV/I and above a specific value of $f_{pv,w}$, the wind-battery system is better than the hybrid PV-wind system; vice versa above a specific value of NPV/I and below a specific value of $f_{pv,w}$. For a value of $f_{pv,w}$ higher than 0.35, all the scenarios of system configuration (III) are above of the Pareto-fronts of the other system configurations. Similarly, for a value of $f_{pv,w}$ higher than 0.50, all the scenarios of system configuration (I) are above the Pareto-fronts of system configuration (II) and (IV). For $f_{pv,w}$ lower than the previous values, the scenarios of the four system configurations are very mixed.

On the Pareto-front, different values of the load are present: a high load assures the highest NPV/I and the lowest $f_{pv,w}$ and vice versa for a low load. As a result, the wind-battery system presents the lowest NPV/I for medium-high loads, while the PV-wind system is characterized by the lowest NPV/I for low loads. In addition, for all the configurations, the vertical dispersion of the points, namely the variation of the NPV/I, not belonging to the Pareto-front grows by increasing the load. This means that the variation of the PV, wind and battery powers has a stronger effect on NPV/I at high loads.

In Table 12, for each system configuration, optimal scenarios that constitute the Pareto-front were reported.

Chapter 3

A novel energy economic-environmental
multi-criteria decision-making
in the optimization of a hybrid renewable system

Table 12. *Optimal scenarios that maximize NPV/I and $f_{pv,w}$ for the four system configurations.*

	System configuration (I)							System configuration (II)							System configuration (III)							System configuration (IV)					
	P_L	P_b	P_{pv}	P_w	$f_{pv,w}$	PI		P_L	P_b	P_{pv}	P_w	$f_{pv,w}$	PI		P_L	P_b	P_{pv}	P_w	$f_{pv,w}$	PI		P_L	P_b	P_{pv}	P_w	$f_{pv,w}$	PI
	(kW)	(kW)	(kW)	(kW)	(-)	(-)		(kW)	(kW)	(kW)	(kW)	(-)	(-)		(kW)	(kW)	(kW)	(kW)	(-)	(-)		(kW)	(kW)	(kW)	(kW)	(-)	(-)
a)-(I)-1	0.5	10	10.0	15.0	1.00	-0.49	a)-(II)-1	0.5	0	10.0	15.0	0.78	-1.09	a)-(III)-1	0.5	10	25.0	0.0	0.99	0.64	a)-(IV)-1	0.5	10	0.0	25.0	0.90	-0.62
a)-(I)-2	0.5	10	10.0	10.0	1.00	-0.47	a)-(II)-2	0.5	0	10.0	10.0	0.75	-1.04	a)-(III)-2	0.5	8	25.0	0.0	0.99	0.71	a)-(IV)-2	0.5	6	0.0	25.0	0.84	-0.50
a)-(I)-3	0.5	10	10.0	7.5	0.99	-0.43	a)-(II)-3	0.5	0	10.0	7.5	0.73	-0.96	a)-(III)-3	0.5	6	25.0	0.0	0.95	0.79	a)-(IV)-3	1.0	10	0.0	25.0	0.73	-0.40
a)-(I)-4	0.5	10	10.0	5.0	0.99	-0.33	a)-(II)-4	1.0	0	10.0	15.0	0.71	-0.93	a)-(III)-4	1.0	10	25.0	0.0	0.89	0.96	a)-(IV)-4	1.0	6	0.0	25.0	0.67	-0.34
a)-(I)-5	0.5	10	10.0	2.5	0.99	-0.16	a)-(II)-5	0.5	0	10.0	5.0	0.70	-0.80	a)-(III)-5	1.0	8	25.0	0.0	0.84	1.00	a)-(IV)-5	1.0	4	0.0	25.0	0.64	-0.33
a)-(I)-6	0.5	8	10.0	2.5	0.98	-0.12	a)-(II)-6	1.0	0	10.0	7.5	0.65	-0.77	a)-(III)-6	1.0	6	25.0	0.0	0.77	1.05	a)-(IV)-6	1.0	2	0.0	25.0	0.59	-0.32
a)-(I)-7	0.5	6	10.0	2.5	0.97	-0.08	a)-(II)-7	0.5	0	10.0	2.5	0.64	-0.48	a)-(III)-7	1.0	4	25.0	0.0	0.69	1.10	a)-(IV)-7	2.5	10	0.0	25.0	0.44	-0.14
a)-(I)-8	1.0	10	10.0	5.0	0.92	-0.02	a)-(II)-8	1.0	0	10.0	2.5	0.56	-0.21	a)-(III)-8	2.5	10	25.0	0.0	0.63	1.52	a)-(IV)-8	2.5	8	0.0	25.0	0.43	-0.13
a)-(I)-9	1.0	6	10.0	5.0	0.84	-0.01	a)-(II)-9	2.5	0	10.0	2.5	0.45	0.41	a)-(III)-9	2.5	8	25.0	0.0	0.60	1.57	a)-(IV)-9	2.5	6	0.0	25.0	0.42	-0.13
a)-(I)-10	1.0	8	10.0	2.5	0.84	0.22	a)-(II)-10	5.0	0	10.0	2.5	0.33	1.04	a)-(III)-10	2.5	6	25.0	0.0	0.57	1.66	a)-(IV)-10	2.5	4	0.0	25.0	0.40	-0.11
a)-(I)-11	1.0	6	10.0	2.5	0.79	0.24	a)-(II)-11	10.0	0	10.0	2.5	0.18	1.17	a)-(III)-11	2.5	4	25.0	0.0	0.54	1.75	a)-(IV)-11	2.5	2	0.0	25.0	0.38	-0.08
a)-(I)-12	1.0	4	10.0	2.5	0.71	0.26								a)-(III)-12	2.5	2	25.0	0.0	0.52	1.89	a)-(IV)-12	5.0	10	0.0	25.0	0.26	-0.01
a)-(I)-13	1.0	2	10.0	2.5	0.64	0.28								a)-(III)-13	5.0	8	25.0	0.0	0.48	2.38	a)-(IV)-13	5.0	8	0.0	25.0	0.25	-0.01
a)-(I)-14	2.5	10	10.0	5.0	0.61	0.42								a)-(III)-14	5.0	6	25.0	0.0	0.47	2.48	a)-(IV)-14	5.0	6	0.0	25.0	0.25	0.02
a)-(I)-15	2.5	8	10.0	5.0	0.58	0.44								a)-(III)-15	5.0	2	25.0	0.0	0.44	2.83	a)-(IV)-15	5.0	4	0.0	25.0	0.24	0.05
a)-(I)-16	2.5	10	10.0	2.5	0.57	0.72								a)-(III)-16	5.0	2	15.0	0.0	0.38	3.06	a)-(IV)-16	5.0	2	0.0	25.0	0.24	0.08
a)-(I)-17	2.5	8	10.0	2.5	0.55	0.76								a)-(III)-17	5.0	2	12.5	0.0	0.36	3.20							
a)-(I)-18	2.5	6	10.0	2.5	0.52	0.80																					
a)-(I)-19	2.5	4	10.0	2.5	0.50	0.88																					
a)-(I)-20	2.5	2	10.0	2.5	0.47	0.95																					
a)-(I)-21	5.0	2	10.0	5.0	0.37	1.03																					
a)-(I)-22	5.0	10	10.0	2.5	0.35	1.04																					
a)-(I)-23	5.0	8	10.0	2.5	0.35	1.15																					
a)-(I)-24	5.0	6	10.0	2.5	0.35	1.29																					
a)-(I)-25	5.0	4	10.0	2.5	0.35	1.44																					
a)-(I)-26	5.0	2	10.0	2.5	0.34	1.61																					
a)-(I)-27	10.0	2	10.0	2.5	0.18	1.67																					

All the optimal system scenarios are characterized by the maximum PV power and by high battery capacities for low loads and low battery capacities for high loads. In the absence of the PV system, the optimal system scenarios present high wind powers, while in the presence of the PV system they require low wind powers for high loads and both low and high wind powers for low loads.

In addition, for system configurations (I) and (II), there are optimal scenarios for each load, while for system configurations (III) and (IV) only for loads up to 5 kW.

With reference to the optimal scenarios, to obtain a PI = 1, system configuration (I) guarantees a maximum $f_{pv,w}$ of 0.37, system configuration (II) of 0.33, system configuration (III) of 0.84, while system configuration (IV) does not allow obtaining PI values higher than 0.08. To obtain $f_{pv,w} = 0.75$ with system configuration (I), the maximum NPV/I obtainable is 0.24, with system configuration (II) NPV/I is negative and –at 1.04, with system configuration (III) it is 1.05, while with system configuration (IV) it is -0.50.

3.1.4.2. *Economic viability versus self-consumption of energy produced*

As regards the image at the centre of Figure 12, for system configurations (I) and (II) there is a scenario, highlighted by means of a dark circle, which maximizes both the energy indicator $f_{u,g}$ and economic indicator NPV/I. Instead, for system configurations (III) and (IV), the trade-off optimal solutions of the Pareto-front were reported, respectively, with a green and blue continuous lines.

The comparison of the optimal scenarios of the different system configurations highlights that the PV-battery system is the best in economic terms, followed by the hybrid PV-wind-battery system, hybrid PV-wind system and wind-battery system. In energy terms, all the system configurations present at least an optimal scenario with a maximum value of $f_{u,g}$ equal to one. For the system

Chapter 3   **A novel energy economic-environmental**
multi-criteria decision-making
in the optimization of a hybrid renewable system

configurations (III) and (IV), the other optimal scenarios increase the NPV/I with a lower value of $f_{u,g}$.

In general, the load increase gives rises to a reduction of $f_{u,g}$ and NPV/I. In addition, for any system configuration, for low values of the load, $f_{u,g}$ present a high dispersion and low values for different scenarios; instead for high loads, $f_{u,g}$ values are very close to one independently of the scenario considered. The dispersion of the different scenarios compared to the optimal ones is according to the system configuration. In particular, the NPV/I has a high dispersion by varying the powers of the system components and load for system configuration (III) and, in a less accentuated manner, for system configuration (I). The other configurations present a lower dispersion.

Table 13 lists optimal scenarios for each system configuration.

Table 13. *Optimal scenarios that maximize NPV/I and $f_{u,g}$ for the four system configurations.*

	P_L	$P_{b,n}$	$P_{pv,n}$	$P_{w,n}$	$f_{u,g}$	PI
	(kW)	(kW)	(kW)	(kW)	(-)	(-)
System configuration (I)						
b)-(I)-1	10.0	2	10.0	2.5	1.00	1.67
System configuration (II)						
b)-(II)-1	10.0	0	10.0	2.5	1.00	1.17
System configuration (III)						
b)-(III)-1	5.0	2	7.5	0.0	1.00	3.01
b)-(III)-2	5.0	2	12.5	0.0	0.89	3.20
System configuration (IV)						
b)-(IV)-1	10.0	2	0.0	7.5	1.00	-0.54
b)-(IV)-2	10.0	10	0.0	15.0	0.99	-0.34
b)-(IV)-3	10.0	2	0.0	15.0	0.98	-0.27
b)-(IV)-4	10.0	10	0.0	25.0	0.96	0.01
b)-(IV)-5	10.0	8	0.0	25.0	0.95	0.02
b)-(IV)-6	10.0	4	0.0	25.0	0.94	0.05
b)-(IV)-7	10.0	2	0.0	25.0	0.93	0.07
b)-(IV)-8	5.0	2	0.0	25.0	0.83	0.08

The optimal system scenarios of system configurations (I) and (II) are characterized by high values of the load equal to the maximum value of 10 kW. Also the eight Pareto-front optimal scenarios of system configuration (IV) are those with a load of 10 kW, except the one with the highest PI value which is characterized by a load of 5 kW. Finally, the two Pareto-front optimal scenarios of system configuration (III) are related to a load of 5 kW. When both PV and wind system are present, the highest PV power of 10 kW and the lowest wind power of 2.5 kW are required. For system configuration (III), the minimum battery power of 2 kW and intermediates PV powers of 7.5 or 12.5 kW constitute the optimal scenarios. Finally, for system configuration (IV), the eight scenarios of the Pareto-front are those with the highest wind power, those with 15 kW of wind power and the minimum and maximum battery power, the one with a battery power of 2 kW and a wind power of 7.5 kW.

Chapter 3

A novel energy economic-environmental
multi-criteria decision-making
in the optimization of a hybrid renewable system

3.1.4.3. *Economic viability versus capacity factor*

As regards the image at the bottom of Figure 12, an optimal scenario that simultaneously assures the highest values of both economic indicator NPV/I and energy indicator $f_{u,hs}$ was found for system configurations (I), (II) and (IV), as shown by the dark circle. Instead, the optimal scenarios of system configuration (III) are represented by a Pareto-front, highlighted by the green continue line. For all the system configurations, the general trend shows a gradual growth in NPV/I by increasing $f_{u,hs}$. Overall, for all the configurations, the load increase determines a rise of $f_{u,hs}$ and NPV/I. Only for system configuration (III), by passing from a load of 5 kW to 10 kW, an NPV/I decrease is observed. The variation range of the indicator $f_{u,hs}$ is different for the four configurations. The indicator represents the normalization of the capacity factor CF with respect to the maximum value $(CF)_{max}$ obtained in all the scenarios considered. The maximum capacity factor $(CF)_{max}$ was obtained in the case of the PV-battery system, as highlighted by the unitary value of $f_{u,hs}$ of the yellow square within the dark circle. For this reason, the other variation ranges of $f_{u,hs}$ are more contained, especially that of the wind-battery system, which presents a maximum $f_{u,hs}$ value of 0.35. The comparison of the optimal scenarios shows that all the points within the Pareto-front of system configuration (III) are characterized by higher NPV/I values than those of the optimal points relative to the other system configurations. The second best configuration in economic terms is the PV-wind-battery system, followed by the PV-wind system and wind-battery system. In energy terms, the PV-battery system assures values of $f_{u,hs}$ higher than those of the optimal scenario of configuration (I) and (IV) for all the optimal scenarios in the Pareto-front.

Table 14 reports the optimal scenarios of each system configuration.

Table 14. *Optimal scenarios that maximize NPV/I and $f_{u,hs}$ for the four system configurations.*

	P_L	$P_{b,n}$	$P_{pv,n}$	$P_{w,n}$	$f_{u,hs}$	PI
	(kW)	(kW)	(kW)	(kW)	(-)	(-)
System configuration (I)						
c)-(I)-1	10.0	2	10.0	2.5	0.84	1.67
System configuration (II)						
c)-(II)-1	10.0	0	10.0	2.5	1.00	1.17
System configuration (III)						
c)-(III)-1	10.0	2	15.0	0.0	0.99	1.82
c)-(III)-2	5.0	2	7.5	0.0	0.89	3.01
c)-(III)-3	5.0	2	12.5	0.0	0.86	3.20
System configuration (IV)						
c)-(IV)-1	10.0	2	0.0	25.0	0.35	0.07

In the presence of a battery system, all the optimal scenarios are characterized by the lowest battery power of 2 kW. Optimal scenarios of system configurations (I), (II) and (IV) present the highest load of 10 kW, while those of system configuration (III) the highest loads of 5 kW and 10 kW. Analogously to the previous section, when both PV and wind system are present, the highest PV power of 10 kW and the lowest wind power of 2.5 kW are required. In the absence of a wind system, the optimal

Chapter 3

**A novel energy economic-environmental
multi-criteria decision-making
in the optimization of a hybrid renewable system**

system is composed of intermediate PV powers between 7.5 kW and 15 kW. In the absence of a PV system, the optimal system is constituted of the maximum wind power of 25 kW.

The comparison of Tables 12-14 highlights that, for system configurations (I), (II) and (III), some combinations of loads and powers of system components belong to the three set of optimal scenarios. The optimal scenarios present in all three tables are:

- the optimal scenario of system configuration (I) with a load of 10 kW, a battery power of 2 kW, a PV power of 10 kW and a wind power of 2.5 kW, which allows obtaining an NPV/I of 1.67, $f_{pv,w}$ of 0.18, $f_{u,g}$ of 1, and $f_{u,hs}$ of 0.84.

- the optimal scenario of system configuration (II) with a load of 10 kW, a battery power of 0 kW, a PV power of 10 kW and a wind power of 2.5 kW, which allows obtaining an NPV/I of 1.17, $f_{pv,w}$ of 0.18, $f_{u,g}$ of 1, and $f_{u,hs}$ of 1.

- the optimal scenario of system configuration (III) with a load of 5 kW, a battery power of 2 kW, a PV power of 12.5 kW and a wind power of 0 kW, which allows obtaining an NPV/I of 3.20, $f_{pv,w}$ of 0.36, $f_{u,g}$ of 0.89, and $f_{u,hs}$ of 0.86.

  In addition, for system configuration (III), the optimal scenario with a load of 5 kW, a battery power of 2 kW, a PV power of 7.5 kW and a wind power of 0 kW, falls within the best scenarios of the two optimizations NPV/I - $f_{u,g}$ and NPV/I - $f_{u,hs}$. Analogously for system configuration (IV) with a load of 10 kW, a battery power of 2 kW, a PV power of 0 kW and a wind power of 25 kW. Finally, for the latter configuration, a load of 5 kW, a battery power of 2 kW, a PV power of 0 kW and a wind power of 25 kW falls within the best scenarios of the two optimizations NPV/I - $f_{pv,w}$ and NPV/I - $f_{u,g}$.

3.1.5. Environmental indicator

The top of Figure 13 reports the CO_2 savings, obtained by system configurations (I), (II), (III) and (IV), as a function of the overall nominal power of the system P_n. For each configuration, the different pointers identify the load value. The different points for a specific configuration and load are related to the scenarios obtained by varying the PV, wind, and battery powers.

Chapter 3

A novel energy economic-environmental
multi-criteria decision-making
in the optimization of a hybrid renewable system
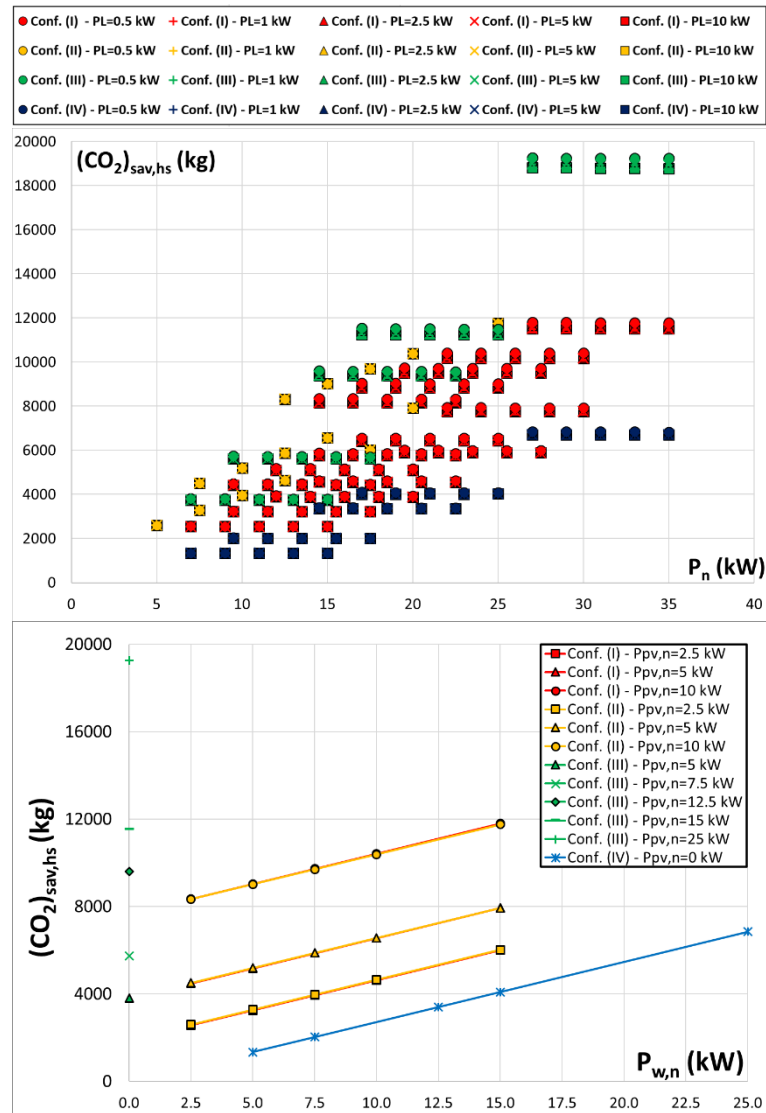
Figure 13. *CO$_2$ savings of system configurations (I), (II), (III) and (IV) for different power loads as a function of the overall nominal power of the system and nominal power of each component*

First of all, the image highlights that the different pointers of the same colour are almost overlapped; as a result, the CO$_2$ savings can be considered independent of the load. In addition, the comparison of the pointers related to the system configurations (II) and system configurations (I), (III) and (IV) shows that CO$_2$ savings result virtually unchanged as a function of the battery power. This result is evident since in configuration (II) there are no pointers arranged horizontally, while in other configurations the five pointers related to increasing system nominal powers, obtained by raising the battery power values and by maintaining unchanged the PV and wind power, are arranged horizontally.

Finally, the highest CO$_2$ savings are obtained with a scenario of system configuration (III), whereas the worst one with a scenario of system configuration (IV). To identify this optimal scenario, the image at the bottom was employed, which shows the CO$_2$ savings by varying the wind power for different values of the PV power for a specific value of the load and battery power, since the latter does not influence the CO$_2$ savings. The overlapping of the trends related to the configuration (I) and (II) confirms the non-dependence of the CO$_2$ savings on the battery power. In general, the CO$_2$ savings

increase linearly as the PV and wind powers increase. Consequently, the lowest and highest values of CO_2 savings obtained are:

- for system configuration (I) and (II), 2597 kg ($P_{pv,n}$=2.5 kW and $P_{w,n}$=2.5 kW) and 11754 kg ($P_{pv,n}$=10 kW and $P_{w,n}$=15 kW);
- for system configuration (III), 1345 kg ($P_{pv,n}$=5 kW and $P_{w,n}$=0 kW) and 6848 kg ($P_{pv,n}$=25 kW and $P_{w,n}$=0 kW);
- for system configuration (IV), 3812 kg ($P_{pv,n}$=0 kW and $P_{w,n}$=5 kW) and 19266 kg ($P_{pv,n}$=0 kW and $P_{w,n}$=25 kW).

The comparison of system configurations (III) and (IV) shows that the PV system allows for obtaining higher CO_2 savings. As a result, configuration (IV) is the best, followed by the two hybrid systems I and II.

3.1.6. Environmental impact of the optimal energy and economic scenarios

Looking at Tables 12-14 for the optimization criteria and results of the environmental analysis, a comparison between all energy-economic optimal scenarios was carried out, obtaining the corresponding CO_2 savings. The comparison shows that only the following scenarios permit the abatement of CO_2 to be maximized:

- with reference to criterion *a)*, scenarios *(I)-1, (II)-1, (II)-4, from (III)-1 to (III)-15* and all the sixteen scenarios of optimal configurations (IV);
- with reference to criterion *b)*, scenarios from *(IV)-4* to *(IV)-8*, while no scenarios of the other configurations allow maximizing CO_2 savings;
- with reference to criterion *c)*, scenario *(IV)-1*, while no scenarios of the other configurations allow maximizing CO_2 savings.

In addition, scenario a)-(IV)-16, which is the same as b)-(IV)-8, is the only one that belongs in the optimal scenarios according to the optimization criteria a) and b) and allows at the same time maximization of CO_2 savings. Instead, scenario b)-(IV)-7, which is the same as c)-(IV)-1, is the only one that belongs in the optimal scenarios according to the optimization criteria b) and c) and allows maximization of CO_2 savings. It is not possible to reach the highest CO_2 savings with a scenario that simultaneously belongs to the optimal scenarios of two criteria, when the PV system is present, namely with configurations (I), (II) and (III).

In general, by maximizing the abatement of CO_2, it is simultaneously possible to find also optimal trade-off scenarios that maximize the load satisfaction and economic convenience, with high values of both energy and economic indicators. Instead, this does not permit the self-consumed energy produced to be maximized when the PV system is present in the system. However, when the PV system is absent, the maximization of CO_2 savings leads to optimal trade-off scenarios with high self-consumed energy produced and a low economic convenience. The same considerations can be also extended to the optimal trade-off scenarios that maximize the normalized capacity factor and the economic viability, also if the normalized capacity factor does not reach high values.

3.1.7. Impact of incentives

The previous analysis highlights the effects produced by the variation of the load magnitude and size of the system components on the economic viability and energy performance. In general, the wind system makes the investment less convenient, while the PV system determines a strong improvement in economic convenience. The presence of the battery allows increasing the NPV/I compared to the

Chapter 3   **A novel energy economic-environmental**
multi-criteria decision-making
in the optimization of a hybrid renewable system

case in the absence. In this section, the effects of the incentives of the PV and wind systems were investigated by considering the different system configurations, changing the tax deductions from 50% to 100% with a step of 10% considering the duration of deductions equal to 10 years for all cases. Figure 14 reports, for an intermediate load of 2.5 kW and system configurations (I), (II) and (IV) equipped with a wind system and a battery capacity of 6 kWh, the NPV and BPF trends by varying the wind power for different levels of incentives of the wind system.

With the current tax deductions of 50% of the initial installation cost, in the presence of a PV system (configurations (I) and (II)), an increase in the wind power reduces NPV by maintaining a positive value. Instead, for the wind-battery system, the NPV trend presents a minimum value by increasing the wind power and a maximum value for the maximum wind power. However, in this case, NPV is always negative.

The growth of wind incentives makes NPV greater and this growth is higher by increasing the wind power. An increase in wind incentives, in addition to increasing the NPV, leads to a gradual modification of the NPV trend, which, for the highest value of tax deductions, presents a trend with a minimum value by increasing the wind power for configurations (I) and (II). As a result, the highest wind power is characterized by an NPV higher than that obtained for the minimum value of the wind power. In the absence of a PV system, with higher wind incentives, the NPV trend becomes always increasing by raising the wind power, allowing the investment to be advantageous above a specific wind power with at least tax deductions higher than 70%, as the NPV passes from negative to positive values.

The BPF has similar trends to those of the NPV. For system configuration (I), an increase in tax deduction up 60% for wind power of 2.5 kW and up 90% for wind powers higher than 7.5 kW would allow obtaining a substantial BPF increase. In the absence of battery (configuration (II)), BPF presents an accentuated growth, by passing from 50% to 70% of tax deductions, for wind powers higher than 7.5 kW. In the absence of a PV system (configuration (IV)), for wind powers higher than 15 kW by increasing tax deductions up to 90 %, the BPF continues to increase and further growth does not lead to significant improvements.

Chapter 3   **A novel energy economic-environmental
multi-criteria decision-making
in the optimization of a hybrid renewable system**
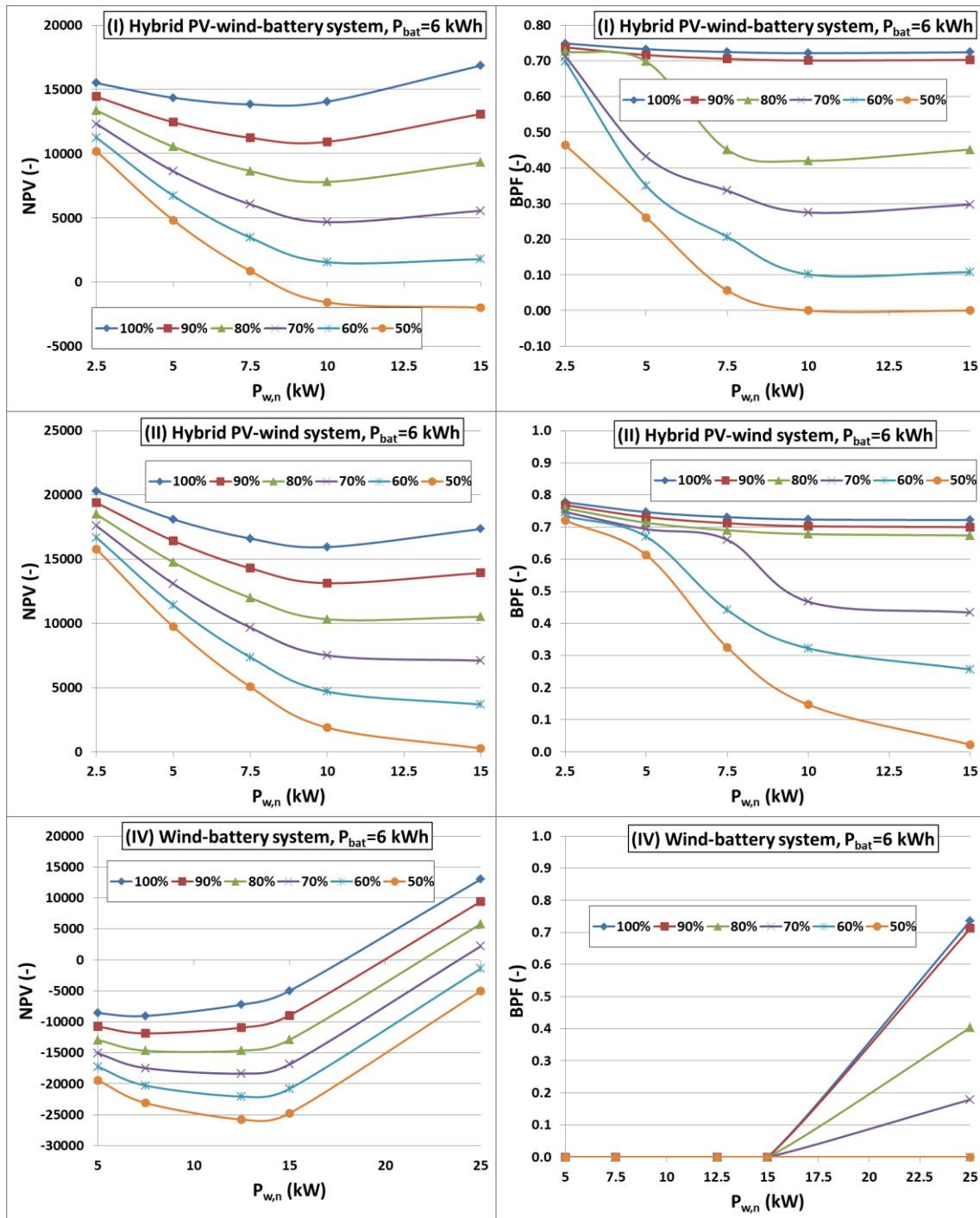
Figure 14. *NPV trend as a function of the wind power for different wind tax deductions and system configurations with a battery capacity of 6 kWh.*

Figure 15 reports, for an intermediate load of 2.5 kW and system configurations (I), (II) and (III) equipped with a PV system and a battery capacity of 6 kWh, the NPV and BPF trends by varying the PV power for different levels of incentives of the PV system.

Chapter 3   **A novel energy economic-environmental**
multi-criteria decision-making
in the optimization of a hybrid renewable system
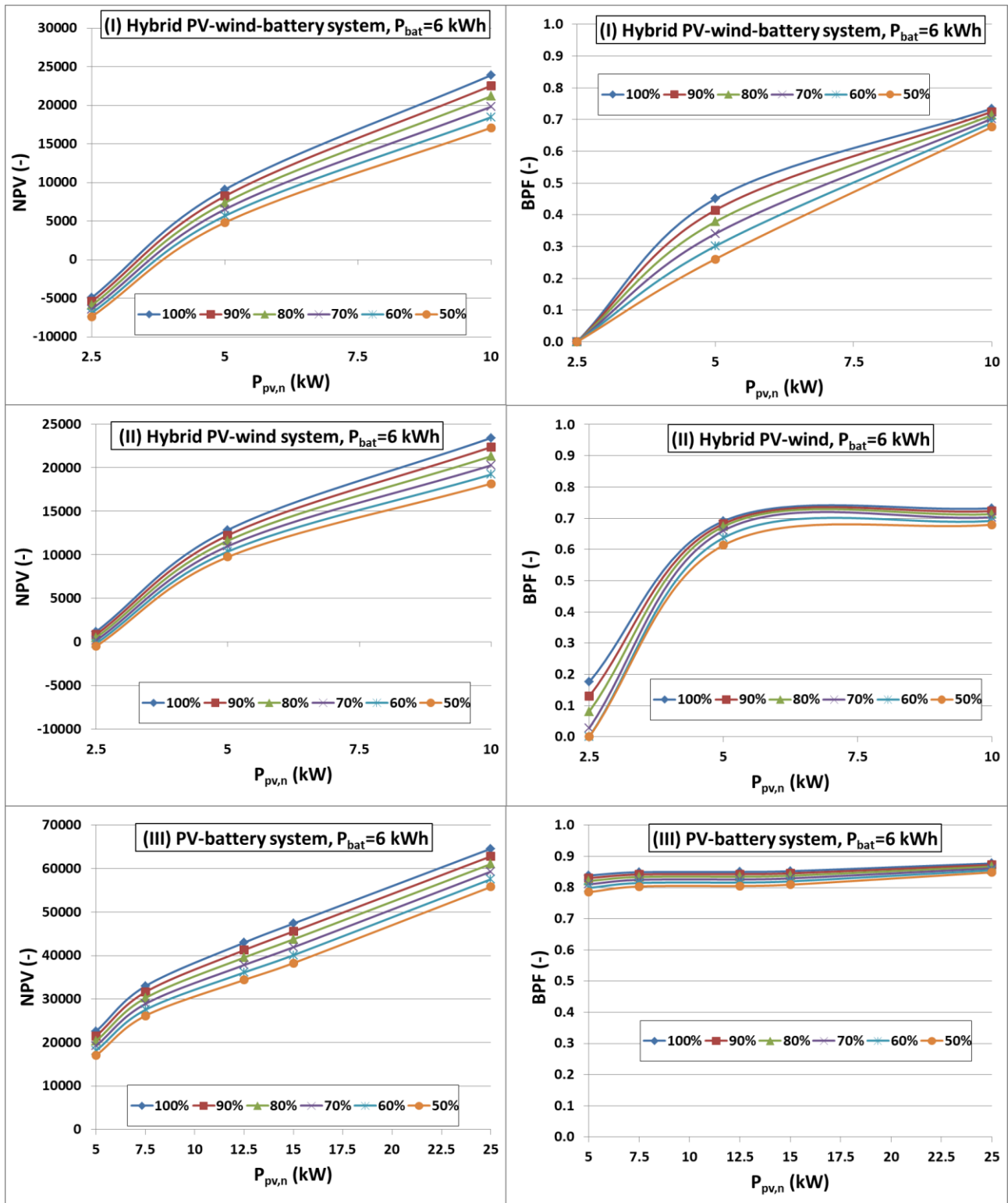
Figure 15. *NPV trend as a function of the PV power for different PV tax deductions and system configurations with a battery capacity of 6 kWh.*

Unlike the previous results, the NPV and BFP trends, by varying the PV power, remain unchanged for the different levels of PV incentives. In addition, the effect of the increase in the PV incentives is less important compared to the increase of wind system ones. In general, for all system configurations, both the NPV and BPF increase as the PV power grows. This growth is very important for the NPV of all the system configurations and the BPF of configuration (I). Instead, the BPF of configuration

Chapter 3

**A novel energy economic-environmental
multi-criteria decision-making
in the optimization of a hybrid renewable system**

(II), for PV power higher than 5 kW, remain constant and that of configuration (III) is not determined by the PV power.

The previous results were obtained by maintaining unchanged battery capacity. The analysis was made again by considering also a reduction and an increase in battery capacity, by considering values of 2 kWh and 10 kWh respectively. Figures 16 and 17 regard the NPV and BPF trends by varying the wind power for different levels of incentives of the wind system.
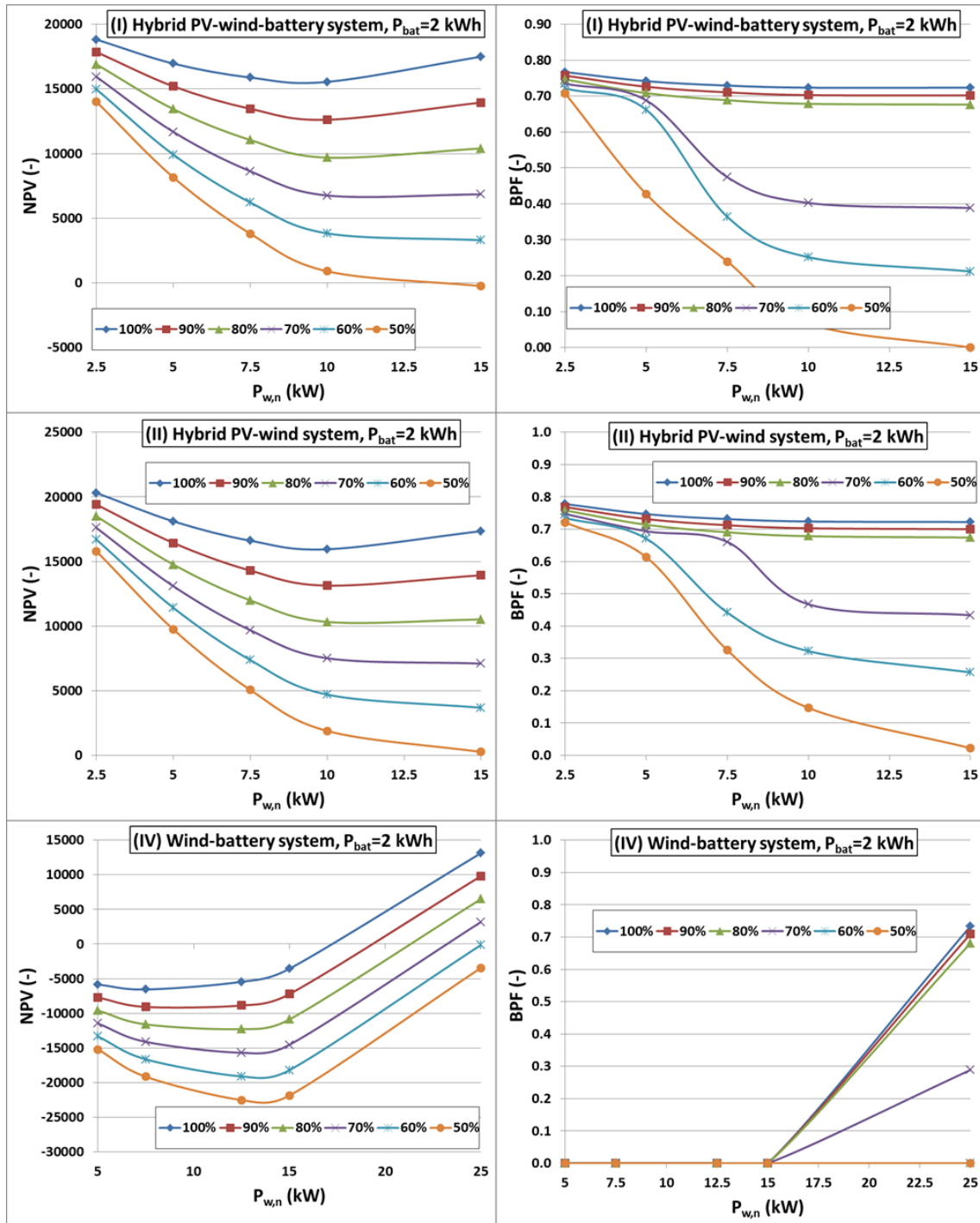
Figure 16. *NPV trend as a function of the wind power for different wind tax deductions and system configurations with a battery capacity of 2 kWh.*

Chapter 3

**A novel energy economic-environmental
multi-criteria decision-making
in the optimization of a hybrid renewable system**
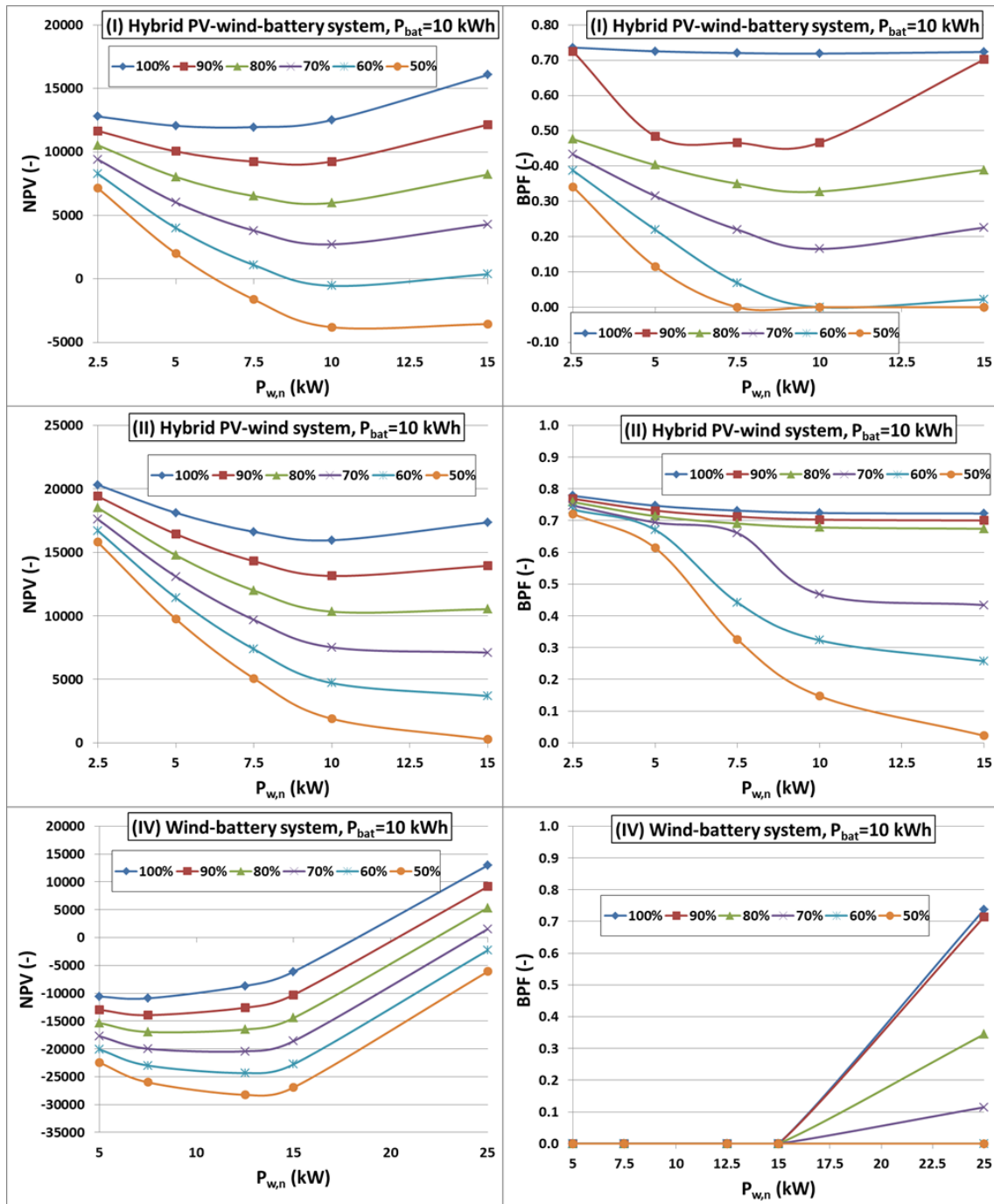
Figure 17. NPV trend as a function of the wind power for different wind tax deductions and system configurations with a battery capacity of 10 kWh.

Compared to the study developed with a battery capacity of 6 kWh, the following statements can be highlighted:

- A reduction up 2 kWh does not lead to any qualitative difference on the NPV and BPF trends for all system configurations; in this case, for system configuration (I), an increase in tax deductions for wind power of 2.5 kW does not produce substantial BPF improvements, while an increase up 80% for wind powers higher than 7.5 kW would allow obtaining a substantial BPF increase.

Chapter 3   **A novel energy economic-environmental**
multi-criteria decision-making
in the optimization of a hybrid renewable system

- An increase up to 10 kWh modifies qualitatively only the BFP for system configuration (I). In particular, the trends for tax reductions of 80% and 90% present minimum values. In this case, an increase in tax deduction leads almost always to substantial BPF improvements.

Figs. 18 and 19 regard the NPV and BPF trends by varying the PV power for different levels of incentives of the PV system.
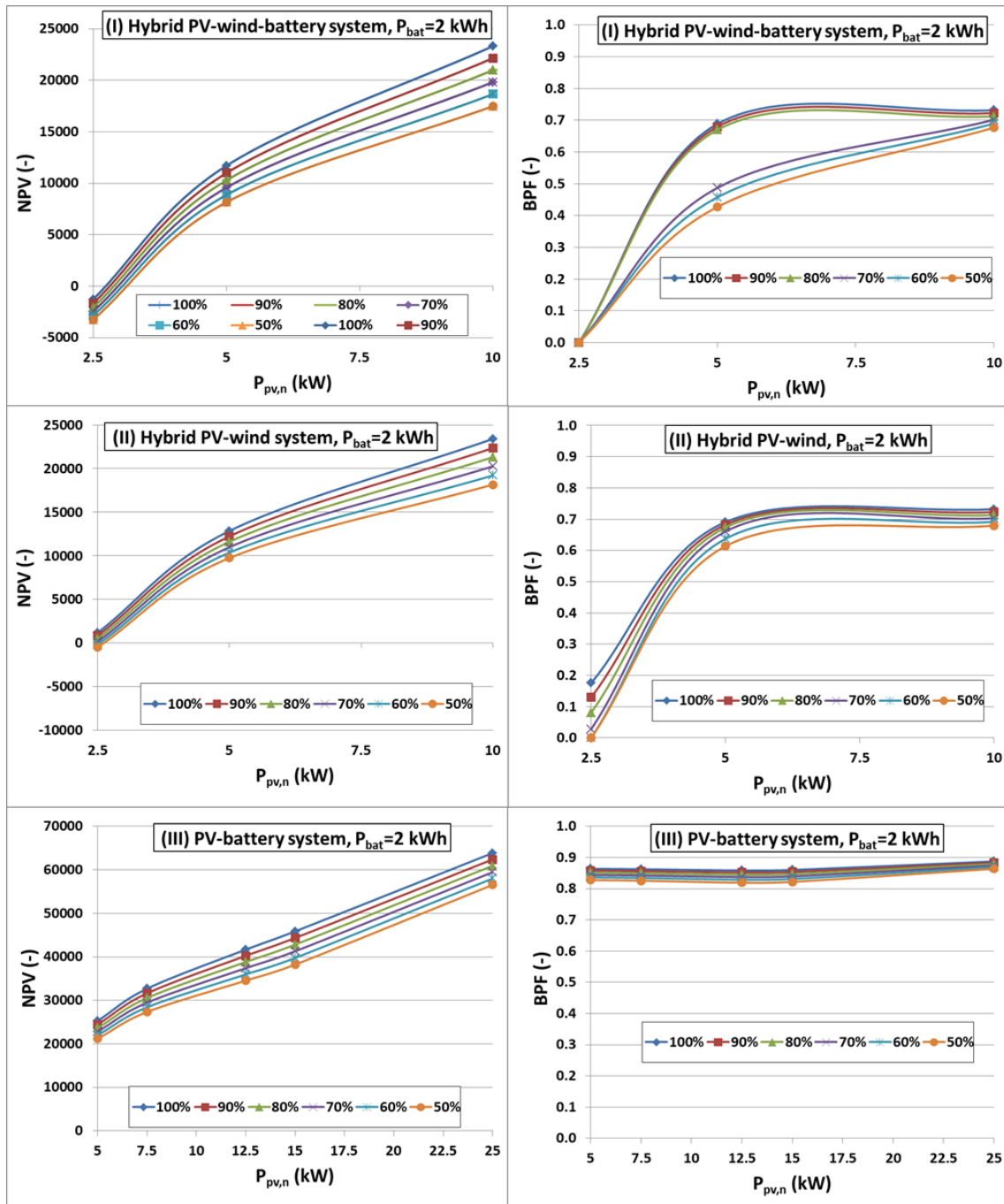
Figure 18. *NPV trend as a function of the PV power for different PV tax deductions and system configurations with a battery capacity of 2 kWh.*

Chapter 3

A novel energy economic-environmental
multi-criteria decision-making
in the optimization of a hybrid renewable system
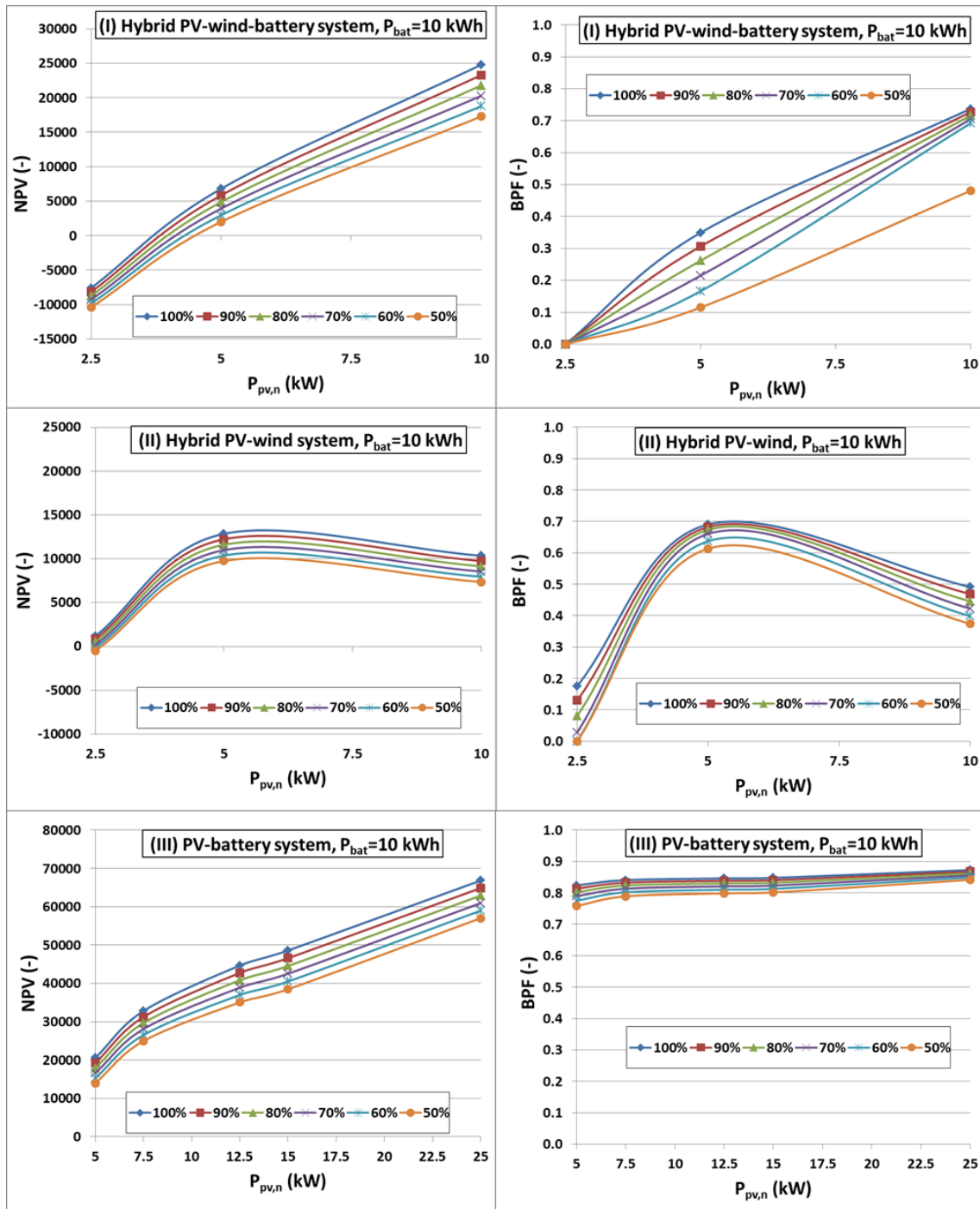
Figure 19. *NPV trend as a function of the PV power for different PV tax deductions and system configurations with a battery capacity of 10 kWh.*

Compared to the study developed with a battery capacity of 6 kWh, the following statements can be highlighted:

- A reduction up 2 kWh does not lead to any qualitative difference on the NPV and BPF trends for all system configurations; the only noticeable modification regards the BPF of the system configuration (I), which for a PV power higher than 5 kW highlights a sharp increase by passing from 70 % to 80% of tax deductions since with 80% the replacement of the battery at the fifteenth year does not lead again to a negative value of the NPV. For this reason, the BPF of the cases 80%, 90% and 100% for a PV power higher than 5 kW remain almost constant.

Chapter 3   **A novel energy economic-environmental**
multi-criteria decision-making
in the optimization of a hybrid renewable system

- An increase up to 10 kWh modifies the NPV and BFP trends of the system configuration (II), which have a trend by varying the PV power with a maximum value. An increase from 50% to 60% of tax deductions for a PV power of 10 kW of the system configuration (I) leads to a significant BPF growth since the NPV does not become negative as a consequence of the battery replacement.

3.2. Impact of technological development of the battery system

The current researches deem it essential to find better methods to store energy efficiently with the development of a battery able to extend the cycle life. Considering the new technological developments in this sector, further analysis was developed, for the system configurations with battery storage, by varying the lifespan of the battery N_{bat} from 15 years to 30 years.

For this analysis, the recent researches developed at the Zentrum für Sonnenenergie- und Wasserstoff Forschung Baden-Württemberg ZSW (Centre for Solar Energy and Hydrogen Research Baden-Württemberg) [62] on enhanced lithium-ion batteries were considered. The new batteries can perform also more than 10000 complete charging and discharging cycles, namely more than 27.4 years of lifespan by considering charge/discharge periodicity of a day, were considered. These lithium-ion batteries are intended for use in electric vehicles and as solar and wind power storage systems.

Table 15 shows the powers of the PV and wind generator for the case a), b) and c) considered. Fig. 20 shows, for an intermediate load of 2.5 kW, the NPV and BPF variations as a function of the battery power installed in the case of a battery lifespan of 15 years and 30 years.

Table 15. *PV and wind powers considered for the study of the effect produced by the battery replacement.*

Case	System configuration	PV power (kW)	Wind power (kW)
a)	System configuration (I)	5	5
	System configuration (III)	5	0
	System configuration (IV)	0	5
b)	System configuration (I)	10	10
	System configuration (III)	7.5	0
	System configuration (IV)	0	7.5
c)	System configuration (I)	10	10
	System configuration (III)	12.5	0
	System configuration (IV)	0	12.5

Chapter 3

**A novel energy economic-environmental
multi-criteria decision-making
in the optimization of a hybrid renewable system**
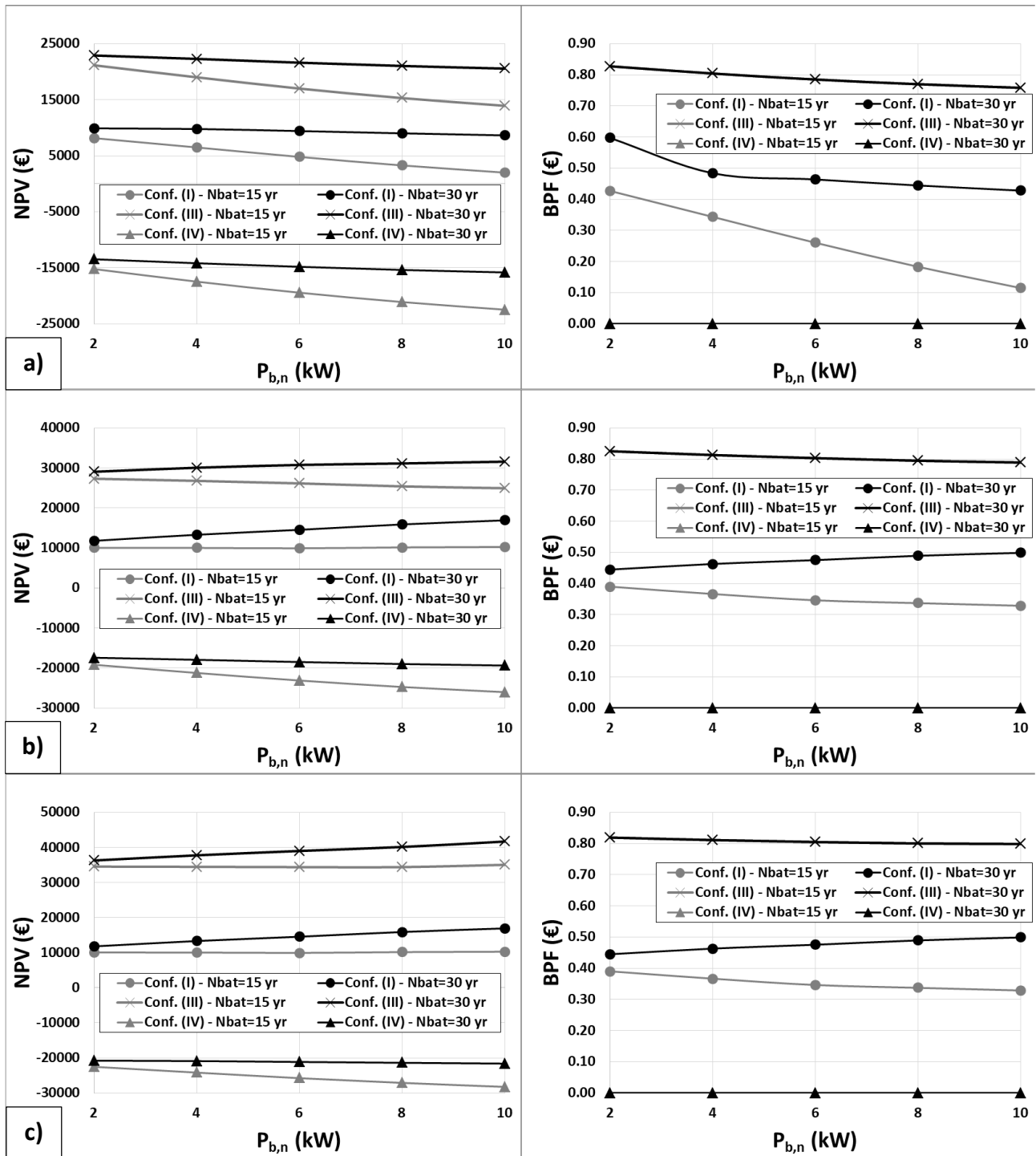
Figure 20. *NPV and BPF trends as a function of the battery power installed for system configuration (I), (III) and (IV) for a battery lifespan of 15 years and 30 years in the case of low PV and wind powers case a) and of high PV and wind powers case b) and c).*

In the case a), for a specific battery power installed, the battery lifespan increase gives rise to a constant NPV growth for all three configurations, and this rise is higher by increasing the battery powers. On the one hand, the battery lifespan increase allows making the investment even more convenient in the case of system configurations (I) and (III), while on the other hand, it does not permit the investment of a wind-battery system to be repaid, as the NPV remains negative. These results are also reflected in the BPF, which presents a substantial increase by raising the battery

Chapter 3

**A novel energy economic-environmental
multi-criteria decision-making
in the optimization of a hybrid renewable system**

lifespan only for system configuration (I). For system configuration (III), the NPV increases without a BPF growth and, for system configuration (IV), BPF is nil for each battery power value. The BPF in the presence of advanced battery storage systems is higher than that of conventional battery storage systems only when the cost of the conventional battery substitution at the 15th year make again negative the NPV. There are two Payback Periods PP in this case, of which only the highest must be considered. By avoiding the battery substitution only, the lowest PP is present by allowing to increase the BPF.

In the case b) and c), namely by considering PV and wind powers higher than those of case a), the NPV of system configurations (I) and (III) equipped with a PV system undergoes a growth, while that of system configuration (IV) shows a reduction. Also in these cases, a battery lifespan of 30 years permits to increase NPV and this growth is higher by increasing the battery power. A noticeable difference between the presence of advanced or conventional battery systems is represented by the NPV trend of system configuration (III), which without the battery replacement highlights an increasing trend by raising the battery power. The BPF of cases b) and c), for system configuration (I) is almost the same as that of case a) without any improvement caused by the use of advanced batteries. For system configuration (III), increasing growth of the BPF is registered by raising the battery power with the presence of advanced battery systems. In addition, in the case b) and c) with advanced batteries, the BFP presents an increasing trend unlike to case a). Finally, in the case of system configuration (IV), the results of case b) and c) remain unchanged compared to those of case a).

4. Conclusions

A novel benchmark procedure was developed consisting of width energy, economic and environmental analysis based on a parametric analysis for the evaluation of a set of indicators and subsequently multi-objective analysis. The entire PV-wind-battery system configuration, PV-wind, PV-battery and wind-battery system sub-configurations, by varying the size of each component and by considering different loads, are considered. The case study has highlighted that there is no system configuration and a combination of nominal powers of the components that, simultaneously, assures:

- from an energy point of view, a high load satisfaction, high utilization of the energy produced and high utilization of the nominal power installed;
- from an economic point of view, the maximum convenience;
- from an environmental point of view, the maximum abatement of CO_2.

Instead, for each specific load, by selecting a suitable system configuration and combining proper values of powers of the components, it is possible to identify three sets of trade-off Pareto optimal system configurations, obtained by comparing the economic convenience with each of the three energy indicators. Some of these configurations belong to all the three sets of trade-off optimal configurations and others that fall within at least two sets of trade-off optimal configurations. Furthermore, some of the latter, in addition to complying with the economic objective and at least two energy objectives, assure the maximum reduction of CO_2 production.

In addition, the results were employed to make a direct comparison of the hybrid PV-wind-battery system with the other three system configurations, each devoid of one of the three components. The comparison of the complete system and the three sub-systems was made in the same conditions,

Chapter 3   **A novel energy economic-environmental**
multi-criteria decision-making
in the optimization of a hybrid renewable system

namely for fixed loads and by maintaining unchanged the powers of the system components that have not been removed. In particular, the results show

- the removal of the storage system leads to: an increase in the system operating time in nominal conditions; a decrease in the load satisfaction, energy produced employed to satisfy the load and economic investment profitability; instead, the CO_2 savings remain substantially unchanged.
- the removal of the wind system leads to: an increase in the load satisfaction, energy produced employed to satisfy the load, and economic investment profitability; a decrease in the CO_2 savings; instead, the system operating time in the nominal conditions undergoes modifications that are the function of the specific value of the load and battery capacity;
- the removal of the PV system leads to: an increase in the load satisfaction, energy produced employed to satisfy the load; a decrease in the economic investment profitability and CO_2 savings; instead, the system operating time in the nominal conditions undergoes modifications that are the function of the specific value of the load and battery capacity;

The procedure developed and the results obtained by means of the use of previous statements and the direct comparison of the configuration without a PV system and that without a wind system has also allowed the identification of the renewable source more appropriate for the loads considered. In particular, the employment of the solar source is the most suitable to maximize the load satisfaction, use of the energy generated, economic investment profitability and to reduce the environmental impact, while the use of the wind source leads to a greater system operating time in the nominal power conditions.

The final analysis related to the study of the impact of the national incentives of the PV and wind systems and of the impact of the technological development of the battery storage system has highlighted the need to develop specific incentives for wind systems to make them competitive in terms of diffusion compared to PV systems in the field of building applications. Their penetration in the market and their economic convenience in a hybrid system is strictly connected also to the current research for the development of battery systems with a higher lifespan.

As demonstrated by the detailed comparisons and analysis developed of the different system configurations, this procedure is proposed as a standard for the next researches in order to provide analogous results in other applications, namely for other load typology and climate conditions. In these conditions, a direct comparison of the future researches that will be developed worldwide can be made and a uniform database can be created.

References

[1] Alkhalidi, L. Qoaider, A. Khashman, Abdel Rahman Al-Alami, Said Jiryes, Energy and water as indicators for sustainable city site selection and design in Jordan using smart grid, Sustainable Cities and Society, Volume 37, 2018, Pages 125-132, ISSN 2210-6707, https://doi.org/10.1016/j.scs.2017.10.037.

[2] J. C. Solano, L. Olivieri, E. Caamaño-Martín, Assessing the potential of PV hybrid systems to cover HVAC loads in a grid-connected residential building through intelligent control, Applied Energy, Volume 206, 2017, Pages 249-266, ISSN 0306-2619, https://doi.org/10.1016/j.apenergy.2017.08.188.

[3] D. B. Richardson, Electric vehicles and the electric grid: A review of modeling approaches, Impacts, and renewable energy integration, Renewable and Sustainable Energy Reviews, Volume 19, 2013, Pages 247-254, ISSN 1364-0321, https://doi.org/10.1016/j.rser.2012.11.042.

[4] D. Mazzeo, Nocturnal electric vehicle charging interacting with a residential photovoltaic-battery system: a 3E (energy, economic and environmental) analysis, Energy, Volume 168, 2019, Pages 310-331, ISSN 0360-5442, https://doi.org/10.1016/j.energy.2018.11.057.

Chapter 3

**A novel energy economic-environmental
multi-criteria decision-making
in the optimization of a hybrid renewable system**

[5] L. Liu, F. Kong, X. Liu, Y. Peng, Q. Wang, A review on electric vehicles interacting with renewable energy in smart grid, Renewable and Sustainable Energy Reviews, Volume 51, 2015, Pages 648-661, ISSN 1364-0321, https://doi.org/10.1016/j.rser.2015.06.036.

[6] C. Roselli, M. Sasso, Integration between electric vehicle charging and PV system to increase self-consumption of an office application, Energy Conversion and Management, Volume 130, 2016, Pages 130-140, ISSN 0196-8904, https://doi.org/10.1016/j.enconman.2016.10.040.

[7] D. Mazzeo, Solar and wind assisted heat pump to meet the building air conditioning and electric energy demand in the presence of an electric vehicle charging station and battery storage, Journal of Cleaner Production, Volume 213, 2019, Pages 1228-1250, ISSN 0959-6526, https://doi.org/10.1016/j.jclepro.2018.12.212.

[8] D. Mazzeo, N. Matera, G. Oliveti, Interaction between a wind-PV-battery-heat pump trigeneration system and office building electric energy demand including vehicle charging, 2018 IEEE International Conference on Environment and Electrical Engineering and 2018 IEEE Industrial and Commercial Power Systems Europe (EEEIC / I&CPS Europe), Palermo, Italy. DOI: 10.1109/EEEIC.2018.8493710.

[9] S. Sinha, S.S. Chandel, Review of recent trends in optimization techniques for solar photovoltaic–wind based hybrid energy systems, Renewable and Sustainable Energy Reviews, Volume 50, 2015, Pages 755-769, ISSN 1364-0321, https://doi.org/10.1016/j.rser.2015.05.040.

[10] Mahesh, K.S. Sandhu, Hybrid wind/photovoltaic energy system developments: Critical review and findings, Renewable and Sustainable Energy Reviews, Volume 52, 2015, Pages 1135-1147, ISSN 1364-0321, https://doi.org/10.1016/j.rser.2015.08.008.

[11] S. Cao, K. Klein, S. Herkel, K. Sirén, Approaches to enhance the energy performance of a zero-energy building integrated with a commercial-scale hydrogen fueled zero-energy vehicle under Finnish and German conditions, Energy Conversion and Management, Volume 142, 2017, Pages 153-175, ISSN 0196-8904, https://doi.org/10.1016/j.enconman.2017.03.037.

[12] Vanhoudt, D. Geysen, B. Claessens, F. Leemans, L. Jespers, J. Van Bael, An actively controlled residential heat pump: Potential on peak shaving and maximization of self-consumption of renewable energy, Renewable Energy, Volume 63, 2014, Pages 531-543, ISSN 0960-1481, https://doi.org/10.1016/j.renene.2013.10.021.

[13] W. Stanek, T. Simla, W. Gazda, Exergetic and thermo-ecological assessment of heat pump supported by electricity from renewable sources, Renewable Energy, Volume 131, 2019, Pages 404-412, ISSN 0960-1481, https://doi.org/10.1016/j.renene.2018.07.084.

[14] B.B Nakomčić-Smaragdakis., N.G Dragutinović, Hybrid renewable energy system application for electricity and heat supply of a residential building, Thermal Science, Volume 20, 2016, Pages 695-706, ISSN 0354-9836, DOI: 10.2298/TSCI150505144N.

[15] Park, S.J. Kwon, Towards a Sustainable Island: Independent optimal renewable power generation systems at Gadeokdo Island in South Korea, Sustainable Cities and Society, Volume 23, 2016, Pages 114-118, ISSN 2210-6707, https://doi.org/10.1016/j.scs.2016.02.017.

[16] M. Hossain, S. Mekhilef, L. Olatomiwa, Performance evaluation of a stand-alone PV-wind-diesel-battery hybrid system feasible for a large resort center in South China Sea, Malaysia, Sustainable Cities and Society, Volume 28, 2017, Pages 358-366, ISSN 2210-6707, https://doi.org/10.1016/j.scs.2016.10.008.

[17] T. Tu, G.P. Rajarathnam, A.M. Vassallo, Optimization of a stand-alone photovoltaic–wind–diesel–battery system with multi-layered demand scheduling, Renewable Energy, Volume 131, 2019, Pages 333-347, ISSN 0960-1481, https://doi.org/10.1016/j.renene.2018.07.029.

[18] L.S.A. Grande, I. Yahyaoui, S.A. Gómez, Energetic, economic and environmental viability of off-grid PV-BESS for charging electric vehicles: Case study of Spain, Sustainable Cities and Society, Volume 37, 2018, Pages 519-529, ISSN 2210-6707, https://doi.org/10.1016/j.scs.2017.12.009.

Chapter 3   **A novel energy economic-environmental**
multi-criteria decision-making
in the optimization of a hybrid renewable system

[19]   Can Duman, Önder Güler, Techno-economic analysis of off-grid PV/wind/fuel cell hybrid system combinations with a comparison of regularly and seasonally occupied households, Sustainable Cities and Society, Volume 42, 2018, Pages 107-126, ISSN 2210-6707, https://doi.org/10.1016/j.scs.2018.06.029.

[20]   D. Akinyele, Techno-economic design and performance analysis of nanogrid systems for households in energy-poor villages, Sustainable Cities and Society, Volume 34, 2017, Pages 335-357, ISSN 2210-6707, https://doi.org/10.1016/j.scs.2017.07.004.

[21]   León-Vargas, M. García-Jaramillo, E. Krejci, Pre-feasibility of wind and solar systems for residential self-sufficiency in four urban locations of Colombia: Implication of new incentives included in Law 1715, Renewable Energy, Volume 130, 2019, Pages 1082-1091, ISSN 0960-1481, https://doi.org/10.1016/j.renene.2018.06.087.

[22]   M.A.M. Ramli, A. Hiendro, Y. A. Al-Turki, Techno-economic energy analysis of wind/solar hybrid system: Case study for western coastal area of Saudi Arabia, Renewable Energy, Volume 91, 2016, Pages 374-385, ISSN 0960-1481, https://doi.org/10.1016/j.renene.2016.01.071.

[23]   V. Bakić, M. Pezo, Ž. Stevanović, M. Živković, B. Grubor, Dynamical simulation of PV/Wind hybrid energy conversion system, Energy, Volume 45, Issue 1, 2012, Pages 324-328, ISSN 0360-5442, https://doi.org/10.1016/j.energy.2011.11.063.

[24]   S. Ahmadi, S. Abdi, Application of the Hybrid Big Bang–Big Crunch algorithm for optimal sizing of a stand-alone hybrid PV/wind/battery system, Solar Energy, Volume 134, 2016, Pages 366-374, ISSN 0038-092X, https://doi.org/10.1016/j.solener.2016.05.019.

[25]   O. Nadjemi, T. Nacer, A. Hamidat, H. Salhi, Optimal hybrid PV/wind energy system sizing: Application of cuckoo search algorithm for Algerian dairy farms, Renewable and Sustainable Energy Reviews, Volume 70, 2017, Pages 1352-1365, ISSN 1364-0321, https://doi.org/10.1016/j.rser.2016.12.038.

[26]   Buonomano, F. Calise, M. Dentice d'Accadia, M. Vicidomini, A hybrid renewable system based on wind and solar energy coupled with an electrical storage: Dynamic simulation and economic assessment, Energy, Volume 155, 2018, Pages 174-189, ISSN 0360-5442, https://doi.org/10.1016/j.energy.2018.05.006.

[27]   Askarzadeh, L. dos Santos Coelho, A novel framework for optimization of a grid independent hybrid renewable energy system: A case study of Iran, Solar Energy, Volume 112, 2015, Pages 383-396, ISSN 0038-092X, https://doi.org/10.1016/j.solener.2014.12.013.

[28]   J. B. Fulzele, M.B. Daigavane, Design and Optimization of Hybrid PV-Wind Renewable Energy System, Materials Today: Proceedings, Volume 5, Issue 1, Part 1, 2018, Pages 810-818, ISSN 2214-7853, https://doi.org/10.1016/j.matpr.2017.11.151.

[29]   Q. Huang, Y. Shi, Y. Wang, L. Lu, Y. Cui, Multi-turbine wind-solar hybrid system, Renewable Energy,Volume 76, 2015, Pages 401-407, ISSN 0960-1481, https://doi.org/10.1016/j.renene.2014.11.060.

[30]   S. Sinha, S.S. Chandel, Improving the reliability of photovoltaic-based hybrid power system with battery storage in low wind locations, Sustainable Energy Technologies and Assessments, Volume 19, 2017, Pages 146-159, ISSN 2213-1388, https://doi.org/10.1016/j.seta.2017.01.008.

[31]   C. Li, X. Ge, Y. Zheng, C. Xu, Y. Ren, C. Song, C. Yang, Techno-economic feasibility study of autonomous hybrid wind/PV/battery power system for a household in Urumqi, China, Energy, Volume 55, 2013, Pages 263-272, ISSN 0360-5442, https://doi.org/10.1016/j.energy.2013.03.084.

[32]   A. Kaabeche, M. Belhamel, R. Ibtiouen, Sizing optimization of grid-independent hybrid photovoltaic/wind power generation system, Energy, Volume 36, Issue 2, 2011, Pages 1214-1222, ISSN 0360-5442, https://doi.org/10.1016/j.energy.2010.11.024.

[33]   A. Kaabeche, R. Ibtiouen, Techno-economic optimization of hybrid photovoltaic/wind/diesel/battery generation in a stand-alone power system, Solar Energy, Volume 103, 2014, Pages 171-182, ISSN 0038-092X, https://doi.org/10.1016/j.solener.2014.02.017.

Chapter 3

A novel energy economic-environmental
multi-criteria decision-making
in the optimization of a hybrid renewable system

[34]   K. Anoune, A. Laknizi, M. Bouya, A. Astito, A. Ben Abdellah, Sizing a PV-Wind based hybrid system using deterministic approach, Energy Conversion and Management, Volume 169, 2018, Pages 137-148, ISSN 0196-8904, https://doi.org/10.1016/j.enconman.2018.05.034.

[35]   N. Ghorbani, A. Kasaeian, A. Toopshekan, L. Bahrami, A. Maghami, Optimizing a hybrid wind-PV-battery system using GA-PSO and MOPSO for reducing cost and increasing reliability, Energy, Volume 154, 2018, Pages 581-591, ISSN 0360-5442, https://doi.org/10.1016/j.energy.2017.12.057.

[36]   V. Behravesh, A. A. Foroud, R. Keypour, Optimal sizing methodology for photovoltaic and wind hybrid rooftop generation systems in residential low voltage distribution networks, Solar Energy, Volume 173, 2018, Pages 17-33, ISSN 0038-092X, https://doi.org/10.1016/j.solener.2018.07.054.

[37]   M. Gökçek, C. Kale, Techno-economical evaluation of a hydrogen refuelling station powered by Wind-PV hybrid power system: A case study for İzmir-Çeşme, International Journal of Hydrogen Energy, Volume   43,   Issue   23,   2018,   Pages   10615-10625,   ISSN   0360-3199, https://doi.org/10.1016/j.ijhydene.2018.01.082.

[38]   A. Maleki, M. G. Khajeh, M. Ameri, Optimal sizing of a grid independent hybrid renewable energy system incorporating resource uncertainty, and load uncertainty, International Journal of Electrical Power &   Energy   Systems,   Volume   83,   2016,   Pages   514-524,   ISSN   0142-0615, https://doi.org/10.1016/j.ijepes.2016.04.008.

[39]   L. Bilir, N. Yildirim, Modeling and performance analysis of a hybrid system for a residential application,   Energy,   Volume   163,   2018,   Pages   555-569,   ISSN   0360-5442, https://doi.org/10.1016/j.energy.2018.08.089.

[40]   M. Kottek, J. Grieser, C. Beck, B. Rudolf, F. Rubel, World Map of the Köppen-Geiger climate classification updated, Meteorologische Zeitschrift 15.3, 2006, Pages 259-263. DOI: 10.1127/0941-2948/2006/0130.

[41]   S. Cao, K. Sirén, Impact of simulation time-resolution on the matching of PV production and household electric demand, Applied Energy, Volume 128, 2014, Pages 192-208, ISSN 0306-2619, https://doi.org/10.1016/j.apenergy.2014.04.075.

[42]   A. Ayala-Gilardón, M. Sidrach-de-Cardona, L. Mora-López, Influence of time resolution in the estimation of self-consumption and self-sufficiency of photovoltaic facilities, Applied Energy, Volume 229, 2018, Pages 990-997, ISSN 0306-2619, https://doi.org/10.1016/j.apenergy.2018.08.072.

[43]   E.J. Hoevenaars, Curran A. Crawford, Implications of temporal resolution for modeling renewables-based power systems, Renewable Energy, Volume 41, 2012, Pages 285-293, ISSN 0960-1481, https://doi.org/10.1016/j.renene.2011.11.013.

[44]   TRNSYS; Version 17. (2012) Solar Energy Laboratory University of Wisconsin-Madison: Madison, WI, USA.

[45]   D. Mazzeo, G. Oliveti, C. Baglivo, P. M. Congedo, Energy reliability-constrained method for the multi-objective optimization of a photovoltaic-wind hybrid system with battery storage, Energy, Volume 156, 2018, Pages 688-708, ISSN 0360-5442, https://doi.org/10.1016/j.energy.2018.04.062.

[46]   S.A. Klein, W.A. Beckman, J.W. Mitchell, TRNSYS 17 (a TRaNsient System Simulation program): Mathematical reference, vol. 4, rapport, University of Wisconsin-Madison, 2012

[47]   B. Fry, Simulation of Grid-Tied Building Integrated Photovoltaic Systems. M. S. Thesis –Solar Energy Laboratory, University of Wisconsin, Madison: 1998.

[48]   P. J. A. Quinlan, Time series modeling of hybrid wind photovoltaic diesel power systems. M. S. Thesis –Solar Energy Laboratory, University of Wisconsin, Madison: 1996.

[49]   S. Sinha, S.S. Chandel, Review of software tools for hybrid renewable energy systems, Renewable and Sustainable Energy Reviews, Volume 32, 2014, Pages 192-205, ISSN 1364-0321, https://doi.org/10.1016/j.rser.2014.01.035.

Chapter 3

A novel energy economic-environmental
multi-criteria decision-making
in the optimization of a hybrid renewable system

[50]   H. Sharma, É. Monnier, G. Mandil, P. Zwolinski, S. Colasson, Comparison of environmental assessment methodology in hybrid energy system simulation software, Procedia CIRP, Volume 80, 2019, Pages 221-227, ISSN 2212-8271, https://doi.org/10.1016/j.procir.2019.01.007.

[51]   S. Sichilalu, T. Mathaba, X. Xia, Optimal control of a wind–PV-hybrid powered heat pump water heater, Applied Energy, Volume 185, Part 2, 2017, Pages 1173-1184, ISSN 0306-2619, https://doi.org/10.1016/j.apenergy.2015.10.072.

[52]   L. Al-Ghussain, H. Ahmed, Fa. Haneef, Optimization of hybrid PV-wind system: Case study Al-Tafilah cement factory, Jordan, Sustainable Energy Technologies and Assessments, Volume 30, 2018, Pages 24-36, ISSN 2213-1388, https://doi.org/10.1016/j.seta.2018.08.008.

[53]   M. Baneshi, F. Hadianfard, Techno-economic feasibility of hybrid diesel/PV/wind/battery electricity generation systems for non-residential large electricity consumers under southern Iran climate conditions, Energy Conversion and Management, Volume 127, 2016, Pages 233-244, ISSN 0196-8904, https://doi.org/10.1016/j.enconman.2016.09.008.

[54]   G. Mulder, D. Six, B. Claessens, T. Broes, N. Omar, J. Van Mierlo, The dimensioning of PV-battery systems depending on the incentive and selling price conditions, Applied Energy, Volume 111, 2013, Pages 1126-1135, ISSN 0306-2619, https://doi.org/10.1016/j.apenergy.2013.03.059.

[55]   C. Jones, V. Peshev, P. Gilbert, S. Mander, Battery storage for post-incentive PV uptake? A financial and life cycle carbon assessment of a non-domestic building, Journal of Cleaner Production, Volume 167, 2017, Pages 447-458, ISSN 0959-6526, https://doi.org/10.1016/j.jclepro.2017.08.191.

[56]   J. Zhang, H. Cho, R. Luck, P.J. Mago, Integrated photovoltaic and battery energy storage (PV-BES) systems: An analysis of existing financial incentive policies in the US, Applied Energy, Volume 212, 2018, Pages 895-908, ISSN 0306-2619, https://doi.org/10.1016/j.apenergy.2017.12.091.

[57]   C. Yuan, S. Liu, Y. Yang, D. Chen, Z. Fang, L. Shui, An analysis on investment policy effect of China's photovoltaic industry based on feedback model, Applied Energy, Volume 135, 2014, Pages 423-428, ISSN 0306-2619, https://doi.org/10.1016/j.apenergy.2014.08.103.

[58]   G. Simpson, J. Clifton, Testing Diffusion of Innovations Theory with data: Financial incentives, early adopters, and distributed solar energy in Australia, Energy Research & Social Science, Volume 29, 2017, Pages 12-22, ISSN 2214-6296, https://doi.org/10.1016/j.erss.2017.04.005.

[59]   Servizio Elettrico Nazionale - Servizio di maggior tutela SEN (National Electric Service - Protected categories market), Rome (Italy), Website: https://www.servizioelettriconazionale.it/it-IT, last access: 30/10/2018.

[60]   Gestore dei Servizi Energetici GSE (Manager of Energy Services), Rome (Italy), Website: https://www.gse.it/, last access: 30/10/2018.

[61]   Legislative Decree N.49/2014 of the Italian Parliament – Photovoltaic panel classified as "WEEE", enactment of the European Directive 2012/19/EU on the Waste of electric and electronic equipment (WEEE).

[62]   Zentrum für Sonnenenergie- und Wasserstoff-Forschung Baden-Württemberg (ZSW) (Center for Solar Energy and Hydrogen Research Baden-Württemberg), Website: https://www.zsw-bw.de, 30/10/2018.

[63]   Revenue Agency, Rome (Italy), Website: https://www.agenziaentrate.gov.it, last access: 30/10/2018.

[64]   Istituto Nazionale di Statistica ISTAT (National Institute of Statistics), Rome (Italy), Website: https://www.istat.it/en, last access: 30/10/2018.

[65]   European Central Bank (ECB), Frankfurt (Germany), Website: https://www.ecb.europa.eu/, last access: 30/10/2018.

[66]   Autorità di Regolazione per Energia Reti e Ambiente (Italian Regulatory Authority for Energy, Networks and Environment) ARERA, Italy, Website: https://www.arera.it, last access: 30/10/2018.

Chapter 3   **A novel energy economic-environmental
multi-criteria decision-making
in the optimization of a hybrid renewable system**

[67]   Ministero dell'Ambiente e della Tutela del Territorio e del Mare MATTM (Ministry of the Environment and Protection of Land and Sea), Italy, Website: http://www.minambiente.it, last access: 30/10/2018.

[68]   P. Limleamthong, G. Guillén-Gosálbez, Rigorous analysis of Pareto fronts in sustainability studies based on bilevel optimization: Application to the redesign of the UK electricity mix, Journal of Cleaner Production,   Volume   164,   2017,   Pages   1602-1613,   ISSN   0959-6526, https://doi.org/10.1016/j.jclepro.2017.06.134.

[69]   L. G. Acuña, R. V. Padilla, A. S. Mercado, Measuring reliability of hybrid photovoltaic-wind energy systems: A new indicator, Renewable Energy, Volume 106, 2017, Pages 68-77, ISSN 0960-1481, https://doi.org/10.1016/j.renene.2016.12.089.

Nomenclature

Symbols

BPF	benefit period fraction (-)
c_{bat}	battery degradation factor (%/year)
c_{PV}	PV degradation factor (%/year)
C	cash flow (€)
C_n	yearly charge/discharge cycles made by the battery (-)
C_{max}	maximum charge/discharge cycles in the battery lifespan (-)
CF	capacity factor of the hybrid system (Wh/Wh)
$CO_{2,ahs}$	CO_2 emissions in the absence of a hybrid system (kg)
$CO_{2,phs}$	CO_2 emissions in the presence of a hybrid system (kg)
$(CO_2)_{sav,hs}$	CO_2 emission savings in the presence of a hybrid system (kg)
e_{dtl}	energy fraction sent directly to the load (-)
e_{fb}	energy fraction drawn from the battery (-)
e_{fg}	energy fraction drawn from the grid (-)
e_g	energy fraction produced by the generators (-)
e_{tb}	energy fraction sent to the battery (-)
e_{tg}	energy fraction in excess sent to the grid (-)
E_g	yearly energy produced by the generators (Wh)
E_L	yearly energy required by the load (Wh)
E_{tl}	yearly energy produced sent to the load (Wh)
f_E	electrical emission factor (kg/Wh)
$f_{pv,w}$	photovoltaic-wind fraction (-)
$f_{u,g}$	utilization factor of the generated energy (-)
$f_{u,hs}$	normalized capacity factor (-)
i_r	real interest rate (-)
I	initial investment (€)
I_{mp}	Current at the maximum power point (A)
N	investment lifespan (years)
N_{bat}	battery lifespan (years)
N_{PV}	PV lifespan (years)
NPV	net present value (€)
P(t)	power (W)
$P_{b,n}$	nominal battery power (W)
$P_g(t)$	overall power generated (W)
$P_{fb}(t)$	power drawn from the battery (W)

Chapter 3   **A novel energy economic-environmental**
multi-criteria decision-making
in the optimization of a hybrid renewable system

$P_{fg}(t)$ power drawn from the grid (W)

$P_L(t)$ power required by the load (W)

P_{mp} power at the maximum power point (W)

P_n overall nominal power of the hybrid system (W)

$P_{pv}(t)$ power produced by the photovoltaic generator (W)

$P_{pv,eff}(t)$ effective power produced by the photovoltaic generator (W)

$P_{pv,n}$ nominal power of the photovoltaic generator (W)

$P_{tb}(t)$ power sent to the battery (W)

$P_{tg}(t)$ power in excess sent to the grid (W)

$P_{tl}(t)$ power produced sent to the load (W)

$P_w(t)$ power produced by the wind generator (W)

$P_{w,eff}(t)$ effective power produced by the wind generator (W)

$P_{w,n}$ nominal power of the wind generator (W)

PI   profitability index (-)

PP   payback period (years)

r   discount rate (-)

R_d discount factor (-)

SOC   state of charge of the battery (Wh)

t   time (s)

T   number of hours in a year (hours)

V_{mp} voltage at the maximum power point (V)

Greek letters

$\eta_{DC/DC}$ DC/DC converter efficiency (-)

$\eta_{AC/DC}$ AC/DC rectifier efficiency (-)

η_{bat} battery efficiency (-)

η_{inv} inverter efficiency (-)

η_{reg} regulator efficiency (-)

τ τ-th year of the investment (year)

Subscripts

i   i-th cash flow

max   maximum value

pv   related to the photovoltaic system

w   related to the wind system

Chapter 4

**Nocturnal electric vehicle charging
interacting with a residential photovoltaic-battery system:
a 3E (energy, economic and environmental) analysis**

Chapter 4

Nocturnal electric vehicle charging interacting with a residential photovoltaic-battery system: a 3E (energy, economic and environmental) analysis

Chapter 4

Nocturnal electric vehicle charging interacting with a residential photovoltaic-battery system: a 3E (energy, economic and environmental) analysis

Chapter 4

Nocturnal electric vehicle charging interacting with a residential photovoltaic-battery system: a 3E (energy, economic and environmental) analysis

Abstract

Increasing costs of petroleum derivatives, limitations on pollutant emissions and development of photovoltaic (PV) and electrical storage systems make it possible to spread the use of electrically powered vehicles.

In this work, a 3E (energy, economic and environmental) feasibility study was carried out regarding a nocturnal electric vehicle (EV) charging in a residential user. In particular, three different EV charging scenarios were considered: use of the grid; use of a grid-connected PV system with a storage battery; use of a grid-connected PV system with a storage battery in the presence also of a residential user. Two sub-scenarios were examined that foresee the purchase of the EV as an alternative to a vehicle powered, respectively, by petrol and diesel.

By considering different daily average distances travelled, a parametric study was developed in order to assess the influence of the size of the PV and storage system on the load satisfaction and solar energy utilization, economic convenience and emission savings.

In general, it is not possible to simultaneously comply with all the 3E objectives and constraints. However, it is possible to select optimal EV-PV-battery combinations from a unique point of view or those that lead to a trade-off.

Keywords: Electric vehicle; Photovoltaic; Battery Storage; Energy reliability; Economic feasibility; Emission savings

- A PV-battery system coupled with nocturnal electric vehicle charging was analysed.
- Energy, economic and environmental feasibility study was developed.
- The electric vehicle was considered as an alternative to diesel and petrol vehicles.
- The absence and presence of an electric residential load were taken into account.
- Different daily distances travelled and PV-battery system sizes were investigated

Chapter 4

**Nocturnal electric vehicle charging
interacting with a residential photovoltaic-battery system:
a 3E (energy, economic and environmental) analysis**

1. Introduction

The reduction of greenhouse gas emissions is seen as an important factor to accelerate and support the growth of electric vehicle (EV) use. The EV falls in the alternatively-powered vehicles category and can be seen as an element capable of promoting sustainable mobility, integrated with the energy sector, for the improvement of air quality levels in urban environments [1]. The global EV stock surpassed 2 million vehicles in 2016 after crossing the 1 million thresholds in 2015 [2]. In the next decades, by taking into account country targets, original equipment manufacturer announcements and scenarios on EV deployment, EVs could reach a market share considerably higher than that nowadays, implying an exponential growth of EVs in relation to new registrations. This will lead to an EV stock that will range between 9 million and 20 million by 2020, and between 40 million and 70 million by 2025 [2-4]. For instance, in the first quarter of 2018, fuel types of new vehicles sold registered the following variations compared with 2017: diesel -17%; petrol +14.6%; electric +47% [5]. Moreover, this development could be supported by new EU-level regulation such as the Clean Mobility Package, which plans to reduce vehicle emissions by 30% by 2030 compared to 2021 [6]. The feasibility of EV spread is closely linked to their purchase and maintenance costs, the price of "fuel", autonomy with a complete recharge cycle, distribution of the charging infrastructure, as well as to the time necessary for a full recharge. The spread of EVs could change the electrical energy peak demand and, more generally, the hourly consumption profile, which is of particular interest from the point of view of the electricity grid. This causes degradation of power quality and destabilizing the electrical system [7]. The behaviour of the consumer (namely when the owner of an EV performs charging) and the recharging infrastructure (namely as an EV is recharged) are the main factors that determine the impact of EV charging on the total profile of the electrical energy demand. The economic feasibility and environmental sustainability of EV strongly depend on the required energy generation mode.

The coupling between charging of the EV batteries and electricity generated from renewable energy sources, owing to also the depletion of fossil fuels and the required increase of distributed generation systems, could be an interesting solution to reduce the utility grid overload [8] and to extend the production of energy from renewable sources to the transport sector. The use of renewable energy sources, such as solar or wind energy, is the most feasible solution for urban areas [9]. In particular, the photovoltaic (PV) has undergone development and has experienced the largest growth of all renewable energy sources in recent years making it accessible to a wider audience owing to a reduction in the costs of PV panels [10-11]. The main issue of PV generation is its intermittence [12-13] with an alternated energy generation, which leads to the need to modify the power supplied by thermoelectric plants or to disconnect the renewable generators to comply with the instantaneous energy balance on the electricity grid. The mutual benefits of coupling the PV non-dispatchable and time-floating energy supply with the controllable and storable energy required by the EVs [14] allows for all these issues to be overcome. In this way, the grid does not have to integrate a large PV capacity and does not need a great integration to satisfy the increasing EV demand [15]. In addition, the combination of PVs and EVs is advantageous since it allows for higher penetration in the market of both technologies [16]. On the one hand, EVs could be used as storage devices and dispatchable loads, helping the grid maintaining the supply-demand balance and allowing a larger renewable penetration [17]. On the other hand, PV production could also enable a larger diffusion of EVs.

A growing recent literature has treated the EV-PV integration in power grids [15, 18-21], identifying the main technical features and issues of such integration in the city, residential or office scale. In

Chapter 4

**Nocturnal electric vehicle charging
interacting with a residential photovoltaic-battery system:
a 3E (energy, economic and environmental) analysis**

accordance with these reviews, the objectives of the researches on the subject can be grouped into three main categories: optimization of load satisfaction and renewable energy utilization, reduction of costs or increase profits, minimization of emissions.

By considering the market, technical and behavioural constraints, Fattori et al. [22] have concluded that a high PV power could cover only a small portion of the transportation demand if EV charging is uncontrolled determining a burden increase of electrical energy demand in the late afternoon hours. The feasibility of EV charging at workplaces in the Netherlands using solar energy was investigated [23]. For this purpose, various dynamic EV charging profiles are compared to minimize the energy drawn from the grid, by considering a first scenario in which EVs have to be charged only on weekdays and a second scenario where EVs have to be charged during the entire week. Similarly, Sasso et al. [24] analysed the EV charging during working hours by means of a PV system in an office building located in southern Italy in the presence of an electrical heat pump, used to satisfy the space heating and cooling load and a pure electrical demand (personal computers, printers, lighting, etc.) and an EV charging. For different PV peak powers (4.5–9.0 kW), EV distance per day (40–120 km) and charging mode, they assessed the primary energy saving and equivalent carbon dioxide emission reduction. Analogously, a similar investigation was addressed in the presence of also a wind system to study, in the presence and absence of battery storage, the dynamic interaction between the solar and wind energy renewable sources and the three electrical loads [25]. Instead, Coffman et al [26] have compared the lifecycle costs and greenhouse gas emissions of EVs charged by a residential solar PV, considering the interaction of EV costs with Hawaii's rapid solar PV uptake, using a scenario planning approach for future fuel and electricity prices. Other authors investigated the potential benefits of PV panels on the roof of EVs and below the windshield to increase energy capture when the vehicle is parked [27]. Recently, an optimal technical design of an off-grid PV-battery system, considering technical, economic and environmental aspects, was developed in Spain for the supply of a public charging station during the daytime [28].

The actual reliability of the PV system to supply EV charging is closely linked to the charging time during the day. A daytime charge is more appropriate to increase the self-consumed produced solar energy. This condition appears to be very probable when the EV is charged during working hours using a PV system installed in the workplace. When the EV charging time is shifted compared to the renewable energy availability time, an electrical storage system is strongly mandatory to develop a feasible combination between the two technologies. This situation appears to be very possible in the residential sector, where EV charging is planned after working hours.

Despite the growing interest in this topic in recent decades, the literature survey has shown that nowadays further researches are requested to provide worldwide qualitative and quantitative results useful to optimize PV-battery system size for EV charging simultaneously taking into account the 3E objectives. In addition, a higher number of researches regarded daytime EV charging, when the solar energy availability makes this combination quite promising. None of the above-mentioned papers analysed in-depth the effect of nocturnal EV charging by using PV and battery system in the presence and absence of a residential load.

Special attention must also be paid to the nocturnal EV charge, a scenario very likely in the residential sector, in those real estate units where users tend to move to the workplace during the daytime and then recharge the EV in the evening or at night. In these conditions, the coupling between EV-PV is feasible only in the presence of an appropriate storage system.

Chapter 4   **Nocturnal electric vehicle charging**
interacting with a residential photovoltaic-battery system:
a 3E (energy, economic and environmental) analysis

In this work, an in-depth analysis is developed regarding the energy reliability, economic rentability and emission abatement achievable by combining a PV-battery system with the nocturnal EV charging in a residential user. In particular, the self-consumed solar energy produced, the net present value of the investment and abatement of CO_2 emissions were evaluated for different daily distances travelled in various scenarios of EV charging: presence and absence of the PV-battery system, with or without electrical residential load; EV purchased as an alternative to a diesel or petrol vehicle. Furthermore, a wide range of variation of the PV power and battery capacity was considered to evaluate the effects produced on the satisfied EV load, surplus energy sent to the grid, investment profitability and reduction of emissions. For this purpose, the system configurations that comply with these objectives were selected. The PV-battery and EV coupling performance was assessed by modelling and simulating the dynamic behaviour of each component and the entire system, by considering the temporal trend of the fuel, management and maintenance costs in the Italian territory.

2. Methodology

2.1. Electric vehicle charging scenarios

In this study, the EV is charged in three different scenarios, see Figure 1:
- Scenario 1: using a "wall box" home charging station that takes energy directly from the grid;
- Scenario 2: using in part the energy sent by the PV generator and storage system, and in part that from the grid;
- Scenario 3: using in part the energy sent by the PV generator and storage system, and in part from the grid, assuming that the total electrical load also includes a residential user.
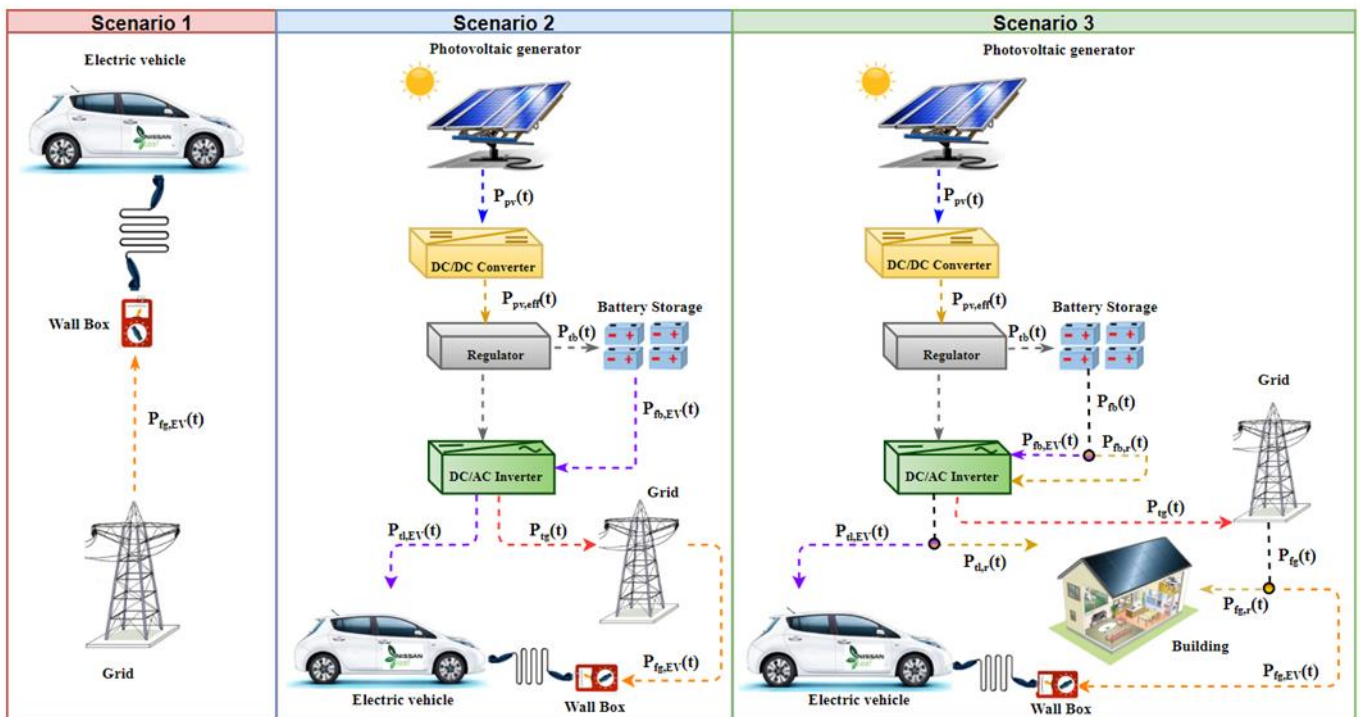
Figure 1. EV charging scenarios and power flows in various system components.

Chapter 4

**Nocturnal electric vehicle charging
interacting with a residential photovoltaic-battery system:
a 3E (energy, economic and environmental) analysis**

In scenarios 2 and 3, the energy produced by the PV generator is used to supply the electrical load, for the charging of the storage system, and the surplus energy is sent to the grid. Two economic sub-scenarios were considered for each scenario:

a) purchase of the EV as an alternative to a diesel vehicle;

b) purchase of the EV as an alternative to a petrol vehicle.

2.2 Energy model

Scenario 1: the energy analysis consists of determining the yearly energy to be taken from the grid $E_{fg,EV}$, given the yearly consumption of the EV for the yearly km travelled. Eq. (1) represents the dimensionless balance equation of the yearly energy required by the load $E_{L,EV}$:

$$1 = \frac{E_{fg,EV}}{E_{L,EV}} = e_{fg,EV} \tag{1}$$

Scenarios 2 and 3: the energy analysis consists of the evaluation of energy fluxes entering and exiting the components of the PV-battery system in the absence in scenario 2 and in the presence in scenario 3 of the residential load. The energy performances of the PV-battery system were evaluated in dynamic conditions using sophisticated mathematical models implemented in specific Types in the TRNSYS [29] environment. In particular, the following ones were used: Type 94 which uses the 5-parameter Fry model for the PV field; Type 47 which calculates the battery state of charge (SOC) at each time instant; Type 48 which models the regulator and the inverter, and the efficiency method for the static converters; Type 9 which processes climatic data; Type 16 which reports the incident solar radiation on the horizontal plane on the inclined plane; Type 25 which allows results to be printed.

With reference to Figure 1, at each time instant, the regulator compares the net power produced by the PV system, $P_{pv}(t)$, reduced by the static converter to $P_{pv,eff}(t)$ and successively by the inverter and the regulator to $P_{pv,eff}(t)\eta_{inv}\eta_{reg}$, with the instantaneous load to be supplied $P_L(t)$:

- if $P_{pv,eff}(t)\eta_{inv}\eta_{reg} > P_L(t)$, the load is completely satisfied by the power sent by the PV generator directly to the load $P_{dtl}(t)$, and the surplus power is used to charge the battery $P_{tb}(t)$ and, if this is completely charged, it is sent to the grid $P_{tg}(t)$;

- if $P_{pv,eff}(t)\eta_{inv}\eta_{reg} < P_L(t)$, the PV generator sends to the load all the power produced $P_{dtl}(t)$ and the lacking power is taken from the battery $P_{fb}(t)$ and, if necessary, from the grid $P_{fg}(t)$.

On a yearly basis, the energy balance equations required by the load in scenario 2, $E_{L,EV}$, and in scenario 3, $E_{L,EV} + E_{L,r}$, are represented respectively by Eq. (2) and Eq. (3). In these equations, the dimensionless terms e are equal to the corresponding energy E compared to the overall yearly load E_L.

$$1 = \frac{E_{dtl,EV}}{E_{L,EV}} + \frac{E_{fb,EV}\eta_{inv}}{E_{L,EV}} + \frac{E_{fg,EV}}{E_{L,EV}} = e_{dtl,EV} + e_{fb,EV} + e_{fg,EV} \tag{2}$$

$$1 = \frac{E_{dtl,EV}}{E_{L,EV} + E_{L,r}} + \frac{E_{fb,EV}\eta_{inv}}{E_{L,EV} + E_{L,r}} + \frac{E_{fg,EV}}{E_{L,EV} + E_{L,r}} + \frac{E_{dtl,r}}{E_{L,EV} + E_{L,r}} + \frac{E_{fb,r}\eta_{inv}}{E_{L,EV} + E_{L,r}} + \frac{E_{fg,r}}{E_{L,EV} + E_{L,r}}$$

$$= e_{dtl,EV} + e_{fb,EV} + e_{fg,EV} + e_{dtl,r} + e_{fb,r} + e_{fg,r} \tag{3}$$

Chapter 4

Nocturnal electric vehicle charging interacting with a residential photovoltaic-battery system: a 3E (energy, economic and environmental) analysis

In Eq. (2), the yearly electrical load required by the EV charging is, in part, satisfied by the energy produced by the PV generator sent directly to the user $E_{dtl,EV}$, in part by the energy taken from the battery $E_{fb}\eta_{inv}$, and in part by the grid $E_{fg,EV}$. Additionally, to the latter, in Eq. (3), the yearly electrical load required by the residential user is satisfied by three contributions $E_{dtl,r}$, $E_{fb,r}\eta_{inv}$ and $E_{fg,r}$. The overall yearly energy sent by the PV system and by the storage system to the EV is $E_{tl,EV} = E_{dtl,EV} + E_{fb,EV}\,\eta_{inv}$, while that sent to the residential user is $E_{tl,r} = E_{dtl,r} + E_{fb,r}\eta_{inv}$. Consequently, the overall yearly energy sent by the PV system and the storage system to the electricity user in scenario 2 is $E_{tl} = E_{tl,EV}$, while in scenario 3 it is $E_{tl} = E_{tl,EV} + E_{tl,r}$. Similarly, the overall energies E_{dtl}, E_{fb}, E_{fg}, and E_{tg} in scenario 2 take into consideration only the relative contribution owing to the EV, while in scenario 3 it is necessary to sum the relative contributions owing to the residential user. The same considerations can be extended also to dimensionless energy contributions e_{dtl}, e_{fb}, and e_{fg}.

In Eq. (3), the sum ($e_{dtl,EV} + e_{fb,EV} + e_{fg,EV}$) represents the fraction of overall electrical energy that is required by the EV, or rather $E_{L,EV}/(E_{L,EV} + E_{L,r})$, while the sum ($e_{dtl,r} + e_{fb,r} + e_{fg,r}$) represents the fraction of overall electrical energy that is required by residential user, that is $E_{L,r}/(E_{L,EV} + E_{L,r})$.

2.3 Economic model

To evaluate the cost-effectiveness of the investments in scenarios 1, 2 and 3 and in the related sub-scenarios, the Net Present Value NPV, expressed by Eq. (4), was used:

$$NPV = -I_0 + \sum_{k=1}^{N}\sum_{h=1}^{H} S_{k,h}\left(\frac{1+g_{r,h}}{1+d}\right)^k - \sum_{k=1}^{N}\sum_{j=1}^{J} C_{k,j}\left(\frac{1+g_{c,j}}{1+d}\right)^k - \sum_{k=1}^{N} I_k + \sum_{k=1}^{N} R_k \qquad (4)$$

Where, I_0 is the initial investment, see Eq. (5), $S_{k,h}$ savings obtained per year k for the h-th contribution, $C_{k,j}$ costs to be incurred per year k for the j-th contribution, I_k extraordinary investment per year k, see Eq. (6), R_k extraordinary revenues per year k, $g_{r,h}$ inflation rate of the h-th contribution to the total saving, $g_{c,j}$ inflation rate of the j-th contribution to the total cost, d discount rate, N investment lifespan, H number of contributions to the total saving, and J number of contributions to the total cost.

$$I_0 = (I_{EV} - I_{TV}) + I_{PV} + I_{inv} + I_{bat,PV} \qquad (5)$$

$$I_m = I_{bat,PV} + I_{inv} + I_{bat,EV} \qquad (6)$$

In the hypothesis that the costs C_k to be incurred and the savings S_k obtained per year k are constant and equal to that predicted for year k=0:

$$C_0 = C_{0,EV} + C_{0,PV} \qquad (7)$$

$$S_0 = S_{0,TV} + S_{0,PV-EV} + S_{0,PV-r} + R_{0,PV-tg} + INC_0 \qquad (8)$$

In successive years, each term of Eqs. (7) and (8), $C_{0,j}$ and $S_{0,h}$, is inflated considering the relative inflation rate $g_{c,j}$ and $g_{r,h}$.

In Eqs. (5)-(8) the various contributions represent:

Chapter 4   **Nocturnal electric vehicle charging**
interacting with a residential photovoltaic-battery system:
a 3E (energy, economic and environmental) analysis

- I_{EV} EV purchase cost, I_{TV} traditional vehicle (TV) purchase cost, I_{PV} PV system purchase and installation cost (PV generator and DC/DC static converter), I_{inv} inverter purchase cost, $I_{bat,PV}$ purchase cost of the PV storage battery;
- I_m extraordinary investment required per year k=m for the substitution of the PV battery $I_{bat,PV}$, inverter I_{inv}, and EV battery $I_{bat,EV}$;
- for k=0, $C_{0,EV}$ EV management and maintenance cost, $C_{0,PV}$ management and maintenance cost of the PV system with storage battery;
- for k=0, $S_{0,TV}$ savings for the management and maintenance of a TV, $S_{0,PV-EV}$ savings connected to the EV charging from PV, $S_{0,PV-r}$ savings related to the satisfaction of the electrical load of the residential user by means of the PV, $R_{0,PV-tg}$ revenue for the sale of electricity to the grid, INC_0 benefits for national incentives supplied for the purchase and installation of PV systems. In particular, the PV system with electrical storage installed on the roofs of buildings, like restructuring interventions, benefits from a form of incentive, i.e. tax deductions of 50% of the initial investment cost on a straight-line basis in the first 10 years of the lifespan of the system [30], see Eq. (9):

$$INC_0 = \frac{0.5(I_{PV} + I_{inv} + I_{bat,PV})}{10} \tag{9}$$

The management and maintenance costs of the EV $C_{0,EV}$ include the cost of electricity for the F23 nocturnal time band, cost of insurance, cost of road tax and cost of ordinary maintenance. The savings for the management and maintenance of the TV $S_{0,TV}$ are instead given by the cost of fuel, cost of insurance, cost of road tax and cost of ordinary maintenance.

The extraordinary revenues R_k are owing to the non-replacement of the mechanical components of TVs.

For scenario 1, the economic model requires the cancellation of all investments, costs, savings and revenues related to the PV system and the storage system. For scenarios 2 and 3, the investment lifespan is that of the PV system, since the lifespan of the EV is lower. Consequently, in the years following the end of the EV lifespan, the relative costs and savings are not considered in the calculation of the NPV. In these years, in scenario 2, the energy produced by the PV-battery system is entirely sold to the grid, determining only revenues, while in scenario 3 it continues to satisfy the sole requirement for electrical residential load and, in the case of surplus electricity production, is sold to the grid.

2.4. CO2 emissions and savings

The yearly CO_2 emissions of the TVs $CO_{2,TV}$ are calculated as a function of the related emission factor f_{TV} (kg/km) for each km travelled, Eq. (10), while the yearly CO_2 emissions of the EV $CO_{2,EV}$ depend on the electrical emission factor f_E (kg/kWh) for each kWh drawn from the grid, Eq. (11):

$$CO_{2,TV} = f_{TV} \, D \tag{10}$$

$$CO_{2,EV} = f_E \, E_{L,EV} \tag{11}$$

Chapter 4

**Nocturnal electric vehicle charging
interacting with a residential photovoltaic-battery system:
a 3E (energy, economic and environmental) analysis**

Where, D is the yearly overall distance travelled by the TV and $E_{L,EV}$ is the energy drawn from the grid required to travel the distance D.

As a consequence, in scenario 1, the yearly CO_2 savings obtained by considering the EV as an alternative to a TV are:

$$(CO_2)_{sav1} = CO_{2,TV} - CO_{2,EV} \tag{12}$$

The yearly CO_2 emissions of the electrical residential load are expressed by Eq. (13).

$$CO_{2,r} = f_E \, E_{L,r} \tag{13}$$

$CO_{2,EV}$ and $CO_{2,EV} + CO_{2,r}$ are the CO_2 emissions in the absence of a PV system in scenario 2 and 3 respectively.

In the presence of a PV generator, only a part of the energy required by the load is drawn from the grid, while the surplus energy contributes to reducing the overall emissions since it is sent to the grid. In these conditions, the yearly CO_2 emissions are:

$$CO_{2,PV} = f_E \left(E_{fg} - E_{tg} \right) \tag{14}$$

Instead, the yearly CO_2 savings owing to the PV system, both for scenario 2 and 3, are:

$$(CO_2)_{sav,PV} = f_E \left(E_{tl} + E_{tg} \right) \tag{15}$$

The overall yearly CO_2 savings in scenario 2 and 3 are:

$$(CO_2)_{sav,2-3} = (CO_2)_{sav1} + (CO_2)_{sav,PV} \tag{16}$$

2.5 Optimization problem

The dimensionless energy balance Eqs. (2) and (3) are to be used to identify the PV-battery system configurations, i.e. the PV power and the storage capacity to be installed, which guarantee values of the fraction of energy taken from the grid e_{fg} and surplus energy fraction sent to the grid e_{tg}, lower than a predetermined value. The fraction e_{tg} is defined as the ratio between the yearly surplus energy sent to the grid E_{tg} and the yearly energy required by the load E_L. The constraints on the fractions e_{fg} and e_{tg} allow avoiding, respectively, an undersizing and an oversizing of the PV power to be installed, and identifying the minimum required storage capacity. The optimal system configurations, among those selected, are characterized by the maximum NPV and CO_2 saving.

The economic and environmental optimization functions and the energy constraints can be placed in the form of Eq. (17).

$$\max \left[NPV \left(P_{pv}, C_{bat}, E_L \right), (CO_2)_{sav} \left(P_{pv}, C_{bat}, E_L \right) \right]$$

subject to constraints

Chapter 4

Nocturnal electric vehicle charging interacting with a residential photovoltaic-battery system: a 3E (energy, economic and environmental) analysis

$$e_{fg}(P_{pv}, C_{bat}, E_L) < \bar{e}_{fg} => \begin{cases} P_{pv} > \overline{P}_{pv,fg} \\ C_{bat} > \overline{C}_{bat,fg} \end{cases} \tag{17}$$

$$e_{tg}(P_{pv}, C_{bat}, E_L) < \bar{e}_{tg} => \begin{cases} P_{pv} < \overline{P}_{pv,tg} \\ C_{bat} > \overline{C}_{bat,tg} \end{cases}$$

Where, $\bar{e}_{fg}$ and $\bar{e}_{tg}$ are respectively the constraint values to be fixed as a function of the specific application, $\overline{P}_{pv,fg}$ and $\overline{C}_{bat,fg}$ are the minimum PV power and battery capacity required to comply with the e_{fg} constraint, and $\overline{P}_{pv,tg}$ and $\overline{C}_{bat,tg}$ are the maximum PV power and the minimum battery capacity required to comply with the e_{tg} constraint. In the optimization analysis, the two constraints are first applied individually and then it is evaluated if there are configurations that allow limiting them simultaneously.

3. Case study

This section shows: the measured climate data for the location considered in Section 3.1, the technical characteristics of all the system components in Section 3.2, the EV and residential loads in Section 3.3, the description of the economic sub-scenarios considered in Section 3.4, the economic and financial data, and emission factors in Section 3.5.

3.1. Climatic data

The hourly meteorological data used in the dynamic simulation of the PV-battery system were detected during the entire year 2015 at the University of Calabria, Cosenza (Italy). The climate is of a Mediterranean type, identified as Csa in the Köppen climate classification [31], and is characterized by an average value of the external air temperature of 16.87 °C and yearly solar radiation on the horizontal plane of 1580.83 kWh/m^2.

3.2. System components

The PV generator consists of modules [32] with polycrystalline silicon cells with an area of 156.5 cm^2 and efficiency in standard conditions of 15.2%. The PV inclination angle is equal to 33°, optimal in the locality considered, and it is exposed to the South. The storage system used consists of lithium-ion batteries. The technical data of all the system components shown in Figure 1 are reported in Table 1. Data are to be considered as average values through the lifespan of the PV and battery systems.

Table 1. *Technical data of the PV-battery system.*

PV module		Storage system		Inverter	
Nominal power peak P_{pv} (W)	250	Nominal capacity C_{bat} (kWh)	1	Efficiency η_{inv} (-)	0.97
Open circuit voltage (V)	37.6	Max continuous power (kW)	1-1.5	**Regulator**	
Short circuit current (A)	8.68	Max battery voltage (V)	150	Efficiency η_{reg} (-)	0.98
Voltage at the maximum power (V)	30.9	Charging efficiency η_{bat} (-)	0.98	**Static converter**	
Current at the maximum power (A)	8.10	High limit on f_{SOC} (-)	0.97	Efficiency $\eta_{DC/DC}$ (-)	0.94
Module efficiency (%)	15.2	Low limit on f_{SOC} (-)	0.1		
Nominal operative cell temperature NOCT (°C)	47.5	Charge to discharge limit (-)	0		

Chapter 4

Nocturnal electric vehicle charging interacting with a residential photovoltaic-battery system: a 3E (energy, economic and environmental) analysis

In the table, f_{SOC} is the fraction of the SOC, namely the ratio of the SOC to the nominal battery capacity C_{bat}.

An overall number of 100 different PV-battery system configurations were considered, obtained by varying the power of the PV generator from 1 kW to 10 kW with a range of 1 kW, and the battery capacity from 1 kWh to 27 kWh with an interval of 3 kWh.

3.3. Electrical load

The electrical load consists in the EV charging in scenarios 1 and 2, while for scenario 3 also the electrical residential load is considered.

3.3.1. EV charging load

The EV considered in this study is the Nissan Leaf 24 kWh, which is the most sold and competitive on the international market for the advantageous quality/cost ratio [33]. It is powered by an extremely quiet synchronous engine 109 hp/80 kW with a top speed of around 140 km/h and its dimensions are Length/Width/Height 445/117/115 cm. The EV is characterized by a charge capacity of 24 kWh, a declared autonomous range of 200 km [34] and a corresponding declared specific average consumption of 0.12 kWh/km. Instead, in the current analysis, vehicle consumptions under real-life conditions, collected and delivered by the Spritmonitor database [35], were considered. In this database, different users can introduce their consumptions for each route and the final data provided are those related to the averaged lifestyle of drivers. Spritmonitor is largely used in scientific studies, for example by the International Council on Clean Transportation (ICCT) [36] as well as the European Federation for Transport and Environment [37], owing to the substantial size and quality reached. For the Nissan Leaf 24 kWh, Spritmonitor provides a specific average consumption of 0.1714 kWh/km, obtained considering urban travels at low speeds, suburb travels at average speeds and highway travels at high speeds, and it includes the contribution of the brake energy regeneration system. As a consequence, the real consumption is significantly higher than that declared by Nissan and the real maximum distance that the Nissan Leaf can be travelled is 140 km. The vehicle is recharged in the home during the evening and nocturnal hours starting from the hour 22:00, as it was supposed that the owner is not present during daytime working hours. In accordance with the relevant European regulation [38], which defines the different charging methods, the EV is recharged in the slow mode, type 1, envisaged in a domestic private environment in alternating current at 16 A at a recharging power of 3 kW. The time required to charge the EV at constant power, in the hypothesis of a "rectangular" schedule analogously to the relevant literature [23-24, 28], can be evaluated using the Eq. (18):

$$t_{charge}(h) = \frac{\text{kWh consumed by vehicle}}{\text{Charge power (3 kW)}} \tag{18}$$

The electrical energy consumed by the Nissan Leaf battery depends on the daily kilometres travelled, gears used, speed, acceleration, breaking and gear changes. With reference to the average consumption of 0.1714 kWh/km, the time necessary to charge the vehicle depends exclusively on the daily kilometres travelled and the recharging power. Eight different daily distances travelled are considered ranging between 17.5 km and 140 km with a step of 17.5 km. A charging time of 1 hour and consumption of 3 kWh are required every 17.5 km.

Chapter 4   **Nocturnal electric vehicle charging**
interacting with a residential photovoltaic-battery system:
a 3E (energy, economic and environmental) analysis

3.3.2. Electrical residential load

The electrical residential load is relative to a family of five people, which consumes a total of 5158 kWh/year, with an average of 15 kWh per day.

To determine the hourly trend of domestic consumptions, the bill of a residential user was used. Monthly electrical consumption was divided into three-time bands F1 (Monday-Friday from 8:00 to 19:00 excluding national holidays), F2 (Monday-Friday from 19:00 to 23:00) and F3 (Monday-Friday from 23:00 to 7:00, weekends and national holidays from 00:00 to 24:00) foreseen by the Italian electrical grid [39]. Thus, the hourly trend for each month and day was reconstructed taking into consideration electricity consumption in the three-time bands and the residential electricity hourly consumption per capita in the Italian territory. The monthly electrical consumption in the three hourly time bands and yearly average hourly trend of the load requested is reported in Figure 2.
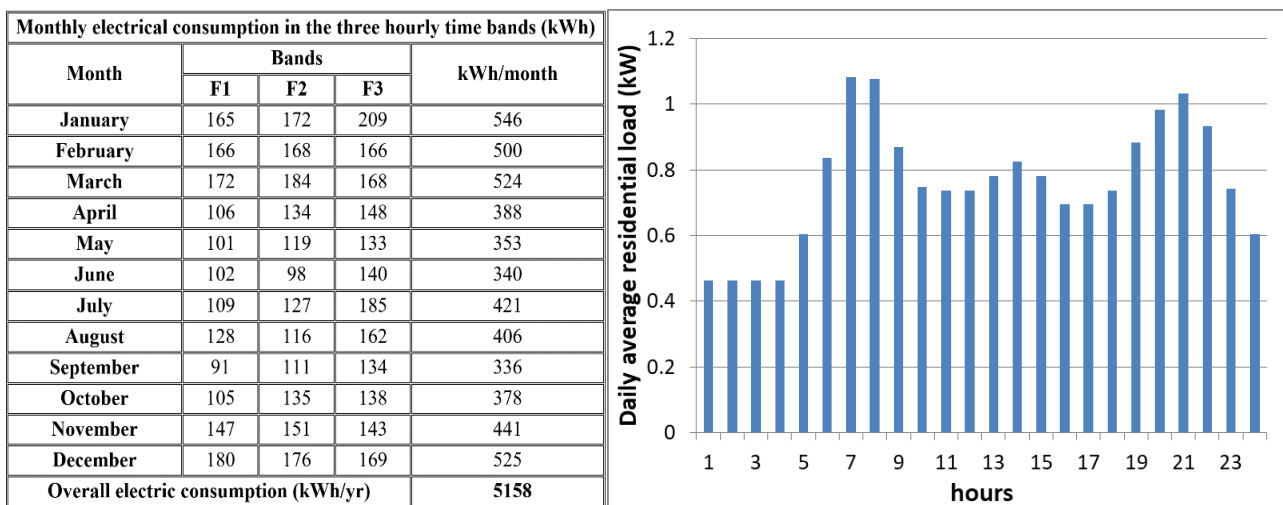
Monthly electrical consumption in the three hourly time bands (kWh)				
Month	Bands			kWh/month
	F1	F2	F3	
January	165	172	209	546
February	166	168	166	500
March	172	184	168	524
April	106	134	148	388
May	101	119	133	353
June	102	98	140	340
July	109	127	185	421
August	128	116	162	406
September	91	111	134	336
October	105	135	138	378
November	147	151	143	441
December	180	176	169	525
Overall electric consumption (kWh/yr)				5158

Figure 2. Monthly electrical consumption in the three hourly time bands and yearly average hourly trend of the electrical load for a residential user.

3.3.3. Overall electrical load for scenario 3

In scenario 3, the overall electrical load was obtained by summing the required load for the EV charging and residential user. Also, in this scenario, eight load configurations were obtained. The yearly average hourly trends for a daily average distance travelled of 17.5 km/day and 140 km/day are reported in Figure 3.

Chapter 4

**Nocturnal electric vehicle charging
interacting with a residential photovoltaic-battery system:
a 3E (energy, economic and environmental) analysis**
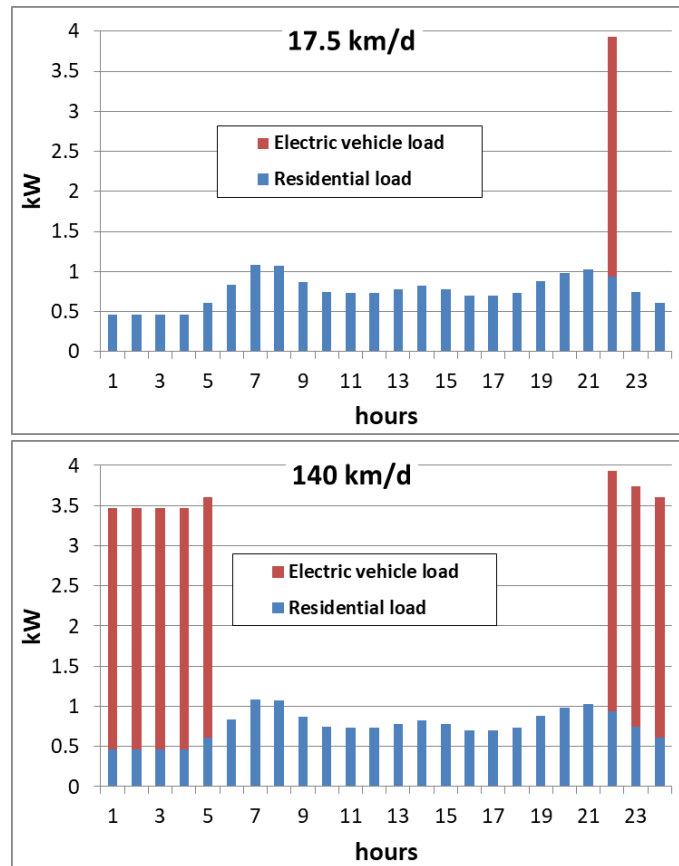
Figure 3. Yearly average hourly trend of the electrical load in scenario 3 for a daily average distance travelled of 17.5 km/day and 140 km/day.

3.4. Economic sub-scenarios

For each scenario, two economic sub-scenarios were considered:

a) purchase of the Nissan Leaf as an alternative to the diesel Nissan Micra 1.5;

b) purchase of the Nissan Leaf as an alternative to the petrol Nissan Micra 1.2.

Table 2 reports the main technical properties of the two vehicles [34] and consumptions taken from the Spritmonitor database [35].

Table 2. Technical features of the Nissan Micra 1.5 and Nissan Micra 1.2.

Traditional vehicle	Supply	Power (hp/kW)	Length/Width/Height (cm)	Consumption (l/km)
NISSAN Micra 1.5	Diesel	90/66	400/174/146	0.0576
NISSAN Micra 1.2	Petrol	90/66	400/174/146	0.0823

3.5. Economic and environmental data

This section contains all the economic and financial data necessary for the application of the NPV method described in Section 2.3, and emission factors for the CO_2 emissions evaluation.

3.5.1 Photovoltaic and storage system

The purchase and installation cost of the PV generator and the DC/DC converter is $I_{PV} = 1460 \, €/kW$, while that of the inverter is $I_{inv} = 1240 \, €/kW$. The lifespan of the PV generator is set equal to $N_{PV} = 24$ years, while that of the inverter is $N_{inv} = 12$ years, so at the end of the twelfth year of ownership it

Chapter 4

**Nocturnal electric vehicle charging
interacting with a residential photovoltaic-battery system:
a 3E (energy, economic and environmental) analysis**

is necessary to replace it. The cost of the storage battery is $I_{bat,PV} = 750$ €/kWh and it has a lifespan of $N_{bat,PV} = 12$ years [40, 41]. The PV and battery lifespan derive from the more relevant papers in the recent scientific literature, which takes into account the current technological developments in this field [42-46]. Consequently, $I_m = I_{12} = I_{bat,PV} + I_{inv} = 1990$ €/kW. The yearly maintenance and management costs of a PV system $C_{0,PV}$ are set equal to 0.8% of ($I_{PV} + I_{bat,PV} + I_{inv}$). For the calculation of $R_{0,PV\text{-}tg}$, it was considered that the surplus energy produced by the PV generator is sold, in accordance with net energy metering, to the Manager of Energy Services (*Gestore dei Servizi Energetici*, GSE) at a price of 0.039 €/kWh [47].

3.5.2 Electric and traditional vehicle

The total cost for the purchase of the Nissan Leaf 24 kWh [34] is 23910 € and for the installation of the domestic charger is 1130 €, with a total of $I_{EV} = 25040$ €. The EV lifespan is $N_{EV} = 15$ years. In the calculation of $S_{0,PV\text{-}EV}$, $S_{0,PV\text{-}r}$ and $C_{0,EV}$, the bihourly tariff is applied to the hourly cost of electrical energy of the domestic user. The bihourly tariff is the sum of the following contributions: electrical energy cost, consisting of a constant contribution and a dependent on the time band contribution; cost of the transport and management of the meter, consisting of a fixed, power installed and energy contribution (€/kWh) in relation to the kWh billed in a year; cost of system charges, taxes and VAT. As the yearly consumption is above 1800 kWh/year and falls in the 2nd category for the energy contribution, the hourly average cost of electricity is 0.176772 €/kWh for the F1 band, and 0.168432 for the F23 band [47].

The purchase cost of the diesel Nissan Micra 1.5 is $I_{TV} = 13800$ €, while the purchase cost of the petrol Nissan Micra 1.2 is $I_{TV} = 12600$ €.

In calculating $S_{0,TV}$, variable petrol and diesel fuel prices were considered. In particular, the daily values, shown in Figure 4, provided by the database of the Italian Ministry of Economic Development (MISE) [48] were employed. The yearly average prices are, respectively, 1.443 €/l and 1.282 €/l.
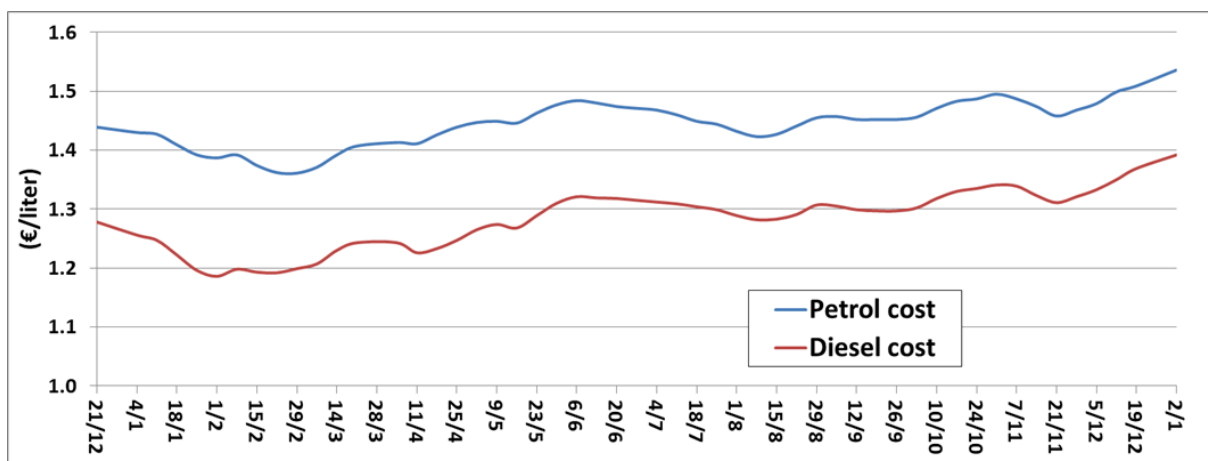
Figure 4. *Trend of petrol and diesel prices in 2016 [48]*

Regarding further contributions to the management and maintenance costs of the EV $C_{0,EV}$ and the further contributions to savings for the management and maintenance of TVs $S_{0,TV}$: the insurance of the Nissan Leaf benefits from a discount and is equal to 410 €/year, while those of the Nissan Micra 1.5 and Nissan Micra 1.2 are respectively 687 €/year and 657 €/year. The cost of road tax for the Nissan Micra 1.5 is 230.04 €/year, for the Nissan Micra 1.2 it is 241.40 €/year, while EVs are exempt

Chapter 4

**Nocturnal electric vehicle charging
interacting with a residential photovoltaic-battery system:
a 3E (energy, economic and environmental) analysis**

for the first 5 years from their registration, and in successive years it is equal to 1/4 of the cost of the corresponding petrol/diesel vehicles.

Ordinary maintenance costs have been assumed to be identical for the EV and for TVs and the differences have been calculated for extraordinary maintenance. In particular, in the calculation of R_k and I_k, extraordinary revenues and investments related to the extraordinary maintenance of the TV and EV, the replacement of components present in all three vehicles, such as the change of tires, the replacement of windscreen wipers and the coolant, the change of brake pads and brake fluid was not taken into account. As a consequence, the EV has extraordinary maintenance at no cost until the battery is replaced, with lifespan $N_{bat,EV} = 12$ years, which contributes in the calculation of $I_m = I_{12}$ with a cost of 275 €/kWh and a total cost of $I_{bat,EV} = 6000$ €. For TVs, Table 3 shows the replacement interval and the costs of the components not present in the EV used for the calculation R_k.

Table 3. Extraordinary maintenance for petrol and diesel Nissans.

Spare part	Fuel filter	Battery	Engine Oil	Distribution belt	Air Filter	Oil Filter
Substitution interval (years)	2	5	2	6	3	3
Price (€)	20	200	60	300	20	20

3.5.3 Financial parameters

The average rate of discount and general inflation for the decade 2006/2016, calculated with reference to the European Central Bank ECB [49] and the National Institute of Statistics ISTAT [50], are equal respectively to d = 1.56 % and g = 1.509 %. Instead, the average rate of inflation of the cost of electrical energy is $g_{el} = 3.50$ %, while that of petrol is $g_p = 1.60\%$ and diesel $g_d = 2.10$ %.

3.5.4 CO2 emission factors

For the environmental analysis, the CO_2 savings were calculated by considering diesel and petrol emission factors related to the two TVs considered [34], equal respectively to 103 g_{CO2}/km and 85 g_{CO2}/km. The emission factor of the electrical energy is related to the Italian average emissions of the thermoelectric plants [51] and equal to 0.531 kg_{CO2}/kWh.

4. Results and discussion

4.1. Electric and traditional vehicle consumption

Figure 5 reports, varying the daily distance travelled, the yearly consumption of electrical energy drawn from the grid, equal to the overall electrical energy required by the EV, and the fuel consumption of petrol and diesel vehicles. It can easily be seen that the electrical energy, petrol and diesel consumptions rise steadily respectively, from 1095 kWh/yr, 526 l/yr, and 368 l/yr, to 8760 kWh/yr, 4206 l/yr and 2944 l/yr, by varying the distance from 17.5 km/d to 140 km/d. The petrol consumption is slightly higher than diesel consumption.

Chapter 4

**Nocturnal electric vehicle charging
interacting with a residential photovoltaic-battery system:
a 3E (energy, economic and environmental) analysis**
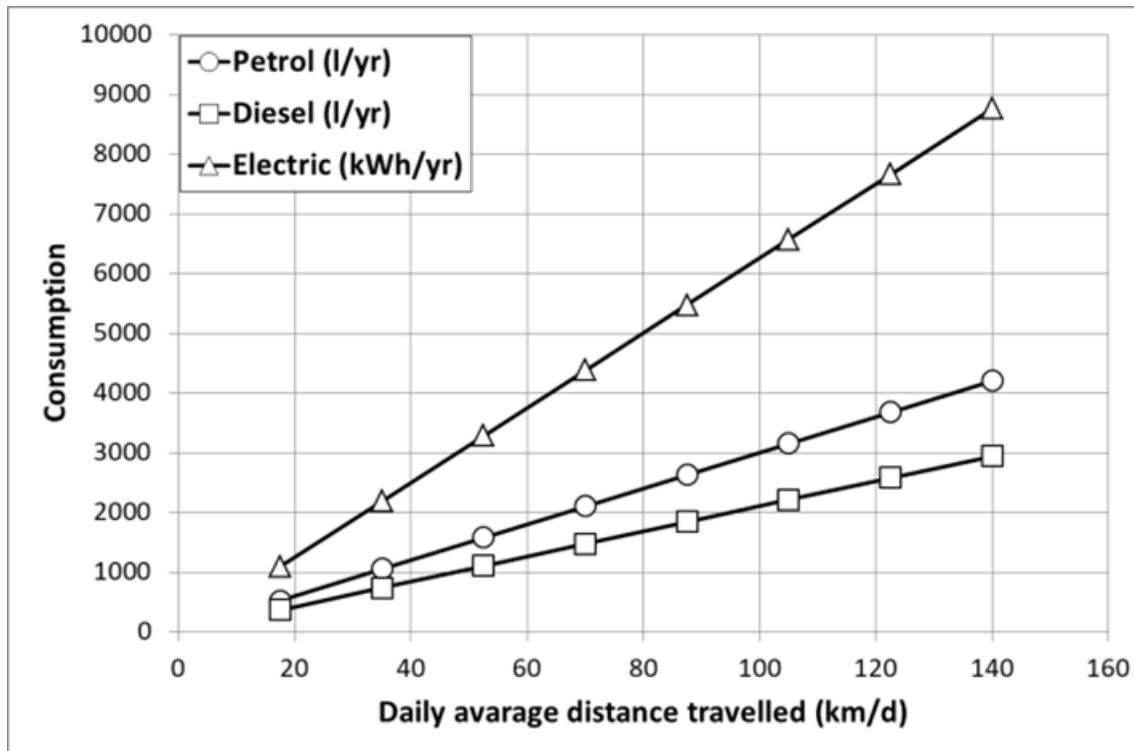
Figure 5. *Trend of consumption of electric and traditional vehicles by varying the daily distance travelled.*

4.2. Energy analysis

4.2.1. Energy performance of PV-battery system

The Figures 6-8 show, respectively, the energy sent to the load by the PV-battery system E_{tl}, energy drawn from the grid E_{fg} and surplus energy sent to the grid E_{tg}, by varying the nominal PV power P_{pv} for different battery capacities C_{bat}, in scenario 2 (blue) and scenario 3 (red). The four images of each figure are related to four different daily average distances travelled.

Chapter 4

**Nocturnal electric vehicle charging
interacting with a residential photovoltaic-battery system:
a 3E (energy, economic and environmental) analysis**
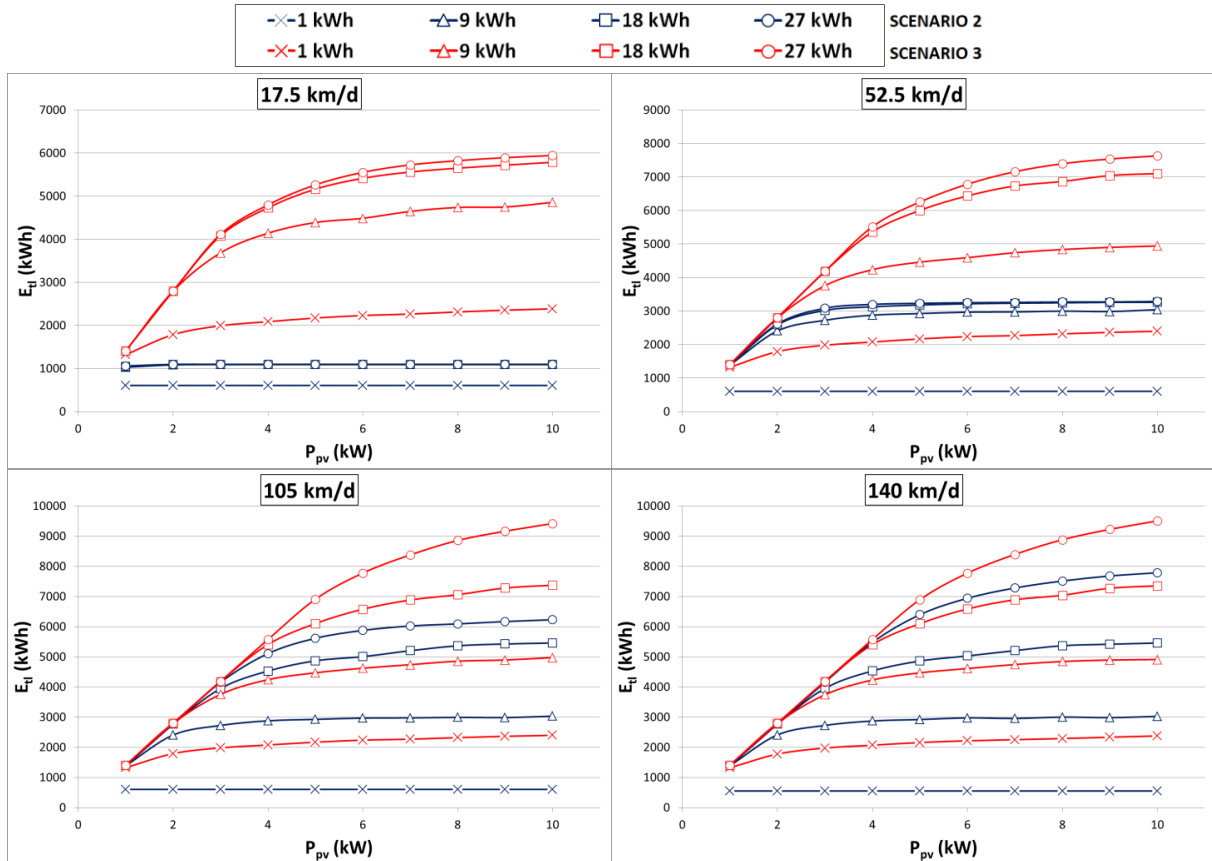
Figure 6. *Energy sent to the load by the PV-battery system for different distances, in scenarios 2 and 3, by varying the PV power and battery capacity.*

As an overall trend, it is clear that E_{tl} grows and E_{fg} decreases by increasing the nominal PV power and battery capacity. These variations are fairly rapid for low nominal PV powers and high battery capacities and gradual for high nominal PV powers and low battery capacities. Instead, Etg rises steadily by increasing the nominal PV power, and it reduces by increasing the battery capacity. In general, the greatest availability of electrical energy generated and stored, obtained by employing the highest nominal PV power and battery capacity, determines an increase of the energy sent to the load, a drop of the energy drawn from the grid and a slump in the surplus energy sent to the grid. The presence of the residential load in scenario 3 determines higher values of E_{tl} and E_{fg} and lower values of E_{tg} than those of scenario 2. The trends of E_{tl} and E_{fg} in scenario 3 vary considerably more across the values of PV powers and battery capacities than those of scenario 2. For instance, in scenario 2 for a battery capacity of 1 kWh, they remain constant in the entire range of PV powers. Instead, the qualitative trends E_{tg} are independent of the scenario considered. The variation of the daily average distance travelled only influences the values of the three energy contributions without affecting the qualitative trends. In particular, a high distance travelled lead to significant growth of E_{tl} and E_{fg}, and a sharp reduction of E_{tg}. The rate of change is more marked in scenario 2, determining a higher influence of the PV power and battery capacity on the three energy contributions

Chapter 4

**Nocturnal electric vehicle charging
interacting with a residential photovoltaic-battery system:
a 3E (energy, economic and environmental) analysis**
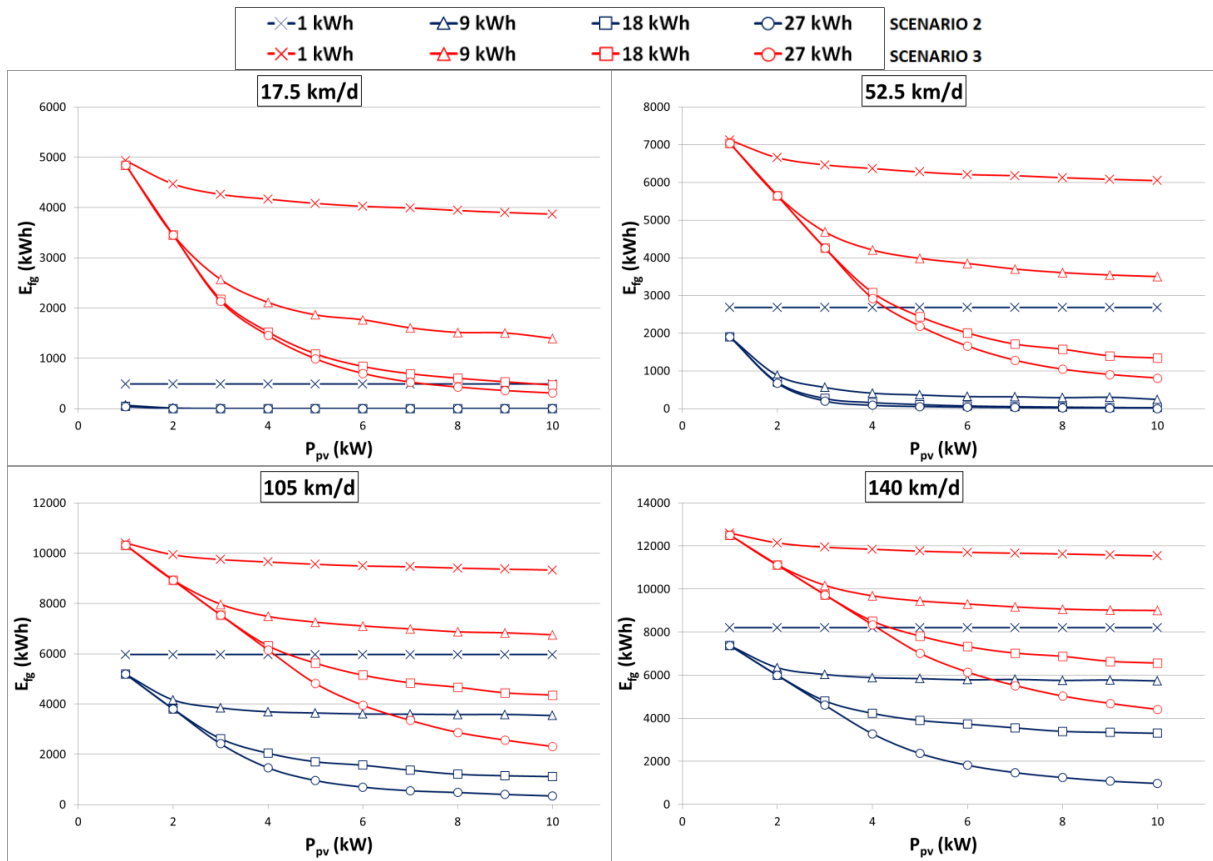
Figure 7. *Energy drawn from the grid for different distances, in scenarios 2 and 3, by varying the PV power and battery capacity.*

Chapter 4

**Nocturnal electric vehicle charging
interacting with a residential photovoltaic-battery system:
a 3E (energy, economic and environmental) analysis**
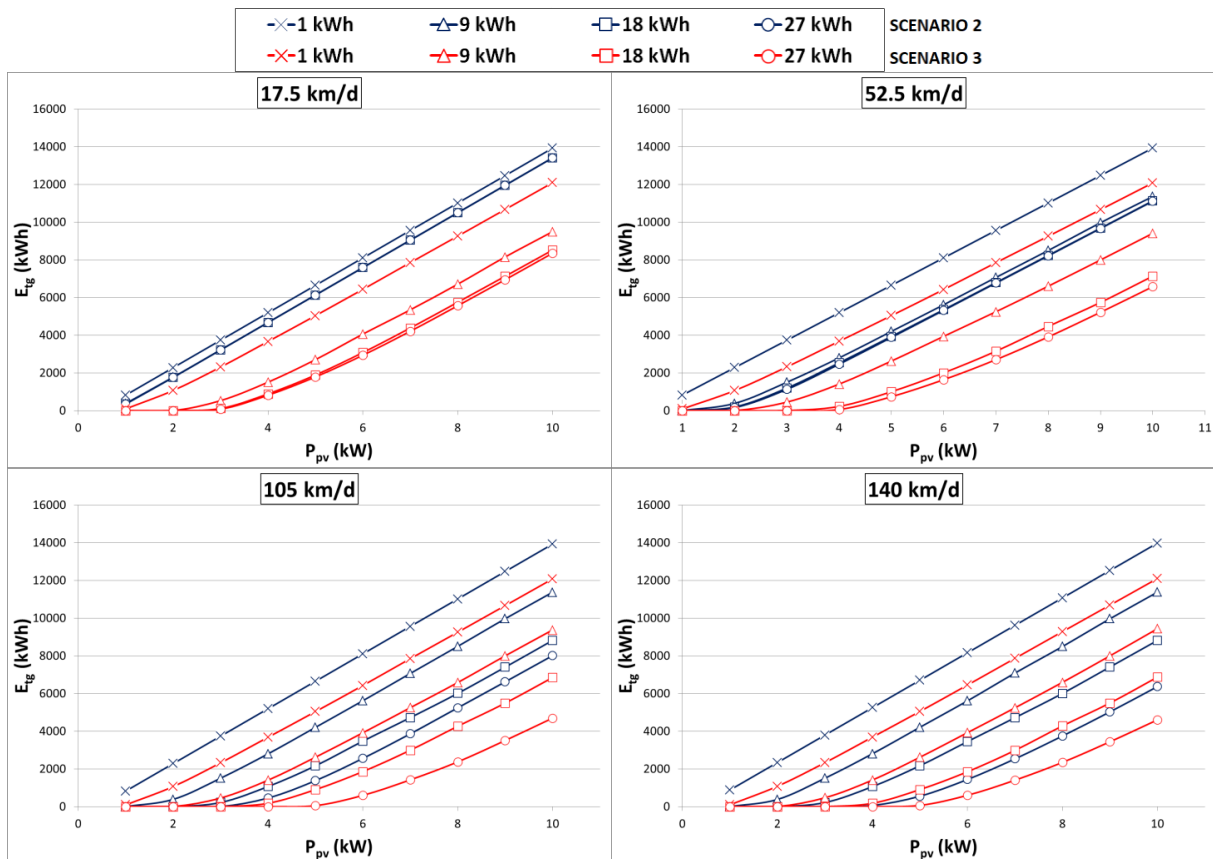
Figure 8. Surplus energy sent to the grid for different distances, in scenarios 2 and 3, by varying the PV power and battery capacity.

4.2.2. Dimensionless energy analysis

This analysis aims to identify, for each daily average distance travelled, the PV-battery configurations that assure high values of E_{tl}, and then reduced values of E_{fg}, and low values of E_{tg}. For this purpose, a dimensionless energy analysis was developed and is reported in Figures 9 and 10. The two figures, related to the minimum and maximum distance travelled of 17.5 km/d and 140 km/d, report: respectively on the top for scenario 2 and on the bottom for scenario 3, the effects produced by the variation of PV power and battery capacity on the dimensionless balance of the energy required by the load. A specific image shows the cumulative histograms of the dimensionless energy contributions that appear in Eqs. (2) and (3) respectively, for scenario 2 and 3. The sum of these contributions is always equal to one, while the surplus energy sent to the grid is the blue bar placed above the cumulative bars of the balance.

First of all, both in scenario 2 and 3, the fraction of energy produced sent directly to the load $e_{dtl,EV}$ is nil for any value of PV power, battery capacity, and distance travelled. This is owing to the nocturnal charge scheduled for the EV that does not allow direct use of the energy produced by the PV generator, but only that stored in the battery. Consequently, the fraction of energy sent to the load $e_{tl,EV}$ is equal to the fraction of energy drawn from the battery $e_{fb,EV}$, that grows by increasing the PV power and battery capacity. In scenario 3, it is evident that growth of the distance travelled leads to a higher fraction of overall energy that it is required by the EV, with a consequent increase of the sum $(e_{dtl,EV} + e_{fb,EV} + e_{fg,EV})$ and a reduction of the sum $(e_{dtl,r} + e_{fb,r} + e_{fg,r})$. This is highlighted by Figures 9 and 10 at the bottom considering the sum of red and green bars, which starting from a value of 0.18 for 17.5 km/d rises to 0.63 for 140 km/d.
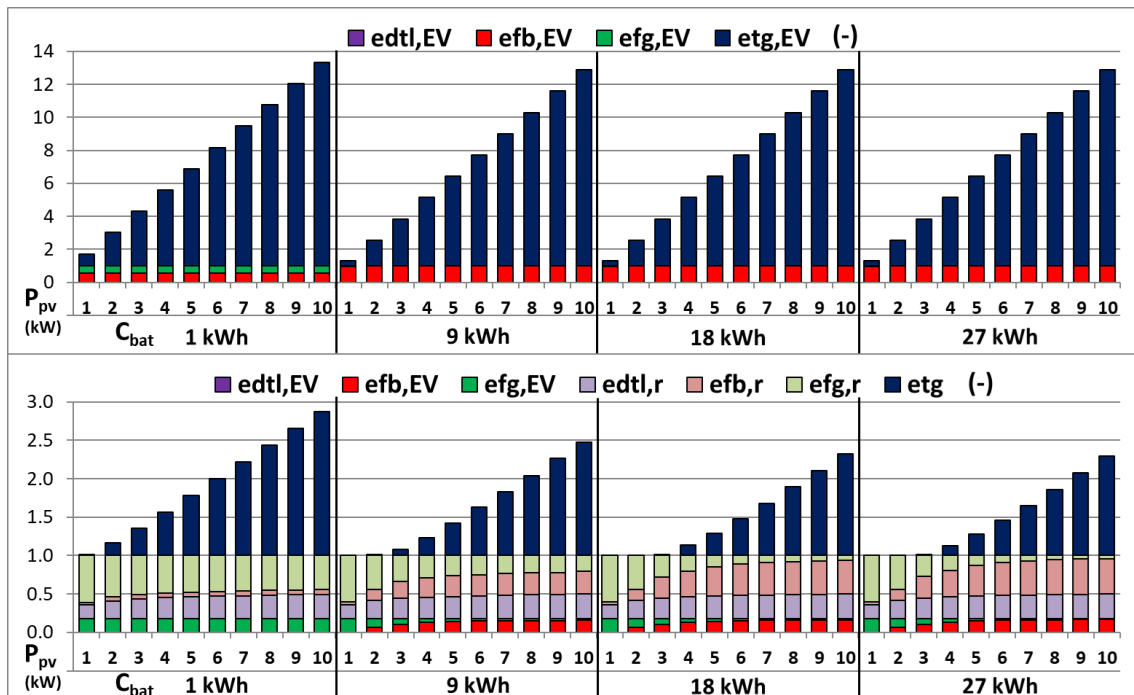
Figure 9. Cumulative histograms of the dimensionless energy contributions of the energy required by the load, for scenarios 2 and 3 and sub-scenarios (a) and (b), as a function of the PV power and capacity battery; 17.5 km/d travelled.

Chapter 4

**Nocturnal electric vehicle charging
interacting with a residential photovoltaic-battery system:
a 3E (energy, economic and environmental) analysis**
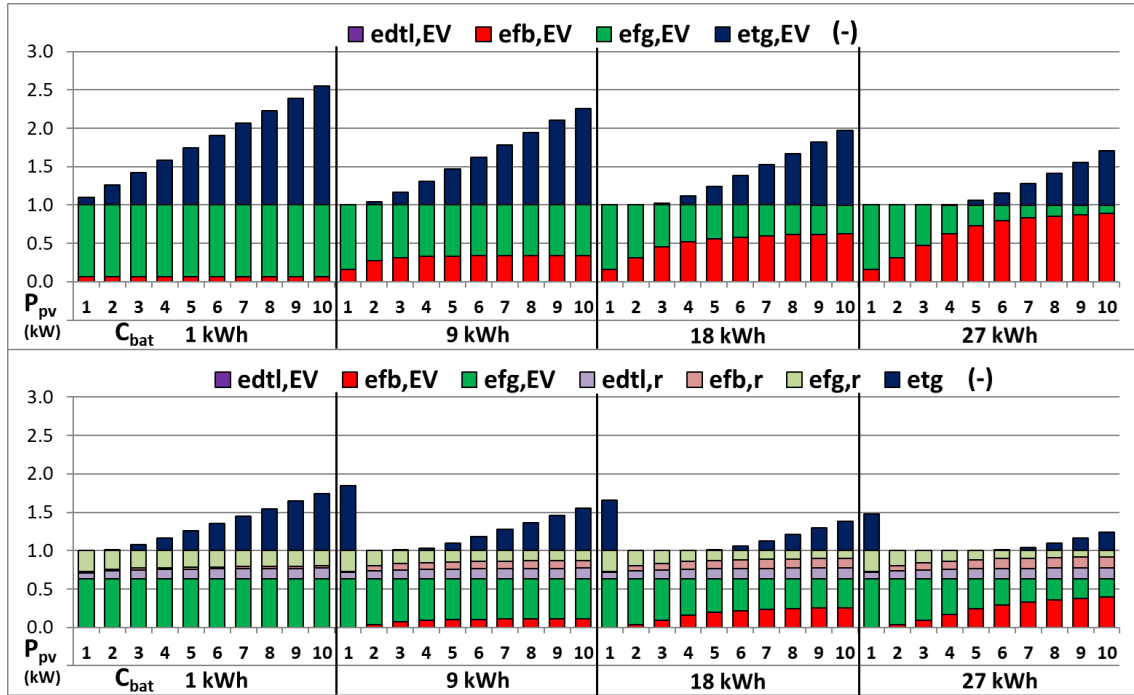
Figure 10. *Cumulative histograms of the dimensionless energy contributions of the energy required by the load, for scenarios 2 and 3 and sub-scenarios (a) and (b), as a function of the PV power and capacity battery; 140 km/d travelled.*

The residential load, unlike the EV load, employs both the energy directly sent by the PV $e_{dtl,r}$ and battery $e_{fb,r}$. Independently of the distance travelled, the energy fraction $e_{dtl,r}$ increases by raising the PV power and is not affected by the battery capacity, since the residential nocturnal load has priority compared to the storage in the battery. Instead, the energy fraction $e_{fb,r}$ also rises with battery capacity growth. The fraction e_{tg} augments as the PV power increases and becomes lower with battery storage and distance travelled growth.

In addition, the figures allow highlighting of the apportionment of the energy required by the load in the absence and presence of the residential load. In particular, a greater PV power or battery capacity produce an increase in the fraction of energy sent to the load with a consequent drop of the fraction of energy drawn from the grid. For each distance travelled, there are different PV power and battery capacity combinations that allow extinguishing the fraction of energy drawn from the grid. In addition, other combinations permit to limit the surplus energy sent to the grid.

4.2.3. Energy-constrained PV-battery configurations

In scenario 2, Table 4 shows, by changing the distance travelled, the minimum PV power $\overline{P}_{pv,fg}$ and battery capacity $\overline{C}_{bat,fg}$ required to limit e_{fg} to values lower than 20 %. Instead, Table 5 reports, by changing the distance travelled, the maximum PV power $\overline{P}_{pv,tg}$ and minimum battery capacity $\overline{C}_{bat,tg}$ required to limit e_{tg} to values lower than 20 %. In both tables, the values of energies E_{dtl}, E_{fb}, and E_{tg}, appearing in the energy balance of the energy required by the load, Eq. (2), are inserted. Finally, in Table 4 and Table 5, respectively, the values that e_{fg} and e_{tg} assume are also reported. Higher PV powers or battery capacities than those reported in Table 4 allow respecting the constraint on e_{fg}; instead, lower PV powers or higher battery capacities than those reported in Table 5 allow respecting the constraint on e_{tg}.

Chapter 4   **Nocturnal electric vehicle charging**
interacting with a residential photovoltaic-battery system:
a 3E (energy, economic and environmental) analysis

Table 4. Minimum PV power and battery capacity required to limit e_{fg} to values lower than 20 %, energy contributions, and fraction of surplus energy sent to the grid, for different distances; scenario 2.

Daily distance travelled (km/d)	$\bar{C}_{bat,fg}$ (kWh)	$\bar{P}_{pv,fg}$ (kW)	$E_{dtl,EV}$ (kWh)	$E_{fb,EV}$ (kWh)	$E_{fg,EV}$ (kWh)	E_{tg} (kWh)	e_{tg} (-)
				$\bar{e}_{fg} < 0.20$			
17.5	3	1	0.00	936.00	159.00	457.10	0.42
35.0	6	2	0.00	1858.82	330.00	926.22	0.42
52.5	9	3	0.00	2722.28	561.00	1456.73	0.44
70.0	12	5	0.00	3519.74	858.00	3465.40	0.79
	15	3	0.00	3516.76	861.00	644.80	0.15
87.5	15	7	0.00	4410.18	1062.00	5380.40	0.98
	18	4	0.00	4494.18	978.00	1060.10	0.19
105.5	18	8	0.00	5360.64	1206.00	5824.31	0.89
	21	5	0.00	5444.57	1122.00	1501.67	0.23
122.5	21	9	0.00	6302.03	1359.00	6274.54	0.82
	24	6	0.00	6385.96	1275.00	1952.14	0.25
140.0	24	9	0.00	7015.60	1740.00	5546.60	0.63
	27	7	0.00	7276.38	1479.00	2454.29	0.28

For e_{fg} limitation, by increasing the distance, increasingly greater battery capacities, and higher values of the minimum PV powers are required. For distances smaller than 70 km/d, only with a battery capacity equal to the portion of EV battery employed in a day, the e_{fg} limitation is guaranteed. Instead, for distances equal to or higher than 70 km/d, two different PV-battery configurations guarantee to respect the constraint set. The first is characterized by a battery capacity equal to the portion of EV battery employed in a day; instead, the second one by battery capacities 3 kWh greater than the portion of EV battery employed in a day, and by PV powers lower than those relative to the first configuration. For example, in the case of 70 km/d, the EV consumes 12 kWh of the energy stored in its battery and the battery capacity required for a PV system is 12 or 15 kWh. For the PV-battery configurations selected, the fraction of surplus energy sent to the grid e_{tg} in the second configuration is lower considerably than the first one, while the energy drawn from the grid E_{fg} is slightly lower.

Chapter 4

**Nocturnal electric vehicle charging
interacting with a residential photovoltaic-battery system:
a 3E (energy, economic and environmental) analysis**

Table 5. *Maximum PV power and minimum battery capacity required to limit e_{tg} to values lower than 20 %, energy contributions, and fraction of energy drawn from the grid, for different distances; scenario 2.*

	$\bar{e}_{tg} < 0.20$						
Daily distance travelled (km/d)	$\bar{C}_{bat,tg}$ (kWh)	$\bar{P}_{pv,tg}$ (kW)	$E_{dtl,EV}$ (kWh)	$E_{fb,EV}$ (kWh)	$E_{fg,EV}$ (kWh)	E_{tg} (kWh)	e_{fg} (-)
35.0	6	1	0.00	1310.16	879.00	73.94	0.40
52.5	3	1	0.00	935.41	2349.00	457.10	0.72
	9	2	0.00	2404.46	879.00	368.39	0.27
70.0	1	1	0.00	602.62	3777.00	796.83	0.86
	9	2	0.00	2404.46	1974.00	368.39	0.45
	15	3	0.00	3516.76	861.00	644.80	0.20
87.5	1	1	0.00	602.62	4872.00	796.83	0.89
	6	2	0.00	1861.82	3612.00	923.16	0.66
	12	3	0.00	3136.02	2337.00	1034.31	0.43
	18	4	0.00	4494.18	978.00	1060.10	0.18
105.5	1	1	0.00	602.62	5967.00	796.83	0.91
	6	2	0.00	1861.82	4707.00	923.16	0.72
	12	3	0.00	3136.02	3432.00	1034.31	0.52
	18	4	0.00	4524.16	2043.00	1029.53	0.31
122.5	1	1	0.00	536.66	7128.00	864.18	0.93
	6	2	0.00	1861.82	5802.00	923.16	0.76
	9	3	0.00	2722.28	4941.00	1456.73	0.64
	18	4	0.00	4524.16	3138.00	1029.53	0.41
	21	5	0.00	5459.56	2202.00	1486.24	0.29
140.0	1	1	0.00	548.65	8211.00	851.93	0.94
	6	2	0.00	1861.82	6897.00	923.17	0.79
	9	3	0.00	2722.28	6036.00	1456.81	0.69
	15	4	0.00	3996.48	4761.00	1567.79	0.54
	21	5	0.00	5462.56	3294.00	1483.27	0.38
	27	6	0.00	6934.64	1821.00	1392.57	0.21

For e_{tg} limitation, the maximum PV powers employable increase with the distance growth, as long as greater battery capacities are employed. To these configurations, correspond e_{fg} values, which are extremely variable between 0.18 and 0.94. Greater PV powers and battery capacities determine an e_{fg} reduction but they do not guarantee the minimum surplus energy E_{tg}. By increasing the distance travelled, an augment of the number of selected configurations is highlighted and for a distance of 17.5 km/d, corresponding to the minimum electrical load, no configuration allows keeping e_{tg} below 0.20.

Finally, the comparison of the two tables highlights that e_{fg} and e_{tg} cannot be limited simultaneously, since a PV power growth determines a reduction of e_{fg} and a growth of e_{tg}. Instead, the battery capacity augment allows reducing both the dimensionless energies, allowing simultaneously respecting, only for some distances travelled, the two constraints.

Chapter 4

**Nocturnal electric vehicle charging
interacting with a residential photovoltaic-battery system:
a 3E (energy, economic and environmental) analysis**

The same analysis was developed in scenario 3 in the presence of the residential load. Table 6 and 7 show the PV-battery configurations that respect the limitation respectively of e_{fg} and e_{tg} to 0.20. In the tables, the energy contributions that appear in the balance of the energy required by the load, Eq. (3), and the surplus energy are also inserted. Finally, in the case of e_{fg} limitation, the corresponding values of e_{tg} in Table 6 and vice versa in Table 7 are reported.

Table 6. *Minimum PV power and battery capacity required to limit e_{fg} to values lower than 20 %, energy contributions, and fraction of surplus energy sent to the grid, for different distances; scenario 3.*

Daily distance travelled (km/d)	$\bar{C}_{bat,fg}$ (kWh)	$\bar{P}_{pv,fg}$ (kW)	$E_{dtl,EV}$ (kWh)	$E_{fb,EV}$ (kWh)	$E_{fg,EV}$ (kWh)	$E_{dtl,r}$ (kWh)	$E_{fb,r}$ (kWh)	$E_{fg,r}$ (kWh)	E_{tg} (kWh)	e_{tg} (-)
						$\bar{e}_{fg} < 0.20$				
17.5	12	6	0.00	927.00	168.00	1892.33	2252.53	1013.14	3335.93	0.53
	15	5	0.00	894.00	201.00	1843.25	2348.55	966.20	1908.08	0.31
35.0	15	7	0.00	1848.00	342.00	1929.04	2188.48	1040.48	3835.56	0.52
	18	6	0.00	1797.00	393.00	1893.98	2344.73	919.29	2352.09	0.32
52.5	18	8	0.00	2760.00	525.00	1965.44	2141.26	1051.29	4328.41	0.51
	21	7	0.00	2721.00	564.00	1932.93	2316.22	908.84	2810.91	0.33
	27	6	0.00	2607.00	678.00	1893.98	2283.58	980.44	1588.62	0.19
70.0	21	8	0.00	3567.00	813.00	1965.44	2118.39	1074.17	3529.24	0.37
	27	7	0.00	3480.00	900.00	1932.93	2296.16	928.90	2058.13	0.22
87.5	24	9	0.00	4437.00	1038.00	1993.41	2108.99	1055.59	4036.81	0.38
	27	8	0.00	4344.00	1131.00	1965.44	2253.39	939.16	2598.76	0.24
105.5	27	10	0.00	5301.00	1269.00	2016.85	2099.69	1041.47	4552.22	0.39

All the qualitative considerations done in scenario 2 continue to be valid also in scenario 3. Unlike scenario 2, the minimum PV powers and battery capacities, necessary to maintain e_{fg} lesser than 0.20 are substantially higher, with the addition of respectively from 2 to 5 kW and from 6 kWh and 9 kWh. These latter allow also supplying the residential load. In the case of 122.5 km/d and 140 km/d, no configurations allow limiting e_{fg} since PV powers greater than 10 kW or battery capacities higher than 27 kWh are needed. On the contrary, by considering also the residential load in scenario 3, the e_{tg} variation is more significantly contained than that of scenario 2. As highlighted by Table 7, also the e_{tg} limitation requires minimum battery capacities and maximum PV power higher than those of scenario 2 and the variation range of e_{fg} is less wide. To complete the analysis, among the numerous system configurations resulted as being the most reliable from an energy point of view, those more profitable from an economic point of view were selected. Finally, the most economically rentable system configurations were identified.

Chapter 4

**Nocturnal electric vehicle charging
interacting with a residential photovoltaic-battery system:
a 3E (energy, economic and environmental) analysis**

Table 7. *Maximum PV power and minimum battery capacity required to limit e_{tg} to values lower than 20 %, energy contributions, and fraction of energy drawn from the grid, for different distances; scenario 3.*

Daily distance travelled (km/d)	$\bar{C}_{bat,tg}$ (kWh)	$\bar{P}_{pv,tg}$ (kW)	$E_{dtl,EV}$ (kWh)	$E_{fb,EV}$ (kWh)	$E_{fg,EV}$ (kWh)	$E_{dtl,r}$ (kWh)	$E_{fb,r}$ (kWh)	$E_{fg,r}$ (kWh)	E_{tg} (kWh)	e_{fg} (-)
					$\bar{e}_{tg} < 0.20$					
17.5	1	1	0.00	0.00	1095.00	1147.31	172.43	3838.26	88.55	0.79
	3	2	0.00	0.00	1095.00	1508.85	744.12	2905.02	556.07	0.64
	6	3	0.00	549.00	546.00	1640.04	1069.57	2448.39	946.87	0.48
	12	4	0.00	825.00	270.00	1771.88	1967.87	1418.26	1026.11	0.27
35.0	1	2	0.00	0.00	2190.00	1460.74	322.63	3374.63	1034.27	0.76
	6	3	0.00	573.00	1617.00	1631.01	1059.97	2467.03	941.93	0.56
	9	4	0.00	1230.00	960.00	1719.98	1284.75	2153.27	1362.22	0.42
	18	5	0.00	1680.00	510.00	1843.91	2149.15	1164.94	1309.26	0.23
52.5	1	2	0.00	0.00	3285.00	1472.79	316.79	3368.42	1028.24	0.79
	3	3	0.00	0.00	3285.00	1670.51	866.84	2620.65	1681.56	0.70
	9	4	0.00	1248.00	2037.00	1717.63	1269.13	2171.23	1361.98	0.50
	15	5	0.00	2226.00	1059.00	1840.98	1551.48	1765.53	1367.66	0.33
	24	6	0.00	2592.00	693.00	1893.98	2249.35	1014.67	1638.84	0.20
70.0	1	2	0.00	0.00	4380.00	1472.79	316.79	3368.42	1028.24	0.81
	3	3	0.00	0.00	4380.00	1670.44	865.17	2622.39	1683.37	0.73
	9	4	0.00	1257.00	3123.00	1716.46	1266.72	2174.82	1356.68	0.56
	12	5	0.00	1815.00	2565.00	1821.04	1472.74	1864.22	1884.65	0.46
	18	6	0.00	3042.00	1338.00	1893.24	1649.70	1615.06	1791.55	0.31
87.5	1	2	0.00	0.00	5475.00	1472.79	316.79	3368.42	1028.24	0.83
	3	3	0.00	0.00	5475.00	1670.51	867.83	2619.67	1680.58	0.76
	6	4	0.00	705.00	4770.00	1714.64	1123.90	2319.46	2067.00	0.67
	12	5	0.00	1821.00	3654.00	1819.90	1473.53	1864.57	1878.85	0.52
	18	6	0.00	3027.00	2448.00	1893.98	1653.77	1610.25	1802.42	0.38
	24	7	0.00	4035.00	1440.00	1932.93	1960.24	1264.83	1833.72	0.25
105.5	1	3	0.00	0.00	6570.00	1636.36	343.12	3178.52	2249.82	0.83
	6	4	0.00	711.00	5859.00	1712.77	1121.05	2324.18	2065.58	0.70
	12	5	0.00	1827.00	4743.00	1815.37	1476.99	1865.64	1873.52	0.56
	18	6	0.00	3045.00	3525.00	1893.98	1638.32	1625.70	1799.35	0.44
	21	7	0.00	3774.00	2796.00	1932.93	1776.86	1448.21	2286.62	0.36
	27	8	0.00	4899.00	1671.00	1965.44	1991.87	1200.69	2299.20	0.24
122.5	1	3	0.00	0.00	7665.00	1629.85	347.92	3180.22	2251.60	0.85
	6	4	0.00	711.00	6954.00	1714.12	1123.82	2320.06	2064.73	0.72
	9	5	0.00	1371.00	6294.00	1782.25	1315.35	2060.40	2539.23	0.65
	15	6	0.00	2505.00	5160.00	1888.15	1597.07	1672.78	2398.69	0.53
	21	7	0.00	3795.00	3870.00	1932.93	1748.40	1476.67	2294.49	0.42
	27	8	0.00	4989.00	2676.00	1965.44	1937.10	1255.45	2263.54	0.31
140.0	1	3	0.00	0.00	8760.00	1628.63	344.61	3184.76	2256.29	0.86
	6	4	0.00	693.00	8067.00	1718.35	1132.49	2307.16	2067.15	0.75
	9	5	0.00	1374.00	7386.00	1780.20	1313.62	2064.18	2539.93	0.68
	15	6	0.00	2490.00	6270.00	1888.95	1596.24	1672.81	2414.45	0.57
	21	7	0.00	3786.00	4974.00	1932.93	1752.27	1472.79	2299.48	0.46
	27	8	0.00	4986.00	3774.00	1965.44	1930.47	1262.09	2274.14	0.36

Chapter 4   **Nocturnal electric vehicle charging**
interacting with a residential photovoltaic-battery system:
a 3E (energy, economic and environmental) analysis

4.3 Economic analysis

4.3.1. Energy-constrained PV-battery configurations and optimum economic

In this Section, the results of an economic analysis that consists of the selection of the system configurations more feasible economically, among those resulted to be the most reliable from an energy point of view, are reported. In particular, considering all the system configurations that have complied with the constraints imposed on e_{fg} and e_{tg}, of which the limit values were reported in Tables 4-7, the highest NPV was identified for each criterion, scenario and sub-scenario.

Figure 11 shows, by varying the distance travelled, the maximum NPV obtained for the three scenarios in sub-scenarios (a) e (b), respectively in the image at the top and bottom, namely when the EV is purchased as an alternative, respectively, to a diesel vehicle and petrol vehicle. In scenarios 2 and 3, the highest NPV values were identified both in the case of e_{fg} and e_{tg} limitation.

In Scenario 1, the NPV steadily rises for increasingly higher distances travelled and, for reduced distances, lower than 50 km/d, the NPV is negative for both fuels. Consequently, in these cases, it is more profitable to opt for the purchase of a TV rather of an EV. NPV ranges between -4084 € and 20754 € in sub-scenario (a) and between -2129 € and 50974 € in sub-scenario (b). By comparing the two images in scenario 1, for a given distance, despite the investment cost in sub-scenario (a) being higher than that in sub-scenario (b), the petrol as alternative fuel leads to higher NPV than those obtained considering diesel as an alternative fuel.

Chapter 4

**Nocturnal electric vehicle charging
interacting with a residential photovoltaic-battery system:
a 3E (energy, economic and environmental) analysis**
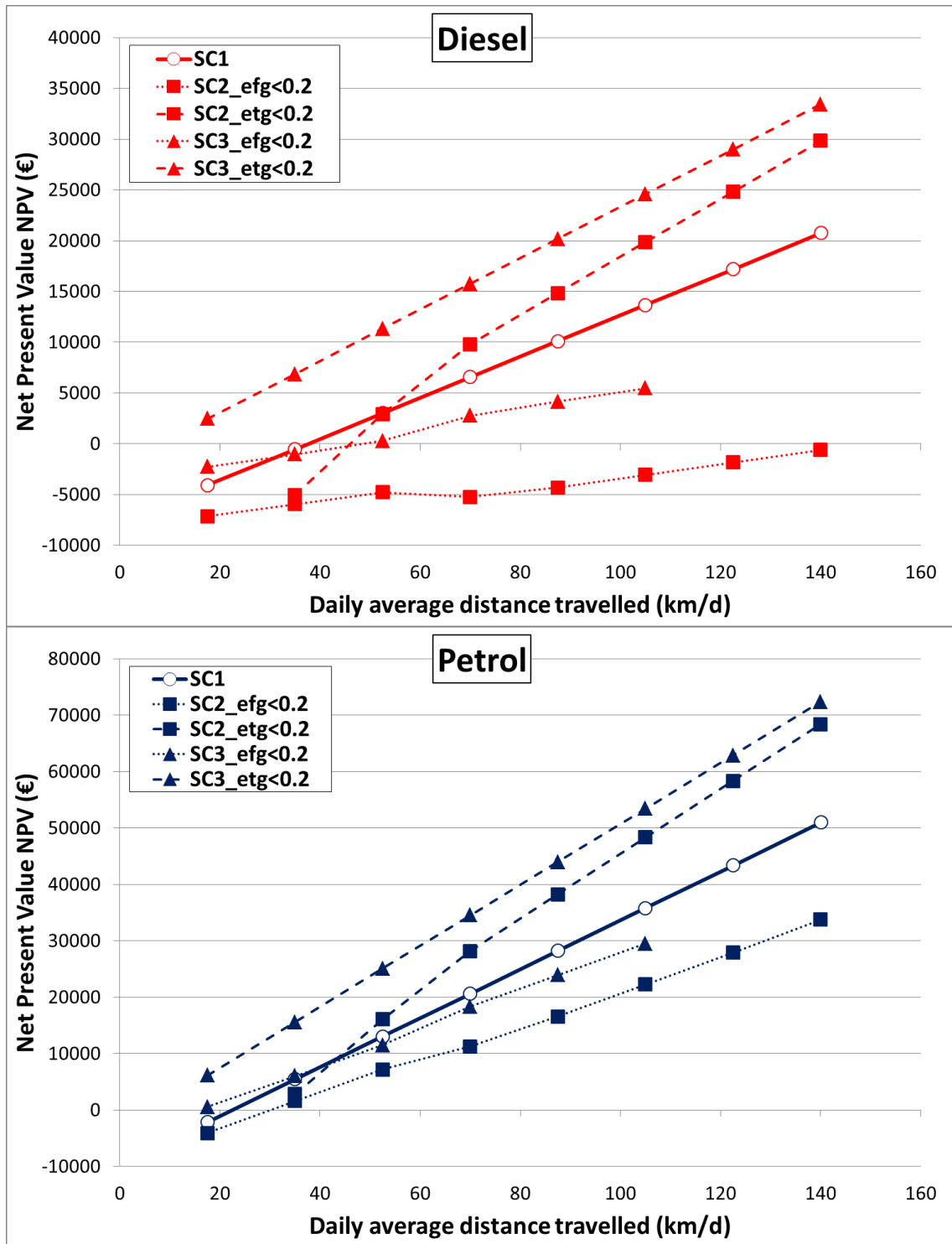
Figure 11. *Maximum NPV as a function of the daily distance travelled in scenario 1, and in scenarios 2 and 3 with e_{fg} and e_{tg} limitation, in sub-scenario (a) at the top and sub-scenario (b) at the bottom.*

The difference between the two sub-scenarios rises gradually, from 2000 € to 30000 €, by augmenting the distance travelled. This higher saving in sub-scenario (b) is owing to the greater petrol cost compared with that of diesel, and to the much higher petrol cost than the electrical energy cost. This scenario represents a reference to identify when, in scenarios 2 and 3, the purchase of a PV-battery system is economically feasible. In other words, the figure allows identifying when further investment in the PV and battery purchase is convenient both in the presence and in absence of a residential load.

By comparing scenario 1 with scenarios 2 and 3, in both sub-scenarios, it emerges that it is convenient to purchase the PV-battery system only when the e_{tg} limitation criterion is employed. The comparison between the two scenarios shows that the presence of residential load leads to a higher NPV increase, independently of the distance travelled, determining higher economic feasibility of the investment. Instead, in scenario 2, the PV-battery system is convenient only above of a specific daily distance travelled, while below a specific daily distance travelled, it is more appropriate to charge the EV by means of the use of the grid. In particular, with reference to a diesel vehicle, starting from 52.5 km/d travelled, the NPV in scenario 2 is higher than that of scenario 1. Instead, for the petrol vehicle, 35.5 km/d are required. From a quantitative point of view, by considering the maximum daily distance and the e_{tg} limitation criterion, the NPV reaches values of 20839 € in sub-scenario (2a) and 33440 € in sub-scenario (3a), while it attains values of 68403 € in sub-scenario (2b) and 72360 € in sub-scenario (3b). By employing the e_{fg} criterion, the maximum NPV is -613 € in sub-scenario (2a) and 33765 € in sub-scenario (2b), while in sub-scenario (3a) and (3b) the highest NPV is reached for a distance of 105 km/d, since no system configurations were found for higher distances, and is equal to, respectively, 5461 € and 29496 €.

Table 8 shows the optimal PV and battery sizes for each distance travelled, scenario and criterion adopted. These optimal sizes are independent of sub-scenario, diesel or petrol.

Table 8. Optimal PV and battery sizes for each scenario and criterion for the different daily distances.

		Scenario 2							
	km/d	17.5	35.0	52.5	70.0	87.5	105.0	122.5	140.0
$e_{fg} < 0.20$	$C_{bat,fg,opt}$ (kWh)	3	6	9	12	18	21	24	24
	$P_{pv,fg,opt}$ (kW)	1	2	3	5	4	5	6	9
	km/d	17.5	35.0	52.5	70.0	87.5	105.0	122.5	140.0
$e_{tg} < 0.20$	$C_{bat,tg,opt}$ (kWh)	/	6	3	1	1	1	1	1
	$P_{pv,tg,opt}$ (kW)	/	1	1	1	1	1	1	1
		Scenario 3							
	km/d	17.5	35.0	52.5	70.0	87.5	105.0	122.5	140.0
$e_{fg} < 0.20$	$C_{bat,fg,opt}$ (kWh)	12	15	18	21	24	27	/	/
	$P_{pv,fg,opt}$ (kW)	6	7	8	8	9	10	/	/
	km/d	17.5	35.0	52.5	70.0	87.5	105.0	122.5	140.0
$e_{tg} < 0.20$	$C_{bat,tg,opt}$ (kWh)	3	3	3	3	3	3	3	3
	$P_{pv,tg,opt}$ (kW)	2	2	3	3	3	3	3	3

As regards the optimal combination PV-battery in scenario 2, among the system configurations that satisfy the e_{fg} constraint, the NPV maximization, for a specific daily distance travelled, requires the highest PV power with the minimum battery capacity. The battery capacity is exactly equal to the portion of the battery capacity of the EV employed to travel the corresponding daily distance. Instead, to limit e_{tg} and maximize NPV simultaneously, the minimum PV power of 1 kW is required for all the distances, while the battery capacity decreases as the distance rises.

Unlike scenario 2, the limitation of e_{fg} in scenario 3 needs, for distances between 17.5 km/d and 70 km/d, battery capacities 9 kWh higher than those selected in scenario 2, while for distances greater than 70 km/d an addition of 6 kWh is enough to limit e_{fg} and maximize NPV at the same time. Instead, the PV powers required rises by 1 kW for each 17.5 km/d travelled, and they are 3-5 kW greater than

Chapter 4

Nocturnal electric vehicle charging interacting with a residential photovoltaic-battery system: a 3E (energy, economic and environmental) analysis

those identified in scenario 2. For the limitation of e_{tg} in scenario 3, since a greater electrical load is considered, PV powers higher than those employable in scenario 2, until to 3 kW can be installed. The optimal battery capacity is independent of the daily distance and equal to 3 kWh. Finally, the optimal PV powers and battery capacities obtained applying the two constraints are different. As a result, a lower maximum NPV value will be obtained by satisfying both constraints.

4.3.2. Economically optimal PV-battery configurations

The second economic analysis concerns the identification of the most economically profitable system configurations independently of the system energy performance.

Figures 12 and 13 present the NPV as a function of the investment cost, for each daily average distance travelled, respectively in sub-scenario (a) and (b). Each image is related to a specific scenario. The one hundred points of the same colour for a specific distance are related to the NPV obtained for the ten values of PV power and the ten values of battery capacity, of which the increase direction is indicated with an arrow. In addition, each full point identifies the corresponding NPV and the investment cost, for a given distance, obtained in scenario 1.

In all scenarios and sub-scenarios, a greater daily distance travelled, corresponding to higher electrical energy consumed by the battery of the vehicle, determines the growth of the NPV and therefore of the investment profitability. This increase is more marked in sub-scenario (b) than sub-scenario (a), as highlighted from the comparison of Figures 12 and Figure 13. In the petrol fuel case, the group of points of the same colour are more spaced one from the other compared with those of the diesel fuel case. Furthermore, the variation range of the NPV, identified by the difference of the maximum and minimum NPV, when petrol is considered results as being higher than that obtained in the case of diesel fuel. As regards the comparison of scenario 2 with scenario 3, in the presence of the residential load, for each distance travelled, the NPV appears to be slightly higher and the discrete surface formed presents a nonlinear trend, while in the absence of the residential load the discrete surface is almost a plane. For a given distance, an investment cost increase does not guarantee a higher NPV. In general, the figures allow identification of when it is convenient to purchase the PV-battery system as an alternative to using the grid to supply the EV or also the residential load. In particular, for a specific distance, by comparing the point related to scenario 1, characterized by a lesser investment cost (absence of PV and battery systems), with the group of points for the same distance in a given sub-scenario of scenario 2 and 3, the convenient PV-battery system configurations can be identified. By increasing the distance travelled, the number of PV-battery configurations with a higher NPV than that of scenario 1 rises. For example, for 17.5 km/d travelled in sub-scenarios (2a) and (2b), no system configurations allow the NPV to be increased, while in sub-scenarios (3a) and (3b), system configurations that invest in solar technologies profitable always exist. In addition, in scenario 3 compared with scenario 2, the number of system configurations that comply with this economic improvement is greater. Broadly, also the NPV values appear to be greater in scenario 3 than scenario 2.

Chapter 4

**Nocturnal electric vehicle charging
interacting with a residential photovoltaic-battery system:
a 3E (energy, economic and environmental) analysis**
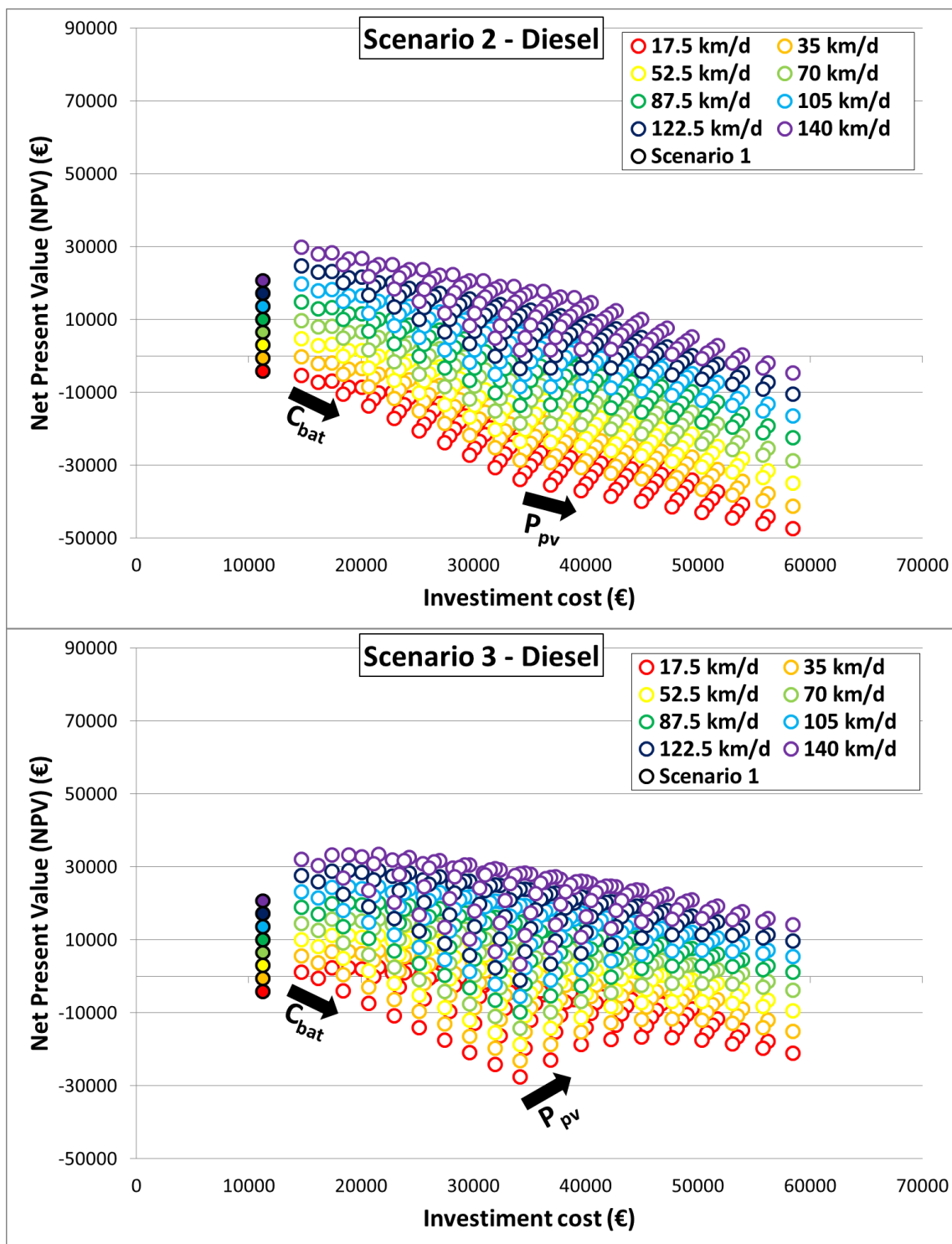
Figure 12. *NPV values as a function of the initial investment cost for different daily distances, PV powers and battery capacities, sub-scenario (a).*

Chapter 4

**Nocturnal electric vehicle charging
interacting with a residential photovoltaic-battery system:
a 3E (energy, economic and environmental) analysis**
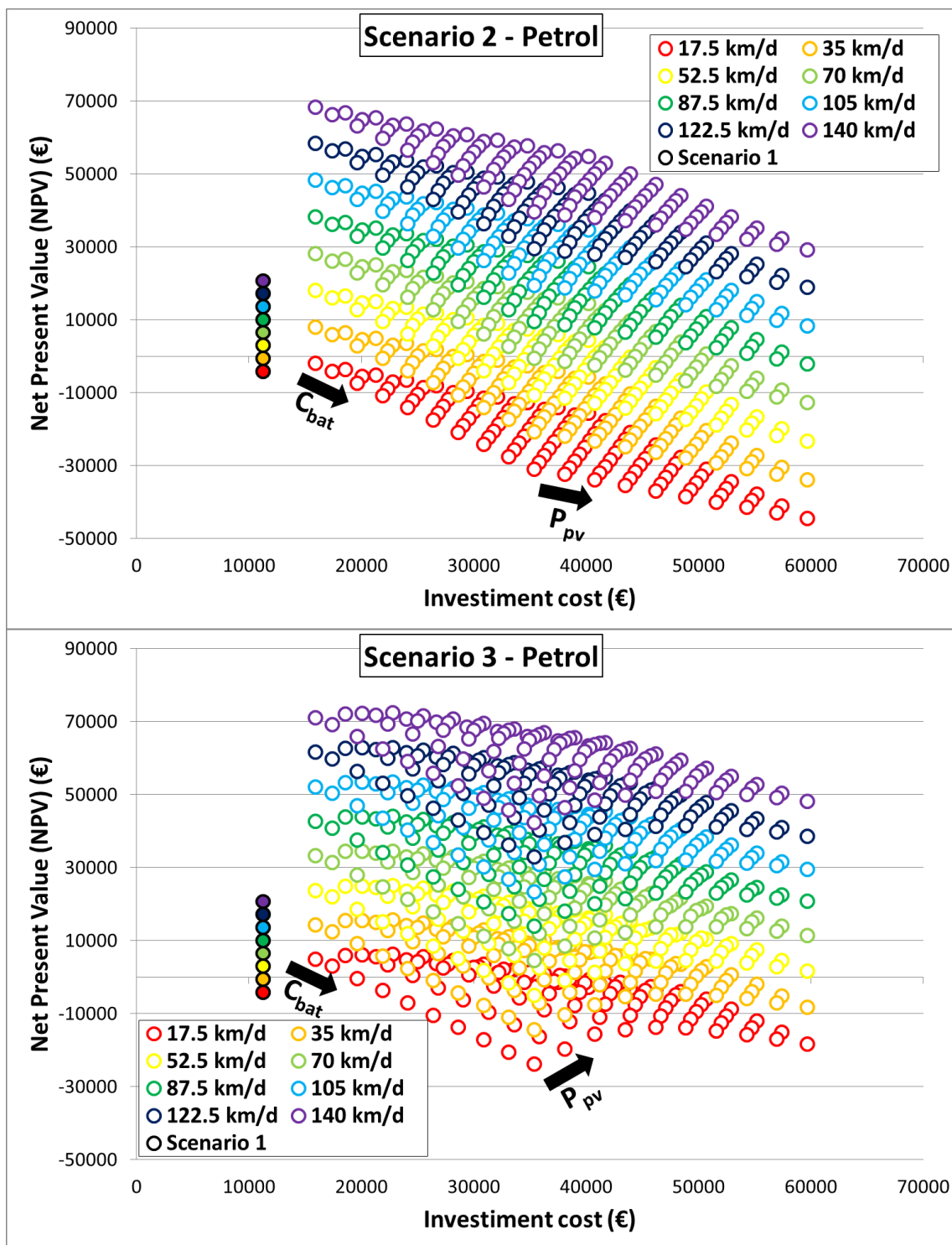
Figure 13. *NPV values as a function of the initial investment cost for different daily distances, PV powers
and battery capacities, sub-scenario (b).*

However, another representation was made to identify for which values of PV and battery sizes a
scenario or sub-scenario is better than the other. Figure 14 shows the trend of NPV as a function of
the investment cost; each curve is related to a given battery capacity value, a specific scenario and
sub-scenario, while each point of the curve, characterized by increasingly higher investment cost,
regards increasing PV powers from 1 kW to 10 kW. Each image is related to a different value of the

Chapter 4

**Nocturnal electric vehicle charging
interacting with a residential photovoltaic-battery system:
a 3E (energy, economic and environmental) analysis**

daily distance travelled. The points identify the NPV and investment cost in sub-scenario (1a) and (1b).
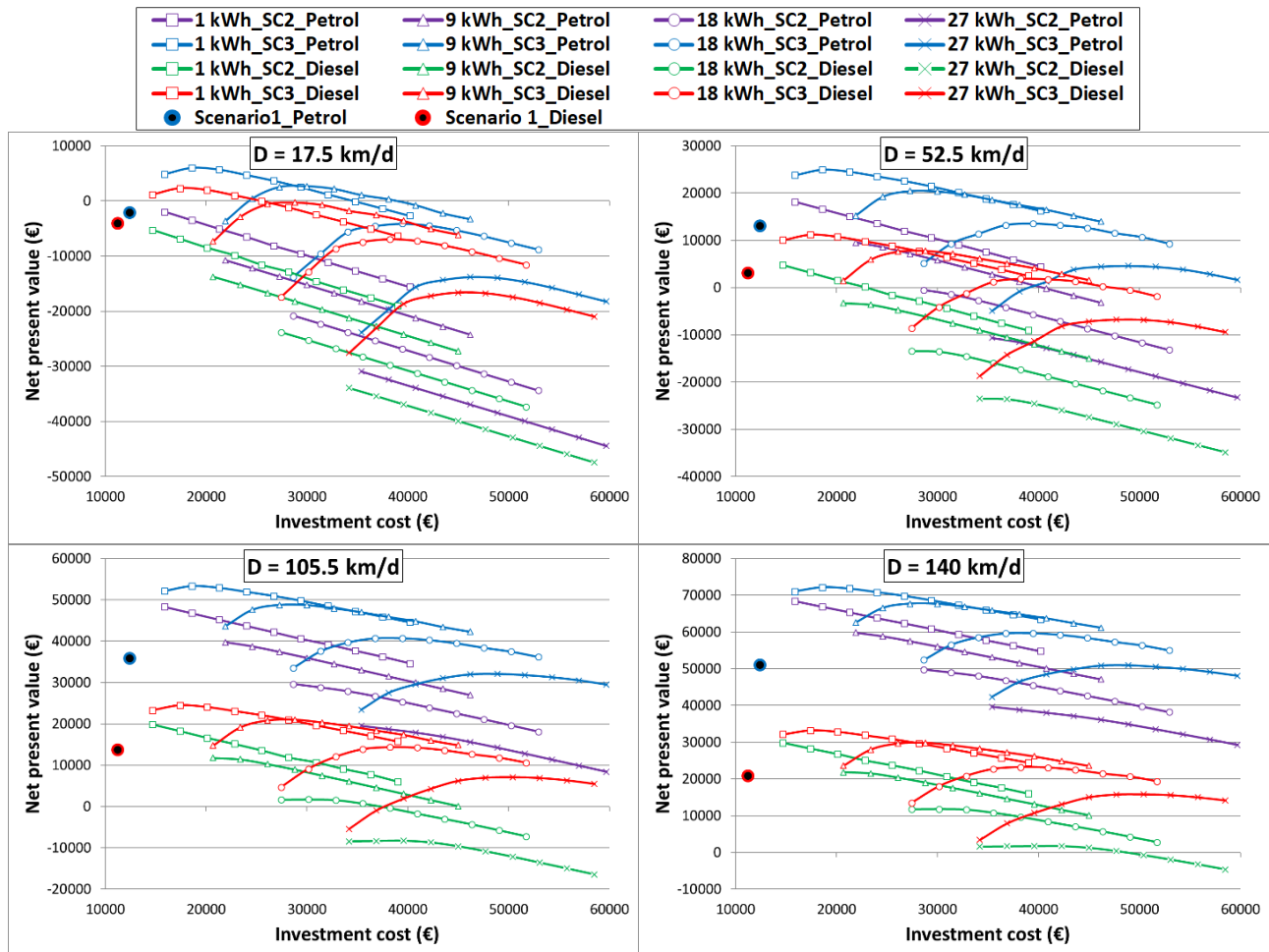
Figure 14. NPV as a function of the initial investment cost, namely PV powers, for the different battery capacities, scenarios and sub-scenarios and daily distance travelled.

Figure 14 highlights that, for any battery capacity value, the PV power increase determines a gradual reduction, almost linear, of the NPV in both sub-scenario (2a) and (2b), while leading to a substantial NPV increase until it reaches a maximum value and then it decreases both in sub-scenario (3a) and (3b). Consequently, an optimal PV power exists for each capacity battery value in scenario 3. Among the different battery capacities considered, the lowest value assures the highest NPV for a given PV power. Scenario 3, considering petrol as the alternative fuel, is more convenient for any distance travelled and given values of PV and battery sizes. For the minimum distance travelled of 17.5 km/d, in the order the sub-scenario (3a), sub-scenario (2b) and sub-scenario (2a) follow in the ranking. However, no configuration appears to be more profitable than scenario 1, except few system configurations in scenario 3. The increase of the distance travelled, in addition to increasing the NPV, gives rise to a modification of the scenario ranking. In particular, for a given PV and battery sizes, sub-scenario (2b) becomes increasingly better than sub-scenario (3a). In these conditions, the employment of solar technologies to supply the EV, in the alternative to the use petrol fuel, and also to supply the residential load, is more appropriate economically than the scenario in which the TV is supplied by diesel fuel. Finally, as the distance grows, also in scenario 2 some PV-battery system

configurations are more convenient than scenario 1. The number of PV-battery configurations that allows obtaining an NPV higher than those related to scenario 1 is increasingly greater by travelling a higher distance.

Figure 15 shows for which PV and battery sizes it is economically feasible to invest in solar technologies to satisfy the EV load in the presence and absence of residential load, considering both petrol and diesel as the alternative TV. In particular, each image, relative to a given scenario and sub-scenario, reports a grid in which each coloured cell detects for which minimum distance a PV-battery combination allows the NPV to be increased. The various distances considered are identified by a different colour. For example, a cell coloured in yellow means that for a distance travelled higher than 52.5 km/d the PV-battery configuration, related to the cell considered, leads to an increase of the NPV compared to the relative case in scenario 1. In the sub-scenario (2a) with a combination of 2 kW and 1 kWh, in the sub-scenario (2b) with a combination of 10 kW and 2 kWh, in the sub-scenario (3a) with a combination of 3 kW and 2 kWh, and in the sub-scenario (3b) with a combination of 4 kW and 18 kWh, a distance higher than 52.5 km/d travelled leads to a more profitable investment compared with the relative cases in scenario 1.

In all sub-scenarios considered, an elevated daily distance travelled assures a wider variation range of PV powers and battery capacities that give rise to a more convenient investment compared to scenario 1. In particular, in scenario 2 a greater battery capacity can be installed, while for a fixed capacity battery a higher PV power can be combined. Analogously in scenario 3, the maximum battery capacity employable is higher and instead, for each capacity battery, the profitable PV powers are contained within a sub-range of the entire variation range between 1 kW and 10 kW of the PV power. This range grows as the distance rises. These growths, both for scenario 2 and 3, are higher when the petrol vehicle is considered as an alternative.

Chapter 4

**Nocturnal electric vehicle charging
interacting with a residential photovoltaic-battery system:
a 3E (energy, economic and environmental) analysis**
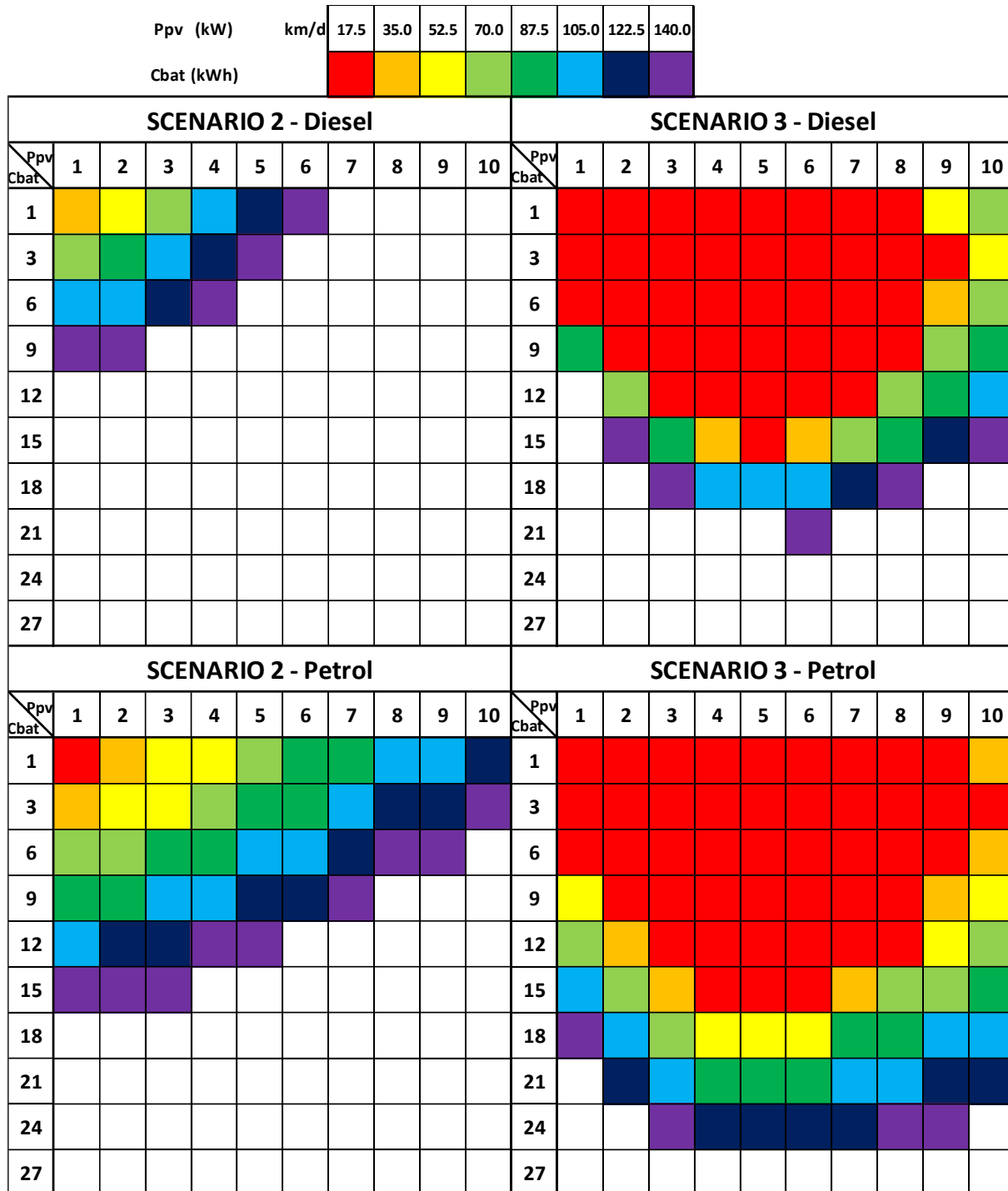
Figure 15. Grid for the identification of the minimum distance for which a PV-battery combination allows increasing the NPV compared to scenario 1; scenario 2 at the left and scenario 3 at the right, for sub-scenario (a) at the top and sub-scenario (b) at the bottom

To evaluate the global economic convenience of the selected system configurations, Table 9 in scenario 2 and Table 10 in scenario 3 show the maximum and minimum values of the NPV and investment costs, for each sub-scenario and daily distance. Furthermore, the resulting highest and lowest energy and dimensionless energy contributions, obtained without constraining the dimensionless indicators, were inserted.

Chapter 4

Nocturnal electric vehicle charging interacting with a residential photovoltaic-battery system: a 3E (energy, economic and environmental) analysis

Table 9. *For the PV-battery system configurations in scenario 2 better than those of scenario 1, maximum and minimum values of NPV, investment cost, energy and dimensionless energy contributions for each sub-scenario and daily distance.*

Scenario 2											
Diesel											
km/d		**I**	**NPV**	$E_{dtl,EV}$	$E_{fb,EV}$	$E_{fg,EV}$	E_{tg}	$e_{dtl,EV}$	$e_{fb,EV}$	$e_{fg,EV}$	e_{tg}
17.5	min				/						
	max										
35.0	min	14690	-251.3	0.0	605.6	1584.0	793.8	0.00	0.28	0.72	0.36
	max										
52.5	min	14690	3179.7	0.0	602.6	2682.0	796.8	0.00	0.18	0.82	0.24
	max	17390	4772.8	0.0	602.6	2682.0	2208.9	0.00	0.18	0.82	0.67
70.0	min	14690	6585.5	0.0	602.6	3444.0	457.1	0.00	0.14	0.79	0.10
	max	20090	9798.5	0.0	935.4	3777.0	3621.0	0.00	0.21	0.86	0.83
87.5	min	14690	11539.0	0.0	602.6	4464.0	457.1	0.00	0.11	0.82	0.08
	max	20090	14824.2	0.0	1010.4	4872.0	3621.0	0.00	0.18	0.89	0.66
105.0	min	14690	14171.7	0.0	602.6	4707.0	73.9	0.00	0.09	0.72	0.01
	max	22790	19849.8	0.0	1861.8	5967.0	5033.1	0.00	0.28	0.91	0.77
122.5	min	14690	17827.1	0.0	536.7	5685.0	73.9	0.00	0.07	0.74	0.01
	max	25490	24800.1	0.0	1978.7	7128.0	6512.6	0.00	0.26	0.93	0.85
140.0	min	14690	21404.9	0.0	548.7	6351.0	73.9	0.00	0.06	0.73	0.01
	max	28190	29839.2	0.0	2407.5	8211.0	7912.5	0.00	0.27	0.94	0.90
Petrol											
km/d		**I**	**NPV**	$E_{dtl,EV}$	$E_{fb,EV}$	$E_{fg,EV}$	E_{tg}	$e_{dtl,EV}$	$e_{fb,EV}$	$e_{fg,EV}$	e_{tg}
17.5	min	15890	-1981.3	0.0	606.0	489.0	793.8	0.00	0.55	0.45	0.72
	max										
35.0	min	15890	5995.3	0.0	605.6	1254.0	457.1	0.00	0.28	0.57	0.21
	max	18590	8077.4	0.0	935.4	1584.0	2205.9	0.00	0.43	0.72	1.01
52.5	min	15890	13098.7	0.0	602.6	2241.0	457.1	0.00	0.18	0.68	0.14
	max	23990	18136.6	0.0	1043.3	2682.0	5033.1	0.00	0.32	0.82	1.53
70.0	min	15890	21667.1	0.0	602.6	2517.0	73.9	0.00	0.14	0.57	0.02
	max	26690	28195.3	0.0	1861.8	3777.0	6445.2	0.00	0.43	0.86	1.47
87.5	min	15890	28664.8	0.0	602.6	3069.0	73.9	0.00	0.11	0.56	0.01
	max	32090	38254.0	0.0	2404.5	4872.0	9269.5	0.00	0.44	0.89	1.69
105.0	min	15890	35911.7	0.0	602.6	3693.0	73.9	0.00	0.09	0.56	0.01
	max	37490	48312.7	0.0	2875.2	5967.0	12093.7	0.00	0.44	0.91	1.84
122.5	min	15890	44274.3	0.0	536.7	4527.0	73.9	0.00	0.07	0.59	0.01
	max	40190	58339.0	0.0	3136.0	7128.0	13573.1	0.00	0.41	0.93	1.77
140.0	min	15890	51168.2	0.0	548.7	5217.0	3.9	0.00	0.06	0.60	0.00
	max	41690	68403.2	0.0	3540.7	8211.0	13560.9	0.00	0.40	0.94	1.55

Chapter 4

Nocturnal electric vehicle charging interacting with a residential photovoltaic-battery system: a 3E (energy, economic and environmental) analysis

Table 10. For the PV-battery system configurations in scenario 3 better than those of scenario 1, maximum and minimum values of NPV, investment cost, energy and dimensionless energy contributions for each sub-scenario and daily distance.

km/d		I	NPV	$E_{dtl,EV}$	$E_{fb,EV}$	$E_{fg,EV}$	$E_{dtl,r}$	$E_{fb,r}$	$E_{fg,r}$	E_{tg}	$e_{dtl,EV}$	$e_{fb,EV}$	$e_{fg,EV}$	$e_{dtl,r}$	$e_{fb,r}$	$e_{fg,r}$	e_{tg}
Scenario 3																	
Diesel																	
17.5	min	14690	-4042.8	0.0	0.0	141.0	1147.3	172.4	936.9	0.0	0.00	0.00	0.02	0.18	0.03	0.15	0.00
	max	39590	2527.3	0.0	954.0	1095.0	1971.2	2348.5	3838.3	9650.4	0.00	0.15	0.18	0.32	0.38	0.61	1.54
35.0	min	14690	-21690.4	0.0	0.0	399.0	1150.2	172.0	1132.0	0.0	0.00	0.00	0.05	0.16	0.02	0.15	0.00
	max	40040	-251.3	0.0	1791.0	2190.0	1974.9	2132.9	3835.8	9666.9	0.00	0.24	0.30	0.27	0.29	0.52	1.32
52.5	min	14690	3140.7	0.0	0.0	753.0	1175.7	231.8	1535.6	0.0	0.00	0.00	0.10	0.14	0.02	0.19	0.00
	max	40490	11325.5	0.0	2532.0	3285.0	1990.6	1691.8	3750.6	11713.5	0.00	0.29	0.39	0.24	0.19	0.45	1.31
70.0	min	14690	6568.9	0.0	0.0	1737.0	1153.0	168.7	1607.0	0.0	0.00	0.00	0.18	0.12	0.02	0.17	0.00
	max	42740	15736.0	0.0	2643.0	4380.0	1991.7	1623.6	3836.3	11713.5	0.00	0.28	0.46	0.21	0.17	0.40	1.23
87.5	min	14690	10162.8	0.0	0.0	2715.0	1153.0	168.7	1522.8	0.0	0.00	0.00	0.26	0.11	0.02	0.14	0.00
	max	44990	20171.0	0.0	2760.0	5475.0	1984.8	1671.3	3836.3	11713.5	0.00	0.26	0.51	0.19	0.16	0.36	1.10
105.0	min	14690	13685.8	0.0	0.0	3525.0	1153.0	168.7	1529.5	0.0	0.00	0.00	0.30	0.10	0.01	0.13	0.00
	max	47240	24593.8	0.0	3045.0	6570.0	1995.6	1667.3	3836.3	11713.2	0.00	0.26	0.56	0.17	0.14	0.33	1.00
122.5	min	14690	17617.9	0.0	0.0	4377.0	1147.3	171.5	1512.2	0.0	0.00	0.00	0.34	0.09	0.01	0.12	0.00
	max	47240	28980.6	0.0	3288.0	7665.0	2000.0	1676.2	3839.3	11710.3	0.00	0.26	0.60	0.16	0.13	0.30	0.91
140.0	min	14690	20822.8	0.0	0.0	5271.0	1146.8	170.9	1477.4	0.0	0.00	0.00	0.38	0.08	0.01	0.11	0.00
	max	49490	33440.4	0.0	3489.0	8760.0	2010.1	1708.4	3840.3	11735.1	0.00	0.25	0.63	0.14	0.12	0.28	0.84
Petrol																	
km/d		I	NPV	$E_{dtl,EV}$	$E_{fb,EV}$	$E_{fg,EV}$	$E_{dtl,r}$	$E_{fb,r}$	$E_{fg,r}$	E_{tg}	$e_{dtl,EV}$	$e_{fb,EV}$	$e_{fg,EV}$	$e_{dtl,r}$	$e_{fb,r}$	$e_{fg,r}$	e_{tg}
17.5	min	15890	-1877.0	0.0	0.0	132.0	1147.3	172.4	775.6	0.0	0.00	0.00	0.02	0.18	0.03	0.12	0.00
	max	43040	6215.1	0.0	963.0	1095.0	1998.7	2488.4	3838.3	11024.8	0.00	0.15	0.18	0.32	0.40	0.61	1.76
35.0	min	15890	5758.3	0.0	0.0	342.0	1150.2	172.0	1040.5	0.0	0.00	0.00	0.05	0.16	0.02	0.14	0.00
	max	43940	15626.4	0.0	1848.0	2190.0	2000.9	2188.5	3835.8	11718.0	0.00	0.25	0.30	0.27	0.30	0.52	1.59
52.5	min	15890	13189.7	0.0	0.0	603.0	1174.1	231.7	1108.0	0.0	0.00	0.00	0.09	0.14	0.02	0.15	0.00
	max	46190	25079.5	0.0	2682.0	3285.0	1997.3	2117.1	3750.8	11713.5	0.00	0.30	0.39	0.24	0.24	0.45	1.39
70.0	min	15890	20689.2	0.0	0.0	1338.0	1153.0	168.7	1495.9	0.0	0.00	0.00	0.14	0.12	0.02	0.16	0.00
	max	48440	34523.1	0.0	3042.0	4380.0	1996.1	1676.6	3836.3	11713.5	0.00	0.32	0.46	0.21	0.18	0.40	1.23
87.5	min	15890	28258.8	0.0	0.0	1998.0	1153.0	168.7	1474.9	0.0	0.00	0.00	0.19	0.11	0.02	0.14	0.00
	max	50690	43991.1	0.0	3477.0	5475.0	2011.2	1706.3	3836.3	11713.5	0.00	0.33	0.51	0.19	0.16	0.36	1.10
105.0	min	15890	36181.3	0.0	0.0	2541.0	1153.0	168.7	1373.7	0.0	0.00	0.00	0.22	0.10	0.01	0.12	0.00
	max	52940	53446.9	0.0	4029.0	6570.0	2016.8	1808.9	3836.3	11713.2	0.00	0.34	0.56	0.17	0.15	0.33	1.00
122.5	min	15890	43445.1	0.0	0.0	3384.0	1147.3	171.5	1280.6	0.0	0.00	0.00	0.26	0.09	0.01	0.10	0.00
	max	55190	62863.9	0.0	4281.0	7665.0	2016.8	1860.5	3839.3	11710.3	0.00	0.33	0.60	0.16	0.15	0.30	0.91
140.0	min	15890	51683.6	0.0	0.0	4020.0	1146.8	170.9	1244.3	0.0	0.00	0.00	0.29	0.08	0.01	0.09	0.00
	max	55190	72359.5	0.0	4740.0	8760.0	2016.8	1920.3	3840.3	11735.1	0.00	0.34	0.63	0.14	0.14	0.28	0.84

Tables show that, despite these configurations assuring higher NPV than those of scenario 1, for reduced distances the NPV can still be negative or very low. Instead, for a greater use of the vehicle, NPV grows and becomes much higher than those of scenario 1, especially when the petrol vehicle is considered. As regards the energy and dimensionless energy contributions, a wider range of variation is observed compared to the criterion that foresees the e_{fg} or e_{tg} limitation. Consequently, by employing this criterion high energy performances of the solar system are not assured. However, the comparison with Figure 11 highlights that the use of this criterion assures considerable higher maximum NPV values than those obtained by limiting the energy drawn from the grid, and lead to maximum NPV values that are equal to or very close to that selected by constraining the surplus energy sent to the grid. In these conditions, the containment of the surplus energy, associated with a substantial amount of energy drawn from the grid, assures also NPV very close to the highest obtainable.

4.4 Environmental analysis

The results of the environmental analysis described in Section 2.4 are reported in Figure 16. The image at the top shows the yearly CO_2 emissions of the diesel and petrol vehicles and EV, and the CO_2 savings $(CO_2)_{sav1}$ in sub-scenarios (1a) and (1b) by varying the distance. The CO_2 emissions by varying the distance in scenario 2 and 3, in the absence and presence of a PV system of 1 kW and 10

Chapter 4

Nocturnal electric vehicle charging interacting with a residential photovoltaic-battery system: a 3E (energy, economic and environmental) analysis

kW, and the CO_2 savings owing to the PV system, by varying the PV power, are reported in the image at the bottom.
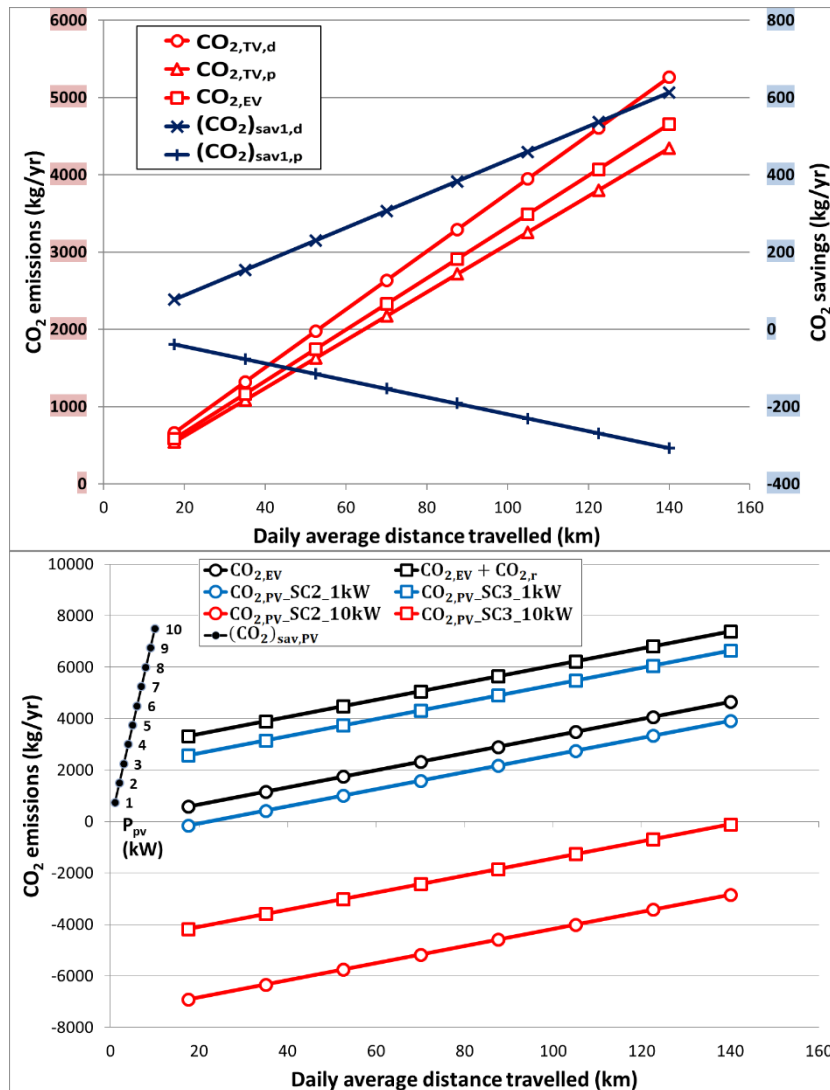
Figure 16. CO_2 emissions and savings in scenario 1, 2 and 3.

The emissions grow gradually for increasing distances. The diesel vehicle leads to the greatest values, followed respectively by the electric and petrol vehicle. Consequently, increasing emission savings of 16 % for higher distances are produced in sub-scenario (1a), while the CO_2 emissions increases by 6 % with the distance in sub-scenario (1b). The higher electrical load in scenario 3 leads to higher emissions than scenario 2, and the difference between two curves of the same colour identifies the CO_2 emissions of the residential load $CO_{2,r}$. In the absence of the PV system, the CO_2 emissions range between 581 kg/yr and 4651 kg/yr in scenario 2, and between 3320 kg/yr and 7390 kg/yr in scenario 3, by considering the minimum and maximum distance respectively.

The PV system allows such emissions to be reduced; moreover, this drop is independent of the battery capacity size. All the energy produced by the PV system, that is sent to the load, stored or sent to the grid, contributes in the same way to reduce the emissions. For example, in the case of a lower battery capacity, the missing stored energy is sent to the grid. In particular, the CO_2 savings realized with the PV system rise from 743 kg/yr to 7492 kg/yr with an increasing PV power from 1 kW to 10 kW. The blue and red curves, related to 1 kW and 10 kW, highlight the CO_2 emissions in the presence of the

Chapter 4

Nocturnal electric vehicle charging
interacting with a residential photovoltaic-battery system:
a 3E (energy, economic and environmental) analysis

PV system. For 10 kW of PV power, the negative values indicate that the energy drawn from the grid is lower than the surplus energy sent to the grid, determining a missing emission of CO_2. From the comparison between the two images, it emerges that the PV system permits to avoid greater CO_2 emissions than the EV. The latter reaches the maximum value of 612.6 kg/yr for the highest distance and considering diesel as the alternative fuel.

5. Conclusions

The study has allowed the identification of the optimal nocturnal EV charging scenarios and optimal PV-battery system configurations by considering the 3E objectives. The energy reliability, economic profitably and emission savings, in the absence and presence of PV-battery system, with and without residential load, were evaluated for different daily average distances travelled, and by considering both diesel and petrol as the alternative TVs.

From an energy point of view, the minimum PV powers and battery capacities required to limit the energy drawn from the grid to charge the EV are considerably lower than those required when also the residential load is present. In particular, to limit the energy drawn from the grid to 20%, a battery capacity of the solar system very close to that employed by the EV is required in absence of the residential load, and addition of respectively from 2 to 5 kW and from 6 kWh and 9 kWh in the presence of residential load. Instead, the limitation of the surplus energy sent to the grid in the presence of residential load requires minimum battery capacities and maximum PV power higher than those required when only EV charging is present as a load. In general, the limitation of the energy drawn from the grid does not guarantee low values of the surplus energy and vice versa. Only the battery capacity increase permits both the energy contributions to be limited.

From an economic point of view, the rentability of the EV-PV coupling is higher when the petrol vehicle is considered as the alternative TV to be purchased, owing to the higher price of petrol compared to diesel, despite the diesel vehicle investment cost is higher. In addition, when the residential load is present, for given PV and battery sizes, the renewable energy produced and utilized is higher, with consequent reduction of the energy fraction purchased from the grid compared to the case when only the EV load is considered. Both in the absence and presence of solar technologies, with or without residential load, the NPV is negative for reduced distances travelled. In this case, the purchase of a TV is more feasible than that of the EV, without employing a solar system. The economic convenience increases with the distance and reaches the maximum value for the highest distance. In particular, for each distance, PV-battery configurations exist that allow improvement of the economic feasibility of the investment compared to that in absence of a solar system. However, even though the investment in the solar system permits an improvement in convenience, if the constraint is characterized by load satisfaction, the NPV becomes positive only when the distance travelled is higher than a determined value. Instead, if the constraint is to limit the surplus energy, for all distances, the investment is rentable. Removing energy constraints, the global economic analysis of the PV-battery and EV combination has highlighted that an optimal PV power exists for each capacity battery value in the presence of the residential load. Consequently, an upward of the initial investment cost does not guarantee a higher NPV. In addition, by maximizing NPV, high energy performances of the solar system are not assured. However, this criterion assures considerable higher maximum NPV values than those obtained by limiting the energy drawn from the grid. Instead, the

Chapter 4
                        Nocturnal electric vehicle charging
interacting with a residential photovoltaic-battery system:
a 3E (energy, economic and environmental) analysis

highest NPVs are very close to those obtained by containing the surplus energy, even if there is a substantial amount of energy drawn from the grid.

From an environmental point of view, the analysis has shown that in the absence of renewable energy, the EV allows containment of emissions compared to the diesel vehicle while, compared to the petrol vehicle, it leads to higher emission production by the national thermoelectric plants employed for electricity generation, even though the emissions in the urban context are reduced. The solar technologies connected to the grid are able, in increasing manner with the power installed, to reduce markedly the emissions independently of the battery capacity installed, since the missing renewable energy employed is sent to the grid, thus reducing the emissions of electricity production plants. In these conditions, the solar system size with the highest emission savings cannot coincide with that with the best economic convenience. Instead, the solar system configurations with a high load satisfaction also permit attainment of CO_2 savings that are very close to maximum savings.

In general, an optimal EV charging scenario by means of a PV-battery system that simultaneously complies with the economic and environmental objectives and the two constraints was not found. The satisfaction of both constraints leads to a lower maximum NPV value than that found applying a single constraint. However, in the design phase, the combination to be selected should depend on the specific application and who invests, whether it is a private individual or a public entity. The procedures proposed and the results obtained can be employed for the PV-battery system design for nocturnal EV charging with high energy reliability, and/or economic profitability, and/or abatement of emissions. Furthermore, with the current cost framework, the research constitutes a reference in order to develop an incentive plan to facilitate the combined purchase of EVs and solar technologies. In addition, the results and considerations were outlined in a conservative context, where the spread of such systems will lead in the short term, owing to the scale factors, to a further reduction in the purchase cost of solar technologies and EVs. Finally, these results are also very useful to foresee the emission savings achievable in an immediate future by considering the exponential growth of EV registrations worldwide.

References

[1] N. Hooftman, L. Oliveira Messagie, M. Coosemans, T., J. Van Mierlo, Environmental Analysis of petrol, diesel and electric passenger cars in a Belgian urban setting. Energies, Volume 9, 2016, EISSN 1996-1073, https://doi.org/10.3390/en9020084.

[2] International Energy Agency (IEA), Global EV Outlook 2017: Two million and counting, 2017, Paris (France), ISBN 9789264278882, http://dx.doi.org/10.1787/9789264278882-en.

[3] TERNA Group, Document description of the scenarios, Edition 2018, Rome (Italy), Website: http://www.terna.it/it-it/home.aspx, last access: 28/05/2018.

[4] TERNA Group, Monthly report on the electrical system, January 2018, Rome (Italy), Website: http://www.terna.it/it-it/home.aspx, last access: 28/05/2018.

[5] ACEA (European Automobile Manufacturers Association), New passenger cars by fuel type in the European union, Quarter 1 2018, Brussels (Belgium), Website: www.acea.be/statistics/tag/category/electric-and-alternative-vehicle-registrations, last access: 28/05/2018.

[6] European Commission - Mobility and transport, Energy Union: Commission takes action to reinforce EU's global leadership in clean vehicles, 2017, Brussels (Belgium), Website: https://ec.europa.eu/transport/modes/road/news/2017-11-08-driving-clean-mobility_en, last access: 28/05/2018.

Chapter 4

Nocturnal electric vehicle charging interacting with a residential photovoltaic-battery system: a 3E (energy, economic and environmental) analysis

[7] A. Poullikkas, Sustainable options for electric vehicle technologies, Renewable and Sustainable Energy Reviews, Volume 41, 2015, Pages 1277-1287, ISSN 1364-0321, https://doi.org/10.1016/j.rser.2014.09.016.

[8] N. Sujitha, S. Krithiga, RES based EV battery charging system: A review, Renewable and Sustainable Energy Reviews, Volume 75, 2017, Pages 978-988, ISSN 1364-0321, https://doi.org/10.1016/j.rser.2016.11.078.

[9] D. Mazzeo, G. Oliveti, C. Baglivo, P. M. Congedo, Energy reliability-constrained method for the multi-objective optimization of a photovoltaic-wind hybrid system with battery storage, Energy, Volume 156, 2018, Pages 688-708, ISSN 0360-5442, https://doi.org/10.1016/j.energy.2018.04.062.

[10] D. Mazzeo, N. Matera, P. Bevilacqua, N. Arcuri, Energy and economic analysis of solar photovoltaic plants located at the University of Calabria, International Journal of Heat and Technology, Volume 33, 2015, Pages 41-50, 10.18280/ijht.330406.

[11] International Energy Agency (IEA), World energy outlook 2017, Paris (France), 2017 ISBN: 9789264282308, http://dx.doi.org/10.1787/weo-2017-en.

[12] J. Wong, Y. Seng Lim, J. Huat Tang, E. Morris, Grid-connected photovoltaic system in Malaysia: A review on voltage issues, Renewable and Sustainable Energy Reviews, Volume 29, 2014, Pages 535-545, ISSN 1364-0321, https://doi.org/10.1016/j.rser.2013.08.087.

[13] P. Denholm, R. M. Margolis, Evaluating the limits of solar photovoltaics (PV) in traditional electric power systems, Energy Policy, Volume 35, Issue 5, 2007, Pages 2852-2861, ISSN 0301-4215, https://doi.org/10.1016/j.enpol.2006.10.014.

[14] P. Nunes, T. Farias, M. C. Brito, Day charging electric vehicles with excess solar electricity for a sustainable energy system, Energy, Volume 80, 2015, Pages 263-274, ISSN 0360-5442, https://doi.org/10.1016/j.energy.2014.11.069.

[15] P. Nunes, R. Figueiredo, M.C. Brito, The use of parking lots to solar-charge electric vehicles, Renewable and Sustainable Energy Reviews, Volume 66, 2016, Pages 679-693, ISSN 1364-0321, https://doi.org/10.1016/j.rser.2016.08.015.

[16] D. P. Birnie, Solar-to-vehicle (S2V) systems for powering commuters of the future, Journal of Power Sources, Volume 186, Issue 2, 2009, Pages 539-542, ISSN 0378-7753, https://doi.org/10.1016/j.jpowsour.2008.09.118.

[17] M. Honarmand, A. Zakariazadeh, S. Jadid, Integrated scheduling of renewable generation and electric vehicles parking lot in a smart microgrid, Energy Conversion and Management, Volume 86, 2014, Pages 745-755, ISSN 0196-8904, https://doi.org/10.1016/j.enconman.2014.06.044.

[18] D.B. Richardson, Electric vehicles and the electric grid: A review of modeling approaches, Impacts, and renewable energy integration, Renewable and Sustainable Energy Reviews, Volume 19, 2013, Pages 247-254, ISSN 1364-0321, https://doi.org/10.1016/j.rser.2012.11.042.

[19] F. Mwasilu, J. J. Justo, E.-K. Kim, T. D. Do, J.-W. Jung, Electric vehicles and smart grid interaction: A review on vehicle to grid and renewable energy sources integration, Renewable and Sustainable Energy Reviews, Volume 34, 2014, Pages 501-516, ISSN 1364-0321, https://doi.org/10.1016/j.rser.2014.03.031.

[20] L. Liu, F. Kong, X. Liu, Y. Peng, Q. Wang, A review on electric vehicles interacting with renewable energy in smart grid, Renewable and Sustainable Energy Reviews, Volume 51, 2015, Pages 648-661, ISSN 1364-0321, https://doi.org/10.1016/j.rser.2015.06.036.

[21] M. Shepero, J. Munkhammar, J. Widén, J. D.K. Bishop, T. Boström, Modeling of photovoltaic power generation and electric vehicles charging on city-scale: A review, Renewable and Sustainable Energy Reviews, Volume 89, 2018, Pages 61-71, ISSN 1364-0321, https://doi.org/10.1016/j.rser.2018.02.034.

[22] F. Fattori, N. Anglani, G. Muliere, Combining photovoltaic energy with electric vehicles, smart charging and vehicle-to-grid, Solar Energy, Volume 110, 2014, Pages 438-451, ISSN 0038-092X, https://doi.org/10.1016/j.solener.2014.09.034.

Chapter 4

**Nocturnal electric vehicle charging
interacting with a residential photovoltaic-battery system:
a 3E (energy, economic and environmental) analysis**

[23] G.R. Chandra Mouli, P. Bauer, M. Zeman, System design for a solar powered electric vehicle charging station for workplaces, Applied Energy, Volume 168, 2016, Pages 434-443, ISSN 0306-2619, https://doi.org/10.1016/j.apenergy.2016.01.110.

[24] C. Roselli, M. Sasso, Integration between electric vehicle charging and PV system to increase self-consumption of an office application, Energy Conversion and Management, Volume 130, 2016, Pages 130-140, ISSN 0196-8904, https://doi.org/10.1016/j.enconman.2016.10.040.

[25] D. Mazzeo, N. Matera, G. Oliveti. Interaction between a wind-PV-battery-heat pump trigeneration system and office building electric energy demand including vehicle charging, 18° EEEIC International Conference on Environment and Electrical Engineering, 2018, Palermo (Italy), 12-15 June 2018. DOI: 10.1109/EEEIC.2018.8493710.

[26] M. Coffman, P. Bernstein, S. Wee, Integrating electric vehicles and residential solar PV, Transport Policy, Volume 53, 2017, Pages 30-38, ISSN 0967-070X, https://doi.org/10.1016/j.tranpol.2016.08.008.

[27] S. De Pinto, Q. Lu, P. Camocardi, C. Chatzikomis, A. Sorniotti, C. Lekakou, Electric vehicle driving range extension using photovoltaic panels, IEEE Vehicle Power and Propulsion Conference (VPPC) 2016, Pages 1-6, 10.1109/VPPC.2016.7791674

[28] L. S. A. Grande, I. Yahyaoui, S. A. Gómez, Energetic, economic and environmental viability of off-grid PV-BESS for charging electric vehicles: Case study of Spain, Sustainable Cities and Society, Volume 37, 2018, Pages 519-529, ISSN 2210-6707, https://doi.org/10.1016/j.scs.2017.12.009.

[29] TRNSYS; Version 17, Solar Energy Laboratory University of Wisconsin-Madison: Madison, 2012, WI (USA).

[30] Senato della Repubblica italiana (Senate of the Italian Republic), Legge sulla Stabilità del 2017, Articolo 3, comma 1, Agevolazioni per gli interventi di efficienza energetica negli edifici, di ristrutturazione edilizia e per l'acquisto di mobile, Rome (Italy), Website: https://www.senato.it/japp/bgt/showdoc/17/DOSSIER/0/1048777/index.html?part=dossier_dossier1-sezione_sezione13-h2_h23, last access: 28/05/2018.

[31] Kottek, M.; Grieser, J; Beck, C.; Rudolf, B.; Rubel F. World Map of the Köppen-Geiger climate classification updated. Meteorologische Zeitschrift 15.3 2006, 259-263. DOI: 10.1127/0941-2948/2006/0130.

[32] Sharp Energy Solutions, Hamburg (Germany). Website: www.sharp.eu/cps/rde/xchg/eu/, last access: 28/05/2018.

[33] European Alternative Fuels Observatory EAFO, Brussels (Belgium), Website: http://www.eafo.eu/, last access: 28/05/2018.

[34] Nissan Italia s.r.l., Website: https://www.nissan.it, last access: 28/05/2018.

[35] Fisch und Fischl GmbH, Spritmonitor.de, Website: www.spritmonitor.de, Thyrnau (Germany), last access: 28/05/2018.

[36] International Council on Clean Transportation ICCT, From laboratory to road - a 2017 update of official and "real-world" fuel consumption and CO2 values for passenger cars in Europe, November 2017, Berlin (Germany), Website: https://www.theicct.org/publications/laboratory-road-2017-update, last access: 28/05/2018.

[37] Transport and Environment, Mind The Gap 2016 – Report, December 2016, Brussels (Belgium), Website: https://www.transportenvironment.org/publications/mind-gap-2016-report, last access: 28/05/2018.

[38] International Electrotechnical Commission. "Electric vehicle conductive charging system-Part 1: General requirements, IEC Standard (2001): 61851-1.

[39] Servizio Elettrico Nazionale - Servizio di maggior tutela SEN (National Electric Service - Protected categories market), Rome (Italy), Website: https://www.servizioelettriconazionale.it/it-IT, last access: 28/05/2018.

Chapter 4   **Nocturnal electric vehicle charging
interacting with a residential photovoltaic-battery system:
a 3E (energy, economic and environmental) analysis**

[40] G. de Oliveira e Silva, P. Hendrick, Photovoltaic self-sufficiency of Belgian households using lithium-ion batteries, and its impact on the grid, Applied Energy, Volume 195, 2017, Pages 786-799, ISSN 0306-2619, https://doi.org/10.1016/j.apenergy.2017.03.112.

[41] S. Schopfer, V. Tiefenbeck, T. Staake, Economic assessment of photovoltaic battery systems based on household load profiles, Applied Energy, Volume 223, 2018, Pages 229-248, ISSN 0306-2619, https://doi.org/10.1016/j.apenergy.2018.03.185.

[42] C. D. Rodríguez-Gallegos, O. Gandhi, M. Bieri, T. Reindl, S.K. Panda, A diesel replacement strategy for off-grid systems based on progressive introduction of PV and batteries: An Indonesian case study, Applied Energy, Volume 229, 2018, Pages 1218-1232, ISSN 0306-2619, https://doi.org/10.1016/j.apenergy.2018.08.019.

[43] C. D. Rodríguez-Gallegos, D. Yang, O. Gandhi, M. Bieri, T. Reindl, S.K. Panda, A multi-objective and robust optimization approach for sizing and placement of PV and batteries in off-grid systems fully operated by diesel generators: An Indonesian case study, Energy, Volume 160, 2018, Pages 410-429, ISSN 0360-5442, https://doi.org/10.1016/j.energy.2018.06.185.

[44] P. Hanser, R. Lueken, W. Gorman, J. Mashal, The practicality of distributed PV-battery systems to reduce household grid reliance, Utilities Policy, Volume 46, 2017, Pages 22-32, ISSN 0957-1787, https://doi.org/10.1016/j.jup.2017.03.004.

[45] X. Han, Y. Liang, Y. Ai, J. Li, Economic evaluation of a PV combined energy storage charging station based on cost estimation of second-use batteries, Energy, Volume 165, Part A, 2018, Pages 326-339, ISSN 0360-5442, https://doi.org/10.1016/j.energy.2018.09.022.

[46] S. Schopfer, V. Tiefenbeck, T. Staake, Economic assessment of photovoltaic battery systems based on household load profiles, Applied Energy, Volume 223, 2018, Pages 229-248, ISSN 0306-2619, https://doi.org/10.1016/j.apenergy.2018.03.185.

[47] Gestore dei Servizi Energetici GSE (Manager of Energy Services), Rome (Italy), Website: https://www.gse.it/, last access: 28/05/2018.

[48] Ministero dello Sviluppo Economico MISE (Ministry of Economic Development), Rome (Italy), Website: http://www.sviluppoeconomico.gov.it, last access: 28/05/2018.

[49] European Central Bank (ECB), Frankfurt (Germany), Website: https://www.ecb.europa.eu/, last access: 28/05/2018.

[50] Istituto Nazionale di Statistica ISTAT (National Institute of Statistics), Rome (Italy), Website: https://www.istat.it/en, last access: 28/05/2018.

[51] Ministero dell'Ambiente e della Tutela del Territorio e del Mare MATTM (Ministry of the Environment and Protection of Land and Sea), Italy, Website: http://www.minambiente.it, last access: 28/05/2018.

Nomenclature

Abbreviations

EV   electric vehicle
NOCT   nominal operative cell temperature
SC1   scenario 1
SC2   scenario 2
SC3   scenario 3
TV   traditional vehicle

Symbols

C   cost (€)
$C_{k,j}$ costs to be incurred per year k for the j-th term (€)
C_{bat} nominal battery capacity (Wh)
$\overline{C}_{bat,fg}$ minimum battery capacity to limit e_{fg} (Wh)

Chapter 4

**Nocturnal electric vehicle charging
interacting with a residential photovoltaic-battery system:
a 3E (energy, economic and environmental) analysis**

$\bar{C}_{bat,tg}$	minimum battery capacity to limit e_{tg} (Wh)
CO_2	CO_2 emissions (kg/yr)
d	discount rate (-)
D	yearly distance travelled (km/yr)
e_{dtl}	fraction of energy sent directly to the load (-)
e_{fb}	fraction of energy drawn from the battery (-)
e_{fg}	fraction of energy drawn from the grid (-)
$\bar{e}_{fg}$	minimum fraction of energy drawn from the grid (-)
e_{tg}	fraction of surplus energy sent to the grid (-)
$\bar{e}_{tg}$	minimum fraction of surplus energy sent to the grid (-)
E_{dtl}	yearly energy sent directly to the load (Wh)
E_{fb}	yearly energy drawn from the battery (Wh)
E_{fg}	yearly energy drawn from the grid (Wh)
E_L	yearly energy required by the load (Wh)
E_{tl}	yearly energy produced sent to the load (Wh)
E_{tg}	yearly surplus energy sent to the grid (Wh)
f_E	electrical emission factor (kg/kWh)
f_{TV}	traditional vehicle emission factor (kg/km)
$g_{c,j}$	inflation rate of the j-th term to the total cost (-)
$g_{s,h}$	inflation rate of the h-th term to the total saving (-)
H	number of terms to the total saving
I_0	initial investment cost (€)
INC	benefits for incentives (€)
J	number of terms to the total cost
k	generic year of the investment lifespan
N	lifespan of the investment (yr)
NPV	net present value (€)
P(t)	power (W)
$P_{fb}(t)$	power drawn from the battery (W)
$P_{fg}(t)$	power drawn from the grid (W)
$P_L(t)$	power required by the load (W)
$P_{pv}(t)$	power produced by the photovoltaic generator (W)
$P_{pv,eff}(t)$	effective power produced by the photovoltaic generator (W)
P_{pv}	nominal power of the photovoltaic generator (W)
$P_{tb}(t)$	power sent to the battery (W)
$P_{tg}(t)$	surplus power sent to the grid (W)
$\bar{P}_{pv,fg}$	minimum photovoltaic power to limit e_{fg} (W)
$\bar{P}_{pv,tg}$	maximum photovoltaic power to limit e_{tg} (W)
$P_{tl}(t)$	power produced sent to the load (W)
R	revenue (€)
R_k	extraordinary revenues per year k (€)
S	saving (€)
$S_{k,h}$	savings obtained per year k for the h-th term (€)
SOC	state of charge of the battery (Wh)
t	time (s)
t_{charge}	charge time (s)

Greek letters

Chapter 4   **Nocturnal electric vehicle charging**
interacting with a residential photovoltaic-battery system:
a 3E (energy, economic and environmental) analysis

$\eta_{DC/DC}$ DC/DC converter efficiency (-)

η_{bat} battery efficiency (-)

η_{inv} inverter efficiency (-)

η_{reg} regulator efficiency (-)

Subscripts

0   year zero

bat,PV battery of the PV system

bat,EV battery of the EV

d   referring to the diesel vehicle

EV   electric vehicle

inv   inverter

m   m-th year in which extraordinary investment costs occur

opt   optimal

p   referring to the petrol vehicle

PV   photovoltaic

PV-EV referring to the electric vehicle charging from photovoltaic

PV-r   referring to the electrical residential user supply from photovoltaic

PV-tg   referring to the sale of electricity to the grid

r   electrical residential load

sav1   emission savings in scenario 1

sav2-3 emission savings in scenario 2 and 3

TV   traditional vehicle

Chapter 5

Interaction between a wind-PV-battery-heat pump trigeneration system and office building electric energy demand including vehicle charging

Chapter 5   **Interaction between a wind-PV-battery-
heat pump trigeneration system and office building electric
energy demand including vehicle charging**

Chapter 5

Interaction between a wind-PV-battery-heat pump trigeneration system and office building electric energy demand including vehicle charging

Abstract

The increasingly electric energy demand, owing to the widespread of use heat pumps and electric vehicles in urban contexts, in the next few years will require strong employment of renewable energy systems and appropriate storage systems. The coupling of more renewable systems with storage systems allows mitigation of the high uncertainty and intermittence of the renewable resources and, therefore, the achievement of greater reliability in satisfying the load and reducing energy in excess.

This work presents a dynamic and energy reliability analysis of a renewable hybrid trigeneration system (RHTS) consisting of a photovoltaic generator, a wind micro-generator and an electric storage battery (electric renewable hybrid system ERHS) used to supply a heat pump, electric office devices, and an electric vehicle charging station. The heat pump is employed for heating and cooling air-conditioning of an office building environment. The RHTS and subsystem grid-connected ERHS considered are employed to satisfy the reference office building energy demand in a Mediterranean area. The dynamic simulation results are employed to study the dynamic interaction between the ERHS with the three electric loads in different characteristic weeks. Different indices are defined and evaluated, in the absence and presence of a battery storage system, to identify the most contemporary load compared with the availability of renewable sources and to determine the system energy reliability.

Keywords: Trigeneration system; Hybrid system; Renewable energy; Electric vehicle; Heat pump; Office building

Chapter 5

Interaction between a wind-PV-battery-
heat pump trigeneration system and office building electric
energy demand including vehicle charging

1. Introduction

Anthropogenic emissions have risen substantially in recent years owing to population growth and, consequently, energy demand, which is destined to grow further. In particular, the electric energy demand could undergo a strong increase over the next 20 years, given the expectations on the diffusion of electric vehicles (EVs) and heat pumps (HPs) for building air conditioning [1,2]. In this hypothetical scenario, the achievement of local energy independence can be attained through the use of one or a combination of several renewable energy systems [3]. The distributed use of electric renewable hybrid systems ERHS, consisting of photovoltaic (PV) and wind power generators and storage system, can be validly used to assist HPs and EVs, as demonstrated by different recent studies in the literature [4-5]. In this work, to evaluate the characteristic dynamic performance and reliability of an RHTS, consisting of a PV and wind generator, battery storage and HP, the potential energy demand in the immediate future of a typical office building, located in the Mediterranean area, was considered. The load scenario considered foresees the employment of the ERHS to supply electric energy to an EV charging station, electric office devices, and HP used for building heating and cooling air conditioning.

2. Hybrid trigeneration system

2.1 Description

A renewable hybrid trigeneration system (RHTS) consisting of a PV system (PV generator and DC/DC converter), a wind system (wind micro-generator and AC/DC rectifier) and an electric storage battery (electric renewable hybrid system ERHS) used to supply a heat pump (HP), the electric devices (ED), and an electric vehicle (EV) charging station in an office building was considered. A reversible multi-stage air-source HP is employed for heating and cooling air-conditioning of the building environments by means of fan coils placed in each thermal zone. In particular, the grid-connected ERHS allows sending the power produced in excess to the grid, when the battery is totally charged, and to draw from the grid the energy missing to satisfy the electric load, when the battery is totally discharged.

2.2 Dynamic simulation

RHTS was dynamically simulated by means of the TRNSYS environment [6] by creating three different subroutines, see Figure 1: (1) building system model; (2) HP system model; (3) ERHS model. In particular, subroutine 1 was employed to evaluate the building peak powers in the heating and cooling period, and hourly building energy needs QB starting from the definition of the external and internal loads, building envelope, functioning hours of the air conditioning system, shading and lighting controls. Subroutine 2 allows the evaluation of the hourly electric energy absorbed by the HP system starting from the hourly building primary energy needs, weather data, and adequate HP control. Starting from the hourly building energy needs, this control manages the HP opening and closure, HP heating and cooling mode, nocturnal/daily set point temperature and, by means of activation of one or more compressors, HP partialisation. Finally, subroutine 3 calculates the hourly renewable energy produced by the ERHS – the part that is directly sent to the load, that which is stored in the battery, and that which is in excess − and the energy drawn from the battery and grid, starting from the weather data, the hourly electric energy absorbed by the HP system, EV and EDs. Types employed are: Type 15 for the generation of the weather data; Type 56 in the detailed mode

Chapter 5

Interaction between a wind-PV-battery-heat pump trigeneration system and office building electric energy demand including vehicle charging

for the building; Type 94 for the PV generator; Type 90 for the wind micro-generator; Type 47 for the battery storage; the efficiency model for the static converters and Type 48 for the inverter and regulator; Type 917, relative to single-stage HP, coupled to Type 970 (for heating mode) or Type 971 (cooling mode), relative to N-stage differential controller, to simulate the energy behavior in the partial load of a multi-stage HP; Type 3 for the hydraulic pump; Type 2 for the differential control, employed for the lighting devices; Type 9 for import into the TRNSYS environment of the hourly data of ground temperature, hourly building energy needs and three electric loads; Type 14 for the air conditioning system daily schedules. For the ground floor, the temperature boundary condition was assessed by a numeric finite difference model.
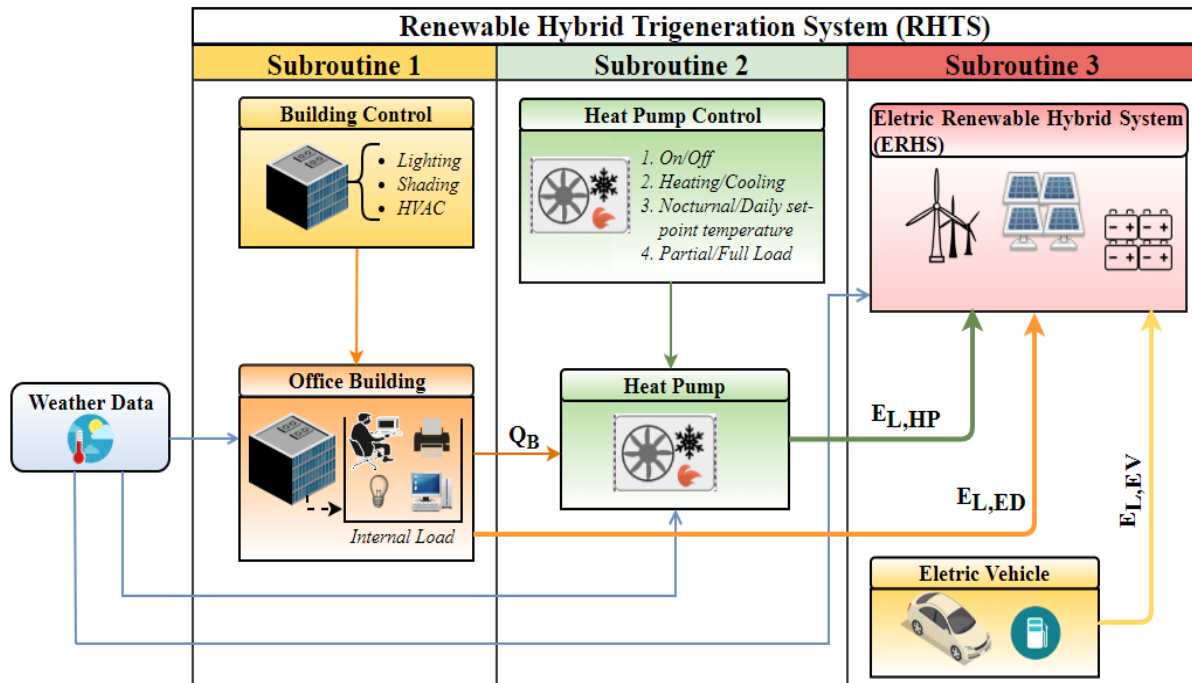
Figure 1. Scheme of the three subroutines for the dynamic simulation of the RHTS.

3. Energy balance of the ERHS

The balance equation of the weekly or yearly energy produced E_g and energy required by the load E_L are:

$$E_g = \frac{E_{dtl}}{\eta_{reg}\eta_{inv}} + \frac{E_{tb}}{\eta_{reg}} + \frac{E_{tg}}{\eta_{reg}\eta_{inv}} \tag{1}$$

$$E_L = E_{L,ev} + E_{L,hp} + E_{L,ed} = E_{dtl} + E_{fb}\,\eta_{inv} + E_{fg} \tag{2}$$

The overall energy produced by the PV and wind generator E_g is partly sent directly to the load, E_{dtl}, partly stored in the battery, E_{tb}, and partly sent to the grid, E_{tg}. The overall energy required by load E_L, the sum of that required by EVs $E_{L,ev}$, HP $E_{L,hp}$ and EDs $E_{L,ed}$, is partly sent directly by the ERHS E_{dtl}, partly received from the battery E_{fb} and partly drawn from the grid E_{fg}. In Eqs. (1) and (2) η_{bat}, η_{inv}, η_{reg} are respectively the battery, inverter and regulator efficiencies.

Chapter 5

**Interaction between a wind-PV-battery-
heat pump trigeneration system and office building electric
energy demand including vehicle charging**

4. Reliability indices

Two different typologies of ERHS reliability indices were defined. The indices defined in relation to the overall load are:

- the overall PV-wind fraction $f_{pv,w}$ measures the fraction of energy required by the load satisfied by the ERHS:

$$f_{pv,w} = \frac{E_{tl}}{E_L} \tag{3}$$

- the utilization factor of the generated energy f_u quantifies the fraction of produced energy by the ERHS employed to satisfy the load:

$$f_u = \frac{E_{tl}}{E_g} \tag{4}$$

The indices defined in relation to the single loads are:

the EV $e_{tl,ev}$, HP $e_{tl,hp}$ and ED $e_{tl,ed}$ energy contemporaneity factors. These factors allow the individuation of the most supplied load, as a consequence of the greater contemporaneity in energy terms between the renewable energy produced trend and the three load trends. The three factors can be calculated considering that the energy sent by the ERHS to the load E_{tl} can be subdivided with reference to the three loads in $E_{tl,ev}$, $E_{tl,hp}$, and $E_{tl,ed}$:

$$\frac{E_{tl,ev}}{E_{tl}} + \frac{E_{tl,hp}}{E_{tl}} + \frac{E_{tl,ed}}{E_{tl}} = e_{tl,ev} + e_{tl,hp} + e_{tl,ed} = 1 \tag{5}$$

the EV $f_{pv,w,ev}$, HP $f_{pv,w,hp}$ and ED $f_{pv,w,ed}$ PV-wind fractions. These fractions are linked to the overall PV-wind fraction by means of the following equation:

$$f_{pv,w} = \frac{E_{tl}}{E_L} = \left(\frac{E_{tl,ev}}{E_{L,ev}}\right)\left(\frac{E_{L,ev}}{E_L}\right) + \left(\frac{E_{tl,hp}}{E_{L,hp}}\right)\left(\frac{E_{L,hp}}{E_L}\right) + \left(\frac{E_{tl,ed}}{E_{L,ed}}\right)\left(\frac{E_{L,ed}}{E_L}\right) =$$

$$= f_{pv,w,ev}\, f_{L,ev} + f_{pv,w,hp}\, f_{L,hp} + f_{pv,w,ed}\, f_{L,ed} \tag{6}$$

where $f_{L,ev}$, $f_{L,hp}$, $f_{L,ed}$ represent the energy fractions required by every single load compared to the overall load. The single products $f_{pv,w}$, f_L correspond to the weighted PV-wind fraction relative to a specific load.

5. Case study

1. _Location:_ the building is located in Rome, Lat = 41° 53', in the Mediterranean area and climate zone D according to the definition given by the standard EN/TR 10349-2 [7]. A typical meteorological year (TMY) data was used to represent the weather conditions [8]. The location is characterized by an annual average hourly temperature of 15.2 °C, annual solar energy on the horizontal plane of 1562.5 kWh/m2 and an annual average hourly and maximum wind speed at a height of 10 m, respectively, of 3.14 m/s and 14.4 m/s.

Chapter 5

**Interaction between a wind-PV-battery-
heat pump trigeneration system and office building electric
energy demand including vehicle charging**

2. _Building:_ is an office with two floors of 100 m2 each. The building envelope vertical surfaces are 50% glazed and the other 50% opaque, and all the building envelope components are those typical of the existing Italian buildings [9]. The opaque and glazed components were designed with steady thermal transmittance lower than those required by the reference national standard [10]. In addition, the shading devices of the glazed walls are activated when the solar radiation is higher than a prederminated limit value. The building was subdivided into eight thermal zones in relation to the wall orientation and occupants' behaviour. In each thermal zone, the heat gains were calculated in relation to the reference standards [11,12]: two people (120 W/per), two personal computers and one printer (75 W) and a LED lighting equipment (125 W), which guarantees an adequate illuminance in the office rooms (400/500 lux). A weekly schedule for the office heat gains was considered in relation to the working hours, between 8:00 and 18:00 from Monday to Friday. Only two zones are different since on Monday, Wednesday and Friday the working hours are from 8:00 to 14:00. In addition, a bright differential control was considered for the lighting devices that allow their closure when the solar radiation is sufficient to guarantee a minimum level of natural lighting. The natural infiltration was set to 1 vol/hour [13]. All the thermal zones are heated to 20°C or cooled to 26°C by an air conditioning system from 7:00 to 18:00 from Monday to Friday. A nocturnal attenuation was considered to avoid excessive cooling in winter and overheating in summer in the thermal zones by opening the air conditioning system again when, respectively, the temperature drops below 12 °C or rises above 34 °C. Dynamic simulations were made to calculate the design peak heating and cooling loads, and the hourly energy needs. The latter were employed to determine the overall yearly heating and cooling energy needs. The design heating and cooling loads [13] are resulted respectively 9.3 kW and 20.6 kW, while the obtained overall yearly heating and cooling energy needs are 987.3 kWh/yr and 19078.8 kWh/yr.

3. _Electric loads_
   - _EV charging_: eight EVs Nissan Leaf 24 kWh were considered to be charged during the working hours. Each EV travels on average 30 km/day and requires two charging hours to recovery this consumption. EV charging station, located in the parking lot of the office building, allows simultaneous charging of four EVs at 2.3 kW. Consequently, the overall schedule of the EV load, required to charge the eight EVs, is 9.2 kW from 9:00 to 13:00 from Monday to Friday. Overall, the yearly electric load owing to the EV charging is 9605 kWh/yr.
   - _HP system_: starting from the peak cooling load, first the design water flow rate m_w at the evaporator was calculated and, considering a water temperature difference of $(T_{w,i}-T_{w,o}) =$
   - $(12 – 7) = 5$ °C, a value of 3780.4 kg/h was obtained. A reversible multi-stage air source HP produced by DAIKIN company with a rated cooling and heating capacity of 21.7 kW and 20.3 kW was considered. The rated cooling and heating electric powers absorbed are 7.25 kW (EER = 2.99) and 7.10 kW (COP = 2.86), while the rated water flow rate is 3720 kg/h. The blower, controller and hydraulic pump powers are respectively 750 W, 40 W and 100 W. The partial load COP and EER were taken in accordance with the manufacturer. By means of a dynamic simulation, the yearly electric energy required by the HP was calculated, resulting in 5999 kWh/yr.
   - _EDs:_ with the weekly schedule of the devices and the bright control described in Section II-E, an overall yearly load of 3101 kWh/yr was obtained. The overall yearly electric load is to be attributed 51 % to the EV, 32 % to the HP, and 17 % to the EDs.

Chapter 5

Interaction between a wind-PV-battery-heat pump trigeneration system and office building electric energy demand including vehicle charging

4. ERHS components

The PV-wind hybrid system analyzed has an overall power of 15 kW and allows the production of almost exactly the energy required by the yearly electric load. Both the PV and the wind micro-generator type were preliminary chosen to maximize, in the location considered, the energy produced for each kW installed. For this reason, 15 different PV generators and 15 different wind micro-generators were independently simulated.

- *PV system:* the best PV module resulted is produced by the Europe Solar Production Company. The polycrystalline silicon module has a rated power of 250 W, efficiency of 15.3 %, and manufacturability in Rome of 1559 kWh/kWp. The overall rated PV power of 7.5 kW was obtained considering 15 modules in series and 2 modules in parallel. The static DC/DC converter efficiency is 0.94.

- *Wind micro-generator system:* the best wind micro-generator resulted is produced by the Tulipower company. It has a rated power of 2.5 kW, rated wind speed of 10 m/s and cut-in wind speed of 3 m/s. The manufacturability in Rome is 1074 kWh/kWp. The overall rated wind power of 7.5 kW was obtained by installing 3 wind micro-generators. The static AC/DC rectifier efficiency is 0.90.

- *Battery, regulator and inverter:* a lithium-ion battery produced by LG Chem, with a storage capacity of 2 kWh and efficiency of 0.85 was employed. The overall storage capacity was increased by using several batteries. The DC/AC inverter and regulator efficiencies are respectively 0.97 and 0.98.

6. Results and discussion

In Section 6.1, the results of the comparison of the ERHS dynamic behavior with overall nominal power of 15 kW in the absence and presence of a battery storage capacity of 20 kWh were reported. In Section 6.2, the increment of the energy reliability owing to the presence of the battery storage, by using the indices defined in Section 6.3, in the characteristic weeks was assessed.

6.1 EHRS dynamic behaviour in characteristic weeks

To study the dynamic interaction between the ERHS and load, three characteristic weeks were identified with the weekly electric energy produced: (a) very close to the weekly electric energy load, 45th week; (b) much lower than the weekly electric energy load, 6th week; (c) much higher than the weekly electric energy load, 7th week. Figs. 2-4, relative respectively to the 45th, 6th, and 7th, show: at the top, both in the presence and absence of the battery storage, the trends of the overall electric load, power produced sent directly to the load, power drawn from the grid, and power sent to the grid (reported on the negative axis); at the centre, the trends of the overall PV and wind power produced, state of charge SOC of the battery, and power sent (positive) or drawn (negative) from the battery; at the bottom, the trends of the solar radiation on the horizontal plane, wind speed and external air temperature. The figures highlight the night/day and weekday/weekend intermittent behavior of the load owing to the occupant.

Chapter 5

**Interaction between a wind-PV-battery-
heat pump trigeneration system and office building electric
energy demand including vehicle charging**
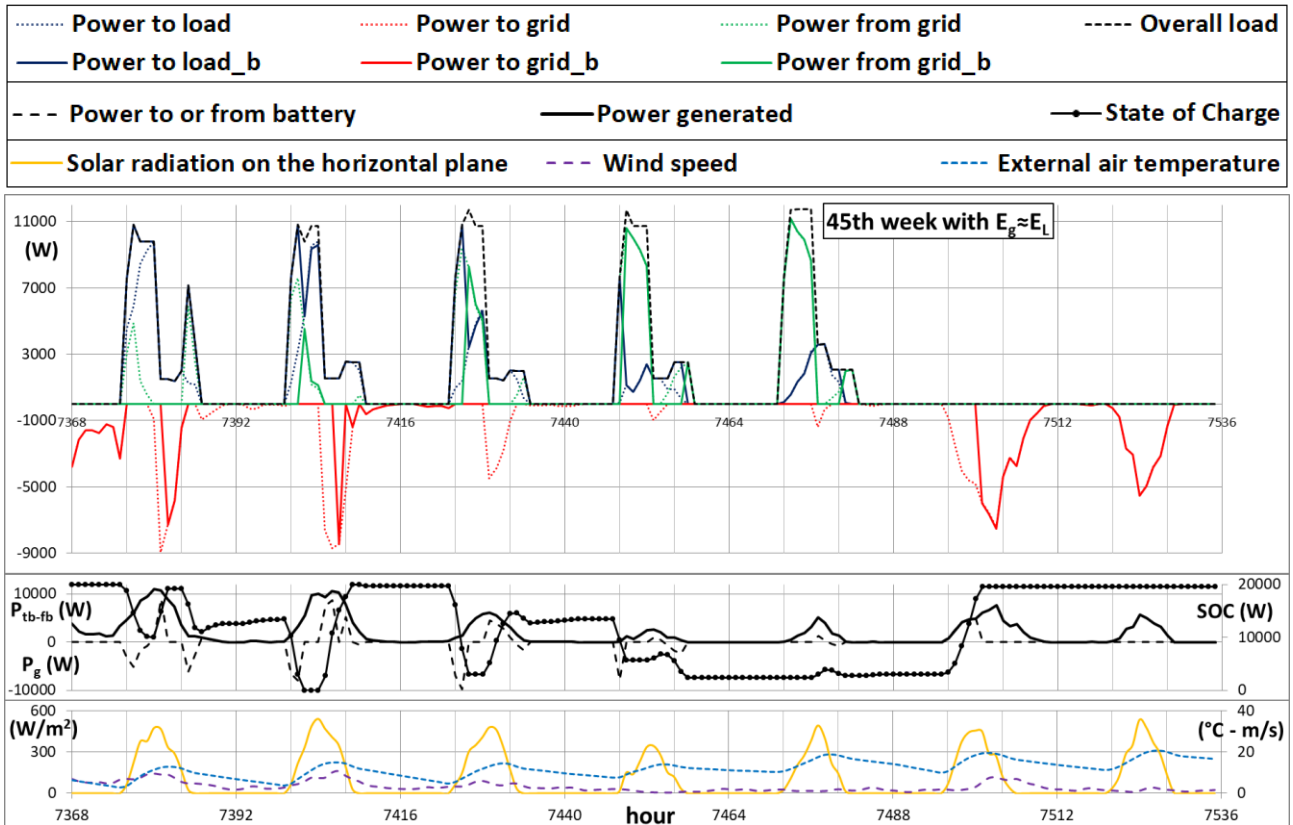
Figure 2. *Dynamic interaction between the ERHS and load when the weekly electric energy produced is very close to the weekly electric energy demand.*
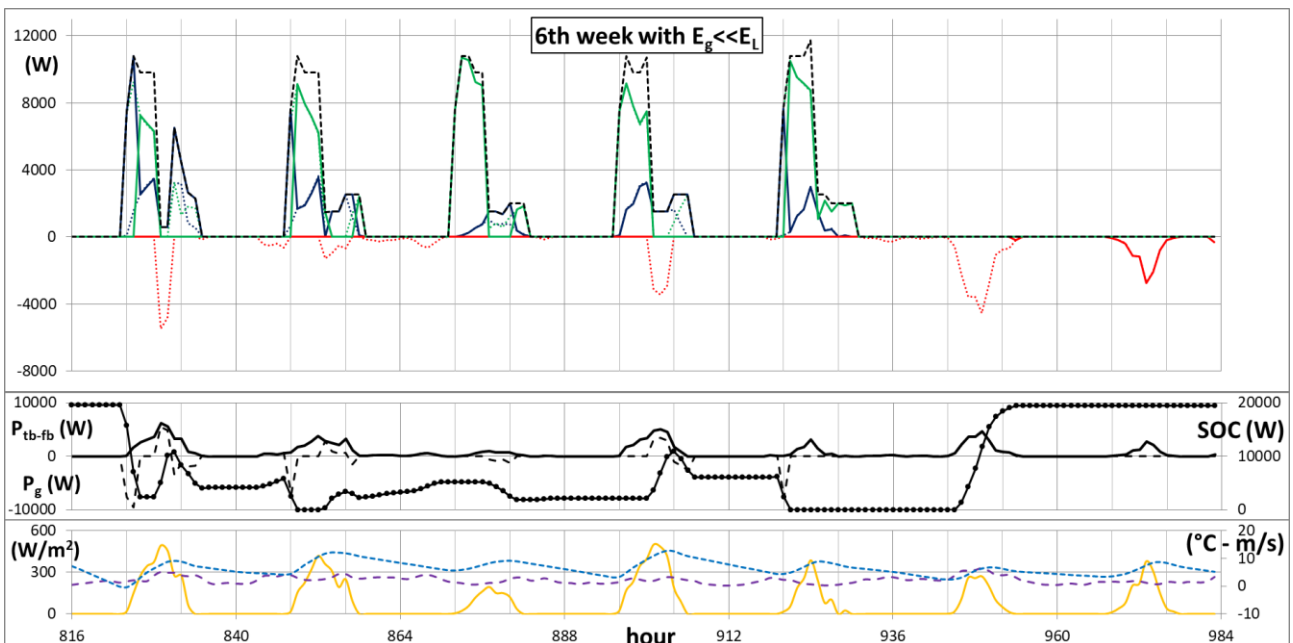
Figure 3. *Dynamic interaction between the ERHS and load when the weekly electric energy produced is much lower than the weekly electric energy demand.*

Chapter 5

**Interaction between a wind-PV-battery-
heat pump trigeneration system and office building electric
energy demand including vehicle charging**
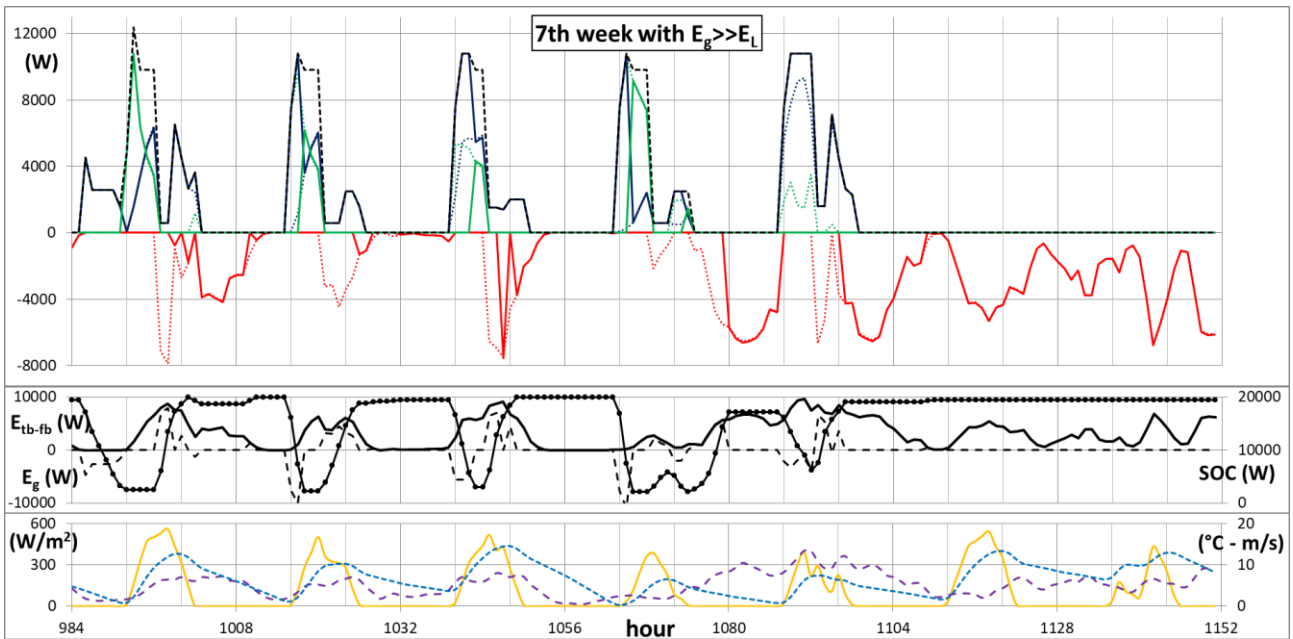
Figure 4. Dynamic interaction between the ERHS and load when the weekly electric energy produced is much higher than the weekly electric energy demand.

In particular, a typical daily trend is characterized by a high load value in the morning mainly owing to the HP opening and the EV charging, while in the afternoon the load is lower and mainly owing to the EDs. In these conditions, during the weekdays, the instantaneous cover of the load is mainly to be attributed to the PV generator, owing to the higher contemporaneity with the load. The wind generator provides the power missing to the load on cloudy days and charges the battery during the night. On sunny days, also the PV generator contributes to charging the battery. At the weekend, in the absence of load, both PV and wind powers produced contribute only to charging the battery. When the PV, wind and battery powers are not enough to satisfy the load, the grid provides the energy missing, while when the power produced is higher than the load and the battery is totally charged, the excess power is sent to the grid. In the absence of the battery, the power in excess and the power drawn from the grid are greater. In particular, in the 45th week ($E_g \approx E_L$), see Fig. 2, the energy produced is almost exclusively originated by the PV generator owing to the reduced wind speeds. On the first two days, characterized by a high PV production: in the absence of the battery, the energy produced sent to the load prevails over the energy drawn from the grid in the load satisfaction, with a significant magnitude of energy in excess; in the presence of the battery, the energy produced sent to the load increases, while the energy drawn from the grid is annulled on the first day and much reduced on the second one. This is a consequence of the partial recovery, by means of the battery, of the energy in excess. The first day starts with a SOC=SOC$_{max}$, reached during the weekend by means of the storage of the energy in excess. Successively, the battery is first partly discharged, then completely recharged and, finally, partly discharged again, as highlighted from the trend of the power sent/drawn. On the second day, in the morning the battery is completely discharged, thus limiting the intervention of the grid, while in the afternoon the battery is completely charged since the load is contained and energy in excess available. The battery intervention is also highlighted by the comparison of the excess power trends in the presence and absence of the battery. On the third day, the PV production is lower: in the absence of the battery, the energy drawn from the grid is higher than energy produced sent to the load, with lower excess power; in the presence of the battery, the

Chapter 5

**Interaction between a wind-PV-battery-
heat pump trigeneration system and office building electric
energy demand including vehicle charging**

load is satisfied to the almost same magnitude by the grid and ERHS. This is a consequence of the complete recovery, by means of the battery, of the excess energy. On this day, the SOC decreases in the morning and increases in the afternoon without charging the battery completely, owing to the reduced energy in excess available. The fourth and fifth day have low PV production. Consequently, both in the absence and presence of the battery storage, the energy sent to the load almost exclusively comes from the grid, energy in excess is almost nil, and there are no significant differences between the case in the presence and absence of the battery. Compared to the fifth day, the fourth day shows a greater difference between the case with and without battery, since it uses the energy stored on the previous day, discharging the battery completely. In these conditions, at the start of the fifth day, there is not the availability of energy stored and, owing to the reduced energy production, the battery remains discharged on the entire day. The charge phase starts then on the first day of the week-end since the load is nil and energy in excess available. This phase ends on the same day since the battery size is not enough to store the high energy in excess available, equal to the overall energy produced in the entire weekend. In these conditions, the weekends with the battery completely charged.

In the 6th week ($E_g \ll E_L$), see Fig. 3, the energy produced is again almost exclusively originated by the PV generator. Compared to the 45th week, the solar radiation on all days is very low. In these conditions, on the weekdays, the energy drawn from the grid prevails over the energy produced sent to the load. In addition, the low PV production gives rise to very low availability of energy in the battery, since the energy in excess recoverable is very limited, which is, however, completely stored. Consequently, the trends of the powers reported in the image at the top, in the presence and absence of the battery are very similar, the SOC is prevalently low during the weekdays, while on the weekend days the SOC reaches the SOC_{max} value by means of the storage of the energy in excess available.

In the 7th week ($E_g \gg E_L$), see Fig. 3, the energy produced is originated by both the PV and wind generator owing to the high solar radiation and wind speeds. Compared to the 45th week, in all the weekdays the energy produced sent to the load prevails over the energy drawn from the grid. The high energy in excess availability leads to a SOC_{max} in the night of the weekdays and at the weekend. In the morning of the weekdays, the battery is discharged, while in the afternoon the SOC_{max} is recovered. Consequently, in the presence of the battery compared with the case of absence of the battery, the energy drawn from the grid is drastically reduced, while the energy produced sent to the load is increased remarkably. Despite the presence of the battery, the energy in excess is not completely recoverable during the weekdays, especially that coming from the wind generator, while that in excess is completely sent to the grid during the weekend. In this week, the trend of the load on the first day shows the activation of the HP system also in the night, and the power requested is provided exclusively by the battery storage since the wind speed is lower than the cut-in wind speed. Consequently, in the morning the battery resulted discharged and the load is satisfied partly by the PV and wind generator and partly by the grid.

6.2. ERHS reliability

As shown in the previous section, during each week the energy reliability of the ERHS is highly variable. To provide a summary indication of the weekly dynamic behavior of the ERHS, the weekly reliability indices were assessed in the absence and presence of the battery storage. Table 1 shows $e_{tl,ev}$, $e_{tl,hp}$ and $e_{tl,ed}$ energy contemporaneity factors, $f_{pv,w,ev}$, $f_{pv,w,hp}$ and $f_{pv,w,ed}$ PV-wind fractions, $f_{pv,w,ev}$, $f_{L,ev}$ $f_{pv,w,hp}$ $f_{L,hp}$ and $f_{pv,w,ed}$ $f_{L,ed}$ weighted PV-wind fractions, and overall PV-wind fraction $f_{pv,w}$.

Chapter 5

Interaction between a wind-PV-battery-heat pump trigeneration system and office building electric energy demand including vehicle charging

In addition, the percentage difference between the reliability indices in the absence and presence of the battery were reported. The energy fractions required by every single load compared to the overall load can be considered constant in the three weeks with values $f_{L,ev}=0.57$, $f_{L,hp}=0.25$, $f_{L,ed}=0.18$, since the overall load is almost unchanged. Only the 6th week is quite different with an EV charging load of 59 %, HP load of 21% and ED load of 19%. The slight differences are owing to the modification of the HP load that is dependent on the energy needs variation.

In the absence of the battery: for all three characteristic weeks, regardless of the E_g and E_L value, the energy contemporaneity factors remain almost unchanged with that relative to the EV almost twice the other factors. This is owing to the higher load requested by the EV charging, despite its being concentrated in a more reduced time interval, and to the greater synchronism with the renewable energy production, especially with the PV one. The comparison of the three PV-wind fractions, in the three characteristic weeks, highlight that: when $E_g \approx E_L$, the three loads are satisfied to almost the same extent; when $E_g \ll E_L$, the lower energy produced gives rise to a drastic reduction of the three fractions, especially that of the EV load; when $E_g \gg E_L$, despite the higher energy produced, the three fractions do not increase in a significant manner, except that of EDs that increases from 0.49 to 0.64.

If the weight of the single loads is considered, the relative PV-wind fractions demonstrate that the EV load is the most incident in the overall PV-wind fraction, owing to the higher energy fraction required by this load.

Table 1. *Reliability indices in the characteristic weeks in the absence and presence of the battery storage.*

Characteristic weeks		*week*	$e_{tl,ev}$	$e_{tl,hp}$	$e_{tl,ed}$	$f_{pv,w,ev}$	$f_{pv,w,hp}$	$f_{pv,w,ed}$	$f_{pv,w,ev} f_{L,ev}$	$f_{pv,w,hp} f_{L,hp}$	$f_{pv,w,ed} f_{L,ed}$	$f_{pv,w}$	$f_{u,g}$
Without battery	$E_g \approx E_L$	45	0.56	0.24	0.21	0.43	0.42	0.49	0.24	0.10	0.09	0.44	0.45
	$E_g \ll E_L$	6	0.50	0.26	0.24	0.19	0.28	0.29	0.11	0.06	0.05	0.23	0.54
	$E_g \gg E_L$	7	0.52	0.24	0.24	0.46	0.49	0.64	0.26	0.12	0.12	0.50	0.31
With battery	$E_g \approx E_L$	45	0.48	0.31	0.21	0.53	0.79	0.73	0.30	0.19	0.13	0.63	0.67
	$E_g \ll E_L$	6	0.36	0.38	0.26	0.23	0.68	0.50	0.14	0.15	0.10	0.38	0.93
	$E_g \gg E_L$	7	0.48	0.31	0.21	0.64	0.94	0.87	0.36	0.23	0.16	0.76	0.49
Percentage difference	**Δ%**	45	-13.74	29.03	3.88	24.93	86.87	50.44	24.93	86.87	50.44	44.82	48.15
	Δ%	6	-27.48	46.78	5.77	20.61	144.12	75.92	20.61	144.12	75.92	66.32	71.04
	Δ%	7	-7.85	27.01	-10.66	39.80	92.69	35.53	39.80	92.69	35.53	51.71	55.93

The comparison of the overall PV-wind fraction and the utilization factor shows their complementary behaviour since, for a given overall load, starting from the case $E_g \approx E_L$ a higher energy produced leads to an increment of the $f_{pv,w}$ and reduction of the $f_{u,g}$. The opposite behaviour is shown for lower energy produced. Finally, in the absence of the battery storage, a maximum satisfied load fraction of 50% is obtained with the maximum energy production, and maximum utilization of the energy generated of 54% is obtained with the minimum energy production.

In the presence of the battery storage, the fractions of overall energy produced sent to the three loads, directly or subsequently to the storage, expressed by means of the energy contemporaneity factors, is considerably modified. In particular, the energy contemporaneity factor of the HP increases remarkably, to the detriment of elevated decrement of energy contemporaneity factor of the EV.

Chapter 5

**Interaction between a wind-PV-battery-
heat pump trigeneration system and office building electric
energy demand including vehicle charging**

These modifications are very pronounced when the energy generated is much lower than the energy required by the overall load. In addition, in the presence of battery storage, all the reliability indices considered undergo a significant increment. In particular, both the non-weighted and weighted PV-wind fractions relative to the HP highlight the most substantial rise, reaching also a value of 144% higher than that obtained in the absence of the battery. In these conditions, the difference between the PV-wind fraction of the EV and that of the HP is reduced, becoming negligible when $E_g \ll E_L$, and they incide to the same extent on the overall PV-wind fraction. $f_{pv,w}$ and $f_{u,g}$ show the same qualitative behaviour highlighted in the absence of the battery storage. Instead, from a quantitative point of view, both $f_{pv,w}$ and $f_{u,g}$ undergo a remarkable augmentation. The maximum $f_{u,g}$ is reached when $E_g \ll E_L$, since all the energy produced is almost sent to the loads and the energy in excess is very limited thanks to the battery intervention. Instead, the maximum $f_{pv,w}$ is attained when $E_g \gg E_L$, limiting the energy drawn from the grid to 24%.

7. Conclusions

The dynamic and energy analysis of an RHTS, in three weeks characterized by different values of the renewable electric energy produced compared to the electric energy required by the three loads, in the absence and presence of battery storage, has highlighted the different interaction between the solar and wind energy renewable sources and loads. The employment of a battery storage system resulted to be fundamental to increase the reliability of an ERHS, being the loads strongly intermittent and energy renewable sources strongly intermittent and random. In particular, the comparison of the three characteristic weeks have shown that in some days the battery is undersized when production and demand are not synchronized or the energy production is very high with substantial energy in excess, and in other days the battery is oversized when production and demand are synchronized or the energy produced is exclusively employed to satisfy the load and the energy in excess is limited. This is also highlighted by the weekly reliability index values that they vary in a wide range.

In the specific RHTS, the trend of the electric vehicle load appears to be the most contemporaneous for a power supply through an ERHS without a battery, employing in this way the vehicle storage system, although if the electric vehicle load is not the most satisfied because of its high value concentrated in a reduced time interval. Instead, in the presence of the battery storage, despite the electric energy required by the heat pump being lower than that of the electric vehicle charging station, the energy produced sent to the two loads and the contribution to the overall PV-wind fraction is comparable, especially when the energy produced is much lower than the overall energy required by the load.

From a qualitative point of view, the reliability increase achieved by means of the battery storage is strongly dependent on the difference of the energy generated and the energy required by the load. In particular, when they are very close, despite there not being a perfect contemporaneity, the ERHS is very reliable both in terms of load satisfaction and complete utilization of the energy produced. In other conditions, the ERHS has partial reliability, since it is not possible to reach simultaneously high values of both the energy indices, because the energy in excess is not recoverable or not available. This objective could be attained with a higher battery storage capacity in order to recover further energy in excess during the weekend when the load is nil. The next step will be to develop a parametric analysis by varying the battery storage capacity in order to highlight the effects produced on the dynamic interaction, and week and yearly energy reliability.

Chapter 5   **Interaction between a wind-PV-battery-
heat pump trigeneration system and office building electric
energy demand including vehicle charging**

References

[1] TERNA Group, Document description of the scenarios, Edition 2018, Website: http://www.terna.it/it-it/home.aspx, last access: 20/04/2018.

[2] TERNA Group, Monthly report on the electrical system, January 2018 Website: http://www.terna.it/it-it/home.aspx, last access: 20/04/2018.

[3] D. Mazzeo, G. Oliveti, C. Baglivo, P. M. Congedo, Energy reliability-constrained method for the multi-objective optimization of a photovoltaic-wind hybrid system with battery storage, Energy, 2018, ISSN 0360-5442, https://doi.org/10.1016/j.energy.2018.04.062.

[4] C. Roselli, M. Sasso, Integration between electric vehicle charging and PV system to increase self-consumption of an office application, Energy Conversion and Management, Volume 130, 2016, Pages 130-140, ISSN 0196-8904, https://doi.org/10.1016/j.enconman.2016.10.040.

[5] J.C. Solano, L. Olivieri, E. Caamaño-Martín, Assessing the potential of PV hybrid systems to cover HVAC loads in a grid-connected residential building through intelligent control, Applied Energy, Volume 206, 2017, Pages 249-266, ISSN 0306-2619, https://doi.org/10.1016/j.apenergy.2017.08.188.

[6] TRNSYS; Version 17. (2012) Solar Energy Laboratory University of Wisconsin-Madison: Madison, WI, USA.

[7] UNI/TR 10349-2, Heating and cooling of buildings Climatic data – Part 2: Data for design load, 2016.

[8] Meteonorm, software version 6.1. 0.20 of April 2010. Meteotest, Switzerland, 2010.

[9] UNI/TR 11552, Opaque envelope components of buildings - Thermo-physical parameters, 2014.

[10]   Decreto interministeriale 26 giugno 2015 - Applicazione delle metodologie di calcolo delle prestazioni energetiche e definizione delle prescrizioni e dei requisiti minimi degli edifici., 2015.

[11]   EN ISO 7730, Ergonomics of the thermal environment - Analytical determination and interpretation of thermal comfort using calculation of the PMV and PPD indices and local thermal comfort criteria, 2005.

[12]   ISO 13790, Energy performance of buildings - Calculation of energy use for space heating and cooling, 2008.

[13]   EN 12831, Heating systems in buildings - Method for calculation of the design heat load, 2003.

Chapter 6

Solar and wind assisted heat pump to meet the building air conditioning and electric energy demand in the presence of an electric vehicle charging station and battery storage

Chapter 6

Solar and wind assisted heat pump to meet the building air conditioning and electric energy demand in the presence of an electric vehicle charging station and battery storage

Chapter 6   **Solar and wind assisted heat pump to**
meet the building air conditioning and electric energy demand
in the presence of an electric vehicle charging station and battery storage

Chapter 6

Solar and wind assisted heat pump to meet the building air conditioning and electric energy demand in the presence of an electric vehicle charging station and battery storage

Abstract

The increasingly widespread use of heat pumps (HPs) for the air conditioning of environments and electric vehicles (EVs) in urban contexts will lead in the short term to an increase in required electricity both on a scale of agglomeration of buildings and of a single building. To address this issue, in this work, an efficient renewable hybrid trigeneration system (RHTS) is analysed to be employed for heating and cooling air conditioning and electricity production. The electric energy is produced by means of an electric renewable hybrid system (ERHS), composed of photovoltaic (PV) and wind systems with battery storage, which is employed to power the HP, an EV charging station and building electric devices.

A methodology that employs different indicators, to be used both in deterministic and statistical system analysis, was proposed to quantify the average reliability and reliability uncertainty of a hybrid system. In particular, in the statistical analysis, each indicator was subdivided into the average and uncertainty contribution, defined with two different perspectives. The first set of indicators allows quantification of the ERHS capability: to satisfy the overall load by means of the overall PV-wind fraction; to utilize the entire renewable energy produced by means of the utilization factor, to operate in nominal conditions by means of the dimensionless manufacturability; to cover the overall load over time by means of the overall time contemporaneity factor. The second set of indicators permits the comparison of the three different electric loads among them in terms of: renewable energy sent by the ERHS to each load by means of the energy contemporaneity factors; satisfaction of every single load by means of the PV-wind fractions; satisfaction of every single load in relation to the overall

load by means of the weighted PV-wind fractions; satisfaction of every single load over time by means of the time contemporaneity factors.

For this issue, a dynamic simulation tool, containing sophisticated models and proper algorithms and made up of three subroutines respectively for the building, HP and ERHS systems, was developed. In particular, a new algorithm to simulate the performance of a reversible multi-stage air-source HP was created.

By considering an RHTS employed for supplying an office building energy demand located in the Mediterranean area, a weekly deterministic analysis has allowed evaluation of the reliability of the ERHS in the presence and absence of electric storage, while a yearly statistical analysis has allowed the identification of the system configurations with the highest average reliability and lowest reliability uncertainty by varying of the battery capacity, PV and wind power.

Keywords: Hybrid system; Photovoltaic; Wind; Storage; Heat pump; TRNSYS; Reliability; Uncertainty

- The average reliability and reliability uncertainty of a renewable hybrid trigeneration system (RHTS) was determined.

Chapter 6   **Solar and wind assisted heat pump to**
meet the building air conditioning and electric energy demand
in the presence of an electric vehicle charging station and battery storage

- PV, wind, and battery system (electric renewable hybrid system ERHS) assist heat pump, electric vehicle and building demand.
- A novel dynamic simulation tool containing building, heat pump and ERHS models was created.
- A new set of indicators were defined and used both in a weekly deterministic and yearly statistical analysis.
- A width parametric analysis as a function of the PV and wind powers and battery storage capacity was developed.

Chapter 6   **Solar and wind assisted heat pump to**
meet the building air conditioning and electric energy demand
in the presence of an electric vehicle charging station and battery storage

1. Introduction

Nowadays the international scientific community and the governing bodies are very sensitive to the issues concerning the emissions of greenhouse gases, which, without a substantial intervention in the efficiency of the energy production systems, are destined to grow further. Different energy sectors are potentially affected by this required turnaround. In particular, the transport and building air conditioning sectors are undergoing a rapid change in terms of the energy sector that are moving toward the electric source. The advent of electric vehicles (EVs) and the spread expected in the coming decades, thanks to continuous technological growth and cost reduction, and the expectations on the diffusion of heat pumps (HPs) for building air conditioning could make the generation and management of electric energy the main issue to be addressed [1].

For this reason, the reduction and decarbonisation of energy in these sectors is a priority objective for the European Union, which with directives - of which the last 2018/844/EU [2] of the European Parliament and of the Council of 30 May 2018, amending Directive 2010/31/EU [3] on the energy performance of buildings and Directive 2012/27/EU [4] on energy efficiency - requires the Member States to enact regulations for the achievement of the defined energy performance of buildings.

Among the novelties of the new directive, "*with regard to new non-residential buildings and non-residential buildings undergoing major renovation, with more than ten parking spaces, Member States shall ensure the installation of at least one recharging point within the meaning of Directive 2014/94/EU of the European Parliament and of the Council and ducting infrastructure, namely conduits for electric cables, for at least one in every five parking spaces to enable the installation at a later stage of recharging points for electric vehicles*". Also, for new residential buildings and residential buildings undergoing major renovation similar provisions are envisaged.
In this way, buildings can support the overall decarbonisation of the transport sector. By citing the recent Directive "*For example, buildings can be leveraged for the development of the infrastructure necessary for the smart charging of electric vehicles and also provide a basis for Member States, if they choose to, to use car batteries as a source of power.*"

With regard to EV, a market share of up to 27% is expected to be achieved by 2030 [5], a development that could be supported by new European regulation such as the "Clean Mobility Package", which aims to reduce vehicle emissions by 30% compared to 2021 [6]. Also, the use of HP is destined to grow, since they are highly efficient technologies that offer the possibility of providing heating and cooling in buildings, reducing the primary energy consumption with respect to traditional systems.

The actions promoted to counter the increase in pollutant emissions concern, on the one hand, the reduction in energy consumption and, on the other, the replacement of conventional energy sources based on fossil fuels, with renewable energy sources. A transition is required that configures consumers no longer as passive figures but rather as active figures in achieving the goals set by international agreements. In accordance with the new Directive, "C*ombined with an increased share of renewable electricity production, electric vehicles produce fewer carbon emissions resulting in better air quality.*".
For this aim, electric renewable hybrid system ERHS, consisting of photovoltaic (PV) and wind micro-generators and storage system, were systematically studied by undergoing a rapid advancement from a technological and cost point of view [7, 8]. Generally, these hybrid systems were employed especially to satisfy the energy demand of a typical office or residential user without considering the

Chapter 6   **Solar and wind assisted heat pump to**
meet the building air conditioning and electric energy demand
in the presence of an electric vehicle charging station and battery storage

recent developments in the air conditioning and mobility sectors with the advent of HPs and EVs [8]. In particular, some researches have addressed the optimization issue in energy, economic and environmental terms of stand-alone hybrid system that utilizes the conventional diesel engine as an integration system in the presence and absence of battery storage [9-12]. In similar studies, the stand-alone system was investigated by using as an integration system only the battery storage [13], or by employing, in addition to the solar and wind energy resources, also the hydropower source [14]. The use of local renewable sources can contribute to smoothing up the electric energy demand peak and, for a typical user, reducing the overall electric energy drawn from the grid. ERHS-assisted HP permits the use of partly locally generated electric renewable energy for high-efficiency building heating and cooling air conditioning, thus obtaining an innovative renewable hybrid trigeneration system (RHTS). In the literature, RHTS was also realized employing geothermal HP assisted by solar collectors to supply thermal storage in the tank [15]. It was demonstrated that the use of the geothermal HP gives rise to different benefits in terms of economic, energy, and greenhouse gas payback time [16].

A well-designed ERHS can also be used to power an EV, thus obtaining important flexibility on the management of the electric energy demand of a user considering the additional storage volume of EV. Laurischkat and Jandt have developed a newly techno-economic model to study the technological synergies between a PV system, a battery storage system and electric vehicles [17].

Ultimately, in the scenario described and considering the continuous reduction of the costs of these technologies, their contemporaneous utilize could become standard practice in new and existing constructions in the short to medium term, to achieve emissions mitigation, to reduce the dependency on fossil fuel, and to considerably improve the system energy efficiency and reliability.

The literature analysis shows that, even if the technologies described have been studied and developed singularly for many years, the study of combined systems is quite recent. It is, therefore, necessary to reinforce theoretical and experimental studies and research to contribute to the more rapid penetration of these combined systems (PVs, winds, storage batteries, HPs and EVs) in the building sector. There are very few scientific studies found in the scientific literature that address in depth these combined systems. For example, recent research that aims to address the topic described by studying, through a deterministic analysis in energy and environmental terms, a PV plant interacting with a reversible HP that satisfies electricity, space heating and cooling demand of an office building located in southern Italy when an EV charging station is present [18]. A similar study has investigated in different characteristic weeks the dynamic interaction between solar and wind generator and battery storage with an electric load owing to an HP, EV charging station and electric devices in an office building [19]. An important role in these system types is conferred to the electric battery storage system. In another recent research, a model of intelligent control of a battery energy storage system is proposed to increase PV self-consumption and grid-peak shaving in a grid-connected residential building prototype integrated with a PV system coupled to a battery energy storage system used for the heating, ventilation, and air-conditioning system by means of a reversible HPs [20].

Finally, renewable generation and electric mobility have attracted the interest of several researchers [21, 22]. A particular analysis that combines the PV generation and the EVs was studied by assuming different levels of PV generation and different penetrations of the EVs under the uncontrolled charging regime and the application of smart charging and vehicle-to-grid strategies [23].

In this work, a novel weekly deterministic and yearly statistical analysis were developed to detect the average reliability and reliability uncertainty of an ERHS, used to supply a HP, the pure

Chapter 6
Solar and wind assisted heat pump to
meet the building air conditioning and electric energy demand
in the presence of an electric vehicle charging station and battery storage

electric energy demand of an office building, and an EV charging station. For this issue, a new dynamic simulation tool in the TRNSYS environment was created for the renewable hybrid trigeneration system RHTS dynamic simulation coupled with the air conditioning and electric energy demand of the office building considered located in the Mediterranean area. Different system configurations and system sizes were parametrically analyzed to identify, by means of the use of a novel set of dimensionless indicators, the ERHS with the most reliable and the least uncertain in reliability terms.

2. Hybrid trigeneration system and user

1. Description

With reference to Figure 1, a renewable hybrid trigeneration system (RHTS) is used to supply heating, cooling and electric energy to an office building user. In particular, a grid-connected electric renewable hybrid sub-system ERHS made up of a PV system (PV generator and DC/DC converter), a wind system (wind micro-generator and AC/DC rectifier) and an electric storage battery, is employed to assist a reversible multi-stage air-source HP for heating and cooling air-conditioning of building environments by means of fan coils placed in each thermal zone. In addition, the ERHS provides for satisfying the electric energy required by the electric office devices (ED), and for supplying an EV charging station.
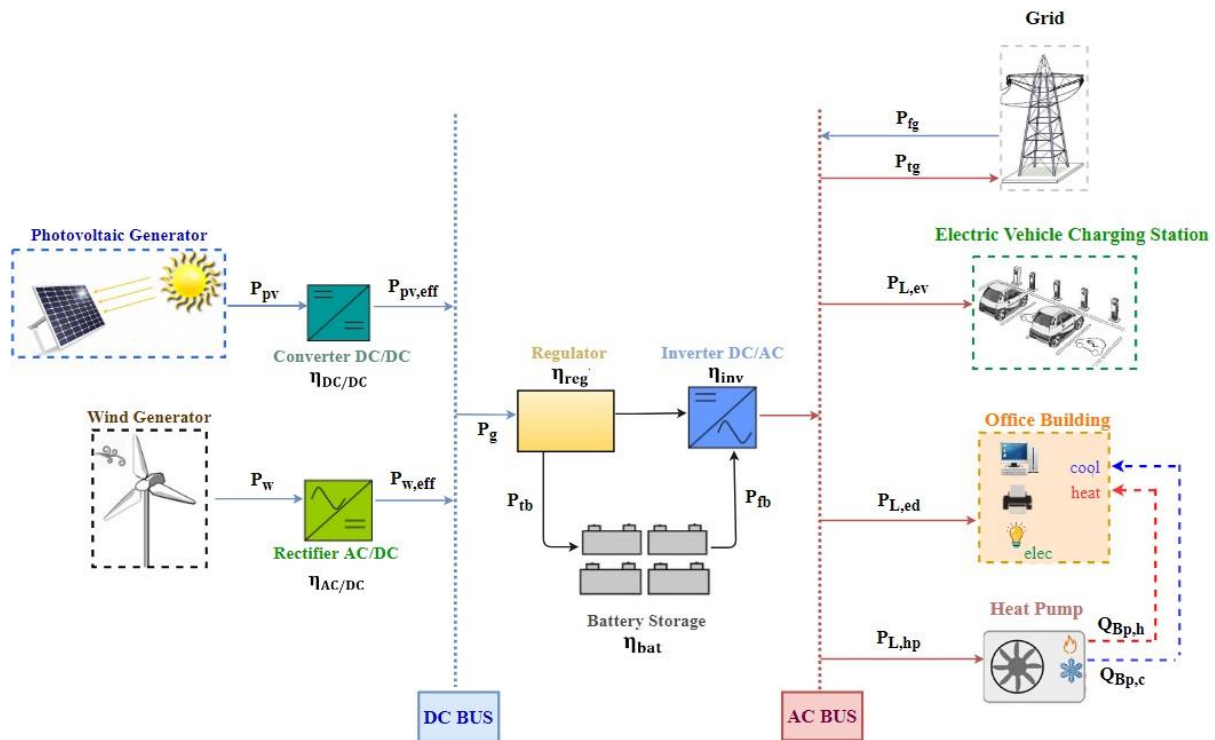
Figure 1. *RHTS and ERHS schematization.*

In particular, the power produced by the PV generator P_{pv}, reduced to $P_{pv,eff}$ by the DC/DC static converter, and by the wind micro-generator P_w, reduced to $P_{w,eff}$ in the rectifier, is used to satisfy the EV load $P_{L,ev}$, HP load $P_{L,hp}$, and building ED load $P_{L,ed}$. In the figure, $\eta_{DC/DC}$, $\eta_{AC/DC}$, η_{reg}, η_{bat}, and η_{inv} are respectively the DC/DC static converter, AC/DC rectifier, regulator, battery and DC/AC inverter efficiencies.

Chapter 6   **Solar and wind assisted heat pump to**
meet the building air conditioning and electric energy demand
in the presence of an electric vehicle charging station and battery storage

When the overall power produced is higher than the overall electric load, the power in excess is stored in the battery P_{tb}, and if the battery is totally charged, is sent to the grid P_{tg}. Otherwise, the missing power is received from the battery P_{fb}, and if the battery is totally discharged, is drawn from the grid P_{fg}. When the grid is overload, the remaining part of power in excess is dissipated. The same considerations can be also extended to stand-alone systems by replacing the power in excess sent to the grid with power to be dissipated.

An inverter is interposed among the ERHS and the three loads which allows converting the overall DC power coming from ERHS P_g, with a given conversion efficiency, in AC power to be sent to the three loads and, when necessary, also to the grid. As regards the HP, $Q_{Bp,h}$ and $Q_{Bp,c}$ are the building heating and cooling primary thermal powers.

2.2. Dynamic simulation tool

A dynamic simulation tool was built for the RHTS capability evaluation in order to satisfy the building heating and cooling air conditioning energy demand, and the electric energy demand of the HP system, EV charging station and the building EDs. With reference to Figure 2, a dynamic simulation tool was developed, divided into three subroutines: (1) building system model; (2) HP system model; (3) ERHS model.

In particular, subroutine (1) achieves a dynamic simulation of the building with the aim of the determination, at any time instant, of building primary energy needs Q_{Bp} to be employed for the dynamic evaluation, by means of the subroutine (2), of the electric power absorbed by the HP system $E_{L,hp}$. This electric power and that required by the EV charging station $E_{L,ev}$ and building EDs $E_{L,ed}$ are used to simulate dynamically the ERHS. The aim is to assess all the electric powers, indicated in Figure 1, in input and output from each ERHS component. The dynamic simulation tool requires as input: the instantaneous weather climatic data; a specific control system for the subroutine (1) to manage the lighting and shading devices, and HVAC opening/closure and nocturnal attenuation; a specific control system for the subroutine (2) to manage the closure-opening, heating-cooling mode, nocturnal-daily set point temperatures and partialization of the HP system; a specific control system for the subroutine (3) to manage the energy flows through the battery storage and grid.

Chapter 6   **Solar and wind assisted heat pump to**
meet the building air conditioning and electric energy demand
in the presence of an electric vehicle charging station and battery storage
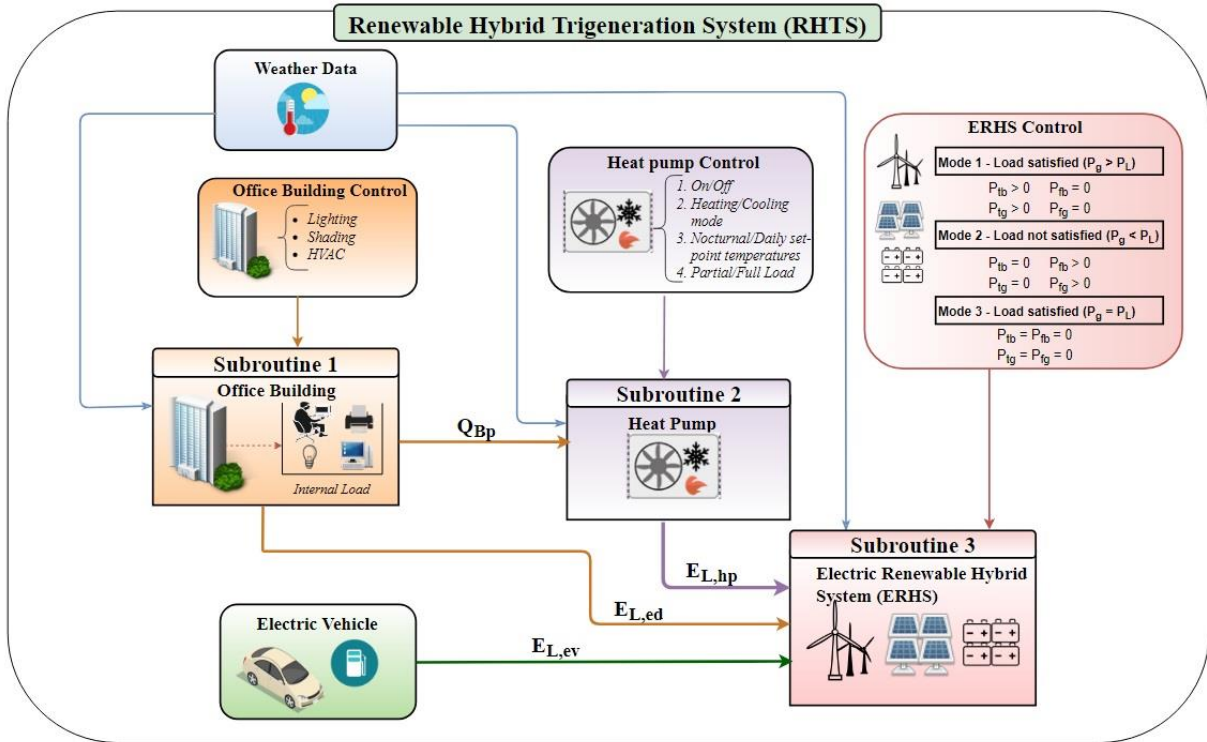
Figure 2. Scheme of the three subroutines of the RHTS dynamic simulation tool.

The three subroutines of the RHTS dynamic simulation tool described were implemented in the TRNSYS environment [24].

2.2.1. Subroutine 1 – Building system model

2.2.1.1. Description

Figure 3 reports the TRNSYS scheme relative to subroutine (1). Subroutine (1) was employed to evaluate the building peak powers in the heating and cooling period, and hourly building energy needs Q_B starting from the definition of the external and internal loads, building shell, functioning hours of the air conditioning system, and shading and lighting controls.
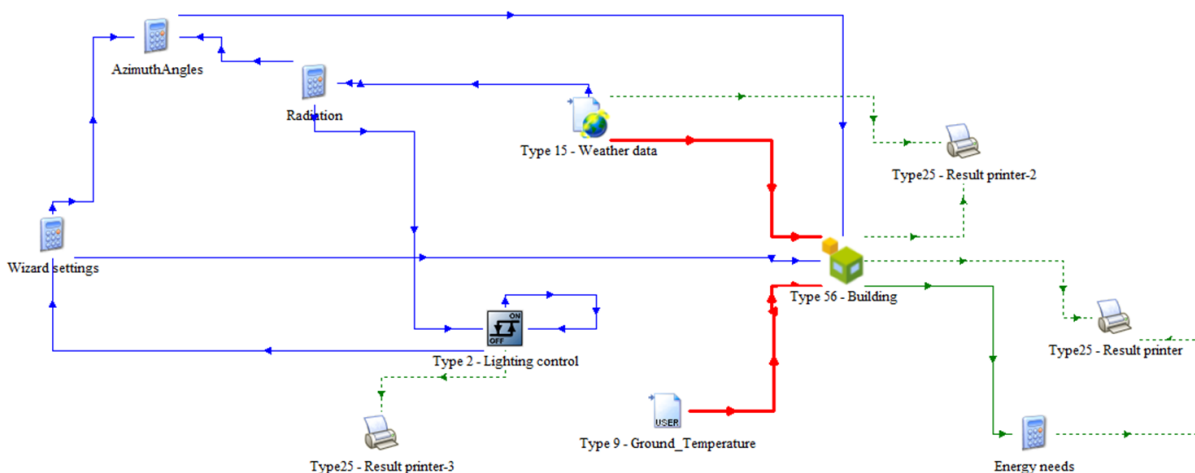
Figure 3. Subroutine (1) in TRNSYS, building system model.

In particular, Type 56 was employed to simulate dynamically the building system in detailed mode. The detailed mode consists of the use of sophisticated models to solve the heat balance in each thermal zone. This mode employs: the 3D shading and insolation matrices for the beam radiation distribution entering through the external window; the view factor matrix for the indoor shortwave diffuse radiation distribution including multi-reflections; the view factor matrix for the indoor longwave radiation exchange between surfaces; the transfer function defined from surface to surface for conductive heat transfer through opaque walls; the optical and thermal models of windows considering transmission, reflection and absorption of solar radiation in detail; analytical correlations for the internal convective heat transfer as a function of the temperature difference between surface and air, and a constant external convective heat transfer; the fictive sky and surface ground temperature and view factors for outdoor longwave radiation exchange; specific schedules for the internal heat gains, infiltrations, air conditioning system opening-closure, and set point temperatures. Moreover, Type 56 requires: climatic data of the locality provided by Type 15, which employs a typical meteorological year (TMY) data [25]; the external surface ground temperature and temperature boundary condition at a depth of 0.4 m from the floor ground – this latter is needed for the calculation of the heat transfer in the ground layer – calculated by a numeric finite-difference model, considering the ground subject to the external loads and a constant temperature at an adequate depth, and imported by Type 9; the bright differential control, made with Type 2, for the closure of the lighting devices when the solar radiation is sufficient to guarantee a minimum level of natural lighting; the shading control to manage the activation of a shading device on the glazed walls when the solar radiation is higher than a predetermined limit value.

2.2.1.2. Data

In the case study, an office building with two 100 m^2 floors was considered. Figure 4 reports a 3D sketch of the office building and the layout of each floor.
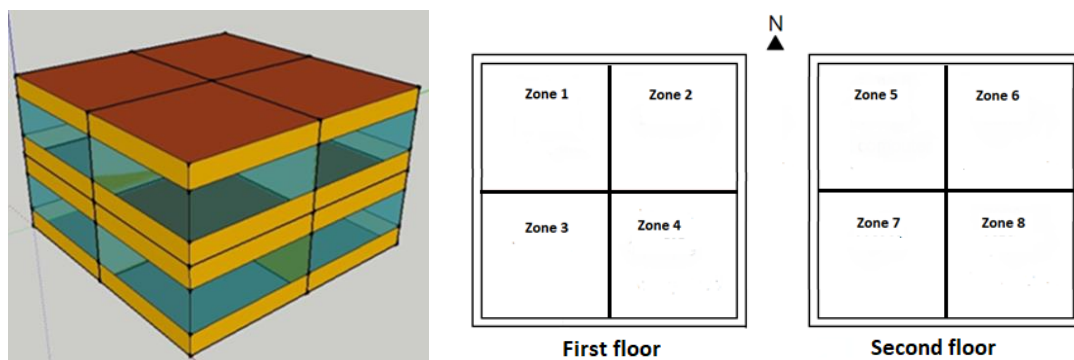
Figure 4. 3D sketch of the office building and layout of each floor.

The building was subdivided into eight thermal zones, corresponding to the number of rooms, each of which is exposed to different orientations and has different occupants' behaviour. The external vertical building walls are 50% glazed. Table 1 reports the thermophysical properties of the opaque building components, chosen in relation to those widespread in the Italian context [26] and designed with steady thermal transmittance U_o lower than those required by the reference national standard [27]. In addition, the wall unitary heat capacities per square meter C, the sum of products of density,

Chapter 6
        **Solar and wind assisted heat pump to
meet the building air conditioning and electric energy demand
in the presence of an electric vehicle charging station and battery storage**

specific heat capacity and thickness of layers, are reported. The windowed walls have a double air chamber of 4/16/4 mm, steady thermal transmittance U_w of 1.4 W/m^2 K and solar heat gain coefficient g of 0.622.

Table 1. Thermophysical properties of the opaque building walls.

Wall Type	Layer	Thickness (m)	Conductivity (W/m K)	Specific heat (J/kg K)	Density (kg/m^3)	Thickness (m)	U (W/m^{2}K)	C (kJ/(m^2 K))
Adjacent ceiling	Indoor flooring - stoneware	0.01	1.47	1000	1700	0.29	1.854	301.0
	Cement mortar	0.02	1.40	1000	2000			
	Concrete slab	0.24	0.75	1000	900			
	Internal plaster	0.02	0.70	1000	1400			
External roof	Internal plaster	0.02	0.70	1000	1400	0.54	0.270	561.4
	Concrete slab	0.24	0.75	1000	900			
	Reinforced concrete	0.04	2.50	1000	2400			
	Cement mortar	0.02	1.40	1000	2000			
	Ordinary concrete screed	0.06	1.06	1000	2000			
	Bitumen	0.01	0.17	1000	1200			
	Insulating	0.12	0.04	1220	30			
	Outdoor flooring - clinker	0.03	0.70	1000	1500			
Floor	Indoor flooring - stoneware	0.015	1.47	1000	1700	0.63	0.352	888.4
	Cement mortar	0.03	1.40	1000	2000			
	Lightweight concrete	0.10	0.33	1000	1200			
	Insulating	0.08	0.04	1220	30			
	Gravel	0.40	1.20	1000	1700			
External walls	Internal plaster	0.02	0.70	1000	1400	0.44	0.296	259.7
	Perforated brick	0.12	0.50	1000	800			
	Air interspace	Thermal resistance = 0.18 m^2/kW		1005	1.2			
	Perforated brick	0.12	0.70	1000	800			
	Insulating	0.10	0.04	1220	30			
	External plaster	0.02	0.90	1000	1800			
Internal partitions	Internal plaster	0.02	0.70	1000	1400	0.10	2.80	91.9
	Hollow flat block	0.06	0.46	1005	595			
	Internal plaster	0.02	0.70	1000	1400			

The external shading device, with a maximum opaque fraction of 70%, is activated when the solar radiation on the horizontal surface is higher than 140 W/m^2 and deactivated when the solar radiation on the horizontal surface is lower than 120 W/m^2.

Heat gains, calculated in relation to the reference standards [28, 29] are owing to the presence in each thermal zone, from Monday to Friday from 8:00 to 18:00, of two people (120 W/per), two personal computers and one printer (75 W) and a LED lighting (125 W) equipment that guarantees an adequate illuminance in the office rooms (400/500 lux). Only two thermal zones are different since on Monday, Wednesday and Friday the working hours are from 8:00 to 14:00.

For the brightness control, the upper and lower dead bands are respectively 200 W/m^2 and 120 W/m^2. Natural infiltration was set to 1 vol./hour [30]. All the thermal zones are heated to 20°C or cooled to 26°C by an air conditioning system from 7:00 to 18:00 from Monday to Friday [29]. A nocturnal

Chapter 6   **Solar and wind assisted heat pump to**
meet the building air conditioning and electric energy demand
in the presence of an electric vehicle charging station and battery storage

attenuation was considered to avoid excessive cooling in winter and overheating in summer in the thermal zones by opening the air conditioning system again when, respectively, the temperature drops below 12 °C or rises above 34 °C.

The building is located in Rome, Lat. = 41° 53', in the Mediterranean area and climate zone D according to the definition given by the standard EN/TR 10349-2 [31]. TMY data was used to represent the weather conditions. The location is characterized by an annual average hourly temperature of 15.2 °C, annual solar energy on the horizontal plane of 1562 kWh/m^2 and an annual average hourly and maximum wind speed at a height of 10 m, respectively, of 3.14 m/s and 14.4 m/s.

2.2.1.3 Preliminary simulations

By using subroutine (1), the first simulation was performed to determine the design peak heating power in steady conditions [32] obtaining a value of 9.3 kW. The second simulation for the design peak cooling power evaluation in dynamic conditions [24] provided a value of 20.6 kW. The third simulation, by considering the actual outside and inside building conditions, allowed the detection of the hourly building energy needs. The energy needs were summarized by means of the overall monthly heating and cooling energy needs, as reported in Figure 5.
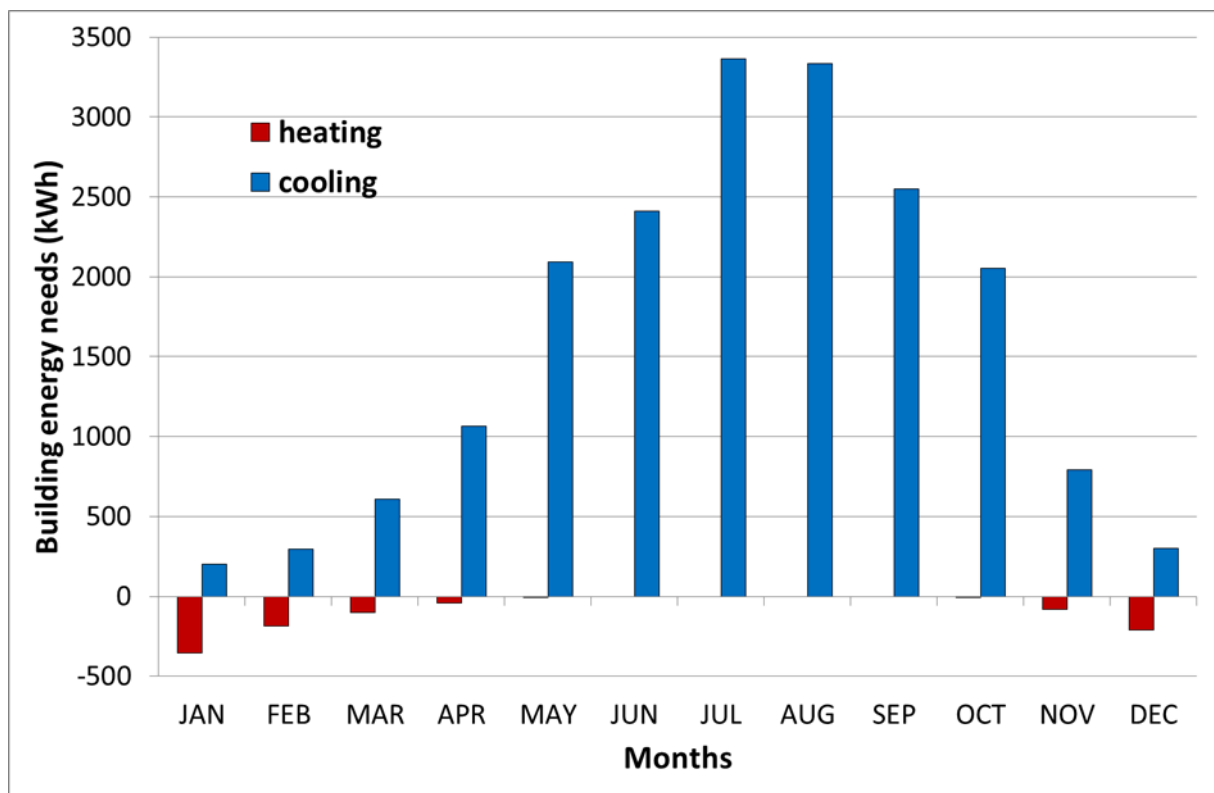
Figure 5. Monthly heating and cooling building energy needs.

The overall yearly heating and cooling energy needs values resulted respectively 987.3 kWh/yr. and 19078.8 kWh/yr., namely 4.94 $kWh/(m^2\ yr.)$ and 95.39 $kWh/(m^2\ yr.)$. This significant discrepancy is due to the noticeable heat gains in the office building (lighting, other EDs, and solar radiation through the wide glazed walls), and air conditioning system closure during the night-time, when the heating demand is the highest, and air conditioning system opening during daytimes, when the cooling demand is the greatest.

Chapter 6   **Solar and wind assisted heat pump to**
meet the building air conditioning and electric energy demand
in the presence of an electric vehicle charging station and battery storage

Overall, the heating and cooling air conditioning hours resulted in 244 and 2177, in 106 hours in some thermal zones heating and others cooling are required, while in the remaining hours the air conditioning system is switched off since they correspond with nocturnal hours or the weekend. When the building requires simultaneously heating in some thermal zones and cooling in other ones, the HP works in the mode to which corresponds the highest demand.

The nocturnal activation hours of the air-conditioning system resulted in 51 and 0 respectively for the heating and cooling period.

2.2.2. Subroutine 2 – Heat pump system model

2.2.2.1. Description

With reference to Figure 6, *Subroutine (2)* allows the evaluation of the hourly electric energy absorbed by a reversible multi-stage air source HP system. The hourly building primary energy needs Q_{Bp}, to be provided by the HP, were evaluated by dividing the hourly building energy needs Q_B to the emission, distribution and control efficiencies.
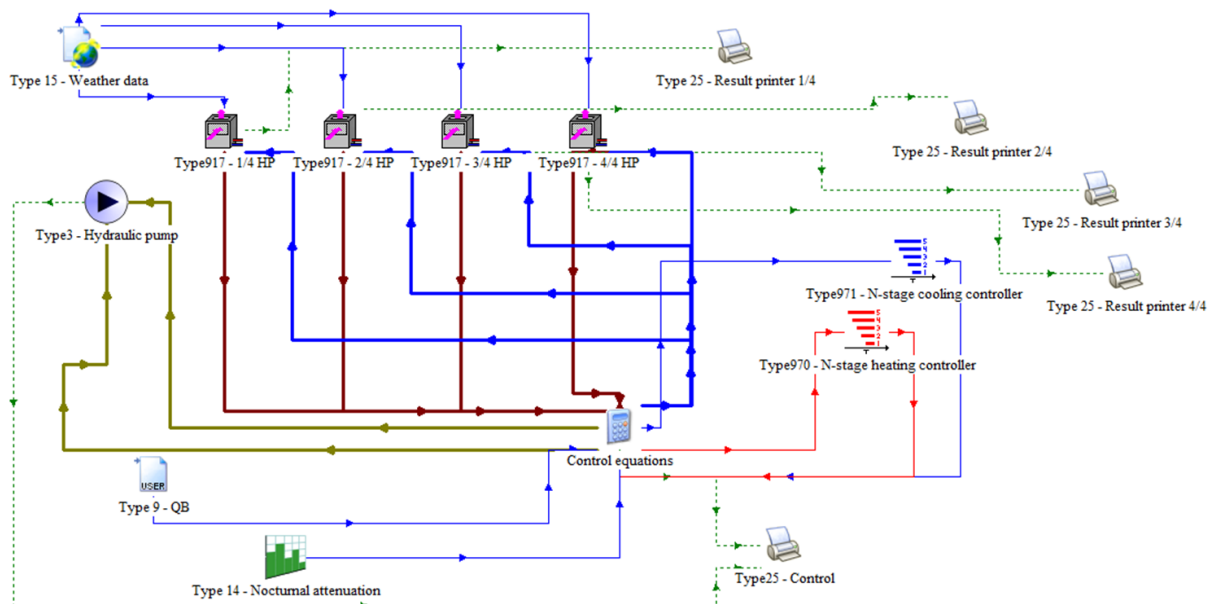
Figure 6. *Subroutine (2) in TRNSYS, heat pump model.*

Starting from the hourly primary energy needs for the building air conditioning − evaluated with subroutine (1) and imported by means of Type 9 −, rated heating and cooling capacity and rated water flow rate of the HP, the electric energy absorbed by the HP system was assessed by implementing the following steps:

1) HP partialization, by means of the activation of one or more compressors, both for heating and cooling mode and both daytime and night-time. Since there is no specific Type in the TRNSYS environment for the dynamic simulation of a reversible multi-stage air source HP, a new algorithm was created, which required the following successive phases:

　　a) individuation of the time instants in which the HP is switched off ($Q_{Bp}=0$) or operates in heating ($Q_{Bp}<0$) or cooling ($Q_{Bp}>0$) mode.

Chapter 6

Solar and wind assisted heat pump to meet the building air conditioning and electric energy demand in the presence of an electric vehicle charging station and battery storage

b) in the HP functioning hours, calculations of the HP return water temperature T_{wi}, namely that in input to the HP, successive to the heat exchange in the fan coils with the air to be sent into the environments, known the HP outlet water set-point temperature T_{wo}, by means of the relation:

$$T_{wi} = T_{wo} + \frac{Q_{Bp}}{\dot{m}_w c_p}$$

(1)

where, T_{wo} is different in heating and cooling mode and, during the weekdays, in daytime and night-time.

c) identification during the entire year, both in daytime and night-time, of the maximum temperature drop $(T_{wo}-T_{wi})_{max}$ in heating mode, and of the maximum temperature rise $(T_{wi}-T_{wo})_{max}$ in cooling mode.

d) subdivision of the four temperature bands, relative to the summer and winter daytime and night-time periods, in N ranges corresponding to the number of the HP stages.

e) employment of N Types 917, each relative to the single-stage HP functioning, coupled to Type 970 (for heating mode) or Type 971 (cooling mode), regarding to N-stage differential controller, to simulate the energy behavior in a partial load of a multi-stage HP. Type 917 dynamically takes into account the effects produced by flow rate and temperature variations of the air and water on the performance coefficient. The external air conditions are provided by Type 15, which generates the weather data in the location considered.

Each Type 917, for the multi-stage HP functioning, has the task of simulating the energy behaviour of the multi-stage HP to a specific partial load. For example, when the HP must operate to a specific partial load, the relative Type 917 that supplies that power is turned on, while the other N-1 Types 917 are not activated. Both the maximum temperature drop in heating mode, see Figure 7a, and maximum temperature rise in cooling mode, see figure 7b, were uniformly subdivided into N ranges to identify the set point water temperatures of every single stage. In addition, for each stage, a dead band was set. The HP return water temperature T_{wi} is employed as monitoring variable by means of which, at each time instant, the number of compressors to be activated is determined following the logic of N-Stage differential controller with multiple deadbands.
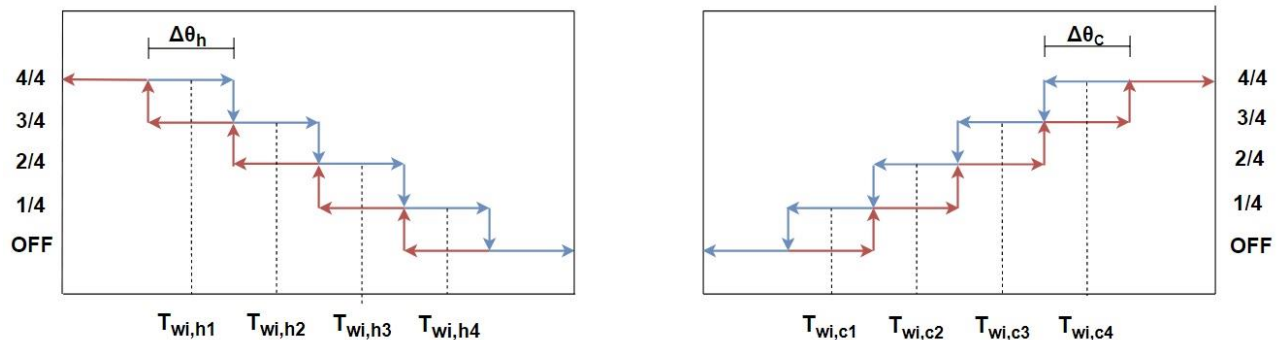
Figure 7. *N-Stage differential controller with multiple deadbands in heating and cooling mode.*

Chapter 6   **Solar and wind assisted heat pump to**
meet the building air conditioning and electric energy demand
in the presence of an electric vehicle charging station and battery storage

In the figures, the controller uses four uniform dead bands $\Delta\theta$ and four set-point values, $T_{wi,1}$, $T_{wi,2}$, $T_{wi,3}$, $T_{wi,4}$, placed at the center of the specific band, for the return water temperature since the HP is composed by four compressors.

For example, in heating mode considering the compressor switched off, the first compressor (1/4) is activated when T_{wi} is lower than $T_{wi,h1}-\Delta\theta_h/2$, the second one (2/4) when T_{wi} decreases below $T_{wi,h2}-\Delta\theta_h/2$ and so on up to work at full load when T_{wi} is lower than $T_{wi,h4}-\Delta\theta_h/2$. Vice versa, starting from a full load functioning, the HP works to partial load with three compressors when the temperature rises up to $T_{wi,h4}+\Delta\theta_h/2$ and similarly in the case of partial load with two or one working compressors. Analogously, in cooling mode considering the compressor switched off, the first compressor (1/4) works when T_{wi} grows above $T_{wi,c1}+\Delta\theta_c/2$, up to reaching a full load functioning when T_{wi} is higher than $T_{wi,c4}+\Delta\theta_c/2$. Vice versa, for decreasing temperatures, the compressors switches off when the temperature drops below the difference between the relative set-point temperature and $\Delta\theta_c/2$.

A further controller, implemented by means of the daily schedule of Type 14, permits the set point outlet water temperatures in the N-Stage differential controller to be modified in the night-time and daytime mode.

f) determination, at each time instant, of the electric energy absorbed by the HP, by using the controller previously described, to identify which Type 917 output must be selected. The electric energy evaluated with Type 917 also includes the electric energy absorbed by the HP controller and blower.

2) Calculation of the electric energy absorbed by the hydraulic pump using Type 3, which employs a variable control function, to switch it off or on, and a fixed maximum flow capacity. The pump power consumption is set to the rated value whenever the control signal indicates that the pump is in operation. A portion of the pump power is converted to fluid thermal energy.

2.2.2.2. Data

First of all, the design water flow rate m_w at the HP evaporator was evaluated considering the peak cooling load and a water temperature difference of $(T_{w,i}-T_{w,o}) = (12 - 7) = 5$ °C. A value of 1.050×10^{-3} m³/s was obtained and maintained constant in the entire year. A reversible multi-stage air source HP produced by DAIKIN company [33] was chosen and the main technical data, taken from the manufacturer and set in TRNSYS environment, were reported in Table 2.

Table 2. *Technical data of the reversible multi-stage air source heat pump.*

	100 %	75 %	50 %	25 %
Cooling				
Rated cooling capacity (kW)	21.70	16.27	10.85	5.42
Rated cooling power (kW)	6.69	4.40	2.27	1.08
EER (-)	3.24	3.70	4.78	5.02
Heating				
Rated heating capacity (kW)	22.19	17.47	11.65	5.82
Rated heating power (kW)	6.78	4.21	2.36	1.05
COP (-)	3.27	4.15	4.94	5.54
Blower power (W)	750			

Chapter 6

Solar and wind assisted heat pump to meet the building air conditioning and electric energy demand in the presence of an electric vehicle charging station and battery storage

Controller power (W)	40
Hydraulic pump power (W)	100
Rated liquid flow rate (m^3/s)	1.033x10^{-3}
Rated air flow rate (m^3/s)	3.08
Air pressure rise across heat pump (kPa)	30

The HP set-point outlet water temperatures T$_{wo}$ were set to 45°C and 27 °C in daytime and night-time heating mode, while 7 °C and 25 °C in the daytime and nighttime cooling mode.

By applying Eq. (1), the minimum return water temperature observed in daytime and night-time heating mode is, respectively, 39.85 °C and 26.32 °C, the maximum return water temperature in daytime cooling mode is 11.87 °C, while in night-time cooling mode, as mentioned in Section 2.2.1.3., the air conditioning system is always switched off.

As regards the HP partialization control system, Table 3 shows the different heating and cooling set point-temperatures and dead bands, both for daytime and night-time.

Table 3. Heating and cooling set point-temperatures and dead bands both for daytime and night-time.

Mode	(°C)				
Daytime heating	T$_{wi,h1}$ = 45	T$_{wi,h2}$ = 43.5	T$_{wi,h3}$ = 42	T$_{wi,h4}$ = 40.5	$\Delta\theta_h$ = 0.125
Nightime heating	T$_{wi,h1}$ = 27	T$_{wi,h2}$ = 26.75	T$_{wi,h3}$ = 26.50	T$_{wi,h4}$ = 26.25	$\Delta\theta_h$ = 0.125
Daytime cooling	T$_{wi,c1}$ = 7	T$_{wi,c2}$ = 8.5	T$_{wi,c3}$ = 10	T$_{wi,c4}$ = 11.5	$\Delta\theta_c$ = 0.125

2.2.2.3. Preliminary simulations

By means of a dynamic simulation, the hourly electric energy required by the HP system was calculated. Figure 8 shows the monthly electric energy required by the HP system.
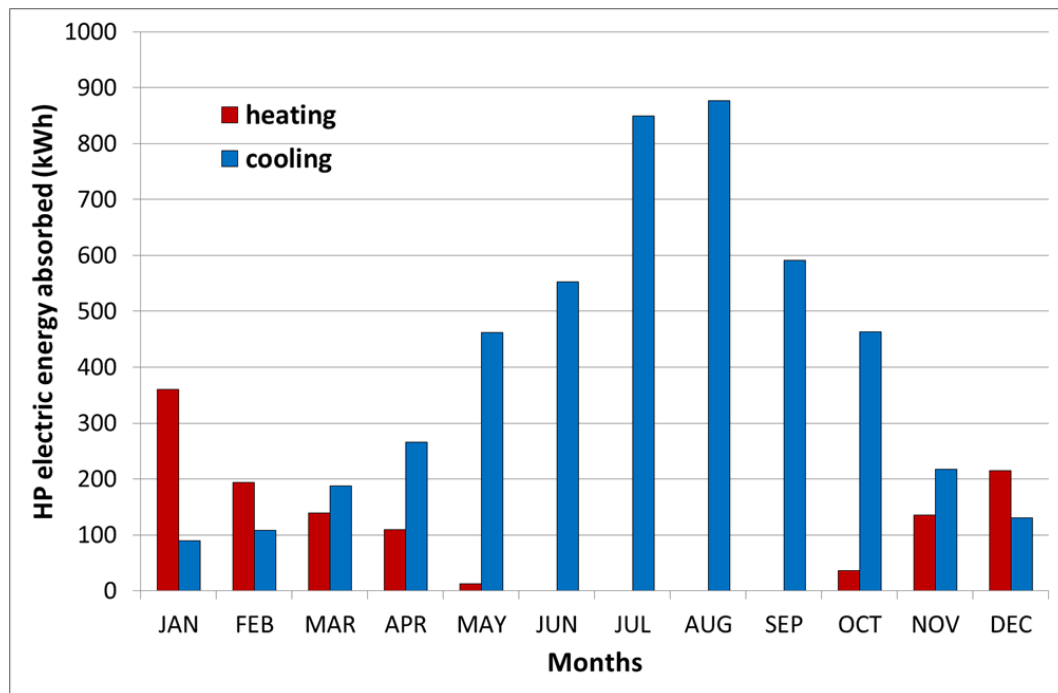
Figure 8. Monthly electric energy required by the HP system in heating and cooling mode.

Chapter 6   **Solar and wind assisted heat pump to**
meet the building air conditioning and electric energy demand
in the presence of an electric vehicle charging station and battery storage

The yearly electric energy required by the HP system resulted in 5999 kWh/yr. Table 4 shows the number of hours in which one, two, three or four HP compressors both in heating and cooling mode are activated.

Table 4. Number of hours with one, two, three and four compressors active.

COMPRESSORS	HEATING MODE				COOLING MODE			
	1	2	3	4	1	2	3	4
HOURS	47.00	58.00	163.00	0.00	852.00	814.00	521.00	11.00

Since the HP is sized on the basis of the cooling peak power, in heating mode all the four compressors are never switched on. In heating mode, the opening of three compressors is the most frequent while in cooling mode prevalently one or two compressors are actives. Overall, in 268 hours the HP works in heating mode and 2198 hours in cooling mode. The comparison of these values with the number of hours of heating and cooling air conditioning reported in Section 2.2.1.3 highlights an imperfect correspondence owing to the discrete N-Stage differential controller and also to the hours in which both heating and cooling are required simultaneously.

2.2.3. Subroutine 3 – ERHS system model

2.2.3.1. Description

Subroutine 3 has the task of solving the energy balance of the ERHS components in order to identify how the load is satisfied and how renewable energy is utilized. In particular, it calculates: the hourly energy sent directly by the PV and wind micro-generator, the energy received from the battery and the energy drawn from the grid for the satisfaction of the load; the part that is directly sent to the load, that which is stored in the battery, and that which is in excess sent to the grid for renewable energy use.

The input data required are the weather data, the hourly electric energy absorbed by the HP system, provided by the subroutine (2), EV charging station and EDs present in the building.

Figure 9 reports the TRNSYS algorithm developed.
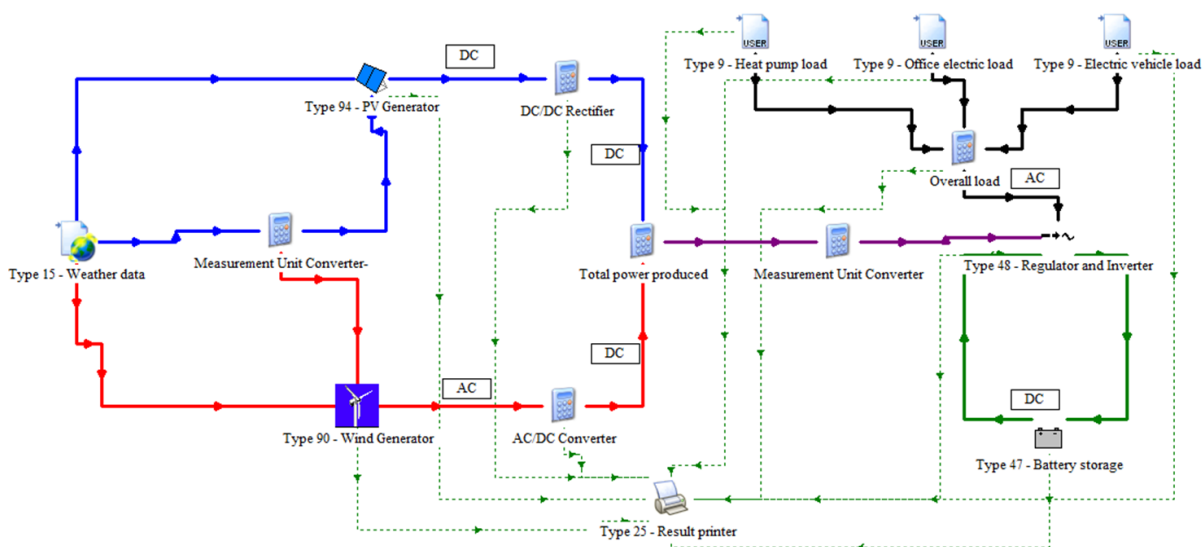
Figure 9. Subroutine (3) in TRNSYS, ERHS model

Chapter 6

Solar and wind assisted heat pump to meet the building air conditioning and electric energy demand in the presence of an electric vehicle charging station and battery storage

Types employed are: Type 15 for the generation of the weather data; Type 94 which uses the 5-parameter Fry model for the PV generator; Type 90 which implements the Quinlan model for the wind micro-generator; Type 47 which employs the state of charge balance for the battery storage; equation block to implement the efficiency model of the static converters; Type 48 for the inverter and regulator; Type 9 for importing the hourly data of three electric loads into the TRNSYS environment. The subroutine contains a controller implemented in Type 48, which at each time instant compares the overall renewable power produced – the sum of the PV power in output from the DC/DC static converter and wind power in output from the AC/DC rectifier − reduced by the DC/AC inverter losses with the overall power required by the three loads, in order to establish the ERHS functioning mode. In particular, the controller identifies when required: to drawn energy from the battery or, if necessary, from the grid; to store energy in the battery or, in the case of battery totally charged, to send to the grid. With reference to Figure 1, the power balance of the power produced by the ERHS sent to the load P_{tl} and power required by the load P_L of the ERHS are expressed respectively by Eqs. (2) and (3).

$$P_{tl}(t) = P_{tl,ev}(t) + P_{tl,ed}(t) + P_{tl,hp}(t)$$
$$= \begin{cases} P_g(t)\eta_{reg}\eta_{inv} - P_{tb}(t)\eta_{inv} - P_{tg}(t) & \text{if } \eta_{reg}\eta_{inv}P_g(t) > P_L(t) \\ P_g(t)\eta_{reg}\eta_{inv} + P_{fb}(t)\eta_{inv} & \text{if } \eta_{reg}\eta_{inv}P_g(t) < P_L(t) \\ P_g(t)\eta_{reg}\eta_{inv} & \text{if } \eta_{reg}\eta_{inv}P_g(t) = P_L(t) \end{cases}$$

$$(2)$$

$$P_L(t) = P_{L,ev}(t) + P_{L,ed}(t) + P_{L,hp}(t)$$
$$= \begin{cases} P_{tl,ev}(t) + P_{tl,ed}(t) + P_{tl,hp}(t) & \text{if } \eta_{reg}\eta_{inv}P_g(t) \geq P_L(t) \\ P_{tl,ev}(t) + P_{tl,ed}(t) + P_{tl,hp}(t) + P_{fg}(t) & \text{if } \eta_{reg}\eta_{inv}P_g(t) < P_L(t) \end{cases}$$

$$(3)$$

Eq. (2) represents the balance equation of the power sent to the load $P_{tl}(t)$ in the case of net renewable power produced $\eta_{reg}\eta_{inv}P_g(t)$ higher than, lower than or equal to the load power $P_L(t)$. In the first case, $P_{tl}(t)$ is the net power produced by the ERHS reduced by the power stored in the battery $P_{tb}(t)$ η_{inv} and in excess sent to the grid $P_{tg}(t)$. In the second case, $P_{tl}(t)$ is the sum of the net power produced and the power drawn from the battery $P_{fb}(t)$ η_{inv}. Finally, in the third case, all the net power produced is sent to the load.

Eq. (3) is the balance equation of the power required by the load $P_L(t)$. In the first and third case, the power required by the load is completely satisfied by the ERHS, while in the second, the missing power is taken from the grid $P_{fg}(t)$.

2.2.3.2. Data
ERHS components

As regards the PV and the wind micro-generator types, 14 different PV generators and 14 different wind micro-generators were independently simulated to identify, in the location considered, the PV and wind generators types that maximize the manufacturability, namely the energy produced for each kW installed.

Chapter 6   **Solar and wind assisted heat pump to**
meet the building air conditioning and electric energy demand
in the presence of an electric vehicle charging station and battery storage

Table 5 reports the technical data of the generators considered and the dynamic simulation results summarized in terms of energy produced E_{pv} and E_w and manufacturability p_{pv} and p_w.

The highest PV manufacturability is obtained by employing the polycrystalline silicon PV module of 250 W produced by the Europe Solar Production Company. Instead, the micro-generator produced by Tulipower resulted in the best in terms of manufacturability and it has a rated power of 2.5 kW. A lithium-ion battery produced by LG Chem, with a storage capacity of 2 kWh and efficiency of 0.98 was employed. Finally, the static DC/DC converter, static AC/DC rectifier, DC/AC inverter and regulator efficiencies are, respectively, 0.94, 0.90, 0.97 and 0.98.

Different ERHS configurations were considered in this study by varying the PV and wind powers, both from 5 kW to 10 kW with a step of 2.5 kW, and battery capacities from 0 kWh to 40 kWh. These variations were obtained by changing the number of PV modules, wind micro-generators and batteries.

Table 5. Technical data, energy produced and manufacturability of the PV and the wind micro-generators.

Photovoltaic generators				Wind micro-generators					
Name	**$P_{pv,n}$ (W)**	**E_{pv} (kWh)**	**p_{pv} (h)**	**Name**	**$P_{w,n}$ (W)**	**V_c (m/s)**	**V_n (m/s)**	**E_w (kWh)**	**p_w (h)**
Sharp	250	385.37	1541.47	Proven	2.50	2.5	12.0	1768.85	707.54
Solarworld	250	368.13	1472.54	Southwest	3.00	3.4	10.5	2624.95	874.98
Vikramsolar	320	496.32	1550.99	Vergnet	10.00	4.5	12.0	3713.94	371.39
CHSM	250	388.15	1552.61	SEI-BNY	3.00	3.5	12.0	3087.29	1029.10
LG	300	458.38	1527.92	Aircon	10.00	2.5	11.0	9964.90	996.49
KCGT	200	299.73	1498.65	Eoltec	6.00	4.0	12.0	3365.49	560.92
MLU	250	332.53	1330.11	Fortis Montana	5.60	2.5	17.0	2320.90	414.45
Europesolar	**250**	**389.67**	**1558.69**	Fortis Wind Energy	10.00	3.0	12.0	5320.62	532.06
Tallmax	320	491.49	1535.92	Iskra Wind Turbines	5.00	3.0	11.0	3700.73	740.15
Jakson	250	385.92	1543.66	Proven Energy Products Ltd	6.00	2.5	12.0	4454.37	742.39
Suntech	250	382.75	1530.98	Travere Industries	3.00	2.8	12.0	1612.91	537.64
Solsonica	250	384.32	1537.27	Travere Industries	5.50	3.0	10.0	4219.22	767.13
Canadiansolar	290	443.68	1529.92	**Tulipower**	**2.50**	**3.0**	**10.0**	**2683.98**	**1073.59**
TP	250	382.68	1530.71	Turby B.V.	2.50	4.0	14.0	646.54	258.62

Electric loads

For the calculation of the electric energy absorbed by the building EDs, the data and the controllers presented in Section 2.2.1. were considered. Instead, the calculation procedure of the absorbed electric energy by the HP was described in Section 2.2.2.

An EV charging infrastructure made up of four charging stations, each of which has a charging power of 2.3 kW was placed in the parking lot of the office building. Eight EVs Nissan Leaf 24 kWh [34] were considered to be charged during the working hours. The average consumption of the EV is 0.1714 KWh/Km, including the energy recovered through the braking regeneration system and evaluated with reference to different types of routes travelled by the EV with variable speeds [35]. By taking into account that each EV travels on average 26.8 km/day, each EV requires two charging hours to recovery the daily consumption of 5.14 kWh/day. Consequently, on weekdays, the daily charging schedule must be made up, during the working hours, of two charging hours at 9.2 kW for the first group of four EVs, and by the other two charging hours at 9.2 kW for the second group of four EVs. The charge period is between 9:00 and 13:00. Figure 10 shows the monthly electric load owing to the ED, HP and EV.

Chapter 6   **Solar and wind assisted heat pump to**
meet the building air conditioning and electric energy demand
in the presence of an electric vehicle charging station and battery storage
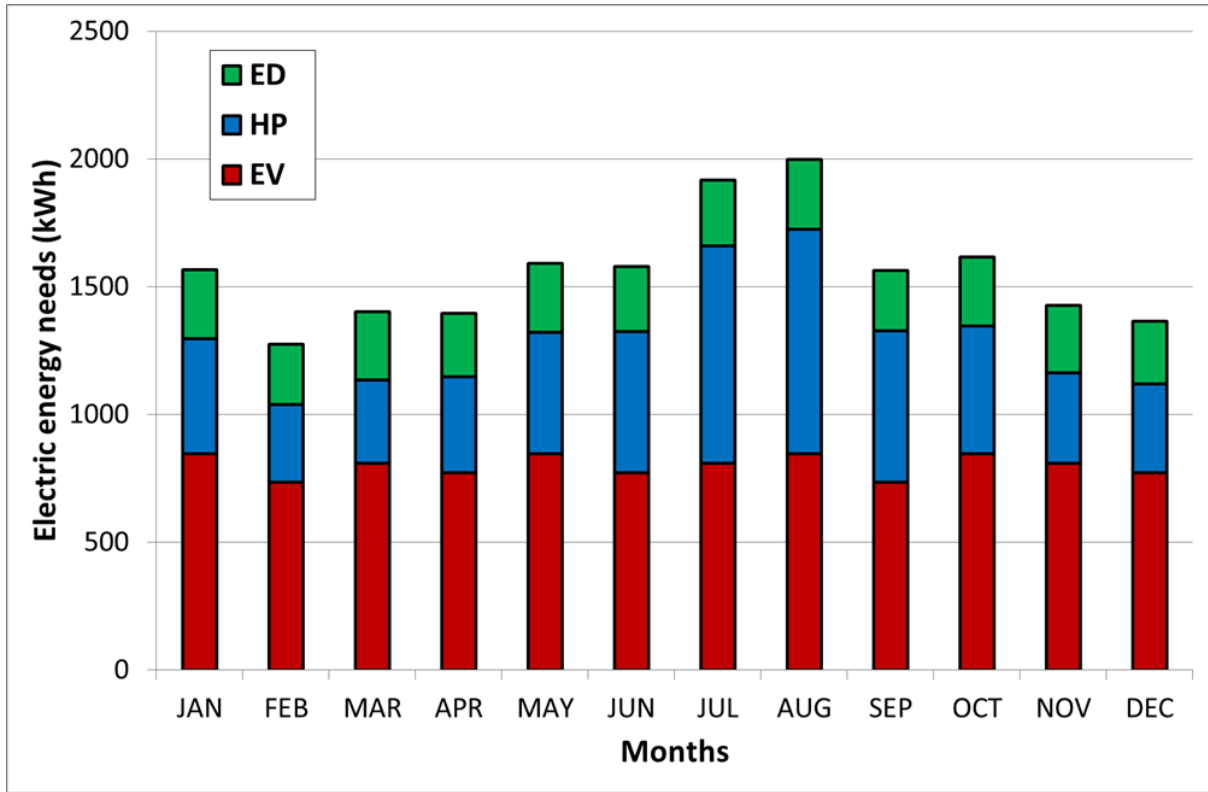
Figure 10. Monthly electric load owing to the ED, HP and EV.

The yearly electric energy required by the ED, HP and EV are resulted, respectively, in 3101 kWh/yr., 5999 kWh/yr. and 9605 kWh/yr. and constitute respectively, 17 %, 32 %, and 51 %, of the overall yearly electric load.

2.3. Energy balance of the ERHS

For a given time interval Δt in which the energy produced E_g is employed to supply the load, to charge the battery and the surplus energy is sent to the grid, the reference balance equation is:

$$E_g \eta_{reg} \eta_{inv} = \left(E_{pv}\, \eta_{DC/DC} + E_w\, \eta_{AC/DC} \right) \eta_{reg} \eta_{inv} = E_{dtl} + E_{tb} \eta_{inv} + E_{tg} \tag{4}$$

Instead, the energy provided by the ERHS, that received from the battery and that drawn from the grid allow satisfaction of the energy required by the three loads in a given time interval Δt. The balance equation of the energy required by the load E_L, sum of that required by the EV $E_{L,ev}$, HP $E_{L,hp}$ and EDs $E_{L,ed}$, is:

$$E_L = E_{L,ev} + E_{L,ed} + E_{L,hp} = E_{dtl} + E_{fb}\, \eta_{inv} + E_{fg} \tag{5}$$

Chapter 6   **Solar and wind assisted heat pump to**
meet the building air conditioning and electric energy demand
in the presence of an electric vehicle charging station and battery storage

By dividing Eqs. (4) and (5) to E_L and multiplying both members of Eq. (4) for the regulator and inverter efficiencies η_{reg} η_{inv} the energy balance equations, per unit of energy required by the load, in dimensionless form were obtained:

$$e_g = e_{dtl} + e_{tb} + e_{tg} \tag{6}$$

$$1 = e_{L,ev} + e_{L,hp} + e_{L,ed} = e_{dtl} + e_{fb} + e_{fg}$$
$$= \left(e_{dtl,w} + e_{dtl,pv}\right) + \left(e_{fb,w} + e_{fb,pv}\right) + e_{fg} \tag{7}$$

Eq. (6) can be rewritten with reference to the overall energy generated E_g, thus obtaining:

$$1 = \frac{e_{dtl}}{e_g} + \frac{e_{tb}}{e_g} + \frac{e_{tg}}{e_g} = \left(\frac{e_{dtl,pv}}{e_g} + \frac{e_{dtl,w}}{e_g}\right) + \left(\frac{e_{tb,pv}}{e_g} + \frac{e_{tb,w}}{e_g}\right) + \left(\frac{e_{tg,pv}}{e_g} + \frac{e_{tg,w}}{e_g}\right) \tag{8}$$

Where, the subscripts *pv* and *w*, respectively, indicate the PV and wind generator contributions.

2.4. Reliability indicators

To study the energy performance of the ERHS, a new set of reliability indicators was introduced subdivided into two different typologies. The first typology of indicators was defined in relation to the overall load:

- the **overall PV-wind fraction $f_{pv,w}$** measures the fraction of energy required by the load satisfied by the ERHS:

$$f_{pv,w} = \frac{E_{tl}}{E_L} \tag{9}$$

- the **utilization factor** of the generated energy $f_{u,g}$ quantifies the fraction of produced energy by the ERHS employed to satisfy the load:

$$f_{u,g} = \frac{E_{tl}}{E_g} \tag{10}$$

- the **dimensionless manufacturability f_m** provides the energy produced referred to the maximum energy that can be produced under nominal operating conditions in a period T:

$$f_m = \frac{E_g}{P_n \Delta t} \quad \text{with} \quad P_n = P_{pv,n} + P_{w,n} \tag{11}$$

Chapter 6   **Solar and wind assisted heat pump to**
meet the building air conditioning and electric energy demand
in the presence of an electric vehicle charging station and battery storage

- the **time contemporaneity factor $\tau_{pv,w}$** identifies the fraction of time in which the load is completely satisfied by the ERHS in a period T:

$$\tau_{pv,w} = \frac{\sum_{t=t_0}^{\Delta t} t_{SL}(t)}{t_L} \qquad \text{with} \qquad t_{SL}(t) = \begin{cases} 1 & \text{if} & P_{tl}(t) = P_L(t) \\ 0 & \text{if} & P_{tl}(t) < P_L(t) \end{cases} \tag{12}$$

Where, t_L is the number of hours in which the overall load is different from zero and t_{SL} is a modified Heaviside step function.

The second typology of indicators was defined in relation to the single loads:

- the **energy contemporaneity factors** of the EV $e_{tl,ev}$, HP $e_{tl,hp}$ and ED $e_{tl,ed}$. These factors allow the individuation of the most supplied load, as a consequence of the greater contemporaneity in energy terms between the renewable energy produced trend and the load trends. The three factors can be calculated considering that the energy sent to the load by the ERHS can be subdivided with reference to the three loads:

$$E_{tl} = E_{tl,ev} + E_{tl,ed} + E_{tl,hp} \tag{13}$$

By dividing into E_{tl}:

$$1 = \frac{E_{tl,ev}}{E_{tl}} + \frac{E_{tl,ed}}{E_{tl}} + \frac{E_{tl,hp}}{E_{tl}} = e_{tl,ev} + e_{tl,hp} + e_{tl,ed} \tag{14}$$

- the **PV-wind fractions** of the EV $f_{pv,w\text{-}ev}$, HP $f_{pv,w\text{-}hp}$ and ED $f_{pv,w\text{-}ed}$ measure, respectively, the fraction of energy required by the EV, HP and ED load satisfied by the ERHS:

$$f_{pv,w-ev} = \frac{E_{tl,ev}}{E_{L,ev}} \qquad f_{pv,w-hp} = \frac{E_{tl,hp}}{E_{L,hp}} \qquad f_{pv,w-ed} = \frac{E_{tl,ed}}{E_{L,ed}} \tag{15}$$

- the **weighted PV-wind fractions** of the EV $\zeta_{pv,w\text{-}ev}$, HP $\zeta_{pv,w\text{-}hp}$ and ED $\zeta_{pv,w\text{-}ed}$. These fractions are evaluable considering that the energy sent to the load by the ERHS can be subdivided with reference to the three loads in the definition of the overall PV-wind fraction. Definitely, each fraction measures the energy sent to a specific load compared to the overall energy required by the load:

$$f_{pv,w} = \frac{E_{tl}}{E_L} = \frac{E_{tl,ev}}{E_L} + \frac{E_{tl,hp}}{E_L} + \frac{E_{tl,ed}}{E_L} = \zeta_{pv,w-ev} + \zeta_{pv,w-hp} + \zeta_{pv,w-ed} \tag{16}$$

Chapter 6   **Solar and wind assisted heat pump to**
meet the building air conditioning and electric energy demand
in the presence of an electric vehicle charging station and battery storage

These fractions are strongly linked to the PV-wind fractions of the EV $f_{pv,w-ev}$, HP $f_{pv,w-hp}$ and ED $f_{pv,w-ed}$ by means of the following equations:

$$\zeta_{pv,w-ev} = f_{pv,w-ev}\, e_{L,ev} \qquad \zeta_{pv,w-hp} = f_{pv,w-hp}\, e_{L,hp} \qquad \zeta_{pv,w-ed} = f_{pv,w-ed}\, e_{L,ed} \quad (17)$$

Where, $e_{L,ev}$, $e_{L,hp}$, and $e_{L,ed}$ represent the energy fractions required by every single load compared to the overall load, Eq. (7).

- the **time contemporaneity factors** of the EV **$\tau_{pv,w-ev}$**, HP **$\tau_{pv,w-hp}$** and ED **$\tau_{pv,w-ed}$** identify the fraction of time in which a specific load is completely satisfied by the ERHS in a period T:

$$\tau_{pv,w-ev} = \frac{\sum_{t=t_0}^{\Delta t} t_{SL,ev}(t)}{t_{L,ev}} \quad \text{with} \quad t_{SL,ev}(t) = \begin{cases} 1 & \text{if} \quad P_{tl,ev}(t) = P_{L,ev}(t) \\ 0 & \text{if} \quad P_{tl,ev}(t) < P_{L,ev}(t) \end{cases} \qquad (18)$$

$$\tau_{pv,w-hp} = \frac{\sum_{t=t_0}^{\Delta t} t_{SL,hp}(t)}{t_{L,hp}} \quad \text{with} \quad t_{SL,hp}(t) = \begin{cases} 1 & \text{if} \quad P_{tl,hp}(t) = P_{L,hp}(t) \\ 0 & \text{if} \quad P_{tl,hp}(t) < P_{L,hp}(t) \end{cases} \qquad (19)$$

$$\tau_{pv,w-ed} = \frac{\sum_{t=t_0}^{\Delta t} t_{SL,ed}(t)}{t_{L,ed}} \quad \text{with} \quad t_{SL,ed}(t) = \begin{cases} 1 & \text{if} \quad P_{tl,ed}(t) = P_{L,ed}(t) \\ 0 & \text{if} \quad P_{tl,ed}(t) < P_{L,ed}(t) \end{cases} \qquad (20)$$

Where, $t_{L,ev}$, $t_{L,hp}$ and $t_{L,ed}$ are the number of hours in which, respectively, the EV, HP and ED loads are present.

The previous reliability indicators R can be employed both for a deterministic and statistical analysis. In the first case, the indicators being variable day per day or week per week, the analysis allows the individuation of the indicator daily or weekly trends and identification the variation ranges of the indicators. In addition to the deterministic analysis, the second analysis permits the determination of the average reliability $\overline{R}$ and the reliability uncertainty of the system to supply the three loads. In this work, to evaluate the average reliability and the reliability uncertainty, the mean and variance values of the statistical distribution are employed. Specifically, to measure the reliability uncertainty, the interquartile range IQR (i.e., first quartile subtracted from the third quartile) is used denoting the dispersion of the reliability (also exhibited by the standard deviation) from the average. The average reliability is associated with the average trend of the renewable sources and loads in a specific period while the reliability uncertainty is determined by the fluctuation of the wind and solar renewable sources and loads around the average trends in the same period. For example, in a weekly analysis, the yearly average weekly trend is responsible for the average reliability of the system, while the reliability uncertainty grows, so much greater is the deviation between the actual weekly trends and the yearly average weekly trend during the whole year. Definitely, each reliability indicator was represented by employing the expression of Eq. (21).

Chapter 6   **Solar and wind assisted heat pump to**
meet the building air conditioning and electric energy demand
in the presence of an electric vehicle charging station and battery storage

$$R = \bar{R} \pm \frac{IQR}{2} \qquad\qquad (21)$$

3. Results and discussion

3.1. Weekly analysis

3.1.1. Energy balance

With reference to Eqs. (4) and (5) of the balance of the energy required by the load and energy generated, Figure 11 shows the different dimensionless energies for the various weeks, at the top in the presence of battery storage of 20 kWh, and at the bottom in the absence of the battery. Moreover, each dimensionless energy is divided into the contribution of the PV generator and wind generator.

The different dimensionless energies are highly variable during the various weeks of the year. In particular, in the presence of the battery, e_{dtl} varies between 0.18 and 0.61, e_{fb} between 0.07 and 0.28, e_{fg} between 0.15 and 0.68, e_{dtl}/e_g between 0.27 and 0.66, e_{tb}/e_g between 0.06 and 0.40, and e_{tg}/e_g between 0.07 and 0.52. In the absence of the battery, the ranges of e_{dtl} and e_{dtl}/e_g remain almost unchanged, while the extreme values of the e_{fg} and e_{tb}/e_g ranges increase, respectively, until to (0.37 - 0.82) and (0.34 - 0.73). Consequently, the battery assures lower exchanges with the grid and greater reliability in terms of satisfied load and self-consumption of the energy generated. However, it does not guarantee a lower variability throughout the year of the previous energy contributions since the range width in the absence and presence of the battery is almost identical. By comparing the PV contributions with the wind contributions, it emerges that, in terms of supplying the load, the PV generator prevails more markedly on the wind generator, in terms of energy in excess sent to the grid, the wind generator contributes in a slightly more significant manner compared to the PV generator and vice versa to this latter case in terms of energy stored.

As shown, during each week the dimensionless energies are strongly variable. To provide a summary indication of the weekly reliability of the ERHS, the weekly reliability indicators were assessed in the absence and presence of the battery storage.

Chapter 6   **Solar and wind assisted heat pump to**
meet the building air conditioning and electric energy demand
in the presence of an electric vehicle charging station and battery storage
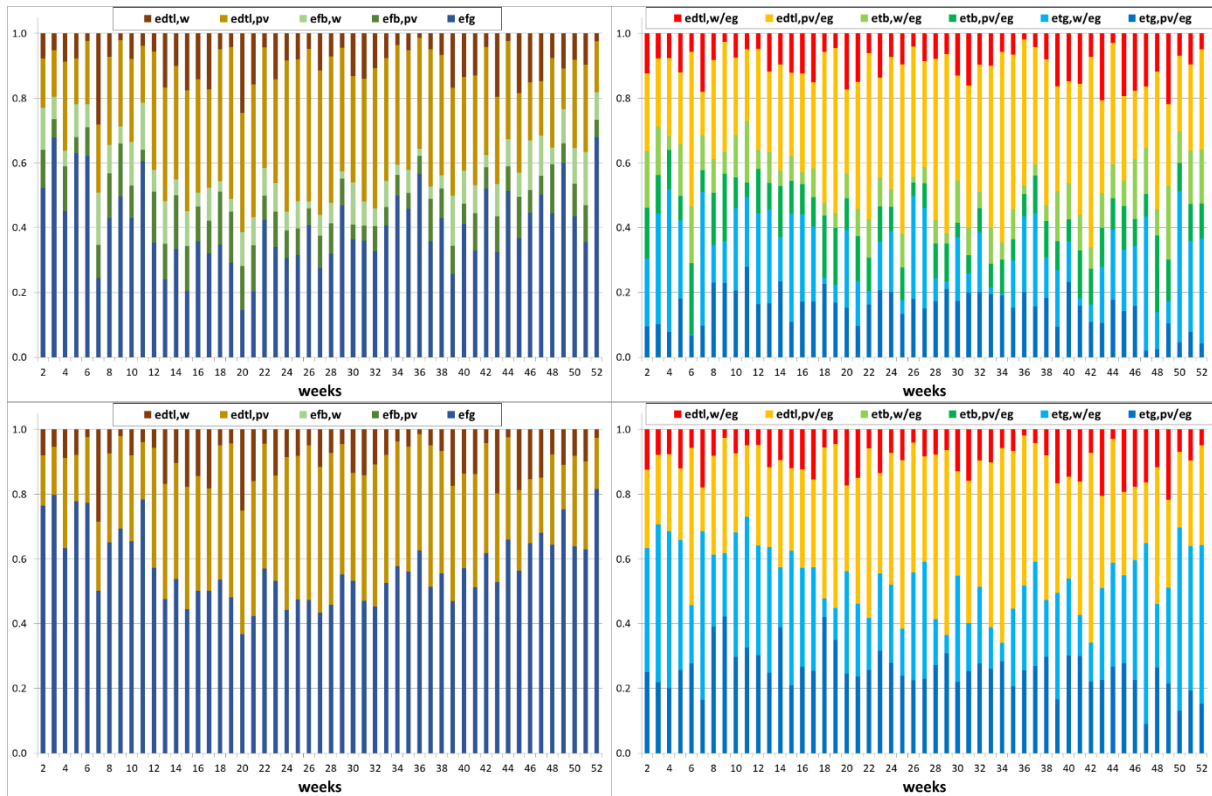
Figure 11. *Dimensionless balance of the energy required by the load on the left and energy generated on the right. In the presence of battery storage of 20 kWh at the top and in the absence of the battery at the bottom.*

3.1.2. Reliability indicators

3.1.2.1. Overall load

Figure 12 reports the weekly energy produced by the ERHS, energy required by the load subdivided into the three contributions due to the HP, EV and EDs, and reliability indicators in relation to the overall load in the presence and absence of the battery, respectively in the image at the top and bottom. The strong variability of the dimensionless energies of the balance equations determines a consequent substantial changeability of the weekly reliability indicators throughout the year. In particular, $f_{u,g}$ is between 0.48 and 0.93, $f_{pv,w}$ between 0.32 and 0.85, and τ between 0.27 and 0.85. In the absence of the battery, the previous values of indicators drastically reduced up to, respectively, 0.27 and 0.66, 0.18 and 0.63, and 0.09 and 0.49. Instead, f_m does not depend on the battery capacity, it is only determined by the energy generated, and varies between 0.05 and 0.22. By comparing $\tau_{pv,w}$ with $f_{pv,w}$, it is possible to identify the weeks in which the load is satisfied in the hours corresponding with the highest or lowest load values. For instance, in the case of the presence of the battery, in the 34th week $f_{pv,w} > \tau_{pv,w}$, namely the load is high in the hours in which it is satisfied; in the fourth week $f_{pv,w} < \tau_{pv,w}$ and prevalently the low loads are satisfied. In the absence of battery $f_{pv,w} > \tau_{pv,w}$ almost in all the weeks.

Chapter 6 **Solar and wind assisted heat pump to**
meet the building air conditioning and electric energy demand
in the presence of an electric vehicle charging station and battery storage
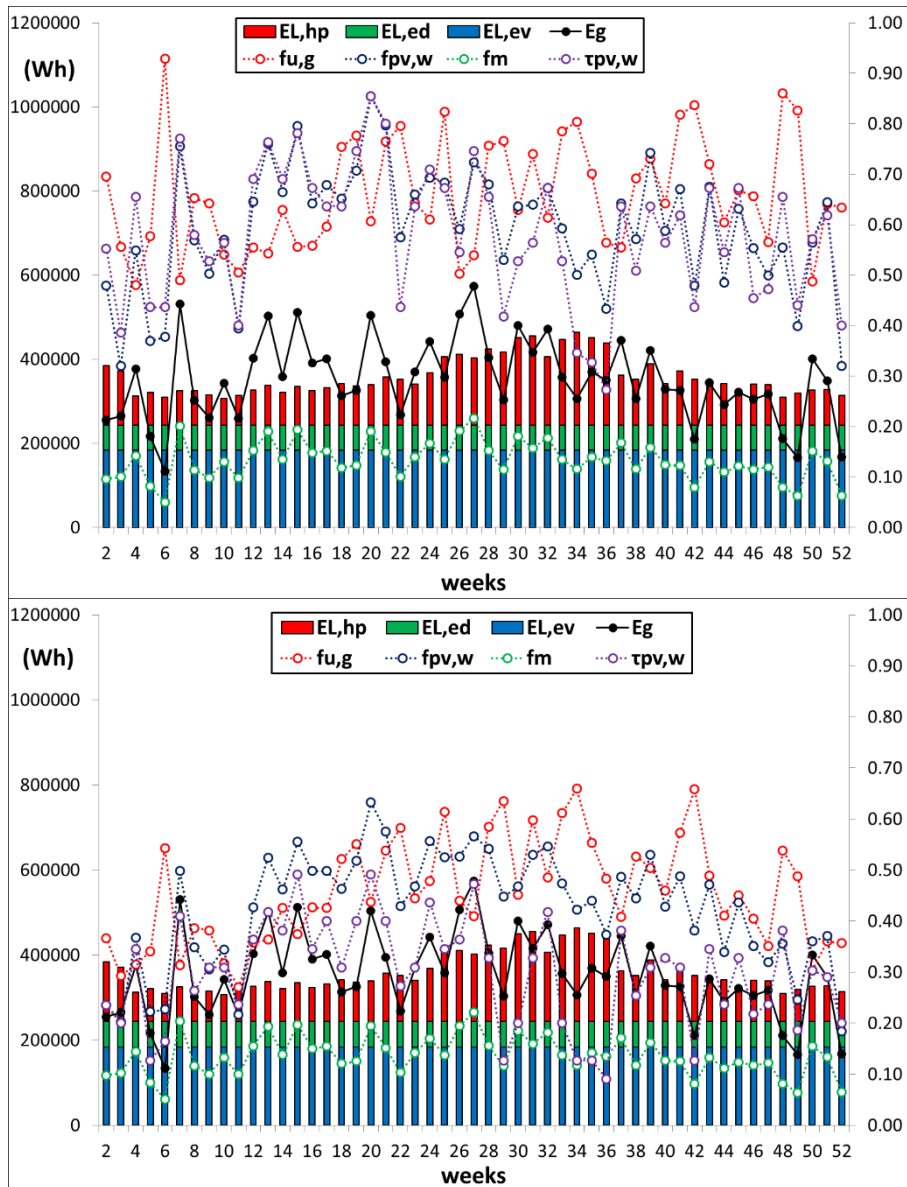
Figure 12. Weekly energy produced by the ERHS, energy required by the load and reliability indicators in relation to the overall load in the presence at the top and absence at the bottom of the battery.

This high variability is determined by the difference between the energy produced and the energy required by the load. In particular, when the energy generated is much lower than the energy required, the load, $f_{u,g}$ presents the highest values, while $f_{pv,w}$ the lowest. Vice versa, when the energy generated is much higher than the energy required for the load. Finally, when the two energies are very close, the two indicators are comparable and they grow by increasing the two values of energies.

3.1.2.2. Single loads

As regards the weekly reliability indicators in relation to the single loads in the presence and absence of the battery, Figures 13, 14, and 15 contain, respectively, the time contemporaneity factors $\tau_{pv,w\text{-}ev}$, $\tau_{pv,w\text{-}hp}$, and $\tau_{pv,w\text{-}ed}$ of the single loads overlapped with the overall time contemporaneity factor $\tau_{pv,w}$ in a polar representation, the cumulative histograms of the energy contemporaneity factors, the non-weighted and weighted PV-wind fractions in polar representations.

Chapter 6   **Solar and wind assisted heat pump to**
meet the building air conditioning and electric energy demand
in the presence of an electric vehicle charging station and battery storage
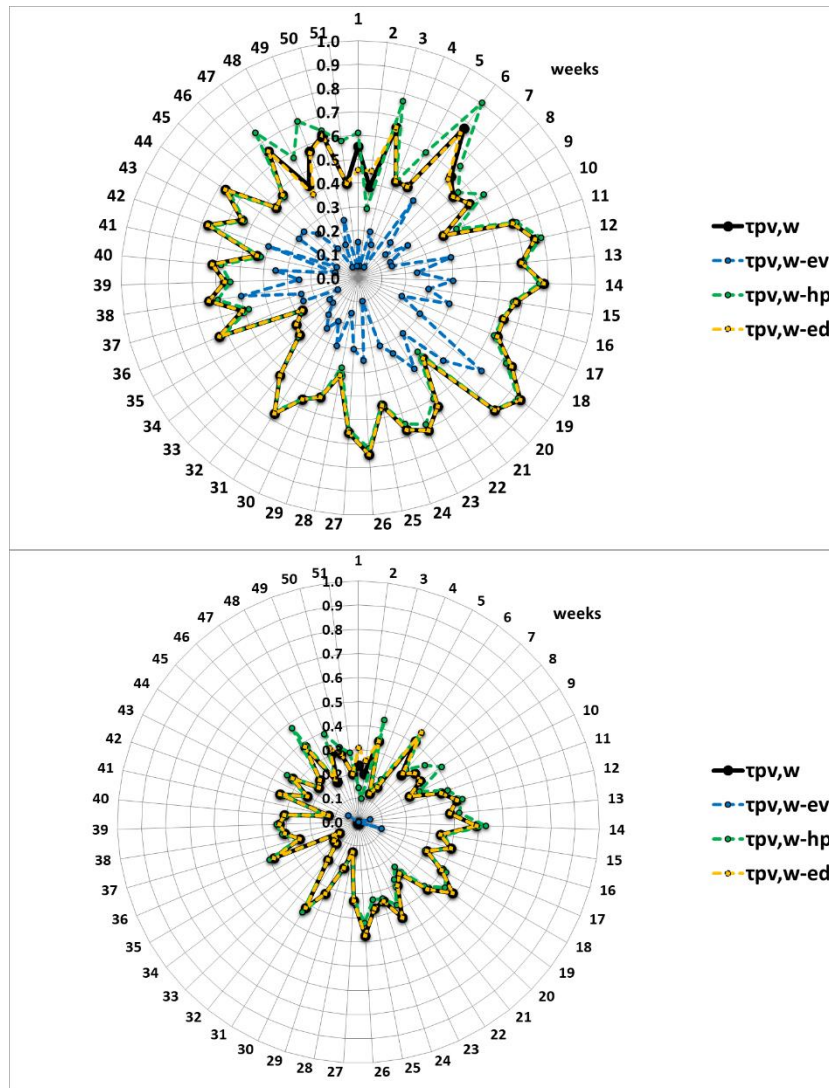
Figure 13. *Overall time contemporaneity factor and time contemporaneity factors of the single loads in the presence at the top and absence at the bottom of the battery.*

By comparing the case with and without battery, the time contemporaneity factors relative to the single loads reduced can be observed, as previously highlighted for the overall time contemporaneity factor. In particular, in the presence of the battery, the electric energy absorbed by the HP presents a time percentage with a satisfied load much higher than that of EV loads. This is owing to the higher energy required by the EVs in a limited period compared to that of the HP that could be distributed in the entire day. In these conditions, the EV load is hardly satisfied. The ED time contemporaneity factor is very close to the overall time contemporaneity factor, since it is the lowest load and the most present, and it is prevalently slightly lower than that of HP, as the HP could be switched off when the building energy needs are nil. In the weeks in which the HP and ED factors are identical, the two electric loads are simultaneously satisfied. In the absence of the battery, the previous considerations remain valid and the EV time contemporaneity factor is nil almost in all the weeks. Consequently, the battery is used for a longer time due to the EV demand.

Chapter 6
         **Solar and wind assisted heat pump to
meet the building air conditioning and electric energy demand
in the presence of an electric vehicle charging station and battery storage**
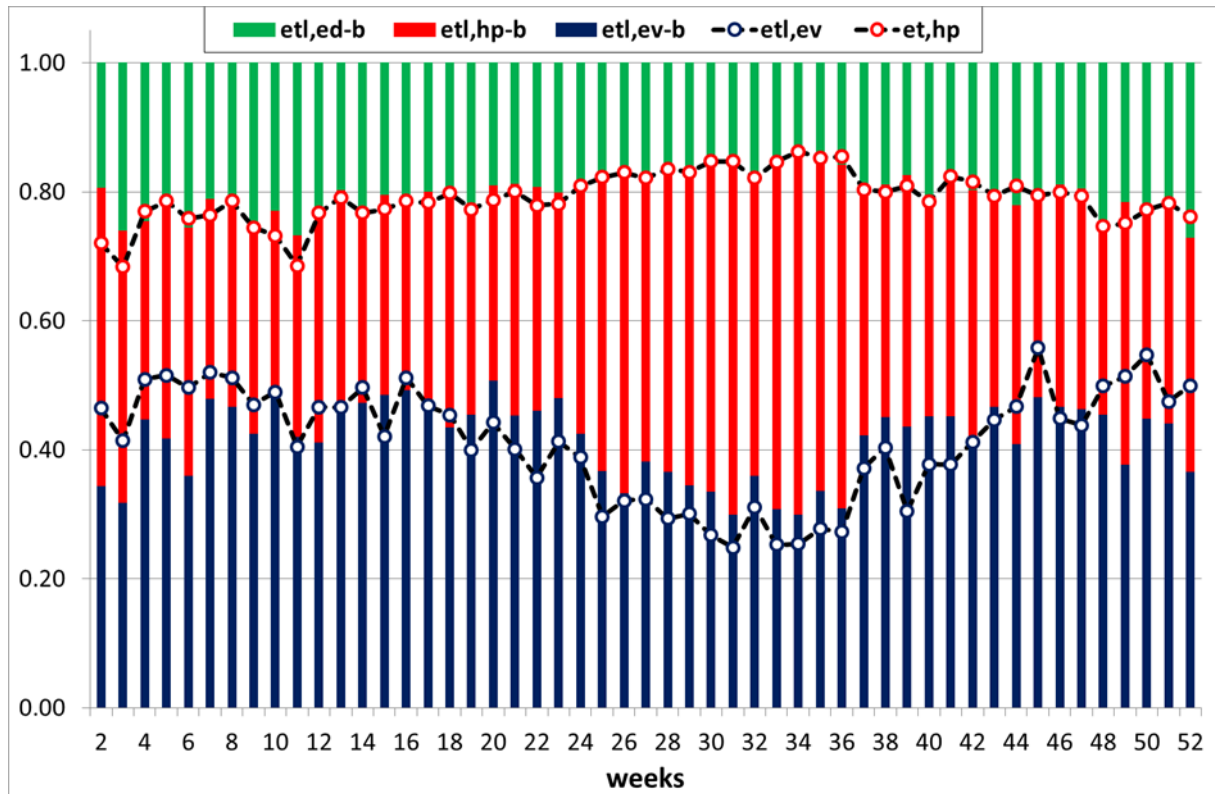
Figure 14. *Energy contemporaneity factors of the single loads in the presence and absence at the bottom of the battery.*

As regards the energy contemporaneity factors, their apportionment, Eq. (14), represented in Figure 14, allows the individuation of the most supplied load by the renewable sources. When ERHS has an electric storage system, in the winter weeks, the renewable energy produced is mainly used to supply the EV charging station, while in the summer period the HP draws the most renewable energy produced. Instead, EDs in the entire year receive the lowest contribution, which is variable on seasonal bases with higher values in the winter and lower values in the summer. The dashed lines show the apportionment when the ERHS is not equipped with a storage system. As an overall trend, it is clear that in winter, compared with the case of the presence of the battery, the EV contribution is reduced, that of EDs slightly increases and consequently, the renewable energy sent to the HP undergoes a reduction, up to becoming comparable with the EDs contribution. In the summer period, the EV contribution increases and that of EDs is almost unchanged. Therefore, renewable energy absorbed by HP reaches the highest values.

In general, the battery is mainly employed by the EVs in the winter owing to the reduced building energy needs for air-conditioning, while in the summer, these energy needs grow and as a consequence, the HP, in addition to being the most supplied by the ERHS, is the electric load that mostly uses the battery. Moreover, the EV and HP loads present greater contemporaneity with the renewable sources in energy terms, respectively, in winter and summer. Such a contemporaneity further rises in the presence of the battery since this latter tends to feed mainly the highest load in the two seasons.

On a yearly basis, the variation range of the ED, HP and EV energy contemporaneity factors resulted (0.15 - 0.27), (0.28 - 0.55), and (0.30 - 0.51) with the battery, while it is (0.14 - 0.32), (0.22 - 0.61) and (0.25 - 0.56) without the battery.

Chapter 6   **Solar and wind assisted heat pump to**
meet the building air conditioning and electric energy demand
in the presence of an electric vehicle charging station and battery storage
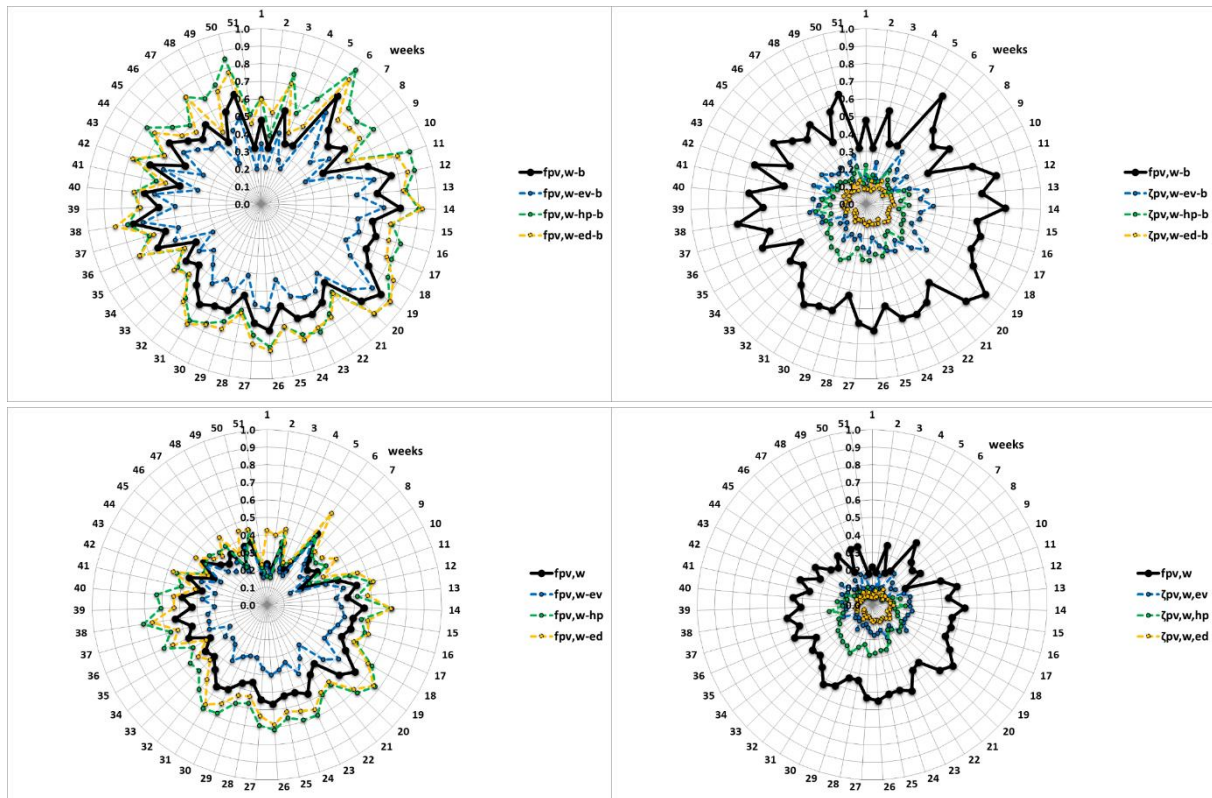
Figure 15. *Non-weighted PV-wind fractions on the left and weighted PV-wind fractions on the right in the presence at the top and absence at the bottom of the battery.*

The EV, HP and ED non-weighted PV-wind fractions, reported at the left of Figure 15, in the presence of the battery, during the entire year, respectively, fall within the ranges (0.20 - 0.80), (0.39 - 0.94) and (0.44 - 0.92), by determining, as described previously, an overall PV-wind fraction variable between (0.32 - 0.85). The weekly variability highlights that the EV fraction is always the lowest, while the HP and ED factors are very close, except in some winter weeks in which the HP factor exceeds the ED factor. In the absence of the battery, it emerges that, in addition to a reduction of the range, the maximum values undergo a slump. Also, as regards the minimum HP and ED factors a substantial decline is observed. These modifications give rise to a fall of the overall PV-wind fraction up to (0.18 - 0.63).

The EV weighted PV-wind fraction, reported on the right of Figure 15, when the ERHS has a storage system, presents the highest variation interval and the highest maximum value, while the ED weighted PV-wind fraction is in all the weeks the lowest. By observing the weekly trends, it is evident that the EV fraction is the most incident on the overall fraction value, except in some summer weeks in which the HP fraction substantially exceeds it. The battery removal in the ERHS has, as a consequence, the more evident reduction of the maximum EV weighted factor; in addition, the minimum HP and ED weighted factors undergo a noticeable reduction. Compared to the case with the storage system, the previous findings in terms of the weekly trends and incidence on the overall fraction remain valid with differences between the EV and HP more pronounced.

The comparison between the non-weighted and weighted PV-wind fractions allows identification of which load is singly most satisfied and which load is the most incident on the overall PV-wind fraction.

Chapter 6   **Solar and wind assisted heat pump to**
meet the building air conditioning and electric energy demand
in the presence of an electric vehicle charging station and battery storage

3.2. Yearly Statistical analysis

The high weekly variability of the reliability indicators both in terms of overall load and in terms of single loads makes necessary a statistical analysis to summarize the results obtained on a yearly basis. In this statistical analysis, the random variables are the reliability indicators each of which varies between zero and one.

As an example, Figure 16 reports the discrete probability distributions $p(x_i)$ of the reliability indicators in relation to the overall load, namely $f_{pv,w}$, $f_{u,g}$, f_m and $\tau_{pv,w}$, in the presence and absence of the storage system.
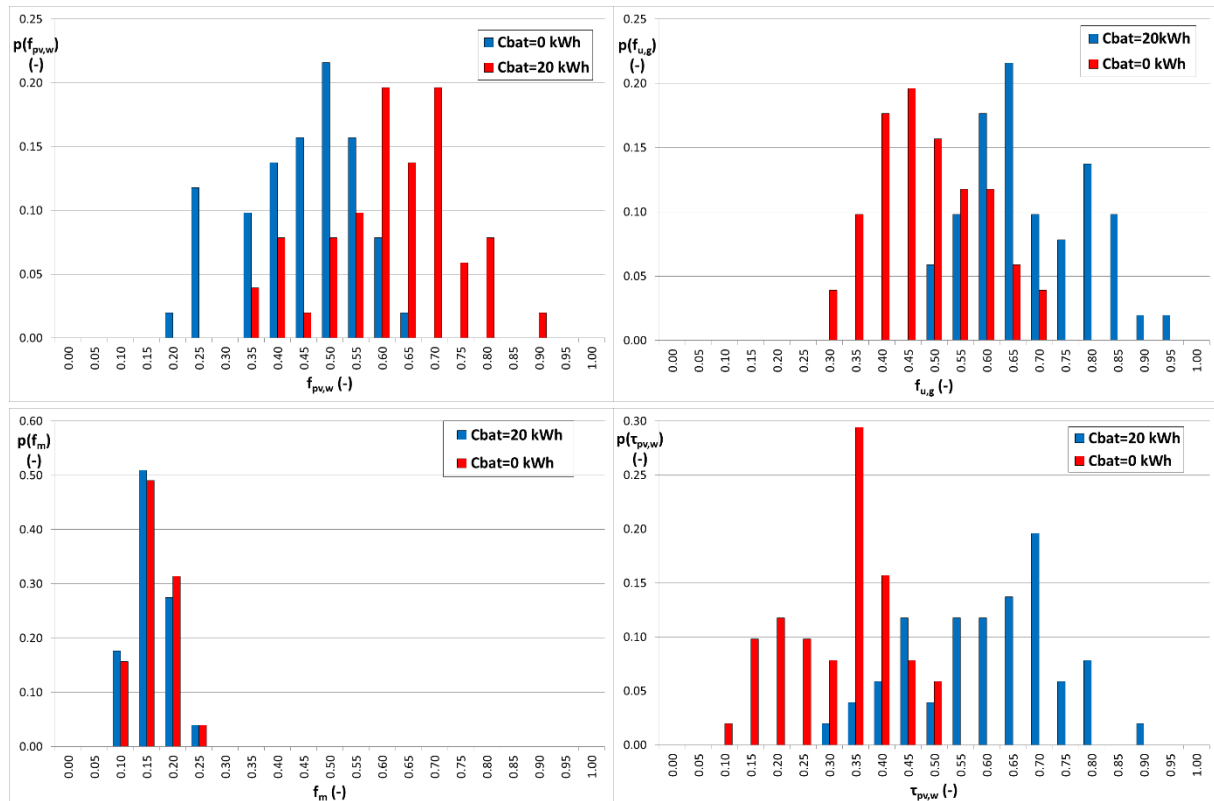
Figure 16. *Discrete probability distributions of the reliability indicators in relation to the overall load in the presence and absence of the storage system.*

The findings described in the previous section are highlighted also by the images. In addition, this representation allows the identification of: the distribution shape within the limit values; the most probable value attributable to each reliability indicator.

In particular, in some cases, the distributions present a bimodal behavior with a maximum frequency not always associated with the peak with the lowest value of the random variable. The battery leads a translation of the discrete probability distributions towards the right by determining higher reliability with a slight modification of the frequency values, except the time contemporaneity factor, which from a range (0, 0.20) extends to a range (0, 0.30). Finally, the dimensionless manufacturability does not depend on the battery capacity and the very small reduction in the lowest values of f_m and the very small increase in the highest values of f_m are owing to the absence of the battery and regulator losses.

In the successive sections, the previous statistical analysis is developed by means of the use of box plots. A box shows the 25th and 75th percentile range, the horizontal line represents the median value, the symbol x identifies the average value, the points detects the outliners and the top whisker and

Chapter 6   **Solar and wind assisted heat pump to**
meet the building air conditioning and electric energy demand
in the presence of an electric vehicle charging station and battery storage

bottom whisker lengths measure respectively the difference between the maximum value and the 75th percentile and between the 25th percentile and the minimum value.

3.2.1. Battery storage capacity effect

This section statistically analyses the effects produced by the battery capacity size on the average reliability and reliability uncertainty with reference to a specific ERHS configuration, namely for a PV and wind power of 7.5 kW. In particular, each reliability indicator by varying the battery storage size was represented by means of box plots.

Figure 17 reports the box plots of the reliability indicators in terms of the overall load.

The reliability on the utilization factor changes from 0.46 ± 0.08 to 0.74 ± 0.08 by comparing the ERHS devoid of the battery storage and the ERHS with battery storage of 40 kWh, denoting a noticeable increase of the average reliability and invariance of the uncertainty. Analogously for the overall PV-wind fraction and time contemporaneity factor that from 0.42 ± 0.08 and 0.30 ± 0.07 become 0.67 ± 0.09 and 0.65 ± 0.10. Instead, the dimensionless manufacturability does not depend on the battery storage size with a reliability of 0.13 ± 0.02.
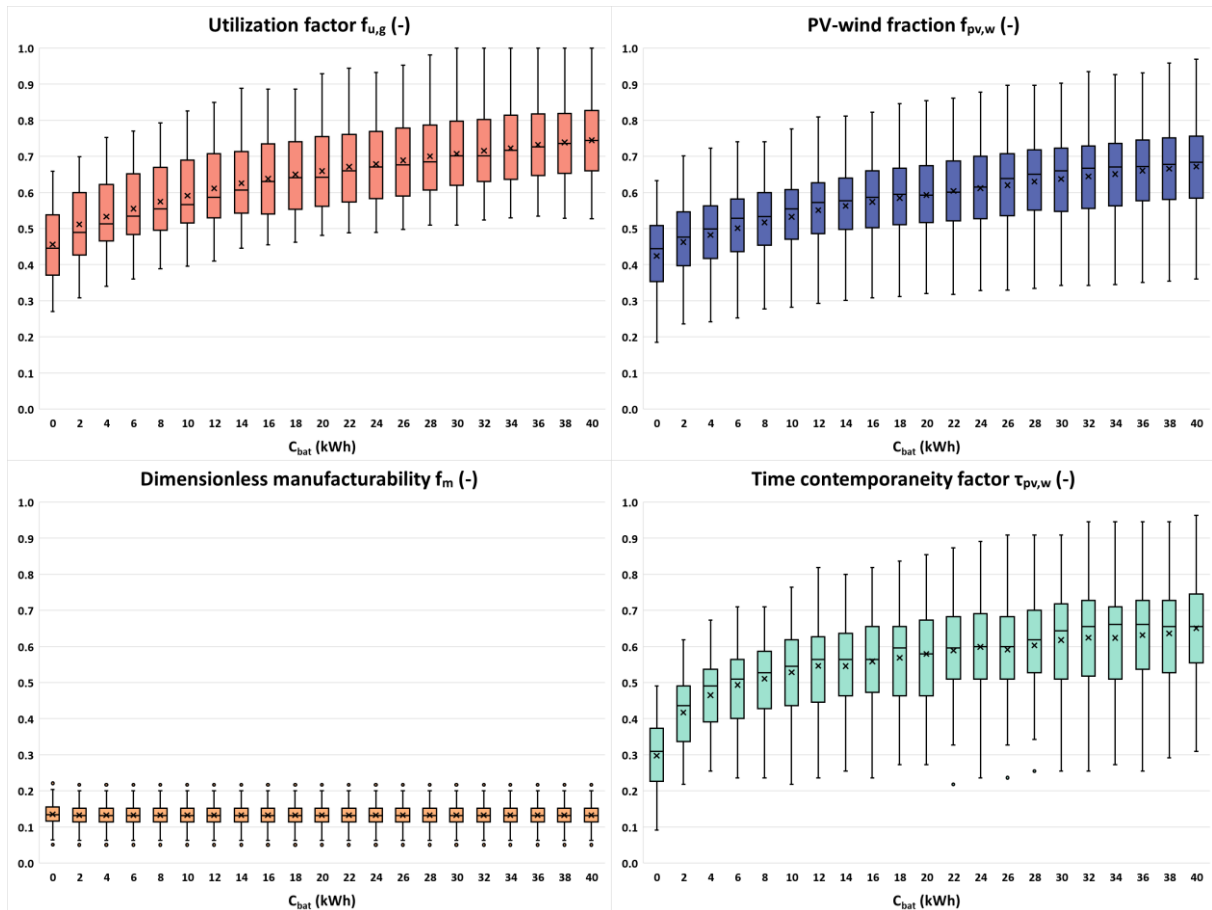
Figure 17. *Box plots of the reliability indicators in terms of overall load as a function of the battery storage size.*

Figures 18-21 are relative to the reliability indicators in terms of single loads.

The average reliability on the PV-wind fractions for all the loads increases considerably across the battery storage. In particular, the battery storage is mainly used to supply the EV, PV-wind fraction of which presents the highest increase with a value of 0.60 at 40 kWh, 81% higher compared to that at 0 kWh. The HP and ED PV-wind fraction average values are very close and higher than those relative to the EV. The maximum value is 0.75. In terms of uncertainty, the three factors are very

comparable and equal to about ± 0.08 in the presence of the battery, while the uncertainty reliability of the factors for the ERHS devoid of battery undergoes a marked increase for the HP and ED and to a marked reduction for the EV.

The average reliability on all the weighted PV-wind fractions grows by increasing the battery capacity. In particular, the HP fraction is the most incident in the overall PV-wind fraction up to a battery capacity value of 6 kWh, above which the EV fraction becomes the highest. Quantitatively, the maximum values reached at 40 kWh are 0.31, 0.24 and 0.12 respectively for the EV, HP and ED. Different trends are observed for the three reliability uncertainties, with an increasing trend as battery capacity grows for the EV fraction, an almost constant trend for the HP and ED uncertainty with a stable value of respectively about ± 0.04 and ± 0.02. In general, the higher uncertainty reliability is detected for the EV fraction with a maximum value of ± 0.07, while the lowest one for the ED fraction. A significant difference is highlighted on the HP fraction in the case of the absence of the battery, the case in which the fraction markedly increases.

Both the average reliability and reliability uncertainty on the EV time contemporaneity factor gradually grows markedly by raising the battery capacity from a nil average reliability and reliability uncertainty to 0.43 ± 0.14. Instead, for the HP and ED factors, the increase in average reliability is less significant, while the reliability uncertainty for both the factors is constant enough around a value of ± 0.09.

Chapter 6   **Solar and wind assisted heat pump to**
meet the building air conditioning and electric energy demand
in the presence of an electric vehicle charging station and battery storage
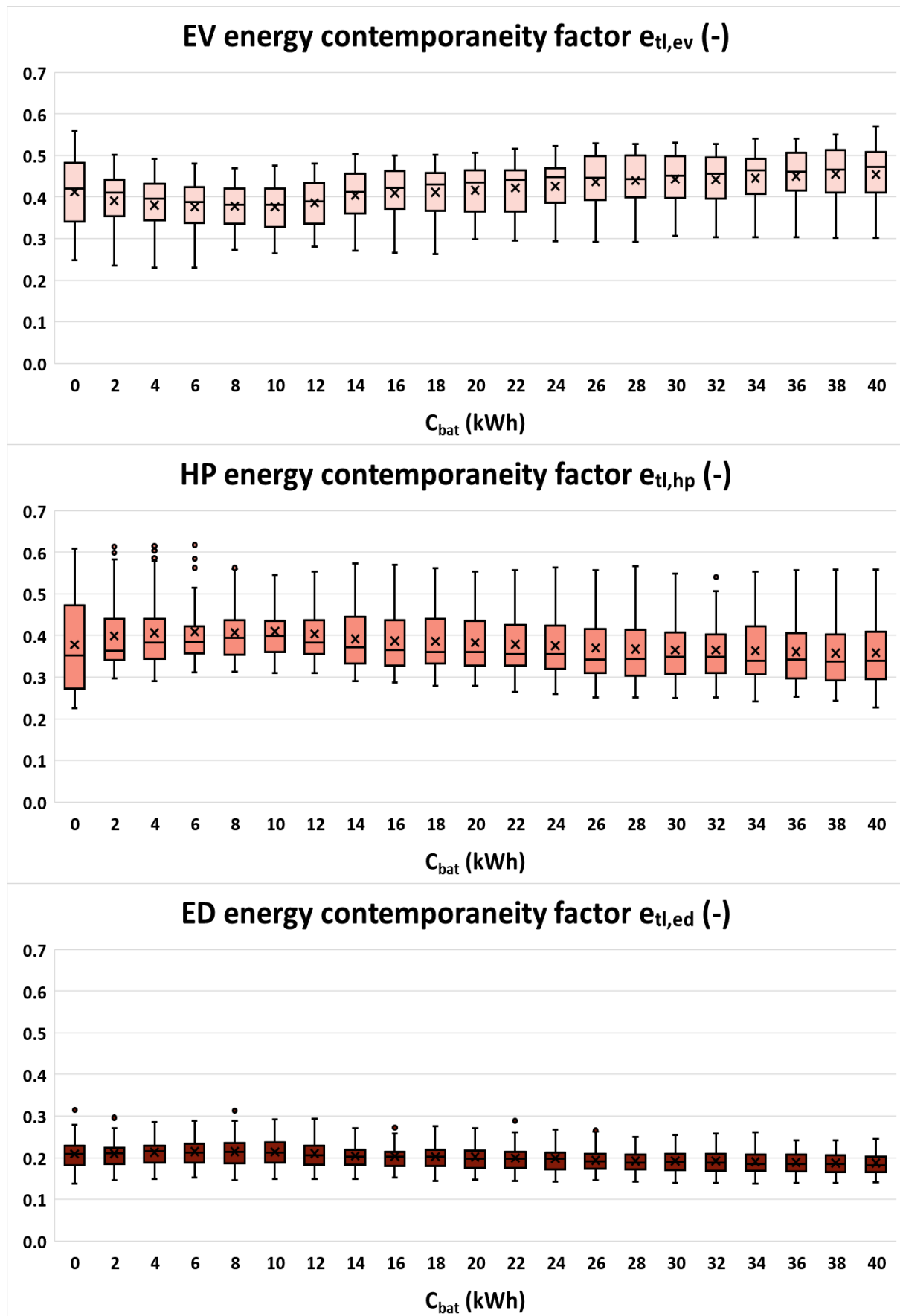
Figure 18. *Box plots of the EV, HP and ED energy contemporaneity factors as a function of the battery storage size.*

Chapter 6   Solar and wind assisted heat pump to
meet the building air conditioning and electric energy demand
in the presence of an electric vehicle charging station and battery storage
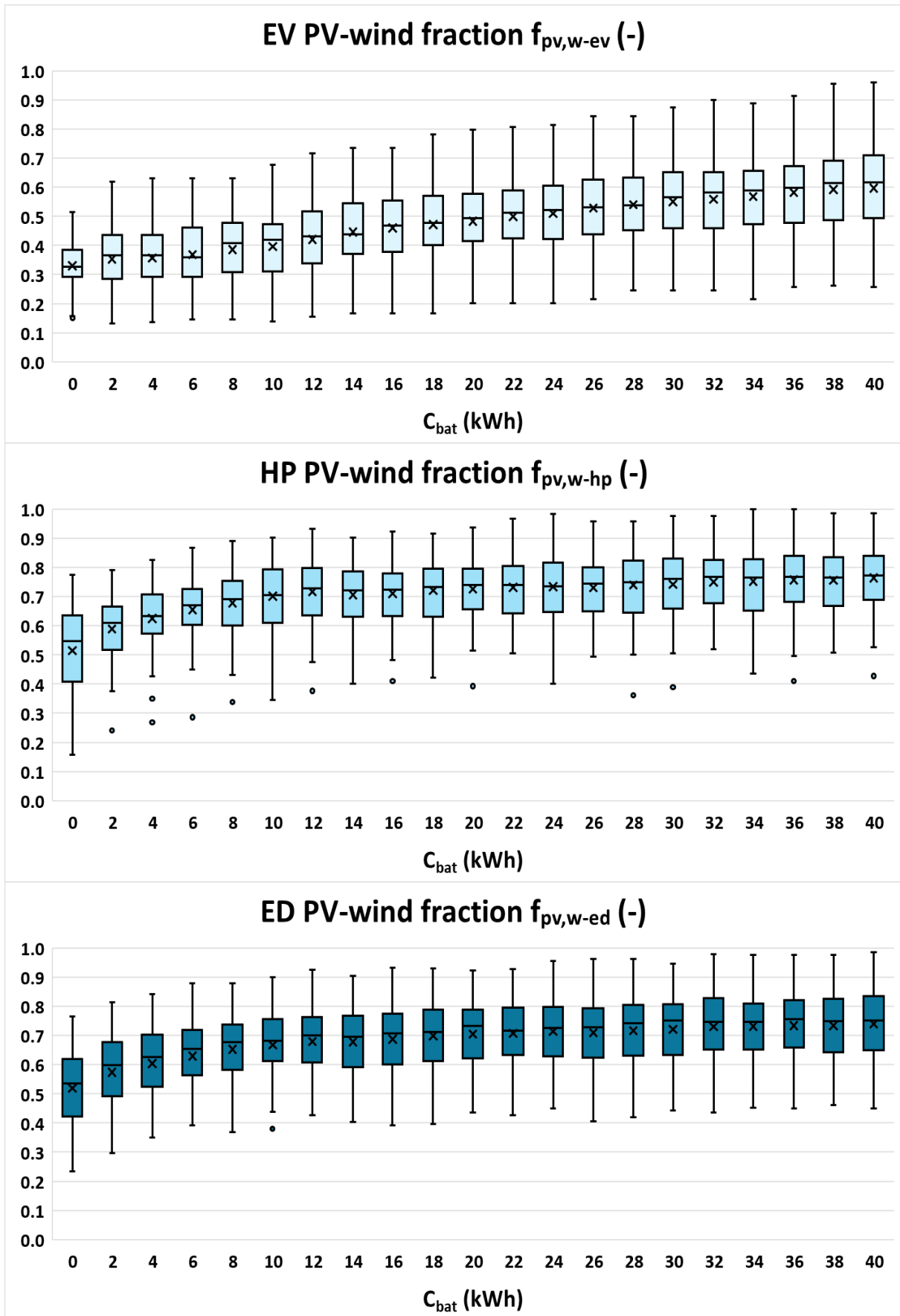
Figure 19. *Box plots of the EV, HP and ED PV-wind fractions as a function of the battery storage size.*

Chapter 6

Solar and wind assisted heat pump to meet the building air conditioning and electric energy demand in the presence of an electric vehicle charging station and battery storage

EV weighted PV-wind fraction ζ$_{pv,w-ev}$ (-)

C$_{bat}$ (kWh)

HP weighted PV-wind fraction ζ$_{pv,w-hp}$ (-)

C$_{bat}$ (kWh)

ED weighted PV-wind fraction ζ$_{pv,w-ed}$ (-)

C$_{bat}$ (kWh)
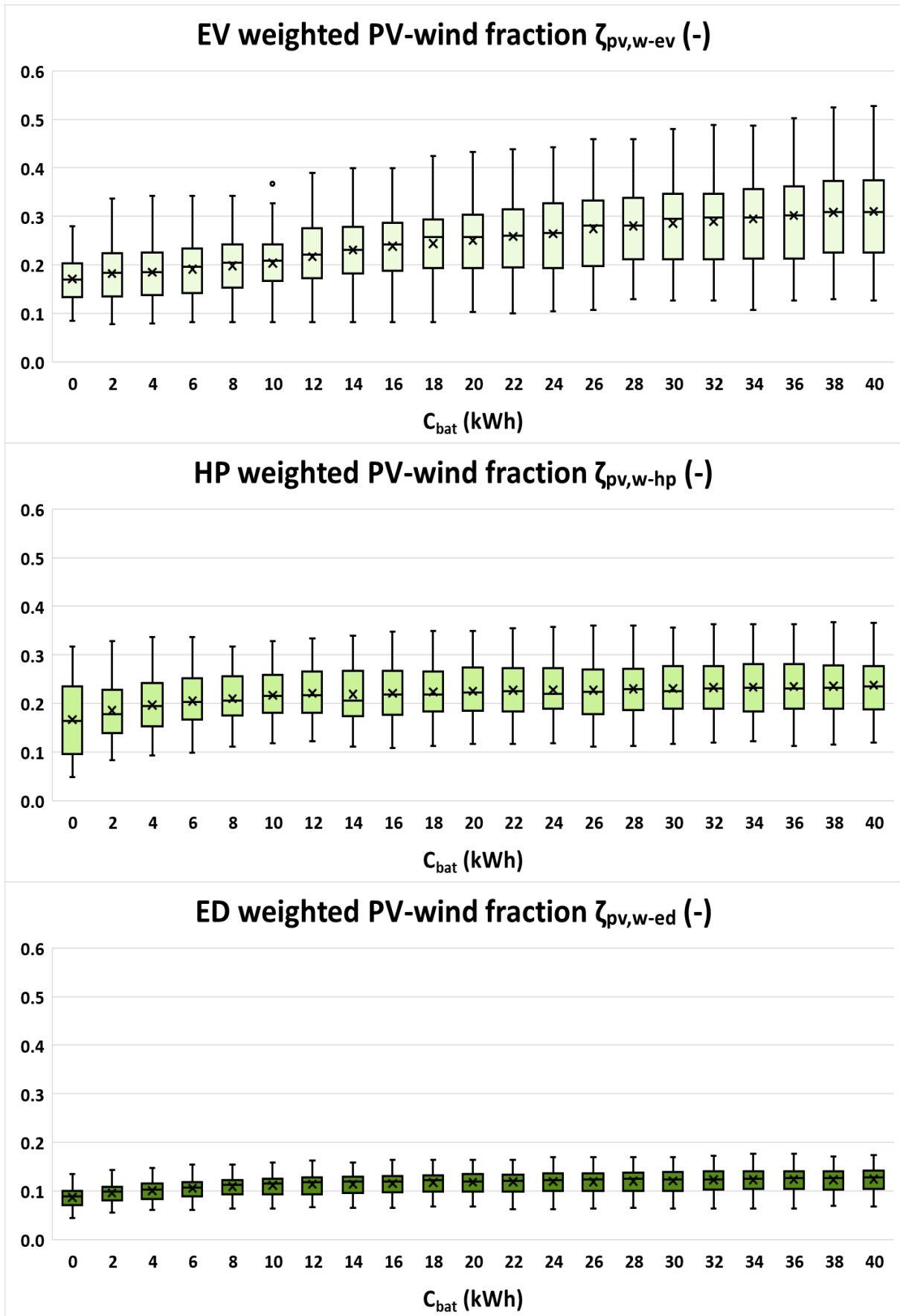
Figure 20. Box plots of the EV, HP and ED weighted PV-wind fractions as a function of the battery storage size.

Chapter 6   **Solar and wind assisted heat pump to**
meet the building air conditioning and electric energy demand
in the presence of an electric vehicle charging station and battery storage

EV time contemporaneity factor $\tau_{pv,w-ev}$ (-)

C_{bat} (kWh)

HP time contemporaneity factor $\tau_{pv,w-hp}$ (-)

C_{bat} (kWh)

ED time contemporaneity factor $\tau_{pv,w-ed}$ (-)

C_{bat} (kWh)
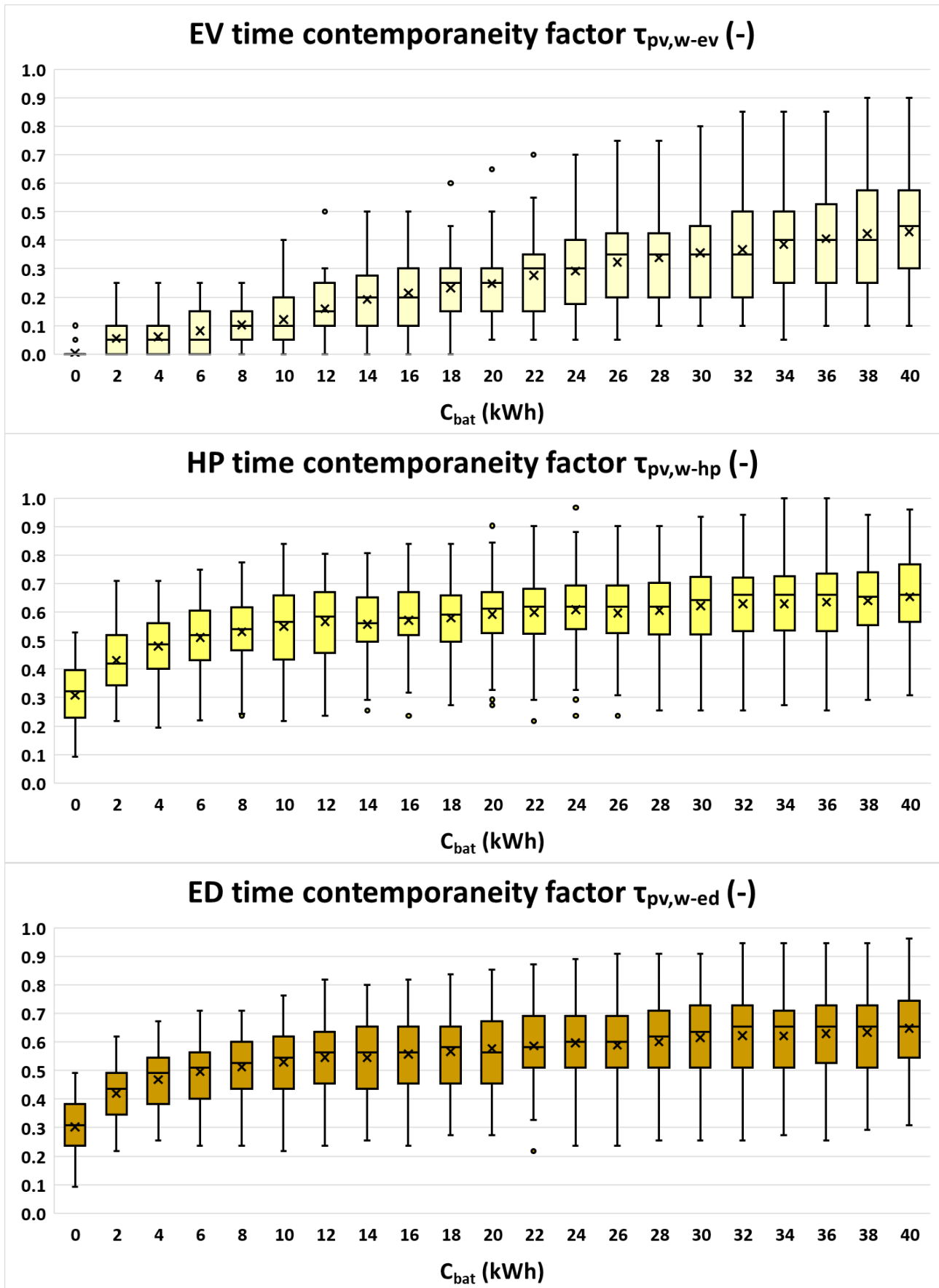
Figure 21. *Box plots of the EV, HP and ED time contemporaneity factors as a function of the battery storage size.*

Chapter 6

Solar and wind assisted heat pump to meet the building air conditioning and electric energy demand in the presence of an electric vehicle charging station and battery storage

3.2.2. Photovoltaic generator power effect

This section statistically analyses the effects produced by the PV power installed on the average reliability and reliability uncertainty, with reference to a specific ERHS configuration, namely for wind power of 7.5 kW in the presence and absence of a battery capacity of 20 kWh. In particular, by varying the PV power, each reliability indicator was represented by means of box plots. Figure 22 reports the box plots of the reliability indicators in terms of the overall load.
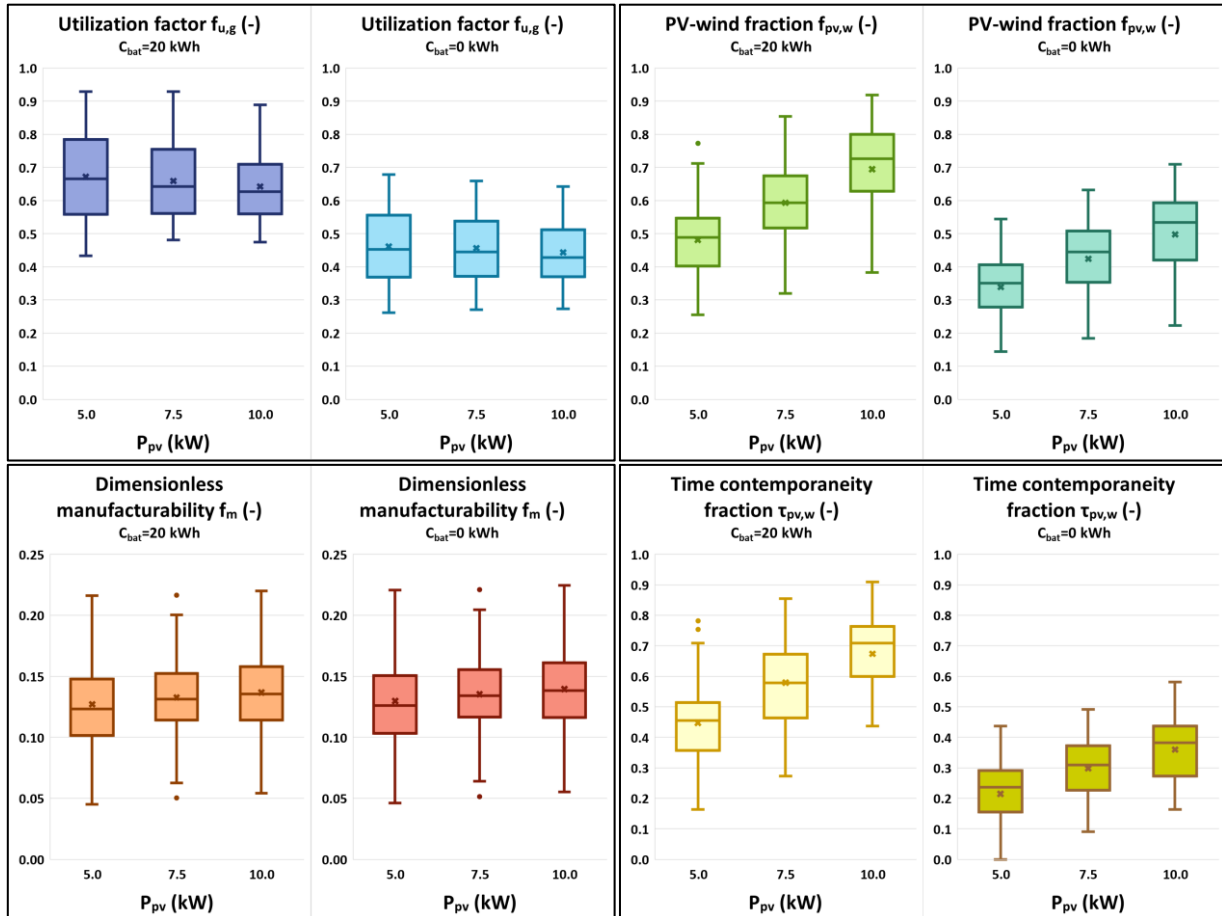
Figure 22. Box plots of the reliability indicators in terms of overall load as a function of the PV power.

The average reliability and reliability uncertainty on the utilization factor undergo a moderate drop as the PV power rises both in the presence and absence of the battery. The maximum value, obtained with 5 kW of PV power and with the ERHS equipped with battery storage is 0.67 ± 0.11. As regards the overall PV-wind fraction, the behavior is contrary. In particular, the average reliability and reliability uncertainty highlight a growth as the PV power increases both in the presence and absence of the battery. The maximum value, obtained with 10 kW of PV power and with the ERHS equipped with battery storage is 0.69 ± 0.09. Compared to the previous case in which the battery size was varied, the average dimensionless manufacturability both for the ERHS equipped with the battery and without the battery shows a slight increase from 0.13 to 0.14, while the uncertainty is almost unchanged to ± 0.02. Finally, the overall time contemporaneity factor has a trend very similar to that of the overall PV-wind fraction with a maximum value, obtained for 10 kW of PV power, of 0.67 ± 0.08.

In Figure 23, the box plots of the reliability indicators defined in terms of single loads are shown. In particular, the images on the left are related to the ERHS equipped with battery storage, while the

Chapter 6

**Solar and wind assisted heat pump to
meet the building air conditioning and electric energy demand
in the presence of an electric vehicle charging station and battery storage**

images on the right to the ERHS without battery. Each image is divided into three sub-images related to the three different loads, in each of which the box plots for three values of the PV power are reported.
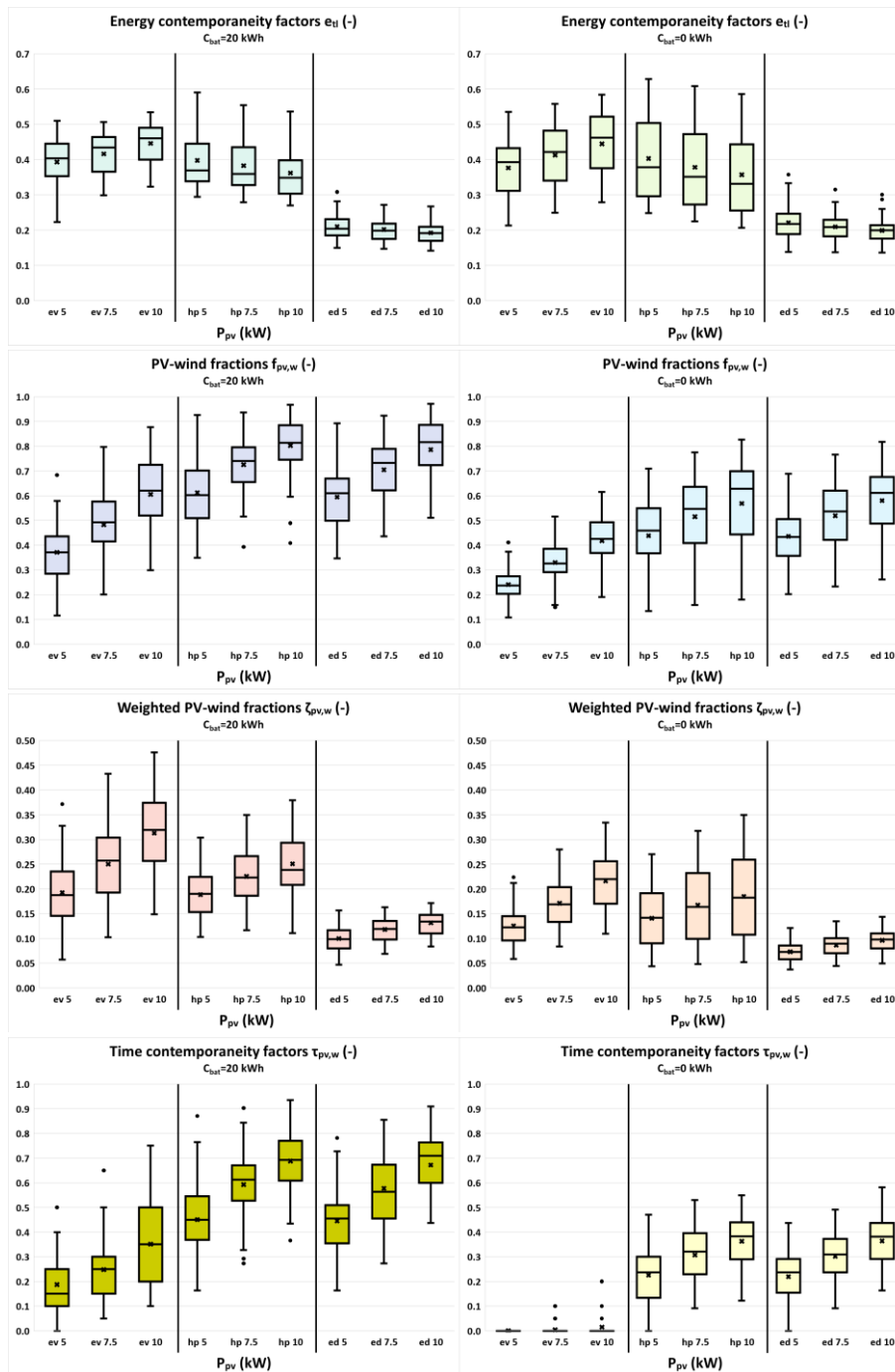
Figure 23. *Box plots of the EV, HP and ED energy contemporaneity factors, non-weighted and weighted PV-wind fractions and time contemporaneity factors as a function of the PV power.*

By increasing the PV power:

a) the average energy contemporaneity factor of the EV grows, while those of the HP and ED are reduced. The uncertainty does not change in a significant manner with the PV power. The removal of battery storage does not produce modifications in qualitative terms by varying the PV power. However, the average reliability on the EV factor is minimally lower than that

Chapter 6   **Solar and wind assisted heat pump to**
meet the building air conditioning and electric energy demand
in the presence of an electric vehicle charging station and battery storage

obtained in the presence of the battery, while that of the HP factor remains almost the same
and that of the ED factor slightly rises;

b) all the average PV-wind fractions rise, while the uncertainties related to the three loads
undergo a slight modification. In the absence of the battery, the previous considerations
remain valid with lower values of the average reliability and uncertainties that are slightly
lower for the EV and are moderately greater for the HP and ED;

c) all the weighted PV-wind fractions are modified in the same way as the non-weighted PV-
wind fraction;

d) all the time contemporaneity factors change analogously to the non-weighted PV-wind
fraction. The only differences regard the uncertainty modification that emerges when the
battery is absent. In particular, the uncertainties for all three factors is minimally reduced when
the battery is removed.

Table 6 contains the maximum reliability obtained for the different indicators defined in relation to
the single loads as a function of the PV power.

Table 6. Maximum reliability indicators in terms of single loads and optimal value of the PV power and battery capacity.

	ev	**hp**	**ed**
e_{tl}	0.45 ± 0.05 (P_{pv}=10 kW, C_{bat}=20 kWh)	0.40 ± 0.05 (P_{pv}=5 kW, C_{bat}=20 kWh)	0.22 ± 0.03 (P_{pv}=5 kW, C_{bat}=0 kWh)
$f_{pv,w}$	0.61 ± 0.10 (P_{pv}=10 kW, C_{bat}=20 kWh)	0.80 ± 0.07 (P_{pv}=10 kW, C_{bat}=20 kWh)	0.79 ± 0.08 (P_{pv}=10 kW, C_{bat}=20 kWh)
$\zeta_{pv,w}$	0.31 ± 0.06 (P_{pv}=10 kW, C_{bat}=20 kWh)	0.25 ± 0.04 (P_{pv}=10 kW, C_{bat}=20 kWh)	0.13 ± 0.02 (P_{pv}=10 kW, C_{bat}=20 kWh)
$\tau_{pv,w}$	0.35 ± 0.15 (P_{pv}=10 kW, C_{bat}=20 kWh)	0.69 ± 0.08 (P_{pv}=10 kW, C_{bat}=20 kWh)	0.67 ± 0.08 (P_{pv}=10 kW, C_{bat}=20 kWh)

3.2.3. Wind micro-generator power effect

This section statistically analyses the effects produced by the wind power installed on the average
reliability and reliability uncertainty, with reference to a specific ERHS configuration, namely for a
PV power of 7.5 kW in the presence and absence of a battery capacity of 20 kWh. In particular, each
reliability indicator by varying wind power was represented by means of box plots. Figure 24 reports
the box plots of the reliability indicators in terms of the overall load.

Chapter 6

Solar and wind assisted heat pump to meet the building air conditioning and electric energy demand in the presence of an electric vehicle charging station and battery storage
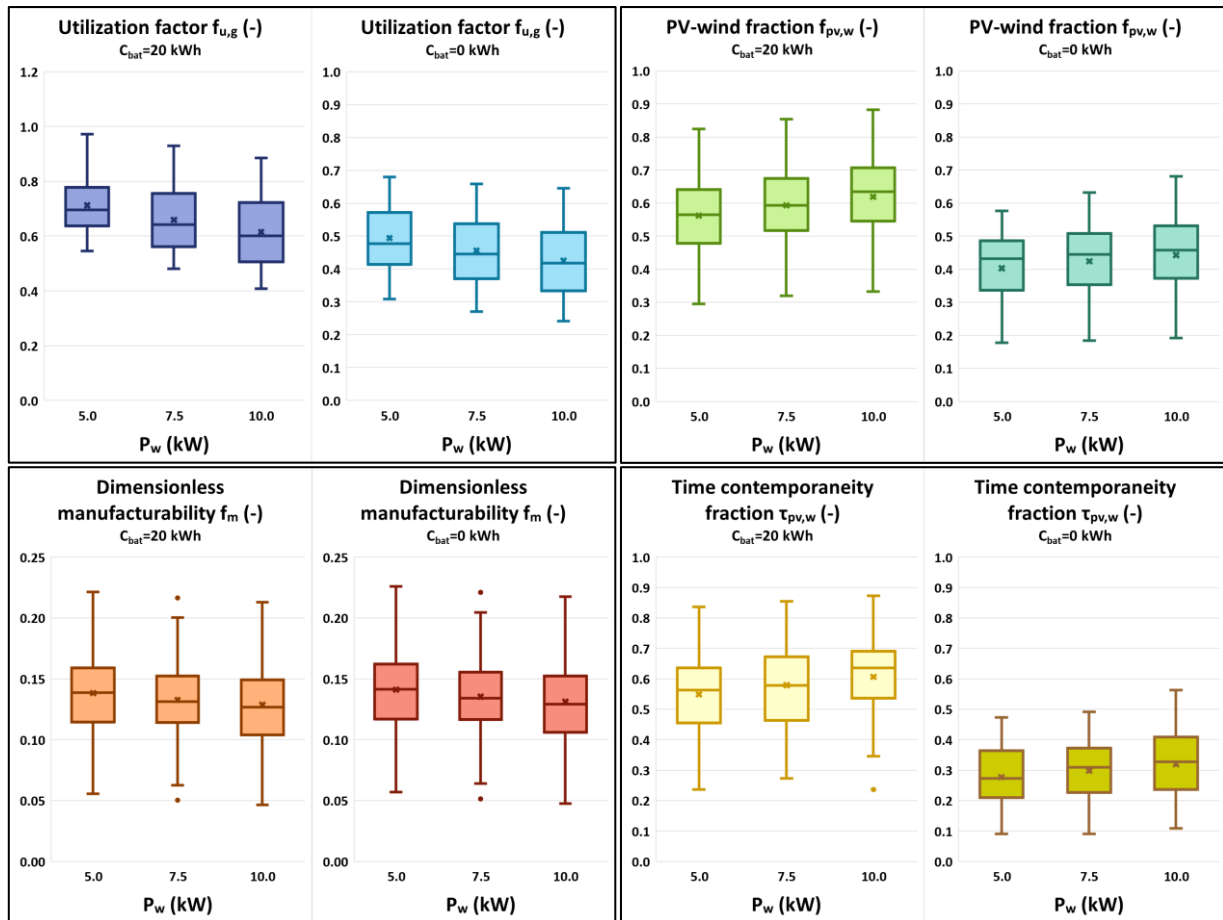
Figure 24. *Box plots of the reliability indicators in terms of overall load as a function of the wind power.*

The average reliability on the utilization factor undergoes a moderate drop as the wind power rises both in the presence and absence of the battery; instead, the reliability uncertainty increases. The maximum value, obtained with 5 kW of wind power and with the ERHS equipped with battery storage is 0.71 ± 0.07. As regards the average overall PV-wind fraction, the behavior is contrary while the uncertainty is reduced in an insignificant manner in the presence of the battery and is slightly increased in the absence of the battery by increasing the wind power. The maximum value, obtained with 10 kW of wind power and with the ERHS equipped with battery storage is 0.62 ± 0.08. Compared to the case in which the battery size was varied, the average dimensionless manufacturability both for the ERHS equipped with the battery and without the battery shows a slight reduction from 0.14 to 0.13, while the uncertainty is almost unchanged at ± 0.02. Finally, the overall time contemporaneity factor has a trend very similar to that of the average overall PV-wind fraction with a maximum value, obtained for 10 kW of wind power, of 0.61 ± 0.08. A different trend is exhibited by the uncertainty, which in the presence of the battery shows the maximum value of ± 0.10 for a $P_w = 7.5$ kW, while in the absence of the battery highlights a minimum value of ± 0.07 at $P_w = 7.5$ kW.

In Figure 25, the box plots of the reliability indicators defined in terms of single loads are shown.

Chapter 6   **Solar and wind assisted heat pump to**
meet the building air conditioning and electric energy demand
in the presence of an electric vehicle charging station and battery storage
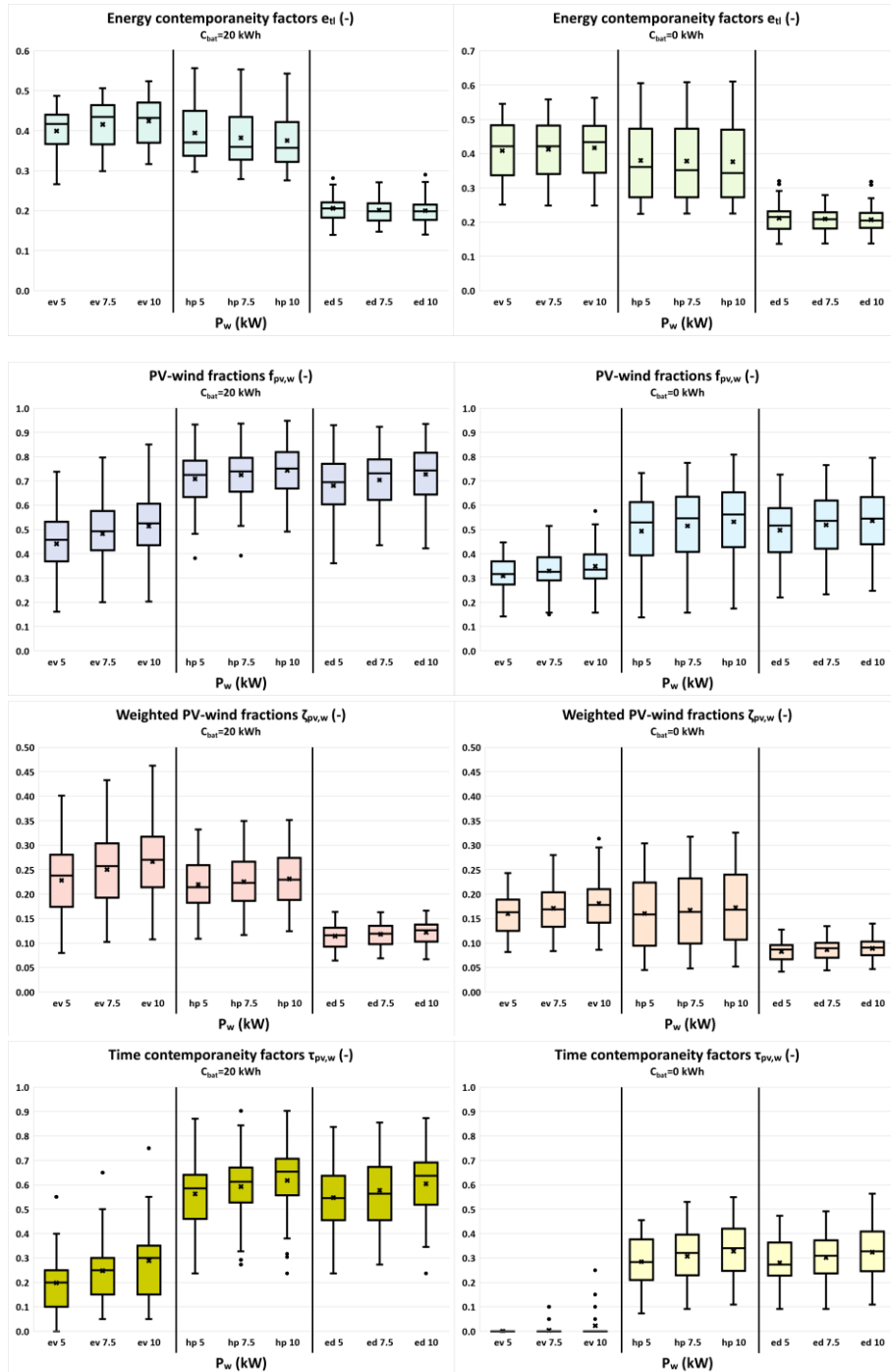
Figure 25. *Box plots of the EV, HP and ED energy contemporaneity factors, non-weighted and weighted PV-wind fractions and time contemporaneity factors as a function of the wind power.*

By increasing the wind power, all the average reliability indicators increase, except the energy contemporaneity factors of the HP and ED, which are reduced. As regards the uncertainty, it generally does not vary substantially. Noticeable modifications are detected only when the battery is removed in the case of EV and HP indicators that respectively are reduced and increased, except the energy contemporaneity factor that always increases. The maximum reduction is obtained for the EV time contemporaneity factor, which is annulled, while the maximum increase is for the HP energy contemporaneity factor, which is doubled.

Table 7 reports the maximum reliability obtained for the different indicators defined in relation to the single loads as a function of the wind power.

Chapter 6   **Solar and wind assisted heat pump to**
meet the building air conditioning and electric energy demand
in the presence of an electric vehicle charging station and battery storage

Table 7. Maximum reliability indicators in terms of single loads and optimal value of the wind power and battery capacity.

	ev	hp	ed
e_{tl}	0.42 ± 0.05 (P_{pv}=10 kW, C_{bat}=20 kWh)	0.39 ± 0.06 (P_{pv}=5 kW, C_{bat}=20 kWh)	0.21 ± 0.03 (P_{pv}=5 kW, C_{bat}=0 kWh)
$f_{pv,w}$	0.51 ± 0.09 (P_{pv}=10 kW, C_{bat}=20 kWh)	0.74 ± 0.07 (P_{pv}=10 kW, C_{bat}=20 kWh)	0.73 ± 0.09 (P_{pv}=10 kW, C_{bat}=20 kWh)
$\zeta_{pv,w}$	0.27 ± 0.05 (P_{pv}=10 kW, C_{bat}=20 kWh)	0.23 ± 0.04 (P_{pv}=10 kW, C_{bat}=20 kWh)	0.12 ± 0.02 (P_{pv}=10 kW, C_{bat}=20 kWh)
$\tau_{pv,w}$	0.29 ± 0.10 (P_{pv}=10 kW, C_{bat}=20 kWh)	0.62 ± 0.07 (P_{pv}=10 kW, C_{bat}=20 kWh)	0.60 ± 0.09 (P_{pv}=10 kW, C_{bat}=20 kWh)

4. Conclusions

A weekly deterministic and yearly statistical analysis was made to determine the performance of a renewable hybrid trigeneration system employed for supplying heating and cooling air conditioning and electricity demand of an office building in the Mediterranean climate. For this issue, a new dynamic simulation tool made up of three subroutines and a new procedure that employs the concepts of the average reliability and reliability uncertainty were developed by means of the definition of a new set of indicators. The deterministic analysis has highlighted the high weekly reliability variability of the electric renewable hybrid system and the impact of the battery storage system on weekly reliability. In particular, the battery allows improvement of the reliability, reducing the effects produced by the no synchronism between the renewable energy production and energy demand; however, the battery capacity resulted undersized in some weeks and oversized in other weeks owing to the high variation of the two renewable sources. For this reason, a statistical analysis was carried out by varying the battery capacity, and also for different PV and wind powers. The main results are summarized as follows:

- the battery storage size increase
    - is able to raise the average reliability of all the indicators in terms of the overall load, except the dimensionless manufacturability that remains almost constant. The reliability uncertainty of all indicators does not present a noticeable modification;
    - has a marked impact also on all the reliability indicators in terms of single loads. In particular, it has a positive effect on the average reliability and it is responsible for how the renewable energy produced is sub-divided to supply the three loads and which load is the most incident in the overall load satisfaction both in energy and time point of view. Instead, the uncertainty is less influenced by it. Only the uncertainty on EV load satisfaction both in energy and time terms undergoes a substantial increase. In addition, the uncertainty is affected by the removal of the battery, especially the indicators related to the EV and HP.
- the PV power increase
    - has a different effect on the average indicators in terms of overall loads. In particular, it gives rise to a reduction of the average utilization factor, a substantial increase in the PV-wind fraction and time contemporaneity factor and a slight rise in dimensionless manufacturability. As regards the uncertainty, modest reductions for the utilization factor, small increases for the PV-wind fraction and a trend with a minimum value for

Chapter 6   **Solar and wind assisted heat pump to**
meet the building air conditioning and electric energy demand
in the presence of an electric vehicle charging station and battery storage

the dimensionless manufacturability were observed. Instead, the time contemporaneity factor presents a trend with a maximum value in the case of ERHS equipped with the battery and an increasing trend in the case of absence of the battery. In general, the removal of the battery produces a reduction in the uncertainty despite a lowering in the average reliability;

- o analogously, also in terms of single loads, a different effect emerged on the average indicators. In particular, the average reliability of all the indicators undergoes a significant increase, except the HP and ED energy contemporaneity factors which are lower. The uncertainty is not determined by the PV power and a noticeable increase is highlighted only by the PV-wind fractions and time contemporaneity factors of the EV and HP.
- the wind power increase:
  - o in terms of indicators related to the overall load, has a very similar effect to that described for the PV power. The effect on the uncertainty is different from that of the PV power, with modest increases for the utilization factor, and invariance of the other indicators. In general, the removal of the battery does not produce a substantial modification of the uncertainty;
  - o in terms of indicators related to the single load, the variations produced on the average reliability are qualitatively the same as that described for the PV power. For all the indicators the variation of the uncertainty can be retained negligible.

In general, the procedure proposed has permitted a direct comparison of the influence of the increase of the PV and wind powers to be made. In the case study considered, all the reliability indicators resulted more affected by the PV power increase rather than the wind power increase, except the utilization factor. Furthermore, the results obtained were employed to identify which PV and wind powers and battery capacities are required to maximize each reliability indicator.

Overall, the results have demonstrated that the average reliability is determined by the system configuration and power, while the uncertainty regards time variation of the renewable sources and loads. In conclusion, the method of analysis developed and used in the specific case study is also employable, in addition to comparing different system configurations and powers, in the system design phase different localities can be compared and, for a specific locality, the most appropriate user can be identified.

References

[1] ENTSO-E - European Network of Transmission System Operators for Electricity, Ten Years National Development Plan 2018 (TYNDP), 2018,   Brussels (Belgium), Website: http://www.entsoe.eu/, last access: 28/07/2018.

[2] Directive 2018/844/EU. European Parliament and of the Council of 30 May 2018 amending Directive 2010/31/EU on the energy performance of buildings and Directive 2012/27/EU on energy efficiency. Official Journal of the European Union (2018), L 156.

[3] Directive 2010/31/EU. European Parliament and of the Council of 19 May 2010 on the Energy Performance of Buildings (recast). Official Journal of the European Union (2010), L 153.

[4] Directive 2012/27/EU. European Parliament and of the Council of 25 October 2012 on energy efficiency, amending Directives 2009/125/EC and 2010/30/EU and repealing Directives 2004/8/EC and 2006/32/EC. Official Journal of the European Union (2012), L 315.

[5] TERNA Group, Monthly report on the electrical system, January 2018, Rome (Italy), Website: http://www.terna.it/it-it/home.aspx, last access: 28/05/2018.

[6] European Commission - Mobility and transport, Energy Union: Commission takes action to reinforce EU's global leadership in clean vehicles, 2017, Brussels (Belgium), Website: https://ec.europa.eu/transport/modes/road/news/2017-11-08-driving-clean-mobility_en, last access: 28/05/2018.

[7] V. Khare, S. Nema, Prashant Baredar, Solar–wind hybrid renewable energy system: A review, Renewable and Sustainable Energy Reviews, Volume 58, 2016, Pages 23-33, ISSN 1364-0321, https://doi.org/10.1016/j.rser.2015.12.223.

[8] D. Mazzeo, G. Oliveti, C. Baglivo, P. M. Congedo, Energy reliability-constrained method for the multi-objective optimization of a photovoltaic-wind hybrid system with battery storage, Energy, Volume 128, 2018, Pages 310-331,ISSN 0360-5442, https://doi.org/10.1016/j.energy.2018.04.062.

[9] L. Ferrari, A. Bianchini, G. Galli, G. Ferrara, E. A. Carnevale, Influence of actual component characteristics on the optimal energy mix of a photovoltaic-wind-diesel hybrid system for a remote off-grid application, Journal of Cleaner Production, Volume 178, 2018, Pages 206-219, ISSN 0959-6526, https://doi.org/10.1016/j.jclepro.2018.01.032.

[10] S.K.A. Shezan, S. Julai, M.A. Kibria, K.R. Ullah, R. Saidur, W.T. Chong, R.K. Akikur, Performance analysis of an off-grid wind-PV (photovoltaic)-diesel-battery hybrid energy system feasible for remote areas, Journal of Cleaner Production, Volume 125, 2016, Pages 121-132, ISSN 0959-6526, https://doi.org/10.1016/j.jclepro.2016.03.014

[11] F. Diab, H. Lan, L. Zhang, S. Ali, An environmentally friendly factory in Egypt based on hybrid photovoltaic/wind/diesel/battery system, Journal of Cleaner Production, Volume 112, Part 5, 2016, Pages 3884-3894, ISSN 0959-6526, https://doi.org/10.1016/j.jclepro.2015.07.008.

[12] S. Mandal, B. K. Das, N. Hoque, Optimum sizing of a stand-alone hybrid energy system for rural electrification in Bangladesh, Journal of Cleaner Production, Volume 200, 2018, Pages 12-27, ISSN 0959-6526, https://doi.org/10.1016/j.jclepro.2018.07.257.

[13] Giallanza, M. Porretto, G. Li Puma, G. Marannano, A sizing approach for stand-alone hybrid photovoltaic-wind-battery systems: A Sicilian case study, Journal of Cleaner Production, Volume 199, 2018, Pages 817-830, ISSN 0959-6526, https://doi.org/10.1016/j.jclepro.2018.07.223.

[14] N. Izadyar, H. C. Ong, W. T. Chong, J. C. Mojumder, K.Y. Leong, Investigation of potential hybrid renewable energy at various rural areas in Malaysia, Journal of Cleaner Production, Volume 139, 2016, Pages 61-73, ISSN 0959-6526, https://doi.org/10.1016/j.jclepro.2016.07.167.

[15] F. Reda, N. Arcuri, P. Loiacono, D. Mazzeo, Energy assessment of solar technologies coupled with a ground source heat pump system for residential energy supply in Southern European climates, Energy, Volume 91, 2015, Pages 294-305, ISSN 0360-5442, https://doi.org/10.1016/j.energy.2015.08.040.

[16] Y. Chang, Y. Gu, L. Zhang, C. Wu, L. Liang, Energy and environmental implications of using geothermal heat pumps in buildings: An example from north China, Journal of Cleaner Production, Volume 167, 2017, Pages 484-492, ISSN 0959-6526, https://doi.org/10.1016/j.jclepro.2017.08.199.

[17] K. Laurischkat, D. Jandt, Techno-economic analysis of sustainable mobility and energy solutions consisting of electric vehicles, photovoltaic systems and battery storages, Journal of Cleaner Production, Volume 179, 2018, Pages 642-661, ISSN 0959-6526, https://doi.org/10.1016/j.jclepro.2017.11.201.

[18] Roselli, M. Sasso, Integration between electric vehicle charging and PV system to increase self-consumption of an office application, Energy Conversion and Management, Volume 130, 2016, Pages 130-140, ISSN 0196-8904, https://doi.org/10.1016/j.enconman.2016.10.040.

[19] Mazzeo, N. Matera, G. Oliveti, Interaction between a wind-PV-battery-heat pump trigeneration system and office building electric energy demand including vehicle charging, 18° EEEIC International Conference on Environment and Electrical Engineering, June 2018, Palermo, Italy.

Chapter 6   **Solar and wind assisted heat pump to**
meet the building air conditioning and electric energy demand
in the presence of an electric vehicle charging station and battery storage

[20]   J. C. Solano, L. Olivieri, E. Caamaño-Martín, Assessing the potential of PV hybrid systems to cover HVAC loads in a grid-connected residential building through intelligent control, Applied Energy, Volume 206,2017, Pages 249-266, ISSN 0306-2619, https://doi.org/10.1016/j.apenergy.2017.08.188.

[21]   B. Richardson, Electric vehicles and the electric grid: A review of modeling approaches, Impacts, and renewable energy integration, Renewable and Sustainable Energy Reviews, Volume 19, 2013, Pages 247-254, ISSN 1364-0321, https://doi.org/10.1016/j.rser.2012.11.042.

[22]   L. Liu, F. Kong, X. Liu, Y. Peng, Q. Wang, A review on electric vehicles interacting with renewable energy in smart grid, Renewable and Sustainable Energy Reviews, Volume 51, 2015, Pages 648-661, ISSN 1364-0321, https://doi.org/10.1016/j.rser.2015.06.036.

[23]   Fattori, N. Anglani, G. Muliere, Combining photovoltaic energy with electric vehicles, smart charging and vehicle-to-grid, Solar Energy,Volume 110,2014,Pages 438-451,ISSN 0038-092X,https://doi.org/10.1016/j.solener.2014.09.034.

[24]   TRNSYS; Version 17. (2012) Solar Energy Laboratory University of Wisconsin-Madison: Madison, WI, USA.

[25]   Meteonorm, software version 6.1. 0.20 of April 2010. Meteotest, Switzerland, 2010.

[26]   UNI/TR 11552, Opaque envelope components of buildings - Thermo-physical parameters, 2014.

[27]   Decreto interministeriale 26 giugno 2015 - Applicazione delle metodologie di calcolo delle prestazioni energetiche e definizione delle prescrizioni e dei requisiti minimi degli edifici, 2015.

[28]   EN ISO 7730, Ergonomics of the thermal environment - Analytical determination and interpretation of thermal comfort using calculation of the PMV and PPD indices and local thermal comfort criteria, 2005.

[29]   ISO 13790, Energy performance of buildings - Calculation of energy use for space heating and cooling, 2008.

[30]   UNI EN 11300-1, Energy performance of buildings – Part 1: Evaluation of energy need far space heating and cooling, 2014.

[31]   UNI/TR 10349-2, Heating and cooling of buildings Climatic data – Part 2: Data for design load, 2016.

[32]   EN 12831, Heating systems in buildings - Method for calculation of the design heat load, 2003.

[33]   Daikin Industries Ltd., Website: https://www.daikin.it/it_it/home.html, last access: 28/07/2018.

[34]   Nissan Italia s.r.l., Website: https://www.nissan.it, last access: 28/07/2018.

[35]   Fisch und Fischl GmbH, Spritmonitor.de, Website: www.spritmonitor.de, Thyrnau (Germany), last access: 28/05/2018.

Nomenclature

Abbreviations

AC   alternating current
DC   direct current
ED   electric devices
ERHS   electric renewable hybrid system
EV   electric vehicle
HP   heat pump
PV   photovoltaic
RHTS   renewable hybrid trigeneration system
TMY   typical meteorological year

Symbols

c_p water specific heat capacity (J/kg K)
C   wall unitary heat capacities per square meter (J/m^2 K)
C_{bat} battery capacity (Wh)

Chapter 6   Solar and wind assisted heat pump to
meet the building air conditioning and electric energy demand
in the presence of an electric vehicle charging station and battery storage

e_{dtl}	energy fraction sent directly to the load (-)	
e_{fb}	energy fraction drawn from the battery (-)	
e_{fg}	energy fraction drawn from the grid (-)	
e_g	energy fraction produced by the generators (-)	
e_L	energy fractions required by each single load compared to the overall load (-)	
e_{tb}	energy fraction sent to the battery (-)	
e_{tg}	energy fraction in excess sent to the grid (-)	
e_{tl}	energy contemporaneity factor (-)	
E_{dtl}	yearly energy sent directly to the load (Wh)	
E_{fb}	yearly energy drawn from the battery (Wh)	
E_{fg}	yearly energy drawn from the power grid (Wh)	
E_g	yearly energy produced by the generators (Wh)	
E_L	yearly energy required by the load (Wh)	
E_{pv}	yearly energy produced by the photovoltaic generator (Wh)	
E_{tb}	yearly energy sent to the battery (Wh)	
E_{tl}	yearly energy produced sent to the load (Wh)	
E_{tg}	yearly energy in excess sent to the grid (Wh)	
E_w	yearly energy produced by the wind generator (Wh)	
$f_{pv,w}$	overall photovoltaic-wind fraction (-)	
f_m	dimensionless manufacturability (-)	
$f_{u,g}$	utilization factor (-)	
g	solar heat gain coefficient of glazed walls (-)	
IQR	interquartile range (-)	
$\dot{m}_w$	HP water flow rate (kg/s)	
p	manufacturability (Wh/W)	
$P_g(t)$	overall power generated (W)	
$P_{fb}(t)$	power drawn from the battery (W)	
$P_{fg}(t)$	power drawn from the grid (W)	
$P_L(t)$	power required by the load (W)	
P_n	overall nominal power of the ERHS (W)	
$P_{pv}(t)$	power produced by the photovoltaic generator (W)	
$P_{pv,eff}(t)$	effective power produced by the photovoltaic generator (W)	
$P_{pv,n}$	nominal power of the photovoltaic generator (W)	
$P_{tb}(t)$	power sent to the battery (W)	
$P_{tg}(t)$	power in excess sent to the grid (W)	
$P_{tl}(t)$	power produced sent to the load (W)	
$P_w(t)$	power produced by the wind generator (W)	
$P_{w,eff}(t)$	effective power produced by the wind generator (W)	
$P_{w,n}$	nominal power of the wind micro-generator (W)	
Q_B	building thermal needs (W)	
Q_{Bp}	primary building thermal requirements (W)	
R	reliability (-)	
$\overline{R}$	average reliability (-)	
t	time (s)	
$t_{SL}(t)$	modified Heaviside step function (-)	
t_L	number of hours in which the overall load is different from zero (-)	
T_{wi}	HP return water temperature (K)	
T_{wo}	HP outlet water temperature (K)	
U_o	steady thermal transmittance of opaque walls (W/m^2 K)	

U_w steady thermal transmittance of windowed walls (W/m^2 K)

Greek letters

Δt period (s)

$\Delta\theta$ temperature deadbands of the N-Stage differential controller (K)

$\zeta_{pv,w}$ weighted PV-wind fraction (-)

$\eta_{DC/DC}$ DC/DC converter efficiency (-)

$\eta_{AC/DC}$ AC/DC rectifier efficiency (-)

η_{bat} battery efficiency (-)

η_{inv} inverter efficiency (-)

η_{reg} regulator efficiency (-)

$\tau_{pv,w}$ overall time contemporaneity factor (-)

Subscripts

c   referring to the cooling period

ed   referring to the electric devices

ev   referring to the electric vehicle

ev   referring to the heat pump

max   maximum value

pv   referring to the PV generator

h   referring to the heating period

w   referring to the wind micro-generator

Chapter 7

Worldwide geographical mapping and optimization of stand-alone and grid-connected hybrid renewable system techno-economic performance across Köppen-Geiger climates

Chapter 7   **Worldwide geographical mapping and**
optimization of stand-alone and grid-connected hybrid renewable
system techno-economic performance across Köppen-Geiger climates
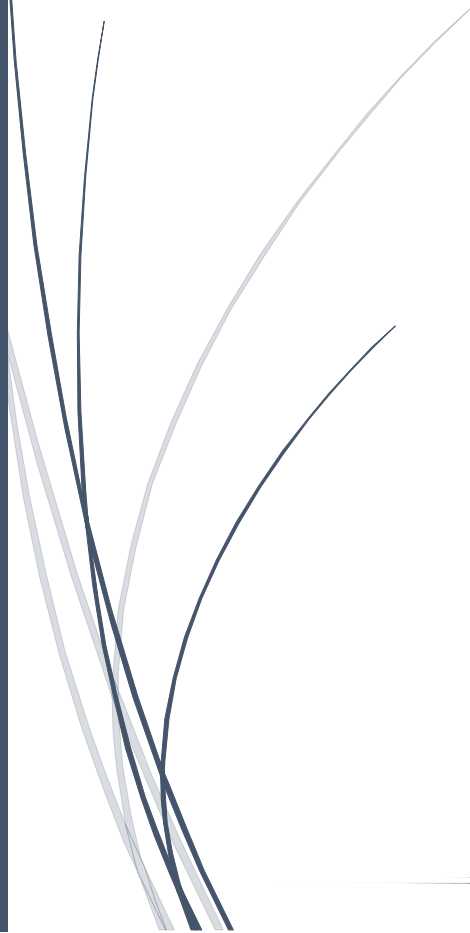
Chapter 7

Worldwide geographical mapping and optimization of stand-alone and grid-connected hybrid renewable system techno-economic performance across Köppen-Geiger climates

Abstract

In the last years, a significant interest in research in stand-alone (SA) and grid-connected (GC) photovoltaic (PV)-wind hybrid renewable energy systems (HRES) is observed for their complementary in the satisfaction of the electrical energy demand in many sectors. However, direct comparisons between the techno-economic performance of two system modes under the same operating conditions are rarely carried out. Additionally, most of the researches are limited to specific weather conditions.

This work aims to bridge the lack of this type of investigations providing a worldwide techno-economic mapping and optimization of SA and GC PV-wind HRES to supply the electrical demand of an office building district. For this purpose, energy and economic optimization problems were formulated to find the optimal SA and GC systems worldwide among 343 HRES system power configurations located in 48 different localities, uniformly divided in the sub-group of the Koppen classification. The energy reliability and economic profitability of optimal systems were geographically mapped worldwide.

In general, the energy or economic optimizations of SA HRES do not lead to highly profitable systems; instead, feed-in-tariff to sell the energy in excess assures viable GC HRES in many localities. However, economically optimal SA and GC HRES, respectively, do not everywhere comply with the threshold value of 70% of the satisfied energy required by the load and are characterized by a high level of energy exchanged with the grid.

The study highlighted that the most suitable climate conditions to install a SA HRES are: (i) Toamasina (Madagascar) from an energy point of view, with 76% of load satisfied and 76% of the energy generated utilized to supply the load; (ii) Cambridge Bay (Canada) from an economic point of view, with 11.1 % of the capital cost recovered each year; instead, the most suitable climate conditions to install a GC HRES are: (iii) New Delhi (India) from an energy point of view, with 48% of energy exchanged with the grid per each kWh required by the load; (iv) Lihue (Hawaii, United States) from an economic point of view, with 24.3 % of the capital cost recovered each year.

- Worldwide techno-economic optimization of PV-wind hybrid renewable energy system (HRES).
- Optimal stand-alone (SA) and grid-connected (GD) HRES in 48 localities were mapped.
- Yearly average solar and wind source around 300–400 W/m^2 and 1.5–2.5 m/s make HRES reliable.
- SA HRES are mainly based on the PV-battery system and are more reliable and cheaper.
- GC HRES are mainly based on the wind system and are very profitable with the feed-in-tariff.

Chapter 7   **Worldwide geographical mapping and**
optimization of stand-alone and grid-connected hybrid renewable
system techno-economic performance across Köppen-Geiger climates

1. Introduction

2.1. Photovoltaic-wind hybrid renewable systems

The growing concern about environmental issues and the progressive depletion of fossil fuels has moved research towards renewable sources. During the Rio Climate Change Conference in Paris in 2015, the 196 participating countries unanimously agreed on a global pact, the so-called Paris Accord, to reduce greenhouse gas emissions, but remarkable results are still far from being achieved [1].
The Renewables Global Status Reports of 2018 and 2019 [2, 3] shows how in recent years the diffusion of renewable energy systems is increasing in different ways in the world continents, through the exploitation of different technologies. They reveal that the renewable energy industry is growing and this growth is not happening as fast as expected.
By 2017, China, Europe and the United States had contributed most to global emissions, being highly industrialized areas, but they are also the largest investors in renewables, accounting for 75% of global investment. This investment declined by 11% in 2018, decreasing mainly in China.
        As shown, there is significant progress in the field of renewable energy sources in almost all parts of the world, especially for photovoltaic (PV) and wind power systems. In general, lower technological costs (particularly for PV systems) have led renewables to play a crucial role especially in remote areas, where access to energy is difficult and the cost of a grid connection would be too high if not supported. Stand-alone systems for rural electrification accounted for 6% of electrical connections between 2012 and 2016 and this value continues to increase.
Solar energy and wind energy are highly uncertain, but they are particularly suitable for the creation of reliable PV-wind hybrid renewable energy system (HRES) due to their complementarity [4-7]. Solar radiation is prevalent during the day of the summer season, while the wind speed compensates for the absence of solar production at night and during the winter season. In this way, one form of energy partly compensates for the other and the HRES operates more continuously than the single system. In the case of stand-alone (SA) systems (not connected to the electrical grid), if both energy sources are deficient, a storage system can be integrated to store excess energy previously produced by the system. Auxiliary energy production systems such as diesel generators can also be integrated into the HRES in the event of failure of renewable sources, but this inevitably leads to an increase in the overall cost of the plant. In the case of grid-connected (GC) systems, if the energy produced by the system is not sufficient to support the load, the energy deficit can be compensated by drawing energy directly from the grid. If, on the other hand, the system production is excessive, the energy can be channelled into the grid or stored in storage systems. These systems are mainly electrical batteries, but solutions such as hydraulic, thermal, compressed air or hydrogen storage with electrolytic cells and fuel cells are also being developed [8, 9]. In addition to PV and wind power, other energy production technologies such as hydropower (there are several cases in particular in China), biomass plants, solar concentration systems and geothermal plants can also be integrated.

2.2. Literature overview

This section provides an overview and objective description of different studies on HRES around the world. Several articles in the scientific databases were selected and analyzed to identify the current trend of the research in this topic around the world. Among these papers, only the most relevant in each continent were selected and described in this section in details.

Table 1 shows four studies for each continent with the highest impact. The location considered is related to the study application and not the author affiliations.

Table 1. Overview of the most influential studies for each continent.

Continent	Rif	Title	Year	Journal	Citations*	Country	Locations	Koppen
Asia	[10]	Optimal sizing method for stand-alone hybrid solar–wind system with LPSP technology by using genetic algorithm	2008	Solar Energy	549	China	Dalajia Island	Cwa
	[11]	Optimal design and techno-economic analysis of a hybrid solar–wind power generation system	2009	Applied Energy	396	China	South-east coasat of China	Cwa/Cfa
	[12]	Size optimization of a PV/wind hybrid energy conversion system with battery storage using simulated annealing	2009	Applied Energy	280	Turkey	Izmir	Csa
	[13]	A feasibility study of a stand-alone hybrid solar–wind–battery system for a remote island	2014	Applied Energy	272	Hong Kong	Small remote island in Hong Kong	Cwa
Europe	[14]	A methodology for optimal sizing of autonomous hybrid PV/wind system	2007	Energy Policy	354	France	Ajaccio	Csb
	[15]	Design and techno-economical optimization for hybrid PV/wind system under various meteorological conditions	2008	Applied Energy	250	France	Ajaccio	Csb
							Figari	
							Solenzara	
							Calvi	Csa
							Ersa	
	[16]	Technical and economic assessment of hybrid photovoltaic/wind system with battery storage in Corsica island	2008	Energy Policy	172	France	Ajaccio	Csb
							Calvi	Csa
							Cape Corse	Csa/Csb
	[17]	Multi-objective design of PV– wind– diesel– hydrogen– battery systems	2008	Renewable Energy	338	Spain	Zaragoza	Bsk
Africa	[18]	Sizing optimization of grid-independent hybrid photovoltaic/wind power generation system	2011	Energy	239	Algeria	Bouzaréah	Csa
	[19]	Feasibility study of small Hydro/PV/Wind hybrid system for off-grid rural electrification in Ethiopia	2012	Applied Energy	220	Ethiopia	Dejen	Cwb
	[20]	Optimal sizing study of hybrid wind/PV/diesel power generation unit	2010	Solar Energy	197	Senegal	Dakar	BSh
	[21]	Economic and technical study of a hybrid system (wind–photovoltaic–diesel) for rural electrification in Algeria	2009	Applied Energy	144	Algeria	Bouzaréah	Csa
							Batna	BSk
							El Oued	
							Ghardaïa	BWh
							Adrar	
							Tamenrasset	
North America	[22]	Unit sizing and cost analysis of stand-alone hybrid wind/PV/fuel cell power generation systems	2005	Renewable Energy	359	USA	Remote location in Montana	BWk/BSk/Cfa /Cfb/Csb/Dfa/ Dfb/Dfc/ Dwb/Dwc/Dsb /Dsc
	[23]	Optimal unit sizing for a hybrid wind/photovoltaic generating system	1996	Electric Power Systems Research	102	USA	Central Montana	BSk/Dfa/Dfc
	[24]	Sizing of a stand-alone hybrid wind-photovoltaic system using a three-event probability density approximation	1996	Solar Energy	101	USA	Boston	Dfa
	[25]	Life cycle cost, embodied energy and loss of power supply probability for the optimal design of hybrid power systems	2014	Mathematics and Computers in Simulation	98	USA	Boulder	BSk
South America	[26]	Techno-economic feasibility of photovoltaic, wind, diesel and hybrid electrification systems for off-grid rural electrification in Colombia	2016	Renewable Energy	102	Colombia	Puerto Estrella	BSh
							Unguia	Am
							Jerico	Aw
	[27]	Business optimal design of a grid-connected hybrid PV (photovoltaic)- wind energy system without energy storage for an Easter Island's block	2013	Energy	81	Chile	Hanga Roa (Easter Island)	Cfa
	[28]	A MILP model to design hybrid wind–photovoltaic isolated rural electrification projects in developing countries	2013	European Journal of Operational Research	57	Peru	El Alumbre	Af/Aw/ Cfb
							Alto Perù	Aw/BSh/Cfb/ Cwc/ET
	[29]	Homeostatic control, smart metering and efficient energy supply and consumption criteria: A means to building more sustainable hybrid micro-generation systems	2014	Renewable and Sustainab	27	Chile	Not specified	Cfb/Cfc/Csa/C sb/Csc/Bsk/B Wk/BWh

Chapter 7   **Worldwide geographical mapping and**
optimization of stand-alone and grid-connected hybrid renewable
system techno-economic performance across Köppen-Geiger climates

				le Energy Reviews				
Oceania	[30]	Technical feasibility and financial analysis of hybrid wind–photovoltaic system with hydrogen storage for Cooma	2005	International Journal of Hydrogen Energy	88	Australia	Cooma	Cfc
	[31]	Optimal sizing of a wind-photovoltaic-battery hybrid renewable energy system considering socio-demographic factors	2016	Solar Energy	43	New Zealand	Auckland	Cfb
	[32]	Hybrid renewable energy integration (HREI) system for subtropical climate in Central Queensland, Australia	2016	Renewable Energy	28	Australia	Rockhampton Yeppoon	Cfa
	[33]	Sustainable energy system design with distributed renewable resources considering economic environmental and uncertainty aspects	2015	Renewable Energy	30	Australia	New South Wales	BSh/BWk/BWh/Csa/Csb/Cfa/Cfb/Cfc/ Dfc

* Citation source is Scopus, analysis carried out on 30 April 2020.

Asia

The studies [10, 11] proposed the optimal sizing of a SA HRES, including battery, to serve a telecommunications station installed on the southeast coast of China, using as decision variables the number and inclination of solar panels, the number and height of wind turbines and the number of batteries. The optimization issue was to minimize the annualized cost of the system (ACS) to obtain the loss of power supply probability value (LPSP) through a genetic algorithm (GA).

Ekren et al. [12] carried out the optimal sizing of a battery-powered HRES to serve a station for the global mobile communications system installed at the campus of the Izmir Institute of Technology, Turkey. In particular, the study used the Simulated Annealing Algorithm (SAA) to minimize the total cost of the system, considering, as variables, the size of the PV string, the rotor area of the wind turbine and the battery capacity. The resulting optimisation was confirmed by calculating the probability of pressure drop (LLP) and autonomy (A). The simulation was performed in ARENA 12.0.

Tao Ma et al. [13] presented a feasibility study and techno-economic evaluation of a SA HRES with a battery system to meet the energy needs of a remote island in the territory of Hong Kong. The analysis was carried out using HOMER software, optimizing the system net present cost (NPC) and cost of energy (COE). The study showed how existing diesel generators could be entirely replaced by renewable energy generation systems capable of providing uninterrupted power at an economical cost.

Europe

The studies [14-16] developed the optimization of a SA HRES with the battery system to be used for residential purposes on the island of Corsica, minimizing LPSP and levelled energy cost (LCE). The paper [15] focuses on the installation of the system in five locations in Corsica to assess the effects of the installation in less windy areas. The results showed the excellent performance of a SA HRES, compared to a single, PV or wind only system. The paper [17] proposed, for the first time, the sizing of a SA HRES with battery, diesel generator and hydrogen storage system as a three-goal optimization problem. A genetic algorithm (GA) and a Multi-Objective Evolutionary Algorithm (MOEA) are used to simultaneously optimize the Net Present Cost of the system (NPC), the pollutant emissions in terms of CO_2 and the unmet load (UL).

Africa

Kaabeche et al. [18] developed the sizing of a SA HRES to serve a residential load in Algeria. The values of the deficiency of power supply probability (DPSP) and Levelised Unit Electricity Costs (LUEC) indicators were varied to find the optimal configuration. Bekele et al. [19] carried out the

Chapter 7   **Worldwide geographical mapping and**
optimization of stand-alone and grid-connected hybrid renewable
system techno-economic performance across Köppen-Geiger climates

simulation, using HOMER software, of an HRES supported by battery and diesel generator coupled with a hydroelectric system for the electrification of a district of 10,500 families in Ethiopia. Belfkira et al. [20] carried out the optimization of a SA HRES coupled to a diesel generator to minimize the total cost of the system (STC). The study presented a comparison of the total costs of the system with and without a battery.

Saheb-Koussa et al. [21] developed the sizing of a SA HRES with battery and diesel generator applied to a residential building for six sites in Algeria, to achieve greater autonomy for low energy costs. The techno-economic optimization has been developed in MATLAB/Simulink.

North America

Nelson et al. [22] carried out an economic analysis of a SA HRES for a residential building in Montana (USA), analyzing the feasibility of a grid connection in MATLAB. In particular, the study compared the system equipped with hydrogen fuel cell storage, with a system with classic battery storage, establishing the latter's superiority in economic terms. The authors hope that the possibility of technological improvements in hydrogen systems can make them more competitive in the future. Kellogg et al. [23] conducted one of the first analyses on a SA HRES with a battery for the energy support of a small ranch in Montana (USA). The analysis is aimed at minimizing the total annual cost of the system. Similarly, Bagul et al. [24] sized a SA PV-wind HRES with a battery for a residential building in New England. Using a probabilistic approach, the optimal number of PV panels and batteries was calculated to allow the system to guarantee a given probability of pressure drop (LOLP) value.

Abbes et al. [25] carried out a multi-objective energy-economic-environmental optimization of a SA residential battery system, using life cycle cost (LCC), embodied energy (EE) and the probability of pressure drop (LPSP) as objective functions. Optimization was performed by MATLAB/Simulink using the NSGA-II algorithm. The methodology has been successfully applied for the sizing of a system that can provide at least 95% of the total annual demand.

South America

Mamaghani et al. [26] analysed a SA system with a battery (with and without a diesel generator) for rural electrification in three villages in Colombia not powered by the electricity grid and with different climatic characteristics. Using HOMER, different combinations of wind turbines, PV panels and diesel generators were modelled and optimized to determine the most energy-efficient and cost-effective system for each location. Caballero et al. [27] used HOMER and MATLAB for the economic optimization of a GC HRES for the energy supply of fifteen buildings on Easter Island. The system was compared with the configurations of PV and wind only systems. Ferrer-Martí et al. [28] proposed a mathematical programming system for the optimization of an HRES with battery for residential and non-residential use in two locations in Peru, using as a criterion the minimization of the initial investment cost. Yanine et al. [29] carried out an economic analysis of a GC system without an accumulation system, serving a simulated load through the real consumption data of a Chilean community. The system was examined using a homeostatic control strategy for energy systems and was, therefore, treated in the same way as a biological system that achieves relative stability in a given environment.

Chapter 7

Worldwide geographical mapping and optimization of stand-alone and grid-connected hybrid renewable system techno-economic performance across Köppen-Geiger climates

Oceania

Shakya et al. [30] used TRNSYS to simulate a SA HRES designed to meet the energy needs of a building located in Cooma, Australia. The system was considered without storage but equipped with a diesel generator and hydrogen system. The analysis was carried out by comparing different Levelized cost of energy (LEC) values to varying percentages of PV and wind power.

Tito et al. [31] presented the optimization of a SA HRES with a storage system for residential use, considering socio-demographic factors. The analysis is aimed at minimizing the cost of the system and the missing energy (by setting the LPSP to 0) by analyzing six different daily load profiles representing different energy demand regimes.

Shafiullah [32] proposed a detailed economic analysis of different configurations of a GC system for residential use in two locations in Australia. The study considered the cost of the system and energy in terms of NPC and COE, as well as the economic return through IRR, cost-benefit ratio and Payback Period. Renewable Fraction (RF) is used for the energy aspect. The analysis is carried out using HOMER software.

Abdullah et al. [33] conducted a multi-objective (energy-economic-environmental) optimization of a battery-powered system to power an electricity distribution network in New South Wales, minimizing the cost of energy (LCOE) and embodied energy (EE). The analysis has been performed in a MATLAB environment.

Overall considerations

Overall, the analysis shows that, given the very high number of citations, the most influential researches on PV-wind HRES topic are in Asia, followed by Europe, Africa and North America. The most discussed topic is the optimization of HRES, especially SA, with a wide range of techniques. Studies from these four continents are all pre-2014, with two North American studies dating as far back as the 1990s.

In South America and Oceania, the most cited studies are almost all more recent and the number of citations is lower, which implies that in these continents research is still in the early stages (especially in South America). In general, each continent has a country that emerges more than the others: China for Asia, France for Europe, Algeria for Africa, the United States for North America, Chile for South America and Australia for Oceania (although the latter two are of dubious statistical relevance, South America for the low activity in the sector, Oceania for the low number of countries).

2.3. Knowledge gap and research contribution

The results of the analysis of the selected papers in the scientific literature have highlighted areas where research on HRES is still rather limited. Considerable interest in research in SA systems, for the satisfaction of energy loads in remote or isolated locations, was observed. GC installations are also highly explored, although to a rather lesser extent. Analyses have shown that a topic on which research is still little focused is the direct comparison between the two system modes, SA and GC, under the same operating conditions. In addition, the techno-economic analysis was extensively performed; however, most investigations are related to a specific locality, country or a Koppen-Geiger climate group [34, 35]. The energy performance and economic profitability of a SA and GC HRES are strongly correlated to the specific weather conditions considered.

To overcome all these gaps and to provide a research of universal value, this work proposes a direct comparison of the techno-economic performance of SA and GC PV-wind HRES in different localities

Chapter 7   **Worldwide geographical mapping and
optimization of stand-alone and grid-connected hybrid renewable
system techno-economic performance across Köppen-Geiger climates**

around the world, considering the different continent and characteristic weather conditions. For this issue, the SA and GC HRES were supposed installed in 48 different localities, two for each sub-group of the Koppen-Geiger classification [34, 35]. Different power installed were considered for the PV and wind systems, by varying the storage capacity of the battery system.

The objective was to identify the energetically and economically optimal system power configurations in each locality for both the SA and GC system. Finally, the most suitable weather conditions in the world, namely localities, for the installation of a SA or a GC HRES were detected both from an energy and economic point of view.

To the best of the authors' knowledge, no previous papers addressed a techno-economic analysis and optimization worldwide of both stand-alone and grid-connected hybrid renewable systems, taking into account all continents and Koppen-Geiger climates, while considering different power configurations. The authors intend to provide reference research of universal value for all climatic conditions according to the Koppen-Geiger classification. From the literature search emerged also that similar researches were made in other topics, such as the mapping of PV energy performance around the world [36], and the worldwide mapping and optimization of the thermal performance of phase change materials integrated into the building envelope for the reduction of the heating and cooling energy requirements [37].
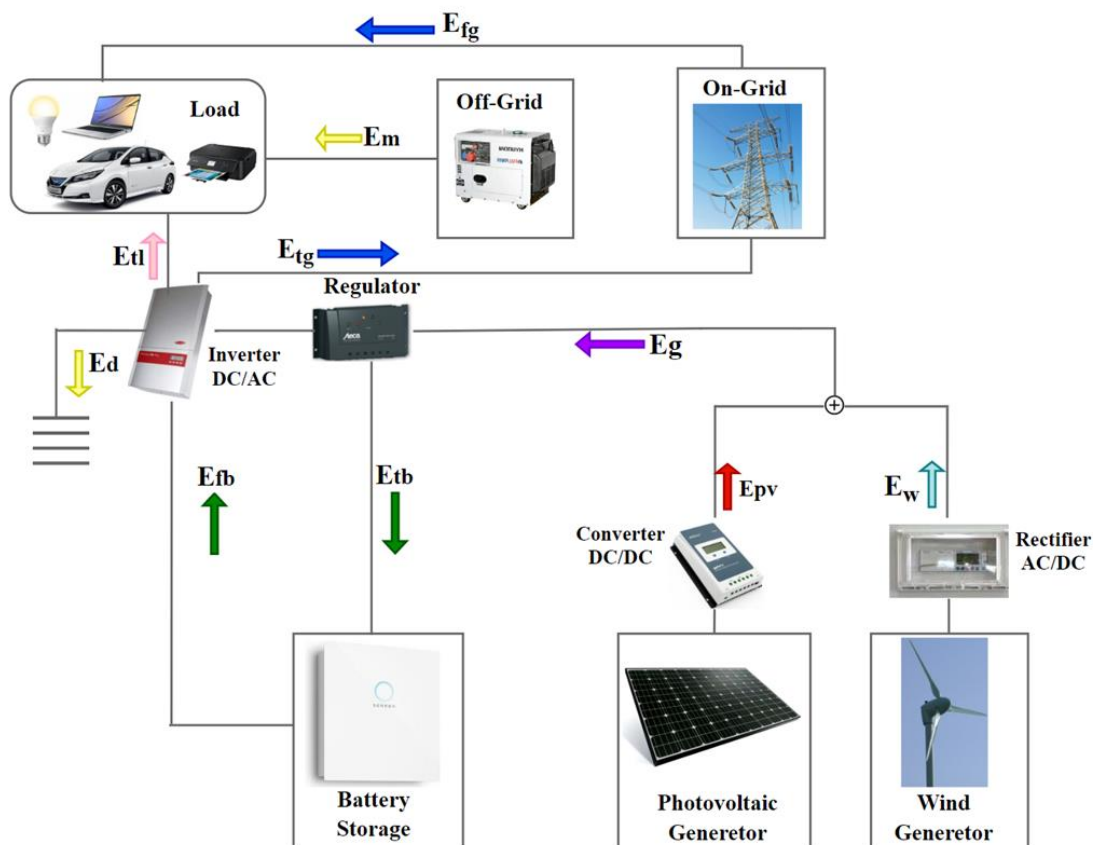

Figure 1. Scheme and energy flow of the stand-alone and grid-connected PV-wind HRES with battery storage.

3. Methods and materials

Figure 1 shows the electrical schemes of the stand-alone (SA) and grid-connected (GC) hybrid renewable energy systems (HRES) and the related energy flows in the different sections of the system.
2. When the energy generated exceeds the energy required by the load, the energy produced is sent directly to the load, when is required, and the remaining part is used to charge the battery. The excess energy is dissipated for the SA system and is sent to the grid for the GC system. When the energy generated is not sufficient to meet the load, the remaining part is extracted from the battery. The missing energy is integrated by an alternative system, such as a diesel generator, for the SA system, and is drawn from the grid for the GC system.

3.1. System component modelling in TRNSYS

TRNSYS 17 (Transient Energy System) is software developed by the University of Wisconsin and the University of Colorado [38]. The main types involved in the simulation of an HRES are:

- Type 94a models the electrical performance of a photovoltaic (PV) module, using the five-parameter model to predict the current-voltage characteristic. It can be used in simulations that provide the grid connection, the presence of storage batteries or the direct coupling to the load. Type is used for panels composed of crystalline or polycrystalline silicon, while for those composed of amorphous silicon or thin films it is advisable to use Type 94b. The parameters to be set in the Type can be found on the datasheets of the panel (short-circuit current and open-circuit voltage of the module, panel area, etc.) while climatic data are set as input.

- Type 90 simulates the performance of a wind turbine by calculating the power produced as a function of wind speed, using both wind turbine characteristic data and analytical solutions. Type uses Quinlan's equations, modelling the density variations and the wind speed as a function of the height. The parameters to be set include the height of the installation site, the height of the hub and the number of turbines. The Type receives as input the wind speed values and the main characteristics of the turbine such as the height above ground of the rotor, the exponent for the determination of the wind speed using the Prandtl model, the air density at 10 meters above ground, the nominal power, the nominal wind speed and the power curve with the corresponding speeds and powers.

- Type 47 models a lithium-ion battery and calculates the SOC as a function of time, known as the charge and discharge rates. In mode 1 (Type 47a), the power input or output from the battery is required as input, while the power exchanged and charge status are given as output. The parameters are the number of cells in series and parallel, battery capacity and charging efficiency.

- The actual output power of the static converters is calculated with coefficients of efficiency using an equation block Type.

Figure 2 shows the TRNSYS workflow, the blue lines are relative to the PV, the red ones to the wind system.
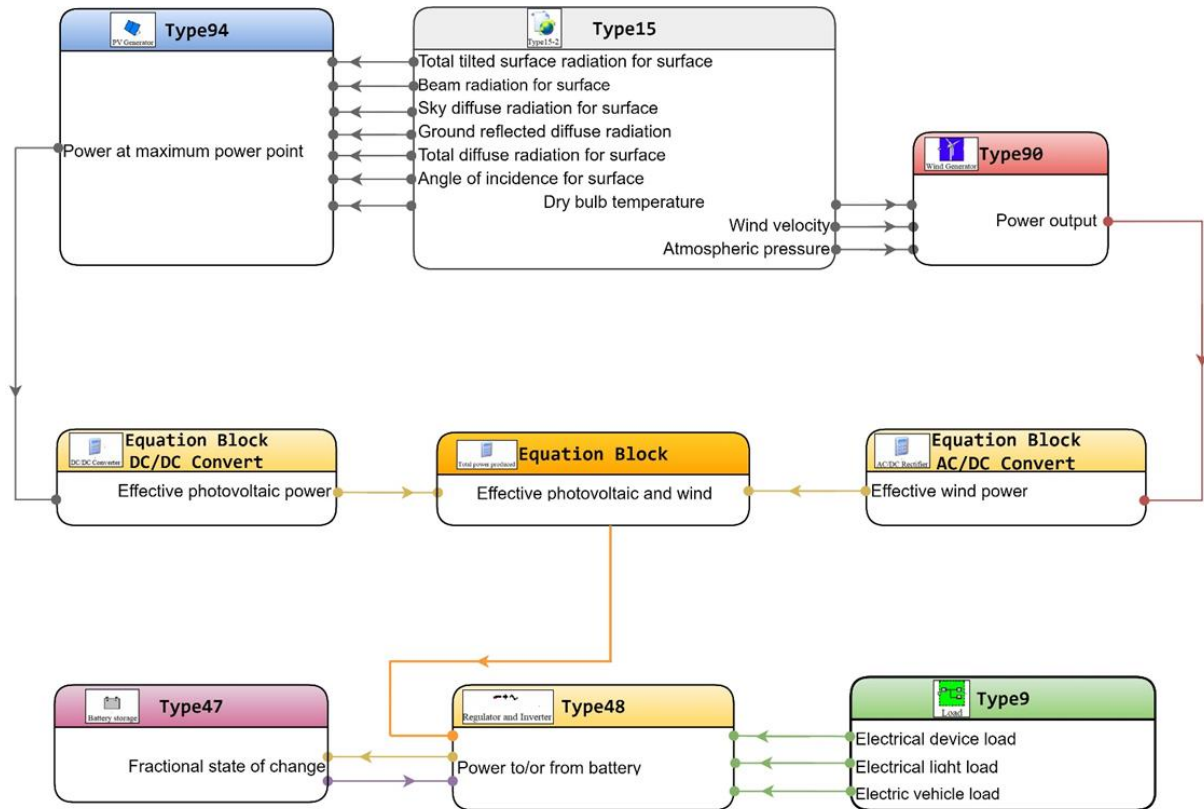
Figure 2. TRNSYS workflow of the PV-wind HRES.

Type 48 simulates the regulator and inverter, Type 15 is used for the importation of the tm2 climatic data of TRNSYS weather library and Type 25 permits to plot the results.

The load is represented grouped in a macro, which involves the Type 9, for the climatic data, the Type 2 that simulates lighting differential controller, to inactive the artificial lighting when solar radiation is sufficient to guarantee adequate levels of natural lighting.

3.1.1. Photovoltaic module

The hourly tilted solar radiation G is the sum of direct, diffuse and reflected radiation [39]:

$$G = G_{b,h}R_b + G_{d,h}R_d + (G_{b,h} + G_{d,h})R_r \tag{1}$$

Where $G_{b,h}$ and $G_{d,h}$ are the direct and diffuse radiation on the horizontal plane, R_b is the inclination factor of direct radiation, R_d are R_r are the inclination factors of diffuse and reflected radiation.

The performance of the PV generator is determined by solving the equation of its equivalent electrical circuit, which consists of an ideal circuit composed of a current generator, a diode and two resistors [40].

The characteristic curve of the circuit is represented by Eq. (2).

$$I = I_L - I_0 \left[e^{\frac{V+IR_s}{a}} - 1 \right] - \frac{V + IR_s}{R_{sh}} \tag{2}$$

Chapter 7   **Worldwide geographical mapping and**
optimization of stand-alone and grid-connected hybrid renewable
system techno-economic performance across Köppen-Geiger climates

The model parameters that characterize the electrical circuit as a function of the absorbed solar radiation and the cell temperature are: the current strength I_L, the saturation current strength I_0, the resistance in series R_s due to the material of the cell, the resistance in parallel (or resistance of shunt) R_{sh} which represents losses caused by leakage currents within the cell, the coefficient of ideality a.

The procedure used to determine the parameters in the reference conditions $I_{l,ref}$, $I_{0,ref}$, $R_{s,ref}$, $R_{sh,ref}$ and a_{ref} is extensively reported in [41].

The parameters under operating conditions are obtained by updating the values of I_L and I_0, as a function of the absorbed solar radiation and cell temperature, respectively. The last one is calculated using the nominal operating temperature of the cell (NOCT). Consequently, the characteristic curve is updated at any time as a function of cell temperature and absorbed solar radiation.

The PV power generated is calculated as the product of the current and voltage at the maximum power point of the characteristic curve:

$$P_{pv}(t) = I_{mp}(t)V_{mp}(t) \qquad (3)$$

3.1.2. Wind generator

The wind power generated is evaluated as a function of wind speed using the experimental reference power curves. This curve is determined for a specific air density value using the wind speed values measured at the turbine hub height.

Under operating conditions, the power output is determined by the Quinlan model [42] considering the air density at real operating height, the wind speed $v_h(t)$ at real operating height z_h of the wind turbine, starting from wind speed $v_{an}(t)$ at anemometric height $z_{an}(t)$, known the exponent α:

$$\frac{v_h(t)}{v_{an}(t)} = \left(\frac{z_h}{z_{an}}\right)^{\alpha(t)} \qquad (4)$$

The corrected power $P_\rho(t)$ and the corrected rated speed $v_{nom,\rho}$ are determined using Eqs. (5) and (6), to consider the updated air density $\rho(t)$, value as a function of the turbine power $P_0(t)$ at real operating height using the experimental power curve determined for reference air density ρ_0:

$$\frac{P_\rho(t)}{P_0(t)} = \frac{\rho(t)}{\rho_0} \qquad (5)$$

$$\frac{v_{nom,\rho}(t)}{v_{nom,\rho_0}} = \left(\frac{\rho_0}{\rho(t)}\right)^{1/3} \qquad (6)$$

Finally, the power produced is reduced by a mixed loss coefficient.

3.1.3. Battery

Battery performance are evaluated through a model that uses the instantaneous state of charge balance equation (SOC).

The SOC value at instant time *t* is determined by Eq. (7):

Chapter 7   **Worldwide geographical mapping and**
optimization of stand-alone and grid-connected hybrid renewable
system techno-economic performance across Köppen-Geiger climates

$$\begin{cases} SOC(t+1) = SOC(t) + P_{tb}(t)\eta_{bat}\Delta t & \text{for} \quad P(t) > 0 \\ SOC(t+1) = SOC(t) - P_{fb}(t)\Delta t & \text{for} \quad P(t) < 0 \end{cases} \tag{7}$$

Where η_{bat} is the battery efficiency, P_{tb} and P_{fb} are the power sent to or drawn from the battery, respectively.

3.2. Energy analysis of the stand-alone and grid-connected hybrid system

The hourly and yearly energy balance of the PV-wind HRES were extensively described in previous works of the authors related to residential and office GC systems [4, 43-45]. In the following sections, the procedure is extended also to SA systems.

3.2.1. Dimensionless power parameters of the hybrid system

A specific HRES power configuration can be identified by using the PV power fraction p_{pv}, the wind power fraction p_w, the battery power fraction p_b, the load power fraction p_l and the overall load power fraction p_{ol}.

$$p_{pv} = \frac{P_{pv}}{P_w + P_{pv}} \tag{8}$$

$$p_w = \frac{P_w}{P_w + P_{pv}} \tag{9}$$

$$p_b = \frac{P_B}{P_n} = \frac{P_b}{P_w + P_{pv} + P_b} \tag{10}$$

$$p_l = \frac{P_l}{P_w + P_{pv}} \tag{11}$$

$$p_{ol} = \frac{P_l}{P_w + P_{pv} + P_b} \tag{12}$$

3.2.1.1.   Energy analysis of the stand-alone and grid-connected hybrid systems

From an energy point of view, the PV fraction $e_{pv,g}$ and wind fraction $e_{w,g}$ of the overall energy generated permits to identify the most active renewable system.

$$e_{pv,g} = \frac{E_{pv}}{E_g} \tag{13}$$

$$e_{w,g} = \frac{E_w}{E_g} \tag{14}$$

However, these parameters can be influenced by the different PV and wind powers installed. Instead, the comparison of fractions $e_{pv,g}$ and $e_{w,g}$, related to the energy produced, with the PV power fraction p_{pv} and the wind power fraction p_w, related to the power installed, permits to identify the predominant renewable source.

3.2.1.2. Energy balance of the stand-alone system

The yearly energy required by the load E_L is the sum of the energy produced by the PV and wind generators sent directly to the load E_{dtl}, the energy drawn from the battery E_{fb} and the missing energy E_m is provided by an alternative system.

$$E_l = E_{dtl} + E_{fb}\eta_{inv} + E_m \tag{15}$$

The yearly energy generated E_g is the sum of the energy produced by the PV and wind generators sent directly to the load E_{dtl}, the energy sent to the battery E_{tb} and the energy dissipated E_d.

$$E_g = \frac{E_{dtl}}{\eta_{reg}\eta_{inv}} + \frac{E_{tb}}{\eta_{reg}} + \frac{E_d}{\eta_{reg}\eta_{inv}} \tag{16}$$

3.2.1.3. Energy balance of the grid-connected system

The yearly energy required by the load E_L is the sum of the energy produced by the PV and wind generators sent directly to the load E_{dtl}, the energy drawn from the battery E_{fb} and the energy drawn from the grid E_{fg}.

$$E_l = E_{dtl} + E_{fb}\eta_{inv} + E_{fg} \tag{17}$$

The yearly energy generated E_g is the sum of the energy produced by the PV and wind generators sent directly to the load E_{dtl}, the energy sent to the battery E_{tb} and the energy in excess sent to the grid E_{tg}.

$$E_g = \frac{E_{dtl}}{\eta_{reg}\eta_{inv}} + \frac{E_{tb}}{\eta_{reg}} + \frac{E_{tg}}{\eta_{reg}\eta_{inv}} \tag{18}$$

3.3. Optimization of the stand-alone and grid-connected hybrid systems

In the current section, the dimensionless energy and economic indicators and the energy and economic optimization algorithms are described.

Chapter 7   **Worldwide geographical mapping and**
optimization of stand-alone and grid-connected hybrid renewable
system techno-economic performance across Köppen-Geiger climates

3.3.1. Energy indicators

The dimensionless energy reliability indicators used in the analysis to identify optimal system configurations are the fraction of satisfied load, the fraction of energy generated and used to satisfy the load, and the level of energy interaction between the system, load and the grid.
The satisfied load fraction SLF, the utilization factor UF and the grid energy interaction factor GEIF are defined by Eqs. (19-21).

$$\text{SLF} = \frac{E_{tl}}{E_l} \tag{19}$$

$$\text{UF} = \frac{E_{tl}}{E_g} \tag{20}$$

$$\text{GEIF} = \frac{E_{fg} + \dfrac{E_{tg}}{\eta_{reg}\eta_{inv}}}{E_l} = (1 - \text{SLF}) + (1 - \text{UF})\frac{E_g}{E_l} \tag{21}$$

When SLF=1, the yearly energy required by the load is entirely provided by the HRES; when UF=1, the yearly energy generated is entirely used to satisfy the load; when $\text{GEIF} = 0$, the interaction with the grid is zero highlighting that the load does not require to extract energy from the grid and neither to send energy to the grid given the presence of excess energy.

3.3.2. Economic indicators

The dimensionless economic indicator used in the analysis to identify optimal system configurations is the non-discount benefit-cost ratio BCR.
The non-discount BCR is defined as the ratio of benefit B achieved in one year by installing the HRES and the capital cost C of the HRES during its life span.

$$\text{BCR} = \frac{B}{C} \tag{22}$$

The capital cost is represented by the sum of the capital cost C_c and replacement cost C_r of system components.

$$C = C_c + C_r = \left(c_{pv}P_{pv} + c_wP_w + c_bP_b + c_{inv}P_{inv}\right) + \left(c_bP_b + c_{inv}P_{inv}\right) \tag{23}$$

Where, P_{pv}, P_w, P_b and P_{inv} are the nominal powers installed of the PV, wind, battery and inverter system, while c_{pv}, c_w, c_b and c_{inv} are the specific costs for the purchase of PV, wind, battery and inverter systems. In Eq. (23), the replacement cost is owing to the shorter battery and inverter lifespan compared to those of the PV and wind generators.
Economies of scale, which indicate the relationship between the increase in the size of the system considered and the decrease in the unit cost of the system, were implemented to take into account, for

each system component, the reduction of the specific purchase cost by increasing the power installed. Consequently, the specific purchase cost of a system component in €/kW is dependent on the power installed $c = f(P)$.

For the SA HRES, the benefit is represented by the economic value EV attributable to the electricity produced by the HRES sent to the load.

$$B = EV = c_e E_{tl} \tag{24}$$

Where c_e is the yearly average electricity cost.

For the GC HRES, the benefit is represented by the sum of the cost saving CS associated with the electricity produced by the HRES sent to the load, no purchased from the grid, and the revenue R deriving from the selling of the solar and wind energy in excess to the grid, namely the so-called Feed-in-Tariff (FiT) subside.

$$B = CS + R = c_e E_{tl} + \left(p_{s,pv} E_{tg,pv} + p_{s,w} E_{tg,w} \right) \tag{25}$$

where $p_{s,pv}$ and $p_{s,w}$ are the yearly average PV and wind electricity selling prices to the grid. For this paper, the economic analysis was developed at the initial time of the investment when the system operation and maintenance cost, the discount rate and the inflation rate are not necessary. However, the indicator can be easily extended to take into account also these further parameters.

3.3.3. Energy optimization algorithm

For the optimization of the HRES in a specific locality, the energy constrained-reliability methods proposed by Mazzeo et al. in previous work [4] was used. The method permits to identify the optimal system power configuration from an energy point of view.

For the SA HRES, only the missing energy to meet the load must be constrained, while the energy produced in excess must be minimized.

Find energy optimal $\left(P_{pv}, P_w, P_b \right)$ *that*

$$max\{UF(P_{pv}, P_w, P_b)\}$$

Subject to the constraints

$$SLF(P_{pv}, P_w, P_b) > \overline{SLF}$$

$$P_{pv,min} < P_{pv} < P_{pv,max}$$

$$P_{w,min} < P_w < P_{w,max}$$

$$P_{b,min} < P_b < P_{b,max}$$

For the GC HRES, the energy drawn from the grid and the energy produced in excess must be limited ($SLF > \overline{SLF}$ and $UF > \overline{UF}$); these limitations can be achieved by minimizing the GEIF.

Chapter 7

Worldwide geographical mapping and optimization of stand-alone and grid-connected hybrid renewable system techno-economic performance across Köppen-Geiger climates

Find energy optimal (P_{pv}, P_w, P_b) *that*

$$min\{\text{GEIF}(P_{pv}, P_w, P_b)\}$$

Subject to the constraints

$$P_{pv,min} < P_{pv} < P_{pv,max}$$

$$P_{w,min} < P_w < P_{w,max}$$

$$P_{b,min} < P_b < P_{b,max}$$

From an energy point of view, the most suitable locality to host a SA HRES is characterized by the highest value of UF among those related to the optimal SA HRES of each locality, while the most suitable locality to host a GC HRES is characterized by the lowest value of GEIF among those related to the optimal GC HRES of each locality.

3.3.4. Economic optimization algorithm

For the optimization of both SA and GC HRES, the BCR must be maximized to identify the optimal system power configuration from an economic point of view.

Find economic optimal (P_{pv}, P_w, P_b) *that*

$$max\{\text{BCR}(P_{pv}, P_w, P_b)\}$$

Subject to the constraints

$$\text{BCR}(P_{pv}, P_w, P_b) > \overline{\text{BCR}}$$

$$P_{pv,min} < P_{pv} < P_{pv,max}$$

$$P_{w,min} < P_w < P_{w,max}$$

$$P_{b,min} < P_b < P_{b,max}$$

An investment with BCR greater than a predetermined acceptable threshold value $\overline{\text{BCR}}$ is economically attractive. This economic indicator can be also used to preliminarily identify the payback period since the BCR provides the percentage of the recovered capital cost in one year. For instance, an investment with a lifespan of 30 years and a BCR=0.10 indicates that the capital cost is recovered at the 10th year. In this example, the capital cost is recovered within 30 years if the BCR > 1/30.

4. The case study

The dynamic simulations, yearly energy balances, and energy and economic indicators were used to carry out a world mapping of the energy performance and economic profitability of the PV-wind HRES both for the SA and GC configurations. The objective is to identify the optimal SA and GC system component powers for each location and to identify the most suitable locality to host a SA or

Chapter 7

Worldwide geographical mapping and
optimization of stand-alone and grid-connected hybrid renewable
system techno-economic performance across Köppen-Geiger climates

a GC system. A parametrical analysis was developed by varying the PV and wind power installed and the battery capacity.

4.1. Locations of study

The data on the typical meteorological years available in the TRNSYS library were used to compare 48 locations, two for each Koppen climatic sub-group, as shown in Figure 3.

In general, it was chosen to operate on locations with different latitudes and homogeneously distributed over the whole globe. The Köppen climate classification consists of five main climate groups: A (tropical), B (dry), C (temperate), D (continental), and E (polar), divided into sub-groups with reference to the second letter that indicates the seasonal precipitation type and the third letter that indicates the level of heat [46, 47].
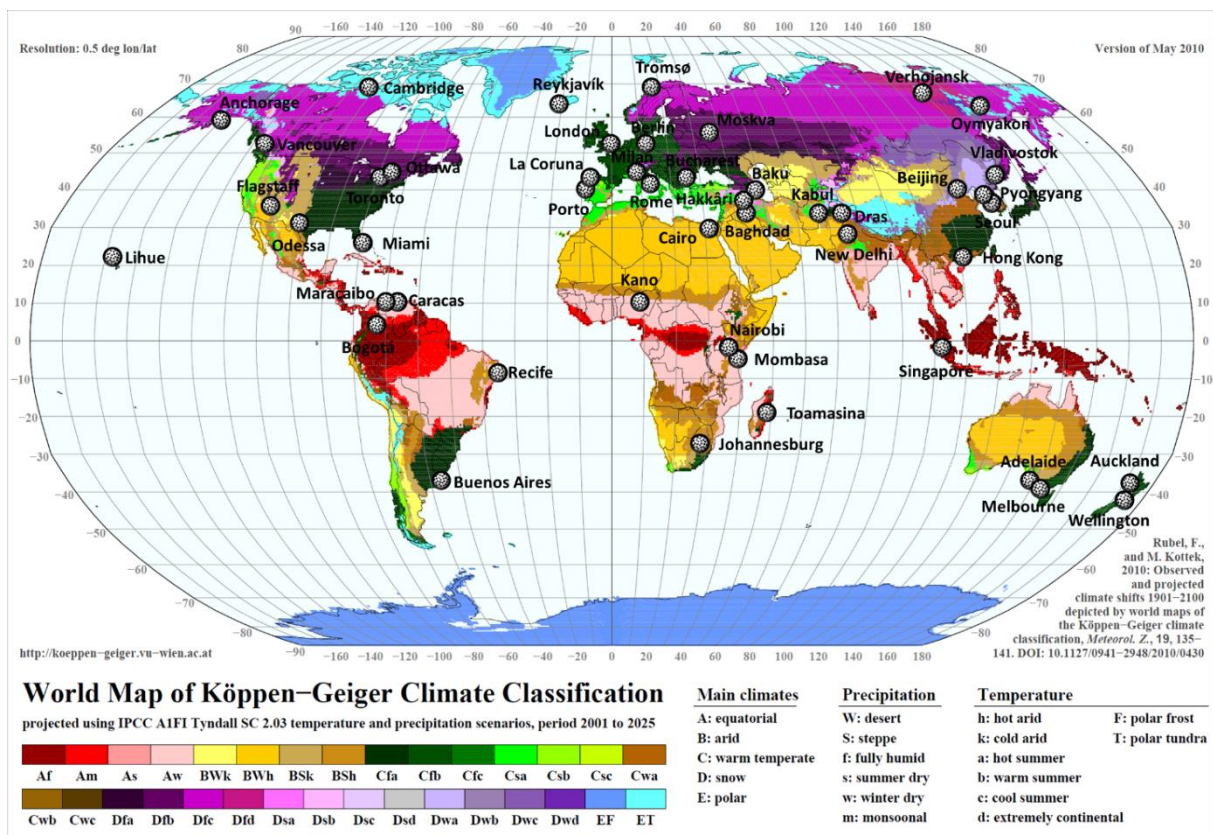
Figure 3. Worldwide locations according to Koppen-Geiger classification selected in this study [35].

The climatic zone Cfb for Oceanic climate has additional climate subgroups, namely the Marine west coast climate and the Subtropical highland climate with uniform rainfall. For this reason, six localities were selected considering the latitude difference as a criterion. The geographical data of the 48 localities considered are reported in Table 2.

The locations have different climatic conditions (very/low windy and/or very/low sunny) as well as different altitudes. In total, eight locations belong to climate group A, six to group B, eighteen to group C and sixteen to group D. The latitudes of the locations vary between a minimum of -41.32° (Wellington, New Zealand) and a maximum of 69.65° (Tromsø, Norway). In terms of longitude, the locations furthest from the Greenwich meridian are Lihue (USA) in Hawaii with - 159.35° and Auckland (New Zealand) with 174.8°. In addition, locations near the equator (Nairobi and Mombasa,

Chapter 7   **Worldwide geographical mapping and**
optimization of stand-alone and grid-connected hybrid renewable
system techno-economic performance across Köppen-Geiger climates

Kenya, Bogota, Colombia, and Singapore) and the Greenwich meridian (London, UK) have been considered. Altitudes vary between 2 (Miami, USA) and 3100 (Dras, India) meters above sea level.

The statistical characteristics of the selected locations are given in Table 3. The table shows the minimum, the first quartile (Q1), the median (Med), the third quartile (Q3), the maximum, the average (Mea) and the maximum/minimum interquartile range values (Int) of the external air temperature, the horizontal solar radiation and the wind speed of the 48 locations during the whole typical meteorological year.

Chapter 7

Worldwide geographical mapping and optimization of stand-alone and grid-connected hybrid renewable system techno-economic performance across Köppen-Geiger climates

Table 2. *Characteristics of the selected locations.*

Group	Koppen	Sub-group	Locality	Country	Latitude (°)	Longitude (°)	Elevation (m)
A Tropical/megathermal climates	**Af**	Tropical rainforest climate	Toamasina	Madagascar	-18.12	49.4	6
			Singapore	Singapore	1.03	103.98	16
	Am	Tropical monsoon climate	Recife, Pernambuco	Brazil	-8.07	-34.85	19
			Miami, Florida	USA	25.8	-80.27	2
	As	Tropical dry or savanna climate	Lihue, Hawaii	USA	21.98	-159.35	45
			Mombasa	Kenya	-4.03	39.62	57
	Aw	Tropical wet or savanna climate	Caracas	Venezuela	10.6	-66.98	43
			Kano	Nigeria	12.05	8.53	481
B Dry (desert and semi-arid) climates	**BWh**	Desert climate	Baghdad	Iraq	33.33	44.43	33
			Cairo	Egypt	31.84	31.28	36
	BSk	Semi-arid, cold	Kabul	Afghanistan	34.55	69.22	1791
			Baku	Azerbaijan	40.38	49.85	5
	BSh	Semi-arid, hot	Odessa, Texas	USA	46.48	-102.36	42
			Maracaibo	Venezuela	10.65	-71.6	40
C Temperate/mesothermal climates	**Cfa**	Humid subtropical climates, Without dry season	Buenos Aires	Argentina	-34.58	-58.48	24
			Milan	Italy	45.62	8.73	211
	Cfb	Oceanic climate, Warm summer	Berlin	Germany	52.47	13.4	50
			London	UK	51.52	-0.12	77
			Vancouver, British Columbia	Canada	49.25	-123.25	87
			Melbourne, Victoria	Australia	-37.82	144.97	38
	Cfb	Highland climates with uniform rainfall	Bogotá, Cundinamarca	Colombia	4.05	-74.15	2548
			Wellington	New Zeland	-41.32	174.77	6
	Cfc	Subpolar oceanic climates	Reykjavík	Iceland	64.13	-21.9	66
			Auckland	New Zeland	-37.02	174.8	6
	Csa	Mediterranean climates, Hot summer	Rome	Italy	41.8	12.58	131
			Adelaide	Australia	-34.93	138.53	4
	Csb	Mediterranean climates, Warm summer	Porto	Portugal	41.13	-8.6	100
			La Coruna	Spain	43.37	-8.42	67
	Cwa	Humid subtropical climates, Dry winter	New Delhi	India	28.58	77.2	212
			Hong Kong	China	22.3	114.17	62
	Cwb	Highland climates	Johannesburg	South Africa	-26.13	28.23	1692
			Nairobi	Kenya	-1.15	36.92	1624
D Continental/microthermal climates	**Dfa**	Hot summer continental climates, Without dry season	Bucharest	Romania	44.5	26.22	91
			Toronto, Ontario	Canada	43.72	-79.23	157
	Dfb	Warm summer continental or hemiboreal climates, Without dry season	Moskva	Russia	55.83	37.62	156
			Ottawa, Ontario	Canada	45.38	-75.72	79
	Dfc	Subarctic or boreal climates	Tromsø	Norway	69.65	18.95	102
			Anchorage, Alaska	USA	61.17	-150.02	35
	Dfd	Subarctic or boreal climates	Oymyakon, Sakha Republic	Russia	63.27	143.15	740
			Verhojansk, Sakha Republic	Russia	67.55	133.38	137
	Dsa	Hot summer continental climates, Dry summer	Hakkâri	Turkey	37.57	43.77	1720
			Cambridge Bay, Nunavut	Canada	69.10	-105.12	23
	Dsb	Warm summer continental or hemiboreal climates, Dry summer	Dras	India	34.43	75.77	3100
			Flagstaff, Arizona	USA	35.13	-111.67	2135
	Dwa	Hot summer continental climates, Dry winter	Beijing	China	39.93	116.28	55
			Seoul	South Korea	37.57	126.97	86
	Dwb	Warm summer continental or hemiboreal climates, Dry winter	Pyongyang	North Korea	39.03	125.78	35
			Vladivostok	Russia	43.12	131.9	80

Chapter 7

Worldwide geographical mapping and optimization of stand-alone and grid-connected hybrid renewable system techno-economic performance across Köppen-Geiger climates

Table 3. *Statistical data of selected locations.*

Locality	External air temperature (°C)							Horizontal global solar radiation (W/m²)							Wind speed (m/s)						
	Min	Q1	Med	Q3	Max	Mea	Int	Min	Q1	Med	Q3	Max	Mea	Int	Min	Q1	Med	Q3	Max	Mea	Int
Toamasina	12.80	20.90	23.40	25.90	32.50	23.30	19.70	0	0	0	376	1105	206	1105	0.00	1.00	1.70	2.70	8.70	2.00	8.70
Singapore	21.00	24.80	26.60	28.40	33.70	26.60	12.70	0	0	0	329	1018	185	1018	0.00	0.70	1.50	2.80	14.20	2.00	14.20
Recife	21.20	26.60	28.60	30.60	36.40	28.60	15.20	0	0	0	483	1090	242	1090	0.10	2.50	4.00	5.90	15.30	4.40	15.20
Miami	3.90	22.30	25.00	27.20	33.40	24.30	29.50	0	0	18	385	1038	205	1038	0.00	2.90	4.10	5.70	11.90	4.30	11.90
Lihue	13.00	22.30	24.20	25.60	29.80	23.90	16.80	0	0	24	388	1093	208	1093	0.25	4.00	5.60	6.70	14.10	5.50	13.80
Mombasa	17.10	23.80	26.10	28.50	36.10	26.20	19.00	0	0	0	431	1093	228	1093	0.10	2.70	4.30	6.30	17.10	4.70	17.00
Caracas	18.20	24.00	25.90	28.00	34.60	26.00	16.40	0	0	6	333	1034	185	1034	0.00	0.40	0.90	1.70	8.60	1.20	8.60
Kano	7.40	22.20	26.50	30.60	43.40	26.30	36.00	0	0	8	548	1040	256	1040	0.05	1.90	3.30	5.00	13.80	3.60	13.70
Baghdad	-2.90	11.60	20.10	28.30	43.70	20.10	46.60	0	0	0	477	1013	238	1013	0.00	1.20	2.10	3.20	10.50	2.40	10.50
Cairo	3.20	16.30	21.30	26.40	39.20	21.30	36.00	0	0	0	467	1012	231	1012	0.05	2.00	3.20	4.70	12.50	3.50	12.50
Kabul	-10.70	2.90	12.40	20.80	35.20	12.10	45.90	0	0	0	408	1132	218	1132	0.00	0.70	1.70	3.20	14.40	2.30	14.40
Baku	-8.00	6.90	14.30	22.00	37.70	14.60	45.70	0	0	0	236	983	152	983	0.15	3.10	5.00	7.10	18.60	5.40	18.40
Odessa	-14.30	2.60	10.40	17.80	33.20	10.20	47.50	0	0	0	222	944	142	944	0.05	2.10	3.60	5.40	14.50	3.90	14.40
Maracaibo	17.10	25.20	27.50	30.00	36.30	27.50	19.20	0	0	0	316	1019	179	1019	0.00	2.00	3.40	5.30	16.20	3.80	16.20
Buenos Aires	2.80	13.00	17.30	22.00	32.90	17.40	30.10	0	0	0	352	1122	195	1122	0.10	2.50	3.90	5.60	13.60	4.20	13.50
Milan	-10.80	4.40	12.10	18.40	32.50	11.60	43.30	0	0	0	210	917	136	917	0.00	0.30	0.80	1.50	9.30	1.10	9.30
Berlin	-16.90	3.10	9.00	15.90	31.70	9.40	48.60	0	0	0	168	876	114	876	0.05	2.50	4.10	6.20	17.20	4.60	17.10
London	-3.00	6.50	10.40	14.90	28.80	10.80	31.80	0	0	0	143	853	106	853	0.05	2.20	3.70	5.50	14.10	4.00	14.10
Vancouver	-5.70	5.20	9.60	14.30	26.20	9.80	31.90	0	0	0	220	953	144	953	0.00	1.60	2.80	4.40	12.50	3.20	12.50
Melbourne	-0.20	9.70	13.50	17.80	37.00	14.00	37.20	0	0	0	302	1096	175	1096	0.15	2.90	4.60	6.70	16.20	4.90	16.00
Bogotá	0.10	10.60	13.30	16.10	24.30	13.30	24.20	0	0	0	328	1185	193	1185	0.00	0.70	1.60	3.10	15.20	2.20	15.20
Wellington	1.60	10.20	13.20	16.50	27.00	13.50	25.50	0	0	0	259	1072	160	1072	0.25	4.20	6.40	9.10	21.50	6.80	21.20
Reykjavík	-11.70	0.40	4.80	8.60	17.40	4.40	29.10	0	0	0	125	792	89	792	0.15	3.40	5.50	7.80	19.20	5.80	19.10
Auckland	2.90	12.00	15.00	18.10	26.30	15.10	23.40	0	0	0	299	1071	175	1071	0.30	4.20	6.40	9.10	20.40	6.80	20.10
Rome	-2.10	9.60	14.90	20.60	34.30	15.20	36.40	0	0	0	320	988	178	988	0.00	1.40	2.60	4.40	14.40	3.10	14.40
Adelaide	2.70	12.10	15.90	20.40	39.70	16.70	37.00	0	0	0	372	1099	204	1099	0.00	2.10	3.70	5.90	18.60	4.20	18.60
Porto	-0.50	10.70	14.50	18.20	33.30	14.50	33.80	0	0	0	307	1030	178	1030	0.05	2.50	4.40	6.80	20.70	5.00	20.60
La Coruna	0.60	11.00	14.10	17.10	27.70	14.10	27.10	0	0	0	220	940	140	940	0.00	1.60	2.80	4.40	12.70	3.20	12.70
New Delhi	4.40	19.20	26.30	31.00	44.60	25.10	40.30	0	0	0	461	1028	225	1028	0.00	0.60	1.20	2.00	7.90	1.40	7.90
Hong Kong	5.40	18.70	23.80	27.40	34.60	22.90	29.20	0	0	3	265	1019	163	1019	0.15	3.20	4.80	6.70	14.90	5.10	14.80
Johannesburg	-3.50	11.40	15.70	19.90	31.40	15.50	34.90	0	0	0	467	1236	236	1236	0.10	1.90	3.10	4.60	12.40	3.40	12.30
Nairobi	6.70	16.30	19.20	22.20	31.00	19.20	24.30	0	0	0	385	1190	211	1190	0.05	2.80	4.60	6.90	18.40	5.10	18.30
Bucharest	-15.30	2.40	10.90	18.40	35.40	10.60	50.70	0	0	0	243	986	151	986	0.00	0.80	1.70	3.10	15.30	2.20	15.30
Toronto	-24.70	-0.60	7.80	16.20	33.00	7.40	57.70	0	0	0	267	979	161	979	0.05	2.60	4.30	6.40	17.20	4.70	17.10
Moskva	-24.40	-3.30	5.30	14.20	29.90	5.00	54.30	0	0	0	152	858	110	858	0.00	0.40	0.90	1.80	8.80	1.30	8.80
Ottawa	-28.80	-3.40	7.00	16.00	33.70	5.90	62.50	0	0	0	270	941	157	941	0.00	1.90	3.20	4.90	14.10	3.60	14.10
Tromsø	-15.20	-2.00	2.60	8.00	20.30	2.90	35.50	0	0	0	88	711	72	711	0.05	2.20	3.70	5.60	15.90	4.10	15.90
Anchorage	-25.30	-4.70	3.30	11.10	25.00	2.60	50.30	0	0	6	141	789	102	789	0.00	2.10	2.90	4.40	11.90	3.30	11.90
Oymyakon	-61.00	-38.50	-14.80	5.90	29.40	-16.10	90.40	0	0	0	191	840	122	840	0.00	0.20	0.60	1.80	13.90	1.30	13.90
Verhojansk	-60.00	-37.50	-12.90	6.90	28.30	-15.10	88.30	0	0	0	161	768	109	768	0.00	0.90	1.90	3.40	14.30	2.40	14.30
Hakkâri	-16.70	0.70	10.00	19.50	34.10	10.10	50.70	0	0	0	343	1063	196	1063	0.00	0.50	1.10	2.10	12.20	1.60	12.20
Cambridge Bay	-44.60	-29.10	-15.70	0.50	17.30	-14.60	61.90	0	0	0	162	797	114	797	0.20	3.60	5.60	7.90	18.80	5.90	18.60
Dras	-23.40	-9.20	2.60	13.00	29.30	2.10	52.70	0	0	0	309	1155	186	1155	0.00	0.80	1.60	2.90	12.50	2.00	12.50
Flagstaff	-25.80	-0.50	7.20	14.70	34.20	7.30	60.00	0	0	23	397	1071	214	1071	0.00	1.80	2.90	4.70	20.60	3.20	20.60
Beijing	-15.00	1.40	12.70	22.20	37.40	11.80	52.30	0	0	0	249	971	148	971	0.00	1.00	2.00	3.50	15.20	2.50	15.20
Seoul	-14.60	2.90	12.90	21.00	33.90	11.80	48.40	0	0	0	220	1000	139	1000	0.00	0.90	1.90	3.40	15.20	2.40	15.20
Pyongyang	-19.20	-0.50	10.60	20.20	34.40	9.60	53.50	0	0	0	241	994	147	994	0.00	0.60	1.20	2.30	15.70	1.70	15.70
Vladivostok	-27.70	-5.60	5.70	14.30	29.10	4.30	56.80	0	0	0	265	966	151	966	0.05	2.20	3.70	5.50	14.30	4.10	14.30

Figure 4 shows the worldwide mapping of the yearly average hourly external air temperature, horizontal solar radiation and wind speed. Considering the average values, Kano is the sunniest location, with medium-high wind speeds, while Auckland and Wellington (both in New Zealand) are the windiest locations. The least sunny place is Tromsø, the northernmost place. The least windy location is, instead, Milan, which is also considerably not very sunny. Lihue, Nairobi, Mombasa and Recife have remarkable average values of both solar radiation and wind speed. In addition to Milan, also Moscow and Oymyakon (both in Russia) have low sun and low wind speeds. In terms of average temperatures, Recife is the warmest and Oymyakon the coldest.
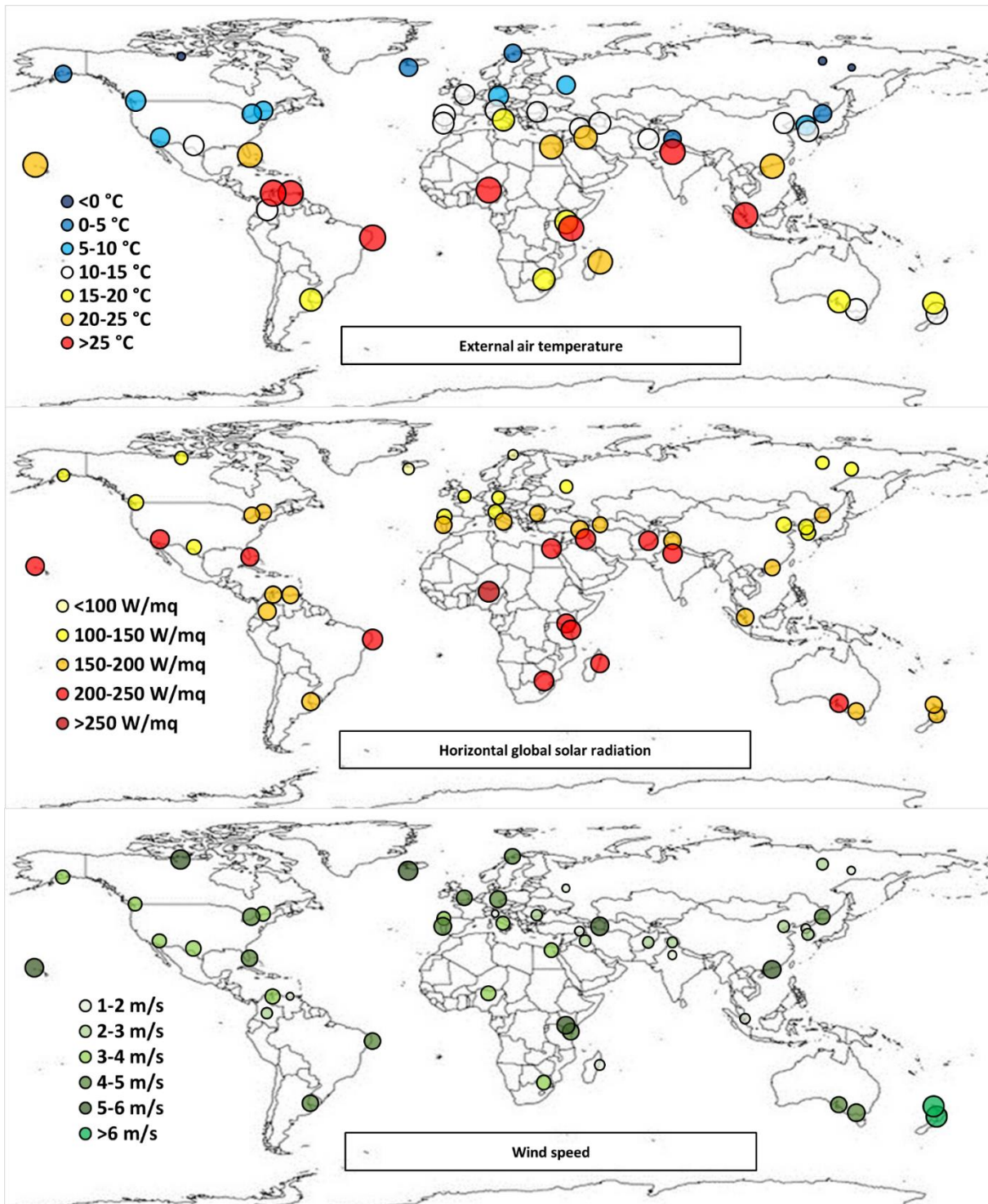
Chapter 7   **Worldwide geographical mapping and**
optimization of stand-alone and grid-connected hybrid renewable
system techno-economic performance across Köppen-Geiger climates

Figure 4. *Worldwide mapping of the yearly average hourly external air temperature, horizontal solar radiation and wind speed.*

4.2. Definition of load

The investigated HRES produces electricity for the energy needs of a district composed of five identical office buildings with a wide windowed envelope [44, 48]. The load requires energy for electrical lighting (EL), electric office devices (ED) and electric vehicle charging stations (EV) located in the parking lots of each building. Each building consists of two floors of 100 m², divided

Chapter 7   **Worldwide geographical mapping and**
optimization of stand-alone and grid-connected hybrid renewable
system techno-economic performance across Köppen-Geiger climates

into eight thermal zones, corresponding to the number of rooms with different orientation and occupant profile.

Six zones have the same occupant profile (OP1) with morning and afternoon working hours during the weekdays, while the other two rooms on some days do not have occupants in the afternoons (OP2).

The load for the LED lighting system requires 125 W in each room when occupants are present, and the solar radiation is lower than a prefixed value. For this reason, this load varies in the localities considered. The On/Off routine of the lighting system is smartly managed by a differential controller. The eight thermal zones have different weekly ED load profiles dependent on the occupant profiles in each zone. When occupants are present, a power 75 W is required for two personal computers and a printer in each zone.

In the district, twenty EV charging stations are supplied to charge forty electric Nissan Leaf of 24 kWh during the occupant profile hours. Each building has four stations, each equipped with 2.3 kW and employed to charge the first group of four vehicles from 9:00 to 11:00 and the second group of four vehicles from 11:00 to 13:00. Overall, the EV load requires 9.2 kW for each building between 9:00 and 13:00.

Each vehicle requires two hours to recover the daily consumption of 5.14 kWh/day owing to an average of 26.8 km per day and an average EV consumption of 0.1714 kWh/km [49].

Figure 5 shows, for one building in the district, the weekly ED loading times in the two characteristic zones with an OP1 and OP2 occupancy profile for the eight zones and the four EV charging stations in the building's parking lot. The EL load cannot be defined as it is different in each location.
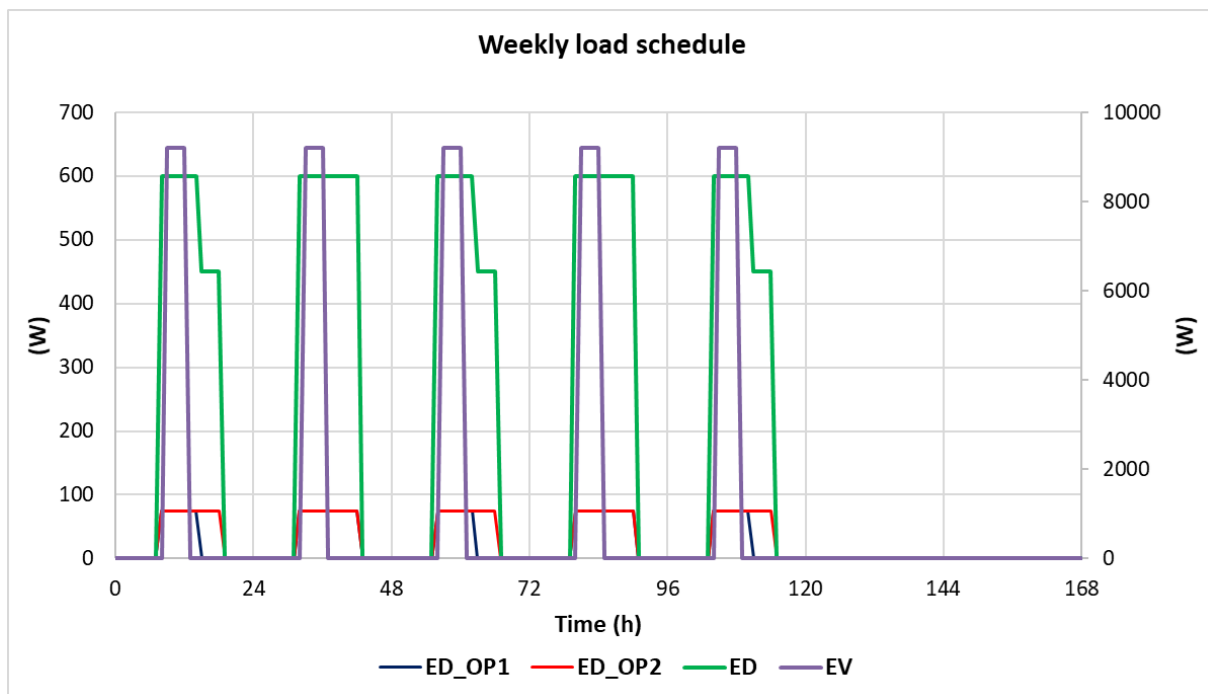

Figure 5. Weekly schedules of the overall electrical device load (ED), electrical device load in zones with occupant profile OP1 (ED_OP1) and occupant profile OP2 (ED_OP2), and electric vehicle charging station load (EV).

In terms of annual load, in all locations, the main contribution is provided by the energy required to recharge EVs (48 MWh), followed by the use of EDs (8 MWh). As can be expected, the maximum

Chapter 7

Worldwide geographical mapping and optimization of stand-alone and grid-connected hybrid renewable system techno-economic performance across Köppen-Geiger climates

annual electricity consumption takes place in the locations with the lowest solar radiation levels, which leads to greater use of the lighting system (see Figure 6). EL consumption varies between 1.7 MWh (Kano) and 9.3 MWh (Tromsø) with corresponding yearly average load powers of 6.59 kW and 7.45 kW.
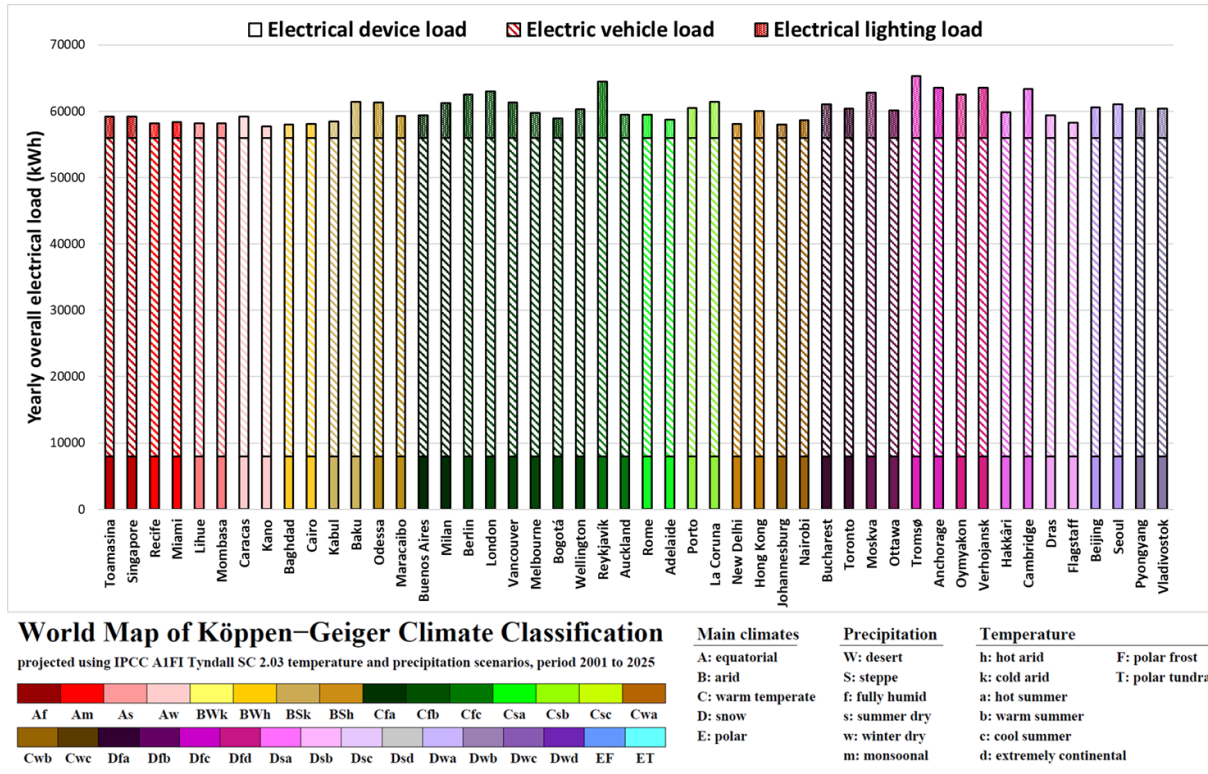

Figure 6. Yearly electrical loads in various locations.

The occupancy profile was supposed identical since, unlike residential uses, the occupancy behaviour and electrical internal loads of typical office building can be assimilated worldwide.

The heating and cooling energy demand and for the domestic hot water demand were supposed satisfied by sources different from the electrical one to not introduce further complexity to the analysis, being these energy demand types dependents on the building envelope thermal characteristics, outdoor climate and internal heat gains.

These aspects were previously addressed in a previous investigation [44] regarding the specific Italian climatic conditions.

4.3. Technical data of the system components

The considered Mitsubishi Electric PV module PV-MLU250HC consists of polycrystalline silicon cells with a nominal power of 250 W, efficiency under operating conditions of 15.3%, nominal operating temperature (NOCT) of 46°C, and area of 1.6236 m^2 [50].

The Tulipower micro wind generator is located 4.5 m above the roof, i.e. 14.5 m above ground level. It is characterized by a rated power of 2500 W, starting speed of 3 m/s, stopping speed of 18 m/s and rated speed of 10 m/s [51]. The SonnenBatterie lithium-ion battery has a capacity of 10 kWh and an efficiency of 0.98 [52]. The FRONIUS IG PLUS V DC/AC inverter has an efficiency equal to 0.97 [53]. Finally, the DC/DC converter has a coefficient of efficiency equal to 0.94, the AC/DC rectifier has an efficiency equal to 0.90, and the regulator has an efficiency equal to 0.98.

Chapter 7

**Worldwide geographical mapping and
optimization of stand-alone and grid-connected hybrid renewable
system techno-economic performance across Köppen-Geiger climates**

3.4. Prices of the system components and electricity

The yearly specific costs for the purchase of PV, wind, battery and inverter systems in €/kW as a function of the installed nominal power were determined by empirical equations obtained by fitting the specific purchase costs for different nominal powers extracted from the market. In particular, for the PV, battery and inverter systems, different powers of the same system typology were considered; instead, different micro-wind generators typology were considered since the Tulipower is available only for 2.5 kW in the market. Figure 7 shows the fitting curves and equations for the specific costs for the purchase of PV, wind, battery and inverter systems in €/kW as a function of the nominal power. Supplementary file S1 contains further data and references related to this market analysis.
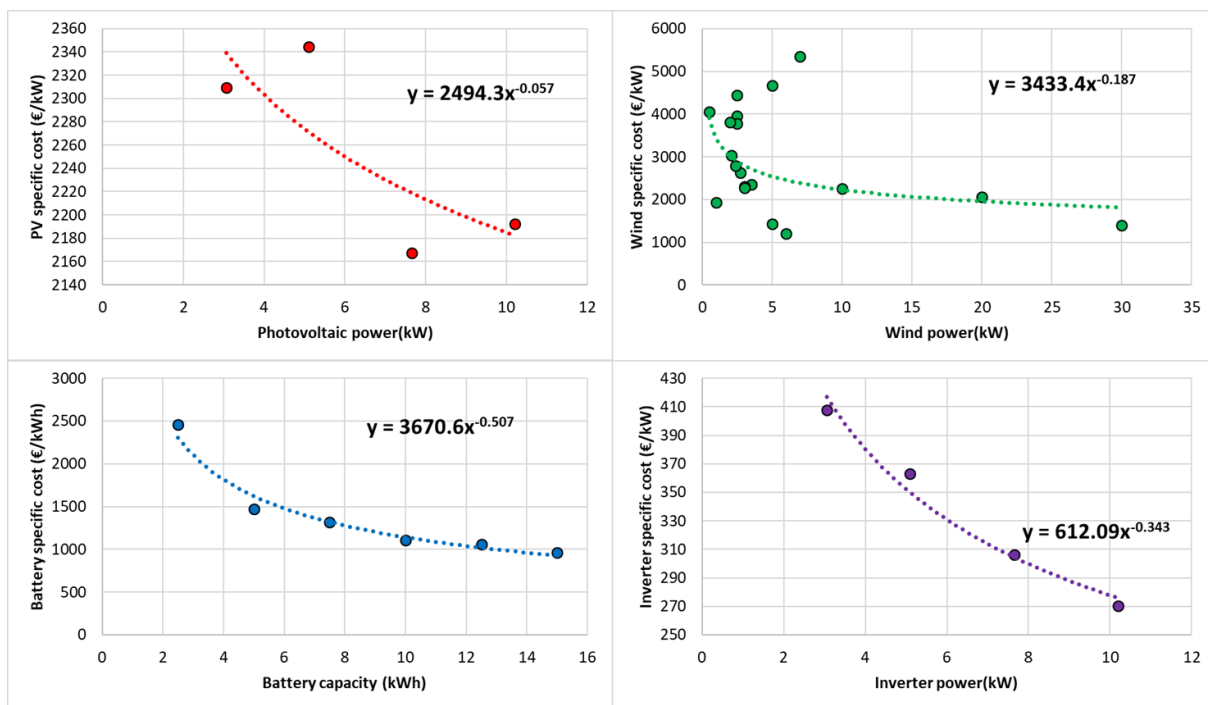
Figure 7. Specific costs for the purchase of different system components as a function of the power installed.

For the different countries selected in this study, an in-depth study of the respective national electrical systems was performed to detect the yearly average electricity price for non-household use. The electricity price in some countries turned out variable as a function of the time and season. In addition, somewhere the electricity price is differentiated over different levels of electricity consumption. In these cases, the yearly average electricity price was determined by averaging the data provided by each official source. When the national electricity price is different in the belonging Regions or States, the electricity price of the region or state of each locality considered in this study was detected.
Similarly, an extensive investigation was performed to collect worldwide data to take into account the FiT electricity policies, which consist of a cost-based compensation to renewable energy producers that sell excess energy to the national grid [54]. The Global status report 2019, published by the multistakeholder governance group Renewable Energy Policy Network for the 21st Century (REN21), has permitted to detect the countries with FiT subsidies currently available [3]. It mentions that 111 countries, states or provinces had FiT policies in place by the end of 2018. An across country analysis was conducted to collect the yearly average PV and wind electricity selling prices to the grid. From this analysis, it emerged that in some countries the FiT is variable on an hourly basis, can be

different Region by Region or State by State and can be exploited only for a specific number of years. Furthermore, it was found that the FiT can be limited by a threshold value of power installed, above which the subside cannot be accessible or by a threshold value of energy supplied to the grid, above which the further energy in excess is not paid. Finally, in some countries, the FiT price is differentiated over different levels of electricity sold to the grid. Taking into account all these factors, the average yearly value was considered.

Table 4 illustrates the worldwide data collected for the yearly average electricity price and PV and wind electricity selling prices.

Table 4. Yearly average electricity and solar and wind FiT price.

Locality	Country	Currency	Exchange Rate (02/06/2020)	c_e (€/kWh)	$p_{s,pv}$ (€/kWh)	$p_{s,w}$ (€/kWh)
Toamasina	Madagascar	Ariary malgascio (MGA)	1 MGA = 0.000237657 EUR	0.0918	0.000	0.000
Singapore	Singapore	Singapore dollar (SGD)	1 SGD = 0.637789 EUR	0.1571	0.000	0.000
Recife	Brazil	Brazilian real (BRL)	1 BRL = 0.168762 EUR	0.0927	0.000	0.000
Miami	United States	U.S. Dollar (USD)	1 USD = 0.900047 EUR	0.0841	0.162	0.162
Lihue	United States	U.S. Dollar (USD)	1 USD = 0.900047 EUR	0.2740	0.174	0.174
Mombasa	Kenya	Kenyan Shilling (KES)	1 KES = 0.00840872 EUR	0.1276	0.108	0.099
Caracas	Venezuela	Venezuelan Bolivar (VEF)	1 VEF = 0.0900758 EUR	0.1156	0.000	0.000
Kano	Nigeria	Nigerian Naira (NGN)	1 NGN = 0.00231842 EUR	0.0458	0.082	0.058
Baghdad	Iraq	Iraqi Dinar (IQD)	1 IQD = 0.000751684 EUR	0.1128	0.000	0.000
Cairo	Egypt	Egyptian Pound (EGP)	1 EGP = 0.0563931 EUR	0.0716	0.076	0.036
Kabul	Afghanistan	Afghanistanian Afghani (AFN)	1 AFN = 0.0117172 EUR	0.1485	0.000	0.000
Baku	Azerbaijan	Azerbaijanian Manat (AZN)	1 AZN = 0.529245 EUR	0.0318	0.000	0.000
Odessa	United States	U.S. Dollar (USD)	1 USD = 0.900047 EUR	0.0706	0.054	0.054
Maracaibo	Venezuela	Venezuelan Bolivar (VEF)	1 VEF = 0.0900758 EUR	0.1156	0.000	0.000
Buenos Aires	Argentina	Argentine Peso (AES)	1 ARS = 0.0131257 EUR	0.0631	0.012	0.012
Milan	Italy	Euro (EUR)	1 EUR = 1 EUR	0.1870	0.040	0.050
Berlin	Germany	Euro (EUR)	1 EUR = 1 EUR	0.1957	0.065	0.108
London	United Kingdom	British Pound Sterling (GBP)	1 GBP = 1.12226 EUR	0.1864	0.028	0.055
Vancouver	Canada	Canadian Dollar (CAD)	1 CAD = 0.662786 EUR	0.0635	0.000	0.000
Melbourne	Australia	Australian Dollar (AUD)	1 AUD = 0.610665 EUR	0.1399	0.080	0.080
Bogotá	Colombia	Colombian Peso (COP)	1 COP = 0.000246204 EUR	0.1353	0.000	0.000
Wellington	New Zealand	New Zealand Dollar (NZD)	1 NZD = 0.568005 EUR	0.0186	0.000	0.000
Reykjavík	Iceland	Icelandic Krona (ISK)	1 ISK = 0.00662244 EUR	0.0672	0.000	0.000
Auckland Islands	New Zealand	New Zealand Dollar (NZD)	1 NZD = 0.568005 EUR	0.0307	0.000	0.000
Rome	Italy	Euro (EUR)	1 EUR = 1 EUR	0.1870	0.040	0.050
Adelaide	Australia	Australian Dollar (AUD)	1 AUD = 0.610665 EUR	0.2153	0.070	0.070
Porto	Portugal	Euro (EUR)	1 EUR = 1 EUR	0.1408	0.095	0.095
La Coruna	Spain	Euro (EUR)	1 EUR = 1 EUR	0.1336	0.000	0.000
New Delhi	India	Indian Rupee (INR)	1 INR = 0.0118929 EUR	0.0864	0.037	0.039
Hong Kong	China	Hong Kong Dollar (HKD)	1 HKD = 0,115958 EUR	0.1251	0.124	0.074
Johannesburg	South Africa	South African Rand (ZAR)	1 ZAR = 0.0520549 EUR	0.0646	0.000	0.000
Nairobi	Kenya	Kenyan Shilling (KES)	1 KES = 0.00840872 EUR	0.1276	0.108	0.099
Bucharest	Romania	Romanian Leu (RON)	1 RON = 0.206263 EUR	0.1206	0.000	0.000
Toronto	Canada	Canadian Dollar (CAD)	1 CAD = 0.662786 EUR	0.0855	0.127	0.083
Moskva	Russia	Russian Rouble (RUB)	1 RUB = 0.0130114 EUR	0.0712	0.000	0.000
Ottawa, Ontario	Canada	Canadian Dollar (CAD)	1 CAD = 0.662786 EUR	0.0855	0.127	0.083

Chapter 7   **Worldwide geographical mapping and**
optimization of stand-alone and grid-connected hybrid renewable
system techno-economic performance across Köppen-Geiger climates

Tromsø	Norway	Norwegian Krone (NOK)	1 NOK = 0.0932880 EUR	0.0948	0.000	0.000
Anchorage	United States	U.S. Dollar (USD)	1 USD = 0.900047 EUR	0.1759	0.000	0.000
Oymyakon	Russia	Russian Rouble (RUB)	1 RUB = 0.0130114 EUR	0.0563	0.000	0.000
Verhojansk	Russia	Russian Rouble (RUB)	1 RUB = 0.0130114 EUR	0.0563	0.000	0.000
Hakkâri	Turkey	Turkish Lira (TRY)	1 TRY = 0.131880 EUR	0.1027	0.120	0.066
Cambridge Bay	Canada	Canadian Dollar (CAD)	1 CAD = 0.662786 EUR	0.4290	0.000	0.000
Dras	India	Indian Rupee (INR)	1 INR = 0.0118929 EUR	0.0541	0.037	0.039
Flagstaff	United States	U.S. Dollar (USD)	1 USD = 0.900047 EUR	0.0863	0.024	0.024
Beijing	China	Chinese Renminbi or Yuán (CNY)	1 CNY = 0.126085 EUR	0.0928	0.111	0.057
Seoul	South Korea	South Korean Won (KRW)	1 KRW = 0.000734275 EUR	0.0644	0.000	0.000
Pyongyang	North Korea	North Korean Won (KPW)	1 KPW = 0.000984159 EUR	0.0344	0.000	0.000
Vladivostok	Russia	Russian Rouble (RUB)	1 RUB = 0.0130114 EUR	0.0396	0.000	0.000

Further information and references related to Table 4 are extensively reported in Supplementary File S2.

4.4. Parametric analysis

A parametric analysis was developed for the 48 locations, making a variation of the powers related to PV, wind and battery systems for a minimum of 10 kW to a maximum of 130 kW, with a step of 20 kW. For each component seven possible power values were considered with overall 343 possible system power configurations for each location, resulting in a total of 16464 scenarios to be evaluated. The analyses were carried out by varying the number of PV strings in parallel (between 1 and 13) in the district, each composed of 40 PV modules of 250 W in series, wind turbines (between 4 and 52) and storage battery modules (between 5 and 13). As regards PV inclination angle, an optimization analysis was made to place PV panels in each locality at their own optimal angle. The optimal angle was obtained by performing a TRNSYS dynamic simulation for inclination angles variable between -90° and 90°. The optimal angles are reported in the supplementary file S1 for each locality.

All scenarios were dynamically simulated in the TRNSYS environment to calculate the hourly power output values of each component, which have been used for the calculation of the yearly energy contributions belonging to the energy balances of the SA and GC systems.

For a specific locality, the optimum power configuration, in terms of energy reliability among all 343 combinations, was identified:

- for the SA HRES, selecting all configurations with $\overline{SLF} > 0.7$ and maximizing the UF value among these configurations.
- for the GC HRES, minimizing the GEIF.

The 16464 scenarios use the same data for both SA and GC systems. For SA systems, the energy sent to the grid E_{tg} was considered as excess energy to be dissipated, while the energy taken from the grid E_{fg} was considered as missing energy (the balance is unchanged).

The yearly energy contributions belonging to the energy balances of the SA and GC systems and specific costs of components, electricity and FiT prices were used to calculate benefits and costs.

For a specific locality and both SA and GC HRES, the optimum power configuration in terms of energy reliability among all 343 combinations was identified:

- maximizing the BCR value and selecting all localities with $\overline{BCR} > 0.10$. In addition, configurations with $\overline{BCR} > 1/30$ will be identified to identify where the capital cost is recovered within the investment lifespan of 30 years.

Chapter 7   Worldwide geographical mapping and
optimization of stand-alone and grid-connected hybrid renewable
system techno-economic performance across Köppen-Geiger climates

5. Discussion of results

The first analysis regards the transient and seasonal behaviour of the HRES investigated in some critical localities. The scope of the second analysis is to identify, in each locality, the optimal power configurations, respectively, with the highest energy performance and profitability, both for a SA and GC HRES. In addition, the most suitable localities worldwide to host a SA and GC system, both from an energy and economic point of view are selected.

The objective of the last analysis is the worldwide geographical mapping of the techno-economic performance of the energetically and economically optimal system configurations.

5.1. Weekly hourly behaviour of the hybrid system in critical weather conditions

To highlight the transient performance over different seasons of SA and GC systems in meeting electrical peak demand, a weekly hourly analysis was developed in few critical climate zones. In particular, the load trend was compared with the missing and excess power trends in the windiest and sunniest localities (Auckland, New Zealand, and Kano, Nigeria) and the least sunny and windy localities (Tromsø, Norway, and Milan Italy) by considering a winter (15-21 January), spring (16-22 April), summer (13-19 August) and autumn (15-21 October) week. The results are valid both for SA and GC HRES, in which the energy is missing or drawn from the grid and the energy in excess is dissipated or sent to the grid, respectively. The analysis considered a system with intermediate power size compared to the range examined (70 kW of PV and wind power, 70 kWh of storage capacity).

Figures 8-11 illustrate the results of this analysis of the four localities selected.

Auckland, extremely productive for all representative weeks, highlights an impending presence of excess energy, so much to cancel (in winter and autumn) or significantly reduce (in summer) the missing energy and thus showing a decided overabundance compared to the load considered. Only the spring week seems to have problems of contemporaneity between the power generated by the HRES and load, showing high values of missing energy but low values of excess energy. Being a location strongly based on wind power, the production of excess energy is extended to all hours of the day.

Kano is also very productive, showing greater load satisfaction in the winter and autumn and showing increasing amounts of missing energy in spring and summer. Being a location heavily dependent on PV production, the peaks of excess energy are concentrated in the daytime hours, immediately after the load request ceases.

Milan is characterized by low load satisfaction and, therefore, a decidedly inadequate system for this building user. In particular, the best performance are obtained in the spring and summer periods, and not every day, with significantly lower missing energy values. Milan is also a location that focuses heavily on PV production and therefore every peak of excess energy is present only during the daytime hours after the load request ceases and during the weekend.

Tromsø also has significant problems with missing energy, especially in the winter-autumn period. The winter period has also high excess energy values mainly owing to the wind energy produced. The peaks of excess power are not synchronized with the diurnal load being a low sunny location.
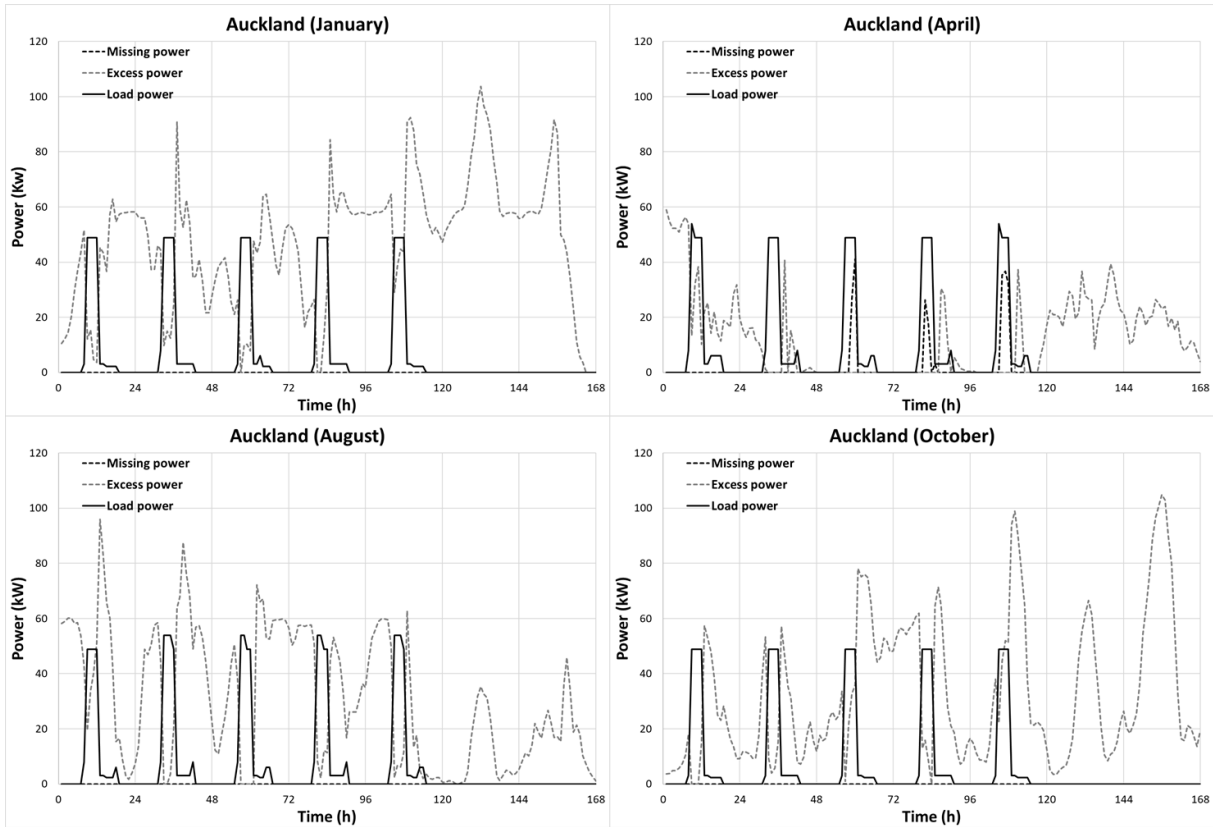
Chapter 7

**Worldwide geographical mapping and
optimization of stand-alone and grid-connected hybrid renewable
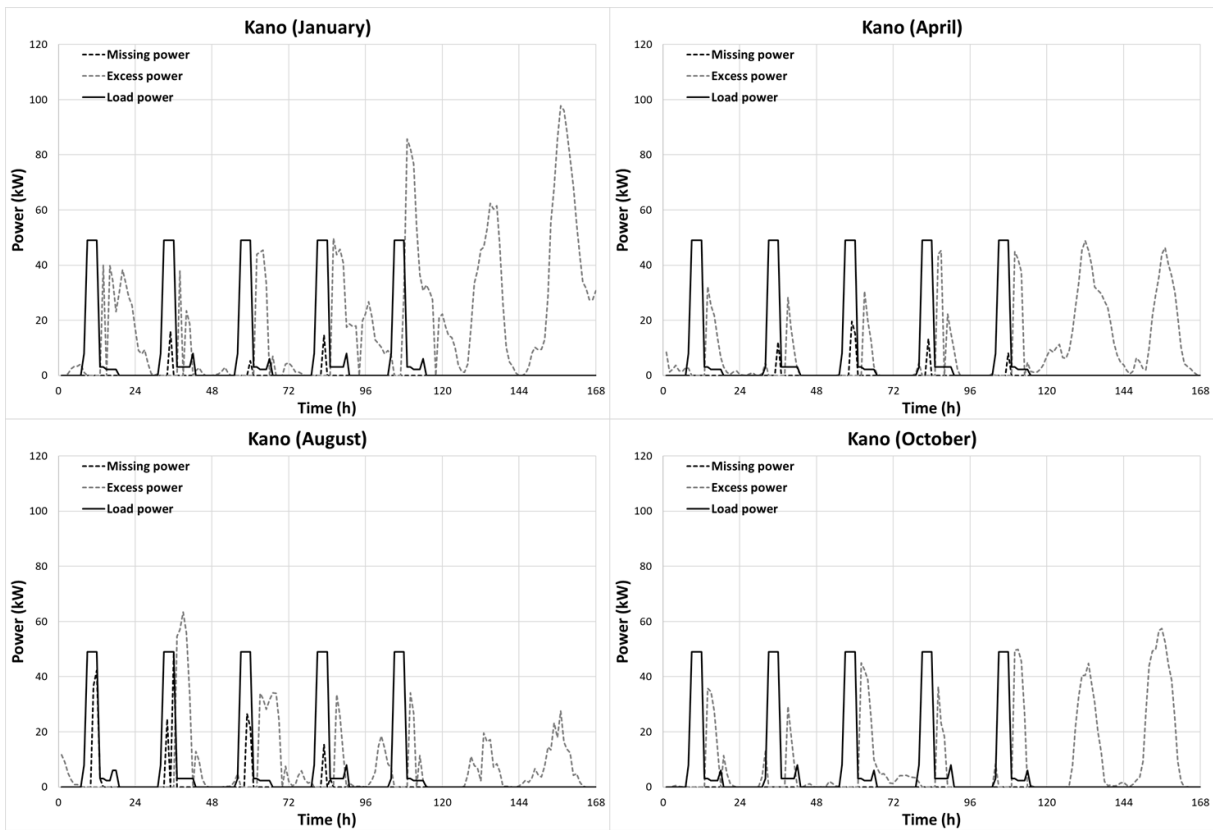system techno-economic performance across Köppen-Geiger climates**

Figure 8. *Winter, spring, summer and autumn weekly hourly trend of the missing, excess and load power in Auckland.*

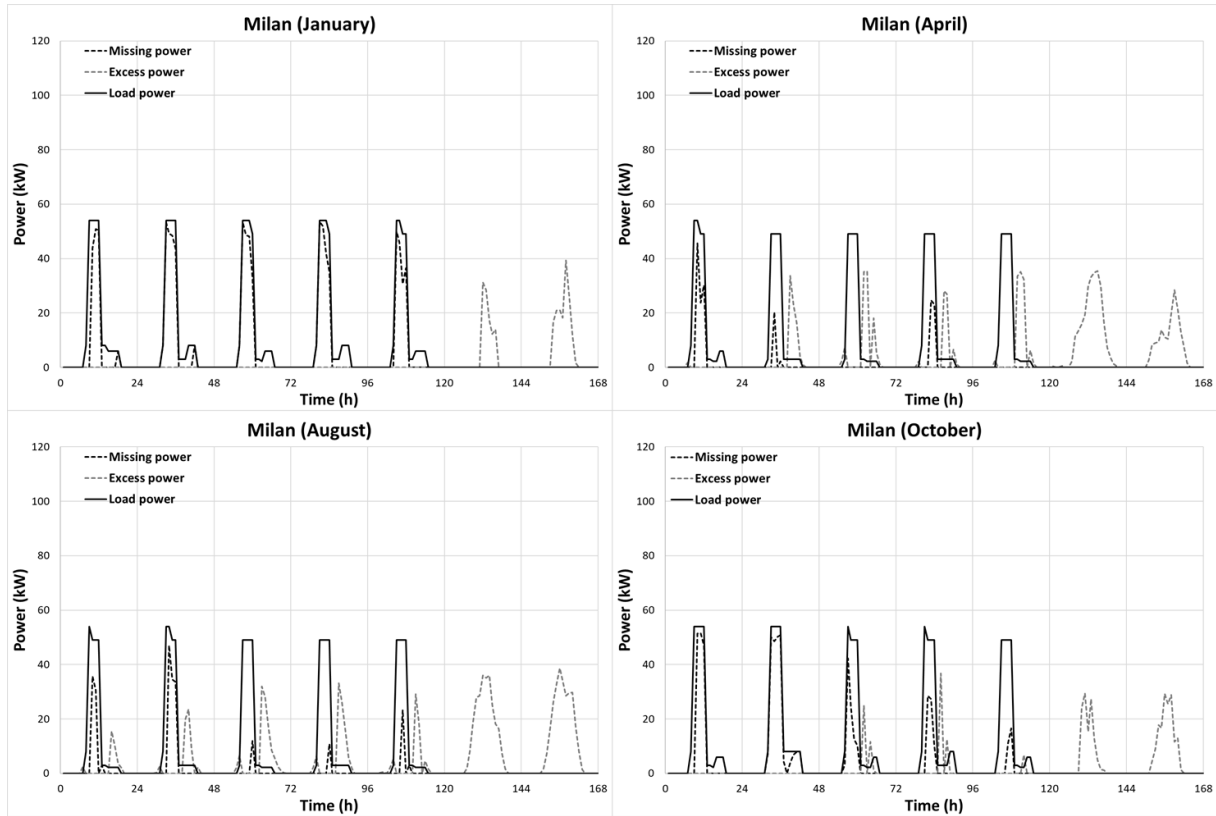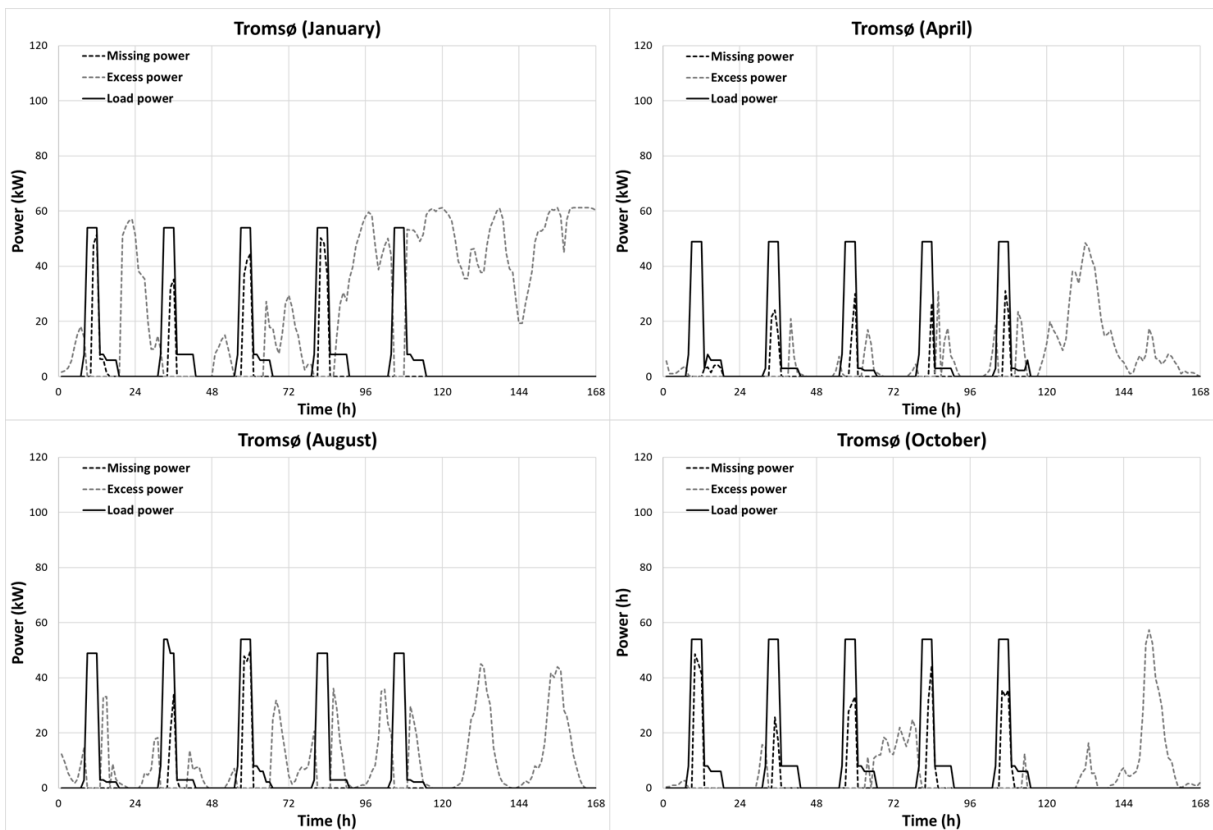**Figure 9.** *Winter, spring, summer and autumn weekly hourly trend of the missing, excess and load power in Kano.*

Chapter 7   **Worldwide geographical mapping and**
optimization of stand-alone and grid-connected hybrid renewable
system techno-economic performance across Köppen-Geiger climates

Figure 10. *Winter, spring, summer and autumn weekly hourly trend of the missing, excess and load power in Milan.*

Figure 11. *Winter, spring, summer and autumn weekly hourly trend of the missing, excess and load power in Tromsø.*

Chapter 7

Worldwide geographical mapping and optimization of stand-alone and grid-connected hybrid renewable system techno-economic performance across Köppen-Geiger climates

5.2. Optimal energetically and economically stand-alone and grid-connected PV-wind HRES across Koppen sub-group climates

The energy and economic optimization algorithms were applied to identify the optimal system power configurations for both SA and GC HRES in each locality. In addition, the most suitable localities to host a SA and GC HRES both from an energy and economic point of view were selected.

For each simulated locality, the energetically and economically optimal power configurations of SA and GC systems are shown in Table 5 and 6, respectively. Also, power fractions p_{pv}, p_w, p_b, p_l and p_{ol}, fractions of wind energy and PV energy generated $e_{g,pv}$ and $e_{g,w}$, energy indicators UF, SLF and GEIF, and economic indicator BCR are reported.

Table 5. Energetically optimal configurations of stand-alone and grid-connected systems.

Locality	Stand-alone system P_{pv} (kW)	P_w (kW)	P_b (kW)	p_{pv} (-)	p_w (-)	p_b (-)	p_l (-)	p_{ol} (-)	$e_{g,pv}$ (-)	$e_{g,w}$ (-)	SLF (-)	UF (-)	BCR (1/yr)	Grid-connected system P_{pv} (kW)	P_w (kW)	P_b (kW)	p_{pv} (-)	p_w (-)	p_b (-)	p_l (-)	p_{ol} (-)	$e_{g,pv}$ (-)	$e_{g,w}$ (-)	SLF (-)	UF (-)	GEIF (-)	BCR (1/yr)
Toamasina	50	10	130	0.83	0.17	0.68	0.11	0.04	0.97	0.03	0.76	0.76	0.019	50	10	130	0.83	0.17	0.68	0.11	0.04	0.97	0.03	0.76	0.76	0.50	0.019
Singapore	50	30	130	0.63	0.38	0.62	0.08	0.03	0.82	0.18	0.70	0.70	0.025	50	10	130	0.83	0.17	0.68	0.11	0.04	0.93	0.07	0.66	0.76	0.56	0.028
Recife	50	10	130	0.83	0.17	0.68	0.11	0.03	0.80	0.20	0.87	0.64	0.021	30	10	130	0.75	0.25	0.76	0.17	0.04	0.70	0.30	0.67	0.72	0.61	0.020
Miami	50	10	130	0.83	0.17	0.68	0.11	0.04	0.79	0.21	0.85	0.68	0.019	50	10	130	0.83	0.17	0.68	0.11	0.04	0.79	0.21	0.85	0.68	0.57	0.036
Lihue	30	10	130	0.75	0.25	0.76	0.17	0.04	0.59	0.41	0.71	0.70	0.063	30	10	130	0.75	0.25	0.76	0.17	0.04	0.59	0.41	0.71	0.70	0.62	0.081
Mombasa	50	10	130	0.83	0.17	0.68	0.11	0.03	0.76	0.24	0.86	0.64	0.029	30	10	130	0.75	0.25	0.76	0.16	0.04	0.66	0.34	0.67	0.72	0.61	0.037
Caracas	70	10	130	0.88	0.13	0.62	0.08	0.03	0.99	0.01	0.80	0.68	0.021	50	10	130	0.83	0.17	0.68	0.11	0.03	0.98	0.02	0.65	0.78	0.55	0.020
Kano	50	10	130	0.83	0.17	0.68	0.11	0.03	0.87	0.13	0.92	0.67	0.011	50	10	130	0.83	0.17	0.68	0.11	0.03	0.87	0.13	0.92	0.67	0.56	0.020
Baghdad	50	10	130	0.83	0.17	0.68	0.11	0.03	0.96	0.04	0.94	0.70	0.028	50	10	130	0.83	0.17	0.68	0.11	0.03	0.96	0.04	0.94	0.70	0.49	0.028
Cairo	50	10	130	0.83	0.17	0.68	0.11	0.03	0.88	0.12	0.91	0.67	0.017	50	10	130	0.83	0.17	0.68	0.11	0.03	0.88	0.12	0.91	0.67	0.56	0.025
Kabul	50	10	130	0.83	0.17	0.68	0.12	0.04	0.95	0.05	0.86	0.67	0.034	30	10	130	0.75	0.25	0.76	0.18	0.04	0.91	0.09	0.64	0.79	0.54	0.031
Baku	50	10	130	0.83	0.17	0.68	0.11	0.04	0.65	0.35	0.74	0.65	0.007	30	10	130	0.75	0.25	0.76	0.17	0.04	0.53	0.47	0.61	0.72	0.64	0.007
Odessa	70	10	130	0.88	0.13	0.62	0.08	0.03	0.82	0.18	0.74	0.59	0.012	30	10	130	0.75	0.25	0.76	0.17	0.04	0.66	0.34	0.51	0.76	0.66	0.015
Maracaibo	70	10	130	0.88	0.13	0.62	0.09	0.03	0.84	0.16	0.81	0.62	0.021	50	10	130	0.83	0.17	0.68	0.12	0.04	0.79	0.21	0.69	0.70	0.62	0.022
Buenos Aires	50	10	130	0.83	0.17	0.68	0.12	0.04	0.80	0.20	0.78	0.62	0.013	30	10	130	0.75	0.25	0.76	0.18	0.04	0.71	0.29	0.60	0.71	0.66	0.014
Milan	90	10	130	0.90	0.10	0.57	0.07	0.03	0.99	0.01	0.74	0.58	0.028	50	10	130	0.83	0.17	0.68	0.11	0.04	0.98	0.02	0.56	0.78	0.61	0.031
Berlin	90	10	130	0.90	0.10	0.57	0.07	0.03	0.78	0.22	0.73	0.54	0.030	50	10	130	0.83	0.17	0.68	0.12	0.04	0.66	0.34	0.60	0.68	0.70	0.040
London	110	10	130	0.92	0.08	0.52	0.06	0.03	0.84	0.16	0.73	0.52	0.025	30	10	130	0.83	0.17	0.68	0.11	0.04	0.70	0.30	0.55	0.73	0.66	0.032
Vancouver	70	10	130	0.88	0.13	0.62	0.08	0.03	0.88	0.12	0.73	0.59	0.011	30	10	130	0.75	0.25	0.76	0.17	0.04	0.76	0.24	0.49	0.79	0.65	0.011
Melbourne	50	10	130	0.83	0.17	0.68	0.11	0.04	0.72	0.28	0.79	0.61	0.030	30	10	130	0.75	0.25	0.76	0.17	0.04	0.61	0.39	0.64	0.70	0.66	0.037
Bogotá	50	10	130	0.83	0.17	0.68	0.11	0.03	0.94	0.06	0.74	0.73	0.027	50	10	130	0.83	0.17	0.68	0.11	0.03	0.94	0.06	0.74	0.73	0.55	0.027
Wellington	50	10	130	0.83	0.17	0.68	0.11	0.04	0.60	0.40	0.80	0.56	0.004	10	10	130	0.50	0.50	0.87	0.33	0.04	0.23	0.77	0.54	0.72	0.69	0.004
Reykjavík	110	10	130	0.92	0.08	0.52	0.06	0.03	0.71	0.29	0.71	0.45	0.009	30	10	130	0.75	0.25	0.76	0.17	0.04	0.40	0.60	0.52	0.69	0.73	0.013
Auckland	30	10	130	0.75	0.25	0.76	0.18	0.04	0.49	0.51	0.73	0.64	0.007	10	10	130	0.50	0.50	0.87	0.35	0.05	0.24	0.76	0.55	0.71	0.69	0.007
Rome	50	10	130	0.83	0.17	0.68	0.11	0.04	0.87	0.13	0.78	0.70	0.039	50	10	130	0.83	0.17	0.68	0.11	0.04	0.87	0.13	0.78	0.70	0.58	0.043
Adelaide	50	10	130	0.83	0.17	0.68	0.12	0.04	0.80	0.20	0.85	0.62	0.048	30	10	130	0.75	0.25	0.76	0.17	0.04	0.70	0.30	0.66	0.72	0.61	0.053
Porto	50	10	130	0.83	0.17	0.68	0.12	0.04	0.73	0.27	0.75	0.57	0.029	30	10	130	0.75	0.25	0.76	0.18	0.04	0.62	0.38	0.61	0.67	0.71	0.039
La Coruna	90	10	130	0.90	0.10	0.57	0.07	0.03	0.90	0.10	0.74	0.52	0.020	30	10	130	0.75	0.25	0.76	0.18	0.04	0.75	0.25	0.44	0.78	0.69	0.020
New Delhi	50	10	130	0.83	0.17	0.68	0.11	0.03	0.99	0.01	0.85	0.73	0.019	50	10	130	0.83	0.17	0.68	0.11	0.03	0.99	0.01	0.85	0.73	0.48	0.022
Hong Kong	50	10	130	0.83	0.17	0.68	0.11	0.04	0.67	0.33	0.74	0.66	0.025	30	10	130	0.75	0.25	0.76	0.17	0.04	0.55	0.45	0.59	0.73	0.65	0.032
Johannesburg	30	30	130	0.50	0.50	0.68	0.11	0.03	0.66	0.34	0.76	0.65	0.013	30	10	130	0.75	0.25	0.76	0.17	0.04	0.85	0.15	0.67	0.75	0.56	0.014
Nairobi	50	10	130	0.83	0.17	0.68	0.11	0.04	0.76	0.24	0.82	0.63	0.028	30	10	130	0.75	0.25	0.76	0.17	0.04	0.65	0.35	0.65	0.71	0.63	0.036
Bucharest	70	10	130	0.88	0.13	0.62	0.09	0.03	0.93	0.07	0.73	0.62	0.021	50	10	130	0.83	0.17	0.68	0.12	0.04	0.91	0.09	0.64	0.74	0.60	0.021
Toronto	50	10	130	0.83	0.17	0.68	0.11	0.04	0.73	0.27	0.78	0.64	0.018	30	10	130	0.75	0.25	0.76	0.17	0.04	0.61	0.39	0.62	0.72	0.63	0.027
Moskva	110	30	130	0.79	0.21	0.48	0.05	0.03	0.96	0.04	0.70	0.51	0.008	50	50	130	0.50	0.50	0.57	0.07	0.03	0.88	0.12	0.52	0.76	0.65	0.008
Ottawa	50	10	130	0.83	0.17	0.68	0.12	0.04	0.83	0.17	0.75	0.68	0.018	30	10	130	0.75	0.25	0.76	0.18	0.04	0.74	0.26	0.57	0.77	0.61	0.023
Tromsø	110	30	130	0.79	0.21	0.48	0.05	0.03	0.55	0.45	0.71	0.44	0.012	50	10	130	0.83	0.17	0.68	0.12	0.04	0.62	0.38	0.47	0.74	0.71	0.013
Anchorage	90	30	130	0.75	0.25	0.52	0.06	0.03	0.72	0.28	0.71	0.48	0.023	50	10	130	0.83	0.17	0.68	0.12	0.04	0.81	0.19	0.51	0.71	0.71	0.026
Oymyakon	70	10	130	0.88	0.13	0.62	0.09	0.03	0.97	0.03	0.70	0.56	0.009	30	10	130	0.75	0.25	0.76	0.17	0.04	0.94	0.06	0.44	0.79	0.68	0.009
Verhojansk	110	50	130	0.69	0.31	0.45	0.04	0.02	0.78	0.22	0.71	0.34	0.006	30	10	130	0.75	0.25	0.76	0.17	0.04	0.83	0.17	0.41	0.76	0.73	0.008
Hakkâri	50	10	130	0.83	0.17	0.68	0.12	0.04	0.97	0.03	0.78	0.72	0.022	50	10	130	0.83	0.17	0.68	0.12	0.04	0.97	0.03	0.78	0.72	0.54	0.031
Dras	50	10	130	0.83	0.17	0.68	0.11	0.04	0.96	0.04	0.74	0.68	0.011	30	10	130	0.75	0.25	0.76	0.17	0.04	0.93	0.07	0.53	0.80	0.61	0.011
Flagstaff	30	30	130	0.50	0.50	0.68	0.11	0.03	0.68	0.32	0.76	0.68	0.018	30	10	130	0.75	0.25	0.76	0.17	0.04	0.86	0.14	0.67	0.77	0.55	0.021
Beijing	50	30	130	0.63	0.38	0.62	0.09	0.03	0.73	0.27	0.71	0.64	0.015	50	10	130	0.83	0.17	0.68	0.12	0.04	0.89	0.11	0.65	0.72	0.62	0.024
Seoul	70	10	130	0.88	0.13	0.62	0.09	0.03	0.92	0.08	0.72	0.65	0.011	50	10	130	0.83	0.17	0.68	0.11	0.04	0.89	0.11	0.61	0.75	0.61	0.011
Pyongyang	70	10	130	0.88	0.13	0.62	0.09	0.03	0.96	0.04	0.75	0.64	0.006	50	10	130	0.83	0.17	0.68	0.11	0.04	0.95	0.05	0.63	0.74	0.61	0.006
Vladivostok	50	10	130	0.83	0.17	0.68	0.12	0.04	0.79	0.21	0.74	0.62	0.008	30	10	130	0.75	0.25	0.76	0.18	0.04	0.69	0.31	0.58	0.72	0.66	0.008

Table 5 highlights that the most suitable locality energetically to install a SA HRES is Toamasina with a UF of 0.76, while to install a GC HRES is New Delhi with a GEIF of 0.48. However, they present a low BCR of 0.019 and 0.022, respectively. Also New Delhi, Bogotà and Hakkari have very high energy performance for SA installations, while Baghdad and Toamasina for GC installations. The

Chapter 7

Worldwide geographical mapping and optimization of stand-alone and grid-connected hybrid renewable system techno-economic performance across Köppen-Geiger climates

worst energetically locality for a SA HRES is Verhojansk with a UF of 0.34, while for a GC HRES are Verhojansk and Reykjavík with a GEIF of 0.73.

Among the energetically optimal SA configurations, the highest profitability is reached in Cambridge Bay with a BCR=0.075 and corresponding low values of UF equal to 0.44. The lowest BCR of 0.004 is highlighted in Wellington that shows a UF of 0.56. Among the energetically optimal GC configurations, the highest profitability is reached in Cambridge Bay with a BCR=0.099 and corresponding GEIF of 0.71. The lowest BCR of 0.004 is highlighted in Wellington that shows a GEIF of 0.69. Both for SA and GC HRES, the profitability in Lihue is very close to the highest obtained.

By considering 48 optimal SA HRES, only 2.1% of localities (Cambridge Bay) comply with the condition BCR>0.1 and only 10.4% of localities (the previous one and Lihue, Adelaide, Rome and Kabul) with the condition BCR>1/30. It highlights that without economic optimization, only in a few climatic conditions the capital cost can be recovered before the investment lifespan. Instead, by considering 48 optimal GC HRES, 4.2% of localities (Cambridge Bay and Lihue) comply with the condition BCR>0.1 and 20.8% of localities (the previous one and Adelaide, Rome, Berlin, Porto, Mombasa, Melbourne, Miami and Nairobi) with the condition BCR>1/30. This highlights the important role of FiT policy also without any economic optimization.

Table 6 highlights that the most suitable locality economically to install a SA HRES is Cambridge Bay with a BCR of 0.111, while to install a GC HRES is Lihue with a BCR of 0.243.

Table 6. Economically optimal configurations of stand-alone and grid-connected systems.

Locality	Stand-alone system													Grid-connected system													
	P_{pv} (kW)	P_w (kW)	P_b (kW)	p_{pv} (-)	p_w (-)	p_b (-)	p_l (-)	p_{ol} (-)	$e_{g,pv}$ (-)	$e_{g,w}$ (-)	SLF (-)	UF (-)	BCR (1/yr)	P_{pv} (kW)	P_w (kW)	P_b (kW)	p_{pv} (-)	p_w (-)	p_b (-)	p_l (-)	p_{ol} (-)	$e_{g,pv}$ (-)	$e_{g,w}$ (-)	SLF (-)	UF (-)	GEIF (-)	BCR (1/yr)
Toamasina	50	10	90	0.83	0.17	0.60	0.11	0.05	0.97	0.03	0.73	0.73	0.019	50	10	90	0.83	0.17	0.60	0.11	0.05	0.97	0.03	0.73	0.73	0.56	0.019
Singapore	70	10	130	0.88	0.13	0.62	0.08	0.03	0.95	0.05	0.81	0.68	0.029	70	10	130	0.88	0.13	0.62	0.08	0.03	0.95	0.05	0.81	0.68	0.60	0.029
Recife	50	10	130	0.83	0.17	0.68	0.11	0.03	0.80	0.20	0.87	0.64	0.021	50	10	130	0.83	0.17	0.68	0.11	0.03	0.80	0.20	0.87	0.64	0.66	0.021
Miami	50	10	130	0.83	0.17	0.68	0.11	0.04	0.79	0.21	0.85	0.68	0.019	10	130	10	0.07	0.93	0.07	0.05	0.04	0.06	0.94	0.62	0.17	3.50	0.121
Lihue	10	30	130	0.25	0.75	0.76	0.17	0.04	0.14	0.86	0.72	0.49	0.067	10	130	10	0.07	0.93	0.07	0.05	0.05	0.04	0.96	0.73	0.13	5.52	0.243
Mombasa	50	10	130	0.83	0.17	0.68	0.11	0.03	0.76	0.24	0.86	0.64	0.029	10	130	10	0.07	0.93	0.07	0.05	0.04	0.05	0.95	0.54	0.12	4.53	0.103
Caracas	70	10	130	0.88	0.13	0.62	0.08	0.03	0.99	0.01	0.80	0.68	0.021	70	10	130	0.88	0.13	0.62	0.08	0.03	0.99	0.01	0.80	0.68	0.60	0.021
Kano	50	10	130	0.83	0.17	0.68	0.11	0.03	0.87	0.13	0.92	0.67	0.011	130	130	10	0.50	0.50	0.04	0.03	0.02	0.57	0.43	0.94	0.17	4.90	0.043
Baghdad	50	10	110	0.83	0.17	0.65	0.11	0.04	0.96	0.04	0.92	0.69	0.028	50	10	110	0.83	0.17	0.65	0.11	0.04	0.96	0.04	0.92	0.69	0.53	0.028
Cairo	50	10	110	0.83	0.17	0.65	0.11	0.04	0.88	0.12	0.89	0.66	0.017	130	10	10	0.93	0.07	0.07	0.05	0.04	0.95	0.05	0.93	0.28	2.53	0.043
Kabul	50	10	90	0.83	0.17	0.60	0.12	0.05	0.95	0.05	0.82	0.63	0.034	50	10	90	0.83	0.17	0.60	0.12	0.05	0.95	0.05	0.82	0.63	0.69	0.034
Baku	10	30	130	0.25	0.75	0.76	0.17	0.04	0.11	0.89	0.64	0.48	0.007	10	30	130	0.25	0.75	0.76	0.17	0.04	0.11	0.89	0.64	0.48	1.11	0.007
Odessa	50	10	130	0.83	0.17	0.68	0.11	0.04	0.77	0.23	0.65	0.68	0.013	10	130	10	0.07	0.93	0.07	0.05	0.04	0.05	0.95	0.46	0.15	3.34	0.042
Maracaibo	50	10	130	0.83	0.17	0.68	0.12	0.04	0.79	0.21	0.69	0.70	0.022	50	10	130	0.83	0.17	0.68	0.12	0.04	0.79	0.21	0.69	0.70	0.62	0.022
Buenos Aires	50	10	130	0.83	0.17	0.68	0.12	0.04	0.80	0.20	0.78	0.62	0.013	10	130	10	0.07	0.93	0.07	0.05	0.05	0.06	0.94	0.50	0.14	3.62	0.015
Milan	70	10	130	0.88	0.13	0.62	0.09	0.03	0.99	0.01	0.67	0.67	0.029	90	10	90	0.90	0.10	0.47	0.07	0.04	0.99	0.01	0.70	0.55	0.92	0.033
Berlin	10	30	130	0.25	0.75	0.76	0.18	0.04	0.11	0.89	0.51	0.50	0.036	10	130	10	0.07	0.93	0.07	0.05	0.05	0.03	0.97	0.52	0.13	4.23	0.118
London	10	50	130	0.17	0.83	0.68	0.11	0.04	0.08	0.92	0.55	0.44	0.032	10	130	10	0.07	0.93	0.07	0.05	0.03	0.03	0.97	0.46	0.15	3.34	0.057
Vancouver	50	10	130	0.83	0.17	0.68	0.11	0.04	0.84	0.16	0.65	0.70	0.011	50	10	130	0.83	0.17	0.68	0.11	0.04	0.84	0.16	0.65	0.70	0.65	0.011
Melbourne	10	30	130	0.25	0.75	0.76	0.17	0.04	0.15	0.85	0.62	0.49	0.030	10	130	10	0.07	0.93	0.07	0.05	0.04	0.04	0.96	0.60	0.12	4.95	0.100
Bogotá	50	10	110	0.83	0.17	0.65	0.11	0.04	0.94	0.06	0.72	0.71	0.027	50	10	110	0.83	0.17	0.65	0.11	0.04	0.94	0.06	0.72	0.71	0.59	0.027
Wellington	10	30	130	0.25	0.75	0.76	0.17	0.04	0.09	0.91	0.75	0.39	0.005	10	30	130	0.25	0.75	0.76	0.17	0.04	0.09	0.91	0.75	0.39	1.47	0.005
Reykjavík	10	30	130	0.25	0.75	0.76	0.17	0.04	0.07	0.93	0.64	0.44	0.016	10	30	130	0.25	0.75	0.76	0.17	0.04	0.07	0.93	0.64	0.44	1.24	0.016
Auckland	10	30	130	0.25	0.75	0.76	0.18	0.04	0.10	0.90	0.77	0.39	0.008	10	30	130	0.25	0.75	0.76	0.18	0.04	0.10	0.90	0.77	0.39	1.49	0.008
Rome	50	10	130	0.83	0.17	0.68	0.11	0.04	0.87	0.13	0.78	0.70	0.039	70	10	10	0.88	0.13	0.11	0.08	0.08	0.90	0.10	0.64	0.42	1.30	0.045
Adelaide	50	10	110	0.83	0.17	0.65	0.12	0.04	0.80	0.20	0.82	0.61	0.048	10	130	10	0.07	0.93	0.07	0.05	0.05	0.06	0.94	0.48	0.13	4.07	0.078
Porto	10	30	130	0.25	0.75	0.76	0.18	0.04	0.15	0.85	0.59	0.48	0.029	10	130	10	0.07	0.93	0.07	0.05	0.04	0.04	0.96	0.53	0.11	4.95	0.114
La Coruña	50	10	130	0.83	0.17	0.68	0.12	0.04	0.83	0.17	0.59	0.69	0.022	50	10	130	0.83	0.17	0.68	0.12	0.04	0.83	0.17	0.59	0.69	0.70	0.022
New Delhi	50	10	130	0.83	0.17	0.68	0.11	0.04	0.99	0.01	0.85	0.73	0.019	130	10	10	0.93	0.07	0.07	0.05	0.04	1.00	0.00	0.87	0.29	2.40	0.028
Hong Kong	10	30	130	0.25	0.75	0.76	0.17	0.04	0.12	0.88	0.62	0.50	0.027	10	130	10	0.07	0.93	0.07	0.05	0.05	0.03	0.97	0.62	0.13	4.91	0.094
Johannesburg	50	10	110	0.83	0.17	0.65	0.11	0.04	0.91	0.09	0.89	0.63	0.016	50	10	110	0.83	0.17	0.65	0.11	0.04	0.91	0.09	0.89	0.63	0.67	0.016
Nairobi	50	10	130	0.83	0.17	0.68	0.11	0.04	0.76	0.24	0.82	0.63	0.028	10	130	10	0.07	0.93	0.07	0.05	0.05	0.05	0.95	0.56	0.13	4.42	0.102
Bucharest	50	10	90	0.83	0.17	0.60	0.12	0.05	0.91	0.09	0.60	0.69	0.021	50	10	90	0.83	0.17	0.60	0.12	0.05	0.91	0.09	0.60	0.69	0.68	0.021
Toronto	50	10	130	0.83	0.17	0.68	0.11	0.04	0.73	0.27	0.78	0.64	0.018	10	130	10	0.07	0.93	0.07	0.05	0.04	0.06	0.94	0.57	0.12	4.64	0.091
Moskva	70	10	130	0.88	0.13	0.62	0.09	0.03	0.98	0.02	0.59	0.69	0.010	70	10	130	0.88	0.13	0.62	0.09	0.03	0.98	0.02	0.59	0.69	0.70	0.010
Ottawa	50	10	130	0.83	0.17	0.68	0.12	0.04	0.83	0.17	0.75	0.68	0.018	130	130	10	0.50	0.50	0.004	0.03	0.03	0.49	0.51	0.86	0.18	4.39	0.059
Tromsø	10	30	130	0.25	0.75	0.76	0.17	0.04	0.10	0.90	0.46	0.57	0.016	10	30	130	0.25	0.75	0.76	0.17	0.04	0.10	0.90	0.46	0.57	0.92	0.016
Anchorage	50	30	130	0.63	0.38	0.62	0.09	0.03	0.59	0.41	0.60	0.61	0.026	50	30	130	0.63	0.38	0.62	0.09	0.03	0.59	0.41	0.60	0.61	0.81	0.026
Oymyakon	50	10	110	0.83	0.17	0.65	0.11	0.04	0.96	0.04	0.59	0.66	0.010	50	10	110	0.83	0.17	0.65	0.11	0.04	0.96	0.04	0.59	0.66	0.73	0.010
Verhojansk	50	10	130	0.83	0.17	0.68	0.11	0.04	0.89	0.11	0.52	0.63	0.008	50	10	130	0.83	0.17	0.68	0.11	0.04	0.89	0.11	0.52	0.63	0.80	0.008
Hakkâri	50	10	90	0.83	0.17	0.60	0.12	0.05	0.97	0.03	0.74	0.69	0.022	130	10	10	0.93	0.07	0.07	0.05	0.05	0.99	0.01	0.84	0.30	2.19	0.059
Cambridge Bay	10	30	130	0.25	0.75	0.76	0.18	0.04	0.09	0.91	0.70	0.41	0.111	10	30	130	0.25	0.75	0.76	0.18	0.04	0.09	0.91	0.70	0.41	1.37	0.111
Dras	50	10	90	0.83	0.17	0.60	0.11	0.05	0.96	0.04	0.69	0.64	0.011	130	10	10	0.93	0.07	0.07	0.05	0.05	0.98	0.02	0.80	0.29	2.26	0.021

Flagstaff	50	10	110	0.83	0.17	0.65	0.11	0.04	0.91	0.09	0.88	0.63	0.021	70	10	10	0.88	0.13	0.11	0.08	0.07	0.94	0.06	0.74	0.39	1.49	0.026
Beijing	50	10	110	0.83	0.17	0.65	0.12	0.04	0.89	0.11	0.64	0.70	0.017	130	10	10	0.93	0.07	0.07	0.05	0.05	0.96	0.04	0.71	0.32	1.88	0.043
Seoul	50	10	130	0.83	0.17	0.68	0.11	0.04	0.89	0.11	0.61	0.75	0.011	50	10	130	0.83	0.17	0.68	0.11	0.04	0.89	0.11	0.61	0.75	0.61	0.011
Pyongyang	70	10	130	0.88	0.13	0.62	0.09	0.03	0.96	0.04	0.75	0.64	0.006	70	10	130	0.88	0.13	0.62	0.09	0.03	0.96	0.04	0.75	0.64	0.70	0.006
Vladivostok	50	10	130	0.83	0.17	0.68	0.12	0.04	0.79	0.21	0.74	0.62	0.008	50	10	130	0.83	0.17	0.68	0.12	0.04	0.79	0.21	0.74	0.62	0.74	0.008

However, the first one presents a low UF of 0.41, while the second one a very high GEIF of 5.52. Also Lihue, Adelaide, Rome, Berlin and Kabul achieve high profitability for SA installations, while Miami, Berlin, Porto and Cambridge Bay for GC installations. The worst economically locality is Wellington with a BCR of 0.05 for both SA and GC HRES.

Among the economically optimal SA configurations, the highest energy performance is reached in Seoul with a UF=0.75 and corresponding low value of BCR equal to 0.011. The lowest UF of 0.39 is highlighted in Wellington and Auckland Islands that show low values of BCR of 0.005 and 0.008, respectively. Among the economically optimal GC configurations, the highest energy performance is reached in Baghdad with a GEIF=0.53 and corresponding low BCR of 0.028. The highest GEIF of 5.52 is highlighted in Lihue that show the highest BCR of 0.243. For SA HRES, energy performance in Toamasina and New Delhi are very close to the highest obtained, while for GC HRES, in Toamasina, Bogotà, Singapore and Caracas.

By considering 48 optimal SA HRES, only 4.2% of localities (Cambridge Bay and Lihue) comply with the condition BCR>0.1 and only 12.5% of localities (the previous one and Adelaide, Rome, Berlin and Kabul) with the condition BCR>1/30. This highlights that without an economic subsidy, only in favourable climatic conditions the capital cost can be recovered before the investment lifespan. Instead, by considering 48 optimal GC HRES, 22.9% of localities (Lihue, Miami, Berlin, Porto, Cambridge Bay, Mombasa, Nairobi, Melbourne, Hong Kong, Toronto and Adelaide) comply with the condition BCR>0.1 and only 41.7% of localities (the previous one and Ottawa, Hakkary, London, Rome, Beijing, Cairo, Kano, Odessa and Kabul) with the condition BCR>1/30. This highlights the important role of FiT policy.

Further graphical elaboration of data included in Tables 4 and 5 are shown in the Data in Brief related to this paper.

With reference to Table 5, for both system modes, in all locations, the energetically optimal configurations include maximum storage capacity (130 kWh) and almost all include minimum wind power (10 kW), with a few exceptions of 30-50 kW in cold locations for SA systems and one exception for GC systems in Moscow with 50 kW. The PV energy is very variable between 30 kW and 110 kW in the SA systems, but no energetically optimal systems have the minimum or maximum power, while in GC ones the range of variation is greatly reduced between 10 kW and 50 kW, allowing wind power to play a more central role. The contribution of the grid permits the setting up of small-scale systems, especially for the PV system.

With reference to Table 6, the economically SA optimal configurations compared to the energetically optimal ones leads, in some localities, to a reduction of the PV power installed that ranges between 10 kW and 50 kW, an increase of the wind power installed that varies between 10 kW and 50 kW, with many localities at 30 kW, and the battery storage is not always the highest and reach also 90 kWh. For GC systems, the economic optimization compared to the energy one leads to unpredictable behaviour with all system components that assume values variable between the minimum and maximum in the different locality. This is owing to the high variability, in addition to that of the electricity price, also that of the FiT. The maximum overall nominal power of system components is required in Verhojansk (290 kW) and Moskva (230 kW) for energetically optimal SA and GC HRES, respectively, while in Singapore, Caracas, Milan, Anchorage, Moskva and Pyongyang

Chapter 7   **Worldwide geographical mapping and**
optimization of stand-alone and grid-connected hybrid renewable
system techno-economic performance across Köppen-Geiger climates

(210 kW) for the economically optimal SA HRES and in Kano and Ottawa (270) for the economically optimal GC HRES.

For both energetically optimal SA and GC systems, the wind power fraction never exceeds 50%, confirming that PV also prevails in terms of installed power. For SA systems, Johannesburg and Flagstaff achieve the greatest balance between PV and wind power (50%). For GC systems, the higher presence of wind power is confirmed, reaching 50% in the windiest locations (Auckland, Wellington, Cambridge Bay and Moscow). Therefore, PV is confirmed as the predominant component for energetically optimal HRES, while wind power is mainly boosted in areas where better availability of the wind resource is guaranteed. As regards economically optimal SA and GC HRES, the wind power fraction exceeds 50% in 12 and 19 localities, respectively. For GC HRES, some localities reach very high wind power fractions until 0.93, similarly to the energetically optimal SA HRES for the PV power fraction.

The energy optimization results have highlighted a consistent use of storage systems, leading the nominal value of the battery always to the maximum level (130 kWh), both for SA and GC systems and all locations. The battery power fraction gives an idea of the importance of the storage system in the HRES. The results highlight that the battery plays an important role in both energetically optimal SA and GC systems. The maximum battery power in GC systems is owing to the lower installed PV and wind power obtained by the energy optimization compared to SA systems. Auckland has the highest battery power fraction for both system modes. For SA systems, lower battery power fractions are observed in some localities belonging to groups C and D. For GC systems, more uniform values are highlighted and, in some cases, the trends are overturned considering that the highest values occur in groups C and D. The economic optimization highlights that the optimal SA HRES can assume higher or lower battery power fractions compared to the energetically optimal ones; instead, for the optimal GC HRES, they undergo a strong reduction in the localities with FiT available since it is preferable to produce energy in excess to be sold to the grid rather than to store a high quantity of energy when an acceptable level of energy required by the load is already satisfied.

The load power fraction permits to verify where the installed power of the system is greater than the yearly average hourly power required by the load. All load power fraction values are less than 1, which means that the installed powers are higher than the yearly average hourly power required by the load. For the energetically optimal HRES, the highest values are observed in the windiest localities, such as Lihue, which is also very sunny, for the SA systems, Wellington and Cambridge Bay, for the GC systems, and Auckland, for both system modes. GC systems have higher load power fractions since they have less installed power. The sunniest locations tend to have the lowest load power fractions. For the economically optimal SA HRES, a global slight increase is observed for the load power fraction, compared to the energetically optimal one, owing to the reduction of the PV and, somewhere, battery power installed. The unpredictable variation of the power installed in the economically optimal GC HRES, compared to the energetically optimal ones, is also reflected in the load power fraction.

Figure 12 and 13 show the energy generated by the PV and wind system for all 48 locations, respectively for the energetically and economically optimal SA and GC HRES.

As expected, the PV and wind generated energies vary with the location, depending on the renewable sources available.

For the energetically optimal HRES, PV energy is predominant in almost all locations. For the 48 locations, this is verified mainly for SA systems and less for GC systems. In SA systems, the only

Chapter 7

Worldwide geographical mapping and optimization of stand-alone and grid-connected hybrid renewable system techno-economic performance across Köppen-Geiger climates

location where wind power slightly prevails over PV is Auckland, namely the windiest location, while in New Delhi and Caracas the wind contribution is almost zero. In GC systems, the fraction of wind energy generated increases giving rise to a prevalence of wind energy in the first four windiest locations, Auckland (this time considerably), Reykjavik, Cambridge Bay and Wellington. GC systems have lower net energy production than SA ones as they have grid support.

For SA systems, locations not particularly sunny, such as Verhojansk, Vladivostok, Milan and La Coruna, have the highest PV energy produced. The largest production of wind energy occurs in Tromsø, Auckland, Wellington and Cambridge Bay. Specifically, Auckland is the windiest but not particularly sunny location and Tromsø is a very little sunny and not particularly windy location. However, both localities have the best balance between PV and wind; Tromsø is one of the locations with the highest nominal PV power. For GC systems, the largest PV energy production comes from the hottest locations (Baghdad, Kano, Cairo, New Delhi), while the highest wind power generation comes from the more windy ones (Auckland, Wellington, Cambridge Bay and Reykjavik) and exceeds the PV one.

Chapter 7

Worldwide geographical mapping and optimization of stand-alone and grid-connected hybrid renewable system techno-economic performance across Köppen-Geiger climates
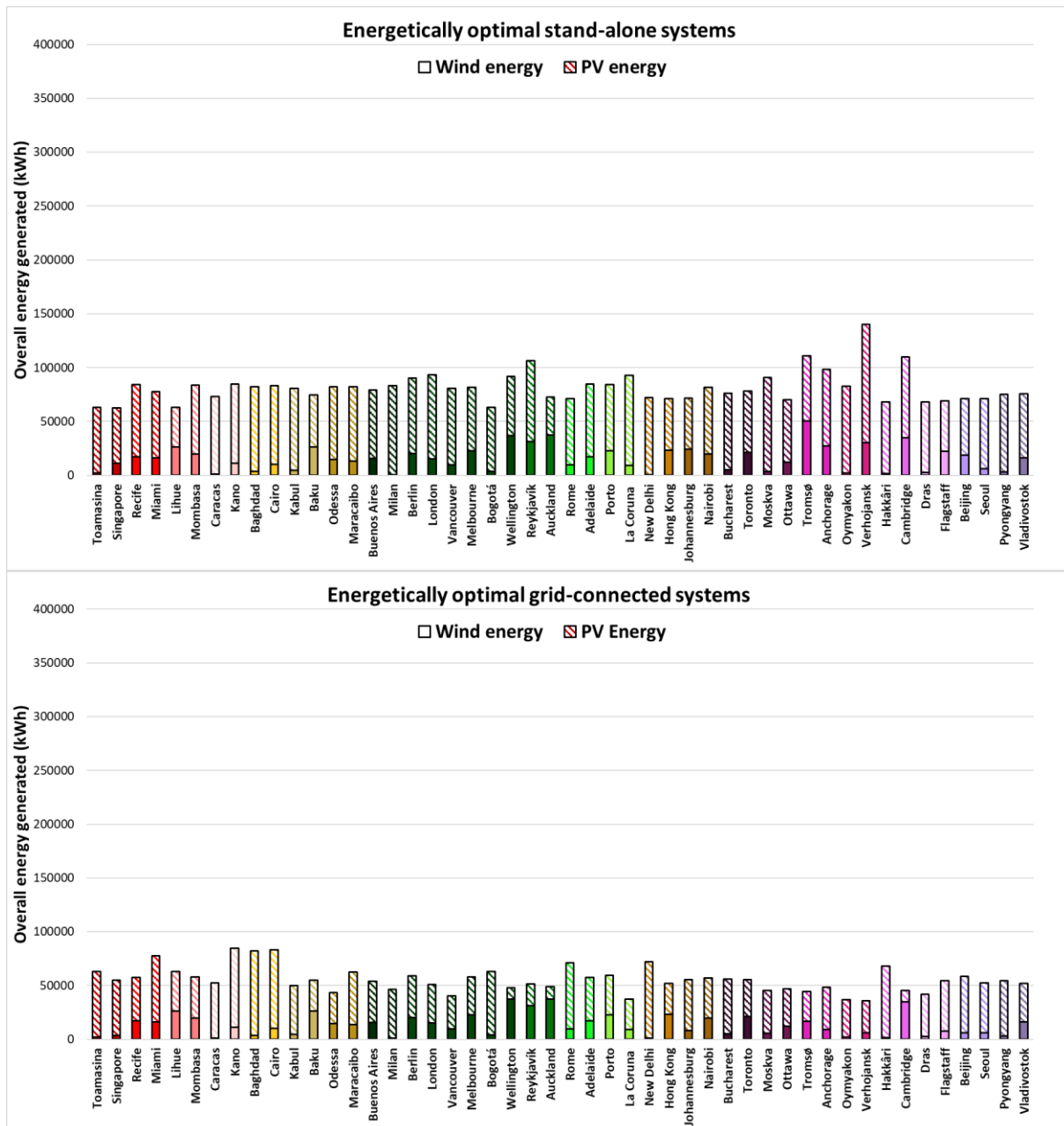
Figure 12. Overall energy generated by the energetically optimal stand-alone and grid-connected systems.
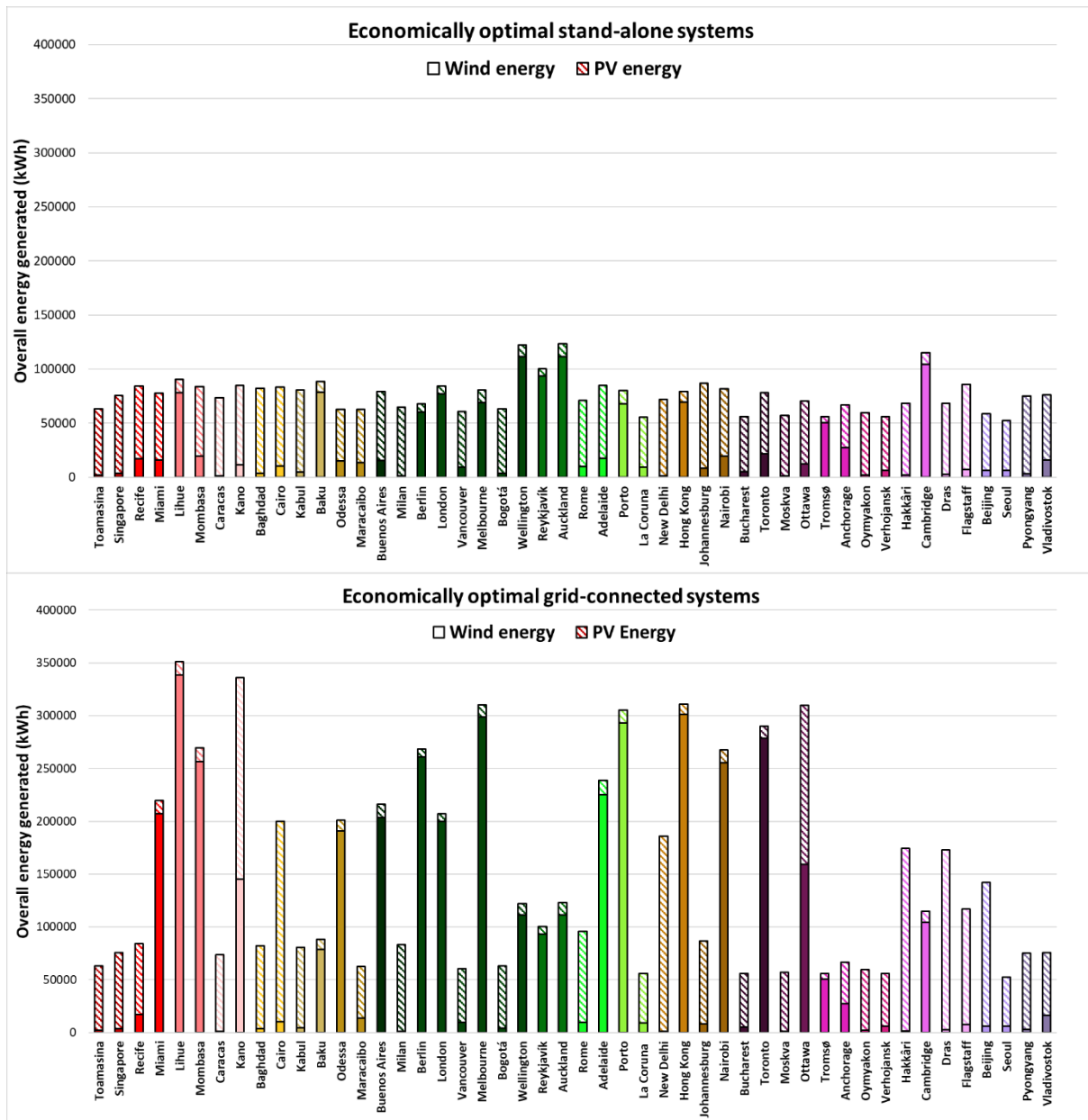
Figure 13. *Overall energy generated by the economically optimal stand-alone and grid-connected systems.*

The location with the best balance between wind and PV is Baku. The results show how, in the energy optimization of SA systems, climate data strongly influence the system power design. Less sunny locations require higher nominal PV powers. The grid provides fundamental support that makes system production less central. In terms of overall energy production, for SA systems, the largest energy production comes from medium windy and less sunny locations (Verhojansk, Cambridge Bay, Tromsø, Reykjavik). In these locations, optimization provides both high nominal PV powers to compensate for the low sun exposure and high nominal wind power to better exploit this source. In GC systems, it is evident that the sunniest locations produce most of the energy (Kano, Cairo, Baghdad, Miami, New Delhi, Rome and Hakkâri). In general, in terms of climate zones, it can be concluded that, for SA HRES, the energy production is quite uniform in groups A and B and it is

Chapter 7

Worldwide geographical mapping and optimization of stand-alone and grid-connected hybrid renewable system techno-economic performance across Köppen-Geiger climates

rather variable in groups C and D. For GC systems, groups A and B have generally higher energy production than that of groups C and D.

For the economically optimal HRES, SA produced energy is quite similar to that of the energetically optimal ones with a strong increase of wind energy produced in some localities. Instead, in the locality with the FiT subsidy, GC system energy production is strongly higher than the energetically optimal GC HRES. In this case, in addition to climate conditions, electricity and FiT prices define optimal power configurations.

The difference between the calculated fractions in terms of installed PV and wind power and PV and wind energy is the effective exploitation of the sources. For example, for energetically optimal GC systems, the PV and wind power fractions have the same value in Cambridge Bay and Moscow (i.e., PV and wind have the same installed power) but, in terms of energy generated, the PV one prevails in Moscow while the wind one prevails in Cambridge Bay.

For all optimal systems, the PV energy fraction and the wind energy fraction closely follow the results obtained for the PV and wind power fractions.

In energetically optimal SA systems, Auckland, the windiest location, is the only location where the wind energy fraction exceeds 50%. In energetically optimal GC systems, wind energy fraction becomes slightly prevalent and, in addition to Auckland, Reykjavik, Wellington and Cambridge Bay present a wind energy fraction greater than 50%. In economically optimal SA and GC systems, the wind energy fraction exceeds 50% in many locations. In this case, the optimal systems turned out less balanced compared to the energetically optimal systems since very high PV and wind fractions are observed. This is especially highlighted in GC systems, where produced energy consists of almost entirely of wind energy or PV energy.

By ordering the wind and solar energy fractions from the windiest locality until to the least windy locality, for the energetically optimal SA systems and especially for GC systems, wind energy is more prevalent in windy locations. This is not so obvious, considering that the same behaviour is not valid for PV energy in locations ordered from the sunniest to the least sunny. For the energetically optimal HRES, the predominant presence of PV power compared to the wind one does not allow to distinguish a scheme in terms of PV energy fraction if the locations are ordered in terms of average solar radiation. By performing the same analysis after an economic optimization, the windiest locations do not lead to the highest wind energy fraction and the sunniest localities to the highest PV energy fraction. This confirms that the wind and PV energy produced by an economically optimal system cannot previously qualitatively detected as a function of the source predominance in a specific locality.

The energy required by the load is supplied by the SA and GC HRES in accordance with the energy balances set out in Section 2.2.2. The graphs in Figures 14 and 15 highlight, respectively, for the energetically and economically optimal HRES, the main energy contributions, i.e. for the GC system, the energy sent directly to the load E_{dtl}, the energy coming from the battery E_{fb}, the energy coming from the grid E_{fg} and the energy sent to the grid E_{tg}, the latter shown on negative vertical axes. In the balance, for SA systems, the energy taken from the grid E_{fg} is considered as missing energy E_m, while the energy fed into the grid E_{tg} is considered as excess energy to be dissipated E_d.

Chapter 7   **Worldwide geographical mapping and**
optimization of stand-alone and grid-connected hybrid renewable
system techno-economic performance across Köppen-Geiger climates
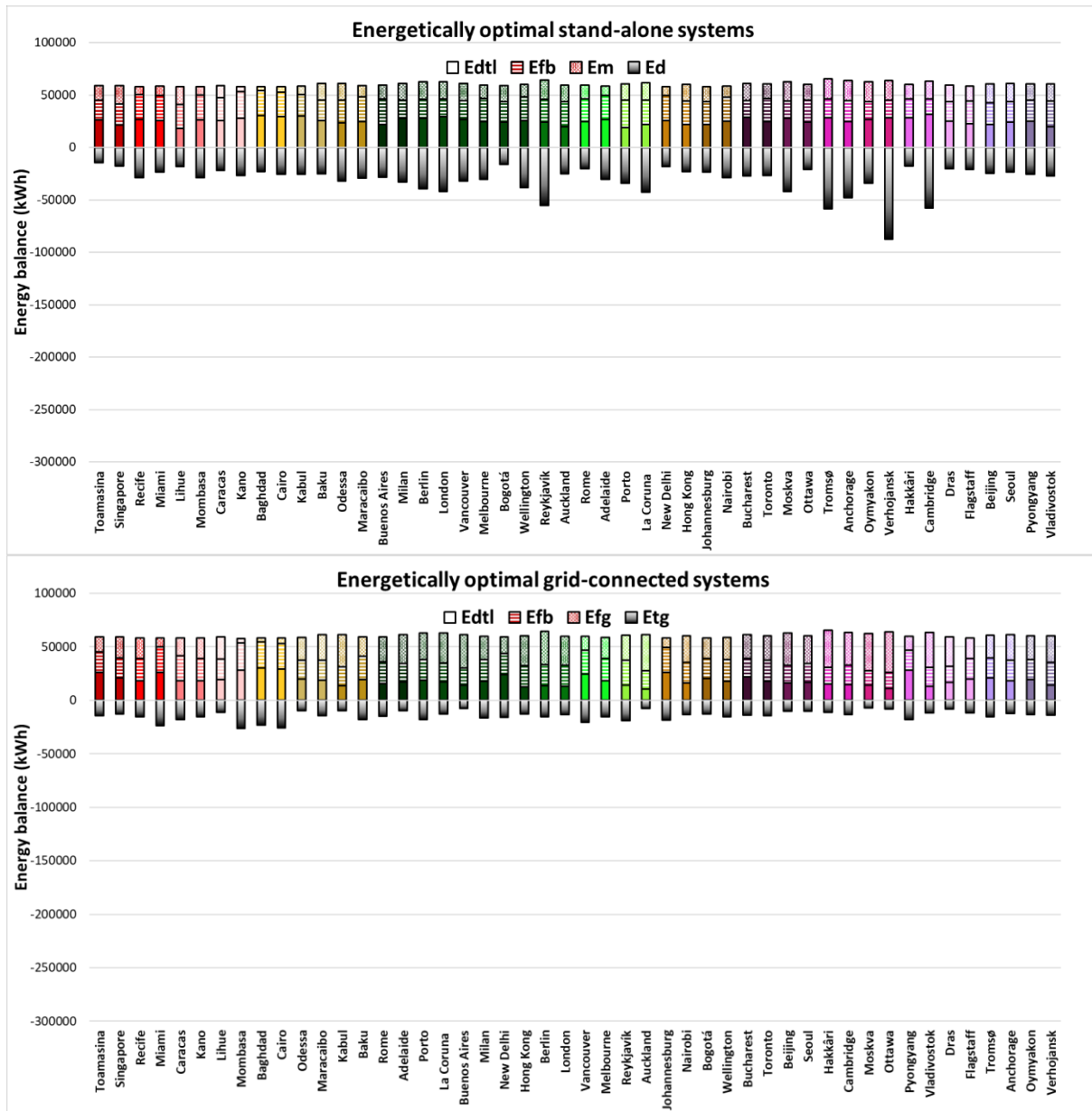
Figure 14. *Energy balance of the energetically optimal stand-alone and grid-connected systems: energy generated sent directly to the load, energy drawn from the battery, energy missing, energy dissipated, energy drawn from and sent to the grid.*
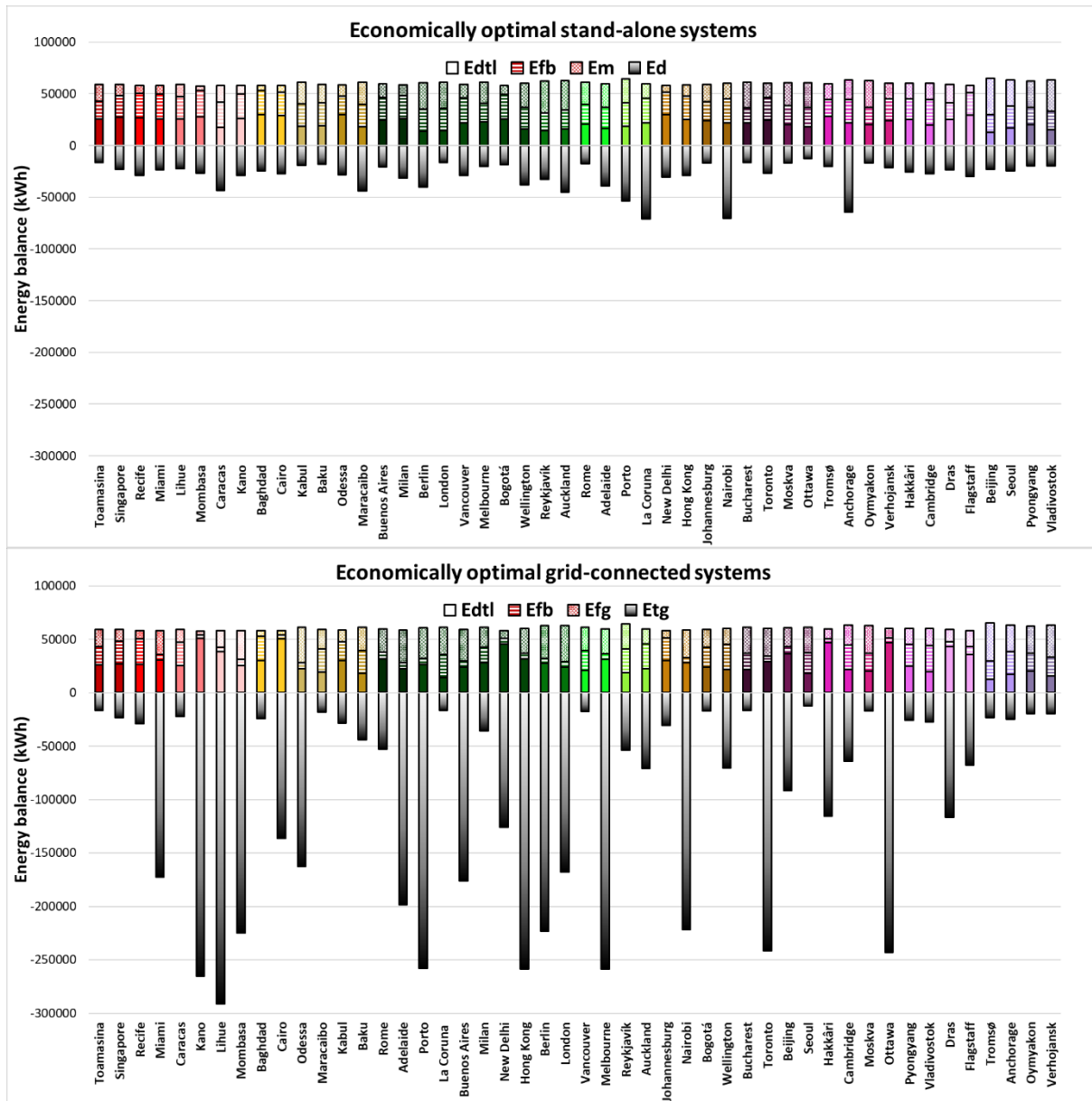
Figure 15. Energy balance of the economically optimal stand-alone and grid-connected systems: energy generated sent directly to the load, energy drawn from the battery, energy missing, energy dissipated, energy drawn from and sent to the grid.

From Figure 14 on the top, it is evident the strong influence of the climatic zone for the optimal energetically SA systems. The zones A and B, which are warmer and with a prevalent presence of PV power, have lower values of unserved energy and excess energy. This is owing to the more synchronism between the PV power generated and the power load. In the other groups, characterized by windier locations, there is a slight increase in unserved load and a significant increase in excess energy, especially in those locations where optimization has required a higher nominal PV power. In this case, the energy production and the load requirement are poorly synchronized and the PV energy is abundant. The battery is used equally in all locations since the energy drawn from it is quite constant. The energetically optimal GC systems exploit significantly the energy drawn from the grid, compared to the optimal SA systems, which have lower unserved energy to be compensated with auxiliary components. The percentage energy contribution of the grid to meet the load is very high, while the energy sent directly to the load is slightly lower. The contribution of the battery is

Chapter 7

Worldwide geographical mapping and optimization of stand-alone and grid-connected hybrid renewable system techno-economic performance across Köppen-Geiger climates

approximately equal for energetically optimal SA and GC HRES. The most significant variation is the excess energy to be sent to the grid, which is much lower than that of the SA systems since the net production of the system is generally lower. This implies a greater simultaneity between energy production and load requirements and a more energy balanced GC system. In GC systems, it is also evident that the largest quantities of excess energy to be sent to the grid occur in the hottest locations, which are also the most productive. In SA systems, the locations with the highest excess energy values are also those with the highest installed power, highlighting the lack of simultaneity between energy production and load requirements. The optimization for SA systems that require high satisfied load fractions, for some locations, has the disadvantage of not considering a simultaneity factor giving rise to very high installed powers. In general, energy optimization has shown that GC systems are more balanced in terms of the distribution of the energy produced and are generally more reliable than a SA system. In addition, SA systems have shown a greater dependence on the climatic zone.

As regards economic optimization, the energy balance of the SA HRES has more energy in excess compared to those obtained with energy optimization. This is owing to the increase of the power installed needed to increase the benefit cost ratio. The other contributions are quite similar. The energy balance of economically optimal GC systems strongly depends on the presence of FiT subsidies. In the absence of FiT, the energy in excess is slightly higher compared to that of the energetically optimal GC HRES. This is owing to the request to maximize the benefit cost ratio, namely the ratio of the economic value of the energy sent to the load and capital cost. This can be reached:

- by modifying the PV and wind powers installed while maintaining capital costs identical compared to the ones of the energetically optimal SA systems, to increase benefits
- by increasing the power installed until the further benefits produced are higher than the further capital costs required.

In the presence of FiT, the energy balance is completely modified by an increase of the energy sent directly to the load, a reduction of the energy drawn from the grid and a strong increase of the energy in excess. The economically optimal GC HRES can satisfy the load without a strong use of the battery storage, producing high energy in excess. This condition permits to exploit as much as possible FiT. The capital costs and benefits deriving by the installation of the energetically optimal SA and GC HRES are reported for all locations in Figures 16 and 17.
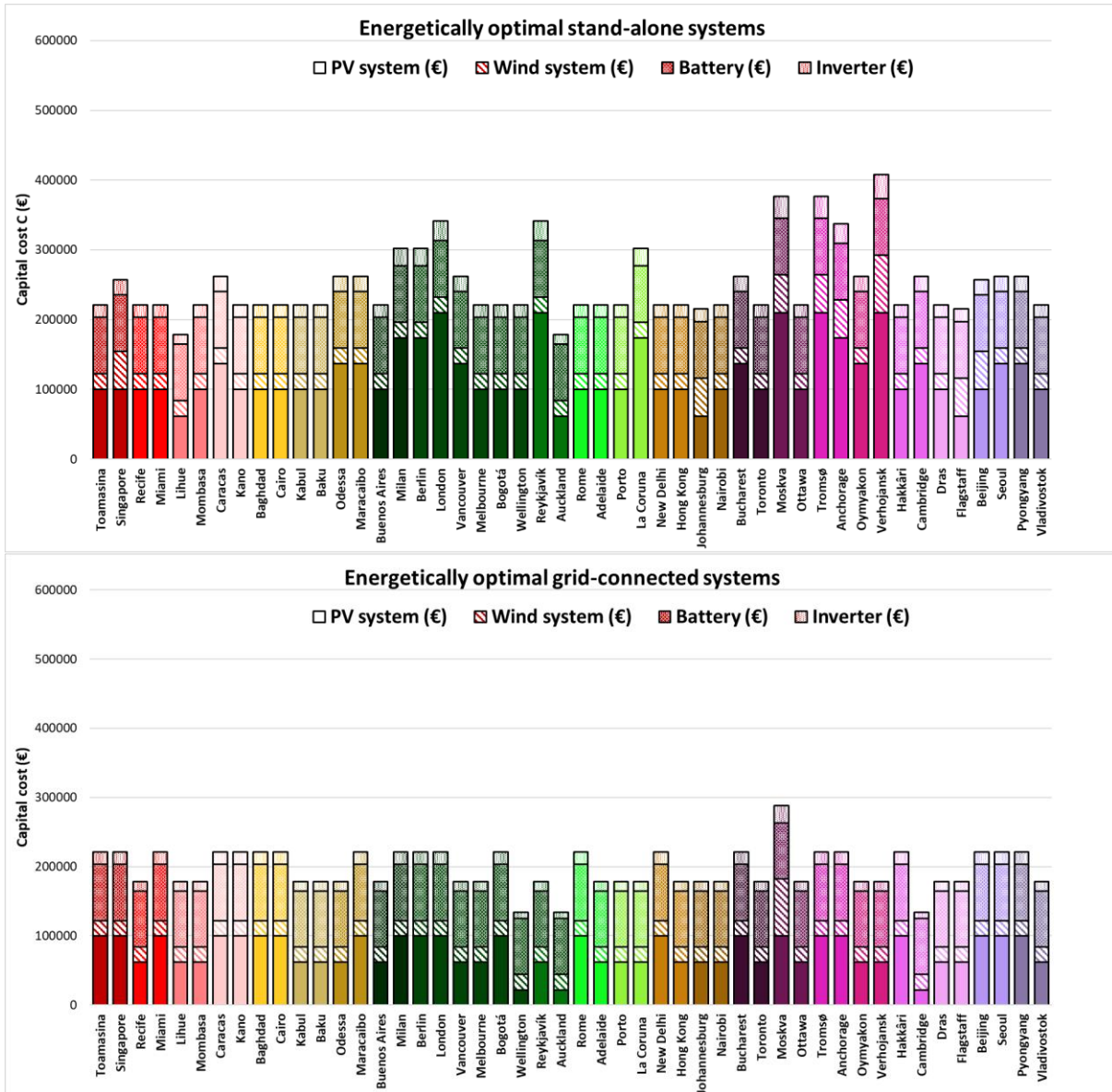
Figure 16. *Capital costs of the energetically optimal stand-alone and grid-connected systems.*

Chapter 7

Worldwide geographical mapping and optimization of stand-alone and grid-connected hybrid renewable system techno-economic performance across Köppen-Geiger climates
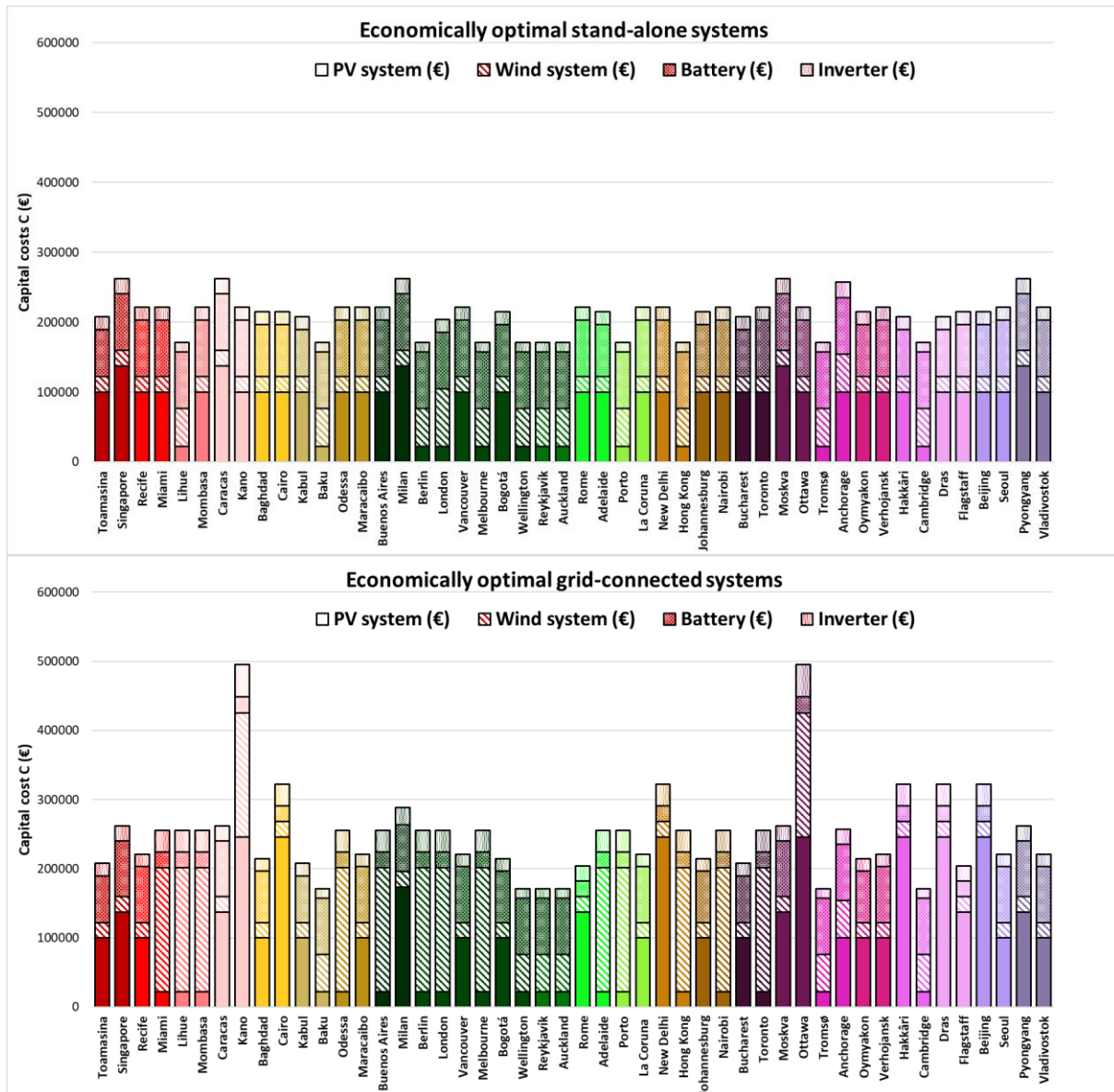
Figure 17. Benefits of the economically optimal stand-alone and grid-connected systems.

By taking into account that specific costs for the purchase of the system components were maintained identical in all locations, the differences highlighted in Figure 16 in the different locations are owing to the different powers to be installed required by the energetically optimal HRES. For the battery and inverter also the replacement costs were considered. The highest capital costs are addressed in Group D, namely in Verhojansk, Tromsø for SA HRES and both for SA and GC HRES in Moskva. The lowest one is realized both for SA and GC HRES in Auckland. Capital costs are quite uniform in the other groups for GC HRES compared to the SA ones, which generally are more expensive than the GC ones.

As regards the benefits, the comparison between SA and GC permits to appreciate the effects of FiT subsidies. Energetically optimal SA systems in some localities are characterized by slightly higher cost savings; however, in localities where the FiT is available, GC systems permit to increase the benefits, even if not significantly. The highest benefit is recorded in Cambridge Bay, followed by Lihue and Adelaide, for SA HRES and in Lihue, followed by Cambridge Bay, for GC HRES.

Chapter 7

Worldwide geographical mapping and optimization of stand-alone and grid-connected hybrid renewable system techno-economic performance across Köppen-Geiger climates

Figures 18 and 19 illustrate the same previous economic parameters for the economically optimal SA and GC HRES.
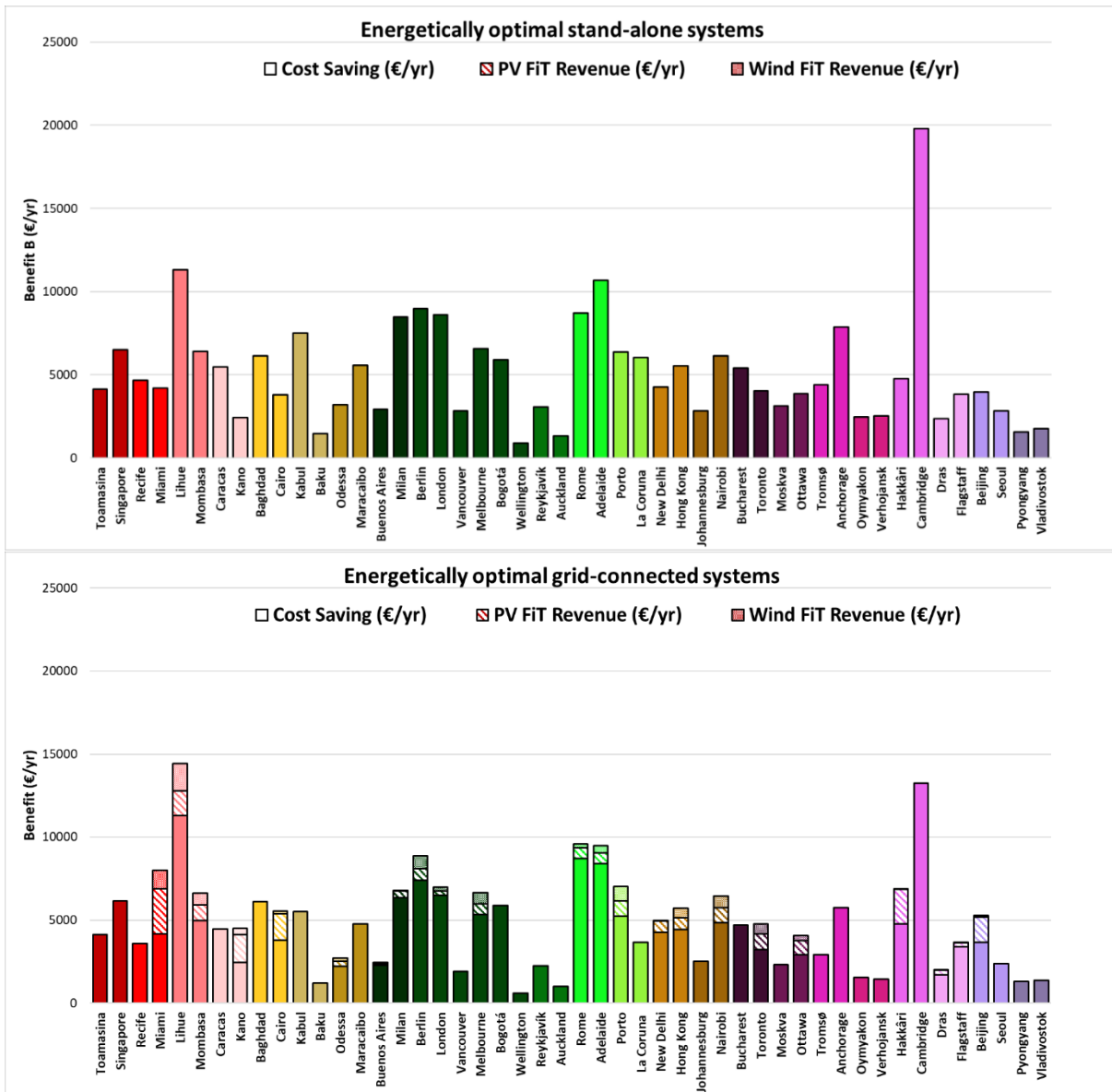
Figure 18. *Capital costs of the energetically optimal stand-alone and grid-connected systems.*
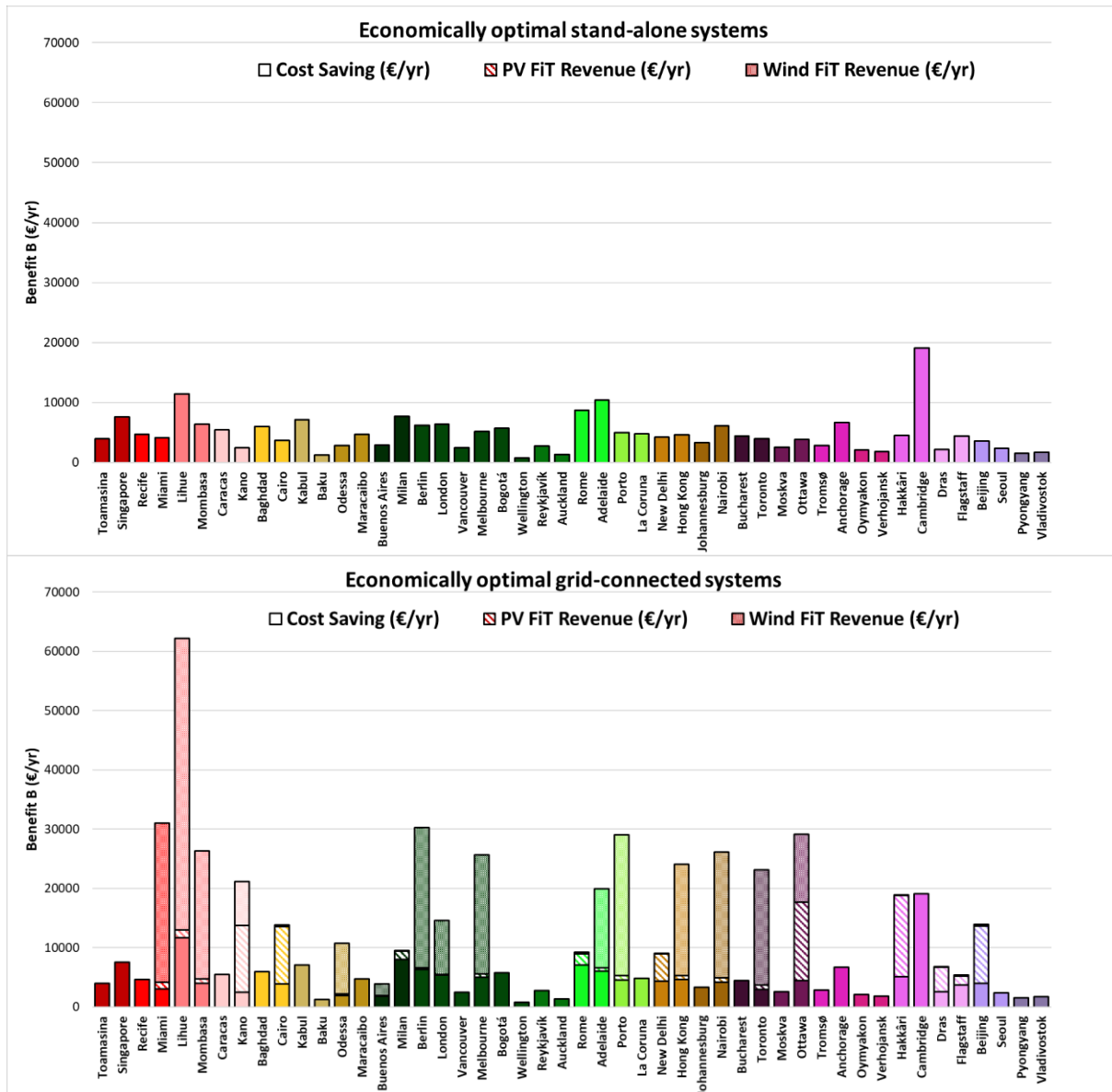
Figure 19. Capital costs of the economically optimal stand-alone and grid-connected systems.

As expected, in some localities, the economically optimal SA HRES are cheaper than those deriving from the energy optimization, while maintaining almost unchanged the benefits. In other localities, the SA HRES capital costs are quite similar to those of the energetically optimal SA ones. This indicates that it is sufficient to modify the subdivision of the overall nominal power installed in the different components to produce higher benefits. As regards the economically optimal GC HRES, in the absence of FiT the capital costs and benefits are identical to the economically optimal SA HRES and very close to the optimal systems from an energy point of view. Instead, localities with FiT subsidies reach very high benefits with an increase in capital costs compared to the energetically optimal GC HRES. In general, the GC systems deriving from economic optimization are more expensive than those obtained with energy optimization.

Figure 20 shows the energy and economic indicators, namely the satisfied load fraction, utilization factor, and also grid energy interaction factor for GC HRES, and benefit cost ratio of the energetically optimal SA and GC systems.

Chapter 7

Worldwide geographical mapping and optimization of stand-alone and grid-connected hybrid renewable system techno-economic performance across Köppen-Geiger climates
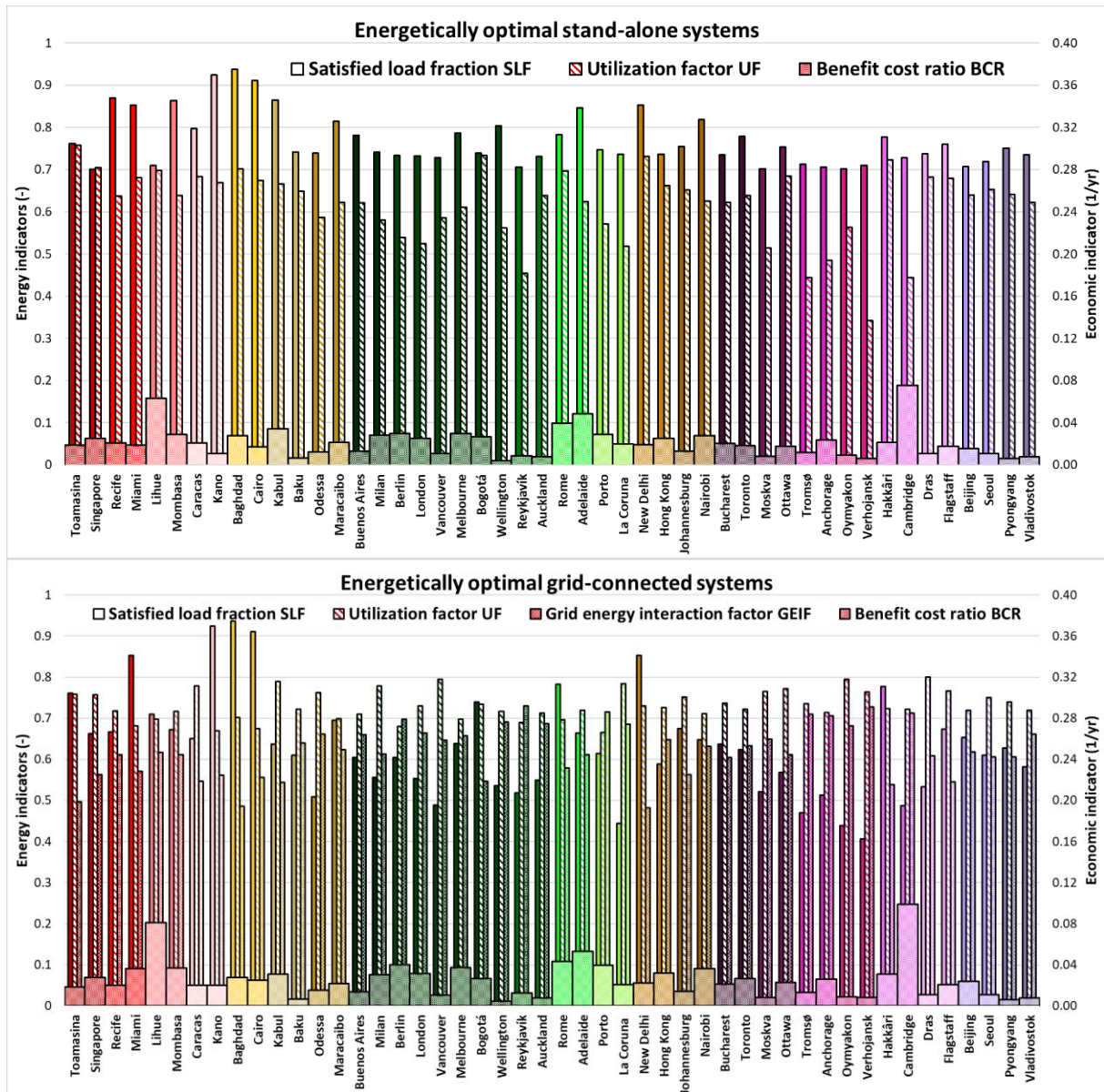
Figure 20. *Satisfied load fraction, utilization factor, and also grid energy interaction factor for the grid-connected systems, and benefit cost ratio of the energetically optimal stand-alone and grid-connected systems.*

In general, it can be noted that the satisfied load fraction and the utilization factor are higher in the sunniest locations (Baghdad, Kano, Cairo, Recife) and decrease with increasing windiness. The windiest locations, where more PV power is installed, Moscow, Reykjavík, Tromsø have utilization factors around 0.5 or less. Similarly to the SA systems, GC systems have variable satisfied load fractions and utilization factors passing from group A to Group D. GC systems are characterized by lower SLF and higher UF compared to SA ones.

Very windy and very sunny locations have low utilization factors, while hot and cold locations in terms of external air temperature have high values.

All GEIF values are below 1, sunny locations (Toamasina, Baghdad and New Delhi) have the lowest value. In particular, the trend shows that smaller values are concentrated in climate groups A and B. The highest values can be found in groups C and D and especially in the windy and coldest locations (Reykjavík, Tromsø, Anchorage, Oymyakon and Verhojansk). By considering energy indicators, the

Chapter 7   **Worldwide geographical mapping and**
optimization of stand-alone and grid-connected hybrid renewable
system techno-economic performance across Köppen-Geiger climates

analysis so far has highlighted the inadequacy of Group D for the installation of HRES, and this explains the lack of studies carried out in this climatic zone.

The benefit cost ratio is quite variable along with the different climatic groups. It is worth mentioning that the FiT for GC HRES does not lead to significant economic improvements. This is owing to the energy optimization that does not select the best economic conditions to significantly exploit economic subsidies. The BCR rank does not strongly depend on the climatic group since it is substantially affected by electricity prices and FiT subsidies, which are determined by local national perspectives.

Finally, the energy and economic indicators are also reported in Figure 21 for the economically optimal SA and GC HRES.
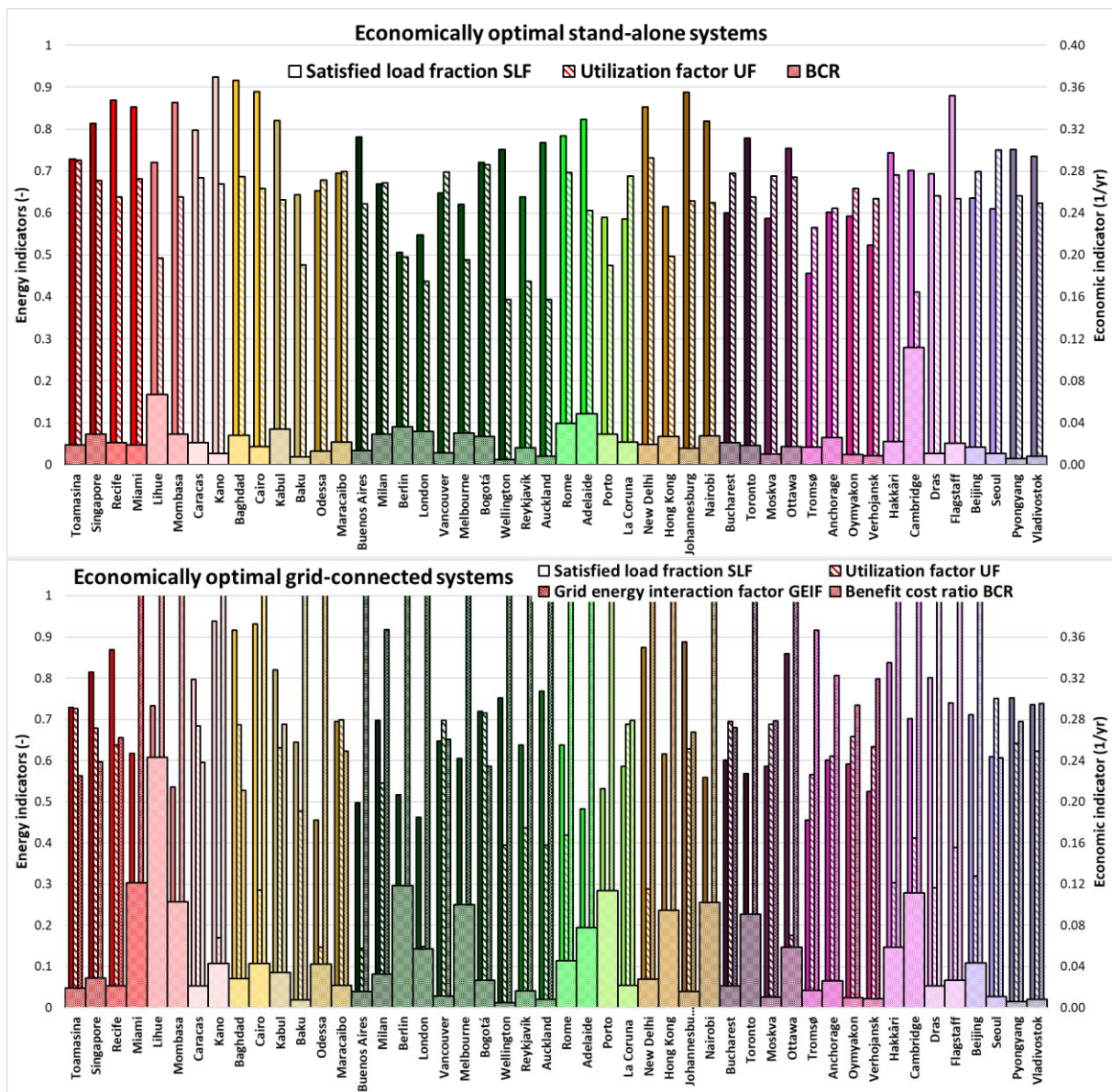
Figure 21. Satisfied load fraction, utilization factor, and also grid energy interaction factor for the grid-connected systems, and benefit cost ratio of the economically optimal stand-alone and grid-connected systems.

Economically optimal SA HRES do not everywhere comply with the threshold value of 0.70 for the satisfied load fraction. Both in the case of SA and GC systems, economic optimization leads to a

reduction of both energy indicators, especially the utilization factor, compared to energy optimization. In addition, the grid energy interaction factor increase in an extensive manner, also reaching a value higher than 1, in localities with FiT subsidies available. Contrarily, the economic profitability both in SA and GC is significantly higher than energetically optimal systems, especially when the two optimal GC HRES are compared.

In some localities, energetically and economically optimal SA systems coincide, namely in Recife, Miami, Mombasa, Caracas, Kano, Buenos Aires, Rome, New Delhi, Nairobi, Toronto, Ottawa and Vladivostok. In all localities, the same PV, wind and battery power of, respectively, 50 kW, 10 kW and 130 kW are required. Instead, the energy and economic optimization of GC HRES lead to the same system power configurations (50 kW, 10 kW and 130 kW) in Maracaibo and Seoul.

5.3. Worldwide mapping of the techno-economic

In this section, the worldwide mapping of techno-economic performance of optimal SA and GC HRES are shown in terms of energy and economic indicators. Additional worldwide mapping of the energy performance and economic profitability of the energetically and economically optimal HRES are illustrated in the Data in Brief related to this paper. These maps are useful for rapid evaluation and comparison of the distribution of the techno-economic performance of the optimal HRES from a geographical point of view. The bubble size is proportional to the value of the parameter or indicator in the locality considered. For a specific parameter or indicator, the sizes of bubbles in the four images related to the energetically and economically optimal SA and GC HRES are between the absolute maximum and minimum values observed in the four datasets.

Figures 22-27 illustrate the maps of the PV, wind and battery powers to be installed for energetically and economically optimal SA and GC HRES.
Instead, Figures 28-34 show the maps of the utilization factor, satisfied load fraction, grid energy interaction factor and benefit cost ratio for energetically and economically optimal SA and GC HRES.

Chapter 7
Worldwide geographical mapping and
optimization of stand-alone and grid-connected hybrid renewable
system techno-economic performance across Köppen-Geiger climates
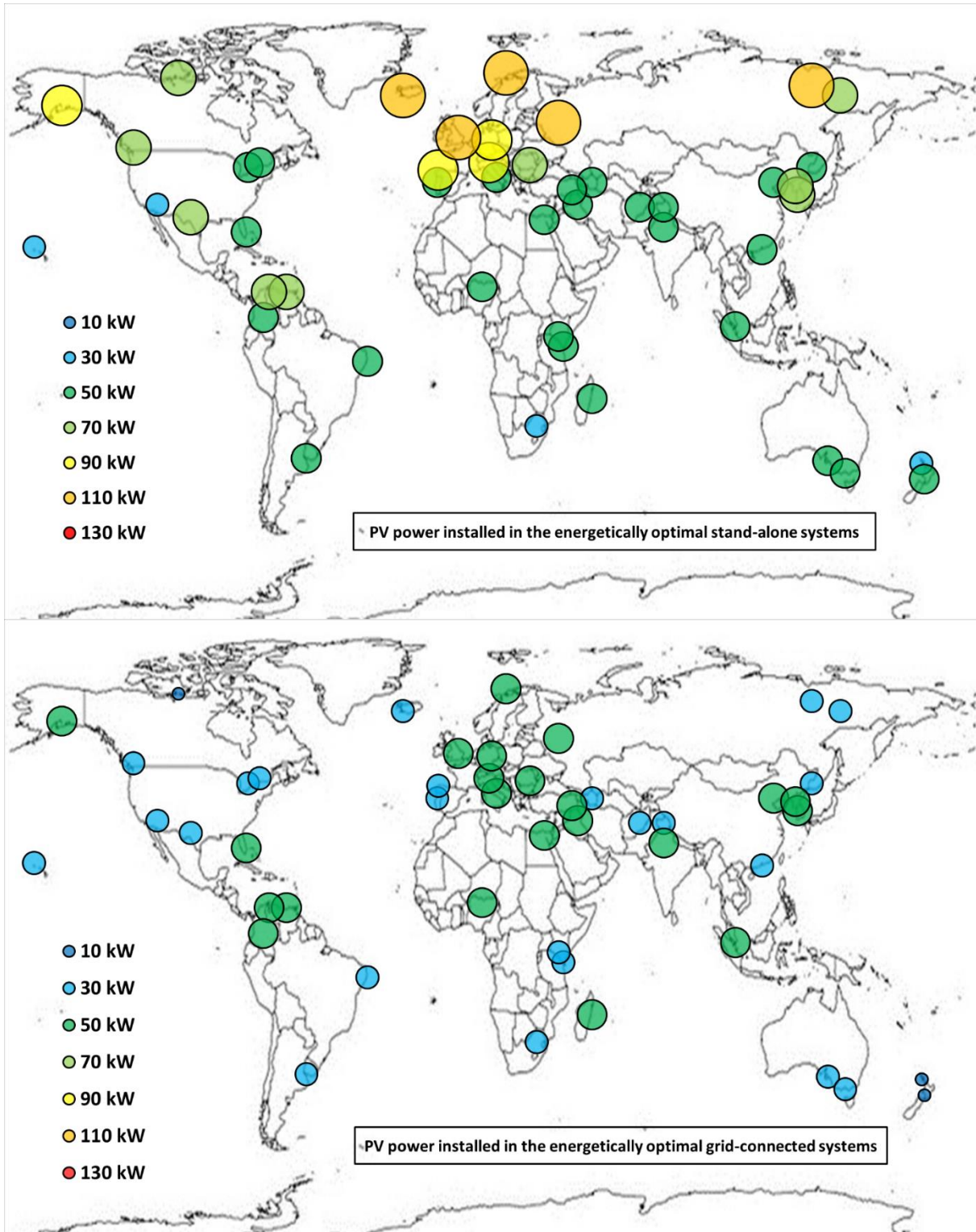
Figure 22. *Worldwide mapping of the PV power installed in the energetically optimal stand-alone and grid-connected systems.*

Chapter 7   **Worldwide geographical mapping and**
optimization of stand-alone and grid-connected hybrid renewable
system techno-economic performance across Köppen-Geiger climates
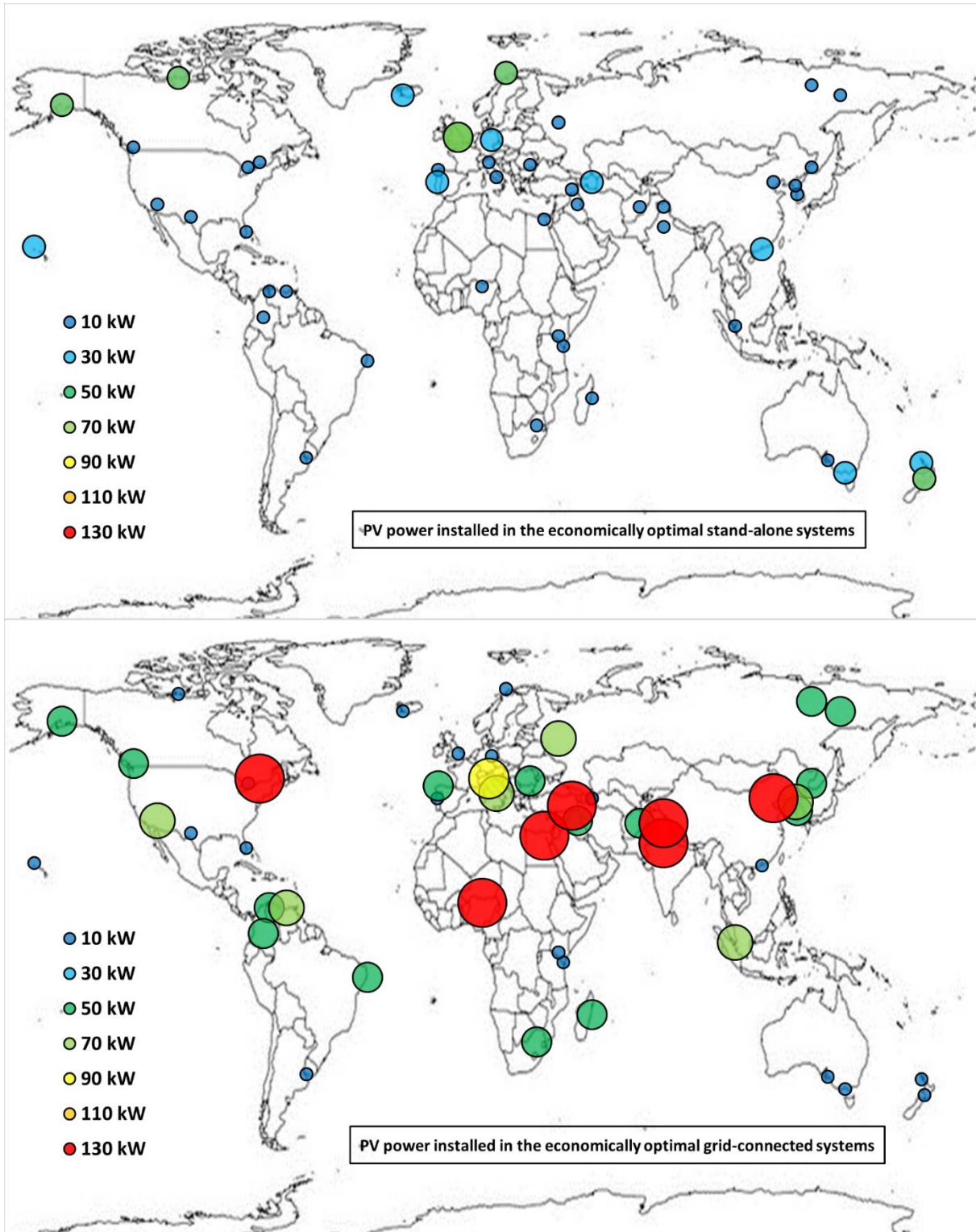
Figure 23. *Worldwide mapping of the PV power installed in the economically optimal stand-alone and grid-connected systems.*
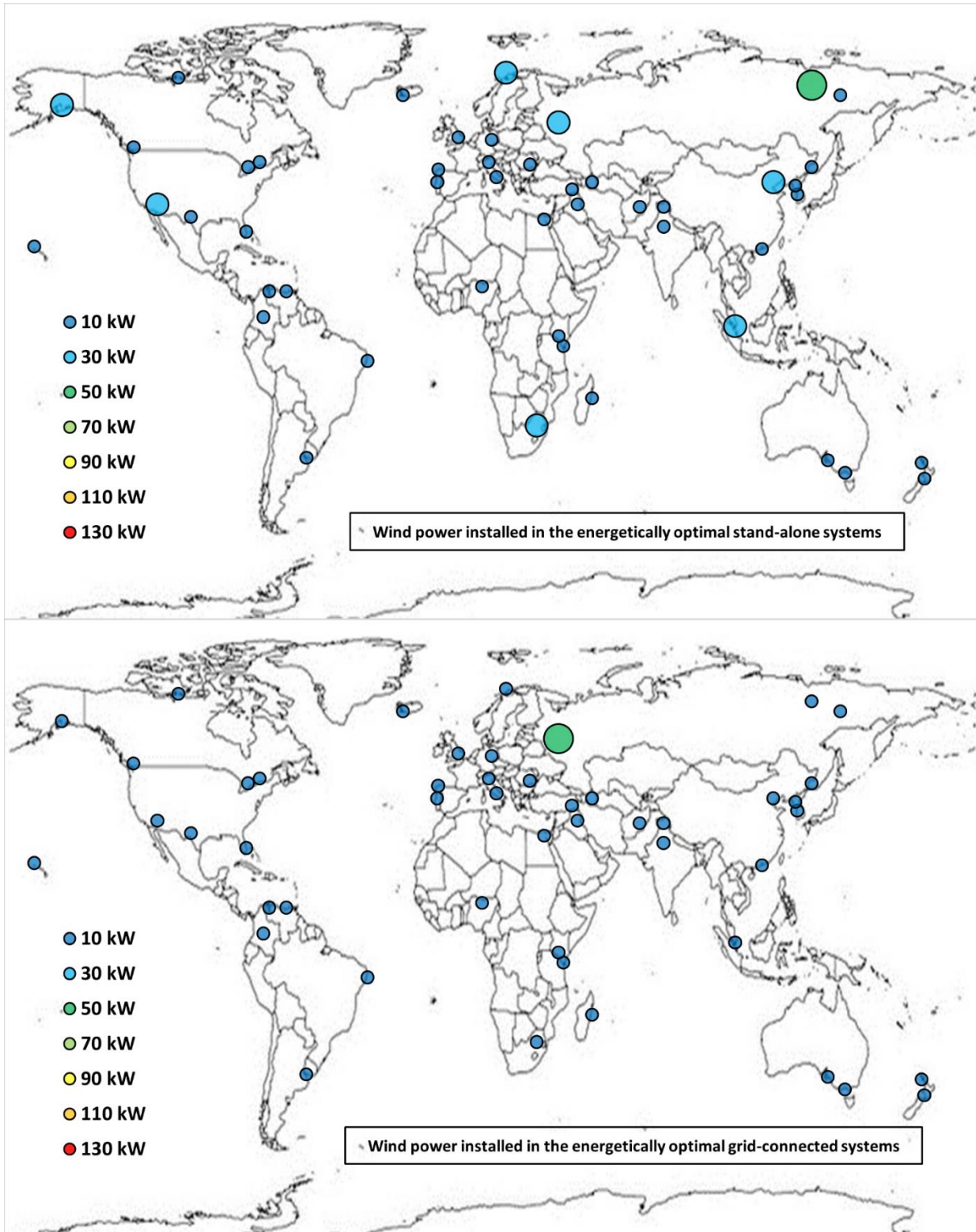
Figure 24. *Worldwide mapping of the wind power installed in the energetically optimal stand-alone and grid-connected systems.*

Chapter 7   **Worldwide geographical mapping and**
optimization of stand-alone and grid-connected hybrid renewable
system techno-economic performance across Köppen-Geiger climates
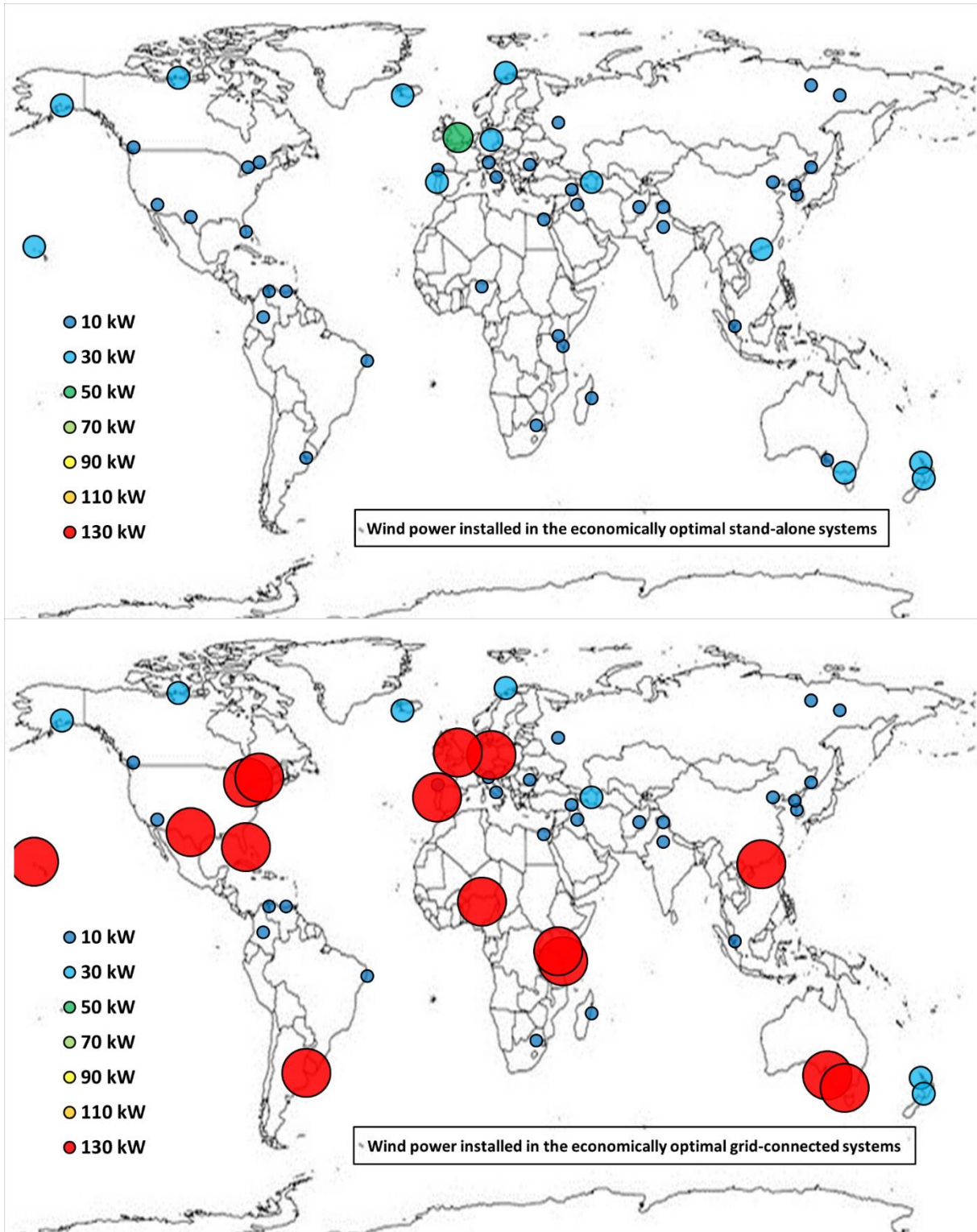
Figure 25. *Worldwide mapping of the wind power installed in the economically optimal stand-alone and grid-connected systems.*

Chapter 7   **Worldwide geographical mapping and**
optimization of stand-alone and grid-connected hybrid renewable
system techno-economic performance across Köppen-Geiger climates
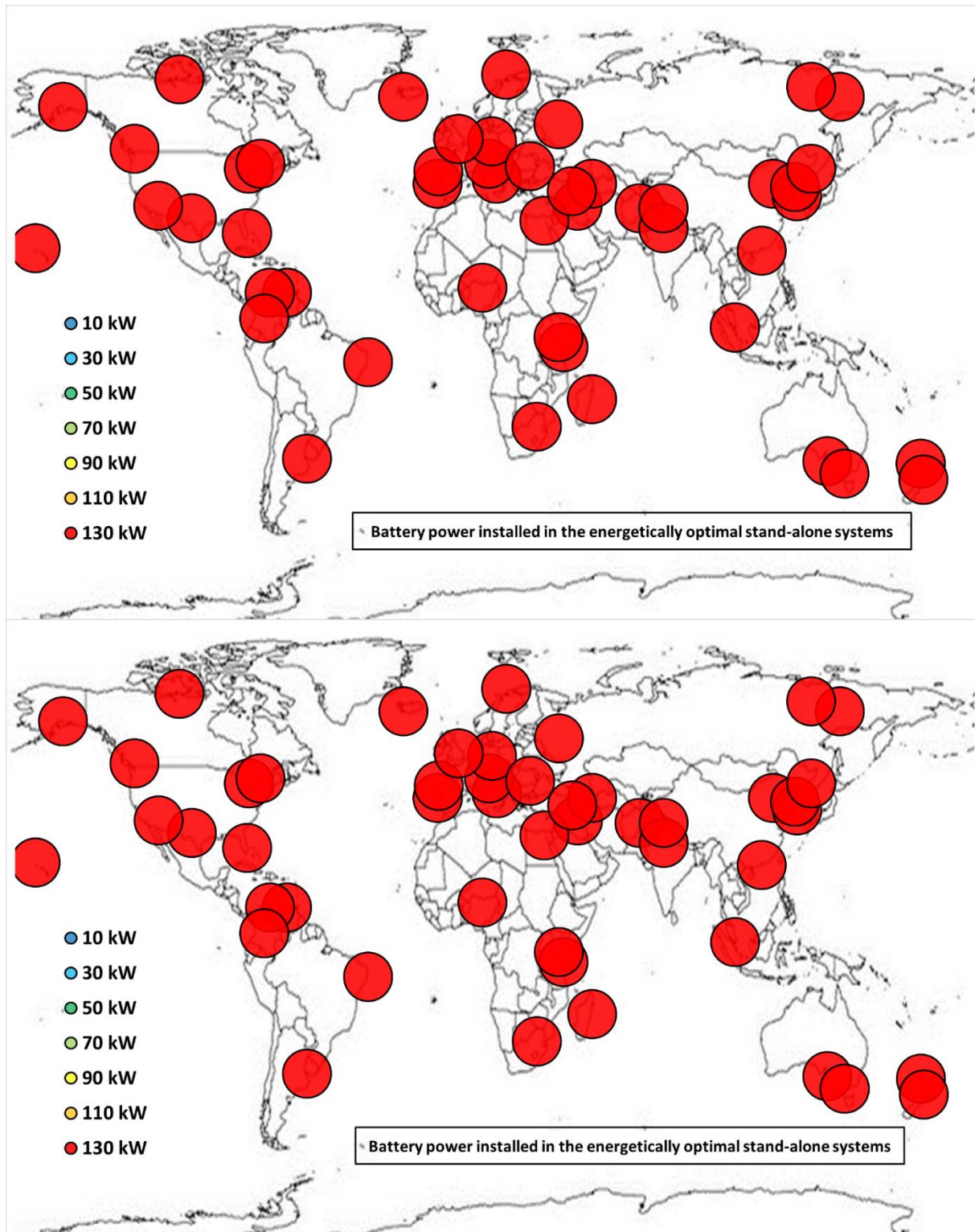
Figure 26. *Worldwide mapping of the battery power installed in the energetically optimal stand-alone and grid-connected systems.*

Chapter 7
                                    Worldwide geographical mapping and
                      optimization of stand-alone and grid-connected hybrid renewable
                      system techno-economic performance across Köppen-Geiger climates
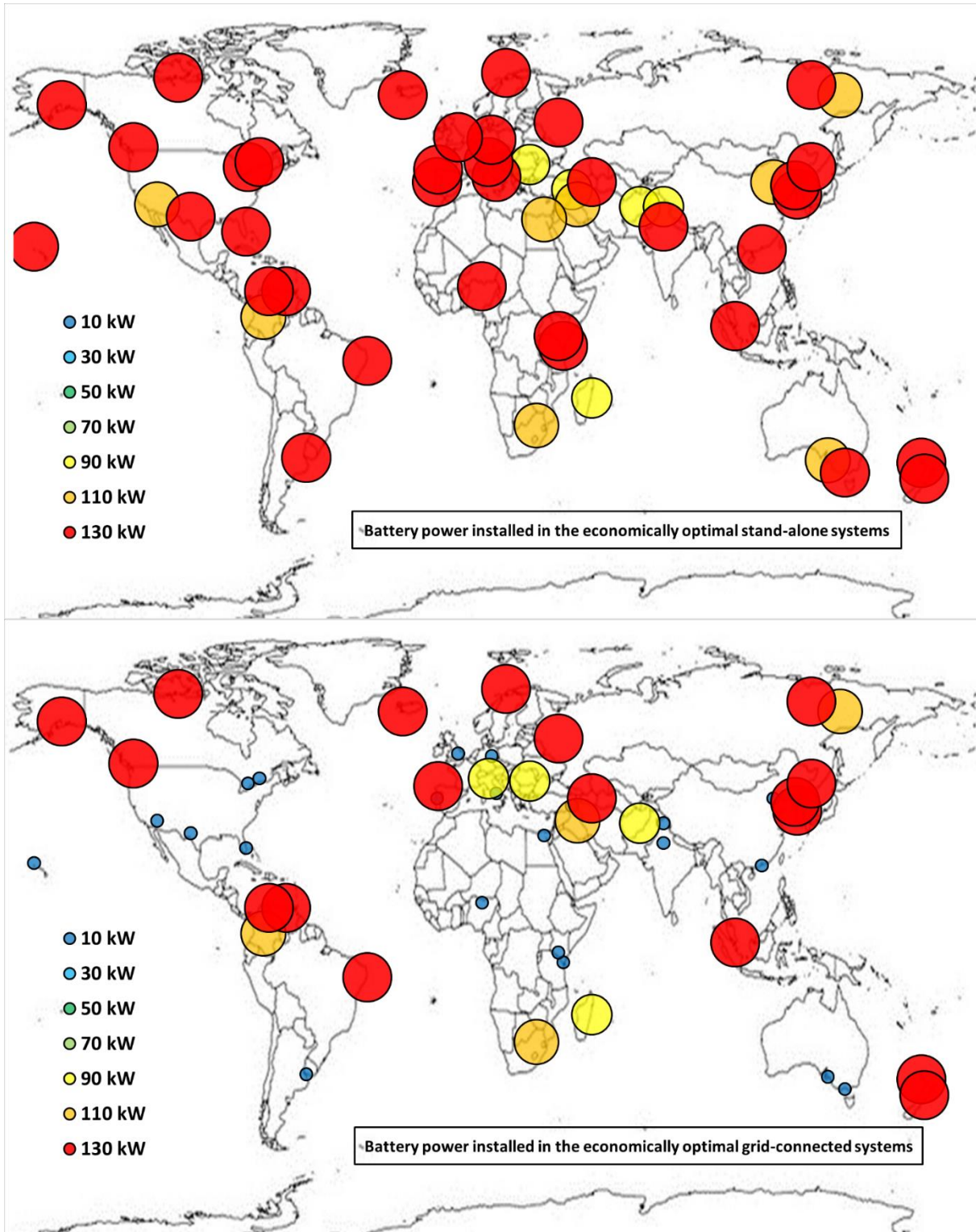
Figure 27. *Worldwide mapping of the battery power installed in the economically optimal stand-alone and grid-connected systems.*
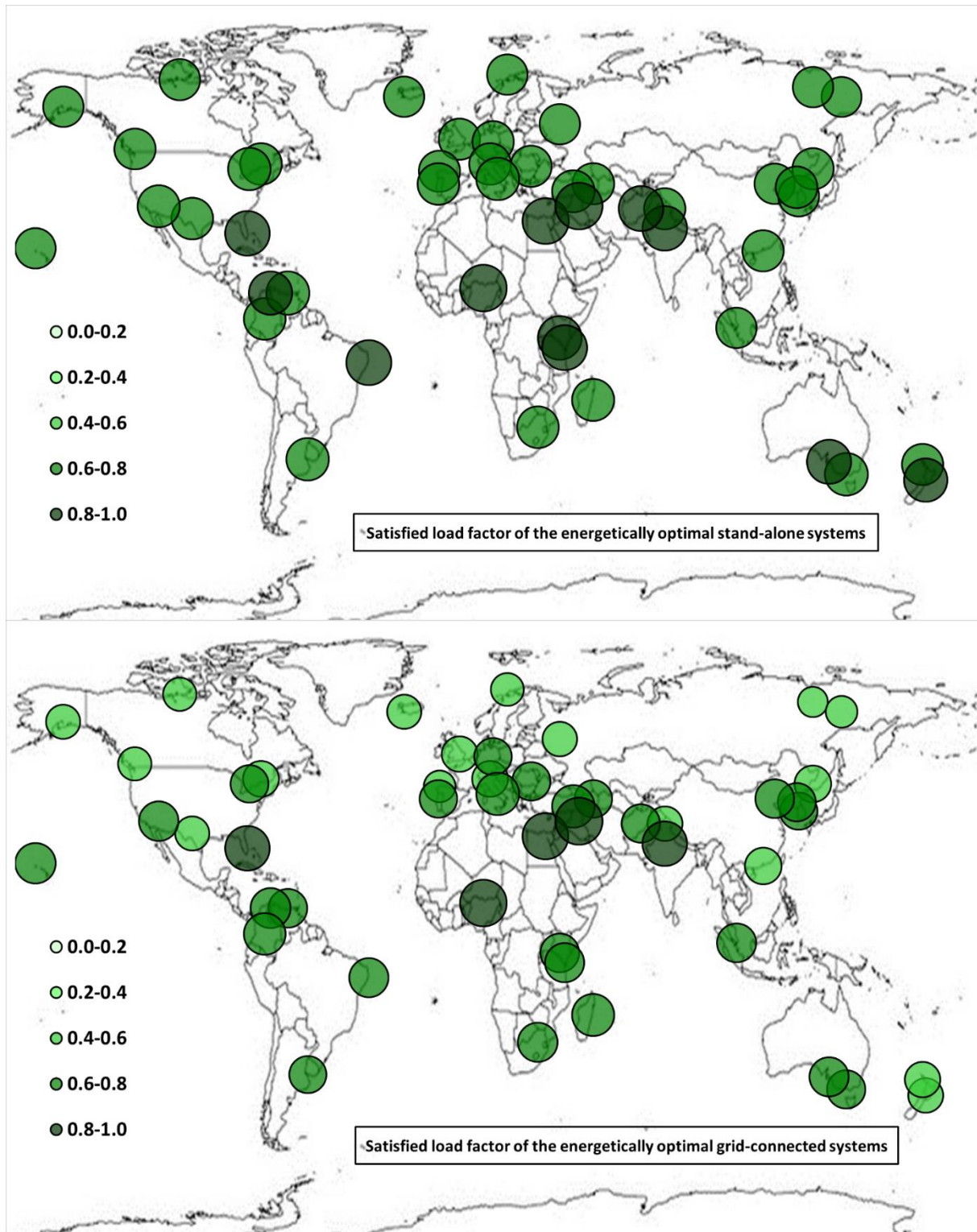
Figure 28. *Worldwide mapping of the satisfied load fraction of the energetically optimal stand-alone and grid-connected systems.*

Chapter 7

Worldwide geographical mapping and optimization of stand-alone and grid-connected hybrid renewable system techno-economic performance across Köppen-Geiger climates
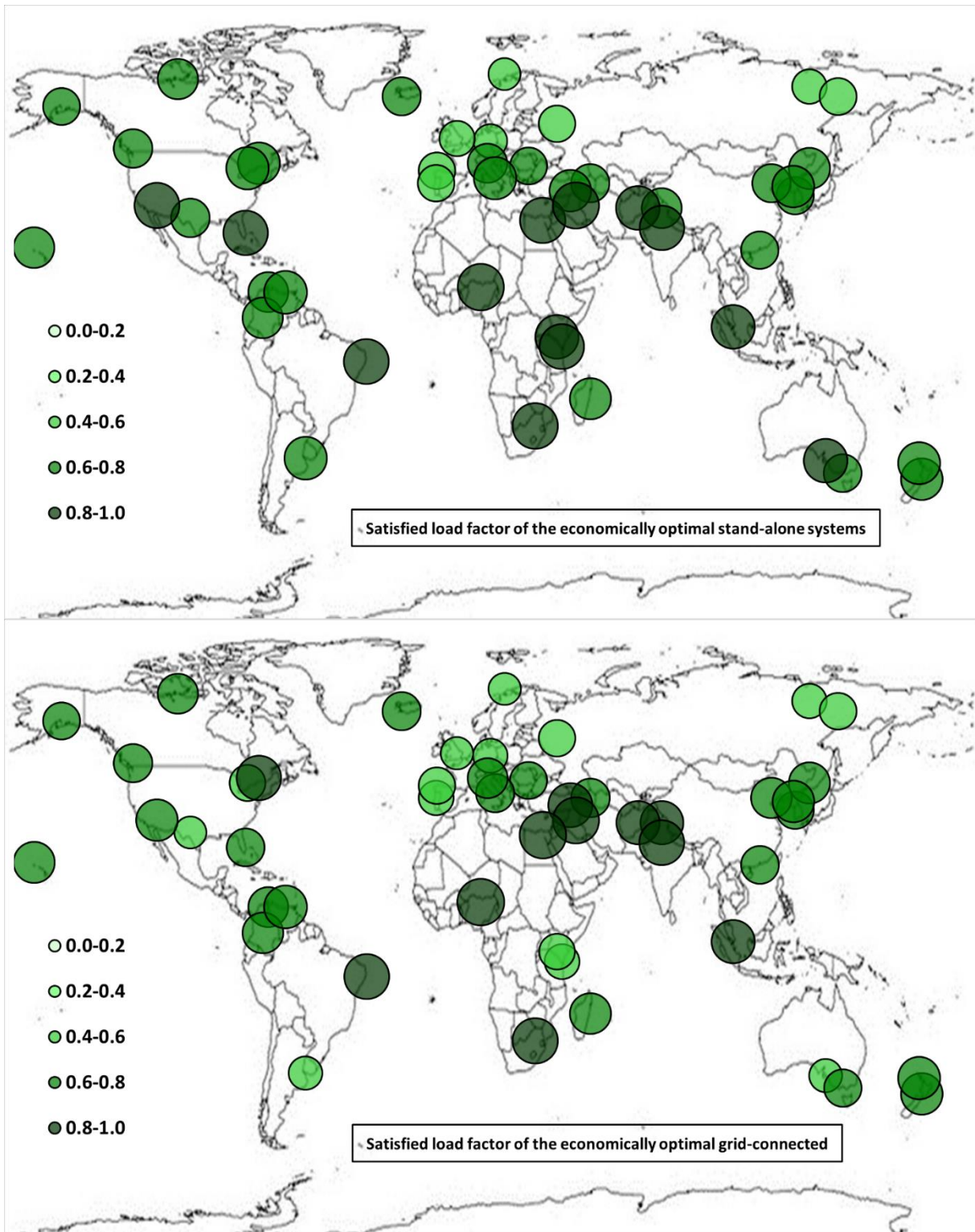
Figure 29. *Worldwide mapping of the satisfied load fraction of the economically optimal stand-alone and grid-connected systems.*

Chapter 7
                                    Worldwide geographical mapping and
                          optimization of stand-alone and grid-connected hybrid renewable
                          system techno-economic performance across Köppen-Geiger climates
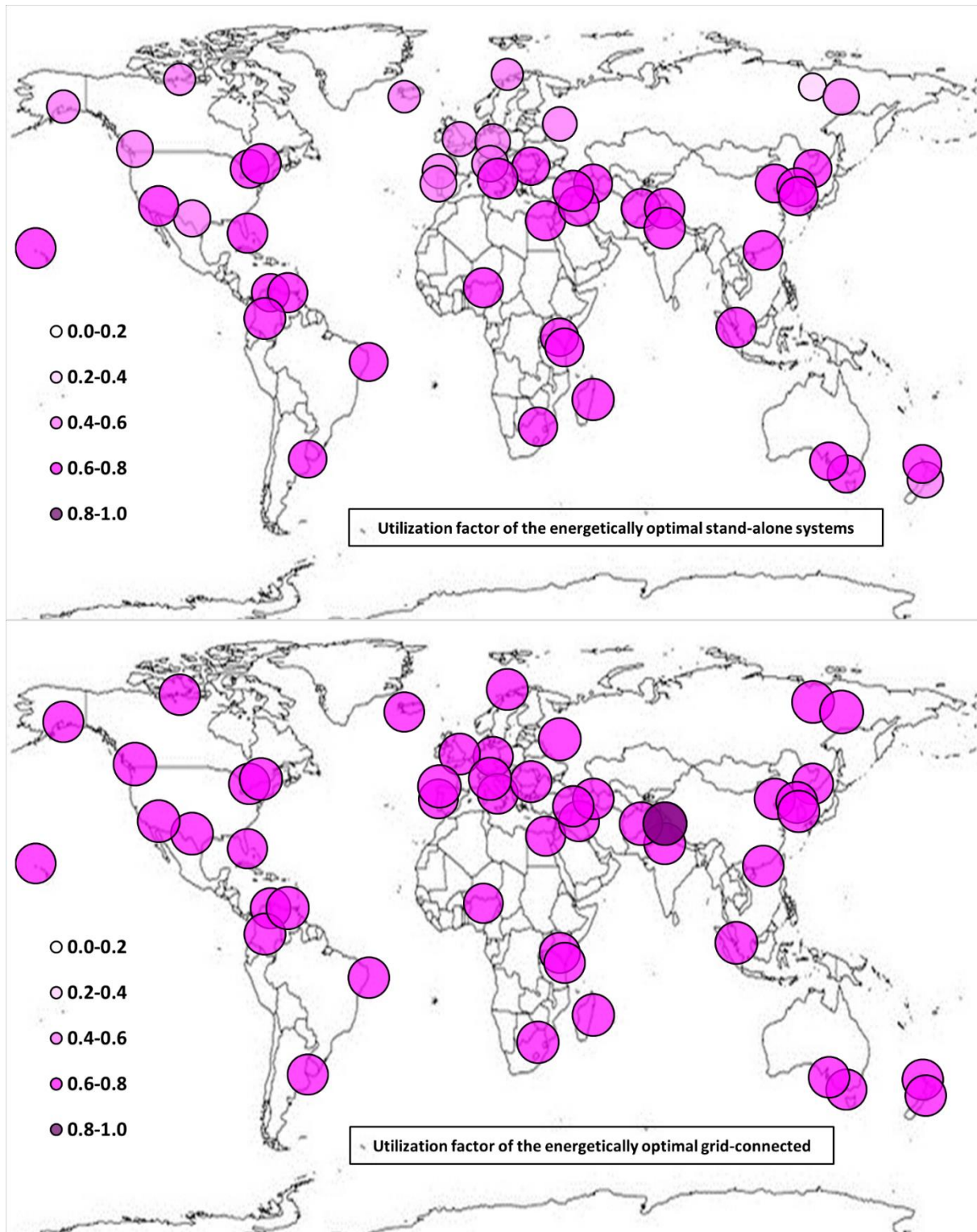
Figure 30. *Worldwide mapping of the utilization factor of the energetically optimal stand-alone and grid-connected systems.*

Chapter 7

Worldwide geographical mapping and optimization of stand-alone and grid-connected hybrid renewable system techno-economic performance across Köppen-Geiger climates
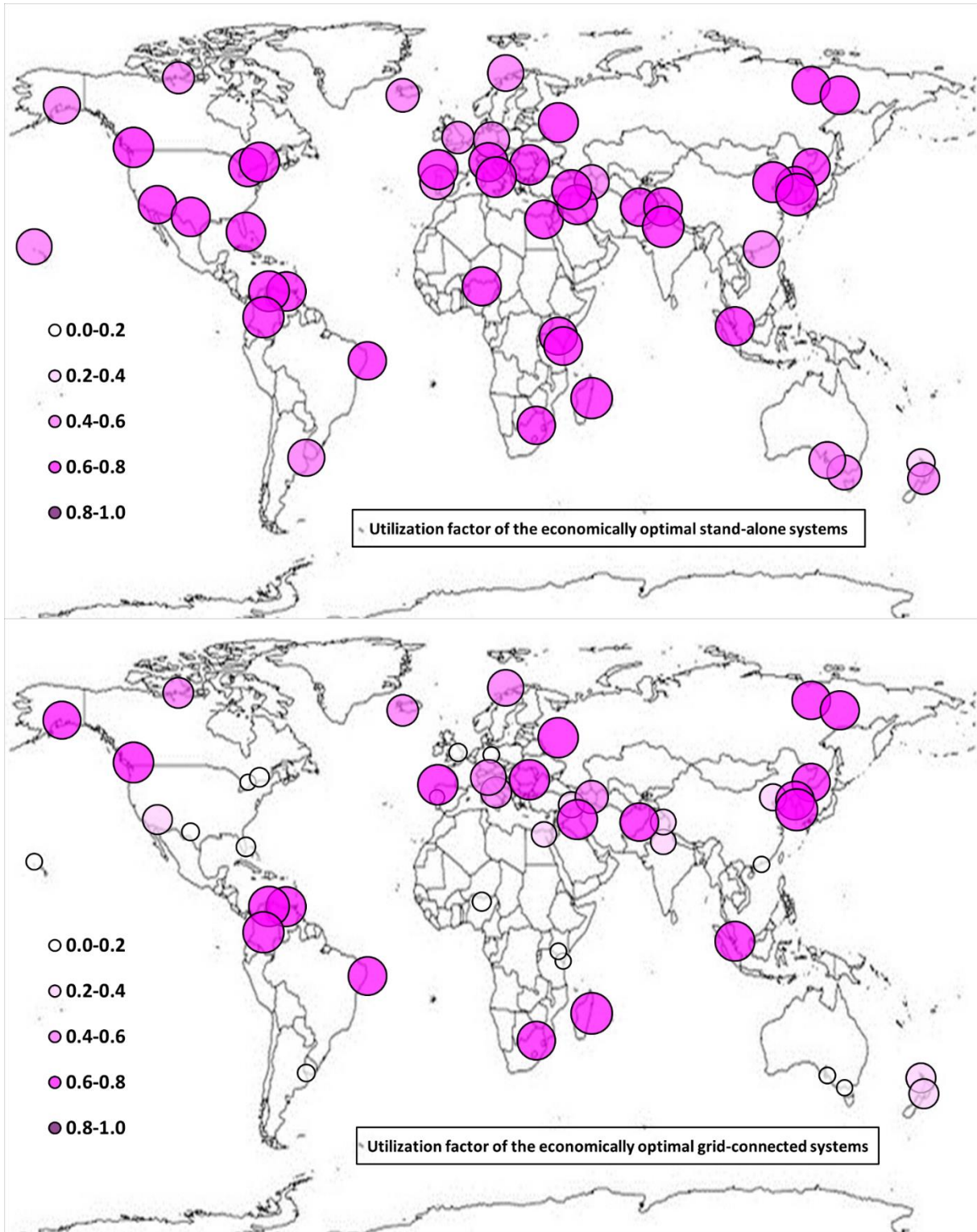
Figure 31. *Worldwide mapping of the utilization factor of the economically optimal stand-alone and grid-connected systems.*

Chapter 7

**Worldwide geographical mapping and
optimization of stand-alone and grid-connected hybrid renewable
system techno-economic performance across Köppen-Geiger climates**
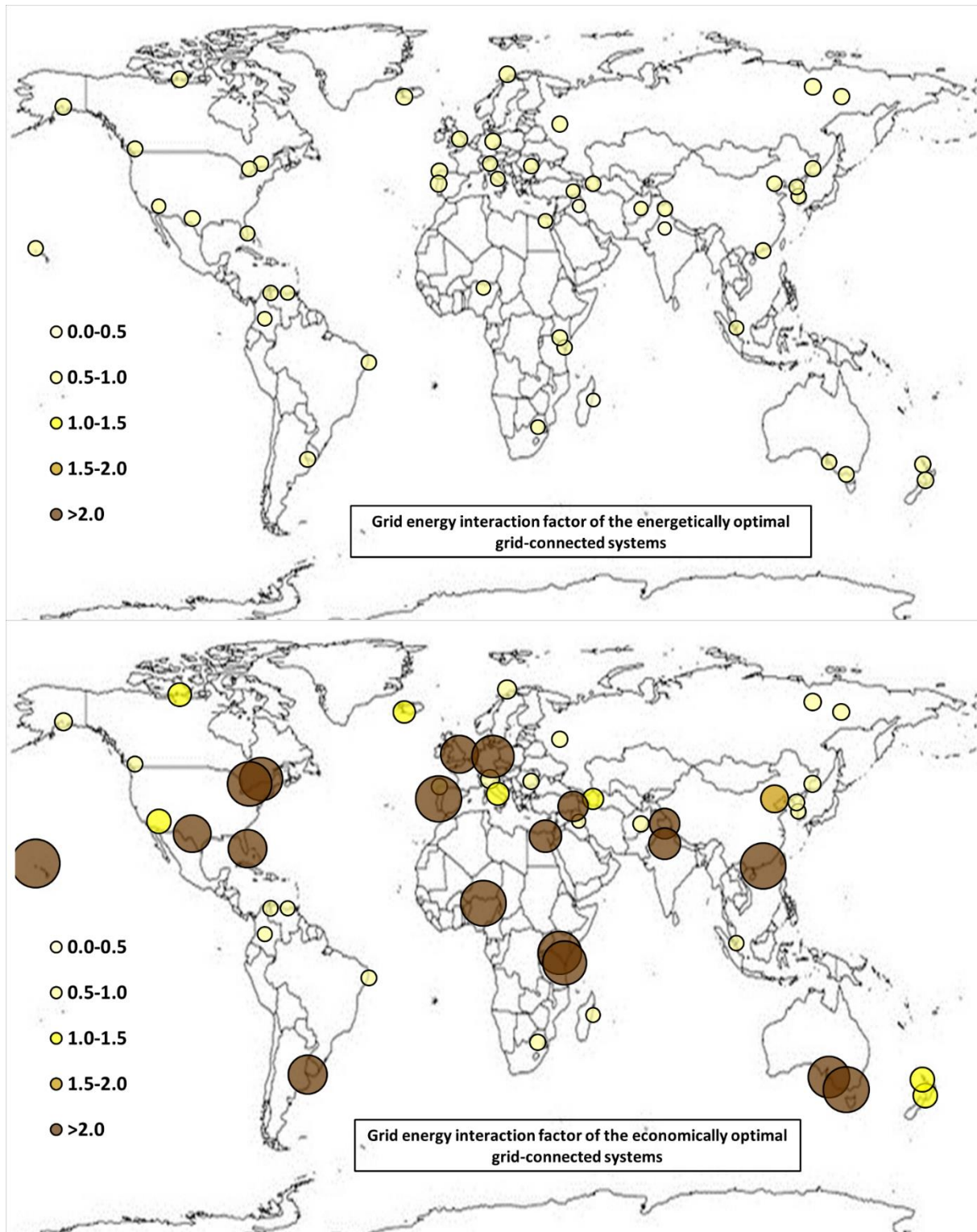
Figure 32. *Worldwide mapping of the grid energy interaction factor of the energetically and economically optimal grid-connected systems.*
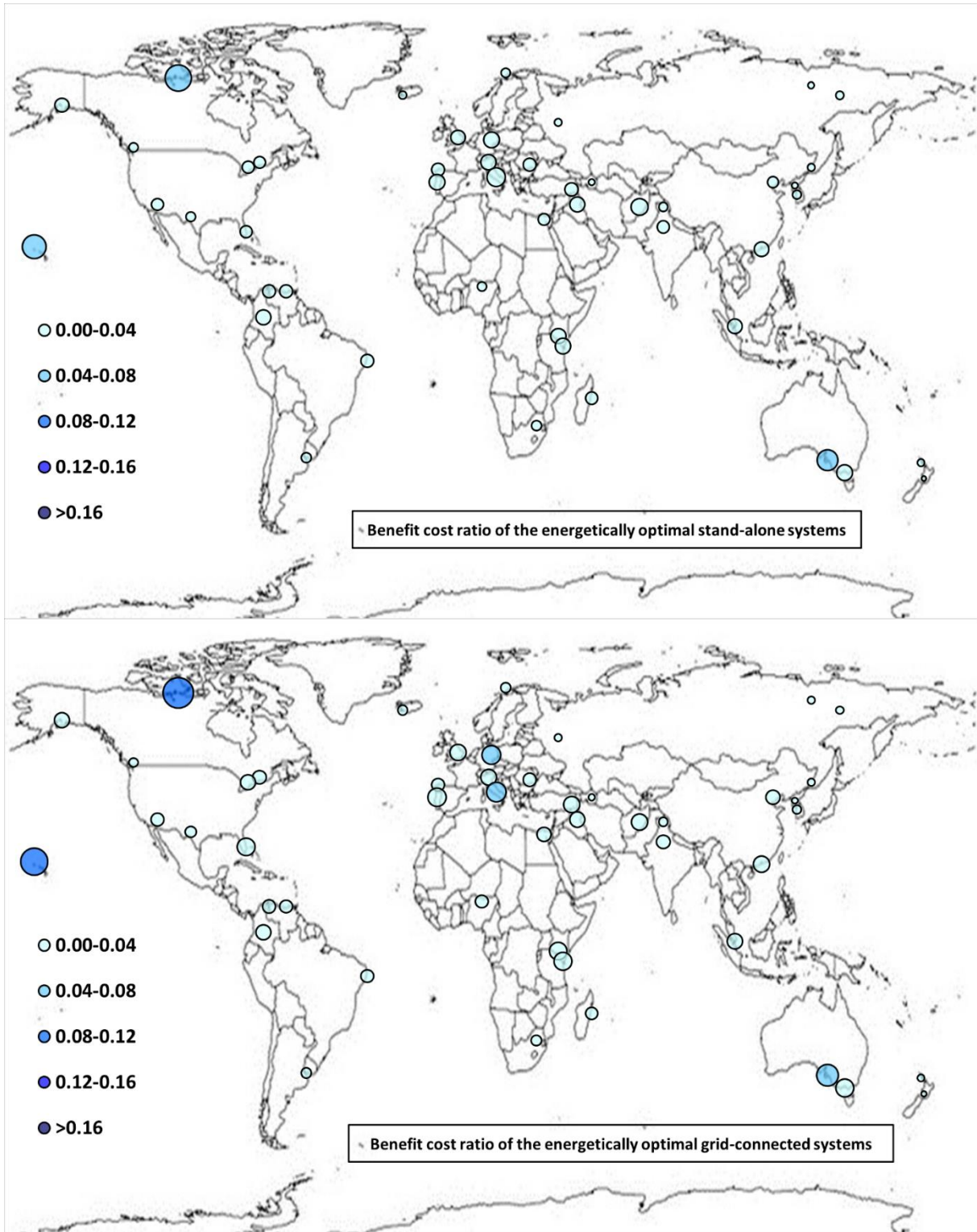
Figure 33. *Worldwide mapping of the benefit cost ratio of the energetically optimal stand-alone and grid-connected systems.*

Chapter 7   **Worldwide geographical mapping and**
optimization of stand-alone and grid-connected hybrid renewable
system techno-economic performance across Köppen-Geiger climates
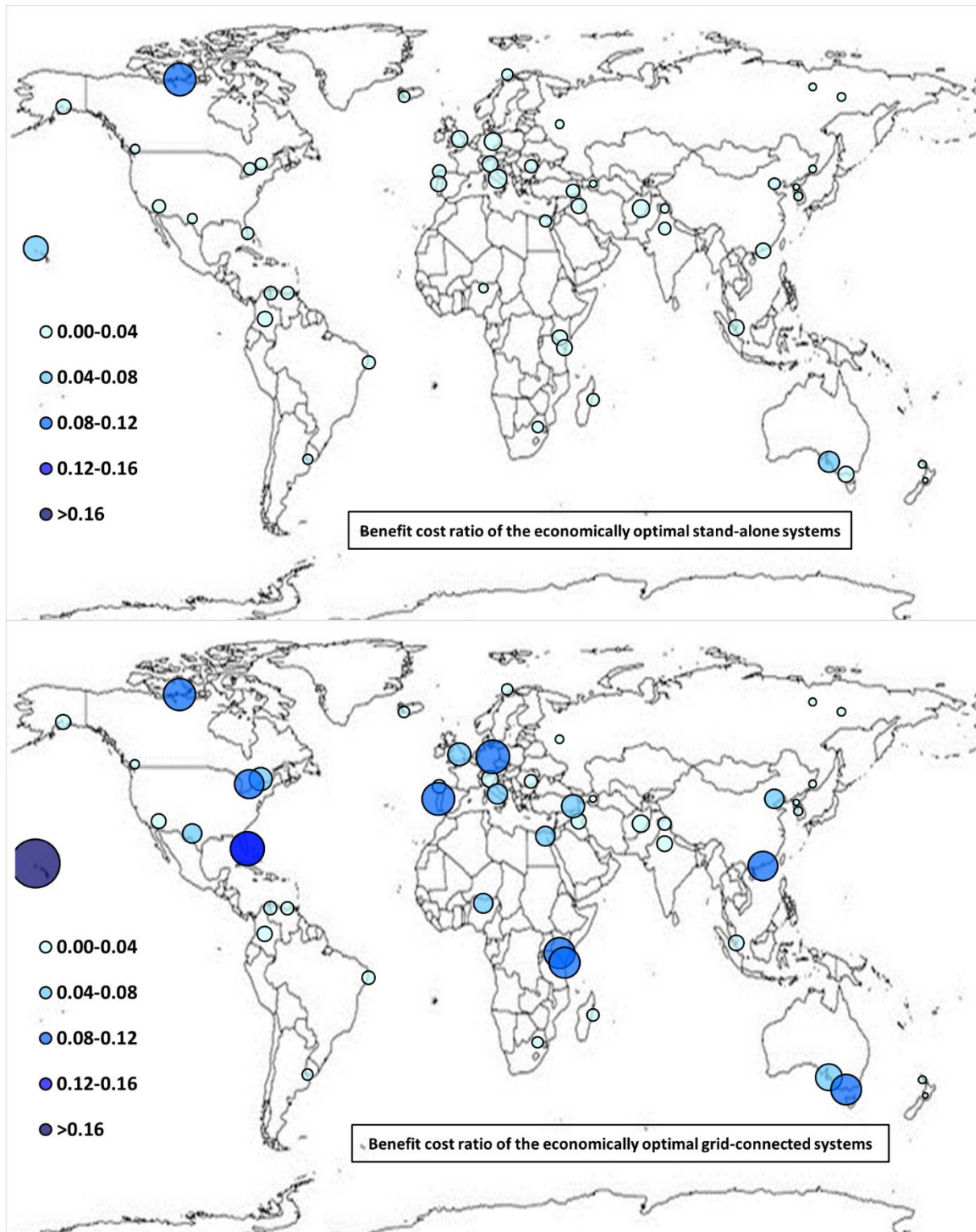
Figure 34. *Worldwide mapping of the benefit cost ratio of the economically optimal stand-alone and grid-connected systems.*

6. Conclusions

This study presents a mapping and energy and economic optimization of the techno-economic performance of stand-alone (SA) and grid-connected (GC) PV-wind hybrid renewable systems (HRES) worldwide for a typical office building district. The simulations were carried out for 343

Chapter 7

Worldwide geographical mapping and optimization of stand-alone and grid-connected hybrid renewable system techno-economic performance across Köppen-Geiger climates

different system power configurations to obtain the energetically and economically optimal configurations for 48 locations around the world both for stand-alone and grid-connected systems. For this purpose, 16464 dynamic simulations were performed and summarized in yearly energies in output from each component and energy and economic indicators. The last ones were calculated by considering market component costs and searching for electricity and FiT prices worldwide. The energy optimization of SA HRES foresees the maximization of the utilization of the energy generated and a constraint on the percentage of load satisfied; instead, the GC HRES one consists of the minimization of the energy exchange with the grid. The economic optimization of SA and GC HRES has the objective to maximize the benefit cost ratio.

As regards energy reliability and economic profitability, the investigation has revealed that:

- only in few localities, the energy or economic optimizations of SA HRES lead to profitable systems without a FiT to sell the energy in excess to the grid; instead, FiT policy for GC HRES assures that 20.8% of localities are viable also without an economic optimization, while the economically optimal systems are profitable in 41.7% of localities and the benefit cost ratio increases in an extensive manner compared to that of the energetically optimal systems;

- however, economically optimal SA HRES do not everywhere comply with the threshold value of 70% of the energy required by the load satisfied leading also to a reduction of the percentage of energy generated utilized to meet the load compared to the energetically optimal ones. Instead, the level of energy exchanged with the grid of economically optimal GC systems increases extensively in localities with the availability of FiT subsidies;

- among the energetically optimal SA configurations, the highest profitability is reached in Cambridge Bay (Canada), while among the economically optimal SA configurations, the highest energy performance is reached in Seoul. Instead, among the energetically optimal GC configurations, the highest profitability is reached in Cambridge Bay (Canada), while among the economically optimal GC configurations, the highest energy performance is reached in Baghdad.

Finally, the study carried out to identify the most suitable climate conditions has highlighted that:

- the most suitable locality to install a SA HRES is Toamasina (Madagascar) from an energy point of view, while is Cambridge Bay (Canada) from an economic point of view;

- the most suitable locality to install a GC HRES is New Delhi (India) from an energy point of view, while is Lihue (Hawaii, United States) from an economic point of view.

The general trend that can be noted by considering the energy optimization analysis is that locations with a good and not excessive degree of sun exposure, between 300 W/m^2 and 400 W/m^2 in terms of yearly average solar radiation on the horizontal plane, and low-medium yearly average wind speed, around 1.5-2.5 m/s, provide good energy performance for both SA and GC systems. In SA HRES guarantee load satisfaction higher and utilization factor of the energy generated higher than 70%, while in GC HRES percentage of energy exchanged from and to the grid per kWh required by the load lower than 50%. Windier and less sunny localities are inadequate both for GC systems with a very high GEIF and for SA installations with a very low utilization factor. Sunnier and windier localities lead to higher satisfied load fraction while decreasing the utilization factor; instead, the grid energy interaction factor increase but not in a significant manner. Locations without particular climatic characteristics are always suitable to host GC systems.

The general trend that can be noted by considering the economic optimization analysis is that the electricity price affects results significantly more than the climatic conditions and the presence or

absence of FiT in the determination of the most suitable locality. The best localities are characterized by the highest electricity price in the world.

The results obtained employing the extensive energy and economic investigation developed constitutes a concrete device and database to detect the performance of the optimal hybrid system around the world. In addition, the results can be used by other researchers as a reference to compare their investigations.

The continuation of the research will make this study even more general considering, in addition to the climatic conditions and system configuration, the use of the building and the resulting load profile and the size of the district.

References

[1] J. Rogelj, M. den Elzen, N. Höhne, et al. Paris Agreement climate proposals need a boost to keep warming well below 2 °C. Nature 534, 631–639 (2016). https://doi.org/10.1038/nature18307

[2] Renewable energy policy network for the 21st century REN21, Renewables 2018 Global Status Report, Paris: REN21 Secretariat, ISBN 978-3-9818911-3-3, 2018, https://www.ren21.net/wp-content/uploads/2019/05/GSR2018_Full-Report_English.pdf.

[3] Renewable energy policy network for the 21st century REN21, Renewables 2019 Global Status Report, Paris: REN21 Secretariat, ISBN ISBN 978-3-9818911-7-1, 2019, https://www.globalwomennet.org/wp-content/uploads/2019/06/gsr_2019_full_report_en.pdf.

[4] D. Mazzeo, G. Oliveti, C. Baglivo, P. M. Congedo, Energy reliability-constrained method for the multi-objective optimization of a photovoltaic-wind hybrid system with battery storage, Energy, Volume 156, 2018, Pages 688-708, ISSN 0360-5442, https://doi.org/10.1016/j.energy.2018.04.062.

[5] A. Burgio, D. Menniti, A. Pinnarelli and N. Sorrentino, "Reliability studies of a PV-WG hybrid system in presence of multi-micro storage systems," 2009 IEEE Bucharest PowerTech, Bucharest, 2009, pp. 1-5, https://doi.org/10.1109/PTC.2009.5281931.

[6] D. Menniti, A. Pinnarelli and N. Sorrentino, "A method to improve microgrid reliability by optimal sizing PV/Wind plants and storage systems," CIRED 2009 - 20th International Conference and Exhibition on Electricity Distribution - Part 1, Prague, Czech Republic, 2009, pp. 1-4.

[7] L. G. Acuña, R. V. Padilla, A. S. Mercado, Measuring reliability of hybrid photovoltaic-wind energy systems: A new indicator, Renewable Energy, Volume 106, 2017, Pages 68-77, ISSN 0960-1481, https://doi.org/10.1016/j.renene.2016.12.089.

[8] P. M. Congedo, C. Baglivo, L. Carrieri, Hypothesis of thermal and mechanical energy storage with unconventional methods, Energy Conversion and Management, Volume 218, 2020, 113014, ISSN 0196-8904, https://doi.org/10.1016/j.enconman.2020.113014.

[9] P. M. Congedo, C. Baglivo, L. Carrieri, Application of an unconventional thermal and mechanical energy storage coupled with the air conditioning and domestic hot water systems of a residential building, Energy and Buildings, 2020, 110234, ISSN 0378-7788, https://doi.org/10.1016/j.enbuild.2020.110234.

[10] H. Yang, W. Zhou, L. Lu, Z. Fang, Optimal sizing method for stand-alone hybrid solar–wind system with LPSP technology by using genetic algorithm, Solar Energy, Volume 82, Issue 4, 2008, Pages 354-367, ISSN 0038-092X, https://doi.org/10.1016/j.solener.2007.08.005.

[11] H. Yang, Z. Wei, L. Chengzhi, Optimal design and techno-economic analysis of a hybrid solar–wind power generation system, Applied Energy, Volume 86, Issue 2, 2009, Pages 163-169, ISSN 0306-2619, https://doi.org/10.1016/j.apenergy.2008.03.008.

[12] O. Ekren, B. Y. Ekren, Size optimization of a PV/wind hybrid energy conversion system with battery storage using simulated annealing, Applied Energy, Volume 87, Issue 2, 2010, Pages 592-598, ISSN 0306-2619, https://doi.org/10.1016/j.apenergy.2009.05.022.

Chapter 7

**Worldwide geographical mapping and
optimization of stand-alone and grid-connected hybrid renewable
system techno-economic performance across Köppen-Geiger climates**

[13]   T. Ma, H. Yang, L. Lu, A feasibility study of a stand-alone hybrid solar–wind–battery system for a remote island, Applied Energy, Volume 121, 2014, Pages 149-158, ISSN 0306-2619, https://doi.org/10.1016/j.apenergy.2014.01.090.

[14]   S. Diaf, D. Diaf, M. Belhamel, M. Haddadi, A. Louche, A methodology for optimal sizing of autonomous hybrid PV/wind system, Energy Policy, Volume 35, Issue 11, 2007, Pages 5708-5718, ISSN 0301-4215, https://doi.org/10.1016/j.enpol.2007.06.020.

[15]   S. Diaf, G. Notton, M. Belhamel, M. Haddadi, A. Louche, Design and techno-economical optimization for hybrid PV/wind system under various meteorological conditions, Applied Energy, Volume 85, Issue 10, 2008. Pages 968-987, ISSN 0306-2619, https://doi.org/10.1016/j.apenergy.2008.02.012.

[16]   S. Diaf, M. Belhamel, M. Haddadi, A. Louche, Technical and economic assessment of hybrid photovoltaic/wind system with battery storage in Corsica island, Energy Policy, Volume 36, Issue 2, 2008, Pages 743-754, ISSN 0301-4215, https://doi.org/10.1016/j.enpol.2007.10.028.

[17]   R. Dufo-López, J. L. Bernal-Agustín, Multi-objective design of PV–wind–diesel–hydrogen–battery systems, Renewable Energy, Volume 33, Issue 12, 2008, Pages 2559-2572, ISSN 0960-1481, https://doi.org/10.1016/j.renene.2008.02.027.

[18]   A. Kaabeche, M. Belhamel, R. Ibtiouen, Sizing optimization of grid-independent hybrid photovoltaic/wind power generation system, Energy, Volume 36, Issue 2, 2011, Pages 1214-1222, ISSN 0360-5442, https://doi.org/10.1016/j.energy.2010.11.024.

[19]   G. Bekele, G. Tadesse, Feasibility study of small Hydro/PV/Wind hybrid system for off-grid rural electrification in Ethiopia, Applied Energy, Volume 97, 2012, Pages 5-15, ISSN 0306-2619, https://doi.org/10.1016/j.apenergy.2011.11.059.

[20]   R. Belfkira, L. Zhang, G. Barakat, Optimal sizing study of hybrid wind/PV/diesel power generation unit, Solar Energy, Volume 85, Issue 1, 2011, Pages 100-110, ISSN 0038-092X, https://doi.org/10.1016/j.solener.2010.10.018.

[21]   D. Saheb-Koussa, M. Haddadi, M. Belhamel, Economic and technical study of a hybrid system (wind–photovoltaic–diesel) for rural electrification in Algeria, Applied Energy, Volume 86, Issues 7–8, 2009, Pages 1024-1030, ISSN 0306-2619, https://doi.org/10.1016/j.apenergy.2008.10.015.

[22]   D. B. Nelson, M. H. Nehrir, C. Wang, Unit sizing and cost analysis of stand-alone hybrid wind/PV/fuel cell power generation systems, Renewable Energy, Volume 31, Issue 10, 2006, Pages 1641-1656, ISSN 0960-1481, https://doi.org/10.1016/j.renene.2005.08.031.

[23]   W. Kellogg, M. H. Nehrir, G. Venkataramanan, V. Gerez, Optimal unit sizing for a hybrid wind/photovoltaic generating system, Electric Power Systems Research, Volume 39, Issue 1, 1996, Pages 35-38, ISSN 0378-7796, https://doi.org/10.1016/S0378-7796(96)01096-6.

[24]   A. D. Bagul, Z. M. Salameh, B. Borowy, Sizing of a stand-alone hybrid wind-photovoltaic system using a three-event probability density approximation, Solar Energy, Volume 56, Issue 4, 1996, Pages 323-335, ISSN 0038-092X, https://doi.org/10.1016/0038-092X(95)00116-9.

[25]   D. Abbes, A. Martinez, G. Champenois, Life cycle cost, embodied energy and loss of power supply probability for the optimal design of hybrid power systems, Mathematics and Computers in Simulation, Volume 98, 2014, Pages 46-62, ISSN 0378-4754, https://doi.org/10.1016/j.matcom.2013.05.004.

[26]   A. H. Mamaghani, S. A. A. Escandon, B. Najafi, A. Shirazi, F. Rinaldi, Techno-economic feasibility of photovoltaic, wind, diesel and hybrid electrification systems for off-grid rural electrification in Colombia, Renewable Energy, Volume 97, 2016, Pages 293-305, ISSN 0960-1481, https://doi.org/10.1016/j.renene.2016.05.086.

[27]   F. Caballero, E. Sauma, F. Yanine, Business optimal design of a grid-connected hybrid PV (photovoltaic)-wind energy system without energy storage for an Easter Island's block, Energy, Volume 61, 2013, Pages 248-261, ISSN 0360-5442, https://doi.org/10.1016/j.energy.2013.08.030.

[28]   L. Ferrer-Martí, B. Domenech, A. García-Villoria, R. Pastor, A MILP model to design hybrid wind–photovoltaic isolated rural electrification projects in developing countries, European Journal of

Chapter 7

Worldwide geographical mapping and optimization of stand-alone and grid-connected hybrid renewable system techno-economic performance across Köppen-Geiger climates

Operational Research, Volume 226, Issue 2, 2013, Pages 293-300, ISSN 0377-2217, https://doi.org/10.1016/j.ejor.2012.11.018.

[29]   F. F. Yanine, F. I. Caballero, E. E. Sauma, F. M. Córdova, Homeostatic control, smart metering and efficient energy supply and consumption criteria: A means to building more sustainable hybrid micro-generation systems, Renewable and Sustainable Energy Reviews, Volume 38, 2014, Pages 235-258, ISSN 1364-0321, https://doi.org/10.1016/j.rser.2014.05.078.

[30]   B. D. Shakya, L. Aye, P. Musgrave, Technical feasibility and financial analysis of hybrid wind–photovoltaic system with hydrogen storage for Cooma, International Journal of Hydrogen Energy, Volume 30, Issue 1, 2005, Pages 9-20, ISSN 0360-3199, https://doi.org/10.1016/j.ijhydene.2004.03.013.

[31]   S. R. Tito, T. T. Lie, T. N. Anderson, Optimal sizing of a wind-photovoltaic-battery hybrid renewable energy system considering socio-demographic factors, Solar Energy, Volume 136, 2016, Pages 525-532, ISSN 0038-092X, https://doi.org/10.1016/j.solener.2016.07.036.

[32]   G. M. Shafiullah, Hybrid renewable energy integration (HREI) system for subtropical climate in Central Queensland, Australia, Renewable Energy, Volume 96, Part A, 2016, Pages 1034-1053, ISSN 0960-1481, https://doi.org/10.1016/j.renene.2016.04.101.

[33]   M.A. Abdullah, K.M. Muttaqi, A.P. Agalgaonkar, Sustainable energy system design with distributed renewable resources considering economic, environmental and uncertainty aspects, Renewable Energy, Volume 78, 2015, Pages 165-172, ISSN 0960-1481, https://doi.org/10.1016/j.renene.2014.12.044.

[34]   M. Kottek, J. Grieser, C. Beck, B. Rudolf, F. Rubel, World Map of the Koppen-Geiger climate classification updated, Meteorologische Zeitschrift, 15.3 (2006), pp. 259-263, 10.1127/0941-2948/2006/0130.

[35]   F. Rubel, M. Kottek, Observed and projected climate shifts 1901-2100 depicted by world maps of the Köppen-Geiger climate classification. Meteorol Z 2010;19:135–41. http://koeppen-geiger.vu-wien.ac.at/shifts.htm.

[36]   J. Ascencio-Vásquez, K. Brecl, M. Topič, Methodology of Köppen-Geiger-Photovoltaic climate classification and implications to worldwide mapping of PV system performance, Solar Energy, Volume 191, 2019, Pages 672-685, ISSN 0038-092X, https://doi.org/10.1016/j.solener.2019.08.072.

[37]   M. Saffari, A. de Gracia, C. Fernández, L. F. Cabeza, Simulation-based optimization of PCM melting temperature to improve the energy performance in buildings, Applied Energy, Volume 202, 2017, Pages 420-434, ISSN 0306-2619, https://doi.org/10.1016/j.apenergy.2017.05.107.

[38]   University of Wisconsin, Solar Energy Laboratory, TRNSYS 17: A transient system simulation program, 2012, http://www.trnsys.com/ (accessed on 26 April 2020).

[39]   D. G. Erbs, S. A. Klein, J. A. Duffie, Estimation of the diffuse radiation fraction for hourly, daily and monthly-average global radiation, Solar Energy, Volume 28, Issue 4, 1982, Pages 293-302, ISSN 0038-092X, http://dx.doi.org/10.1016/0038-092X(82)90302-4.

[40]   J. A. Duffie, W. A. Beckman, Solar Engineering of Thermal Processes 4th Edition, Solar Energy Laboratory University of Wisconsin-Madison, John Wiley & Sons, 2013.

[41]   A. Bryan Fry, Simulation of Grid-Tied Building Integrated Photovoltaic Systems. M. S. Thesis –Solar Energy Laboratory, University of Wisconsin, Madison: 1999.

[42]   P. J. A. Quinlan, Time series modeling of hybrid wind photovoltaic diesel power systems. M. S. Thesis –Solar Energy Laboratory, University of Wisconsin, Madison: 1996.

[43]   D. Mazzeo, C. Baglivo, N. Matera, P. M. Congedo, G. Oliveti, A novel energy-economic-environmental multi-criteria decision-making in the optimization of a hybrid renewable system, Sustainable Cities and Society, Volume 52, 2020, 101780, ISSN 2210-6707, https://doi.org/10.1016/j.scs.2019.101780.

[44]   D. Mazzeo, Solar and wind assisted heat pump to meet the building air conditioning and electric energy demand in the presence of an electric vehicle charging station and battery storage, Journal of Cleaner

Chapter 7   **Worldwide geographical mapping and**
optimization of stand-alone and grid-connected hybrid renewable
system techno-economic performance across Köppen-Geiger climates

Production,   Volume   213,   2019,   Pages   1228-1250,   ISSN   0959-6526,
https://doi.org/10.1016/j.jclepro.2018.12.212.

[45]   C. Baglivo, D. Mazzeo, G. Oliveti, P. M. Congedo, Technical data of a grid-connected
photovoltaic/wind hybrid system with and without storage battery for residential buildings located in a
warm   area,   Data   in   Brief,   Volume   20,   2018,   Pages   587-590,   ISSN   2352-3409,
https://doi.org/10.1016/j.dib.2018.08.083.

[46]   A. J. Arnfield, Köppen climate classification, Encyclopædia Britannica, Encyclopædia Britannica,
inc., 2020, https://www.britannica.com/science/Koppen-climate-classification.

[47]   D. Chen, H. W. Chen, Using the Köppen classification to quantify climate variation and change: An
example for 1901–2010. Environmental Development, 6, 69-79, 2013, 10.1016/j.envdev.2013.03.007.

[48]   D. Mazzeo, N. Matera, G. Oliveti, Interaction Between a Wind-PV-Battery-Heat Pump Trigeneration
System and Office Building Electric Energy Demand Including Vehicle Charging, 2018 IEEE
International Conference on Environment and Electrical Engineering and 2018 IEEE Industrial and
Commercial   Power   Systems   Europe   (EEEIC / I&CPS   Europe),   Palermo,   2018,   pp.   1-5,
https://doi.org/10.1109/EEEIC.2018.8493710.

[49]   D. Mazzeo, Nocturnal electric vehicle charging interacting with a residential photovoltaic-battery
system: a 3E (energy, economic and environmental) analysis, Energy, Volume 168, 2019, Pages 310-331,
ISSN 0360-5442, https://doi.org/10.1016/j.energy.2018.11.057.

[50]   Mitsubishi Electric & Electronics USA, Inc,   Mitsubishi PV-MLU250HC, Available at:
https://www.mitsubishielectricsolar.com/images/uploads/documents/specs/MLU_spec_sheet_250W_255
W.pdf, last access: 23/06/2020.

[51]   Renugen - Renewable Generation, Tulipower 2.5kW Wind Turbine, Available at:
https://www.renugen.co.uk/tulipower-2-5kw-wind-turbine-discontinued, last access: 23/06/2020

[52]   Electric Car Home, sonnenBatterie, https://electriccarhome.co.uk/battery-storage/sonnen-battery, last
access: 23/06/2020.

[53]   Solaris Technology Industry, Inc., Fronius, Available at: https://www.solaris-shop.com/fronius-ig-
plus-v-5-0-1-uni-5-0kw-inverter-4-210-113-800, last access: 23/06/2020.

[54]   W. Rickerson, Feed-in tariffs as a policy instrument for promoting renewable energies and green
economies in developing countries, United Nations Environment Programme UNEP, 2012, Available at:
http://wedocs.unep.org/bitstream/handle/20.500.11822/8102/-Feed-
in%20tariffs%20and%20a%20policy%20instrument%20for%20promoting%20renewable%20energies%
20and%20green%20economies%20in%20developing%20countries-
20121117.pdf?sequence=3&isAllowed=y, last access: 23/06/2020.

Nomenclature

Abbreviations

A	Autonomy
ACS	Annualized Cost of the System (€)
BCR	Benefit cost ratio (1/yr)
COE	Cost of Energy (€/kWh)
DPSP	Deficiency of Power Supply Probability (%)
ED	Electrical Device
EE	Embodied Energy
EL	Electrical Lighting
EV	Electric Vehicle
FiT	Feed-in-Tariff
GA	Genetic Algorithm
GC	Grid-Connected

GEIF	Grid Energy Interaction Factor (-)
HRES	Hybrid renewable energy systems
IRR	Internal Rate of Return
LCC	Life Cycle Cost
LEC	Levelled Energy Cost (€/kWh)
LCE	Levelized Cost of Energy (€/kWh)
LCOE	Renewable Fraction
LOLP	Loss of Load Probability
LPSP	Loss of Power Supply Probability (%)
LUEC	Levelised Unit Electricity Costs (€/kWh)
MOEA	Multi-Objective Evolutionary Algorithm
NOCT	nominal operating temperature of the cell (°C)
NPC	Net Present Cost (€)
OP	Occupant Profile
PV	Photovoltaic
RF	Renewable Fraction
SA	Stand-Alone
SAA	Simulated Annealing Algorithm
SOC	State Of Charge of the battery (Wh)
STC	Total Cost of The System (€)
SLF	Satisfied load fraction (-)
UF	Utilization factor (-)
UL	Unmet Load (kWh)

Symbols

a	Modified ideality factor (eV)
B	Yearly benefit (€/yr)
c_b	Battery specific cost (€/kWh)
c_e	Yearly average electricity price (€/kWh)
c_{inv}	Inverter specific cost (€/kW)
c_{pv}	Photovoltaic specific cost (€/kW)
c_w	Wind specific cost (€/kW)
C	Overall system cost (€)
C_c	Capital cost (€)
C_r	Replacement cost (€)
$e_{pv,g}$	PV energy fraction (-)
$e_{w,g}$	Wind energy fraction (-)
E_d	Yearly energy dissipated (Wh)
E_{dtl}	Yearly energy sent directly to the load (Wh)
E_{fb}	Yearly energy drawn from the battery (Wh)
E_{fg}	Yearly energy drawn from the grid (Wh)
E_g	Yearly overall energy produced by the generators (Wh)
E_L	Yearly energy required by the load (Wh)
E_m	Yearly missing energy (Wh)
E_{pv}	Yearly energy produced by the photovoltaic generator (Wh)
E_{tb}	Yearly energy sent to the battery (Wh)
E_{tl}	Yearly energy produced sent to the load (Wh)

E_{tg}	Yearly energy produced sent to the grid (Wh)
E_w	Yearly energy produced by the wind generator (Wh)
G	Hourly solar radiation on the inclined surface (W/m^2)
$G_{b,h}$	Hourly beam solar radiation on the horizontal surface (W/m^2)
$G_{d,h}$	Hourly diffuse solar radiation on the horizontal surface (W/m^2)
I	Current (A)
I_0	Diode reverse saturation current (A)
I_L	Light current (A)
$I_{mp}(t)$	Current at maximum power point (A)
$P_0(t)$	Wind turbine power at the actual operating height for a reference air density (W)
p_b	Battery power fraction (-)
p_l	Load power fraction (-)
p_{ol}	Overall load power fraction (-)
p_{pv}	Photovoltaic power fraction (-)
$p_{s,pv}$	Photovoltaic Feed-in-tariff price (€/kWh)
$p_{s,w}$	Wind Feed-in-tariff price (€/kWh)
p_w	Wind power fraction (-)
P_b	Nominal battery power (kW)
P_{inv}	Nominal inverter power (kW)
P_l	Yearly average load power (kW)
P_{pv}	Nominal photovoltaic power (kW)
P_w	Nominal wind power (kW)
$P_{pv}(t)$	Power produced by the photovoltaic generator (W)
$P_{tb}(t)$	Power sent to the battery (W)
$P_\rho(t)$	Wind turbine power as a function of air density (W)
R	Yearly revenue (€/yr)
R_b	Geometry factor of the beam radiation (-)
R_d	Geometry factor of the diffuse radiation (-)
R_r	Geometry factor of the reflected radiation (-)
R_s	Series resistance (Ω)
R_{sh}	Shunt resistance (Ω)
V	Voltage (V)
v_{an}	Wind speed at the anemometric height (m/s)
$v_h(t)$	Wind speed at the actual operating height of the wind turbine (m/s)
$V_{mp}(t)$	Voltage at maximum power point (V)
$v_{nom,\rho}$	Nominal wind speed as a function of air density (m/s)
v_{nom,ρ_0}	Nominal wind speed at the reference air density (m/s)
z_{an}	Anemometric height (m)
z_h	Actual operating height of the wind turbine (m)
Greek letters	
$\alpha(t)$	Wind shear exponent (-)
Δt	Time interval (s)
η_{bat}	Battery efficiency (-)
η_{inv}	Inverter efficiency (-)
η_{reg}	Regulator efficiency (-)
$\rho(t)$	Air density (kg/m^3)
ρ_0	Power curve air density (kg/m^3)

Artificial intelligence application for the performance prediction of a clean energy community

Chapter 8

Artificial intelligence application for the performance prediction of a clean energy community

Abstract

Artificial Neural Networks (ANNs) are proposed for sizing and simulating a clean energy community (CEC) that employs a PV-wind hybrid system, coupled with energy storage systems and electric vehicle charging stations, to meet the building district energy demand. The first ANN is used to forecast the energy performance indicators, which are satisfied load fraction and the utilization factor of the energy generated, while the second ANN is used to estimate the grid energy indication factor. ANNs are trained with a very large database in any climatic conditions and for a flexible power system configuration and varying electrical loads. They directly predict the yearly CEC energy performance without performing any system dynamic simulations using sophisticated models of each CEC component. Only eight dimensionless input parameters are required, such as the fractions of wind and battery power installed, yearly mean and standard deviation values of the total horizontal solar radiation, wind speed, air temperature and load. The Garson algorithm was applied for the evaluation of each input influence on each output. Optimized ANNs are composed of a single hidden layer with twenty neurons, which leads to a very high prediction accuracy of CECs which are different from those used in ANN training.

Keywords: Machine learning; Artificial neural network; Solar PV; Wind turbines; Electric vehicle charging; Battery storage

- Artificial neural network (ANN) tools to predict the performance of a clean energy community (CEC)
- PV and wind systems, battery storage and electric vehicle charging stations compose the novel CEC
- ANNs are validated for any power installed and for any load trend, without geographical restrictions
- ANNs are capable to determine the yearly performance without performing any dynamic simulation
- Optimized ANNs are composed of a single hidden layer with twenty neurons

1. Introduction

Big data and artificial intelligence (AI) have received significant attention in recent years from research communities and the energy industry. There are two main reasons for this interest (i) increasing computational power, and (ii) exponential growth of data around the world [1]. Particularly, big data and AI are useful tools for wind and solar energy due to their interruptible nature. Big data and AI can be applied to wind and solar generation forecasting, grid stability and reliability, demand forecast, demand-side management, optimised energy storage operation, market design, and operation for wind and solar integration [2].
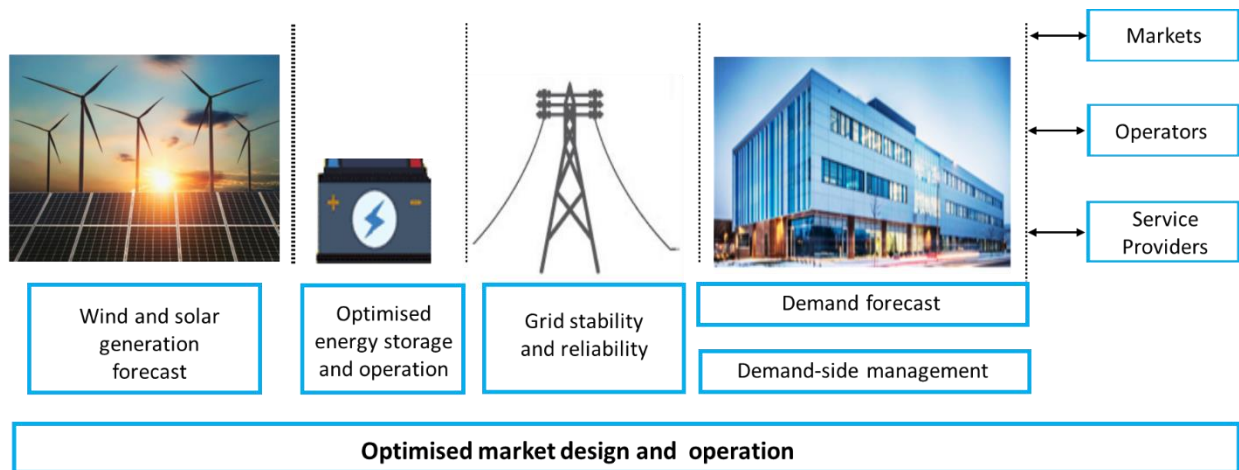
Figure 1. *Artificial intelligence applications for wind and solar integration (modified from [2]).*

1.1 State-of-the-art

Many research papers have been published in recent years with increasing attention in regards to AI applications for wind energy, solar energy and hybrid renewable energy systems. Jha *et al.* [3] summarized the review papers on AI applications in renewable energy (RE) that were published up until 2017. The AI methods have been used for [3]: (i) wind energy: wind power prediction, wind speed prediction, design of wind generation systems, missing wind data interpolation, wind turbine fault diagnosis, risk optimization in wind energy trading; (ii) solar energy: solar irradiance prediction, daily ambient temperature prediction, daily solar irradiation prediction, solar energy prediction, solar power prediction, maximum power point tracking (MPPT) of PV arrays, size optimization of PV systems; (iii) hybrid renewable energy: power and generator status prediction, energy management, PV/wind system optimization, size optimization, power flow control. The various AI methods [3] used for RE can be listed as: artificial neural network (ANN), back propagation neural network (BPNN), radial basis function neural networks (RBFNN), adaptive linear element network (ADALINE), recurrent high order ANN, naïve Bayes (NB), Trigonometric point cumulative semivariogram (TPCSV), Autoregressive moving average (ARMA), neural logic network (NLN), fuzzy, support vector machines (SVM), adaptive neuro fuzzy inference system (ANFIS), wavelet analysis (WT), genetic algorithm (GA), ant colony optimization (ACO), particle swarm optimization (PSO), bee algorithm, Markov based GA, and hybrid methods such as the combination of Fuzzy and GA or ACO and PSO.

A comprehensive literature search was also conducted for this study while considering the scope of our paper. The sources published between 2016 and 2020 were identified through Scopus using this

string: (Wind OR Solar OR "Wind Turbine" OR "Solar PV" OR "Solar Photovoltaic") AND ("Artificial Intelligence" OR "Machine Learning") AND (building* OR house* OR residential OR home* OR household). The search was limited to the journals: Applied Energy, Energies, Energy, Energy Conversion and Management, Journal of Cleaner Production, Renewable Energy, Renewable and Sustainable Energy Reviews, and Solar Energy. However, other journals were also searched using the snowball method after completing the Scopus search. There were 25 papers concluded to be most relevant for our literature search and they are summarized in Table 1.

Table 1. Selected papers about AI applications in solar, wind and hybrid systems published between 2016 and 2020 (Refs. [4-28])

Author & Year	Application	Method(s)	Comments
Li *et al.,* **2016**	Solar PV power generation estimation	ANN, SVR	The authors compared ANN and SVR for predicting energy productions from a solar PV system in Florida.
Klingler & Teichtmann, **2017**	Predicting solar PV production and household demand	ANN	The studied system in this paper is the grid connect PV-battery system. PV production and household demand were estimated using ANN and the battery operation was controlled by applying a linear optimization approach.
Al-Dahidi *et al.*, **2018**	Predicting solar PV power production	ELM	ELM was used to predict solar PV power production. The ELM model was compared with BP-ANN, and the results revealed that the ELM predicted the PV power production slightly more accurately, with negligible computational effort, compared to the BP-ANN model.
Yu *et al.*, **2018**	Identifying the GPS databased for solar PV installations.	MARS, one-stage random Forest, two-stage models utilizing a second stage with LR or MARS, two-stage Random Forest (SolarForest), and FFNN (SolarNN)	The authors developed DeepSolar, a novel semi-supervised deep learning framework to generate a national solar installation database from satellite images.
Kim & Lim, **2018**	EMS for a smart energy building	Q-learning	Q-learning, one of the methods in RL, was used as an energy management algorithm for a smart energy building. The energy system includes PV generation, an energy storage system and a vehicle to grid station. The building was also connected to an external grid.
Priyadarshi *et al.*, **2019**	MPPT	ACO	Maximum power point was achieved by using ACO-based MPPT.
Zhang *et al.*, **2019**	Optimal sizing of a stand-alone hybrid solar and wind energy system	Hybrid (CS- HS- SA)	Three hybrid systems: solar/hydrogen, wind/hydrogen, and solar/wind/hydrogen were optimized using CS-HS-SA. The ANN model was also used in the study for weather forecasting.
Zhang *et al.*, **2019**	Load forecasting, optimal design of a small independent hybrid system	ANN, TS	ANN was applied for load forecasting, and the TS method was used for the optimal design of the hybrid system that consists of wind, solar and battery.
Le & Benjapolakul, **2019**	Evaluation of lifetime energy yield of roof top PV systems	Bootstrap, MLR	The researchers in this paper investigated PV system configurations and component contributions to energy yield.
Marinescu *et al.*, **2019**	Optimal EV residential charging	P-MARL	A control algorithm, prediction-based P-MARL, was developed to the problem of optimal EV residential charging under intermittent wind availability and variable household baseload demands,
Zhang *et al.*, **2019**	Energy management of an IES	DRL	The results showed that the proposed algorithm can effectively minimize the operating cost of the system.
Bingham *et al.*, **2019**	Optimal design of building envelope and renewable energy integration	NSGA-II	The authors showed that the life cycle cost of the system and yearly energy consumption of the building could be significantly decreased using optimal design algorithms.
Sundaram, **2019**	Predicting solar PV plant performance	ANN	The final yield and performance ratio for 1 MWp PV system on a monthly average daily basis were estimated by using ANN.
Pang *et al.*, **2020**	Solar radiation prediction	ANN, RNN	ANN and RNN were compared for solar radiation prediction. The results revealed that RNN has a higher prediction accuracy than ANN.

Lee & Choi, **2020**	EMS	DRL	DRL was used for scheduling energy consumption of smart home appliances and DERs including an ESS and an EV.
Ahmad *et al.*, **2020**	Forecasting of renewable energy and electricity requirement	ML algorithms, ensemble-based approaches, ANNs	This paper is a review study on renewable energy and electricity prediction models using different AI methods.
Nezhad *et al.*, **2020**	Determining wind energy production potential	ANFIS	The authors proposed a new combined model to integrate wind speed assessment, mapping and forecasting using Sentinel 1 satellite data through image processing and ANFIS.
Mirza *et al.*, **2020**	MPPT	SSO	SSO method was proposed for effective MPPT under various weather conditions.
Zhou & Zheng, **2020**	Demand-side controller for high-rise office buildings	MLR, SVR, BPNN	A data-driven model was formulated for the building demand prediction with a short-term prediction for energy management.
Feng *et al.*, **2020**	Capacity and operation method optimization of PV-PV-BSS	PSO	PSO was applied to optimize the economic and environmental impacts of integrated PV-BSS.
Mayer *et al.*, **2020**	Optimization of a household level hybrid renewable energy system	GA	The household hybrid RE system was optimized by using GA. The hybrid system consists of solar PV, wind turbine, solar heat collector, heat pump, heat storage, and battery. Backup power was provided from the grid or a diesel generator.
Nyong-Bassey *et al.*, **2020**	Energy management strategies	RL	Energy management of stand-alone hybrid energy storage systems was investigated by applying RL based adaptive power pinch analysis.
Dhunny *et al.*, **2020**	Assessing and optimizing wind turbine placement	GA	The method that was proposed by the authors can be used for design and economic assessment of offshore wind farms in any location in the world.
Kim *et al.*, **2020**	Forecasting of the optimal panel tilt angle of PV system	LR, LASSO, RF, SVM, GB	LR, LASSO, RF, SVM and GB were used to forecast the solar power generation and define the optimal panel tilt angle of a PV system considering various conditions such as weather, dust level, and aerosol level.
Sui & Song, **2020**	Battery scheduling	RL	The authors developed an RL framework for solving battery scheduling problems to extend the battery lifetimes for various applications that include EVs, cellular phones and embedded systems.

Abbreviation: ELM: extreme learning machine, LR: linear regression, MARS: multivariate adaptive regression splines, FFNN: feedforward neural network, EMS: energy management system, RL: reinforcement learning, MPPT: maximum power point tracker, CS: chaotic search, HS: harmony search, SA: simulated annealing, TS: tabu search, MLR: multiple linear regression, P-MARL: multi-agent reinforcement learning, EV: electric vehicle, IES: integrated energy system, DRL: deep reinforcement learning, NSGA-II: non-sorting generic algorithm, RNN: recurrent neural network, DERs: distributed energy resources, ESS: energy storage system, ML: machine learning, SSO: Salp swarm optimization, SVR: support vector regression, PV-BSS: PV-battery swapping station, LASSO: least absolute shrinkage and selection operator, RF: random forest, GB: gradient boosting.

Based on the comprehensive literature search and to the best of our best knowledge, there is no published paper in the literature estimating the performance of a hybrid wind-solar PV-battery and EV station integrated into buildings at any location in the world. Therefore, ANN was applied and validated for the pre-sizing and energy performance prediction of a PV-wind-battery hybrid renewable energy system (HRES) in this paper. The developed ANN algorithms aim to directly determine the yearly energy reliability of a PV-wind HRES without using hourly climatic data and to implement sophisticated dynamic models to predict the thermo-electrical performance of a PV system and the electrical performance of a wind-turbine. In addition, the yearly energy performance evaluated by the ANN considers the hourly balance of the system that changes if the power generated

is lower or greater than the power load. An ANN optimization was performed by determining the number of neurons that permit accuracy optimization, quantified by using some indices, such as the MSE and R-square. MATLAB source codes were used in this study, which have been made open-source and are available to the readers in the Appendix and through LAPSE: Living Archive for Process Systems Engineering at PSEcommunity.org.

1.2 Research objectives and novelties

An Artificial Neural Network (ANN) for the sizing and energy performance prediction of a CEC consisting of PV-wind-battery hybrid renewable energy system (HRES) used to supply electrical energy for office buildings equipped with electric vehicle charging stations was developed and validated.

The ANN was trained using an extremely large database composed of 49392 yearly simulations carried out on an hourly basis considering 48 locations around the world. These simulations were conducted according to the Koppen climate classification and, different system power configurations and loads, which were obtained by changing the number of buildings in the district.

The training phase was developed using:

- As outputs: some dimensionless indicators that estimate interactions between load demand, the hybrid system and the electrical grid, such as the fraction of satisfied load, the fraction of energy generated employed to satisfy the load and the level of energy interaction with the grid;

- As inputs: some dimensionless indicators that consider the yearly average values of the hourly external weather data and load, and the yearly standard deviations of the hourly load as a function of the system component nominal powers installed.

In this way, the ANN summarizes the hourly behaviour of the PV-wind HRES in relation to the existing climate and load conditions to directly provides the yearly energy performance.

This ANN algorithm can directly determine the yearly energy performance of the PV-wind HRES deriving from the implementation of sophisticated dynamic models to predict the thermo-electrical performance of a PV system coupled to the electrical performance of a wind turbine in dynamic simulations that requires hourly climatic data. The ANN requires component powers installed, yearly mean and standard deviations values of dynamic variables, such as external air temperature, horizontal solar radiation, wind speed and electrical load. In addition, the yearly energy performance evaluated by the ANN considers the hourly balance of the system that changes if the power generated is lower or greater than the power load.

The ANN was validated by considering different localities, system power configurations and power loads that differ from those used to create the database. This demonstrated the universal validity, namely, for any locality around the world, any system power configuration, and power load level.

An ANN optimization was performed by determining the number of neurons needed to optimize the accuracy, quantified by using some accuracy metrics, such as the root mean square error RMSE and regression R.

Definitively, the ANN proposed allows designers and researchers to immediately obtain the yearly energy performance of a PV-wind HRES in any location and for any power installed and load. The result obtained from ANN is almost equivalent to what would be obtained by a sophisticated hourly simulation based on detailed component electrical models. The advantages are related to the reduction of input data required, only yearly average and standard deviations, and the lack of required expertise needed to use specific transient simulation tools that in many cases require an expensive license to be used.

2. Materials and Methods

Figure 2 illustrates the steps to develop an ANN to forecast the energy performance of a hybrid system for any location in the world. The hybrid system consists of solar PV and wind power generators, and a battery storage system to supply electricity to a building district containing electric vehicle charging (EV) stations.
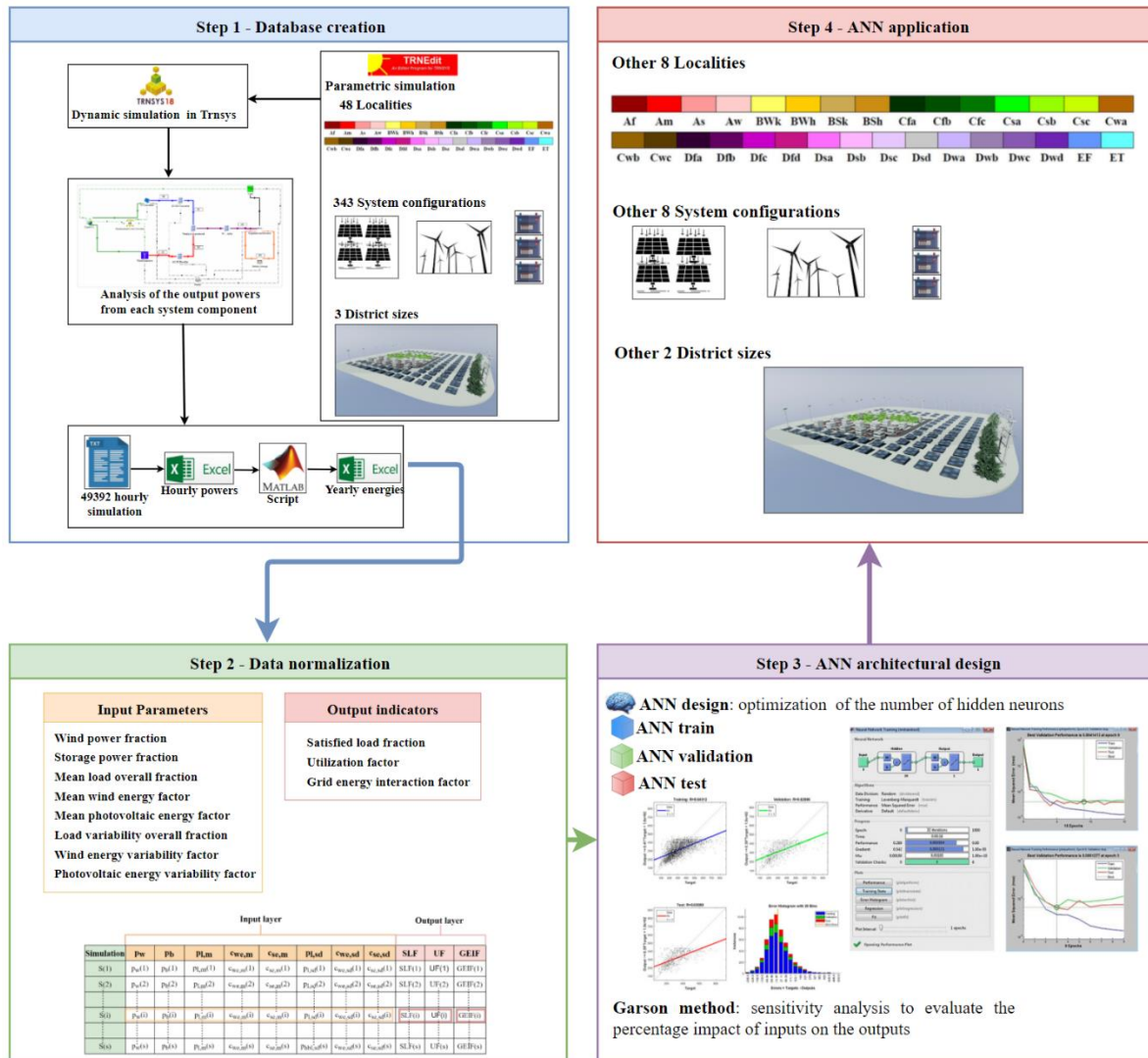
Figure 2. *Framework of the artificial neural network creation*

Step 1 consists of the database creation that requires:

- the implementation of a simulation algorithm in the TRNSYS environment [29] to evaluate dynamically the power flows in the different sections of the system for different installed powers, locations worldwide and district sizes by using the TrnEdit tool;
- the development of a Matlab script for the instantaneous verification of the balances of the system power flows, the calculation of the yearly energies in the different sections of the system and the verification of the yearly energy balances.

Step 2 involves the data normalization using the definition of input dimensionless parameters dependent on the technical characteristic of the hybrid system, climatic data variables and load trend and output indicators defining the energy reliability and performance of the system.

Step 3 has the objective to design, train, validate and test the ANN architecture using the previously created database. The Neural Net Fitting tool in MATLAB [30] was used for the training phase, which allows the user to create a neural network with a hidden layer and train it through an error reduction algorithm. Some accuracy indices were used to optimize the number of neurons.

Step 4 concerns the application, validation and testing of the ANNs created under other climatic conditions and for other system configurations and district sizes, namely by employing external data to the initial database.

Each step is explained in detail in the following sections.

The forecasting tool is proposed as a design support tool for the energy performance verification of an HRES configuration located in a specific locality and used to supply electricity to a building district with a known size. In addition, the forecasting tool can be used for the optimization purpose, by means of extensive parametric simulations, to identify the optimal HRES configuration for a specific locality and load or vice versa.

2.1. Step 1 – Database creation

The database for the studied hybrid system in this work was built in two steps. In the first step, the simulation model of the system was created in the TRNSYS environment. TRNSYS was selected for simulation of the system because with its extensive library, it has an advanced capability for transient simulation of renewable energy systems [29]. Furthermore, TRNSYS can be easily connected with other applications such as Excel, MATLAB, and Engineering Equation Solver (EES). In the simulation, the output powers from each component in the system were hourly calculated and summarized by means of yearly energies. In the second step, a normalized database was created to develop an ANN model for the proposed system in this work. The hourly results were summarized in terms of yearly energies by means of a homemade Matlab Script and normalized by defining some dimensionless parameters and indicators.

2.1.1. Case study

The clean energy community (CEC) shown in Figure 3 is composed of office buildings equipped with electric vehicle charging stations powered by a PV-wind-battery hybrid renewable system. The community is connected to the grid to import and export energy when, respectively, the generated energy from the system is lower or higher than the overall electrical load of the CEC.

The main components of the hybrid renewable system are a PV generator, a wind turbine and a battery electrical storage unit. Three different district sizes were analysed by considering a CEC composed of five, ten and twenty buildings that require electrical energy for electric devices, lighting systems and EV charging stations. A video of the 3D model of the CEC can be downloaded with this paper.

The studied system was considered in 48 different locations around the world. The locations were selected based on the Koppen climate classification. The locality selection phase includes at least two localities for each Koppen climate sub-group, a uniform distribution in different continents and latitudes on the basis of continent size and population, and climatic conditions very different with very and low sunny localities, very hot and cold localities and very and low windy localities. There are five main groups in Koppen climate classification: tropical, dry, temperate, continental, and polar. Some subcategories further classify the climate into major categories. The selected locations mostly

belong to macro-regions C and D, which turn out to be those of greatest interest since they are most populated. The parameters considered for each location are: (i) wind speed; (ii) total solar radiation in the horizontal plane; (iii) external air temperature. The first two variables are needed to calculate the energy generated from the wind and solar systems, respectively, while the temperature is an essential parameter that affects the performance of both systems. Distributions of the locations chosen for this study are shown in Figure 3 and Table 2. Details about the Koppen climate classification can be found in the supplementary file.

Figure 3. Grid-connected system considered in this study.
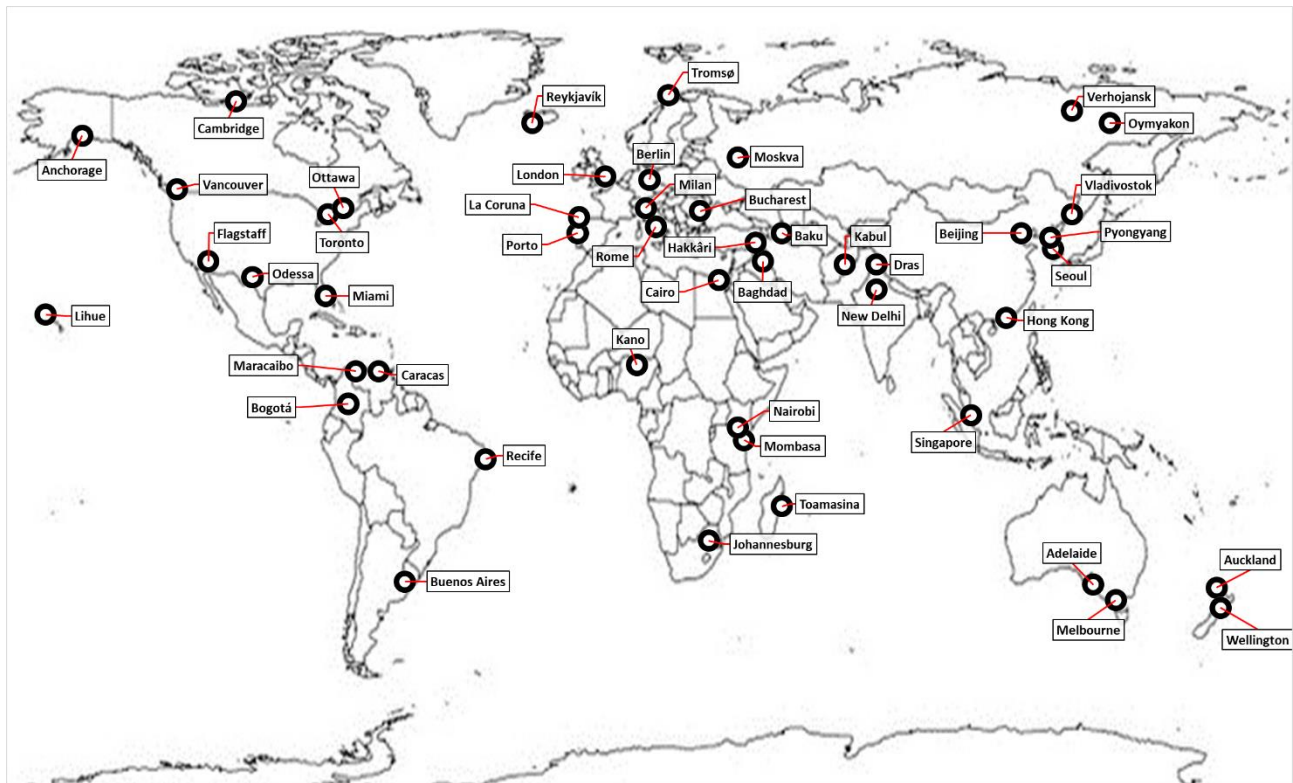
Figure 4. Geographical distribution of the locations chosen for this study.

As regards PV inclination angle, a preliminary optimization analysis was made to place PV modules in each locality at their optimal angle that maximize the yearly electrical energy produced. The optimal angle derives from a TRNSYS dynamic simulation for inclination angles variable between −90° and 90°. As regards the PV azimuth angle, PV modules are exposed to the South for the Northern hemisphere localities and to the North for the Southern hemisphere localities. In this way, the forecasting tool directly provides results considering the optimal PV inclination angle for each locality worldwide.

Table 2. Selected cities for ANN training.

Number	Locality	Country	Koppen group	Latitude	Longitude	Optimal PV angle
1	Toamasina	Madagascar	Af	-18.12	49.40	-16
2	Singapore	Singapore	Af	1.03	103.98	2
3	Recife, Pernambuco	Brazil	Am	-8.07	-34.85	-4
4	Miami, Florida	United States	Am	25.80	-80.27	26
5	Lihue, Hawaii	United States	As	21.98	-159.35	20
6	Mombasa	Kenya	As	-4.03	39.62	0
7	Caracas	Venezuela	Aw	10.60	-66.98	10
8	Kano	Nigeria	Aw	12.05	8.53	16
9	Baghdad	Iraq	BWh	33.33	44.43	32
10	Cairo	Egypt	BWh	30.08	31.28	28
11	Kabul	Afghanistan	BSk	34.55	69.22	34
12	Baku	Azerbaijan	BSk	40.38	49.85	28
13	Odessa, Texas	United States	BSh	46.48	-30.63	34
14	Maracaibo	Venezuela	BSh	10.65	-71.60	10
15	Buenos Aires	Argentina	Cfa	-34.58	-58.48	-28
16	Milan	Italy	Cfa	45.62	8.73	36

17	Berlin	Germany	Cfb	52.47	13.40	38
18	London	United Kingdom	Cfb	51.52	-0.12	36
19	Vancouver, British Columbia	Canada	Cfb	49.25	-123.25	36
20	Melbourne, Victoria	Australia	Cfb	-37.82	144.97	-30
21	Bogotá, Cundinamarca	Colombia	Cfb	4.05	-74.15	2
22	Wellington	New Zealand	Cfb	-41.32	174.77	-32
23	Reykjavík	Iceland	Cfc	64.13	-21.90	44
24	Auckland Islands	New Zealand	Cfc	-37.02	174.80	-30
25	Rome	Italy	Csa	41.80	12.58	36
26	Adelaide	Australia	Csa	-34.93	138.53	-28
27	Porto	Portugal	Csb	41.13	-8.60	34
28	La Coruna	Spain	Csb	43.37	-8.42	32
29	New Delhi	India	Cwa	28.58	77.20	32
30	Hong Kong	China	Cwa	22.30	114.17	20
31	Johannesburg	South Africa	Cwb	-26.13	28.23	-26
32	Nairobi	Kenya	Cwb	-1.15	36.92	4
33	Bucharest	Romania	Dfa	44.50	26.22	34
34	Toronto, Ontario	Canada	Dfa	43.72	-79.23	36
35	Moskva	Russia	Dfb	55.83	37.62	42
36	Ottawa, Ontario	Canada	Dfb	45.38	-75.72	40
37	Tromsø	Norway	Dfc	69.65	18.95	46
38	Anchorage, Alaska	United States	Dfc	61.17	-150.02	48
39	Oymyakon, Sakha Republic	Russia	Dfd	63.27	143.15	52
40	Verhojansk, Sakha Republic	Russia	Dfd	67.55	133.38	52
41	Hakkâri	Turkey	Dsa	37.57	43.77	30
42	Cambridge Bay, Nunavut	Canada	Dsa	69.10	-105.12	52
43	Dras	India	Dsb	34.43	75.77	30
44	Flagstaff, Arizona	United States	Dsb	35.13	-111.67	36
45	Beijing	China	Dwa	39.93	116.28	38
46	Seoul	South Korea	Dwa	37.57	126.97	34
47	Pyongyang	North Korea	Dwb	39.03	125.78	36
48	Vladivostok	Russia	Dwb	43.12	131.90	44

To summarize the behaviour of each climate variable in different localities, box plots of hourly variations were built, as reported in Figure 5. The typical meteorological year (TMY) weather data file, already available in the TRNSYS library in the version tm2, was used for the localities considered. The figure highlights the strong difference in climatic conditions in the localities considered.
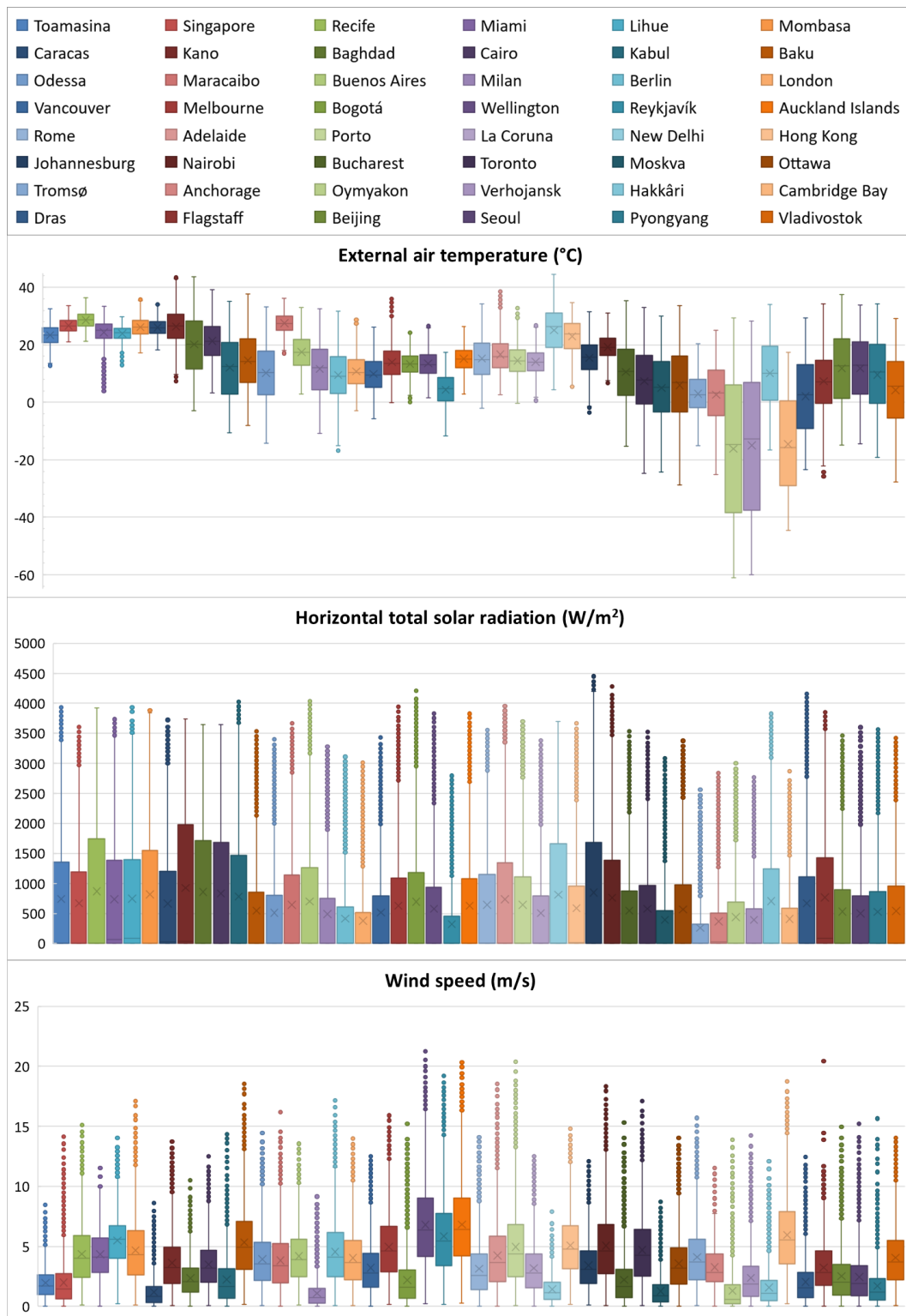
Figure 5. *Yearly box plots of the hourly external air temperature, horizontal total solar radiation and wind speed in the selected locations for the ANN design.*

2.1.2. The system dynamic simulation in the TRNSYS environment

The schema of the hybrid plant studied in the TRNSYS simulation studio is illustrated in Figure 6. The version used for this study was TRNSYS 17. Each component in the system is simulated in the TRNSYS environment using a specific type. In addition, several calculator tools, a printer, and a controller were added for simulation purposes.
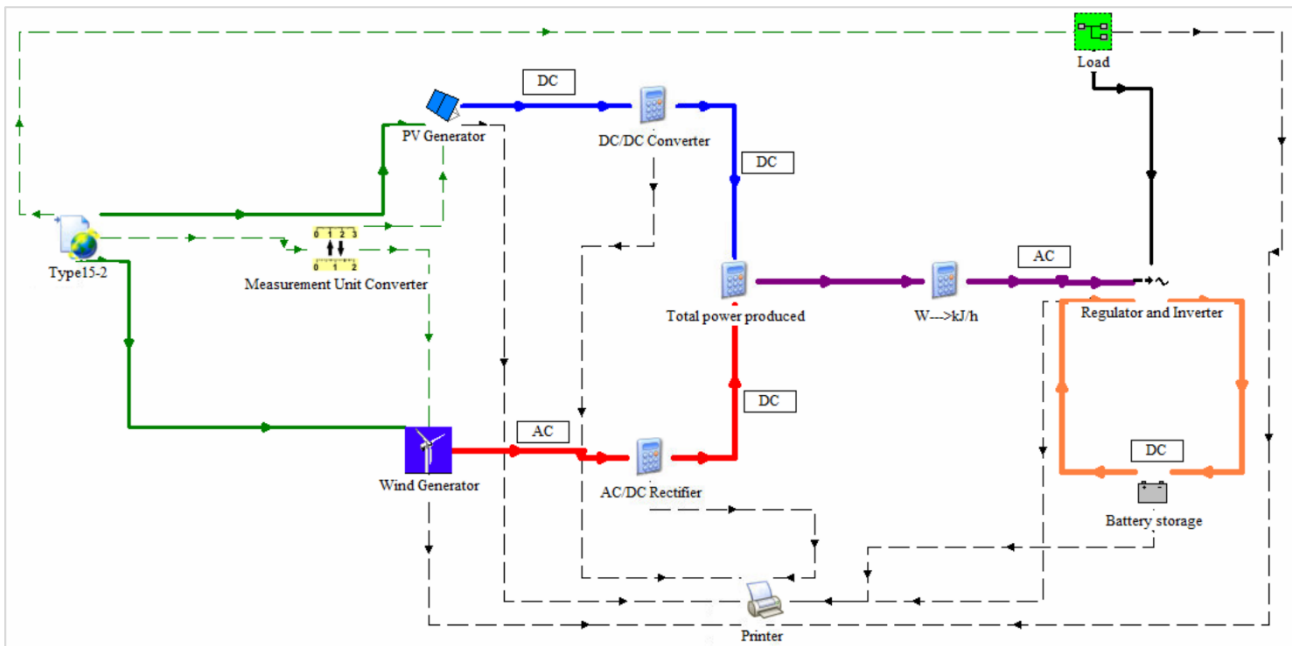
Figure 6. Schema of the hybrid plant in the TRNSYS environment.

Type15 in TRNSYS was used to obtain the weather data of each location investigated in this study. This type provides a typical meteorological year (TMY) that is a collation of selected weather data for a specific location listing hourly values of meteorological elements for one year. Total tilted surface radiation, beam radiation, total diffuse radiation, angle of incidence, ambient temperature, atmospheric pressure, and wind velocity are given to the solar PV and wind generators as input parameters. The solar PV generator and wind generator are simulated in the TRNSYS environment to estimate time-dependent power output from the generators. The solar PV generator can be simulated in TRNSYS using a five parameters model [31]. The four-parameter model is suitable for crystalline silicon panels while the five-parameter model is preferred for the simulation of amorphous silicon or thin-film panels. In this study, monocrystalline silicon panels are selected; thus, the five-parameter model is used for the simulation with Type94a. The wind generator is simulated using Type90. The power output of the wind generator at a given wind speed is estimated in TRNSYS.

The power output value from the solar generator is sent to the DC/DC converter while the output value from the wind generator is sent to the AC/DC rectifier. The calculator in TRNSYS is used to estimate the effective output power of the solar generator at the exit of the converter and the effective power of the wind generator at the exit of the rectifier. The efficiency of the converter is assumed to be 0.94 while the efficiency of the rectifier is assumed to be 0.9 to estimate the effective solar power and wind generator power. In addition, another calculator tool is used to determine combined power produced by solar and wind generators.

A regulator is added in the simulation to manage the energy flows of solar and wind generators, grid, and battery bank. Furthermore, an inverter is also used to convert direct current to alternating current, which can be sent to the load or the grid. The regulator and inverter are simulated using Type48. Excess power from the solar and wind generators is stored using a lithium-ion battery bank. Type47 is implemented in the TRNSYS environment for the simulation of the battery bank. Type47 calculations are based on the remaining state of charge (SOC) according to the power supplied or drawn over time from the battery. The characteristics and the input parameters of the components in the hybrid system are given in the supplementary file.

The electrical load requirement of the office buildings should also be incorporated into the simulation. The implementation of the load profile in the TRNSYS environment is explained in detail in the next section.

2.1.3. Load profiles of the office buildings

Various Types were used for implementing the load profile in the TRNSYS environment. The Types used for the simulation of load profile were grouped in a macro (see Figure 7), which includes Type9 for reading climate data, and Type2 for simulating the lighting differential controller using the time-dependent solar radiation values.
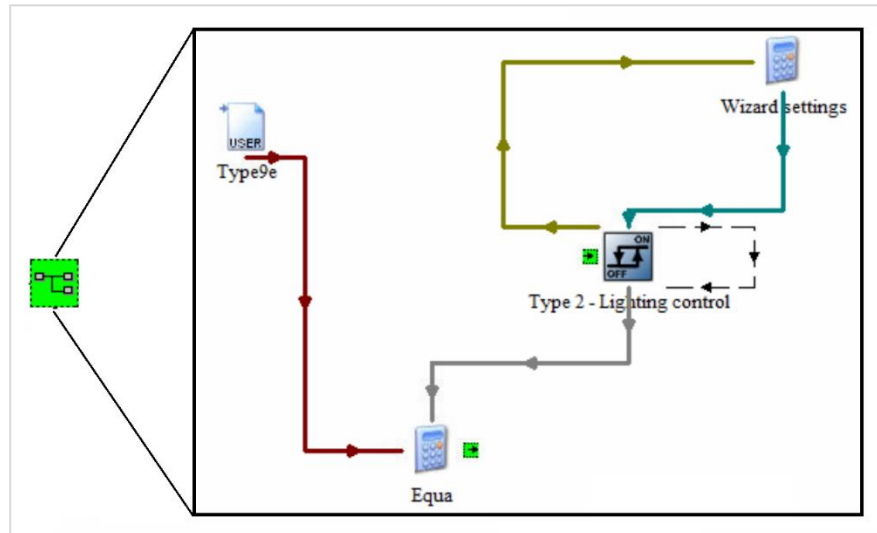
Figure 7. Load macro diagram in the TRNSYS environment.

The electrical load was estimated for an office building that includes two floors and four offices on each floor. The electrical load was also calculated for 5, 10 and 20 buildings to reveal the energy behaviour of the hybrid system with the change in the load profile.

For each building, the load considered in this work is the sum of three contributions: two independent and one as a function of the location.

- The first thing that contributes to the building's electrical load is the electrical instruments in the offices such as personal computers and printers. Their room consumption is taken to be equal to 75 W and they are only used during business hours.
- The second contributor to the electrical load is the lighting with a consumption of 125 W per room. It is considered an intelligent lighting system in which the lights are switched on only when the irradiance on the vertical surface is less than 120 W/m^2; thus, this contribution is a function of location because of varying solar radiation.
- The last contribution to the electrical load is the set of charging stations for electric vehicles. It was assumed that there were four charging stations, and each station had an electric power equal to 2.3 kW. In addition, it was assumed that eight Nissan Leaf 24 kWh vehicles are recharged during working hours. The average electricity consumption per vehicle was taken to be equal to 0.1714 kWh/km due to the energy recovered through the regenerative braking system [32, 33]. The average daily distance was assumed to be 26.8 km; thus, each vehicle requires two hours of charging to recover the daily consumption of 4.6 kWh/day.

Consequently, the hybrid system must work for four hours, from 9:00 to 13:00, at 9.2 kW of power to recharge the 8 electric vehicles.

The full-time working hours are determined to be 8:00 to 18:00 in six rooms from Monday to Friday, while the part-time working hours in the other two rooms are between 8:00 to 14:00 on Monday, Wednesday, and Friday to estimate the load profile. Three figures that are available in the Supplementary file were prepared to better show the change in load profile with variation in the number of buildings and the location.

2.1.4. The hybrid system power analysis

After setting the system in the TRNSYS environment, the power produced by the photovoltaic $P_{pv}(t)$ and wind $P_w(t)$, the power output from the AC/DC rectifier $P_{w,eff}(t)$, the DC/DC converter $P_{pv,eff}(t)$ and the DC/AC inverter $P_{inv,out}(t)$, the power input and output from the battery $P_{tb}(t)$ and $P_{fb}(t)$, the power sent to the load $P_{tl}(t)$, the excess power $P_{tg}(t)$; and the power extracted from the grid $P_{fg}(t)$ at all times were determined. Three operating modes are identified for the energy management of the system:

1) $\eta_{reg}\eta_{inv}P_g(t) > P_L(t)$:

When the total net power generated from the solar and wind generator is greater than the power required by the load $P_L(t)$, the load is directly completely compensated by the hybrid system $P_{dtl}(t)$ and the excess power is used to charge the battery $P_{tb}(t)$. If the battery is fully charged, the excess power is sent to the grid ($P_{tg}(t)$). In this operating mode, the power drawn from the battery $P_{fb}(t)$ and from the grid $P_{fg}(t)$ is null. The balance equations of the generated power $P_g(t)$ and load $P_L(t)$ are:

$$P_g(t) = \left[P_{pv,eff}(t) + P_{w,eff}(t)\right] = \frac{P_{dtl}(t)}{\eta_{reg}\eta_{inv}} + \frac{P_{tb}(t)}{\eta_{reg}} + \frac{P_{tg}(t)}{\eta_{reg}\eta_{inv}} \quad ; \quad P_L(t) = P_{dtl}(t) \qquad (1)$$

2) $\eta_{reg}\eta_{inv}P_g(t) < P_L(t)$:

When the total net power generated is less than the power required by the load, the remaining power for the load is drawn from the battery. If the power is still insufficient, the power from the grid is also drawn to obtain enough power for the load. In this mode, the power sent to the battery $P_{tb}(t)$ and the excess power sent to the grid $P_{tg}(t)$ are equal to zero. The balance equations of the generated power $P_g(t)$ and load $P_L(t)$ are:

$$P_g(t) = \frac{P_{dtl}(t)}{\eta_{reg}\eta_{inv}} \quad ; \quad P_L(t) = P_{dtl}(t) + P_{fb}(t)\eta_{inv} + P_{fg}(t) \qquad (2)$$

3) $\eta_{reg}\eta_{inv}P_g(t) = P_L(t)$:

When the total generated power from the system is equal to the load, the power sent or drawn from the battery and the grid are equal to zero. The balance equations of the generated power $P_g(t)$ and load $P_L(t)$ are:

$$P_g(t) = \frac{P_{dtl}(t)}{\eta_{reg}\eta_{inv}} \quad ; \quad P_L(t) = P_{dtl}(t) \qquad (3)$$

2.1.5. The hybrid system energy analysis

Estimating power based on the system operating modes was integrated for the energy analysis of the hybrid system.

The produced energy by the solar PV and wind generators is:

$$E_g = E_{pv}\, \eta_{DC/DC} + E_w\, \eta_{AC/DC} \qquad (4)$$

The produced energy from the system based on the system operating mode can be directly sent to the load E_{dtl}, partially stored in the battery E_{tb} or can be sent to the grid E_{tg}. Thus, the produced energy can be written as a function of E_{dtl}, E_{tb} and E_{tg} as:

$$E_g = \frac{E_{dtl}}{\eta_{reg}\eta_{inv}} + \frac{E_{tb}}{\eta_{reg}} + \frac{E_{tg}}{\eta_{reg}\eta_{inv}} \qquad (5)$$

The energy required by the load is calculated as:

$$E_L = E_{dtl} + E_{fb}\eta_{inv} + E_{fg} = E_{tl} + E_{fg} \qquad (6)$$

Where E_{tl} is the total energy sent to the load (wind, photovoltaic and battery energies) from the hybrid system, E_{dtl} is the produced energy from the solar PV and wind generators and sent directly to the load, and $E_{fb}\eta_{inv}$ is the total effective energy sent to the load from the battery, while E_{fg} is the energy sent to the load from the grid.

2.1.6. Parametric analysis

Parametric analyses were conducted using the TrnEdit tool to create a comprehensive database for the forecasting tool. The parametric analyses were conducted while considering the following ranges of variation for each parameter:

- Nominal PV powers, from 10 kW to 130 kW in steps of 20 kW, namely from 40 to 520 PV modules of 0.25 kW (from 1 to 13 strings in parallel, of which each string composed by 40 modules in series);
- Rated wind turbine powers, from 10 kW to 130 kW in steps of 20 kW, namely from 4 to 52 turbines of 2.5 kW in steps of 8;
- Battery capacity, from 10 kW to 130 kW in steps of 20 kWh, namely from 1 to 13 batteries of 10 kW in steps of 1;
- 48 localities worldwide with different climates according to the Koppen climate classification;
- A small district with 5 buildings, a medium district with 10 buildings and a big district with 20 buildings.

Overall, 343 HRES system configurations, 48 localities and 3 building district sizes were considered. To complete the parametric analyses, 49 392 simulations were performed for 8760 hourly values of the input and output powers. TrnEdit was used in the TRNSYS environment to create this comprehensive database.

The parametric dynamic simulation provided 49 392 text files containing the hourly powers in the different sections of the system.

A MATLAB script was created to verify the hourly power balance equations of Section 2.1.4. for each time step and all simulations. In addition, the script elaborates upon the 49 392 text files to calculate, for each simulation, the yearly energies related to the power flows outgoing from the different system components which are provided in an output Excel file constituted by 49 392 rows. Subsequently, in the Excel file, an automatic calculation was implemented to verify that the yearly energy balances also comply with the conditions of Section 2.1.5. The Matlab Script is reported in Appendix A.

2.2 Step 2 – Data normalization

The objective of this step is to normalize the input and output data to be used to train and create the hybrid system ANN. The dimensionless input parameters and output indicators calculable starting from the dynamic simulation and yearly energy synthesis are defined in the following sections.

2.2.1. The input parameters

The dimensionless parameters that characterize the system size and the time variability of the climatic conditions and load were evaluated based on the following parameters:

- **Wind power fraction** p_w (0, 1) is the ratio between the rated wind power P_W and the total rated power installed P_n. It can be between 0 and 1.

$$p_w = \frac{P_W}{P_n} = \frac{P_W}{P_W + P_{PV} + P_B} \tag{7}$$

- **Storage power fraction** p_b (0, 1) is the ratio between the rated power of the battery P_B (maximum stored energy in one hour) and the total rated power of the system P_n. It can be between 0 (system without battery) and 1 (system with the only battery since $P_n=0$).

$$p_b = \frac{P_B}{P_n} = \frac{P_B}{P_W + P_{PV} + P_B} \tag{8}$$

- **Mean load overall fraction** $p_{l,m}$ (0, +∞) is the ratio between the yearly average load $P_{L,m}$ and the rated power of the system P.

$$p_{l,m} = \frac{P_{L,m}}{P_n} = \frac{P_{L,m}}{P_W + P_{PV} + P_B} \tag{9}$$

- **Mean wind energy factor** $c_{we,m}$ (0, +∞) is dependent on the available yearly average wind energy that is directly proportional to the cube of the yearly cubic average wind speed V_{m3} and is inversely proportional to the yearly average external air temperature T_m. This energy availability is normalized with respect to the available yearly average wind energy in the reference conditions.

$$c_{we,m} = \frac{V_{m3}^3}{V_{m3,ref}^3} \frac{T_{ref,w}}{T_m} \tag{10}$$

Where $V_{m3,ref}$ is set equal to 6.5 m/s that is representative of the worldwide average of the yearly cubic average wind speed, while $T_{ref,w}$ is equal to 288.15 K that is the reference temperature for the characteristic power curve of a wind turbine.

- **Mean photovoltaic energy factor** $c_{se,m}$ (0, +∞) is dependent on the available yearly average solar energy that is directly proportional to the yearly average horizontal solar radiation G_m and is inversely proportional to the yearly average external air temperature T_m. This energy availability is normalized with respect to the available yearly average solar energy in the reference conditions.

$$c_{se,m} = \frac{G_m}{G_{ref}} \frac{T_{ref,PV}}{T_m} \tag{11}$$

Where G_{ref} and $T_{ref,PV}$ are set equal to, respectively, 1000 W/m² and 298.15 K that are the reference absorbed total solar radiation and temperature for the characteristic I-V curve of a PV cell.

- **Load variability overall fraction** $p_{l,sd}$ (0, +∞) is the ratio between the standard deviation of the yearly load $P_{L,sd}$ and the rated power of the system.

$$p_{l,sd} = \frac{P_{L,sd}}{P_n} = \frac{P_{L,sd}}{P_W + P_{PV} + P_B} \tag{12}$$

- **Wind energy variability factor** $c_{we,sd}$ (0, +∞) represents the yearly standard deviation of the wind energy availability normalized with respect to the available yearly average wind energy in the reference conditions. The standard deviation of the wind energy availability is directly proportional to the standard deviation of the cube of the cubic mean wind speed $V_{m3,sd}^3$ and inversely proportional to the yearly standard deviation of the external air temperature T_{sd}.

$$c_{we,sd} = \frac{V_{m3,sd}^3}{V_{m3,ref}^3} \frac{T_{sd,ref}}{T_{sd}} \tag{13}$$

Where $T_{sd,ref}$ is set equal to 8 K that is representative of the worldwide average of the yearly average standard deviation of the temperature.

- **Photovoltaic energy variability factor** $c_{se,sd}$ (0, +∞) represents the yearly standard deviation of the solar energy availability normalized with respect to the available yearly average solar energy in the reference conditions. The standard deviation of the solar energy availability is directly proportional to the yearly standard deviation of the horizontal solar radiation G_{sd} and inversely proportional to the yearly standard deviation of the external air temperature T_{sd}.

$$c_{se,sd} = \frac{G_{sd}}{G_{ref}} \frac{T_{sd,ref}}{T_{sd}} \tag{14}$$

2.2.2. The output energy reliability indicators

The dimensionless energy reliability indicators that were defined to identify the energy performance of the hybrid system in a specific location and load are as follows:

- **Satisfied load fraction** *SLF* (0, 1) is defined as the ratio between the energy supplied by the HRES E_{tl} to the load and the energy required of the load E_L.

$$SLF = \frac{E_{tl}}{E_L} = 1 - \frac{E_{fg}}{E_L} \tag{15}$$

   SLF measures the fraction of energy required of the load that is met by the system. It varies between 0 and 1 (in which case all the energy required of the load is supplied by the system, and the energy supplied by the grid is zero).

- **Utilization factor of the energy generated** *UF* (0, 1) is the ratio of the yearly energy supplied by the HRES E_{tl} to the load and yearly energy generated E_g.

$$UF = \frac{E_{tl}}{E_g} = 1 - \eta_{reg}\eta_{inv}\frac{E_{tg}}{E_g} \tag{16}$$

   It can vary between 0 and 1 (in which case all the energy generated is delivered to the load and the excess energy is zero).

- **Grid Energy Interaction Factor** *GEIF* (0, +∞) is the ratio of the yearly energy exchanged with the grid $E_{fg} + E_{tg}/(\eta_{reg}\eta_{inv})$ and the yearly energy required of the load E_L.

$$GEIF = \frac{E_{fg} + \dfrac{E_{tg}}{\eta_{reg}\eta_{inv}}}{E_L} = (1 - SLF) + (1 - UF)\frac{E_g}{E_L} \tag{17}$$

   The *GEIF* makes it possible to identify the most suitable locations for the hybrid plants considered, quantifying the interaction of the system and the load with the grid, i.e. the energy imported from the grid or exported to the grid.

Finally, each of the dimensionless inputs and outputs are to be normalized to confer at each input the same initial importance during the ANN training phase, by using the following equations:

$$\chi_i = 2\frac{x_{0,i} - x_{0,i,min}}{x_{0,i,max} - x_{0,i,min}} - 1 \qquad \psi_i = 2\frac{y_i - y_{i,min}}{y_{i,max} - y_{i,min}} - 1 \tag{18}$$

Where, χ_i and ψ_i are the i-th normalized input and output.
With this type of normalization, the minimum and maximum values become, respectively -1 and 1.
After the ANN training process, the outputs are denormalized with the inverse formula.

2.3 Step 3 – Artificial neural network architectural design

ANN is a powerful forecasting tool that can be used for predicting the energy performance of a hybrid renewable energy system. Collection of data, creating and configuring the network, initializing the

weights and bias, training the network, validating, and using the network are the steps that are used to design an ANN. Brief information about ANN theory and the design and implementation of ANN theory for this work are given in the following sections.

2.3.1. ANN theory and its implementation in the hybrid renewable energy system

ANN is a powerful forecasting technique that is used for a wide range of disciplines such as computing, science, engineering, medicine, mining, business, nanotechnology, etc. **[34]**. The components of an ANN can be listed as (i) input layer, (ii) hidden layer(s), (iii) output layer, (iv) weights and biases between layers and (v) activation function. Each ANN layer includes neurons like our brains, which are the core processing units of the networks. A generalized representation of an ANN can be seen in Figure 8.
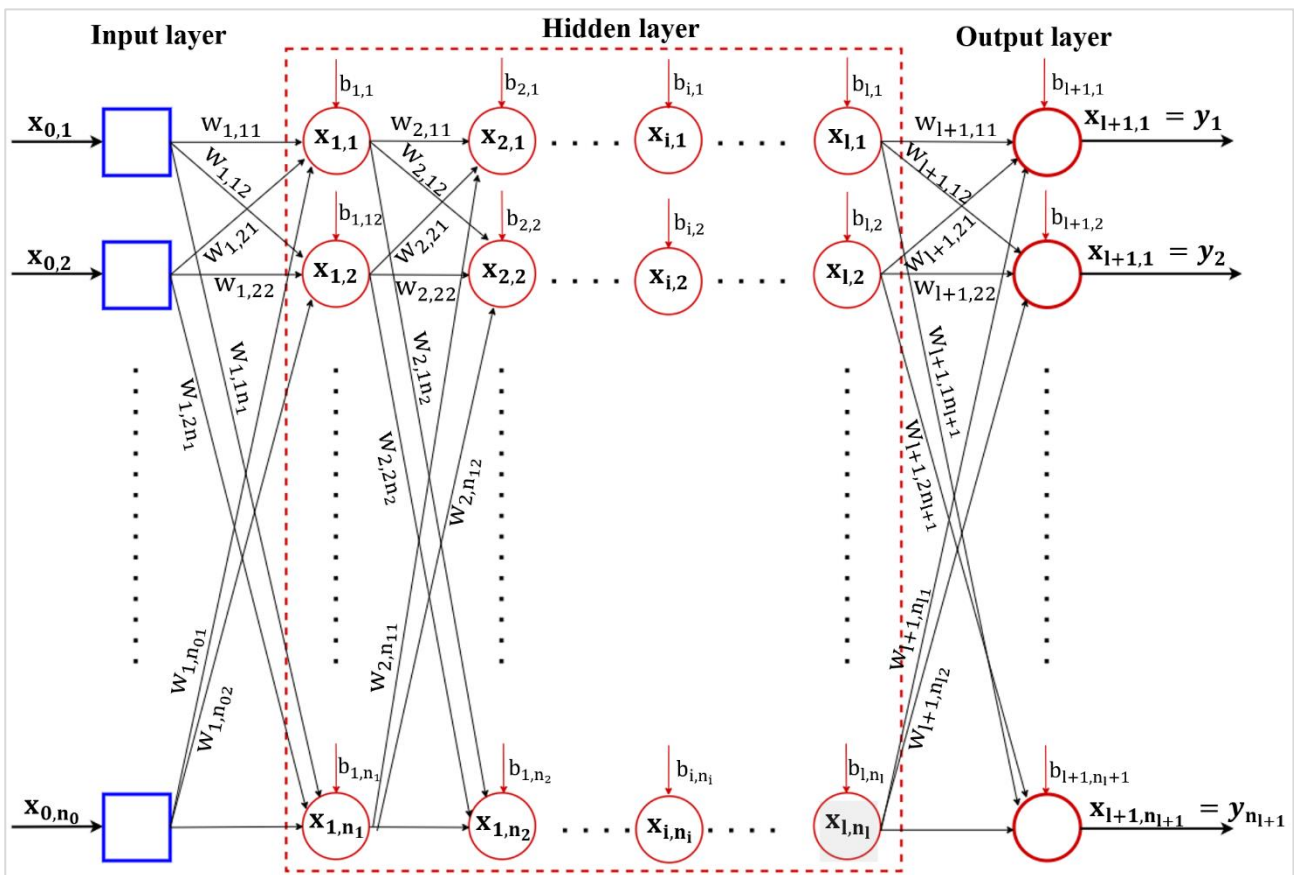
Figure 8. *Generalized representation of an artificial neural network with n_0 inputs, n_{l+1} outputs and l hidden layers.*
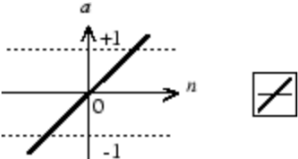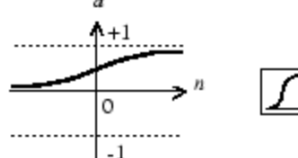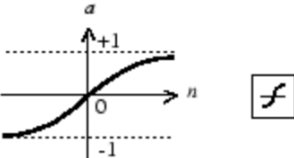
The square nodes constitute the input layer with n_0 nodes that transmit the input signal only. They do not calculate the weighted sum and do not use the activation function. This is why we use square nodes to distinguish them from other nodes. The rightmost nodes constitute the output layer with n_{l+1} nodes.

The first component in an ANN architecture is the input layer which receives the input. The input vector x_0 with n_0 nodes can be expressed in a vectorial form:

$$X_0 = \begin{bmatrix} X_{0,1} \\ X_{0,2} \\ X_{0,3} \\ \vdots \\ X_{0,n_0} \end{bmatrix} \tag{19}$$

The input layer in an ANN architecture moves to the hidden layer or multiple hidden layers in which most of the calculations in the architecture take place. The last layer in an ANN architecture is the output layer which forecasts the desired output values. There are weights and biases between each layer in the neural network architecture which provides some sort of computation by the neurons. The other component in an ANN architecture is an activation function that is used to determine the response of the neuron. There are several types of activation functions in the literature; the most commonly used are reported in Table 3.

Table 3. ANN activation functions

Name	Function	Equation	Codomain	Graph
Linear transfer function	$purelin(x)$	x	$(-\infty, +\infty)$	$a = purelin(n)$ Linear Transfer Function
Log-sigmoid transfer function	$logsig(x)$	$\dfrac{1}{1 + e^{-x}}$	$(0, 1)$	$a = logsig(n)$ Log-Sigmoid Transfer Function
Hyperbolic tangent sigmoid transfer function	$tansig(x)$	$\dfrac{2}{1 + e^{-2x}} - 1$	$(-1,1)$	$a = tansig(n)$ Tan-Sigmoid Transfer Function

The weights between the *(i-1)*-th layer and the *i*-th layer can be expressed in a matrix form:

$$W_i = \begin{bmatrix} w_{i,11} & w_{i,21} & w_{i,31} & \cdots & w_{i,1n_i} \\ w_{i,12} & w_{i,22} & w_{i,32} & \cdots & w_{i,2n_i} \\ w_{i,13} & w_{i,23} & w_{i,33} & \cdots & w_{i,3n_i} \\ \vdots & \vdots & \vdots & & \vdots \\ w_{i,n_{i-1}1} & w_{i,n_{i-1}2} & w_{i,n_{i-1}3} & \cdots & w_{i,n_{i-1}n_i} \end{bmatrix} \tag{20}$$

By considering the *i*-th hidden layer, the first digit represents the destination neuron of the weight, while the second digit indicates which source is the input for that weight. The weights of the first node of the *i*-th layer are in the first row and the weights of the second node of the *i*-th layer are in the second row and so on.

The higher the weight, the greater the effect is. When weight is zero, the corresponding signal will not be transmitted and do not affect the network.

Each node of the *i*-th layer is characterized by a bias value. The bias vector b_i of the *i*-th layer can be expressed by:

$$b_i = \begin{bmatrix} b_{i,1} \\ b_{i,2} \\ b_{i,3} \\ \vdots \\ b_{i,n_i} \end{bmatrix} \tag{21}$$

The output vector from a previous *(i-1)*-th hidden layer is multiplied by the weight matrix w_i and is summed to the bias vector b_i before entering the successive i-th layer. In addition, the activation function calculates how strongly the neuron fires and delivers the output value x_i for the successive layer.

The output x_i from the *i*-th hidden layer can be represented with a generalized equation:

$$x_i = \begin{bmatrix} x_{i,1} \\ x_{i,2} \\ x_{i,3} \\ \vdots \\ x_{i,n_i} \end{bmatrix} = \varphi(w_i x_{i-1} + b_i) \tag{22}$$

In this way, the output from the *i*-th hidden layer can be calculated starting from the output from the previous *(i-1)*-th layer. This output is transmitted to the successive layer. So, the input to the first node of the successive layer is $x_{i,1}$ and the input to the last node of the successive layer is x_{i,n_i}.

Similarly, the output of the neural network with *l* hidden layer can be expressed in a matrix form:

$$x_{l+1} = y = \begin{bmatrix} y_1 \\ y_2 \\ y_3 \\ \vdots \\ y_{n_{l+1}} \end{bmatrix} = \varphi(w_{l+1} x_l + b_{l+1}) \tag{23}$$

Where x_{l+1} x is the output y from the neural network, b_{l+1} is the bias vector of the output layer and w_{l+1} represent the weight matrix between the *n*-th hidden layer and the output layer.

The calculation is pretty simple and straightforward.

When a linear activation function is used, mathematically Eq. (22) gives an output the same as the input, as shown in Eq. (24). A multi-layer neural network becomes similar to a single layer neural network and the hidden layers become ineffective.

By substituting the outputs of the previous hidden layers backwards in the ANN output $y=x_{l+1}$, Eq. (24) is obtained.

$$y = \varphi(w_{l+1}x_l + b_{l+1}) = w_{l+1}x_l + b_{l+1} = x_0 \sum_{i=1}^{l+1} w_i + \sum_{k=1}^{l+1} b_k \left(\prod_{i=k+1}^{l+1} w_i \right) \qquad (24)$$

A forecasting tool based on ANN was created to estimate the performance of the hybrid photovoltaic-wind-battery storage system in any location in the world after creating a comprehensive database. An overview of the structure used to create the forecasting tool is summarized in Figure 9.

A multilayer perceptron (MLP) neural network was adopted as a pattern of the ANN with only one hidden layer. Eight parameters that are p_w, p_b, $p_{l,m}$, $c_{we,m}$, $c_{se,m}$, $p_{l,sd}$, $c_{we,sd}$ and $c_{se,sd}$ were used as an input layer of the neural network while *SLF*, *UF*, and *GEIF* were used as an output layer of the neural network.
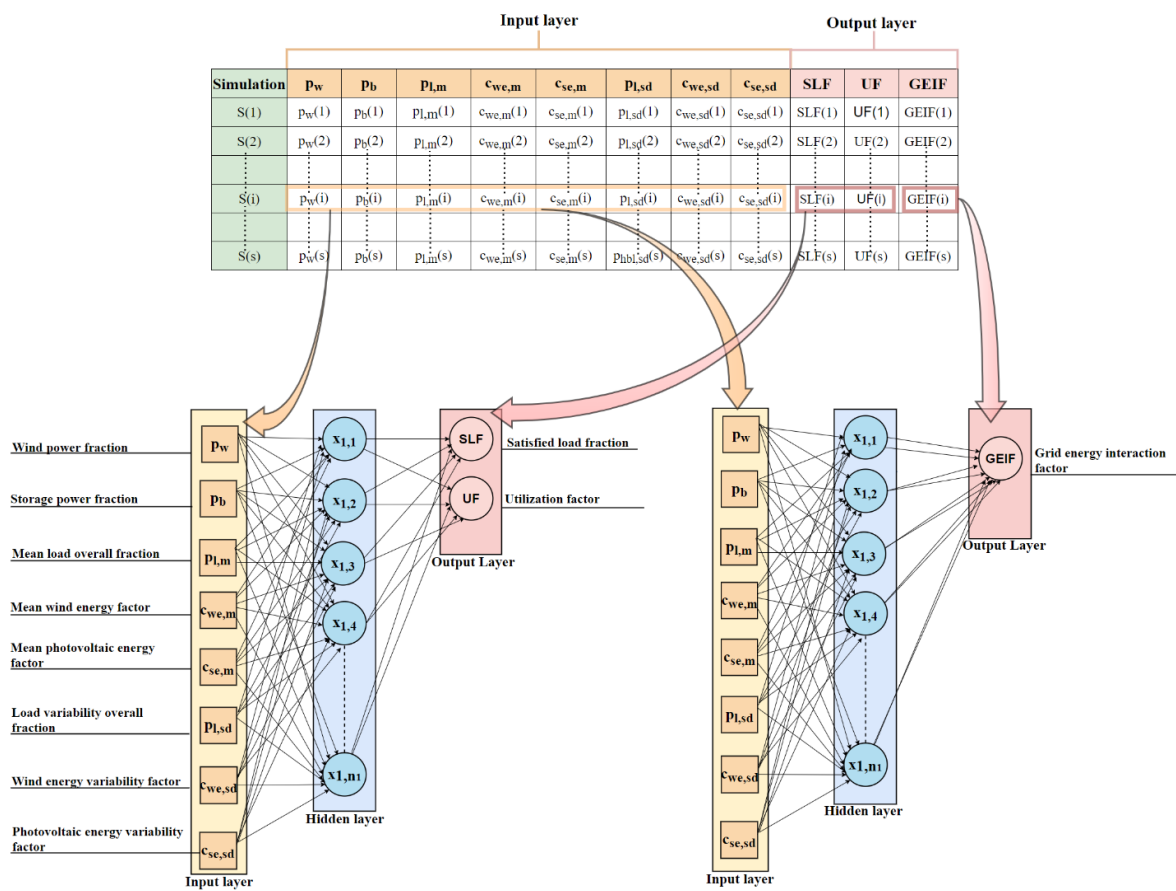
Figure 9. *An overview of the structure of the forecasting tool.*

Five characteristics were defined for the creation of the network: (i) architecture type; (ii) number of inputs; (iii) number of outputs; (iv) number of neurons; (v) activation function.

Two ANN were created for the hybrid system performance prediction: the first one composed of eight input neurons, one hidden layer and two output neurons; the second one differs only for the number of output neurons equal to one. The first ANN can predict the satisfied load fraction and the utilization factor, while the second one the grid energy interaction factor starting from the dimensionless input parameters defined in Section 2.2.1.

For the design of the two ANNs, the number of neurons in the hidden layer is considered variable between 1 and 40 neurons with a step of 2 neurons. Consequently, $n_0 = 8$, $l = 1$, and $n_{l+1} = 2$ for the first ANN and $n_{l+1} = 1$ for the second ANN. Assuming that the number of hidden neurons is $n_1 = 20$.

With reference to the first ANN, Eq. (23) becomes:

$$x_2 = y = \begin{bmatrix} y_1 \\ y_2 \end{bmatrix} = \varphi(w_2 x_1 + b_2) = \varphi\left[w_2\big(\varphi(w_1 x_0 + b_1)\big) + b_2\right] \tag{25}$$

The activation functions φ used are *tansig* in the hidden neurons and *purelin* in the output neurons.

2.3.2. ANN training, validation, testing and accuracy

2.3.2.1. ANN training, validation, and testing

The forecasting tool based on the neural network built in this study is a supervised learning tool. The neural network for supervised learning is trained based on already known correct output. The steps of the training process for supervised learning can be listed as [35]: (1) initialize the weights; (2) calculate the error from the difference between output and correct input; (3) calculate the weights updates; (4) adjust the weights to reduce the error; (5) repeat steps 2 to 4 for all training data; (6) repeat steps 2 to 5 until the error reaches an acceptable level. When all training data goes through step 2 to 5 it is called an epoch.

The process required for the determination of the numerical value of the weights is called learning or training. The weights are adjusted iteratively until the error E_i between the targets t_i and outputs y_i is reasonably small.

$$E_i = t_i - y_i \tag{26}$$

At each step, the generic weight w_{ij} between node i and node j of the previous layer is updated.

$$w_{ij,new} = w_{ij,old} + \Delta w_{ij} = w_{ij,old} + \alpha E_i x_j \tag{27}$$

Where x_j is the output from node j and α is the learning rate, variable between 0 and 1. The learning rate determines how much the weights are changed every time

The updated weight w_{ij} between the node i and the node j of the previous layer is:

$$w_{ij,new} = w_{ij,old} + \Delta w_{ij} = w_{ij,old} + \alpha \delta_i x_j \tag{28}$$

The term δ_i is expressed by the equation:

$$\delta_i = \varphi'(x_i) E_i \tag{29}$$

x_i is the weighted sum of the output node i and φ' is the derivative of the activation function φ of node i.

Different methods for weight updates are available [35]:

- in the stochastic gradient descent (SGD), errors are calculated for all training data and single weight updates are used to modify the weights;
- in the Batch method, errors are calculated for all training data and the average value of all of the weight updates is used to modify the weights.
- in the Mini Batch method, sets of training data are selected to apply the batch method and, in each group, a single weight update is used to modify the weights, like the SGD method.

In this research, the Matlab Neural network fitting toolbox 8.3 [30] was used to train, test and validate the ANN of the hybrid system. The tool allows users to train a two-layer feed-forward network as a function of the number of hidden neurons, to evaluate its performance using mean squared error and regression analysis, and to analyse the results using visualization tools such as a regression fit or histogram of the errors. It randomly divides data into training, validation, and testing sets: 70% of the data was used for training; 15% was used for validation; 15% was used for testing. The validation and testing sets are used to stop training early and to measure the ANN generalization and to independently check the potential error that the network can provide. The default activation functions used are the sigmoid transfer function in the hidden layer and the linear transfer function in the output layer.

For the training phase, the batch Levenberg-Marquardt backpropagation algorithm process (*trainlm* function was selected [36, 37, 38] and all training data set are applied to the network before the weights are updated. The method is a variation of Newton's method and employs the Jacobian matrix to minimize errors, by approximating the Hessian matrix and the error gradient employing the matrix first derivatives of the network errors concerning the weights and biases.

The default performance function for feedforward networks is the mean square error (MSE), which measures the network's performance according to the mean of squared errors.

For the training phase, an important target is the proper design of the ANN architecture in terms of hidden neurons and training data. The optimal number of hidden neurons depends on the number of training data. An ANN with many nodes predicts the training data excellently but loses generalization capabilities. This phenomenon is called overfitting and the model produces good results on the training data but performs poorly on the test data. This issue can be overcome by reducing the ANN architecture complexity, by increasing the training data, by early stopping the training process or by reducing the number of neurons.

In this work, the number of hidden neurons varies between 1 and 20 neurons with a step of 1 neuron and the optimal ANN architecture is chosen by identifying the ANN with the highest accuracy in the training, validation and testing data to avoid overfitting phenomenon and to maximize some accuracy metrics.

2.3.2.2. ANN accuracy

The prediction accuracy of the neural network is evaluated by comparing the output values obtained using the neural network with the values obtained in TRNSYS that are considered the desired or target values. The following regression performance metrics are used to evaluate the accuracy of the prediction algorithm (ANN algorithm).

Two metrics are used to measure and optimize the ANN accuracy: the first one is the Performance P measured by means of the mean square error (MSE) and the second one is the Regression R measured using the correlation coefficient (CC).

$$P = MSE = \frac{\sum(t_i - y_i)^2}{N} \quad ; \quad R = CC = \frac{N\sum_{i=1}^{N} t_i\, y_i - \left(\sum_{i=1}^{N} t_i\right)\left(\sum_{i=1}^{N} y_i\right)}{[N(\sum_{i=1}^{N} t_i{}^2) - (\sum_{i=1}^{N} t_i)^2][N(\sum_{i=1}^{N} y_i{}^2) - (\sum_{i=1}^{N} y_i)^2]} \quad (30)$$

Where t_i is the reference value of the output parameter obtained from the TRNSYS simulations, y_i is the value predicted by the neural network and N is the total number of comparisons.

In addition to these metrics, additional metrics are used to evaluate ANN accuracy:

- the minimum E_{min}, maximum E_{max}, mean E_m and standard deviation E_{sd} values of the error, the difference between the target t and output y.

$$E_{min} = min(t_i - y_i) \quad ; \quad E_{max} = max(t_i - y_i) \quad ; \quad E_m = \frac{\sum(t_i - y_i)}{N} \quad ; \quad E_{sd} = \sqrt{\frac{\sum(E_i - E_m)^2}{N}} \quad (31)$$

- the root mean square error (*RMSE*) (0, +∞)

$$RMSE = \sqrt{MSE} \quad (32)$$

- the coefficient of residual mass (*CRM*) (-∞, +∞)

$$CRM = \frac{\sum_{i=1}^{N} y_i - \sum_{i=1}^{N} t_i}{\sum_{i=1}^{N} t_i} \quad (33)$$

- the mean absolute deviation (*MAE*) (0, +∞)

$$MAE = \frac{\left(\sum_{i=1}^{N}|E_i|\right)}{N} \quad (34)$$

Where t_m and y_m are the mean values of the target and output values, respectively.

The model characterized by E_{min}, E_{max}, E_m, E_{sd}, *RMSE* and *MAE* values equal to zero indicates the highest accuracy of this algorithm. RMSE is a parameter that gives a relatively high weight to large errors, unlike *MAE*. *CRM* is a measure of the tendency of the model. The optimal *CRM* value is equal to 0 when the target values approximate the ANN outputs. Positive values indicate that the model tends to underestimate data, while negative values show that the model tends to overestimate data. The comparison of the target values with the predicted ANN outputs generates a linear regression with a specific value of the coefficient of determination R^2, calculated as:

$$R^2 = CC^2 \quad (35)$$

When the mean squared deviation of the model is much lower than that produced by the fixed arithmetic mean model, the value of R^2 will be close to 1. In addition, to have an R^2 close to 1, the linear regression curve must be very close to the bisector, namely the angular coefficient m of the linear regression curve must be very close to 1 and the intercept b very close to 0.

2.3.3 Sensitivity analysis by Garson method

A sensitivity analysis of the best ANN model was conducted using Garson's algorithm illustrated, in his reference [39], for the case with two input neurons, one hidden layer with two neurons and one output neuron. The method quantitatively demonstrates the importance of each input in predicting each output, namely to determine the influence of each input variable and its contribution to the output. This method is also used to eliminate irrelevant input; namely, the most significant explanatory variables are determined, then the variables below a fixed threshold are excluded from the network. This allows the size of the network to be reduced and thus minimises redundancy in the training data. The same method was illustrated by Gevrey et al. [40], called the weight method, considering the neural network with three input neurons, one hidden layer with four neurons and one output neuron.

In this paper, a generalized procedure of the Garson method is proposed with reference to Figure 8.

To determine the relative importance of each input to each output, the computation process is as follows:

(1) Identification of all routes between $x_{0,i}$ and y_j through the neurons of the l hidden layers, for a couple constituted by a neuron of the input layer $x_{0,i}$ and a neuron of the output layer y_j. The number of routes between each couple $x_{0,i}$ and y_j is equal to the overall hidden neurons $N_R = n_1 + n_2 + .. + n_i + \cdots + n_l$.

(2) Calculation of the r-th overall weight $W_{r,ij}$, namely the product of all absolute value of weights of a specific route r between the i-th input $x_{0,i}$ and the j-th output y_j:

$$W_{r,ij} = \prod_{k=1}^{l+1} |w_k| \tag{36}$$

This product is composed of $l+1$ weights $w_{k,ij}$; namely, as many as there are, the weight connections are required to move from the input neuron to the output neuron. In addition; only one weight for each hidden layer appears in Eq. (37) as highlighted by subscript k.

(3) Determination of the sum s_{ij} of the r overall weights $W_{r,ij}$, summed overall weights, between the i-th input $x_{0,i}$ and the j-th output y_j:

$$s_{ij} = \sum_{r=1}^{N_R} W_{r,ij} \tag{37}$$

(4) Application of Steps (1)-(3) for all $(n_0 \cdot n_{l+1})$ couples of input neurons-output neurons

(5) Calculation of the percentage sensitivity S_{ij} of each i-th input on the j-th output with the following equation:

$$S_{ij} = \frac{s_{ij}}{\sum_{i=1}^{n_0} s_{ij}} 100 \tag{38}$$

(6) Repeat Steps (5) for the n_{l+1} output neurons.

The hybrid system ANN reported in Figure 9 has eight input neurons $n_0 = 8$, one hidden layer $l = 1$ and one output neuron $n_{l+1} = 1$. Assuming that the number of hidden neurons is $n_1 = 20$, twenty routes are available between a given input neuron and the output neuron and the overall weight $W_{r,ij}$ of each route is composed of the product of two weights.

2.3.4. Step 4 – ANN application

The ANNs created were used to predict the energy performance of additional case studies, external from the database used to train, test and validate the ANN.

For this scope, 128 other simulations by seven other localities and a repeated locality (Hakkari), eight other hybrid systems with the main components characterized by different powers installed and two other office building district sizes were simulated directly with the ANNs developed:

- The eight localities considered belong to different Koppen climatic groups, as reported in Table 4, characterized by the external air temperature, horizontal total solar radiation and wind speed variations illustrated in Figure 10; the optimal PV angle for the different localities as a function of the latitude was obtained by an empirical correlation obtained by using as linear regression data those of Table 2.

- The component powers of the hybrid systems considered have PV, wind and battery nominal powers of 40 kW and 100 kW for a total of eight hybrid systems. These values were within the interval of validity of the ANN (from 10 kW to 130 kW in steps of 20 kW for each component), but they were not used for the ANN training;

- The number of buildings in the district is the intermediate cases of the values chosen for the ANN training (5-10-20); namely, a small-medium district with 7 buildings and a medium-large district with 15 buildings.

The eight localities belong to different subgroups of the main Koppen climate groups A, B, C and D and are characterized by a different hourly distribution of external air temperature, solar radiation and wind speed as shown in Figure 10. Hakkari, already used for the training phase, was used also for the ANN application to verify the ANN reliability when only the system power configuration and district size is changed.

Table 4. Selected cities for the ANN application.

Location	Country	Koppen Classification	Climate	Latitude (°)	Longitude (°)	Optimal PV angle (°)
Havana	Cuba	Aw	Tropical savanna, wet	22.98	-81.60	19
Bechar	Algeria	BWh	Hot desert climate	31.62	-1.77	26
Vienna	Austria	Cfb	Temperate oceanic climate, Marine west coast climate	48.12	16.57	39
Valencia	Spain	Csa	Hot-summer Mediterranean climate	39.48	23.22	32
Mexico City	Mexico	Cwb	Subtropical highland climate or temperate oceanic climate with dry winters	19.43	-98.92	17
Warsaw	Poland	Dfb	Warm-summer humid continental climate	52.27	20.98	42
Hakkari	Turkey	Dsa	Hot, dry-summer continental climate	37.57	43.77	31
Irkutsk	Russia	Dwb, bordering on Dwc	Monsoon-influenced warm-summer humid continental climate	52.27	104.35	42

Figure 10. *Yearly box plots of the hourly external air temperature, horizontal total solar radiation, and wind speed in the selected locations for the ANN application.*

The same 128 simulations were also performed by using TRNSYS software to verify the accuracy of the ANN model.

3. Results and discussion

In this section, the optimal ANN architectures created by using the normalized data of 49000 dynamic simulations summarized in yearly normalized input and output data is presented. In particular, 20 ANN architectures were trained for two cases, namely by using as outputs the pair of indicators *SLF* and *UF* and the single indicator *GEIF*. For the optimal ANN architectures, the Garson method was applied to identify the effects produced by each input on each output. This method has permitted the determination of the most relevant inputs on which the hybrid system performance depends.

3.1. Step 1 – Database creation

The input climatic data of the 48 localities and load data of the three-building districts considered, required for the calculation of the eight dimensionless input data for the ANN training, are reported in Tables 5 and 6.

Table 5. Climatic data for the dimensionless input data calculation for ANN training.

Locality	T_m (°C)	G_m (W/m²)	V_{m3}^3 (m³/s³)	T_{sd} (°C)	G_{sd} (W/m²)	$V_{m3,sd}^3$ (m³/s³)
Toamasina	23.30	205.87	19.48	3.59	287.75	42.18
Singapore	26.62	185.30	39.66	2.46	264.60	137.80
Recife	28.58	241.68	180.58	2.78	324.87	313.87
Miami	24.31	204.69	138.25	4.28	279.76	175.28
Lihue	23.92	207.60	231.62	2.63	278.78	240.16
Mombasa	26.15	227.54	219.65	3.26	310.19	381.67
Caracas	25.98	184.66	9.26	2.84	263.84	32.09
Kano	26.29	256.41	115.14	6.18	335.16	219.29
Baghdad	20.12	238.15	33.46	10.11	316.64	70.03
Cairo	21.32	231.37	91.76	6.53	308.61	157.29
Kabul	12.06	217.73	53.76	10.58	302.55	163.06
Baku	14.57	152.41	311.56	9.42	235.40	513.03
Odessa	10.16	141.77	138.12	9.47	219.53	249.43
Maracaibo	27.54	179.50	139.68	3.41	258.76	276.08
Buenos Aires	17.42	194.89	144.50	5.89	277.42	226.85
Milan	11.62	135.71	8.75	8.94	208.70	36.96
Berlin	9.42	114.35	213.80	8.53	184.79	390.48
London	10.78	105.50	146.57	5.79	174.31	261.31
Vancouver	9.84	143.96	85.84	5.83	224.71	173.43
Melbourne	14.00	175.04	248.41	5.82	257.19	407.97
Bogotá	13.26	193.15	53.02	4.03	283.51	180.20
Wellington	13.51	160.44	591.97	4.32	243.43	888.67
Reykjavík	4.37	89.35	397.00	5.31	151.59	636.89
Auckland	15.09	175.10	597.04	4.12	255.73	892.95
Rome	15.21	178.21	96.96	7.19	254.13	233.51
Adelaide	16.65	204.08	207.44	6.14	288.89	449.33

Porto	14.48	178.22	316.22	5.30	258.44	652.90
La Coruna	14.09	139.92	84.87	4.12	215.45	175.07
New Delhi	25.07	225.08	9.87	7.87	299.22	24.80
Hong Kong	22.87	162.66	237.84	5.51	243.38	339.78
Johannesburg	15.47	235.95	85.94	6.04	318.23	151.74
Nairobi	19.23	211.37	291.14	4.19	299.92	521.88
Bucharest	10.58	151.24	51.66	10.07	229.83	165.31
Toronto	7.37	160.65	233.81	10.99	238.66	418.05
Moskva	5.01	109.72	11.14	11.05	180.47	40.26
Ottawa	5.93	157.26	111.54	12.46	230.58	217.23
Tromsø	2.95	72.47	164.47	6.61	129.23	310.26
Anchorage	2.64	101.62	76.91	9.77	165.48	137.07
Oymyakon	-16.15	122.17	23.62	24.05	188.72	108.96
Verhojansk	-15.05	109.11	55.16	23.73	174.86	156.72
Hakkâri	10.11	196.29	21.44	11.16	284.34	81.92
Cambridge	-14.56	113.79	406.70	16.11	183.37	626.69
Dras	2.09	186.47	35.64	12.50	275.34	105.67
Flagstaff	7.30	213.52	83.14	9.81	289.17	194.39
Beijing	11.79	148.15	60.69	11.76	219.17	168.96
Seoul	11.84	138.57	59.87	10.83	211.44	179.29
Pyongyang	9.58	146.57	27.87	11.95	218.39	112.95
Vladivostok	4.27	150.77	149.88	12.15	217.14	268.28

Table 6. Load data for the dimensionless input data calculation for ANN training

Locality	$P_{L,m}$ (kW) 5 buildings	$P_{L,m}$ (kW) 10 buildings	$P_{L,m}$ (kW) 20 buildings	$P_{L,sd}$ (kW) 5 buildings	$P_{L,sd}$ (kW) 10 buildings	$P_{L,sd}$ (kW) 20 buildings
Toamasina	6.76	13.52	27.03	56.53	113.07	226.14
Singapore	6.76	13.53	27.05	57.12	114.23	228.47
Recife	6.64	13.27	26.55	56.79	113.58	227.16
Miami	6.66	13.32	26.64	56.91	113.83	227.65
Lihue	6.65	13.29	26.58	57.02	114.03	228.06
Mombasa	6.64	13.28	26.56	56.79	113.58	227.16
Caracas	6.76	13.53	27.05	57.38	114.77	229.54
Kano	6.59	13.18	26.36	56.54	113.09	226.18
Baghdad	6.62	13.23	26.46	56.68	113.35	226.71
Cairo	6.63	13.25	26.51	56.64	113.28	226.56
Kabul	6.67	13.35	26.69	56.89	113.79	227.58
Baku	7.01	14.01	28.02	57.58	115.16	230.31
Odessa	7.01	14.01	28.02	58.92	117.84	235.68
Maracaibo	6.77	13.53	27.06	57.61	115.22	230.45
Buenos Aires	6.78	13.56	27.12	57.94	115.89	231.77
Milan	6.99	13.99	27.97	58.59	117.17	234.35
Berlin	7.14	14.28	28.57	58.98	117.96	235.91
London	7.19	14.38	28.76	59.19	118.39	236.78
Vancouver	7.01	14.01	28.02	58.56	117.13	234.26
Melbourne	6.82	13.64	27.28	57.76	115.52	231.05
Bogotá	6.73	13.45	26.91	57.09	114.18	228.36
Wellington	6.89	13.77	27.55	58.06	116.11	232.23
Reykjavík	7.36	14.72	29.44	60.18	120.37	240.74

Auckland	6.79	13.57	27.15	57.59	115.17	230.34
Rome	6.79	13.57	27.15	57.53	115.07	230.14
Adelaide	6.71	13.41	26.83	57.23	114.45	228.90
Porto	6.91	13.82	27.64	58.91	117.83	235.66
La Coruna	7.02	14.03	28.06	59.38	118.76	237.52
New Delhi	6.63	13.26	26.52	56.82	113.63	227.27
Hong Kong	6.85	13.71	27.42	57.73	115.47	230.94
Johannesburg	6.62	13.24	26.48	56.68	113.37	226.74
Nairobi	6.69	13.38	26.76	57.19	114.38	228.76
Bucharest	6.97	13.94	27.89	57.85	115.70	231.41
Toronto	6.89	13.78	27.56	58.02	116.04	232.07
Moskva	7.17	14.34	28.69	59.35	118.70	237.40
Ottawa	6.86	13.72	27.45	57.85	115.70	231.39
Tromsø	7.45	14.90	29.80	60.10	120.20	240.41
Anchorage	7.25	14.50	29.01	59.92	119.85	239.69
Oymyakon	7.13	14.27	28.54	59.09	118.19	236.38
Verhojansk	7.26	14.51	29.03	59.80	119.60	239.20
Hakkâri	6.83	13.66	27.33	57.15	114.30	228.61
Cambridge	7.23	14.47	28.93	59.40	118.81	237.61
Dras	6.78	13.56	27.12	57.32	114.64	229.29
Flagstaff	6.65	13.30	26.60	57.08	114.16	228.32
Beijing	6.91	13.82	27.65	57.96	115.91	231.82
Seoul	6.96	13.93	27.86	58.42	116.84	233.68
Pyongyang	6.89	13.79	27.57	58.18	116.36	232.71
Vladivostok	6.89	13.78	27.57	58.67	117.34	234.69

Similarly, the outputs data to be used for the calculation of the three dimensionless output data for the ANN training, are reported in Figure 11 in terms of energy drawn from and sent to the grid.
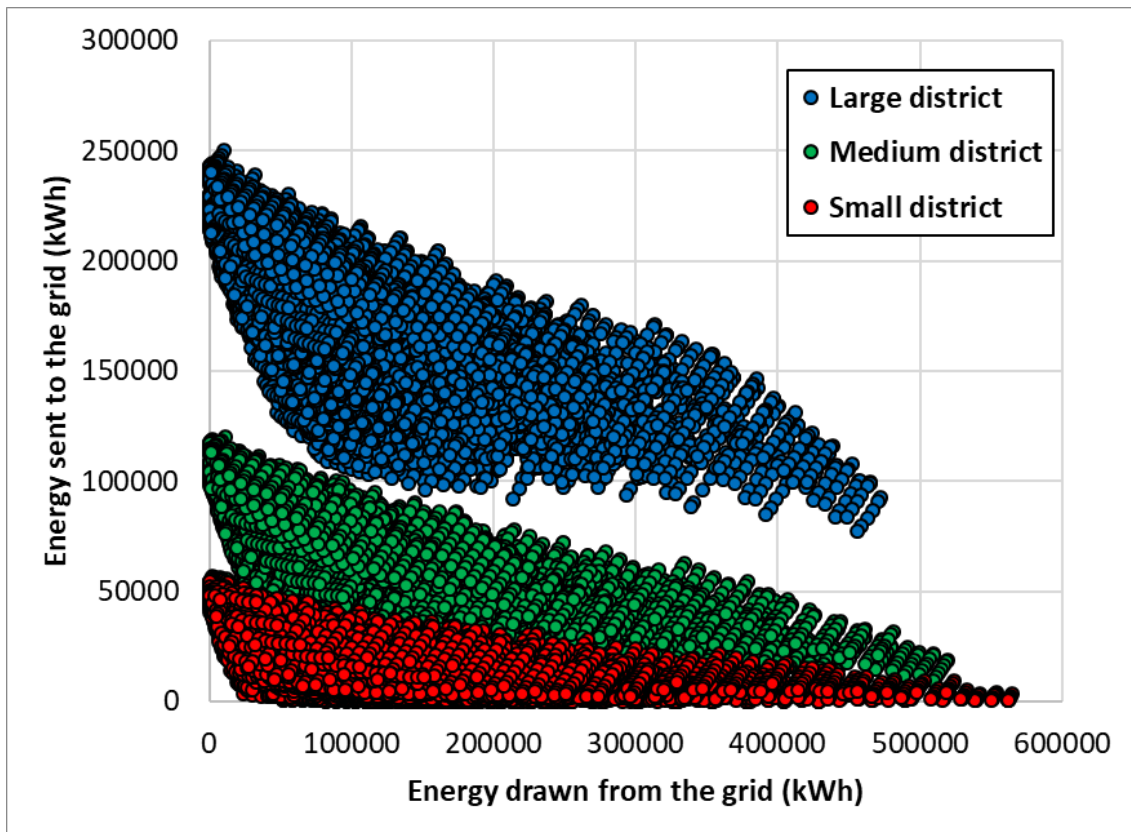
Figure 11. Energy drawn from and sent to the grid for the entire data sample.

The input and outputs data presented summarize yearly the dynamic simulations performed. The database includes a wide range of variation of the climatic and load conditions. The mean values of the climatic variables shown in Table 5 highlights that in the sample are present climates that exhibit wide ranges of temperature, sunshine and wind speed values; the wide range of the standard deviation of the climatic variables testify to the different climatic variability during the year in the localities selected. Similarly, the increase in the number of buildings in the district permits the consideration of different mean and standard deviation values of the hourly power load.

As expected, Figure 11 indicates that the energy drawn from the grid increases while the energy sent to the grid decreases as the load increases. For a specific district, the general trend highlights that an increase of the energy drawn from the grid results in a reduction of the energy sent to the grid. Despite this, this effect depends on the locality and system power configuration considered.

3.2. Step 2 – Data normalization

Starting from the database created, the normalized database was created. The database consists of 49392 combinations of the eight normalized input parameters and three normalized output indicators.

The statistical trend, represented by the box plot, of each input and output normalized parameter is presented in Figures 12 and 13. These box plots are representative of all 49392 simulations by varying the locality, the system power configuration and district size and permit the identification of the mean, the first and third quartile, the interquartile, the minimum and maximum and the variation range values.
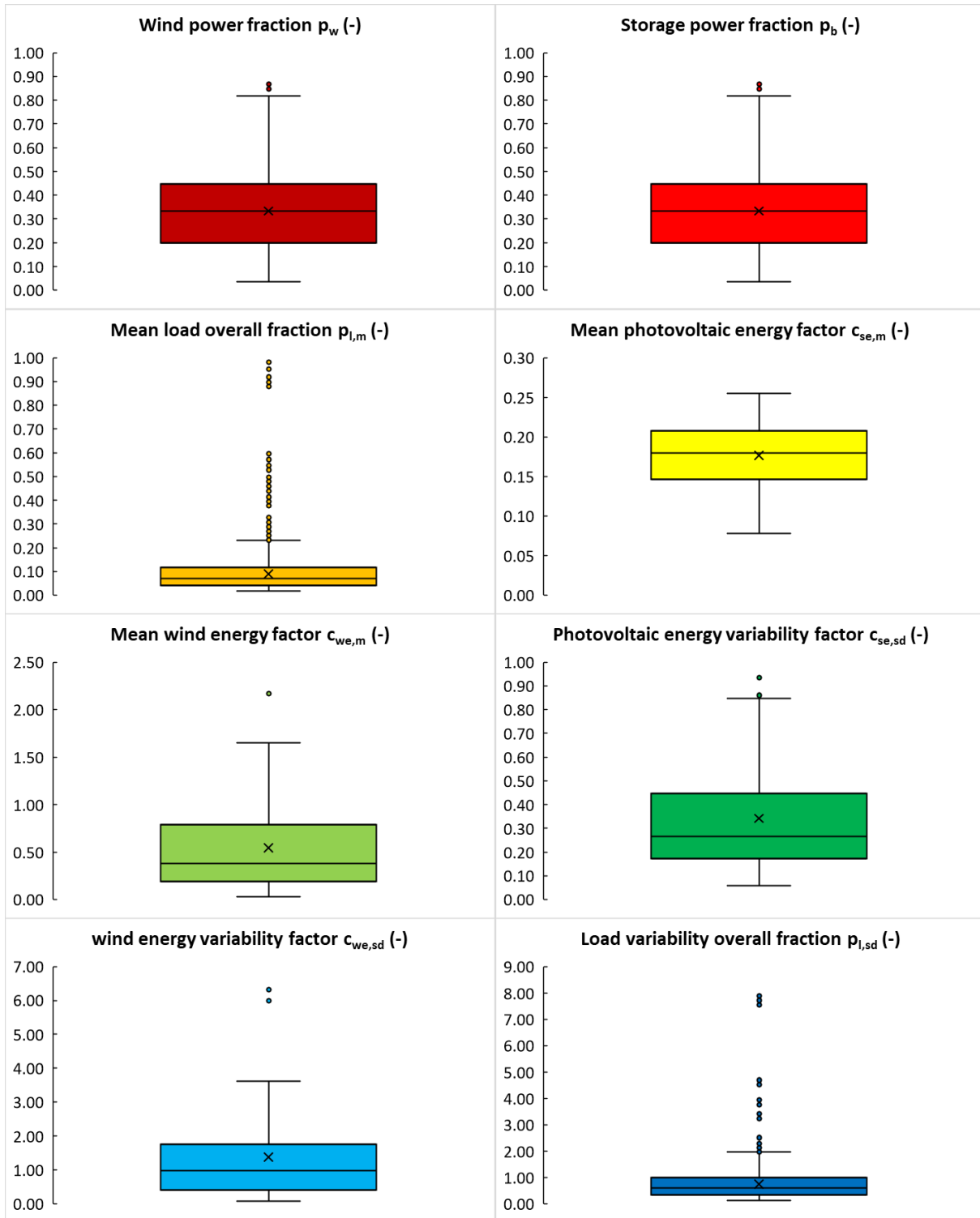
***Figure 12.** Box plots of the input parameters for the ANN training.*
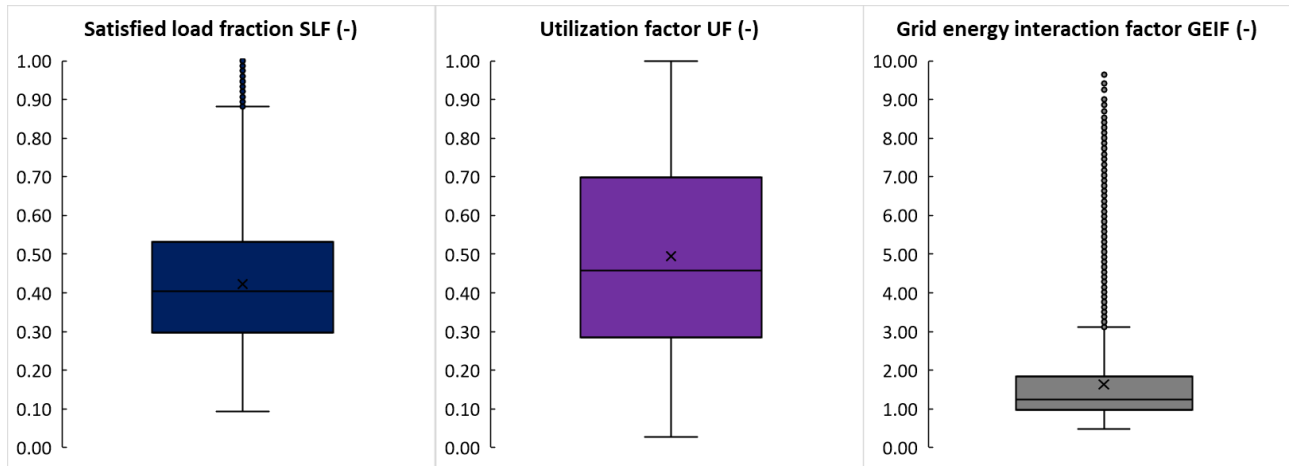
Figure 13. Box plots of the output indicators for the ANN training.

Definitively, the ANN is valid for the variation range of the input and output parameters reported in Table 7.

Table 7. Variation range of validity of the ANNs.

(-)	p_w	p_b	$p_{l,m}$	$c_{se,m}$	$c_{we,m}$	$c_{se,sd}$	$c_{we,sd}$	$p_{l,sd}$	UF	SLF	GEIF
minimum	0.04	0.04	0.02	0.08	0.03	0.06	0.09	0.14	0.09	0.03	0.48
maximum	0.87	0.87	0.99	0.26	2.17	0.93	6.32	8.02	1.00	1.00	9.75

3.3. Step 3 – ANN architectural design

In this section, the results obtained by training two ANNs as a function of the number of neurons is illustrated to identify the best in terms of accuracy. The best ANN was chosen as the one with the lowest mean square error (*MSE*) and the highest regression (*R*) values.
On the optimized ANNs, the Garson method was applied. Finally, the optimal ANNs were used to predict the performance of other hybrid system power configurations located in other localities and districts to measure prediction accuracy.

3.3.1. Optimized ANN architecture

The database composed of 49392 different combinations of the 8 inputs and 3 outputs (two outputs for the first ANN and one for the second ANN) was used to train the two ANNs by changing the number of neurons from 1 to 20. The data sets were randomly divided into training, validation and testing data sets with the following percentage 70%, 15% and 15%, with values of 34574, 7409 and 7409, respectively.

3.3.1.1. ANN for the prediction of the satisfied load fraction and utilization factor

The first ANN was developed by using as outputs the satisfied load fraction and the utilization factor.
The regression points illustrated in Figure 14 as a function of the number of neurons show the results of both network outputs related to all training, validation, and testing data. In the regression curves, the ANN output values are compared with the target values. The points falling closer to the bisector, a 45-degree line, permit the identification of the best fit, namely when the

ANN outputs are equal to the targets. Overall, the graph contains about 2 million (50000x2x20) data points.
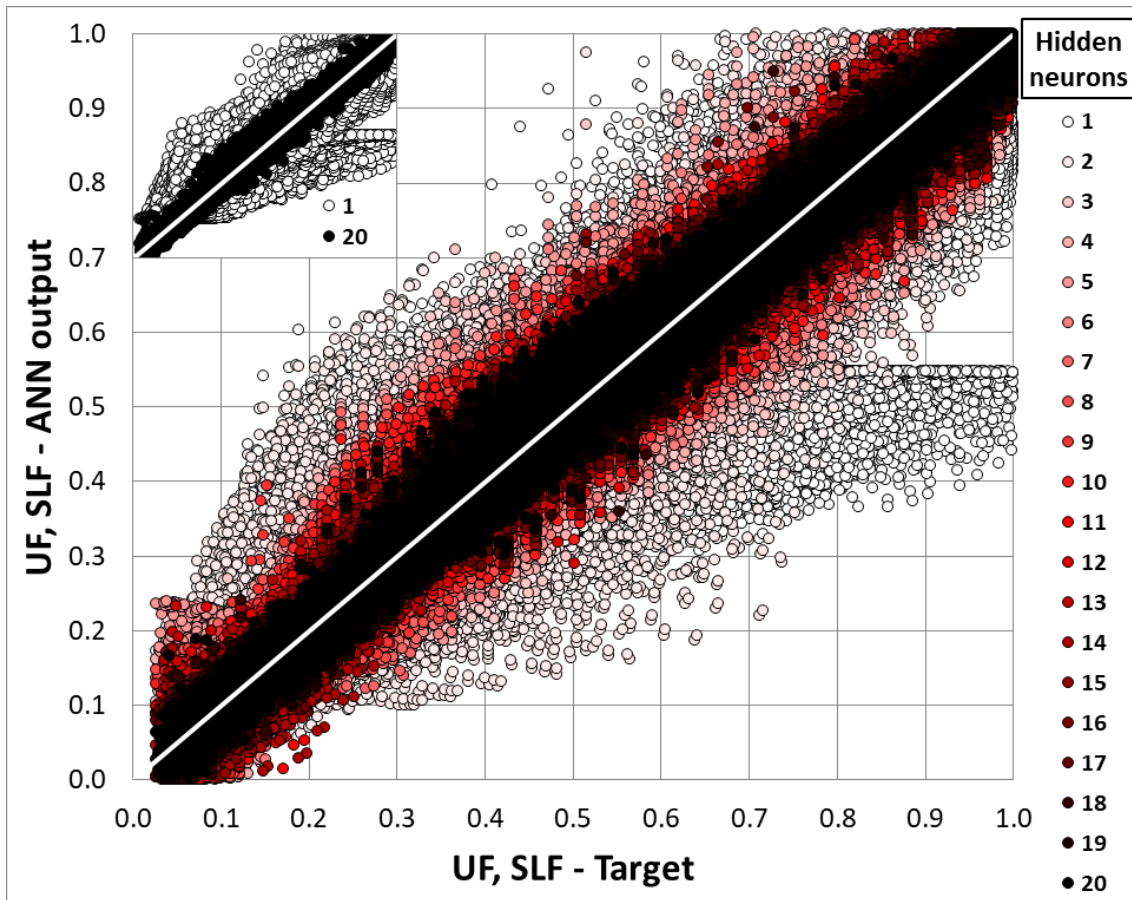
Figure 14. Regression between target and ANN outputs by varying the number of hidden neurons in the first ANN.

The fit is insufficient when the number of neurons is low since the ANN does not accurately predict the two outputs. For example, with 1 neuron, two different groups of points away from the bisector can be distinguished for the two outputs. By increasing the number of neurons, the number of data sets falling on the bisector rises significantly, and with 20 neurons, all the data sets are arranged symmetrically around the bisector.

The results of the training process, by varying the number of hidden neurons, are reported in Figure 15 in terms of absolute errors $|E_i|$, the absolute difference between the target and ANN output values, in predicting the two indicators *SLF* and *UF*.
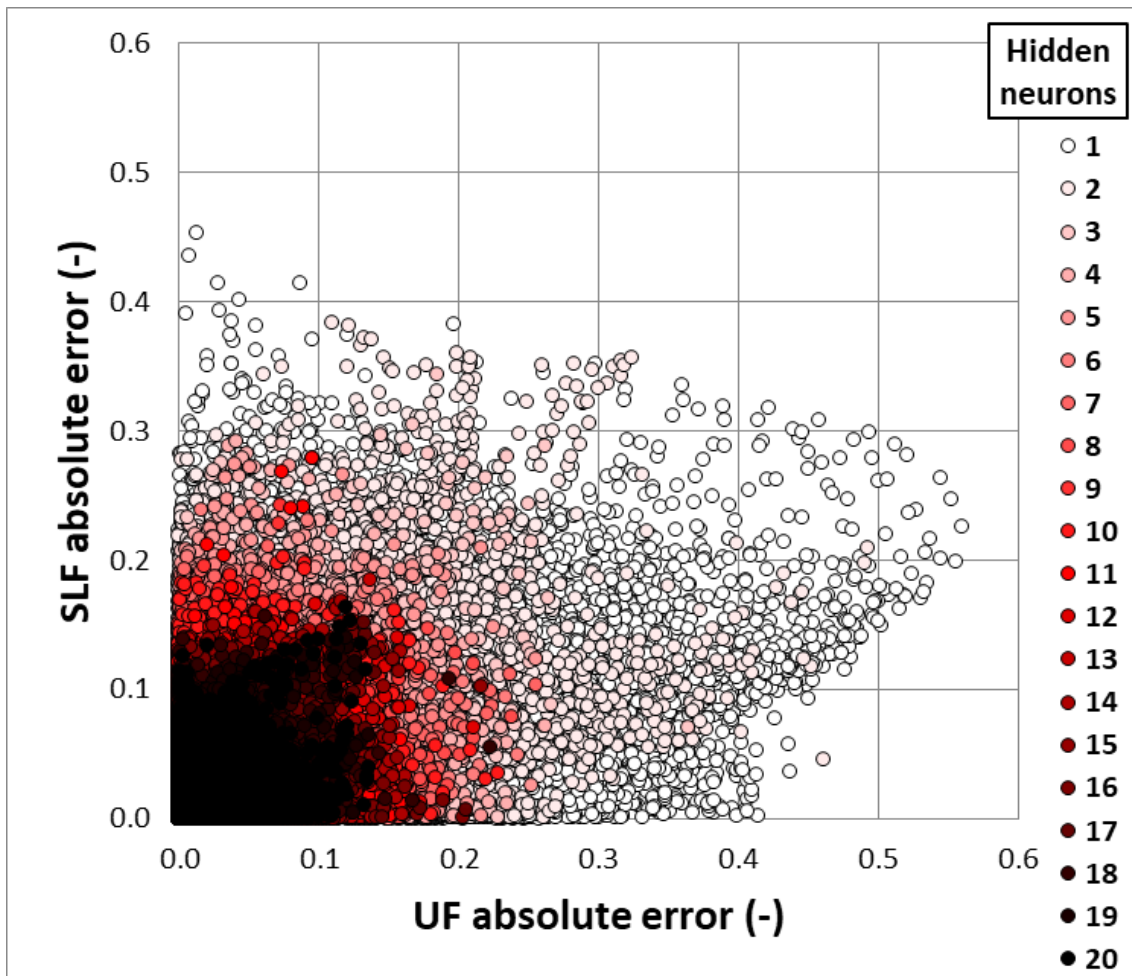
Figure 14. *SLF and UF absolute error comparison by varying the number of hidden neurons in the first ANN.*

The figure contains about 50000 pairs of *SLF* and *UF* errors for each specific number of neurons. It is evident that the increase in the number of hidden neurons from 1 to 20 leads to a reduction of the range of variation of errors of the two indicators approximately from the quadrant (0, 0.4) to the quadrant (0, 0.1).

The errors E_i were also used to draw the box plots separately for the two indicators in Figure 15 as a function of the number of neurons.
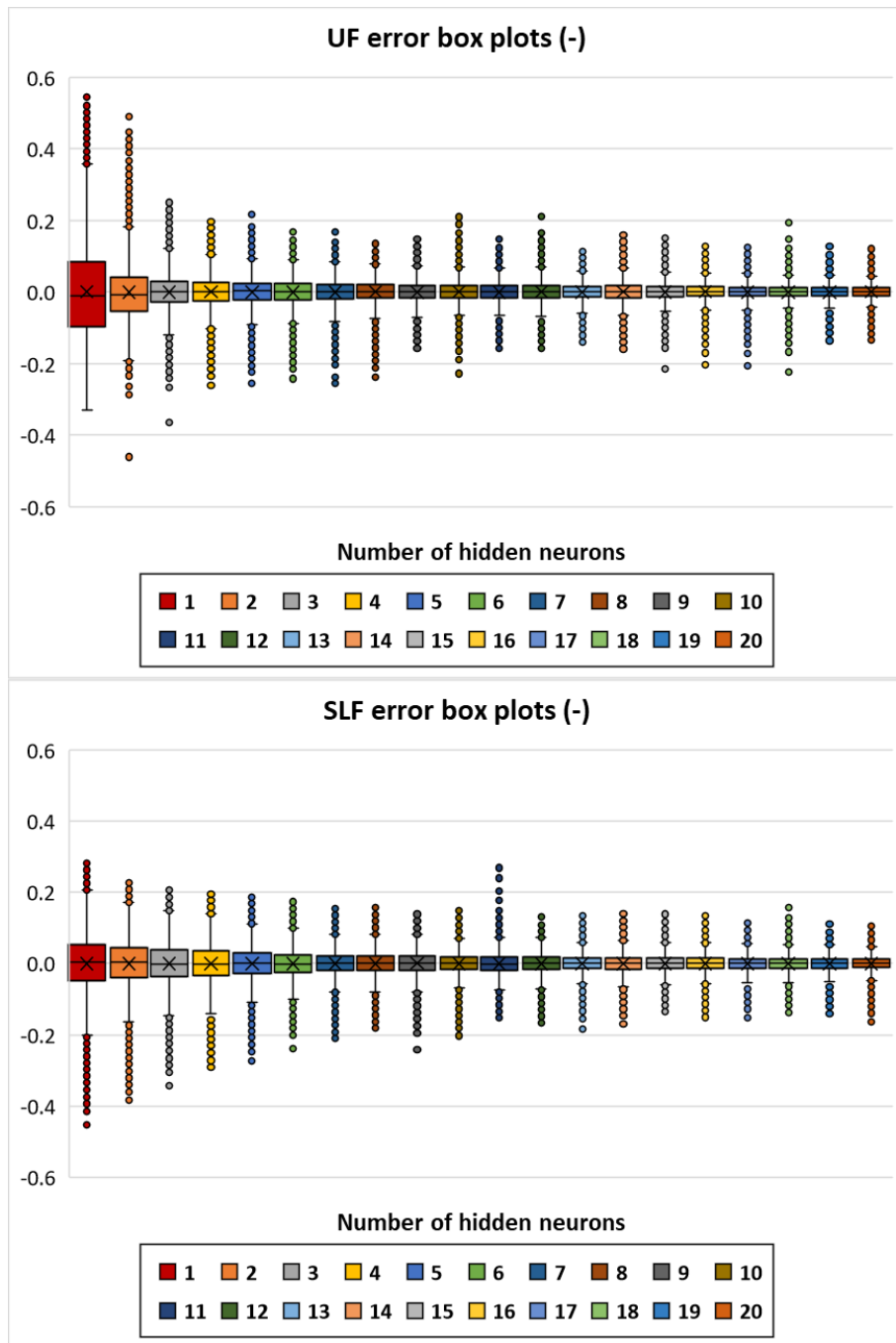
***Figure 15.** UF and SLF error box plots by varying the number of hidden neurons in the first ANN.*

As expected, the box plot underwent a reduction of its interquartile range (the difference between the third and first quartile), mean and size of whiskers by using a high number of neurons. These graphs show that the ANN has a lower prediction capacity for the utilization factor compared to that of the satisfied load fraction since, if the same number of neurons is considered, the *UF* box plot covers a high range of variation of the ordinate.

Finally, the errors were used to calculate the error frequency density distributions starting from the 1-neuron ANN to the 20-neuron ANN to obtain additional verification of the ANN reliability and accuracy. Figure 16 compares the distributions obtained for the two outputs.
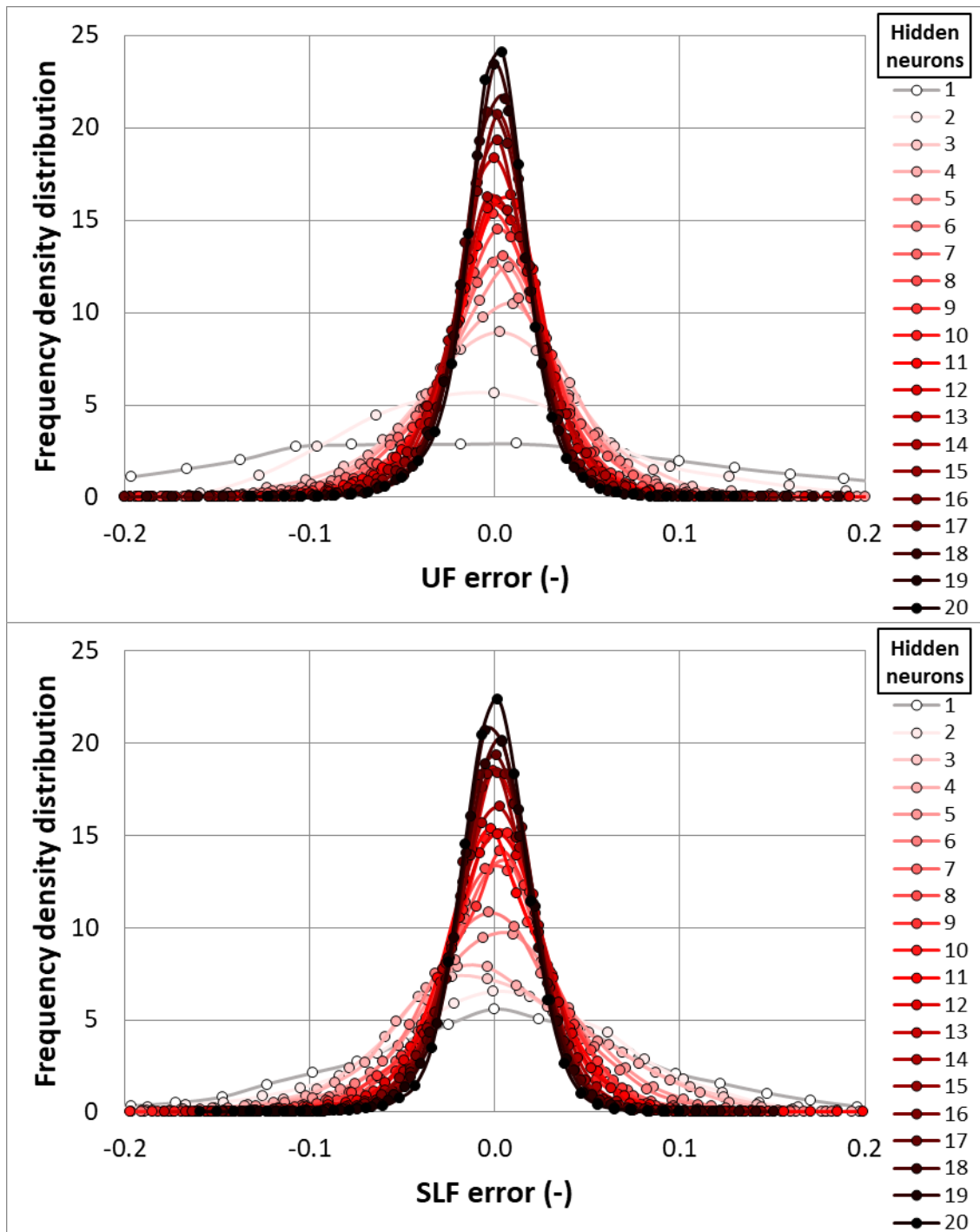
Figure 16. UF and SLF frequency density distributions by varying the number of hidden neurons in the first ANN.

For both outputs, the distribution narrows around the zero value with a higher number of neurons. In addition, this further elaboration confirms that the ANN is more accurate in the prediction of *SLF* and *UF* with 20 neurons since the frequency of nil errors is higher in both cases.

The target, output and error values achieved by changing the number of neurons were used to calculate the metrics described in Section 2.3.2.2.

Figure 17 shows the trend obtained for regression *R* (red pointer) and performance *P* (blue pointers), divided in training, validation, testing and global process, by varying the number of neurons within the hidden layer for the network trained using two outputs.
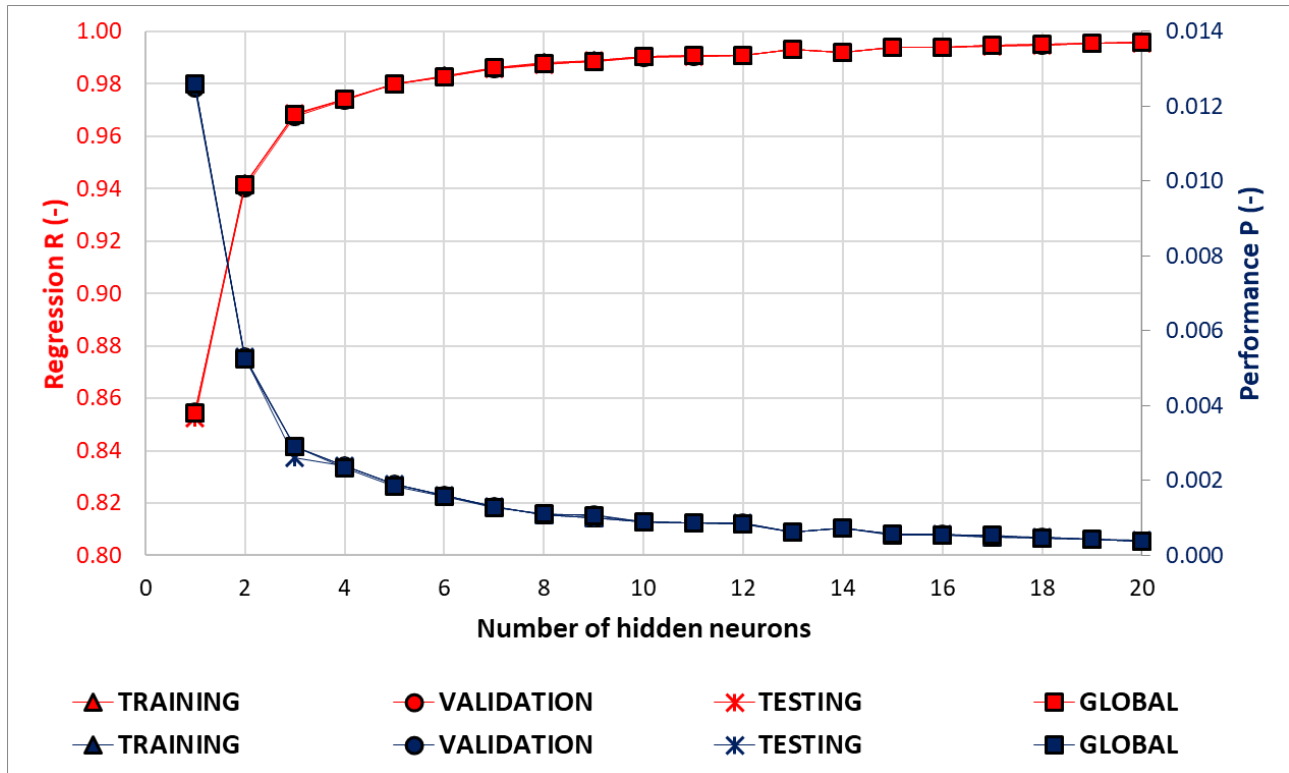
Figure 17. *Regression and Performance indicators for the training, validation, testing and global
processes by varying the number of hidden neurons in the first ANN.*

Figure 17 highlights that the regression and performance indicators are improved by increasing
the number of hidden neurons and no overfitting phenomena occur. This indicates that the
number of training data is sufficient to generalize the ANN in the range of the number of neurons
considered. The curves related to the global process are almost identical to those of the training,
validation, and testing data. The highest increase in accuracy is reached between 1 and 3 neurons
with global *R=0.8543* and global *P=0.0126* for one neuron and global *R=0.9682* and global
P=0.0029 for three neurons. Given the decreasing asymptotic trend and the very low *P* and very
high *R* values, the best ANN can be chosen as the 20-neuron ANN with global *R=0.9958* and
global *P=0.0004*.

Figure 18 shows the computational cost required by the training phase in terms of time and
epochs.
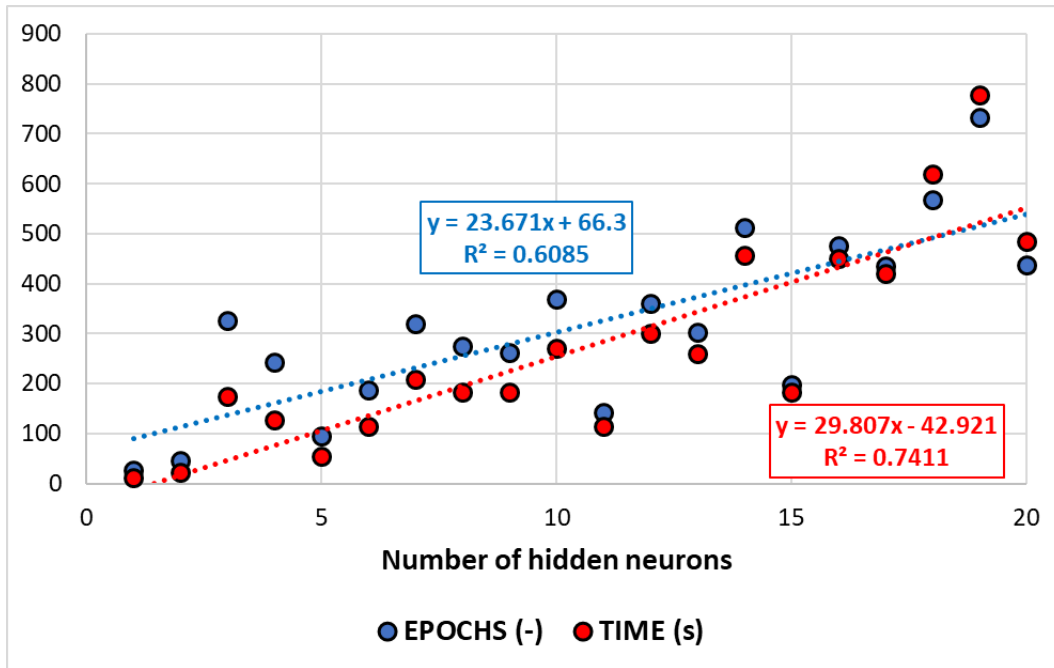
Figure 18. Epochs and time required for the training, validation, and testing processes by varying the number of hidden neurons in the first ANN.

For both computational cost indicators, a noisy increasing trend can be observed. The linear regression demonstrates that a further increase of one neuron determines an increase of about 29.8 s and 23.7 epochs of the training process.

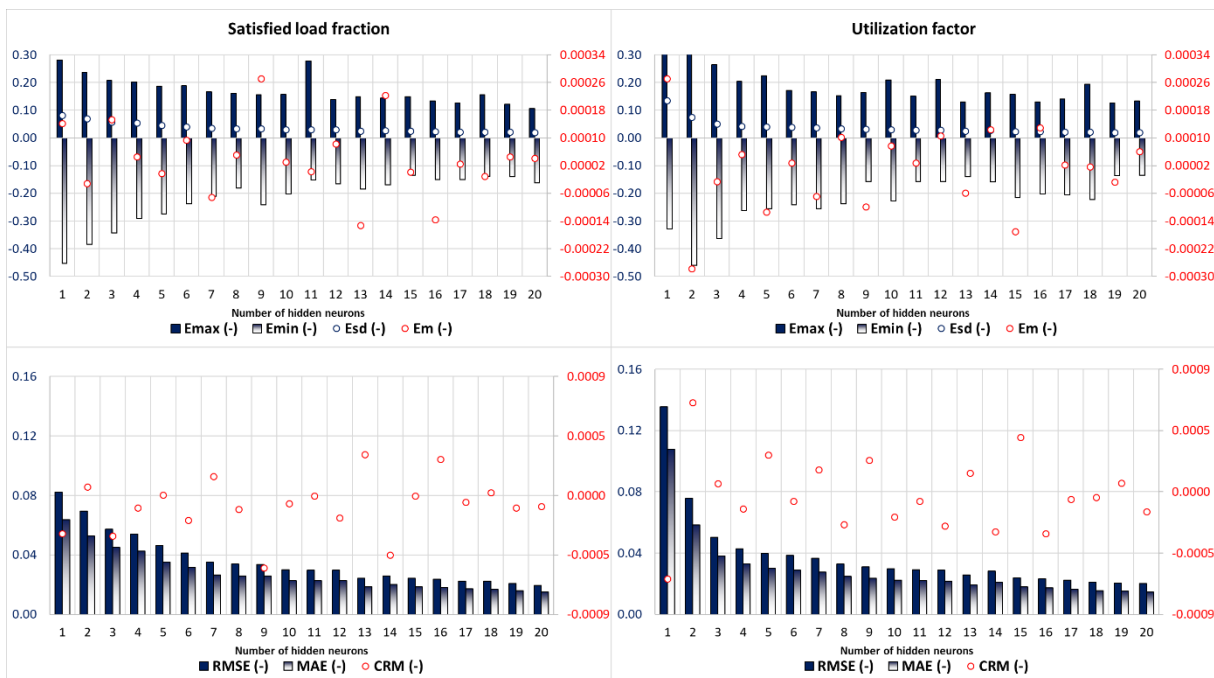The other metrics defined were plotted in Figure 19 for both indicators.

Figure 19. Prediction accuracy metrics for the SLF and UF by varying the number of hidden neurons in the first ANN.

For both outputs, the overall conclusions extractable from these trends as the neurons increase are:

- E_{sd}, *RMSE* and *MAE* decrease;
- E_{min} and E_{max} overall tend to zero, showing some noise in the trend;
- E_m and *CRM* randomly vary, demonstrating that, globally, the ANN can overestimate or underestimate the target values by changing the number of neurons.

All the accuracy metrics are slightly better for *SLF* compared to those of *UF*.

These data can be used to confirm that the best ANN is that the one with 20 neurons, which is characterized by the highest accuracy with, globally, a slight overestimation of both indicators.

Finally, for each regression curve shown in Figure 14, the coefficient of determination R^2, the angular coefficient m and the intercept b were determined and illustrated as a function of the number of neurons in Figure 20 for both indicators both separately and globally.
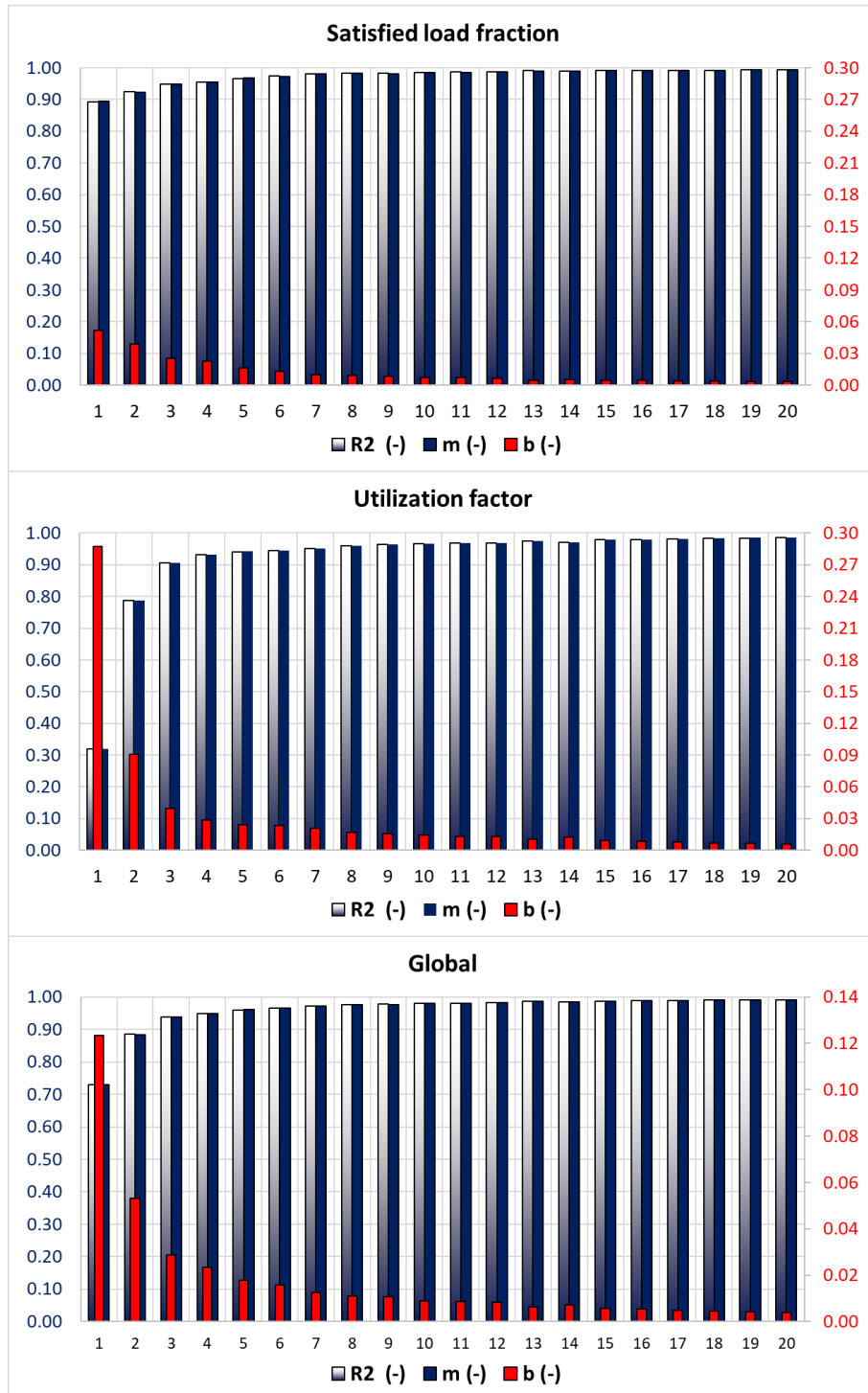
Figure 20. *Regression metrics for the SLF, UF and global output by varying the number of hidden neurons in the first ANN.*

The regression curve becomes closer to the bisector by increasing the number of neurons and on one hand, the SLF metrics respect the bisector constraints with few neurons and the UF metrics are characterized by a high value of the intercept *b* and low values of the angular coefficient *m* and coefficient of determination R^2; on the other hand, the global regression curves present a trade-off behaviour for the metrics values.

Globally, the 20-neuron ANN shows a very satisfactory agreement between the target outputs.

3.3.1.2. ANN for the prediction of the grid energy interaction factor

The second ANN was developed by using as outputs the grid energy interaction factor, a function of the other two output indicators.

The linear regression curves illustrated in Figure 21, by changing the number of neurons, were used to validate the network performance. They also show that in this case, an increase of neurons leads to a better fit between the pointers and the 45° line with the best result obtained with the 20-neuron ANN. For this ANN, the pointers are much closer to the bisector than the first ANN with two outputs. This is owing to the presence of a sole output to be predicted.
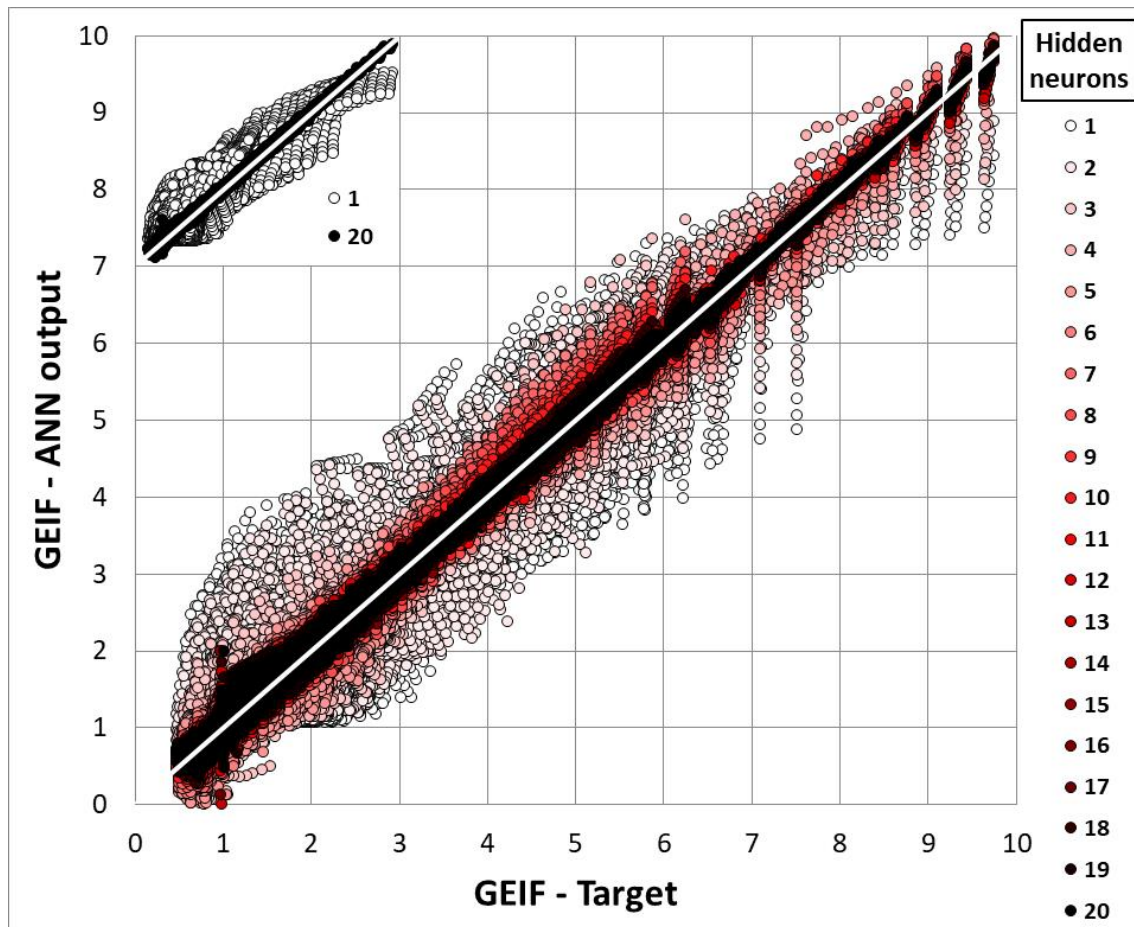
Figure 21. Regression between target and ANN outputs by varying the number of hidden neurons in the second ANN.

All the data elaboration related to the errors E_i performed for the first ANN were also obtained for this case.

Box plots and the frequency density distributions as a function of the number of neurons are reported in Figure 22 and 23, respectively.
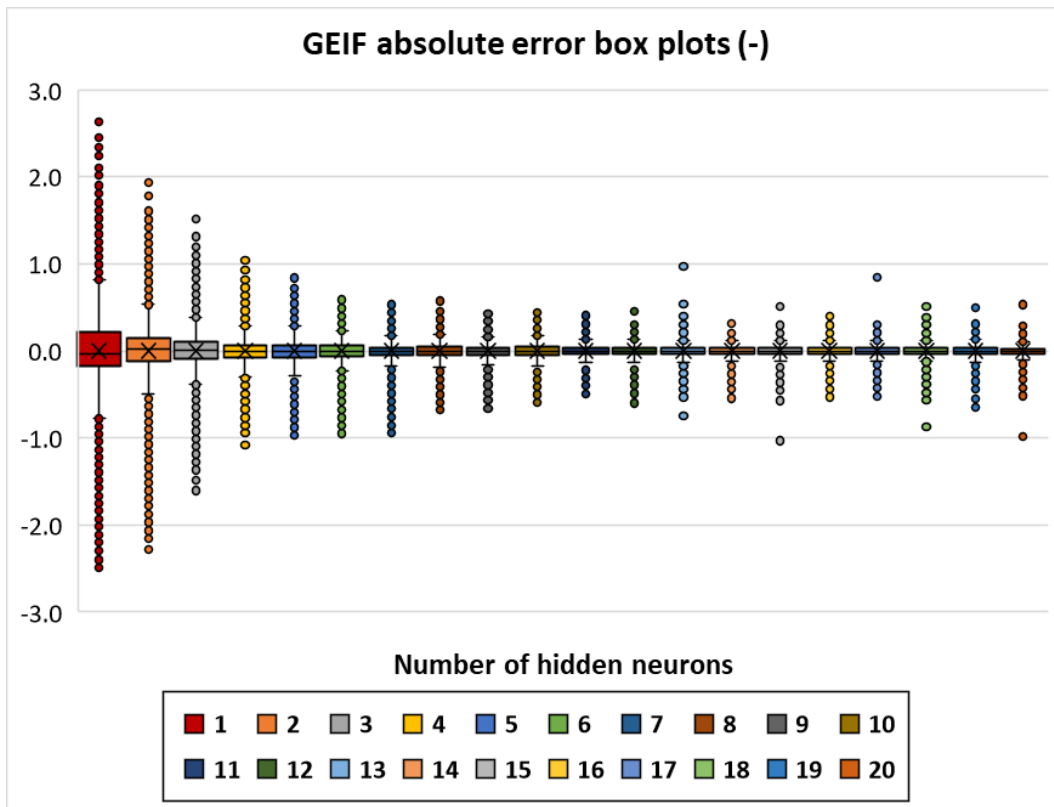
Figure 22. GEIF error box plots by varying the number of hidden neurons in the second ANN.
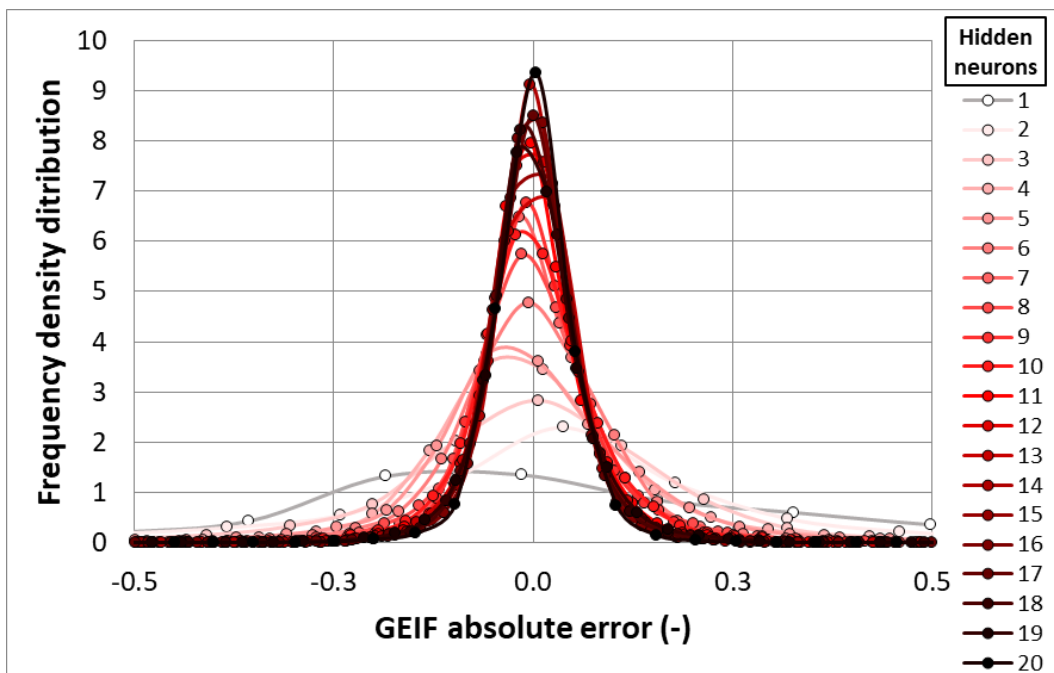

Figure 23. GEIF frequency density distributions by varying the number of hidden neurons in the second ANN.

The same qualitative conclusions drawn from the other ANN with two outputs can also be observed for this ANN. Substantially, an increase in the number of neurons permits the reduction of the interquartile range that remains practically constant after 6 neurons. Similarly, the width of the frequency density distribution, which is representative of the variance value, is reduced

and the occurrences in the proximity of the nil error increase.

Figure 24 shows the trend obtained of regression R (red pointer) and performance P (blue pointers), divided among training, validation, testing and global process, by varying the number of neurons within the hidden layer for the network trained by using one output.
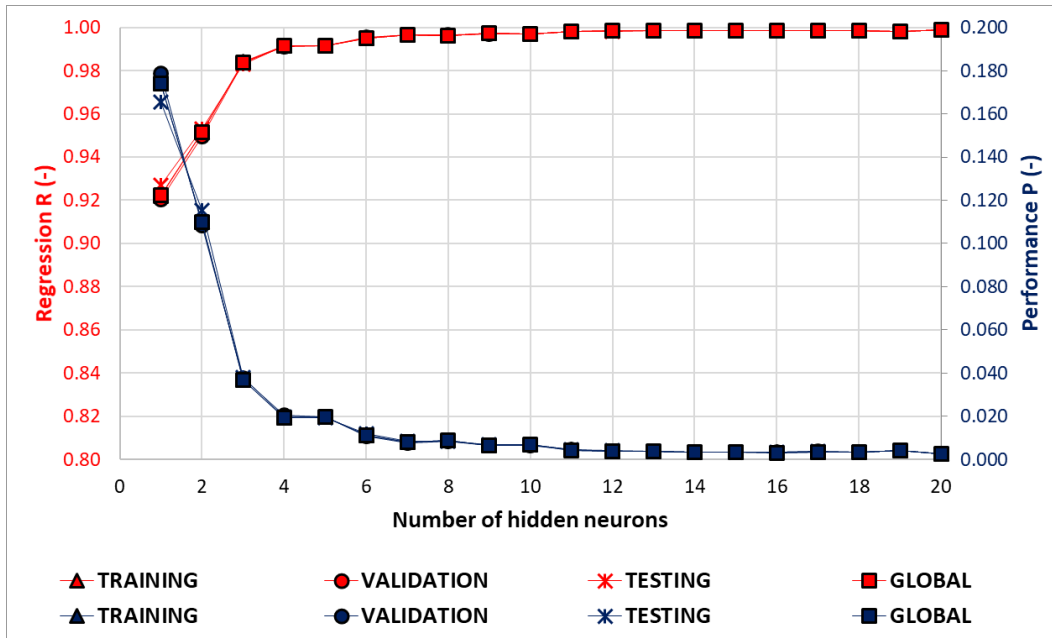

Figure 24. *Regression and Performance indicators for the training, validation, testing and global processes by varying the number of hidden neurons in the second ANN.*

Figure 24 highlights that the regression and performance indicators are improved by increasing the number of hidden neurons. In this case, no overfitting phenomena occur, except for 1 neuron, where the testing data shows a lower accuracy compared with the training data. The number of training data permits the generalization of the ANN in the range of the number of neurons considered. The curves related to the global process is almost identical to those of the training, validation, and testing data. The highest increase in accuracy is reached between 1 and 4 neurons with global *R=0.9225* and global *P=0.1740* for one neuron and global *R=0.9915* and global *P=0.0194* for four neurons. Given the decreasing asymptotic trend and the very low *P* and very high *R* values, the best ANN can be chosen as the 20-neuron ANN with global *R=0.9989* and global *P=0.0025*.
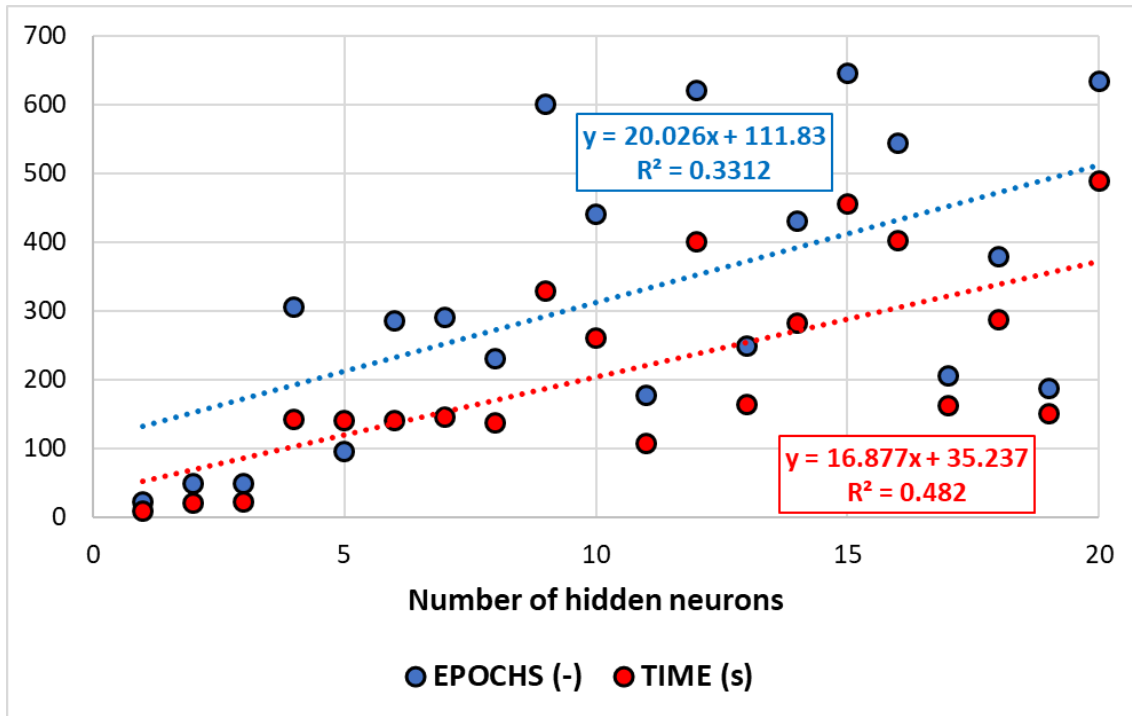
Figure 25. *Epochs and time required for the training, validation and testing processes by varying the number of hidden neurons in the second ANN.*

As shown in Figure 25, the training process was faster than that related to the two-output ANN since 16.9 s and 20.0 epochs per each additional neuron are required.
The additional accuracy metric trends are reported in Figure 26, while the regression metrics are shown in Figure 27.
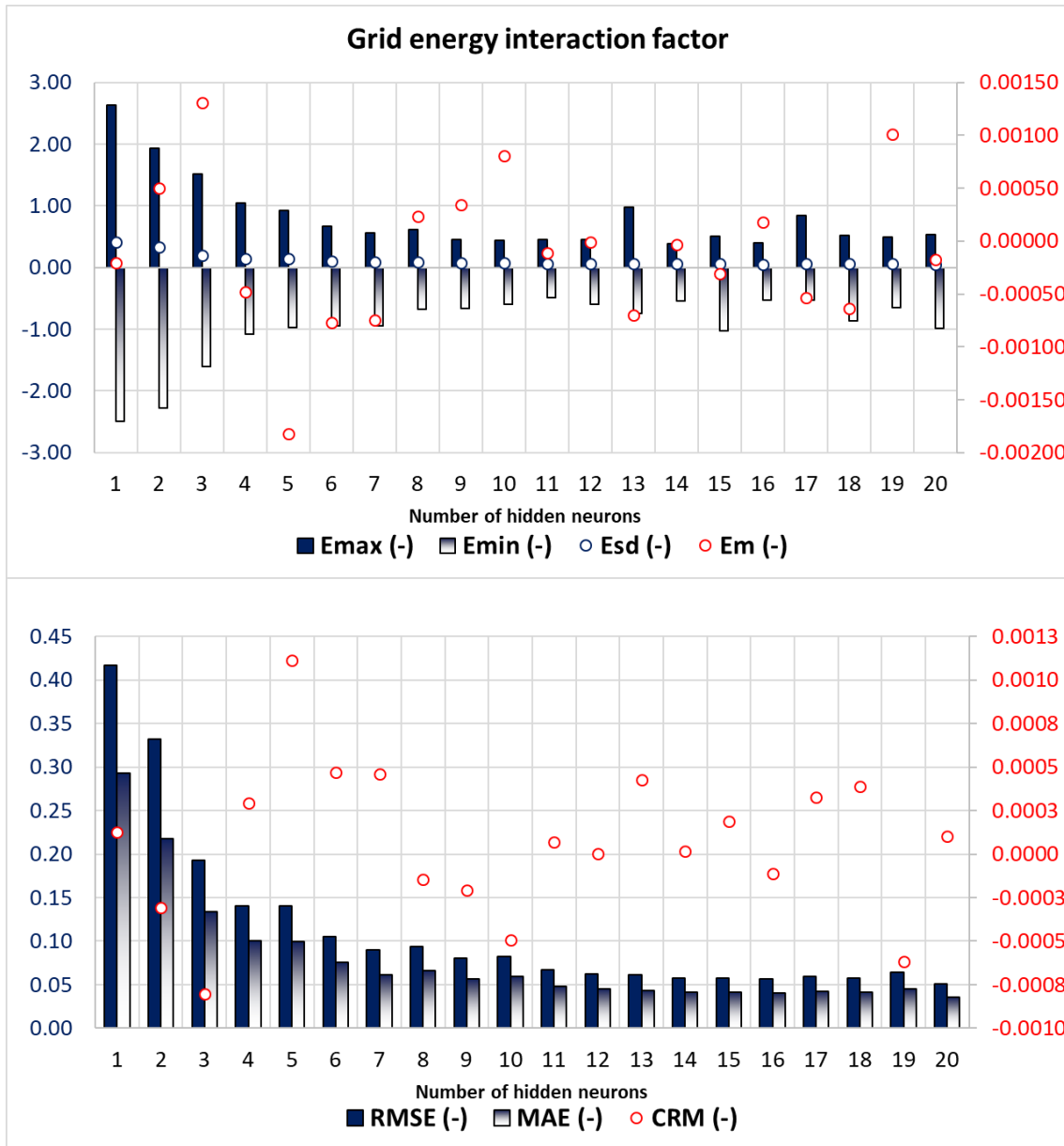
Figure 26. Prediction accuracy metrics for the GEIF by varying the number of hidden neurons in the second ANN.

The same qualitative trend of the metrics obtained with the two output-ANN is observed by increasing the number of neurons. In this case, the optimal 20-neuron ANN has very low values of E_{sd}, *RMSE* and *MAE*. Instead, the very close to zero values of E_m and *CRM* demonstrate that this optimal ANN does not globally tend to overestimate or underestimate the target values.
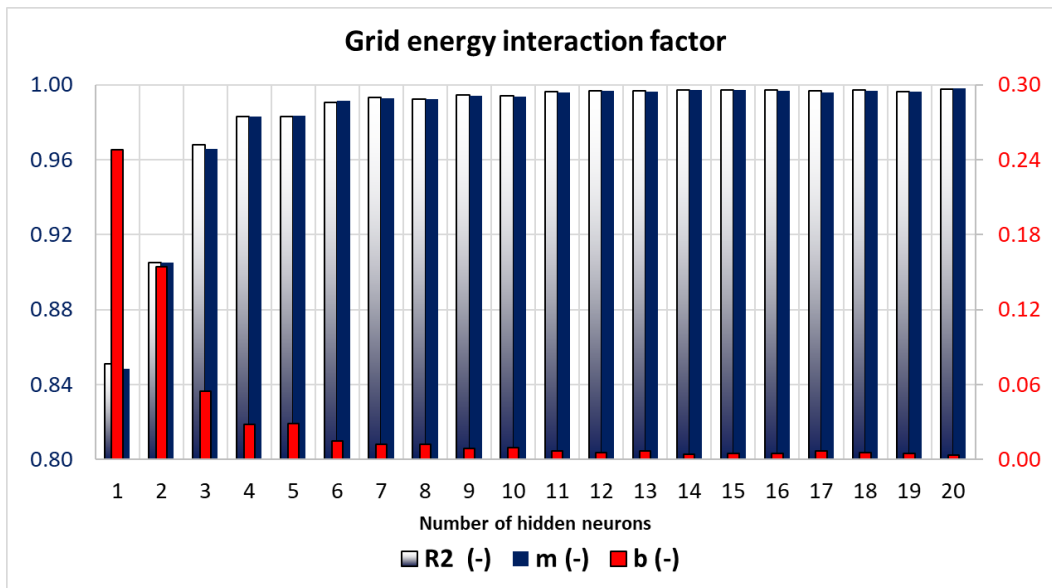
Figure 27. Regression metrics for the GEIF by varying the number of hidden neurons in the second ANN.

The regression curve of the 20-neuron ANN was highly accurate as characterized by an almost unitary value of R^2 and m and an almost nil value of b.
Globally, the 20-neuron ANN showed a very satisfactory agreement between the target output.

3.3.2. Garson method

The Garson method described in Section 2.3.3 was applied to the two optimal ANNs to perform a sensitivity analysis, namely, to determine the inputs that most influence the variation of the outputs.
Weights and biases of the optimal ANNs extracted from pre-defined commands in MATLAB software were used to evaluate the input influence on the outputs of the first and second ANN.

3.3.2.1. ANN for the prediction of the satisfied load fraction and utilization factor

Table 8 contains the weight matrix w_1 (8x20) between the input layer and the hidden layer, the weight matrix w_2 (20x2) between the hidden layer and the output layer, and the biases vector of the hidden and output layers.
Overall, 20 routes can be identified between a generic input $x_{0,i}$ and a specific output y_i. The twenty overall weights $W_{r,ij}$ for the eight inputs, calculated with Eq. (37) for the satisfied load factor and utilization factor, are reported in Table 9. In the same table, the sum of the twenty overall weights s_{ij} is reported for each pair input-output. Finally, Figure 28 shows the percentage sensitivity S_{ij} between the i-th input and j-th output.

Table 8. *Weight matrices w_1 and w_2 and bias vectors b_1 and b_2 of the optimal first ANN.*

	w_1	$x_{1,1}$	$x_{1,2}$	$x_{1,3}$	$x_{1,4}$	$x_{1,5}$	$x_{1,6}$	$x_{1,7}$	$x_{1,8}$	$x_{1,9}$	$x_{1,10}$	$x_{1,11}$	$x_{1,12}$	$x_{1,13}$	$x_{1,14}$	$x_{1,15}$	$x_{1,16}$	$x_{1,17}$	$x_{1,18}$	$x_{1,19}$	$x_{1,20}$
							Input-Hidden Connection Weights														
p_w	$x_{0,1}$	0.48	-0.17	-0.03	-0.62	-0.03	0.04	0.12	0.19	1.15	0.12	-0.10	-0.60	-0.54	-0.44	1.02	-0.88	0.38	0.96	0.12	0.45
p_b	$x_{0,2}$	0.55	-0.16	-0.08	0.36	0.02	0.14	0.62	0.13	0.79	0.18	-0.36	-0.80	-0.74	-0.20	-0.35	-0.22	0.42	0.28	0.32	0.18
$p_{l,m}$	$x_{0,3}$	-2.96	-19.51	0.24	-0.67	1.84	-0.51	4.90	-5.55	-2.36	-1.56	1.17	9.07	23.64	11.22	-7.63	-11.88	11.33	15.11	16.91	-13.48
$c_{se,m}$	$x_{0,4}$	-0.18	0.59	0.07	-0.11	-0.04	-0.03	-14.40	-1.14	-22.92	-0.16	0.09	-0.25	-0.32	0.29	0.10	0.24	0.29	-0.22	-0.09	-0.28
$c_{we,m}$	$x_{0,5}$	-3.64	-1.42	0.02	-0.02	-0.06	0.02	-18.69	-2.26	-19.39	0.09	-0.02	1.70	1.67	-0.26	1.26	-2.08	-0.19	2.08	0.17	0.20
$c_{se,sd}$	$x_{0,6}$	0.14	-14.12	-0.05	-0.02	0.04	0.03	6.98	-1.32	12.36	0.03	-0.02	0.01	0.02	-0.08	-0.01	-0.13	-0.08	0.15	0.05	0.07
$c_{we,sd}$	$x_{0,7}$	-0.09	10.36	-0.04	0.03	0.06	-0.05	2.87	3.02	-3.20	-0.07	0.02	-0.04	0.02	0.05	0.38	0.30	0.18	-0.32	-0.08	-0.02
$p_{l,sd}$	$x_{0,8}$	2.72	18.63	1.77	0.66	-4.61	0.48	-4.77	5.32	1.85	5.38	-1.12	2.94	-7.91	-23.04	7.10	11.18	-12.62	-14.24	-13.09	24.84
	b_1	$b_{1,1}$	$b_{1,2}$	$b_{1,3}$	$b_{1,4}$	$b_{1,5}$	$b_{1,6}$	$b_{1,7}$	$b_{1,8}$	$b_{1,9}$	$b_{1,10}$	$b_{1,11}$	$b_{1,12}$	$b_{1,13}$	$b_{1,14}$	$b_{1,15}$	$b_{1,16}$	$b_{1,17}$	$b_{1,18}$	$b_{1,19}$	$b_{1,20}$
		-5.61	-6.26	3.20	-2.83	-3.13	-0.10	5.63	0.30	-2.84	3.99	0.10	14.89	18.13	-12.48	4.14	-2.85	-2.68	3.10	5.44	12.20
								Hidden-Output Connection Weights														
	w_2	$x_{1,1}$	$x_{1,2}$	$x_{1,3}$	$x_{1,4}$	$x_{1,5}$	$x_{1,6}$	$x_{1,7}$	$x_{1,8}$	$x_{1,9}$	$x_{1,10}$	$x_{1,11}$	$x_{1,12}$	$x_{1,13}$	$x_{1,14}$	$x_{1,15}$	$x_{1,16}$	$x_{1,17}$	$x_{1,18}$	$x_{1,19}$	$x_{1,20}$
UF	y_1	10.69	-0.23	22.96	28.87	6.80	-20.35	0.05	-0.33	0.06	0.72	-7.63	-3.52	1.24	3.95	13.40	6.53	0.42	6.14	6.80	5.70
SLF	y_2	-2.87	-0.13	-48.25	-8.66	-15.05	-21.17	0.07	-0.40	0.07	-6.70	-8.13	35.63	-13.55	10.47	-5.17	0.30	-8.66	0.11	21.26	12.48
	b_2	$b_{2,1}$ 2.08	$b_{2,2}$ -22.41																		

Table 9. *Overall weights $W_{r,ij}$ and summed overall weights s_{ij} of the optimal first ANN.*

Overall weights

Satisfied load fraction

	W_1	W_2	W_3	W_4	W_5	W_6	W_7	W_8	W_9	W_{10}	W_{11}	W_{12}	W_{13}	W_{14}	W_{15}	W_{16}	W_{17}	W_{18}	W_{19}	W_{20}	s_{ij}
p_w	5.08	0.04	0.78	17.96	0.19	0.73	0.01	0.06	0.07	0.09	0.76	2.11	0.67	1.75	13.65	5.73	0.16	5.91	0.84	2.57	59.15
p_b	5.85	0.04	1.88	10.43	0.12	2.79	0.03	0.04	0.05	0.13	2.74	2.80	0.92	0.77	4.70	1.47	0.18	1.71	2.19	1.04	39.88
$p_{l,m}$	31.69	4.43	5.50	19.47	12.55	10.34	0.23	1.81	0.15	1.13	8.94	31.91	29.23	44.33	102.30	77.53	4.81	92.79	114.98	76.79	670.89
$c_{se,m}$	1.94	0.13	1.61	3.25	0.29	0.63	0.69	0.37	1.48	0.11	0.70	0.89	0.40	1.15	1.37	1.53	0.12	1.36	0.63	1.62	20.27
$c_{we,m}$	38.87	0.32	0.37	0.61	0.38	0.34	0.89	0.74	1.25	0.06	0.13	5.97	2.06	1.05	16.96	13.56	0.08	12.79	1.14	1.13	98.68
$c_{se,sd}$	1.50	3.21	1.18	0.50	0.26	0.62	0.33	0.43	0.80	0.02	0.13	0.02	0.02	0.31	0.14	0.86	0.03	0.91	0.33	0.41	12.03
$c_{we,sd}$	0.93	2.35	0.88	0.79	0.44	1.05	0.14	0.98	0.21	0.05	0.18	0.13	0.03	0.19	5.03	1.95	0.08	1.97	0.56	0.11	18.03
$p_{l,sd}$	29.11	4.23	40.72	18.92	31.36	9.82	0.23	1.74	0.12	3.90	8.53	10.33	9.78	91.03	95.12	73.00	5.36	87.42	89.02	141.48	751.21

Utilization factor

|	W_1	W_2	W_3	W_4	W_5	W_6	W_7	W_8	W_9	W_{10}	W_{11}	W_{12}	W_{13}	W_{14}	W_{15}	W_{16}	W_{17}	W_{18}	W_{19}	W_{20}	s_{ij}
p_w	1.37	0.02	1.63	5.39	0.42	0.76	0.01	0.08	0.08	0.79	0.81	21.37	7.31	4.64	5.27	0.27	3.30	0.10	2.62	5.63	61.84
p_b	1.57	0.02	3.94	3.13	0.27	2.90	0.05	0.05	0.05	1.17	2.92	28.37	10.09	2.05	1.81	0.07	3.61	0.03	6.85	2.28	71.25
$p_{l,m}$	8.52	2.62	11.56	5.84	27.74	10.76	0.36	2.22	0.16	10.42	9.51	323.19	320.22	117.44	39.49	3.60	98.05	1.63	359.50	168.19	1521.02
$c_{se,m}$	0.52	0.08	3.38	0.97	0.65	0.65	1.06	0.46	1.53	1.04	0.75	8.98	4.34	3.05	0.53	0.07	2.52	0.02	1.96	3.54	36.11
$c_{we,m}$	10.45	0.19	0.78	0.18	0.84	0.35	1.38	0.91	1.29	0.59	0.13	60.47	22.62	2.77	6.55	0.63	1.61	0.22	3.56	2.47	117.99
$c_{se,sd}$	0.40	1.89	2.49	0.15	0.58	0.64	0.52	0.53	0.82	0.22	0.14	0.25	0.20	0.83	0.05	0.04	0.67	0.02	1.02	0.90	12.37
$c_{we,sd}$	0.25	1.39	1.85	0.24	0.97	1.09	0.21	1.21	0.21	0.45	0.19	1.28	0.33	0.50	1.94	0.09	1.53	0.03	1.75	0.25	15.77
$p_{l,sd}$	7.83	2.50	85.57	5.67	69.33	10.22	0.35	2.13	0.12	36.05	9.08	104.66	107.15	241.18	36.72	3.39	109.29	1.54	278.35	309.89	1421.02
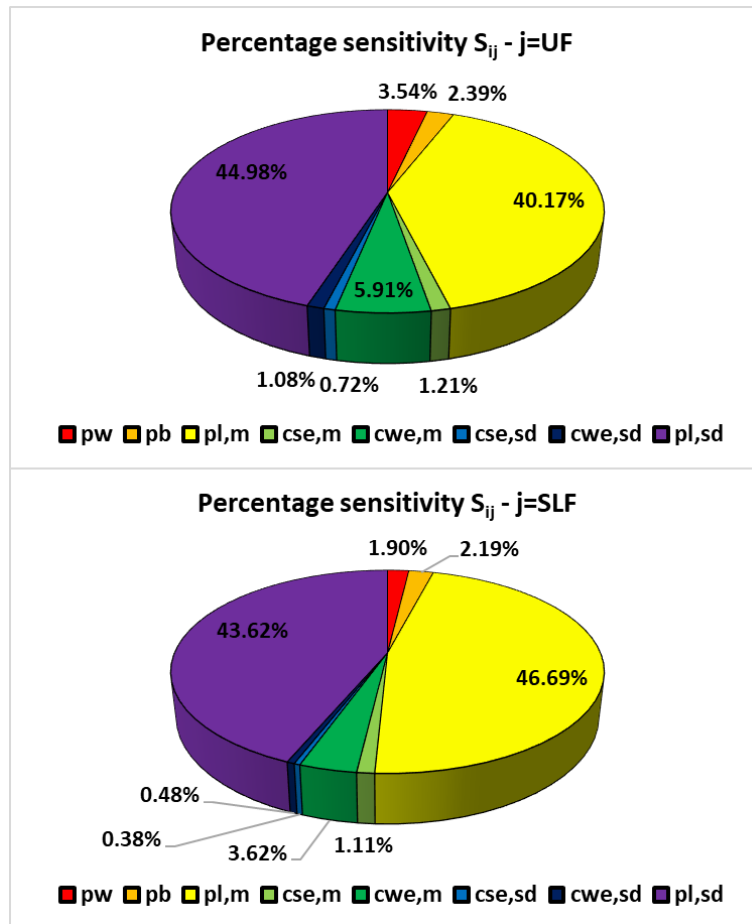
Figure 28. Percentage sensitivity of eight inputs on the UF and SLF.

The figures quantitatively demonstrate the importance of each input parameter for predicting the two outputs and that UF and SLF are mainly affected by the variation of the load variability overall fraction $p_{l,sd}$ and mean load overall fraction $p_{l,m}$. In both cases, the two input percentage sensitivities exceed 40%. Accordingly, the increment of the power installed, or the number of buildings can strongly modify the energy indicators.

For both outputs, the mean wind energy factor $c_{we,m}$ is the third most effective parameter according to the conducted sensitivity analysis with a percentage sensitivity of 5.9% and 3.6%, respectively for the SLF and UF. Finally, the other dimensionless inputs affect the output with a magnitude variable between 0% and 2%. On the other hand, solar availability and variability, wind variability and the subdivision of the power installed in wind, PV and battery may affect the energy performance of the CEC somewhat equally.

3.3.2.2. ANN for the prediction of the grid energy interaction factor

Similar to the previous section, weights and biases of the optimal ANN extracted from pre-defined commands in MATLAB software were used to evaluate the input influence on the output of the second ANN.

Table 10 contains the weight matrix w_1 (8x20) between the input layer and the hidden layer, the weight matrix w_2 (20x1) between the hidden layer and the output layer, and the biases vector of the hidden and output layers.

In addition, in this case, 20 routes can be identified between a generic input $x_{0,i}$ and a specific

output y_i. The twenty overall weights $W_{r,ij}$ for the eight inputs, calculated with Eq. (37) for the grid energy interaction factor, are reported in Table 11. In the same table, the sum between the twenty overall weights s_{ij} is reported for each input-output pair. Finally, Figure 29 shows the percentage sensitivity S_{ij} between the i-th input and j-th output.

Table 10. *Weight matrices w_1 and w_2 and bias vectors b_1 and b_2 of the optimal second ANN.*

	w₁	$x_{1,1}$	$x_{1,2}$	$x_{1,3}$	$x_{1,4}$	$x_{1,5}$	$x_{1,6}$	$x_{1,7}$	$x_{1,8}$	$x_{1,9}$	$x_{1,10}$	$x_{1,11}$	$x_{1,12}$	$x_{1,13}$	$x_{1,14}$	$x_{1,15}$	$x_{1,16}$	$x_{1,17}$	$x_{1,18}$	$x_{1,19}$	$x_{1,20}$
p_w	$x_{0,1}$	0.41	-0.04	-0.12	-0.03	0.34	-0.07	0.08	0.02	0.02	0.03	0.04	0.07	-1.91	0.10	0.07	0.28	0.34	0.11	0.09	0.46
p_b	$x_{0,2}$	0.37	0.04	-0.04	0.16	0.03	0.01	0.10	-0.03	0.00	-0.02	0.01	0.01	-2.88	-0.10	-0.97	-0.05	0.27	0.01	-0.97	0.12
$p_{l,m}$	$x_{0,3}$	3.43	6.59	8.48	7.29	1.26	24.85	-2.31	5.42	23.05	6.21	0.70	0.59	-15.45	-2.93	1.16	-13.80	18.00	2.98	3.72	10.16
$c_{se,m}$	$x_{0,4}$	-1.15	-2.07	0.01	-0.52	0.94	0.02	-0.04	-2.05	0.00	0.54	0.32	0.29	-0.48	0.60	-0.02	0.16	-0.22	0.17	-0.01	0.22
$c_{we,m}$	$x_{0,5}$	-2.25	-3.42	0.81	0.32	1.23	-0.25	-0.94	6.82	-0.21	-2.13	-1.11	-0.78	3.82	-0.57	-0.02	1.01	0.12	0.08	-0.02	-1.78
$c_{se,sd}$	$x_{0,6}$	7.21	-0.52	-0.13	1.94	-2.35	-0.12	0.15	-6.33	-0.10	-0.87	-0.64	-0.65	0.34	-1.85	0.07	-0.26	0.04	-0.47	0.07	-0.71
$c_{we,sd}$	$x_{0,7}$	3.93	3.25	0.01	-1.57	2.08	0.15	0.00	5.81	0.12	2.63	0.92	0.58	-1.33	1.38	-0.04	0.87	0.03	0.18	-0.05	1.28
$p_{l,sd}$	$x_{0,8}$	0.53	7.04	2.76	-5.69	-2.23	-11.96	-9.42	-5.54	-9.04	-6.10	-0.77	-0.72	12.22	1.76	4.39	12.01	-3.21	-3.14	2.17	-6.00
b₁		$b_{1,1}$	$b_{1,2}$	$b_{1,3}$	$b_{1,4}$	$b_{1,5}$	$b_{1,6}$	$b_{1,7}$	$b_{1,8}$	$b_{1,9}$	$b_{1,10}$	$b_{1,11}$	$b_{1,12}$	$b_{1,13}$	$b_{1,14}$	$b_{1,15}$	$b_{1,16}$	$b_{1,17}$	$b_{1,18}$	$b_{1,19}$	$b_{1,20}$
		13.91	18.18	13.40	2.00	-1.60	14.14	-13.31	-2.25	14.69	0.32	-0.26	-0.21	-0.17	-1.89	4.00	-1.63	16.97	0.14	4.23	5.27

	w₂	$x_{1,1}$	$x_{1,2}$	$x_{1,3}$	$x_{1,4}$	$x_{1,5}$	$x_{1,6}$	$x_{1,7}$	$x_{1,8}$	$x_{1,9}$	$x_{1,10}$	$x_{1,11}$	$x_{1,12}$	$x_{1,13}$	$x_{1,14}$	$x_{1,15}$	$x_{1,16}$	$x_{1,17}$	$x_{1,18}$	$x_{1,19}$	$x_{1,20}$
GEIF	y_1	-0.40	11.61	48.13	0.86	-0.51	-57.40	10.85	0.26	18.86	1.26	-8.57	8.47	-0.03	1.21	0.85	0.63	-27.14	-2.44	-0.82	0.49
b₂		$b_{2,1}$ 15.82																			

Table 11. *Overall weights $W_{r,ij}$ and summed overall weights s_{ij} of the optimal second ANN.*

Overall weights — Grid energy interaction factor

	W_1	W_2	W_3	W_4	W_5	W_6	W_7	W_8	W_9	W_{10}	W_{11}	W_{12}	W_{13}	W_{14}	W_{15}	W_{16}	W_{17}	W_{18}	W_{19}	W_{20}	s_{ij}
p_w	0.16	0.48	5.89	0.03	0.17	3.82	0.91	0.00	0.38	0.03	0.37	0.58	0.06	0.12	0.06	0.17	9.25	0.28	0.07	0.22	23.07
p_b	0.15	0.43	1.84	0.14	0.01	0.55	1.08	0.01	0.04	0.03	0.10	0.12	0.09	0.12	0.82	0.03	7.25	0.01	0.79	0.06	13.67
$p_{l,m}$	1.36	76.43	408.19	6.30	0.65	1426.60	25.04	1.41	434.62	7.81	6.01	4.99	0.49	3.53	0.99	8.65	488.50	7.27	3.04	4.95	2916.83
$c_{se,m}$	0.46	24.03	0.59	0.45	0.48	1.13	0.46	0.54	0.09	0.67	2.78	2.46	0.02	0.72	0.02	0.10	5.86	0.41	0.01	0.11	41.39
$c_{we,m}$	0.89	39.70	38.85	0.27	0.63	14.19	10.21	1.78	3.87	2.68	9.49	6.63	0.12	0.68	0.02	0.63	3.24	0.19	0.02	0.87	134.98
$c_{se,sd}$	2.85	6.07	6.09	1.68	1.20	6.92	1.62	1.65	1.88	1.10	5.52	5.49	0.01	2.23	0.06	0.16	1.10	1.14	0.06	0.34	47.16
$c_{we,sd}$	1.56	37.73	0.44	1.36	1.07	8.65	0.03	1.51	2.30	3.31	7.87	4.94	0.04	1.67	0.03	0.54	0.70	0.43	0.04	0.62	74.85
$p_{l,sd}$	0.21	81.74	132.89	4.91	1.14	686.40	102.15	1.44	170.43	7.67	6.61	6.10	0.38	2.12	3.73	7.52	87.11	7.66	1.78	2.92	1314.95

Percentage sensitivity S_{ij} - j=GEIF

0.51% 0.30% 28.79% 1.64% 1.03% 2.96% 0.91% 63.87%

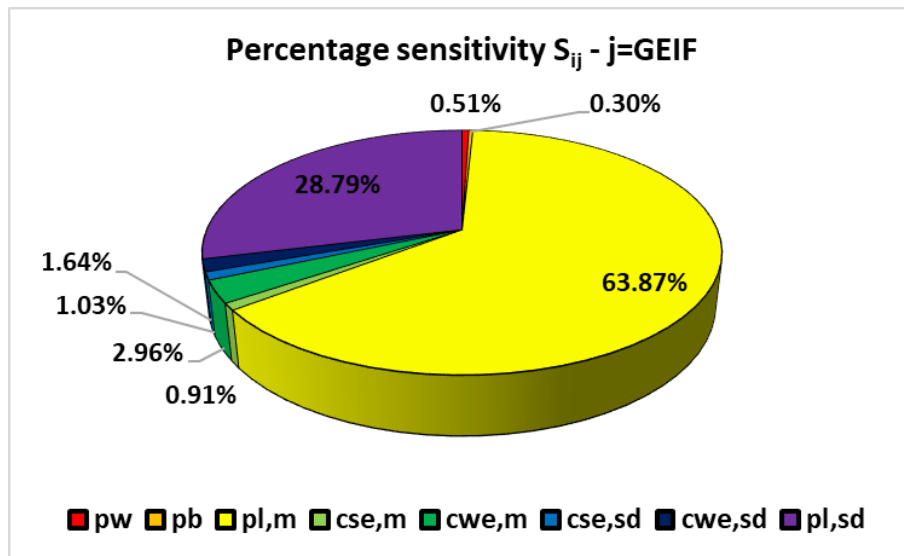☐ pw ☐ pb ☐ pl,m ☐ cse,m ☐ cwe,m ☐ cse,sd ☐ cwe,sd ☐ pl,sd

Figure 29. *Percentage sensitivity of eight inputs on the GEIF.*

For the single-output ANN, the mean load overall fraction $p_{l,m}$ is the most important input parameter in the determination of the *GEIF*. This parameter has a relative importance of about 64% between the eight input parameters demonstrating that the energy performance of the CEC strongly depends on the system and load size. In addition, the variability of the load trend has a

substantial influence with a percentage sensitivity of about 29%. Finally, the other dimensionless inputs affect the output with a magnitude variable between 0% and 3%, by confirming that the solar and wind availability and variability, and subdivision of the power installed in the three main components less significantly modify the interaction with the grid compared to the overall power installed and load requirement and variability.

3.4. Step 4 – ANN application

The accuracy and reliability of the optimal ANNs were verified by providing data derived from case studies not used in the training process. Only the input parameters related to the additional 128 case studies were provided to the optimal ANNs.

Tables 12 and 13 list the climatic and load data required for the calculation of the dimensionless inputs by changing the locality.

Table 12. Climatic data for the dimensionless input data calculation for ANN training.

Locality	T_m (°C)	G_m (W/m²)	V_{m3}^3 (m³/s³)	T_{sd} (°C)	G_{sd} (W/m²)	$V_{m3,sd}^3$ (m³/s³)
Havana	24.28	199.23	64.34	4.08	276.74	118.77
Bechar	20.90	240.87	182.25	9.33	315.70	284.62
Vienna	9.76	126.92	182.29	8.66	200.41	318.85
Valencia	17.33	185.80	98.92	6.37	261.24	241.53
Mexico City	16.41	210.45	40.37	5.13	295.82	77.57
Warsaw	7.81	113.29	127.06	9.03	185.53	237.13
Hakkari	10.11	196.20	21.44	11.16	284.34	81.92
Irkutsk	0.15	128.63	89.41	14.31	197.47	189.61

Table 13. Load data for the dimensionless input data calculation for ANN application.

| Locality	$P_{L,m}$ (kW) 7 buildings	$P_{L,m}$ (kW) 15 buildings	$P_{L,sd}$ (kW) 7 buildings	$P_{L,sd}$ (kW) 15 buildings
Havana	9.38	20.10	80.18	171.81
Bechar	9.24	19.80	79.28	169.89
Vienna	9.88	21.17	81.91	175.52
Valencia	9.52	20.41	81.35	174.32
Mexico City	9.36	20.07	80.12	171.68
Warsaw	10.00	21.43	82.31	176.38
Hakkari	9.87	21.15	82.87	177.58
Irkutsk	9.57	20.50	80.01	171.46

The range of variation of the dimensionless inputs used to apply the optimal ANNs and the range of variation of the dimensionless outputs derived from TRNSYS simulations comply with the range of validity of the dimensionless inputs and outputs reported in Table 14 of the trained ANNs. This guarantees a good preliminary verification of the application chosen.

***Table 14.** Range of variation of the dimensionless inputs used in the ANN application.*

p_w	p_b	$p_{l,m}$	$c_{se,m}$	$c_{we,m}$	$c_{se,sd}$	$c_{we,sd}$	$p_{l,sd}$	UF	SLF	GEIF
0.17	0.17	0.03	0.12	0.08	0.11	0.21	0.26	0.23	0.18	0.68
0.56	0.56	0.18	0.24	0.68	0.54	1.10	1.48	0.77	0.99	3.18

3.4.1. ANN for the prediction of the satisfied load fraction and utilization factor

For the first ANN with two outputs, Figure 30 shows the linear regression curve obtained comparing the ANN outputs and TRNSYS output, both separately (*UF* in red and *SLF* in blue) and globally for the two outputs (in black).
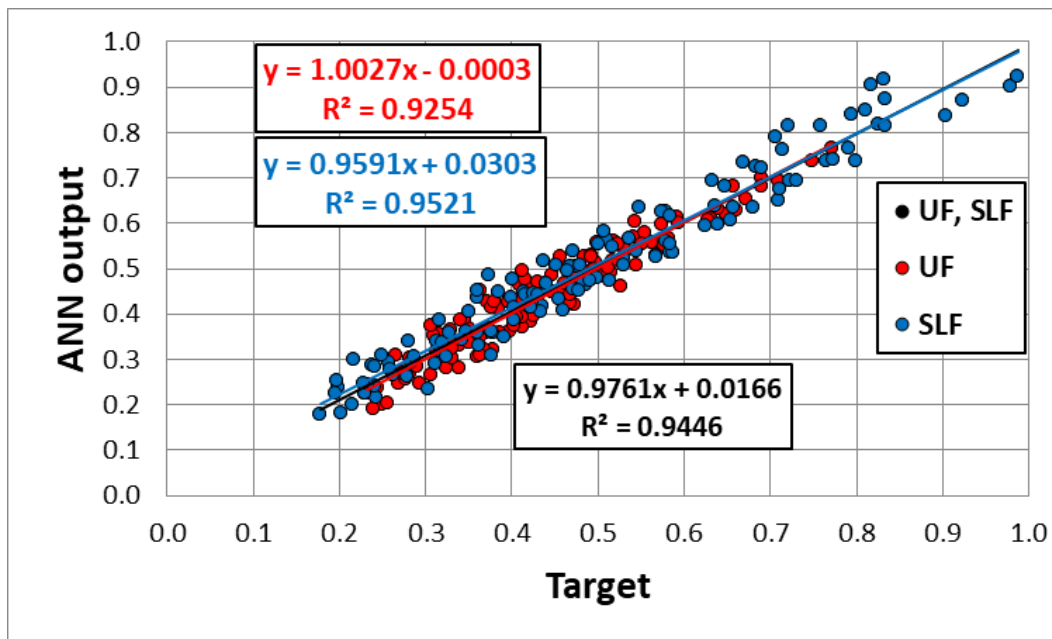
***Figure 30.** Regression curve and metrics for the application of the optimal first ANN.*

The figures ascertain the very high accuracy of the ANN in the prediction of the energy performance of any energy community worldwide. The R^2 is 0.925 for the calculation of the *UF*, 0.952 for the *SLF* and 0.945 globally. Also, the angular coefficients are very close to one and the intercepts very close to zero. As expected, the reliability in the determination of the SLF is slightly higher than that for the calculation of the UF.

To better highlight the real power of the tool created, Figure 31 shows for the eight localities considered, two building districts and eight system power configurations the direct comparison between the *SLF* and *UF* calculated with TRNSYS and with the optimized ANNs.

The **ordinate** contains the indicator **SLF** (-) or **UF** (-) and ranges between **0** and **1**.

The **abscissa** contains the eight system power configurations P_{PV}-P_W-P_B (kW):

    1) **40-40-40**; 2) **40-40-100**; 3) **40-100-40**; 4) **40-100-100**;

    5) **100-40-40**; 6) **100-40-100**; 7) **100-100-40**; 8) **100-100-100.**
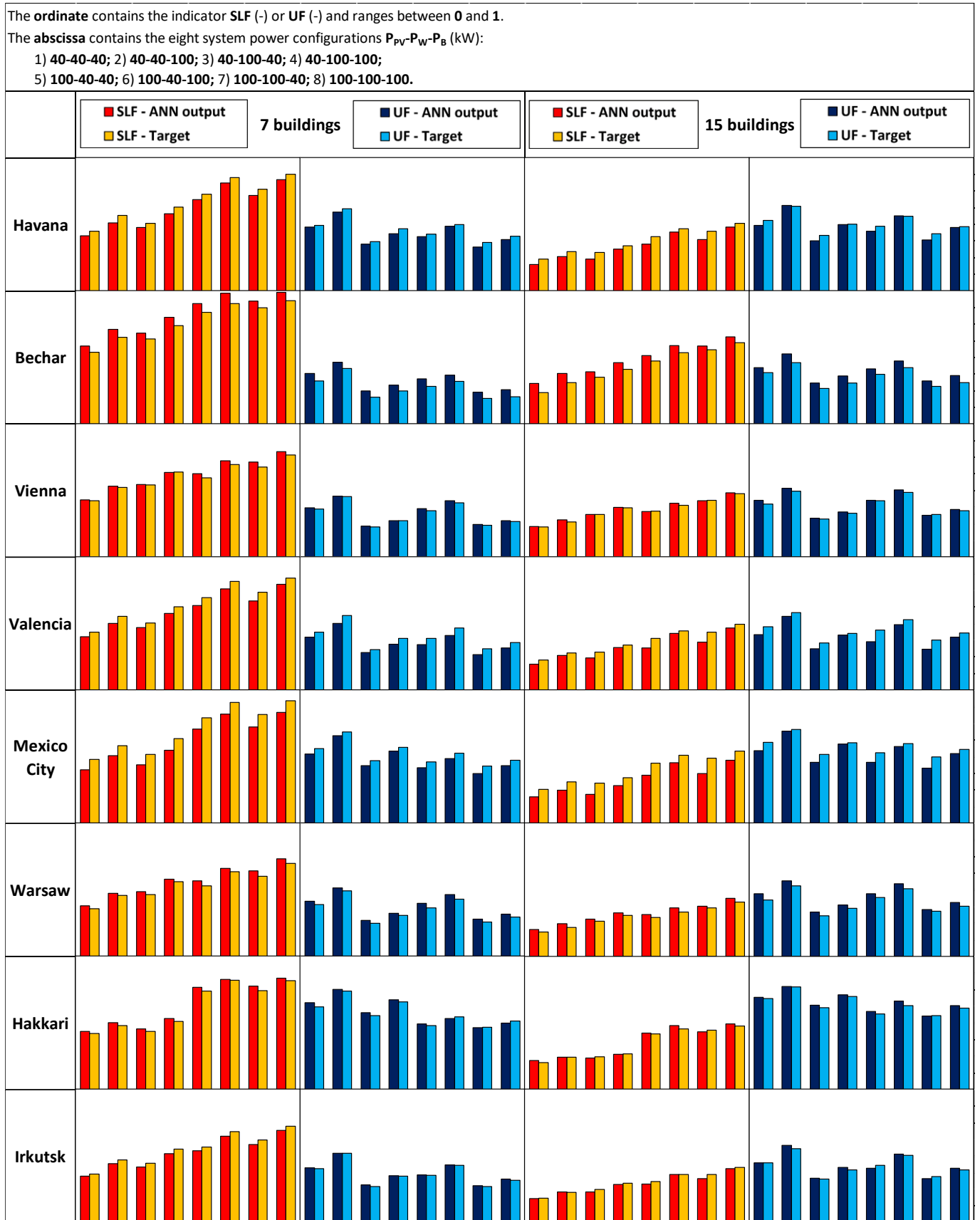
Figure 31. Direct comparison between the SLF and UF calculated with TRNSYS and with the optimized ANN for the eight localities considered, two building districts and eight system power configurations.

In all 128 cases, an excellent agreement between the two estimations can be observed.

3.4.2. ANN for the prediction of the grid energy interaction factor

Similar to the first optimal ANN, a comparison between ANN and TRNSYS output was developed and shown in Figure 32 in terms of a linear regression curve for the ANN with a sole output.
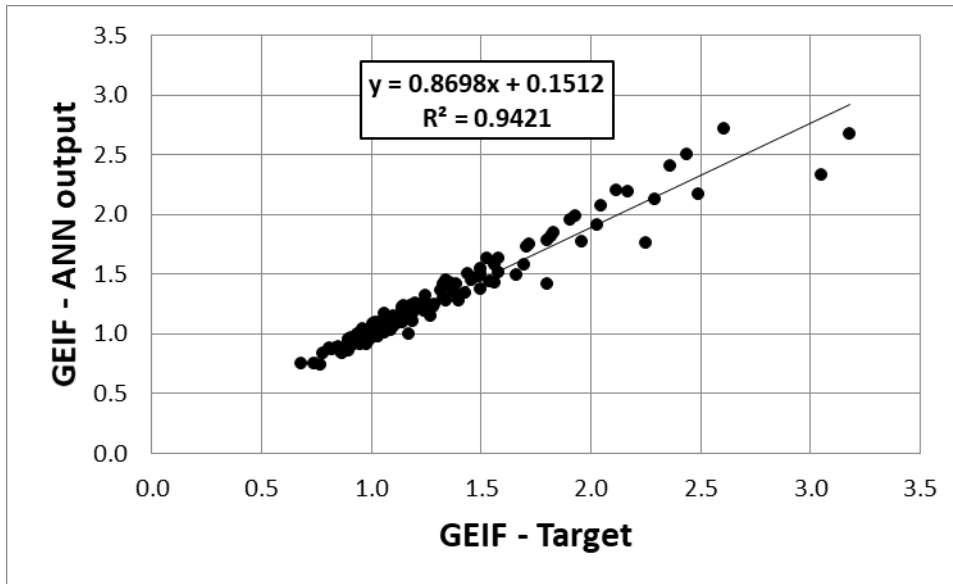
Figure 32. *Regression curve and metrics for the application of the optimal second ANN.*

The regression metrics highlight a high accuracy in the prediction of the *GEIF* by the ANN, which is confirmed when Figure 33, related to the direct comparison between the target and ANN output values of the 128 applications considered, is analysed.
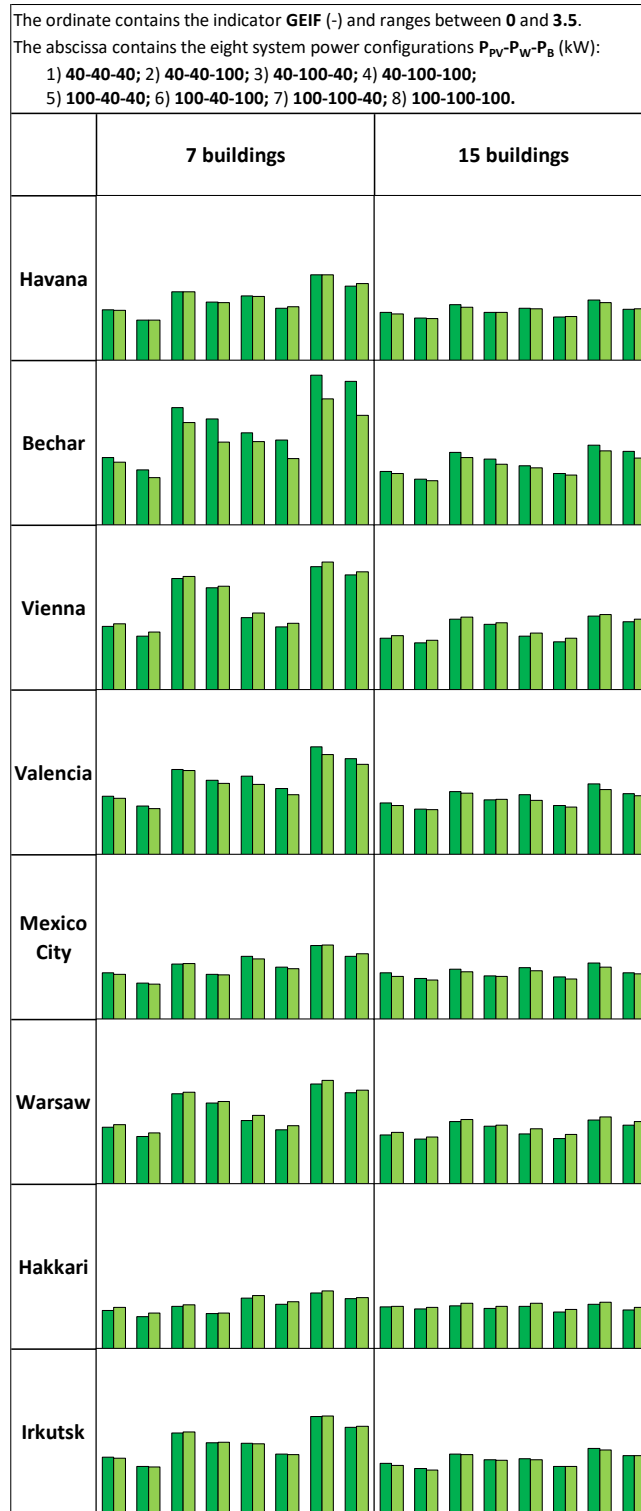
Figure 33. Direct comparison between the GEIF calculated with TRNSYS and with the optimized ANN for the eight localities considered, two building districts and eight system power configurations.

Furthermore, the second optimal ANN can be considered a reliable and accurate tool for the prediction of the level of interaction of the CEC with the grid.

4. Conclusions

A forecasting tool has been developed to predict the electrical performance of a hybrid system (PV panels, a wind turbines and energy storage) placed in a clean energy community where EV charging stations are available outside office buildings. The forecasting tool based on ANN has been created to characterize the defined energy performance indicators of a hybrid system at any locations. A procedure has been developed to describe the following four steps: (1) database generation; (2) data normalization; (3) designing, training, validating, and testing of the ANN architecture; and (4) application, validation, and testing of the created ANNs with different climatic conditions and system configurations. Although several studies have been conducted to create ANN-based forecasting tools for renewable energy systems, this is the first study in the literature, to the best of authors' knowledge, to predict the energy performance of a hybrid renewable energy system with any nominal power installed, without geographical restrictions, to be potentially implemented at any location in the world, and to be coupled with any load trend. In addition, the tool is capable to determine the yearly performance of the system deriving from a dynamic simulation without performing any dynamic simulation. The power of this tool is represented by the requirement to use only yearly mean and standard deviation values of time-dependent variables. The results obtained are almost equivalent to that obtained by a sophisticated hourly simulation based on detailed component electrical models. The input parameters of the forecasting tool were derived from an extremely large database using TRNSYS. To create this database, 49392 simulations were performed for 8760 hourly values of the interested parameters. Two different ANN architectures were developed to forecast SLF, UF and GEIF. Garson's algorithm was used to evaluate the influence of each input variable in the ANN architecture and its contribution to the model output.

The results reveal that for the first ANN architecture, the load variability overall fraction and the mean load overall fraction are the two most important input parameters to determine SLF and UF. However, the mean load overall fraction is the most important parameter for the second ANN architecture to quantify GEIF. Overall, the R^2 values of SLF, UF and GEIF predictions are 0.952, 0.925, 0.942 respectively, in all modelled energy communities external to the training database. The developed framework in this study is expected to help researchers to develop forecasting tools for different energy applications. Furthermore, the proposed ANNs represent user-friendly tools with the advantages in the reduction of input data required and no need of required high expertise to use transient simulation software that in many cases requires an expensive license to be used.

Considerations of the techno-economic assessment and developing energy management strategies by using different artificial intelligence techniques for hybrid renewable energy systems are a subject of future work.

Appendix A– Matlab script for the post-processing and synthesis of the 49392 dynamic hourly simulations

```
%% Calculation of the yearly energies from the hourly powers
intm=zeros(8760,27); % intermediate calculation matrix
Em=zeros(8232,21); % matrix for the calculation of yearly energies
Vm=zeros(8232,2); % matrix for the hourly verification of generated and load power balances
for i=1:49393 % cycles to extract, read and use for calculations the 49392 .txt TRNSYS files
    T=importdata(strcat('sone (',num2str(i),').txt'));
    C=T.data;
```

Chapter 8
Artificial intelligence application for the performance
prediction of a clean energy community

```
M=C(:,2:end); % matrix containing hourly powers outgoing each system component
intm(:,[1:4,6,7])=M(:,[1:4,6,7]);
intm(:,5)=M(:,2)+M(:,4);
intm(:,8:14)=M(:,7:13)/3.6;
for k=1:8760 % cycles to extract, read and use for calculations the 8760 rows (hours) in each TRNSYS files
    if intm(k,5)==0
        intm(k,15)=0;
    else
        intm(k,15)=intm(k,2)/intm(k,5);
        intm(k,16)=intm(k,4)/intm(k,5);
    end

    if intm(k,11)>0
        intm(k,17)=int(k,11)*intm(k,15);
        intm(k,18)=intm(k,11)*intm(k,16);
        intm(k,19)=intm(k,12)*intm(k,15);
        intm(k,20)=intm(k,12)*intm(k,16);
        intm(k,23)=intm(k,5);
        intm(k,24)=intm(k,12)/(0.98*0.97)+intm(k,13)/0.98+intm(k,11)/0.98;
        intm(k,25)=intm(k,12);
    else
        intm(k,17)=0;
        intm(k,18)=0;
        intm(k,19)=(intm(k,12)+intm(k,11)*0.97)*intm(k,15);
        intm(k,20)=(intm(k,12)+intm(k,11)*0.97)*intm(k,16);
        intm(k,23)=0;
        intm(k,24)=0;
        intm(k,25)=intm(k,10)*0.97*0.98-intm(k,11)*0.97;
    end
end
intm(:,21)=intm(:,13).*intm(:,15);
intm(:,22)=intm(:,13).*intm(:,16);
intm(:,26)=intm(:,25)+intm(:,14);
intm(:,27)=M(:,14)/3.6;

vp=abs(intm(:,23)-intm(:,24));
vl=abs(intm(:,26)-intm(:,27));
bvp=vp>0.3; % verification of hourly generated power balances
bvl=vl>0.3; % verification of hourly load power balances
Vm(i,1)=sum(bvp); % calculation of the number of hourly balances generated power not verified
Vm(i,2)=sum(bvl); % calculation of the number of hourly load power balances not verified

Em(i,:)=0;
for j=1:8760
    Em(i,[1:5,8:18,20])=Em(i,[1:5,8:18,20])+intm(j,[1:5,9,10,12:14,17:22,27]);
    if intm(j,8)>0
    Em(i,6)=Em(i,6)+intm(j,8);
    else
    Em(i,7)=Em(i,7)+intm(j,8);
    end
end
Em(:,19)=(Em(:,10)+Em(:,7)*0.97)/(0.97*0.98)+Em(:,11)/0.98+Em(:,6)/0.98;
Em(:,21)=Em(:,10)+Em(:,12);
Em(i,:)=Em(i,:)*10^-3;
end
xlswrite('1_verifica.xlsx',Vm,1); % print of excel file for the verifications
xlswrite('1_parametricresults.xlsx',Em,1); % print of excel file for yearly energies
```

Appendix B - Matlab script for the use of the optimal 20-neuron artificial neural network with the satisfied load fraction and the utilization factor as outputs

```matlab
function [Y,Xf,Af] = myNeuralNetworkFunction(X,~,~)
%MYNEURALNETWORKFUNCTION neural network simulation function.
%
% Generated by Neural Network Toolbox function genFunction, 05-Nov-2020 12:35:49.
%
% [Y] = myNeuralNetworkFunction(X,~,~) takes these arguments:
%
%   X = 1xTS cell, 1 inputs over TS timsteps
%   Each X{1,ts} = 8xQ matrix, input #1 at timestep ts.
%
% and returns:
%   Y = 1xTS cell of 1 outputs over TS timesteps.
%   Each Y{1,ts} = 2xQ matrix, output #1 at timestep ts.
%
% where Q is number of samples (or series) and TS is the number of timesteps.

%#ok<*RPMT0>

% ===== NEURAL NETWORK CONSTANTS =====

% Input 1
x1_step1_xoffset =
[0.037037037037037;0.037037037037037;0.0168945381102915;0.0782597980466159;0.0322527711963764;0.0589599192449892;0.0918006321999447;0.144960981250681];
x1_step1_gain =
[2.41071428571429;2.41071428571429;2.0481716617729;11.2968986244832;0.934102756695385;2.28452759826558;0.321074365843934;0.253818580812862];
x1_step1_ymin = -1;

% Layer 1
b1 = [-5.6104658836916945;-6.2556237377550641;3.1995994643446077;-2.8300355045556622;-3.1321238259223629;-0.10079552686556184;5.6305132305458532;0.30483782053287789;-2.8439284627855268;3.994170250845456;0.095151308162437415;14.887078524206744;18.127482265874939;-12.482313587262249;4.1391418775598172;-2.8502341662497046;-2.6843068363955216;3.1027444721155377;5.4365382188597655;12.200503896860582];
IW1_1 = [0.47513859284114773 0.54686492870946035 -2.9638395011077714 -0.18148485890517246 -3.6354496285332862 0.14061766847699617 -0.086781422848006232 2.7224076863461719;-0.17283106988795521 -0.16169158296460254 -19.510554604798987 0.59319974214946536 -1.4167458073027601 -14.117925875962412 10.359335261499503 18.628218754370479;-0.03375502998081515 -0.081698657064163377 0.23950828193549115 0.0700852613295396 0.016268654517138336 -0.051539545642703723 -0.038310390867143912 1.7734444905354763;-0.62227895445522052 0.36115323448569886 -0.67455567283680307 -0.11240819685660572 -0.021084948618650241 -0.017380106968578869 0.027241600759696269 0.6552295048143165;-0.027834789364377513 0.018236880524741025 1.844023809915933 -0.042954293105613259 -0.055752799008626237 0.038436144370493266 0.064357118222255705 -4.6084364802710676;0.035733375348957833 0.13714489775256189 -0.50821960238325958 -0.030800905764490585 0.016551162094700984 0.030404649491706844 -0.051480997957947423 0.48247660723936414;0.11793481352510211 0.62382742009026571 4.8999645966973677 -14.398254203488328 -18.686787734924778 6.9829864350492725 2.8676857111085279 -4.7737779724560623;0.1922948481795532 0.13096042526706159 -5.5512709866577596 -1.1397745412677305 -2.2626350781068876 -1.3193460348610244 3.0176572805558228 5.3212633721253226;1.1480264000390525 0.79204913896037443 -2.3588761390320743 -22.918747007242843 -19.392251418308295 12.359546213402867 -3.1982057861745044 1.8480495729982165;0.11780763724282889 0.1753256155791868 -1.5561602132992269 -0.15576421039128524 0.08778319098158463 0.033000439817089972 -0.066707866652585684 5.3847329698124025;-0.099574205762121268 -0.35889505483904893 1.1707210811953037 0.092061064597857081 -0.016447886654150135 -0.0171494793321077667 0.023112019847062057 -1.1177531842554922;-0.59969914121578649 -0.79621788284690287 9.0694406161445826 -0.25189845406807049 1.6969116573680654 0.0070661118186901468 -0.036003696643398218 2.9369001528092769;-0.53925240794178952 -
```

```
0.74478893569974502 23.635083826047339 -0.32018747256270685 1.6693790942836366 0.015117953114278854
0.024543502970146448 -7.9087414758260888;-0.44339196099304973 -0.19609269827155817 11.221144875172033
0.29180689636864182 -0.26477106894362962 -0.079667693835337061 0.048129407700001112 -
23.044064595506914;1.0181093291279513 -0.35052040910930371 -7.6314748707738387 0.10247722542807271
1.2649183681604008 -0.010585012840755654 0.37527006226105181 7.0957978965998665;-0.87839509950589512 -
0.22496663604100001 -11.878664499352633 0.23516450445825218 -2.0774297574220393 -0.13149162492257568
0.29902899884578804 11.184941140311524;0.38087307127395231 0.41739044480996573 11.325122698647153
0.29066566413230577 -0.18627609477555884 -0.077195624939410887 0.17702770009063712 -
12.623261792952617;0.96262845577406242 0.27912342365740644 15.109609540382205 -0.22128377716469691
2.0819305803242232 0.14810126989822595 -0.32068456364160519 -14.235915899529182;0.12324508550499604
0.32199722821027704 16.908715693779161 -0.092333032044113625 0.16723792550720981 0.04784277511001752 -
0.08247147740250417 -13.092055529986386;0.45095442710123373 0.18293593775506548 -13.482222002499666 -
0.28372830955374623 0.19801023216483016 0.07200596403267133 -0.019721763199877992
24.840688182160136];
```

```
% Layer 2
b2 = [2.0755997427107391;-22.40502373058878];
LW2_1 = [10.690915372389462 -0.22706174350814751 22.961779731276255 28.869664994195702
6.8040576626588996 -20.350096609378102 0.047790823043871021 -0.32610428153963167 0.064590702711650419
0.72449179017355392 -7.6331241710491824 -3.5179084831312784 1.2367589744675136 3.9502075439394839
13.404612615070208 6.5267412669008023 0.4246053778099963 6.1411521017803761 6.7998344546168674
5.6956427856362426;-2.8749736698201533 -0.13406459017669969 -48.248358462811723 -8.6565900488211387 -
15.045130303519052 -21.174467797864697 0.073961264268137011 -0.40005653541246222 0.066573020102656547
-6.6952356930477634 -8.1272904048175132 35.63470115045692 -13.548498037270489 10.466181334382986 -
5.1746220208905145 0.30297514630542782 -8.6579450770040811 0.10801889305103876 21.26097453196898
12.475179134761158];
```

```
% Output 1
y1_step1_ymin = -1;
y1_step1_gain = [2.20543685627519;2.05519642876897];
y1_step1_xoffset = [0.0931501873157924;0.0268570088952661];
```

```
% ===== SIMULATION =======
```

```
% Format Input Arguments
isCellX = iscell(X);
if ~isCellX, X = {X}; end;
```

```
% Dimensions
TS = size(X,2); % timesteps
if ~isempty(X)
    Q = size(X{1},2); % samples/series
else
    Q = 0;
end
```

```
% Allocate Outputs
Y = cell(1,TS);
```

```
% Time loop
for ts=1:TS
```

```
    % Input 1
    Xp1 = mapminmax_apply(X{1,ts},x1_step1_gain,x1_step1_xoffset,x1_step1_ymin);
```

```
    % Layer 1
    a1 = tansig_apply(repmat(b1,1,Q) + IW1_1*Xp1);
```

```
    % Layer 2
    a2 = repmat(b2,1,Q) + LW2_1*a1;
```

```matlab
  % Output 1
  Y{1,ts} = mapminmax_reverse(a2,y1_step1_gain,y1_step1_xoffset,y1_step1_ymin);
end

% Final Delay States
Xf = cell(1,0);
Af = cell(2,0);

% Format Output Arguments
if ~isCellX, Y = cell2mat(Y); end
end

% ===== MODULE FUNCTIONS ========

% Map Minimum and Maximum Input Processing Function
function y = mapminmax_apply(x,settings_gain,settings_xoffset,settings_ymin)
y = bsxfun(@minus,x,settings_xoffset);
y = bsxfun(@times,y,settings_gain);
y = bsxfun(@plus,y,settings_ymin);
end

% Sigmoid Symmetric Transfer Function
function a = tansig_apply(n)
a = 2 ./ (1 + exp(-2*n)) - 1;
end

% Map Minimum and Maximum Output Reverse-Processing Function
function x = mapminmax_reverse(y,settings_gain,settings_xoffset,settings_ymin)
x = bsxfun(@minus,y,settings_ymin);
x = bsxfun(@rdivide,x,settings_gain);
x = bsxfun(@plus,x,settings_xoffset);
end
```

Appendix C - Matlab script for the use of the optimal 20-neuron artificial neural network with the grid energy interaction factor as output

```matlab
function [Y,Xf,Af] = myNeuralNetworkFunction(X,~,~)
%MYNEURALNETWORKFUNCTION neural network simulation function.
%
% Generated by Neural Network Toolbox function genFunction, 10-Nov-2020 16:43:34.
%
% [Y] = myNeuralNetworkFunction(X,~,~) takes these arguments:
%
%   X = 1xTS cell, 1 inputs over TS timsteps
%   Each X{1,ts} = 8xQ matrix, input #1 at timestep ts.
%
% and returns:
%   Y = 1xTS cell of 1 outputs over TS timesteps.
%   Each Y{1,ts} = 1xQ matrix, output #1 at timestep ts.
%
% where Q is number of samples (or series) and TS is the number of timesteps.

%#ok<*RPMT0>

% ===== NEURAL NETWORK CONSTANTS =====

% Input 1
x1_step1_xoffset =
[0.037037037037037;0.037037037037037;0.0168945381102915;0.0782597980466159;0.0322527711963764;0.0589599192449892;0.0918006321999447;0.144960981250681];
```

```
x1_step1_gain =
[2.41071428571429;2.41071428571429;2.0481716617729;11.2968986244832;0.934102756695385;2.2845275982655
8;0.321074365843934;0.253818580812862];
x1_step1_ymin = -1;
```

```matlab
% Layer 1
b1 = [13.905356904171413;18.181141770709136;13.399337520662707;1.9973307383820311;-
1.5963486545021104;14.139989834385851;-13.312042337317145;-
2.2548525176366248;14.686557372064788;0.3193383042099206;-0.26358447723233541;-0.20555165260860536;-
0.1650170495281551;-1.8886356925120582;3.9993672599994574;-
1.6272184357898059;16.969049374823967;0.13574022144705006;4.2311321312322665;5.2682426327088407];
IW1_1 = [0.41247209096970472 0.37197337293210098 3.4298417452517165 -1.1531298587378234 -
2.2521185859512074 7.2091539253514361 3.9344968736898824 0.52925861722509548;-0.041123378117603811
0.036655252523169125 6.5860006606535535 -2.0710166197532938 -3.4212102239009212 -0.52278149818950226
3.2513648217714652 7.0436487599509849;-0.12237410167750773 -0.038157815984621306 8.4807858568024592
0.012265438618020241 0.80710617571177412 -0.12651669695211942 0.0091287612317893334
2.7610497901580038;-0.034923994053926287 0.16133631682341026 7.2922796431755881 -0.52496843855178854
0.3164371473054689 1.9428292933659346 -1.5708206572907994 -5.6880326320498531;0.33536009027523039
0.029275963415003086 1.2614669025462897 0.94360059923695294 1.231941285711909 -2.349397882171425
2.0826450966145353 -2.2302517283674241;-0.066474280368318844 0.0095935740045000311 24.854406857118491
0.019685007322816854 -0.24721980994162782 -0.1206099773582365 0.15067601410147219 -
11.958520207304481;0.083540326917103128 0.099959279487074795 -2.3078929320557533 -
0.042255817259619355 -0.94141121185877019 0.14889762650334629 -0.0032208803368358593 -
9.415066677512554;0.018333129910036619 -0.025782633695252129 5.423600341457961 -2.0545592412690485
6.8249469581996056 -6.329724945327337 5.8072224396658578 -5.5400511598978754;0.02035289505610257 -
0.0021757270485331308 23.047636716531972 -0.0049603767699790509 -0.20535026218386185 -
0.099483799385008231 0.12175634576963046 -9.0379800435353026;0.02596824842543529 -
0.023183412716954795 6.2116803253072801 0.53590958672585276 -2.133728940870844 -0.8722941747419678
2.6338156487366198 -6.1027404552108822;0.043171301100919622 0.01159110127003677 0.70186625950631509
0.32457217405200556 -1.1077396857734321 -0.644116643988909 0.91835800641600152 -
0.77190415740862828;0.067916469962766304 0.013836832535216132 0.58951765163739955 0.2903205166563978
-0.78322720041736804 -0.64777425865356808 0.58368596891071267 -0.72045027233513625;-1.9117693021612012
-2.882854193539667 -15.448568997300219 -0.48082572376400456 3.8171337951376336 0.34470826557281925 -
1.3267458047959999 12.218812816463878;0.10274790797161197 -0.096716753246369178 -2.9256861346472429
0.59630360812345318 -0.56609262079290346 -1.8502757745395737 1.3825836178332374
1.7553921198829416;0.074997047414807227 -0.96789142270755235 1.1596352784279218 -0.023414595509726098
-0.017675475307022757 0.06711634651850916 -0.037178863916060026
4.3935104681694526;0.27734821387991926 -0.048285558525565167 -13.80123269198616 0.16436583045800326
1.0075148574767465 -0.25937831472391426 0.86858403229015946 12.007360490310509;0.34065108458110893
0.26727701027051143 17.996675911852133 -0.21575536110964444 0.11947406510782682 0.040504393004984318
0.025720544430131807 -3.2091666772782159;0.11467996581765777 0.0059426699627541883 2.9803923219256987
0.16909058975488203 0.076848689703877343 -0.46683793812110475 0.17780695678253755 -
3.1386720202938778;0.088004688453794555 -0.96829227394297379 3.7180702804614021 -
0.0076925133793133548 -0.024501167054664947 0.068863863942549508 -0.047424261238301901
2.1741651789371321;0.45982183761793088 0.11877143620228461 10.164686900572756 0.21749858454446461 -
1.7773148236747232 -0.70600951252220323 1.2822362899878117 -5.9993464867908388];
```

```matlab
% Layer 2
b2 = 15.819800316197659;
LW2_1 = [-0.39596255073086178 11.605031720780044 48.131718936218107 0.86365392772930383 -
0.51210283156876779 -57.398109573417706 10.849977257002525 0.26077400144705765 18.85738332020755
1.2568506404410225 -8.5678171110470789 8.4698181839372566 -0.031472527545683755 1.2066201597546264
0.85002021808098538 0.62662240554841697 -27.14392960104842 -2.4400437086589783 -0.81854807138681007
0.48742696065345426];
```

```matlab
% Output 1
y1_step1_ymin = -1;
y1_step1_gain = 0.215827589025058;
y1_step1_xoffset = 0.481351774190152;
```

```matlab
% ===== SIMULATION ========
```

```matlab
 % Format Input Arguments
isCellX = iscell(X);
if ~isCellX, X = {X}; end;

% Dimensions
TS = size(X,2); % timesteps
if ~isempty(X)
   Q = size(X{1},2); % samples/series
else
   Q = 0;
end

% Allocate Outputs
Y = cell(1,TS);

% Time loop
for ts=1:TS

   % Input 1
   Xp1 = mapminmax_apply(X{1,ts},x1_step1_gain,x1_step1_xoffset,x1_step1_ymin);

   % Layer 1
   a1 = tansig_apply(repmat(b1,1,Q) + IW1_1*Xp1);

   % Layer 2
   a2 = repmat(b2,1,Q) + LW2_1*a1;

   % Output 1
   Y{1,ts} = mapminmax_reverse(a2,y1_step1_gain,y1_step1_xoffset,y1_step1_ymin);
end

% Final Delay States
Xf = cell(1,0);
Af = cell(2,0);

% Format Output Arguments
if ~isCellX, Y = cell2mat(Y); end
end

% ===== MODULE FUNCTIONS ========

% Map Minimum and Maximum Input Processing Function
function y = mapminmax_apply(x,settings_gain,settings_xoffset,settings_ymin)
y = bsxfun(@minus,x,settings_xoffset);
y = bsxfun(@times,y,settings_gain);
y = bsxfun(@plus,y,settings_ymin);
end

% Sigmoid Symmetric Transfer Function
function a = tansig_apply(n)
a = 2 ./ (1 + exp(-2*n)) - 1;
end

% Map Minimum and Maximum Output Reverse-Processing Function
function x = mapminmax_reverse(y,settings_gain,settings_xoffset,settings_ymin)
x = bsxfun(@minus,y,settings_ymin);
x = bsxfun(@rdivide,x,settings_gain);
x = bsxfun(@plus,x,settings_xoffset);
end
```

References

[1] Digitalisation and Energy. IEA, November 2017. Website: https://www.iea.org/reports/digitalisation-and-energy.

[2] IRENA. Innovation landscape brief: Artificial intelligence and big data, International Renewable Energy Agency, Abu Dhabi, 2019.

[3] S. Kr. Jha, J. Bilalovic, A. Jha, N. Patel, H. Zhang, Renewable energy: Present research and future scope of Artificial Intelligence, Renewable and Sustainable Energy Reviews, Volume 77, 2017, Pages 297-317, ISSN 1364-0321, https://doi.org/10.1016/j.rser.2017.04.018.

[4] L. Zhaoxuan, S.M. Rahman, R. Vega, B. Dong, A hierarchical approach using machine learning methods in solar photovoltaic energy production forecasting, Energies, Volume 9, Issue 1, 2016, Pages 55, ISSN 1996-1073, https://doi.org/10.3390/en9010055

[5] A.-L. Klingler, L. Teichtmann, Impacts of a forecast-based operation strategy for grid-connected PV storage systems on profitability and the energy system, Solar Energy, Volume 158, 2017, Pages 861-868, ISSN 0038-092X, https://doi.org/10.1016/j.solener.2017.10.052.

[6] S. Al-Dahidi, O. Ayadi, J. Adeeb, M. Alrbai, B.R. Qawasmeh, Extreme learning machines for solar photovoltaic power predictions, Energies, Volume 11, Issue 10, 2018, Pages 2725, ISSN 1996-1073, https://doi.org/10.3390/en11102725

[7] J. Yu, Z. Wang, A. Majumdar, R. Rajagopal, DeepSolar: A Machine Learning Framework to Efficiently Construct a Solar Deployment Database in the United States, Joule, Volume 2, Issue 12, 2018, Pages 2605-2617, ISSN 2542-4351, https://doi.org/10.1016/j.joule.2018.11.021.

[8] S. Kim, H. Lim, Reinforcement learning based energy management algorithm for smart energy buildings, Energies, Volume 11, Issue 8, 2018, 2010, ISSN 1996-1073, https://doi.org/10.3390/en11082010

[9] N., Priyadarshi, V.K. Ramachandaramurthy, S. Padmanaban, F. Azam, An ant colony optimized MPPT for standalone hybrid PV-wind power system with single Cuk converter, Energies, Volume 12, Issue 1, 2019, 167, ISSN 1996-1073, https://doi.org/10.3390/en12010167

[10] W. Zhang, A. Maleki, M. A. Rosen, J. Liu, Sizing a stand-alone solar-wind-hydrogen energy system using weather forecasting and a hybrid search optimization algorithm, Energy Conversion and Management, Volume 180, 2019, Pages 609-621, ISSN 0196-8904, https://doi.org/10.1016/j.enconman.2018.08.102.

[11] W.Zhang, A. Maleki, M. A. Rosen, A heuristic-based approach for optimizing a small independent solar and wind hybrid power scheme incorporating load forecasting, Journal of Cleaner Production, Volume 241, 2019, 117920, ISSN 0959-6526, https://doi.org/10.1016/j.jclepro.2019.117920.

[12] N.T. Le, W. Benjapolakul, Evaluation of contribution of PV array and inverter configurations to rooftop PV system energy yield using machine learning techniques, Energies, Volume 12(16), 2019, Pages 3158, https://doi.org/10.3390/en12163158

[13] A. Marinescu, A. Taylor, S. Clarke, I. Serban, C. Marinescu, Optimising residential electric vehicle charging under renewable energy: Multi-agent learning in software simulation and hardware-in-the-loop evaluation, International Journal of Energy Research, Volume 43, Issue 8, Pages 3853-3868, 2019, ISSN 1099-114X, https://doi.org/10.1002/er.4559.

[14] B. Zhang, W. Hu, D. Cao, Q. Huang, Z. Chen, F. Blaabjerg, Deep reinforcement learning–based approach for optimizing energy conversion in integrated electrical and heating system with renewable energy, Energy Conversion and Management, Volume 202, 2019, 112199, ISSN 0196-8904, https://doi.org/10.1016/j.enconman.2019.112199.

[15] R. D. Bingham, M. Agelin-Chaab, M. A. Rosen, Whole building optimization of a residential home with PV and battery storage in The Bahamas, Renewable Energy, Volume 132, 2019, Pages 1088-1103, ISSN 0960-1481, https://doi.org/10.1016/j.renene.2018.08.034.

[16] S. Sundaram, Performance assessment with the prediction of final yield and performance ratio employing Artificial Neural Network for a realistic 1 MWp PV plant in India, International Journal of Ambient Energy, 2020, Pages 1-39, ISSN: 2162-8246, https://doi.org/10.1080/01430750.2020.1712239.

[17] Z. Pang, F. Niu, Z. O'Neill, Solar radiation prediction using recurrent neural network and artificial neural network: A case study with comparisons, Renewable Energy, Volume 156, 2020, Pages 279-289, ISSN 0960-1481, https://doi.org/10.1016/j.renene.2020.04.042.

[18]   Lee, S. and Choi, D.H. Energy Management of Smart Home with Home Appliances, Energy Storage System and Electric Vehicle: A Hierarchical Deep Reinforcement Learning Approach, Sensors, Volume 20, Issue 7, 2020, 2157, ISSN 1424-8220, https://doi.org/10.3390/s20072157

[19]   T. Ahmad, H. Zhang, B. Yan, A review on renewable energy and electricity requirement forecasting models for smart grid and buildings, Sustainable Cities and Society, Volume 55, 2020, 102052, ISSN 2210-6707, https://doi.org/10.1016/j.scs.2020.102052.

[20]   M. Majidi Nezhad, A. Heydari, D. Groppi, F. Cumo, D. Astiaso Garcia, Wind source potential assessment using Sentinel 1 satellite and a new forecasting model based on machine learning: A case study Sardinia islands, Renewable Energy, Volume 155, 2020, Pages 212-224, ISSN 0960-1481, https://doi.org/10.1016/j.renene.2020.03.148.

[21]   A. F. Mirza, M. Mansoor, Q. Ling, B. Yin, M. Y. Javed, A Salp-Swarm Optimization based MPPT technique for harvesting maximum energy from PV systems under partial shading conditions, Energy Conversion and Management, Volume 209, 2020, 112625, ISSN 0196-8904, https://doi.org/10.1016/j.enconman.2020.112625.

[22]   Y. Zhou, S. Zheng, Machine-learning based hybrid demand-side controller for high-rise office buildings with high energy flexibilities, Applied Energy, Volume 262, 2020, 114416, ISSN 0306-2619, https://doi.org/10.1016/j.apenergy.2019.114416.

[23]   J. Feng, S. Hou, L. Yu, N. Dimov, P. Zheng, Chunping Wang, Optimization of photovoltaic battery swapping station based on weather/traffic forecasts and speed variable charging, Applied Energy, Volume 264, 2020, 114708, ISSN 0306-2619, https://doi.org/10.1016/j.apenergy.2020.114708.

[24]   M. J. Mayer, A. Szilágyi, G. Gróf, Environmental and economic multi-objective optimization of a household level hybrid renewable energy system by genetic algorithm, Applied Energy, Volume 269, 2020, 115058, ISSN 0306-2619, https://doi.org/10.1016/j.apenergy.2020.115058.

[25]   B. E. Nyong-Bassey, D. Giaouris, C. Patsios, S.Papadopoulou, Athanasios I. Papadopoulos, Sara Walker, Spyros Voutetakis, Panos Seferlis, Shady Gadoue, Reinforcement learning based adaptive power pinch analysis for energy management of stand-alone hybrid energy storage systems considering uncertainty, Energy, Volume 193, 2020, 116622, ISSN 0360-5442, https://doi.org/10.1016/j.energy.2019.116622.

[26]   A.Z. Dhunny, D.S. Timmons, Z. Allam, M.R. Lollchund, T.S.M. Cunden, An economic assessment of near-shore wind farm development using a weather research forecast-based genetic algorithm model, Energy, Volume 201, 2020, 117541, ISSN 0360-5442, https://doi.org/10.1016/j.energy.2020.117541.

[27]   G.Y. Kim, D.S. Han, Z. Lee, Solar Panel Tilt Angle Optimization Using Machine Learning Model: A Case Study of Daegu City, South Korea, Energies, Volume 13, Issue 3, 529, 2020, ISSN 1996-1073, https://doi.org/10.3390/en13030529.

[28]   Y. Sui, S. Song, A Multi-Agent Reinforcement Learning Framework for Lithium-ion Battery Scheduling Problems, Energies, Volume 13, Issue 8, 1982, 2020, ISSN 1996-1073, https://doi.org/10.3390/en13081982.

[29]   TRNSYS, Transient System Simulation Tool, Version 17, Solar Energy Laboratory University of Wisconsin-Madison, Madison, WI (USA), 2012, http://www.trnsys.com.

[30]   Deep Learning Toolbox, ©COPYRIGHT 1992-2004 by The MathWorks, Inc. Natick, Massachusetts, United State. Website: https://www.mathworks.com/help/deeplearning/ref/nftool.html.

[31]   Solar Energy Laboratory, University of Wisconsin-Madison (2012). TRNSYS 17 documentation, Volume 4, Mathematical Reference.

[32]   Fisch und Fischl GmbH, Spritmonitor.de, Available at: www.spritmonitor.de, Thyrnau (Germany), last access: 30/11/2020.

[33]   D. Mazzeo, Nocturnal electric vehicle charging interacting with a residential photovoltaic-battery system: a 3E (energy, economic and environmental) analysis, Energy, Volume 168, 2019, Pages 310-331, ISSN 0360-5442, https://doi.org/10.1016/j.energy.2018.11.057.

[34]   O. I. Abiodun, A. Jantan, A. E. Omolara, K. V. Dada, N. A. Mohamed, H. Arshad, State-of-the-art in artificial neural network applications: A survey, Heliyon, Volume 4, Issue 11, 2018, e00938, ISSN 2405-8440, https://doi.org/10.1016/j.heliyon.2018.e00938.

[35]   P. Kim, Matlab deep learning. With Machine Learning, Neural Networks and Artificial Intelligence,
Volume 130, Issue 21, ISBN 978-1-4842-2845-6, 2017, https://doi.org/10.1007/978-1-4842-2845-6.

[36]   Deep Learning Toolbox, ©COPYRIGHT 1992-2004 by The MathWorks, Inc. Natick,
Massachusetts, United State. Website: https://www.mathworks.com/help/deeplearning/ref/trainlm.html

[37]   M.T. Hagan, H.B. Demuth, M.H. Beale, Neural Network Design, 1996, Boston, MA: PWS Publishing.

[38]   M. T. Hagan and M. B. Menhaj, Training feedforward networks with the Marquardt algorithm," in
IEEE Transactions on Neural Networks, Volume 5, Issue 6, Pages 989-993, ISSN 1941-0093, 1994,
https://doi.org/10.1109/72.329697.

[39]   G. D. Garson, Interpreting Neural Network Connection Weights, AI Expert, Volume Issue 6, 1991,
Pages 47-51, ISSN 0888-3785.

[40]   M. Gevrey, I. Dimopoulos, S. Lek, Review and comparison of methods to study the contribution of
variables in artificial neural network models, Ecological Modelling, 2003, Volume 160, Issue 3, 2003,
Pages 249-264, ISSN 0304-3800, https://doi.org/10.1016/S0304-3800(02)00257-0.

Nomenclature

Acronyms

AI	Artificial intelligence
ANN	Artificial neural network
CRM	Coefficient of residual mass
EV	Electric vehicle
GEIF	Grid energy interaction factor
HRES	Hybrid renewable energy system
MAE	Mean absolute error
MPPT	Maximum power point tracker
MSE	Mean square error
RE	Renewable energy
RMSE	Root mean square error
SLF	Satisfied load fraction
SOC	State of charge
UF	Utilization factor

Symbols

b_i	Bias vector of the i-th layer in an ANN architecture
$c_{se,sd}$	Photovoltaic energy variability factor (-)
$c_{se,m}$	Mean photovoltaic energy factor (-)
$c_{we,m}$	Mean wind energy factor (-)
$c_{we,sd}$	Wind energy variability factor (-)
E_{dtl}	Yearly energy sent directly to the load (Wh)
E_{fb}	Yearly energy drawn from the battery (Wh)
E_{fg}	Yearly energy drawn from the grid (Wh)
E_g	Yearly overall energy produced by the generators (Wh)
E_L	Yearly energy required by the load (Wh)
E_{pv}	Yearly energy produced by the photovoltaic generator (Wh)
E_{tb}	Yearly energy sent to the battery (Wh)
E_{tg}	Yearly energy sent to the grid (Wh)
E_{tl}	Yearly energy produced sent to the load (Wh)
E_w	Yearly energy produced by the wind generator (Wh)
G_m	Yearly average horizontal solar radiation (W/m^2)
G_{ref}	Reference absorbed total solar radiation (W/m^2)
G_{sd}	Yearly standard deviation of the horizontal solar radiation (W/m^2)

GEIF	Grid energy interaction factor (-)
MSE	Mean square error (-)
N	Total number of comparisons (-)
P	Performance (-)
p_b	Storage power fraction (-)
P_B	Nominal battery power (W)
P_{dtl}	Load directly compensated by the hybrid system (W)
P_{fb}	Power drawn from the battery (W)
P_{fg}	Power drawn from the grid (W)
P_g	Generated power (W)
$P_{L,m}$	Yearly average load (W)
$p_{l,m}$	Mean load overall fraction (-)
$p_{l,sd}$	Load variability overall fraction (-)
$P_{L,sd}$	Standard deviation of the yearly load (W)
P_n	Total rated power of the system (W)
P_{pv}	Photovoltaic power produced (W)
P_{PV}	Nominal photovoltaic power (W)
$P_{pv,eff}$	Effective photovoltaic power output from the DC/DC converter (W)
P_{tb}	Power sent to the battery (W)
P_{tg}	Power sent to the grid (W)
p_w	Wind power fraction (-)
P_w	Wind power produced (W)
P_W	Nominal wind power (W)
$P_{w,eff}$	Effective wind power output from the AC/DC rectifier (W)
R	Coefficient of correlation (-)
R^2	Coefficient of determination (-)
s_{ij}	Sum of the r overall weights $W_{r,ij}$,
S_{ij}	Percentage sensitivity
SLF	Satisfied load factor (-)
t_i	Target value (-)
T_m	Yearly average external air temperature (K)
$T_{ref,pv}$	Reference temperature for the characteristic I-V curve of a PV cell (K)
$T_{ref,w}$	Reference temperature for the characteristic power curve of a wind turbine (K)
T_{sd}	Yearly standard deviation of the external air temperature (K)
UF	Utilization factor (-)
V_{m3}	Yearly cubic average wind speed (m/s)
$V_{m3,sd}$	Standard deviation of the cubic mean wind speed (m/s)
$V_{m3,ref}$	Reference cubic mean wind speed (m/s)
w_i	Weights between the (i-1)-th layer and i-th layer in an ANN architecture
$W_{r,ij}$	Overall weight of the route r between the i-th input neuron and the j-th output neuron
x_0	Input vector in an ANN architecture
y	Output vector in an ANN architecture

Greek Letters

η_{inv}	Inverter efficiency (-)
η_{reg}	Regulator efficiency (-)
φ	Activation function in an ANN architecture
χ_i	i-th normalized input
ψ_i	i-th normalized output

Conclusions

The detailed outcomes deriving from this PhD thesis were illustrated in the different chapters. The main proposals, accomplishments and conclusions of this PhD thesis are listed below:

1. an **upgradable matrix literature database** and **literature review** that can be updated for future investigations aiming to detect the research trend in this field. This research is proposed as a valuable tool for engineers, experts and national and international policymakers.

2. an **energy-constrained reliability method for the multi-objective optimization of PV-wind hybrid systems**. It employs several indicators to identify the most energy reliable system configurations and can be applied easily to a grid-connected and stand-alone PV-wind hybrid system with and without storage battery, in any climate context and load conditions and allows optimizing the system in accordance with the specific application and the objectives. In addition, it can be applied in both the design phase and performance verification phase of a specific hybrid system.

3. a **novel energy-economic-environmental multi-criteria decision-making procedure to analyse the PV-wind-battery system configuration, PV-wind, PV-battery and wind-battery system sub-configurations**, by varying the size of each component and by considering different loads. The procedure consists of width energy, economic and environmental analysis that, simultaneously, assures:

   - from an energy point of view, a high load satisfaction, high utilization of the energy produced and high utilization of the nominal power installed;
   - from an economic point of view, the maximum convenience;
   - from an environmental point of view, the maximum abatement of CO_2.

   The effect produced by the battery lifespan and incentives on the multi-criteria decision-making procedure results was investigated.

4. an **energy, economic and environmental (3E) feasibility study regarding a nocturnal electric vehicle (EV) charging in a residential user**. In particular, three different EV charging scenarios were considered: use of the grid; use of a grid-connected PV system with a storage battery; use of a grid-connected PV system with a storage battery in the presence also of a residential user. Two sub-scenarios were examined that foresee the purchase of the EV as an alternative to a vehicle powered, respectively, by petrol and diesel.

5. a **dynamic and energy reliability analysis of a renewable hybrid trigeneration system (RHTS)** consisting of a photovoltaic generator, a wind micro-generator and an electric storage battery (electric renewable hybrid system ERHS) used to supply a heat pump, electric office devices, and an electric vehicle charging station.

6. a **new dynamic simulation tool made up of three subroutines** and a new procedure that employs the concepts of the average reliability and reliability uncertainty **to determine the performance of a renewable hybrid trigeneration system employed for supplying heating and cooling air conditioning and electricity demand**. The method of analysis developed and used in the specific case study is also employable, in addition to comparing different system configurations and powers, in the system design phase. Different localities can be compared and, for a specific locality, the most appropriate user can be identified.

7. a **mapping and energy and economic optimization of the techno-economic performance of stand-alone (SA) and grid-connected (GC) PV-wind hybrid renewable systems (HRES)**

worldwide for a typical office building district. The extensive energy and economic investigations developed constitute a concrete device and database to detect the performance of the optimal hybrid system around the world. In addition, the results can be used by other researchers as a reference to compare their investigations.

8. **Artificial Neural Networks (ANNs) for sizing and simulating a clean energy community (CEC) that employs a PV-wind hybrid system, coupled with energy storage systems and electric vehicle charging stations, to meet the building district energy demand**. Although several studies have been conducted to create ANN-based forecasting tools for renewable energy systems, this is the first study in the literature, to the best of my knowledge, to predict the energy performance of a hybrid renewable energy system with any nominal power installed, without geographical restrictions, to be potentially implemented at any location in the world, and to be coupled with any load trend. The proposed ANNS represent user-friendly tools with the advantages in the reduction of input data required and no need of required high expertise to use transient simulation software that in many cases requires an expensive license to be used.